

## INFORMATION TO USERS

This manuscript has been reproduced from the microfilm master. UMI films the text directly from the original or copy submitted. Thus, some thesis and dissertation copies are in typewriter face, while others may be from any type of computer printer.

**The quality of this reproduction is dependent upon the quality of the copy submitted.** Broken or indistinct print, colored or poor quality illustrations and photographs, print bleedthrough, substandard margins, and improper alignment can adversely affect reproduction.

In the unlikely event that the author did not send UMI a complete manuscript and there are missing pages, these will be noted. Also, if unauthorized copyright material had to be removed, a note will indicate the deletion.

Oversize materials (e.g., maps, drawings, charts) are reproduced by sectioning the original, beginning at the upper left-hand corner and continuing from left to right in equal sections with small overlaps. Each original is also photographed in one exposure and is included in reduced form at the back of the book.

Photographs included in the original manuscript have been reproduced xerographically in this copy. Higher quality 6" x 9" black and white photographic prints are available for any photographs or illustrations appearing in this copy for an additional charge. Contact UMI directly to order.

# UMI

A Bell & Howell Information Company  
300 North Zeeb Road, Ann Arbor MI 48106-1346 USA  
313/761-4700 800/521-0600



**THE MECHANICS OF CURVE PROGRESSION IN  
ADOLESCENT IDIOPATHIC SCOLIOSIS**

by

**Neil Alexander Duncan**

**Department of Mechanical Engineering  
McGill University, Montreal**

A Thesis submitted to the Faculty of Graduate Studies and Research  
in partial fulfilment of the requirements of the degree of  
Doctor of Philosophy.

February 1997

© Neil A. Duncan. 1997



National Library  
of Canada

Acquisitions and  
Bibliographic Services

395 Wellington Street  
Ottawa ON K1A 0N4  
Canada

Bibliothèque nationale  
du Canada

Acquisitions et  
services bibliographiques

395, rue Wellington  
Ottawa ON K1A 0N4  
Canada

*Your file Votre référence*

*Our file Notre référence*

The author has granted a non-exclusive licence allowing the National Library of Canada to reproduce, loan, distribute or sell copies of this thesis in microform, paper or electronic formats.

The author retains ownership of the copyright in this thesis. Neither the thesis nor substantial extracts from it may be printed or otherwise reproduced without the author's permission.

L'auteur a accordé une licence non exclusive permettant à la Bibliothèque nationale du Canada de reproduire, prêter, distribuer ou vendre des copies de cette thèse sous la forme de microfiche/film, de reproduction sur papier ou sur format électronique.

L'auteur conserve la propriété du droit d'auteur qui protège cette thèse. Ni la thèse ni des extraits substantiels de celle-ci ne doivent être imprimés ou autrement reproduits sans son autorisation.

0-612-29926-0

*To my parents,*

*for confidence to explore the reality of imagination*

"The edges of the real landscape became one with the edges of something I dreamed. But what I had dreamed was only a pattern, some beautiful pattern of light. The continuous work of the imagination, I thought, to bring what is actual together with what is dreamed is an expression of human evolution. The conscious desire is to achieve a state, even momentarily, that like light is unbounded, nurturing, suffused with wisdom and creation, a state in which one has absorbed that very darkness which before was the perpetual sign of defeat.

Whatever world that is, it lies far ahead. But its outline, its adumbration is clear in the landscape, and upon this one can actually hope we will find our way."

*Barry Lopez, 1986*

"Eventually, all things merge into one, and a river runs through it."

*Norman Maclean, 1976*

## ABSTRACT

Scoliosis is a deformity of the spine that predominately affects adolescent females. Mild scoliotic curves are most vulnerable to progression during the adolescent growth spurt, however, only an unpredictable 15-25% progress to large incapacitating deformities. The present objective was to identify mechanical factors associated with the adolescent growth spurt which are instrumental to curve progression in adolescent idiopathic scoliosis (AIS). An initially curved and twisted, spatial beam-column model of a spine with a mild scoliosis was developed. The spine was embedded in a three-dimensional elastic medium to represent the ribcage. A finite element model of a ribcage was developed to establish its three-dimensional stiffness through a series of numerical experiments. Parametric analyses of both the ribcage and spine models were conducted to elucidate a better understanding of this mechanical system. The geometry, material properties and applied loads of the spine were then systematically changed to simulate both normal and aberrant growth patterns during the adolescent years. The three-dimensional stiffnesses of the ribcage were found to vary significantly with rib level and orientation, and were most sensitive to changes in the gross ribcage geometry and the material properties of the costotransverse joints. The parametric analysis of the whole spine model indicated that the progression of a mild scoliosis was most sensitive to the initial Cobb angle, the spine length, the body weight and the lateral translational stiffness of the ribcage. The progression of a mild scoliotic curve (Cobb angle  $< 20^\circ$ ) was found to be small due to mechanical changes associated with the normal adolescent growth spurt in both males and females. For an initial Cobb angle of  $30^\circ$ , significant progression was predicted for a female during normal growth. The mechanical changes associated with reported aberrant growth patterns could be key factors in the progression of a mild scoliosis in a female, but not in a male. These results, which considered both the different geometry, stiffness and loads in growing females and males, strongly suggested a distinct difference in the progression tendencies between sexes, consistent with clinical data. Although an aberrant growth pattern cannot fully explain curve progression in AIS, mechanical factors associated with the adolescent growth spurt should be considered to successfully predict the prognosis of a young scoliotic patient.

## RESUME

La scoliose est une déformation de la colonne vertébrale qui affecte essentiellement la population féminine. Les personnes atteintes d'une déformation scoliotique légère sont les plus vulnérables à une progression pathologique pendant la phase de croissance rapide. Toutefois, cette progression mène à une incapacité physique chez seulement 15 à 25% de ces personnes. L'objectif de cette étude est d'identifier les facteurs mécaniques qui sont à la base d'une progression de la courbure spinale durant la phase de croissance rapide chez les adolescents atteints d'une scoliose idiopathique. Une modèle incorporant une courbure et une déformation angulaire initiale a été développé pour simuler une colonne vertébrale avec une scoliotique légère. La cage thoracique a été représentée par des éléments élastiques dont la rigidité spatiale a été déterminée utilisant un modèle tridimensionnel d'éléments finis. Des analyses paramétriques des résultats des modèles de la cage thoracique ainsi que de la colonne vertébrale ont été menées pour une meilleure compréhension de ce phénomène. Les propriétés géométriques et matérielles ainsi que le chargement de la colonne ont été systématiquement adaptés pour simuler aussi bien une croissance normale qu'anormale durant l'adolescence. L'analyse a montré que la rigidité de la cage thoracique varie d'une manière significative en fonction de la position et de l'orientation dans l'espace, et qu'elle est affectée essentiellement par les changements des facteurs géométriques et mécaniques (propriétés des matériaux) des articulations costo-transversaires. Les résultats de l'analyse du modèle de la colonne vertébrale a montré que la progression de la scoliose idiopathique légère est affectée principalement par l'angle de Cobb, par la longueur de la colonne, par le poids ainsi que par la rigidité de déplacement latéral de la cage thoracique. Il a été montré que la progression de la courbure scoliotique (l'angle de Cobb  $< 20^\circ$ ) due aux changements mécaniques associées à la phase de croissance rapide des adolescents est faible chez les deux sexes. Pour une angle de Cobb de  $30^\circ$ , progression de la courbure scoliotique a été montré pour les adolescents féminin pendant la phase de croissance rapide. Cependant les changements mécaniques associés à des croissances anormales sont probablement les facteurs responsables de la progression de la scoliose idiopathique légère, mais seulement chez les adolescents de sexe féminin. Ces résultats, qui tiennent compte des différences

géométriques, de rigidité et de chargement, montrent une nette distinction dans les tendances vers une progression scolio-tique chez les adolescents des deux sexes. Malgré qu'une croissance anormale ne peut expliquer la progression de la courbure chez les adolescents scolio-tiques, les facteurs mécaniques associées à une croissance rapide durant l'adolescence devraient être utilisés pour établir un pronostic satisfaisant chez les adolescents scolio-tiques.

## ACKNOWLEDGMENTS

I wish to express my sincere gratitude to Professor Abdul M. Ahmed who first introduced me to the stimulating area of biomechanical research. It is through his encouragement and original suggestion to study scoliosis that I pursued this project. His invaluable experience and advice on all aspects of biomechanics, engineering, research and teaching have been truly excellent and always readily available. His energy and eternal optimism have been a source of inspiration. By providing opportunities for exposure to all aspects of research and teaching, he enabled me to develop all the skills necessary for an academic career. And by developing challenging projects of broad scope, I learnt the value of doing fundamental and relevant research. It has been an honour to work with him in an atmosphere of constant support and encouragement, and I will forever remember these years for both the intellectual and personal enrichment.

Equally, I must thank my co-supervisor, Professor Arun K. Misra, who provided excellent advice and suggestions on all the theoretical aspects of the project. His outstanding knowledge of engineering mechanics and modelling taught me the value of reducing a problem to its simplest form to gain further insight of the underlying mechanics. His careful reading of the thesis and the equations is deeply appreciated.

I must also thank Ms. Anna Cianci for her truly outstanding work in typing this thesis despite my seemingly never ending changes. Her attention to detail and efforts far beyond my asking were critical in the completion of this thesis. In particular, her help in completing this long distance was amazing and I will never forget this help.

I wish to acknowledge my fellow students and researchers with whom I have worked and spent many hours in the Biomechanics Lab. In particular, I must thank Mr. Christopher McLean and Dr. Mustapha Tissakht for their friendship which made the time spent in the lab and at many conferences so enjoyable. Our many discussions on all aspects of Biomechanics were invaluable in ways that cannot be measured.

I must thank Le Fonds pour la Formation de Chercheurs et l'Aide à la Recherche (FCAR) for a postgraduate scholarship, the Medical Research Council of Canada for very generous financial support and the Department of Computer Science, McGill University, for

extensive computer funding through their excellent mainframe system. I must also thank the members of the Anatomy Lab in the Department of Anatomy, McGill University, who allowed me access to the cadavers and the collection of skeletons.

Finally, I must thank the members of both my immediate and extended family for their never ending support and help in ways that cannot be repaid. Their continual encouragement and acceptance of my chosen career are the key links in completing any such work. My wife, Julia, has always shown the confidence in me that I truly know what I'm doing when it wasn't very evident to even myself. I could not imagine a better partner for such an endeavour.

My parents have always encouraged my interests and given me the necessary freedom to explore any path possible. As fate so often decides, not all managed to see the end, though these losses have been tempered by the timely arrival of Alasdair and Cameron with sheer wonder and questions in their eyes. Why?

# Contents

<b>ABSTRACT</b> . . . . .	i
<b>RESUME</b> . . . . .	ii
<b>ACKNOWLEDGMENTS</b> . . . . .	iv
<b>NOMENCLATURE</b> . . . . .	xxvi
<b>MEDICAL GLOSSARY</b> . . . . .	xxxiv
<b>1 INTRODUCTION</b> . . . . .	<b>1</b>
1.1 General Introduction . . . . .	1
1.2 Scoliosis . . . . .	3
1.2.1 Definition and Classification . . . . .	4
1.2.2 Adolescent Idiopathic Scoliosis (AIS) . . . . .	4
1.3 Motivation . . . . .	5
1.4 Literature Review of the Etiology of Scoliosis . . . . .	8
1.5 Problem Identification and General Objective . . . . .	18
1.6 Thesis Outline . . . . .	21
<b>2 REVIEW OF SPINAL BIOMECHANICS AND FORMULATION OF SPECIFIC OBJECTIVES</b> . . . . .	<b>22</b>
2.1 Introduction . . . . .	22
2.2 Review of Spinal Biomechanics . . . . .	23
2.2.1 Experimental Studies . . . . .	23
2.2.2 Scoliosis Models . . . . .	24
2.3 Formulation of Specific Objectives . . . . .	31

<b>3</b>	<b>SPINAL COLUMN MODEL</b>	<b>36</b>
3.1	Introduction . . . . .	36
3.2	Review of Beam-Column Theory and Behaviour . . . . .	36
3.3	Spatial Beam-Column Model of a Mild Scoliosis . . . . .	45
3.3.1	Assumptions and Features of the Present Model . . . . .	46
3.3.2	Development of the Governing Differential Equations . . . . .	50
3.3.3	Application to the Scoliotic Spine . . . . .	75
3.4	Solution . . . . .	80
3.5	Spinal Column Loads . . . . .	83
3.6	Spinal Column Geometry . . . . .	89
3.6.1	Normal Adult . . . . .	89
3.6.2	Mild Scoliotic Deformity . . . . .	94
3.7	Spinal Column Material Properties . . . . .	96
3.8	Validation Studies of the Spinal Column . . . . .	99
3.9	Procedure for Parametric Analysis of Whole Spine Model . . . . .	102
3.10	Simulation of Adolescent Growth Spurt . . . . .	103
3.10.1	Normal Growth . . . . .	104
3.10.2	Accelerated Growth in Scoliotics . . . . .	107
<b>4</b>	<b>RIBCAGE MODEL</b>	<b>111</b>
4.1	Introduction . . . . .	111
4.2	Finite Element Model of the Ribcage . . . . .	112
4.2.1	Geometry and Nodal Coordinates . . . . .	114
4.2.1.1	Ribs . . . . .	114
4.2.1.2	Costal Cartilages and Sternum . . . . .	116
4.2.1.3	Costovertebral and Costotransverse Joints . . . . .	119
4.2.1.4	Nodal Coordinates of the Assembled Ribcage . . . . .	120
4.2.2	Elements and Material Properties . . . . .	121
4.2.2.1	Ribs . . . . .	123

4.2.2.2	Costal Cartilages and Sternum . . . . .	134
4.2.2.3	Costovertebral and Costotransverse Joints . . . . .	136
4.2.2.4	Intercostal Structures . . . . .	138
4.2.2.5	Assembled Ribcage . . . . .	138
4.3	Solution . . . . .	141
4.4	Equivalent Stiffness of the Ribcage . . . . .	142
4.4.1	Model of the Equivalent Stiffness of the Ribcage . . . . .	142
4.4.2	Procedure for the Numerical Experiments . . . . .	158
4.4.2.1	Sensitivity Analysis . . . . .	159
4.4.2.2	Determination of Adult Ribcage Stiffnesses . . . . .	163
4.4.2.3	Determination of Adolescent Ribcage Stiffnesses . . . . .	165
<b>5</b>	<b>VALIDATION OF THE PRESENT MODEL</b>	<b>170</b>
5.1	Introduction . . . . .	170
5.2	Finite Element Model of the Ribcage . . . . .	170
5.2.1	Individual Ribcage Components . . . . .	171
5.2.2	Assembled Ribcage . . . . .	179
5.3	Spatial Beam-Column Model of the Whole Spine . . . . .	187
<b>6</b>	<b>RESULTS - RIBCAGE ANALYSIS</b>	<b>194</b>
6.1	Introduction . . . . .	194
6.2	Equivalent Ribcage Stiffnesses of an Adult . . . . .	194
6.3	Sensitivity Analysis of Ribcage Stiffnesses . . . . .	202
6.4	Equivalent Ribcage Stiffnesses from Adolescence to Adulthood . . . . .	210
<b>7</b>	<b>RESULTS - SCOLIOTIC SPINE MODEL</b>	<b>220</b>
7.1	Introduction . . . . .	220
7.2	Parametric Analysis of the Scoliotic Spine Model . . . . .	220
7.3	Effect of the Adolescent Growth Spurt on Curve Progression . . . . .	223
7.3.1	Normal Growth Pattern . . . . .	223

7.3.2	Accelerated Growth Pattern . . . . .	227
<b>8</b>	<b>DISCUSSION AND CONCLUSIONS</b>	<b>233</b>
8.1	Introduction . . . . .	233
8.2	Mechanical Factors Affecting Curve Progression in Scoliosis . . . . .	234
8.3	Effect of Adolescent Growth on Curve Progression . . . . .	237
8.4	Comparison with Previous Work . . . . .	241
8.5	Limitations . . . . .	242
8.6	Clinical Significance . . . . .	247
8.7	Summary and Conclusions . . . . .	252
8.8	Future Studies . . . . .	254
	<b>STATEMENT OF ORIGINALITY</b> . . . . .	<b>256</b>
	<b>REFERENCES</b> . . . . .	<b>257</b>
<b>A</b>	<b>Classification System for Spinal Deformities</b>	<b>283</b>
<b>B</b>	<b>Etiological Theories for Idiopathic Scoliosis</b>	<b>286</b>
<b>C</b>	<b>Anatomy of the Spine</b>	<b>296</b>
C.1	Introduction . . . . .	296
C.2	Intervertebral Joint . . . . .	296
C.3	Spinal Column . . . . .	300
C.4	Ribcage . . . . .	303
C.5	Trunk Musculature . . . . .	308
<b>D</b>	<b>Spine Models</b>	<b>311</b>
<b>E</b>	<b>Error Analysis of the Beam-Column Model</b>	<b>317</b>
<b>F</b>	<b>Components of the Main Governing Equations in Matrix Form</b>	<b>319</b>
<b>G</b>	<b>Matrix Components for the Ribcage Loads</b>	<b>328</b>



# List of Figures

1.1	(A) Scoliosis is a three-dimensional deformity of the spinal column, with associated deformity to the ribcage (Keim and Hensinger, 1989). (B) A typical anterior-posterior (A-P) X-ray of a scoliotic patient, illustrating the classic two-dimensional measure of the deformity, the Cobb angle (Leatherman and Dickson, 1988). . . . .	3
1.2	Illustration of the four common curve types found in AIS. A) Thoracic; B) Thoracolumbar; C) Lumbar; D) Double (Keim and Hensinger, 1989). . . .	5
1.3	The vertebrae in AIS are always found to be rotated with the spinous processes oriented towards the concavity of the curve (White and Panjabi, 1990). . . . .	6
3.1	Illustration of the Bernoulli-Euler beam-column assumption that plane sections originally normal to the elastic axis remain normal after deformation. . . . .	38
3.2	A) A beam-column subjected to an axial compression load, $P$ , and a distributed lateral load, $q$ . B) Differential element from the beam-column shown in a displaced position for small displacements. $V$ is the shear force. $N$ is the normal force, which is equal to $P$ in the present example, and $M$ is the bending moment acting on the cross-section. . . . .	38
3.3	Effect of imperfections on the displacement behaviour of a column. An initial displacement, $\Delta$ , causes immediate deflections, which can become large below the critical load. Other imperfections such as a small lateral load, $Q$ , or a load eccentricity, $e$ , causes a further increase in the displacements. . . . .	40

3.4	Illustration of a beam-column subjected to bi-axial bending due to an eccentric compression load $P$ . Moments $M_x$ and $M_y$ are produced in each plane and the resulting deflection is spatial. . . . .	41
3.5	The axis of a spatial rod is specified by the position vector, $\hat{r}$ , in a Cartesian system. At each point along a curve, a Frenet triad formed by the unit tangent vector, $\hat{t}$ , the unit principal normal, $\hat{n}$ , and the unit binormal, $\hat{b}$ , can be defined. Two directors, $d_2$ and $d_3$ , are also shown, which need not lie in the plane defined by $\hat{n}$ and $\hat{b}$ . . . . .	44
3.6	Illustration that the cross-sectional plane of the spine at all positions along the axis cannot remain normal to the elastic axis. Within each motion segment, however, at least one plane should remain normal after deformation.	47
3.7	The axis of the initially curved and twisted beam-column is specified in the fixed system, $\hat{i}_j$ , by the position vector $\hat{r}_0$ . A point B in the plane of the cross-section is specified by the position vector $\hat{r}$ . Also shown is the local system, $\hat{e}_i$ , where $\hat{e}_1$ is the unit tangent vector and $\hat{e}_2, \hat{e}_3$ define the plane of the cross-section. At point B, the basis vectors, $\hat{g}_i$ , are shown. . . . .	53
3.8	The elastic axis of the beam-column before and after deformation. The displacement, $\hat{D}_0$ , of the beam-column is given by the components $w, u$ and $v$ , expressed in the $\hat{e}_i$ system, respectively. Also shown is the $\hat{e}_i^*$ system of the deformed beam-column, where $\hat{e}_1^*$ is the unit tangent vector of the deformed axis, and $\hat{e}_2^*$ and $\hat{e}_3^*$ define the plane of the cross-section of the deformed beam-column. . . . .	55
3.9	Illustration of the relationship between the displacement variables $w, u$ and $v$ , where are a function $d_1, d_2$ and $d_3$ , and the three Euler rotations of the cross-section of the beam-column. The cross-section of the undeformed beam-column, with unit tangent vector, $\hat{e}_1$ , is carried through three Euler type rotations, $\theta_3, \theta_2$ and $\theta_1$ , to the deformed position with unit tangent vector $\hat{e}_1^*$ . . . . .	58

3.10	Illustration of the deformation of the beam-column from the initial to the deformed position. The displacement of a point B on the cross-section is given by $\hat{U}$ . Also shown are the basis vectors, $\hat{G}_i$ , of the deformed beam-column at point B. . . . .	64
3.11	Differential element, $ds$ , of the spatial beam-column subjected to an applied force, $\hat{f}$ , and moment, $\hat{m}$ , per unit length along the elastic axis. . . . .	70
3.12	Location of the tension centre of the spine in relation to the shear centre. Due to symmetry, the tension centre is assumed to be offset only in the $\hat{e}_3$ direction by $\eta_0$ . . . . .	76
3.13	Flowchart of the overall solution procedure. Note that of the solution of each set of nonlinear 1 <sup>st</sup> order equations involved a further loop which proceeded from a solution of the linear equations first, and then to the full nonlinearity using the previous step as a guess. Also, for the parametric analysis only the loop to solve both sets of nonlinear equations was performed. . . . .	84
3.14	Location of the line of action of the body weight in the fixed system. . . . .	86
3.15	The average effective stiffnesses of an adult at each of the spine levels. . . . .	101
3.16	The upper body weight of a male and female from young adolescence to young adulthood. . . . .	108
3.17	The vertical spine height of a male and female from young adolescence to young adulthood. . . . .	108
3.18	The effective stiffnesses at the T8-T9 spine level as a function of age for male and female. (A) Lateral bending stiffness - $EI_{\eta_0}$ ; (B) Axial torsion stiffness - $GJ$ . . . . .	109

4.1	Geometric parameters used to quantify the rib geometry. $R_N$ – radius of a rib in the neck region; $R_S$ – radius of a rib in the shaft region; $l_c$ – chord length of a rib; $\beta$ – arc angle of a rib; $C_x$ – lateral coordinate of the center of curvature of the shaft; $C_y$ – anterior-posterior coordinate of the centre of curvature of the shaft; $A_y$ – anterior-posterior coordinate of the rib angle; $\beta$ – arc angle of the rib shaft. (Adapted from Gray, 1989). . . . .	116
4.2	Geometry of the ribs at each level used in the present model and compared with experiments. A dotted line was added to interconnect the model data from the discreet levels to greater illustrate the changes as a function of rib level. (A) $R_N$ , $R_S$ ; (B) $l_c$ ; (C) $\beta$ ; (D) $C_x$ ; (E) $C_y$ ; (F) $A_y$ . . . . .	117
4.2	(Con'd) Geometry of the ribs at each level used in the present model and compared with epxeriments. A dotted line was added to interconnect the model data from the discreet levels to greater illustrate the changes as a function of a rib level. (A) $R_N$ , $R_S$ ; (B) $l_c$ ; (C) $\beta$ ; (D) $C_x$ ; (E) $C_y$ ; (F) $A_y$ . . . . .	118
4.3	(A) Coordinate system $x_s - y_s$ of the sternum to define the geometry of the costosternal joints; (B) Coordinate system $x_v - y_v$ of a vertebra to define the geometry of the costovertebral and costotransverse joints. (Adapted from Gray, 1989). . . . .	119
4.4	Orientation of a typical rib in space, as defined by the “pump handle” angle, $\beta_1$ , and the “bucket handle” angle, $\beta_2$ . (Adapted from Gray, 1989). . . . .	120
4.5	Flowchart of the assembly procedure to determine the 3-D nodal coordinates of the ribcage. The data was input in the local coordinate systems of the ribs, vertebrae and sternum, and output as three-dimensional data in the fixed global system. . . . .	122
4.6	The thoracic ratio at each rib level in the present model and compared to clinical data in the literature. . . . .	123
4.7	Grid independence check for the finite element representation of the ribs. Comparison between a curved and a straight beam representation are also shown. . . . .	125

4.8	Cross-sectional geometric parameters of a rib. (A) Typical geometries in the shaft and neck regions; (B) Hollow elliptic model of the rib cross-section. $h_0$ - major outer diameter; $h_i$ - major inner diameter; $b_0$ - minor outer diameter; $b_i$ - minor inner diameter; $t_{cort}$ - cortical wall thickness. . . . .	126
4.9	Cross-sectional geometry of the ribs at each level for the neck and shaft (average of 3 locations) regions, based on the measurements from three skeletons. (A) Major outer diameter, $h_0$ ; (B) Minor outer diameter, $b_0$ ; (C) Ratio of the major to minor outer diameters. . . . .	129
4.10	Cross-sectional properties of the ribs used in the beam elements and comparison with values in the literature [A dotted line was added to interconnect the data used in the model to greater illustrate the differences as a function of rib level.] (A) Major moment of inertia, $I_1$ ; (B) Minor moment of inertia, $I_2$ ; (C) Torsional constant, $J_R$ ; (D) Cross-sectional area, $A_R$ . . . . .	131
4.10	(Con'd) Cross-sectional properties of the ribs used in the beam elements and comparison with values in the literature [A dotted line was added to interconnect the data used in the model to greater illustrate the differences as a function of rib level.] (A) Major moment of inertia, $I_1$ ; (B) Minor moment of inertia, $I_2$ ; (C) Torsional constant, $J_R$ ; (D) Cross-sectional area, $A_R$ . . . . .	132
4.11	Costal cartilages and sternum of the finite element model shown in a frontal view. The beam elements of the costal cartilages are only illustrated by a line to represent the elastic axis. . . . .	135
4.12	The structural model of the costovertebral and costotransverse joints. . . .	137
4.13	The finite element model of the assembled ribcage. (A) Lateral view; (B) Frontal view; (C) General view. Note that in (A) and (B) the intercostal elements were removed for clarity and only shown in (C). Also, beam and rod elements are only illustrated by a line to represent the elastic axis. . .	140

4.14	Model of the elastic restraint exerted by the ribcage against the spinal column in response to lateral bending in the coronal plane (Adapted from Gray, 1989). At each vertebral level, the collective actions of the ribcage are replaced by a spring acting in the coronal plane at a point $S_R$ in the transverse plane. (A) Coronal plane view; (B) Transverse plane view at one vertebral level. . . . .	144
4.15	Three-dimensional model of the elastic restraint of the ribcage which surrounds the spinal column (Adapted from Gray, 1989). At each vertebral level, both translational and rotational springs are used to model the 3-D support of the ribcage. . . . .	145
4.16	Translation of the shear centre as viewed in the transverse plane. Note that since the systems are not necessarily co-planar, then only the projections of the axes of the coordinate systems $\hat{e}_i$ and $\hat{e}_i^*$ onto the fixed system $\hat{i}_j$ in the transverse plane are shown. . . . .	150
4.17	The ribcage dimensions as a percentage of the adult value for females and males from young adolescence to adulthood. (A) Gross ribcage width; (B) Gross ribcage depth; (C) Gross ribcage height. The earlier growth spurt of the females is evident. . . . .	166
4.18	Flowchart of the current overall approach to model development, validation and analysis. . . . .	169
5.1	Predictions of the present model for the principal translations of the rib tips subjected to a force of 7.4 N for three different sets of rib cross-sectional properties. In comparison to the experimental results of Schultz et al (1974a) (averaged between opposite loading directions), the predictions using the cross-sectional properties of Case A were in closest agreement, although all cases were in good agreement. (A) Medial/Lateral Force; (B) Anterior/Posterior Force; (C) Superior/Inferior Force. . . . .	174

5.2	Predictions of the present model for the principal translations of the rib tips subjected to a force of 7.4 N for linear and geometrical nonlinear analyses. The predictions were generally in close agreement to other models (Closkey et al, 1992), and in better agreement with experiment (Schultz et al, 1974a) for rib levels 2, 4 and 6 for an anterior force. (A) Lateral Force; (B) Anterior Force; (C) Superior Force. . . . .	175
5.2	(Con'd) Predictions for the present model of the principal translations of the rib tips subjected to a force of 7.4 N for linear and geometrical nonlinear analyses. The predictions were generally in close agreement to other models (Closkey et al, 1992), and in better agreement with experiment (Schultz et al, 1974a) for rib levels 2, 4 and 6 for an anterior force. (D) Medial Force; (E) Posterior Force; (F) Inferior Force. . . . .	176
5.3	Comparison of the predictions of the present finite element model of the ribcage subjected to a lateral squeezing force compared with experiment and previous models. The predictions of the present model are only shown for a linear analysis to maintain clarity. Excellent agreement for the change in the lateral diameter was found in comparison to both experiment and previous models, whereas a better agreement with experiment was found for the change in anterior/posterior diameter. . . . .	181
5.4	Deformed and undeformed configuration of the ribcage finite element model subjected to a lateral squeezing force centered at the level of the xiphoid process at the bottom of the sternum. The intercostal elements between the ribs ensured the coordinated action of all the ribs together. . . . .	182
5.5	Comparison of the predictions of the present finite element model of the ribcage subjected to a sternal compressive load compared with experiment (A) and previous models (B). Excellent agreement with the experiments of unembalmed cadavers was found, and the present model was in general more flexible in the anterior/posterior direction compared with previous models. . . . .	185

5.6	Deformed configuration of the finite element model of the ribcage subjected to a lower sternal load. The sternum undergoes a relatively large rotation due to the larger anterior displacements at the inferior portion. . . . .	186
5.7	Comparison of the axial rotation at each spine level of the present model with experiment and other models for an axial rotation of 54° at T1. . . .	191
5.8	The lateral translations of the present model for an axial compressive load applied with a small imperfection for both a free and a pinned top. The properties used in the analysis matched those of the spines used in the experiment of Lucas and Bresler (1961). . . . .	192
5.9	The model predictions for the lateral translation (A) and axial rotation (B) due to a lateral load applied at vertebra T9. . . . .	193
6.1	The load displacement results for a 100 N lateral load (A) and a 100 N anterior load (B) applied at the shear centres of the spine at all rib levels one at a time. There was a clear variation in the displacements with rib level for both anterior and lateral loads. . . . .	197
6.2	The lateral displacements of the shear centres at all the rib levels due to a lateral load (100 N) applied at the shear centre of rib level 3 and at rib level 8. The maximum displacements occurred at the primary loaded level and significant but lesser displacements were induced at the other rib levels. The principal stiffness determined from the load-displacement response at a given rib level was therefore affected by interaction of that given level with all the other rib levels, primarily through the intercostals due to relative movement between ribs. . . . .	198

6.3	The translational (A) and rotational stiffnesses (B) as a function of rib level. The lateral and anterior translational stiffnesses were very similar at all rib levels except the first and second where the anterior stiffness increased greatly. The axial rotational stiffness was greater at most rib levels and the lateral bending and flexion/extension rotational stiffnesses were similar at all rib levels. . . . .	199
6.4	The percentage change in the lateral translational stiffness ( $k_{11}$ ) due to changes in the geometry (A) and the material properties (B) of the ribcage. The exact parametric changes to the geometry of the ribcage width (G-RW), ribcage depth (G-RD), ribcage height (G-RH), rib cross-section (G-RCS), costal cartilages (G-CC), and the material properties of the cortical rib bone (MP-CRT), the intercostals (MP-IC), the costal cartilages (MP-CC), the costovertebral joints (MP-CV) and the costotransverse joints (MP-CT) are detailed in Table 4.1. . . . .	205
6.5	The percentage change in the anterior/translational stiffness ( $k_{22}$ ) due to changes in the geometry (A) and the material properties (B) of the ribcage. The exact parametric changes to the geometry of the ribcage width (G-RW), ribcage depth (G-RD), ribcage height (G-RH), rib cross-section (G-RCS), costal cartilages (G-CC), and the material properties of the cortical rib bone (MP-CRT), the intercostals (MP-IC), the costal cartilages (MP-CC), the costovertebral joints (MP-CV) and the costotransverse joints (MP-CT) are detailed in Table 4.1. . . . .	206

6.6	The percentage change in the flexion/extension rotational stiffness ( $k_{44}$ ) due to changes in the geometry (A) and the material properties (B) of the ribcage. The exact parametric changes to the geometry of the ribcage width (G-RW), ribcage depth (G-RD), ribcage height (G-RH), rib cross-section (G-RCS), costal cartilages (G-CC), and the material properties of the cortical rib bone (MP-CRT), the intercostals (MP-IC), the costal cartilages (MP-CC), the costovertebral joints (MP-CV) and the costotransverse joints (MP-CT) are detailed in Table 4.1. . . . .	207
6.7	The percentage change in the lateral bending rotational stiffness ( $k_{55}$ ) due to changes in the geometry (A) and the material properties (B) of the ribcage. The exact parametric changes to the geometry of the ribcage width (G-RW), ribcage depth (G-RD), ribcage height (G-RH), rib cross-section (G-RCS), costal cartilages (G-CC), and the material properties of the cortical rib bone (MP-CRT), the intercostals (MP-IC), the costal cartilages (MP-CC), the costovertebral joints (MP-CV) and the costotransverse joints (MP-CT) are detailed in Table 4.1. . . . .	208
6.8	The percentage change in the axial rotational stiffness ( $k_{66}$ ) due to changes in the geometry (A) and the material properties (B) of the ribcage. The exact parametric changes to the geometry of the ribcage width (G-RW), ribcage depth (G-RD), ribcage height (G-RH), rib cross-section (G-RCS), costal cartilages (G-CC), and the material properties of the cortical rib bone (MP-CRT), the intercostals (MP-IC), the costal cartilages (MP-CC), the costovertebral joints (MP-CV) and the costotransverse joints (MP-CT) are detailed in Table 4.1. . . . .	209
6.9	The net changes in the five ribcage stiffnesses at all rib levels due to differences in geometry (A) and material properties (B) of a young adolescent compared to an adult. $k_{11}$ —lateral translational stiffness; $k_{22}$ —anterior translational stiffness; $k_{44}$ —flexion/extension rotational stiffness; $k_{55}$ —lateral bending rotational stiffness; $k_{66}$ —axial rotational stiffness. . . . .	211

6.10	The net changes in the five ribcage stiffnesses at all rib levels due to the collective differences in geometry and material properties of a young adolescent compared to an adult. $k_{11}$ – lateral translational stiffness; $k_{22}$ – anterior translational stiffness; $k_{44}$ – flexion/extension rotational stiffness; $k_{55}$ – lateral bending rotational stiffness; $k_{66}$ – axial rotational stiffness. . . . .	213
6.11	The lateral translational stiffness per unit length ( $k_{11}^o$ ) at each rib level as a function of age for a female (A) and male (B). . . . .	215
6.12	The anterior translational stiffness per unit length ( $k_{22}^o$ ) at each rib level as a function of age for a female (A) and male (B). . . . .	216
6.13	The flexion/extension rotational stiffness per unit length ( $k_{44}^o$ ) at each rib level as a function of age for a female (A) and male (B). . . . .	217
6.14	The lateral bending rotational stiffness per unit length ( $k_{55}^o$ ) at each rib level as a function of age for a female (A) and male (B). . . . .	218
6.15	The axial rotational stiffness per unit length ( $k_{66}^o$ ) at each rib level as a function of age for a female (A) and male (B). . . . .	219
7.1	The model predictions of the effect of normal growth in males and females on curve progression of a mild scoliosis in a spine with an initial Cobb angle of 10°. (A) The Cobb angle of the scoliotic curve at each age of adolescence. (B) The lateral translation of the vertebral centres along the spine at the age of peak increase in Cobb angle. (C) The axial rotation of the vertebrae along the spine at the age of peak increase in Cobb angle. . . . .	224
7.2	The model predictions of the effect of normal growth in males and females on curve progression of a mild scoliosis in a spine with an initial Cobb angle of 20°. (A) The Cobb angle of the scoliotic curve at each age of adolescence. (B) The lateral translation of the vertebral centres along the spine at the age of peak increase in Cobb angle. (C) The axial rotation of the vertebrae along the spine at the age of peak increase in Cobb angle. . . . .	225

7.3	The model predictions of the effect of normal growth in males and females on curve progression of a mild scoliosis in a spine with an initial Cobb angle of 30°. (A) The Cobb angle of the scoliotic curve at each age of adolescence. (B) The lateral translation of the vertebral centres along the spine at the age of peak increase in Cobb angle. (C) The axial rotation of the vertebrae along the spine at the age of peak increase in Cobb angle. . . . .	226
7.4	The model predictions of the effect of the accelerated growth pattern of Case I on the Cobb angle of a mild scoliotic curve with an initial Cobb angle of 10, 20 and 30°. (A) Female; (B) Male. . . . .	229
7.5	The model predictions of the effect of the accelerated growth pattern of Case II on the Cobb angle of a mild scoliotic curve with an initial Cobb angle of 10, 20 and 30°. (A) Female; (B) Male. . . . .	230
7.6	The model predictions of the effect of the accelerated growth pattern of Case III on the Cobb angle of a mild scoliotic curve with an initial Cobb angle of 10, 20 and 30°. (A) Female; (B) Male. . . . .	231
7.7	The correlation of the axial rotation of the spine at the curve apex with the Cobb angle during curve progression for the accelerated growth of Case III in a female. . . . .	232
8.1	The growth velocity of standing height from birth to maturity for a female and male (Tanner et al. 1966). . . . .	251
8.2	The ratio of the upper body weight to the critical load of a fixed-fixed beam-column for a male and female during adolescence. A margin of safety exists between the value of this ratio and when it equals one, which indicates an unstable system. . . . .	252

C.1	A) An intervertebral joint or motion segment comprised of two vertebrae plus the interconnecting disc, ligaments and facet joints (Grant, 1978). B) A typical vertebra from the lumbar region of the spine (Gray, 1989). C) An intervertebral disc is composed of a nucleus, surrounded by a series of fibrous bands. . . . .	297
C.2	The spinal or vertebral column is composed of 33 vertebrae and divided into four regions: sacral, lumbar, thoracic and cervical (Grant, 1978). A) Lateral view; B) Anterior view. . . . .	301
C.3	Typical orientations of the facet joints from two regions of the spine (White and Panjabi, 1990). A) Lumbar facets; B) Thoracic facets. . . . .	304
C.4	Typical views of the ribcage devoid of musculature (Grant, 1978). A) Anterior; B) Lateral. . . . .	305
C.5	Transverse view of the costovertebral joint and costotransverse joint (Gray, 1989). . . . .	308
C.6	An illustration of some of the trunk muscles (Gray, 1989). A) Intrinsic; B) Extrinsic. . . . .	309
C.7	A) An illustration of some of the respiratory muscles which serve to raise and lower the ribcage structure during respiration (Gray, 1989); B) The rib-neck axis (line C-D), about which the rib rotates during respiration (Woodburne, 1983). . . . .	310

# List of Tables

1.1	Summary of the studies related to anthropometry and scoliosis. . . . .	16
2.1	Summary of the models that have been developed to investigate the mechanics of scoliosis. The models are grouped according to the different primary researchers. . . . .	22
3.1	The distributed body weights and locations of the centres of mass in an adult male and female as used in the present model. . . . .	90
3.2	Anthropometric data of an adult male and female for input to the spinal column model. . . . .	95
3.3	The average stiffness coefficients and calculated effective stiffnesses of the thoracic and lumbar regions of an adult. . . . .	97
3.4	Effective stiffnesses of an adult at all spine levels of the present model. . .	100
4.1	Summary of the ten models developed to investigate the sensitivity of the ribcage stiffnesses to changes in geometry and material property parameters.	141
5.1	The present model predictions of the translations of a rib 6 segment loaded in three orthogonal directions about the costovertebral and costotransverse joints were found to be in excellent agreement compared to the model of Andriacchi et al (1974). . . . .	178

5.2	The present model predictions of the translations of a costal cartilage segment attached to rib 7 loaded in orthogonal directions about the costosternal joint were found to be in excellent agreement compared to the model of Andriacchi et al (1974).	178
5.3	Comparison of the present model predictions with experiment for the combined lateral bending and axial rotation response due to a 250 N lateral load applied at vertebra T9.	190
6.1	The principal and coupled displacements of rib 6 subjected to 100 N loads and 1000 N-mm moments applied independently at the shear centre of the spine at this rib level. The coupled displacements are in general much less than the principal displacements.	200
6.2	The principal ribcage stiffnesses per unit length at all the rib levels for an adult ribcage.	201
6.3	The principal ribcage stiffnesses per unit length at all the rib levels of a young adolescent.	214
7.1	The sensitivity of the scoliotic spine model to changes in various mechanical parameters.	222
A.1	Etiological classification system for spinal deformities developed in accordance with the Scoliosis Research Society (Leatherman and Dickson, 1988).	284
B.1	Summary of the various etiological theories for AIS, subdivided according to the primary tissue, structure or system involved.	292
D.1	Summary of spine models to illustrate the various techniques employed. This is only intended as a representative list, and also does not include scoliosis models (See Table 2.1).	315

## NOMENCLATURE

$(\hat{\quad})$	— vector
$(\quad)_{,1}$	— first derivative with respect to axial direction $s$ or $l$
$(\quad)_{,11}$	— second derivative with respect to axial direction $s$ or $l$
$(\quad)_{,111}$	— third derivative with respect to axial direction $s$ or $l$
$(\quad)_{,1111}$	— fourth derivative with respect to axial direction $s$ or $l$
$\hat{t}$	— unit tangent vector of a spatial curve
$\hat{n}$	— unit principal normal of a spatial curve
$\hat{b}$	— unit binormal of a spatial curve
$\hat{i}_j: \hat{i}_1, \hat{i}_2, \hat{i}_3$	— triad of unit vectors in the fixed Cartesian system ( $Z - X - Y$ )
$\hat{e}_i: \hat{e}_1, \hat{e}_2, \hat{e}_3$	— triad of unit vectors along the axis of the undeformed beam-column
$\hat{e}_i^*: \hat{e}_1^*, \hat{e}_2^*, \hat{e}_3^*$	— triad of unit vectors along the axis of the deformed beam-column
$z, x, y$	— coordinates of a point on the beam-column in the fixed Cartesian system $\hat{i}_j$ , respectively
$s, \xi, \eta$	— coordinates of a point on the beam-column in the local system $\hat{e}_i$ , respectively
$x_r - y_r$	— local system on a rib with origin at the costotransverse joint
$x_s - y_s$	— local system on the sternum with origin at the xiphoid process
$x_v - y_v$	— local system on a vertebra with origin at the vertebral center
$\mathcal{K}$	— curvature
$\tau$	— geometric torsion
$\alpha$	— angle between the natural system $\hat{t}, \hat{n}, \hat{b}$ and the $\hat{e}_i$ system, rotated about the tangent $\hat{t}$ or $\hat{e}_1$
$\hat{k}$	— curvature vector of the initially curved and twisted beam-column in the $\hat{e}_i$ system
$\hat{K}$	— curvature vector of the deformed beam-column in the $\hat{e}_i^*$ system
$k_C, k_\xi, k_\eta$	— components of the initial torsion and curvature of the

	beam-column in the $\hat{e}_i$ system, respectively
$K_\zeta, K_\xi, K_\eta$	— components of the torsion and curvature of the beam-column after deformation in the $\hat{e}_i^*$ system, respectively
$\hat{r}_0, \hat{R}_0$	— position vectors of the undeformed and deformed beam-column axis, respectively
$\hat{r}, \hat{R}$	— position vectors of any point on the beam-column before and after deformation, respectively
$\hat{d}_0, \hat{D}_0$	— displacement vectors of the undeformed and deformed beam-column axis, respectively
$\hat{U}$	— displacement vector of any point of the beam-column from undeformed to the deformed position
$w_0, u_0, v_0$	— components of the initial displacement of the beam-column axis in the $\hat{i}_j$ system, respectively
$w, u, v$	— components of the displacement of the beam-column axis after deformation in the $\hat{e}_i$ system, respectively
$\theta_1, \theta_2, \theta_3$	— three Euler angles for the rotation of $\hat{e}_i \rightarrow \hat{e}_i^*$
$\theta$	— axial rotation of the beam-column axis
$T_z, T_x, T_y$	— translations in the fixed system, $\hat{i}_j$
$R_z, R_x, R_y$	— rotations of the ribcage in the fixed system, $\hat{i}_j$
$C_{ij}^o$	— rotation matrix of $\hat{i}_j \rightarrow \hat{e}_i$
$C_{ij}^*$	— rotation matrix of $\hat{e}_i \rightarrow \hat{e}_i^*$
$C_{ij}$	— rotation matrix of $\hat{i}_j \rightarrow \hat{e}_i^*$ , based on the initial and the deformed displacement variables of the beam-column
$C'_{ij}$	— rotation matrix of $\hat{i}_j \rightarrow \hat{e}_i^*$ , based on the three rotations $R_x, R_y$ and $R_z$ of the ribcage
$d_1, d_2, d_3$	— components of the unit tangent vector, $\hat{e}_1^*$ , of the deformed

	—	system expressed in the undeformed system, $\hat{e}_i$ , respectively
$\hat{g}_i: \hat{g}_1, \hat{g}_2, \hat{g}_3$	—	basis vectors in the undeformed system, $\hat{e}_i$
$\hat{G}_i: \hat{G}_1, \hat{G}_2, \hat{G}_3$	—	basis vectors in the deformed system, $\hat{e}_i^*$
$\bar{e}_{11}$	—	axial strain of the beam-column axis
$e_{11}$	—	axial strain at any point of the beam-column
$e_{12}, e_{13}$	—	shear strain at any point of the beam-column
$\epsilon_{11}$	—	engineering axial strain at any point of the beam-column
$\gamma_{12}, \gamma_{13}$	—	engineering shear strain at any point of the beam-column
$\bar{K}_\zeta, \bar{K}_\xi, \bar{K}_\eta$	—	generalized strains
$\sigma_{11}$	—	axial stress at any point of the beam-column
$\tau_{12}, \tau_{13}$	—	shear stresses at any point of the beam-column
$\hat{S}$	—	stress vector
$\hat{F}$	—	internal resultant force vector
$\hat{M}$	—	internal resultant moment vector
$\hat{f}$	—	applied force per unit length
$\hat{m}$	—	applied moment per unit length
$\hat{f}^w$	—	body weight forces per unit length
$\hat{m}^w$	—	body weight moments per unit length
$\hat{f}^r$	—	ribcage forces per unit length
$\hat{m}^r$	—	ribcage moments per unit length
$N, V_\xi, V_\eta$	—	components of $\hat{F}$ in the deformed system, $\hat{e}_i^*$ , respectively
$M_\zeta, M_\xi, M_\eta$	—	components of $\hat{M}$ in the deformed system, $\hat{e}_i^*$ , respectively
$F_1, F_2, F_3$	—	components of $\hat{F}$ in the undeformed system, $\hat{e}_i$ , respectively
$M_1, M_2, M_3$	—	components of $\hat{M}$ in the undeformed system, $\hat{e}_i$ , respectively
$f_1, f_2, f_3$	—	components of $\hat{f}$ in the undeformed system, $\hat{e}_i$ , respectively
$m_1, m_2, m_3$	—	components of $\hat{m}$ in the undeformed system, $\hat{e}_j$ , respectively
$f_z^w$	—	vertical component of the body weight per unit length

	in the fixed system, $\hat{i}_j$
$W$	— total weight of upper body
$\mathcal{F}_z, \mathcal{F}_x, \mathcal{F}_y$	— components of the ribcage forces in the fixed system, $\hat{i}_j$ , respectively
$\mathcal{M}_z, \mathcal{M}_x, \mathcal{M}_y$	— components of the ribcage moments in the fixed system, $\hat{i}_j$ , respectively
$f_z^r, f_x^r, f_y^r$	— components of the ribcage forces per unit length in the fixed system, $\hat{i}_j$ , respectively
$m_z^r, m_x^r, m_y^r$	— components of the ribcage moments per unit length in the fixed system, $\hat{i}_j$ , respectively
$f_1^w, f_2^w, f_3^w$	— components of the body weight forces per unit length in the undeformed system, $\hat{e}_i$ , respectively
$m_1^w, m_2^w, m_3^w$	— components of the body weight moments per unit length in the undeformed system, $\hat{e}_i$ , respectively
$f_1^r, f_2^r, f_3^r$	— components of the ribcage forces per unit length in the undeformed system, $\hat{e}_i$ , respectively
$m_1^r, m_2^r, m_3^r$	— components of the ribcage moments per unit length in the undeformed system, $\hat{e}_i$ , respectively
$L$	— vertical height of the spine
$l_n$	— distance between vertebral centres at each level of the spine ( $n = 1 \rightarrow 17$ )
$h_n$	— average height of a vertebra ( $n = 1 \rightarrow 17$ )
$b_n$	— average width (coronal plane) of a vertebra ( $n = 1 \rightarrow 17$ )
$d_n$	— average depth (sagittal plane) of a vertebra ( $n = 1 \rightarrow 17$ )
$b$	— representative cross-sectional width of the spine in the coronal plane
$d$	— representative cross-sectional depth of the spine in the mid-sagittal plane

$\xi_0, \eta_0$	— location of the tension centre in the cross-section of the beam-column at position, $s$ , along the axis in the $\hat{e}_i$ system
$e_x, e_y$	— point of application of the body weight in the fixed system, $\hat{i}_j$
$\Delta_g$	— location of centre of mass anterior to vertebral centre
$R_N$	— rib radius in the neck region
$R_S$	— rib radius in the shaft region
$l_c$	— chord length of a rib from tip to costotransverse joint
$C_x, C_y$	— lateral and anterior-posterior coordinates, respectively, of the centre of curvature of the rib shaft
$A_y$	— anterior-posterior coordinate of the rib angle
$\beta$	— arc angle of a rib
$\beta_1$	— pump handle angle of a rib
$\beta_2$	— bucket handle angle of a rib
$h_0, h_i$	— major outside and inside diameter of a rib, respectively
$b_0, b_i$	— minor outside and inside diameter of a rib, respectively
$t_{cort}$	— cortical wall thickness of a rib
$t_c$	— ratio of outside to inside diameter of a rib, major or minor
$TI$	— thoracic index: ratio of width to depth of the ribcage at mid-sternum
$TR$	— thoracic ratio: ratio of width at each vertebral level to the length $T1 - T12$
$A$	— cross-sectional area of the spine
$A_R$	— effective cross-sectional area of a rib
$I_{\xi\xi}, I_{\eta\eta}$	— principal moments of inertia of the spine
$I_{\xi\xi_0}, I_{\eta\eta_0}$	— principal moments of inertia of the spine, offset by $\langle \xi_0, \eta_0 \rangle$
$I_1, I_2$	— principal moments of inertia of a rib
$J$	— St-Venant's torsion constant of the spine

$J_R$	—	St-Venant's torsion constant of a rib
$E$	—	representative Young's Modulus of the spine
$E_{can}$	—	Young's Modulus of cancellous bone
$E_{cort}$	—	Young's Modulus of cortical bone
$G$	—	representative Shear Modulus of the spine
$G_{can}$	—	Shear Modulus of cancellous bone
$G_{cort}$	—	Shear Modulus of cortical bone
$E_{IC}$	—	Young's Modulus of the intercostals
$E_{CC}$	—	Young's Modulus of the costal cartilages
$E_{CV}$	—	Young's Modulus of the costovertebral joints
$E_{CT}$	—	Young's Modulus of the costotransverse joints
$EA$	—	axial stiffness of the spine
$EI_{\xi\xi_0}, EI_{\eta\eta_0}$	—	principal bending stiffnesses of the spine
$EI_1, EI_2$	—	principal bending stiffnesses of a rib
$GJ$	—	torsional rigidity of the spine
$GJ_R$	—	torsional rigidity of a rib
$\Delta$	—	initial lateral offset of the spine at the curve apex
$P_{cr}$	—	critical buckling load
$C$	—	Euler constant, dependent on the boundary conditions
$k_{ij}$	—	components of the 3-D ribcage stiffness
$k_{ij}^o$	—	components of the 3-D ribcage stiffness per unit length
$f_{ij}$	—	components of the 3-D ribcage flexibility
$\{t\}$	—	vector of the four unknowns $N, u, v$ and $\theta$
$[M_4], [M_3], [M_2],$ $[M_1], [M_0]$	—	matrices containing the components of the internal reactions of the governing equations

- $[AM_2], [AM_1],$  — matrices and vector containing the components of the  
 $[AM_0], \{AM_c\}$  applied forces and moments of the governing equations
- $[R], [D], \{I\}$  — matrices and vector containing the components of the  
 ribcage forces and moments
- $\{W\}$  — vector containing the components of the applied body  
 weight forces and moments
- $U_n, U_n^{NL},$  — linear and nonlinear components of the lateral  
 $V_n, V_n^{NL},$  “ $U$ ”, sagittal “ $V$ ” and axial rotation  
 $T_n, T_n^{NL}:$  “ $T$ ” equations related to the stiffnesses and  
 $n = 1 - 12$  the initial curvatures and twist
- $UN_n, UN_n^{NL},$  — linear and nonlinear components of the lateral  
 $VN_n, VN_n^{NL}$  “ $U$ ”, sagittal “ $V$ ” and axial rotation “ $T$ ”  
 $TN_n, TN_n^{NL}:$  equations associated with the coupling terms, respectively,  
 $n = 1 - 12$  of the axial load “ $N$ ” equation related to the initial  
 curvatures and twist, and the shear centre
- $UN_n^P, UN_n^{PNL},$  — linear and nonlinear components of the lateral  
 $VN_n^P, VN_n^{PNL}$  “ $U$ ” and sagittal “ $V$ ” equations associated with the  
 $UN_n^{PP}, UN_n^{PPNL}:$   $N_{,1}$  and  $N_{,11}$  coupling terms, respectively,  
 $VN_n^{PP}, VN_n^{PPNL}$  of the axial load “ $N$ ” equation related to the initial curvatures  
 $n = 1 - 12$  and twist, and the shear centre
- $\{ACU\}_n:$  — vector containing components of the lateral “ $U$ ”  
 $n = 1 - 9$  load equation
- $\{ACV\}_n:$  — vector containing components of the sagittal  
 $n = 1 - 9$  “ $V$ ” load equation
- $\{ACT\}_n:$  — vector containing components of the axial rotation

$n = 1 - 9$	—	“ $T$ ” load equation
$N_n: n = 1 - 2$	—	unknown axial load $N_1 = N$ and its first derivative $N_2 = N_{,1}$ for solution in a 1 <sup>st</sup> order system of equations
$u_n: n = 1 - 4$	—	unknown lateral displacement $u_1 = u$ and its derivatives $u_2 = u_{,1}$ , $u_3 = u_{,11}$ , $u_4 = u_{,111}$ for solution in a 1 <sup>st</sup> order system of equations
$v_n: n = 1 - 4$	—	unknown sagittal displacement $v_1 = v$ and its derivatives $v_2 = v_{,1}$ , $v_3 = v_{,11}$ , $v_4 = v_{,111}$ for solution in a 1 <sup>st</sup> order system of equations
$\theta_n: n = 1 - 2$	—	unknown axial rotation $\theta_1 = \theta$ and its first derivative $\theta_2 = \theta_{,1}$ for solution in a 1 <sup>st</sup> order system of equations
$A_n: n = 1 - 2$	—	homogeneous components of the 1 <sup>st</sup> order axial load equation
$A_3$	—	nonhomogeneous component of the 1 <sup>st</sup> order axial load equation
$B_n: n = 1 - 10$	—	homogeneous components of the 1 <sup>st</sup> order lateral displacement equation
$B_{11}$	—	nonhomogeneous component of the 1 <sup>st</sup> order lateral displacement equation
$C_n: n = 1 - 10$	—	homogeneous components of the 1 <sup>st</sup> order sagittal displacement equation
$C_{11}$	—	nonhomogeneous components of the 1 <sup>st</sup> order sagittal displacement equation
$D_n: n = 1 - 8$	—	homogeneous components of the 1 <sup>st</sup> order axial rotation equation
$D_9$	—	nonhomogeneous components of the 1 <sup>st</sup> order axial rotation
$C_{NL}$	—	nonlinear terms of the 1 <sup>st</sup> order equations are multiplied by this term, which is increased from $0 \rightarrow 1.0$ for solution equation

## MEDICAL GLOSSARY

The explanation of some terms used extensively in the thesis are as follows:

anterior	—	towards the front
apical vertebra	—	the most rotated vertebra in a scoliotic curve; usually coincident with the vertebra most laterally deviated from the vertical axis
caudal	—	away from the head
cephalad	—	towards the head
Cobb angle	—	clinical measure of the magnitude of a scoliotic curve, measured on an anterior-posterior (A - P) X-ray
coronal plane	—	any vertical plane which divides the body into front and back, also termed the frontal plane
etiology	—	the study or theory of the factors that cause a disease
extension	—	backward bending
flexion	—	forward bending
idiopathic	—	of unknown origin or cause: occurring spontaneously
kyphosis	—	convexity of the spine towards the back or posterior
lateral	—	towards or pertaining to either side of the body
lordosis	—	concavity of the spine towards the back or posterior
medial	—	towards or pertaining to the middle of the body
median plane	—	the vertical plane of symmetry that divides the body into right and left halves, also termed the mid-sagittal plane
posterior	—	towards the back
prognosis	—	a forecast of the probable outcome or termination of a disease
progression	—	the gradual increase of a scoliotic deformity or curve
sagittal plane	—	any vertical plane that divides the body into right and left sides
scoliosis	—	a three-dimensional deformity of the spinal column
transverse plane	—	any horizontal plane that divides the body into upper and lower parts, also termed the axial plane

# Chapter 1

## INTRODUCTION

### 1.1 General Introduction

Deformity of the spine has probably afflicted humans throughout evolution. Stone age drawings of spinal deformity reveal that the condition predates recorded history. Ancient literature from China, India and Egypt, and parts of the Old Testament, have all made reference to persons with spinal deformities (Roaf, 1980; Robin, 1990). Hippocrates, in about 500 B.C., established the term *scoliosis* to describe a deformity of the spine, but which has come to refer more specifically to a *lateral curvature*. Furthermore, he proposed that the spine could be straightened through the appropriate application of forces. Since that time, both theories as to the cause, and methods for the treatment of scoliosis have been proposed by innumerable researchers and physicians.

A remarkable variety of braces have been designed and employed in the treatment of scoliosis, to lesser and greater degrees of success. Expanding on Hippocrates' technique of using traction and lateral forces, various methods were developed to apply the correction forces in combination with exercise regimes and bed rest (Paré, 1582; Avicenna, 1595; Glisson, 1672). During the industrial revolution the complexity of the braces to apply the forces became increasingly elaborate, with only marginal success. Sayre (1877) introduced the plaster of Paris jacket which was reasonably successful, if used for long periods of time; the consequences of which could be equally devastating. Since then, various forms

of plaster casts have continued to be introduced (Risser, 1953; Cotrel, 1970). The net result of this long history of development has been the realization that though a brace or cast may straighten much of the spinal deformity, it is very difficult to achieve full and permanent correction.

The modern era of scoliosis treatment began with the successful development of inter-segmental fusion of the spine by Hibbs (1917). Harrington (1962) developed the first effective internal fixation system to provide distraction forces directly to the spine. Used in combination with fusion, long term permanent correction of scoliotic deformity was at last possible. To ensure success, patients were placed in an external cast or brace, till the fusion mass had stabilized. Many varieties of internal fixation have been devised with notable contributions by Luque (1982), which applied multi-segmental lateral forces rather than distraction, and by Cotrel and Dubousset (1984), which attempted to address the axial rotational component of the spine in scoliosis.

Today, the physician has available various brace designs and/or surgical procedures to use in the control and correction of spinal deformity, and has given the patient the hope that the deformity can be corrected. Though these procedures have achieved a significant degree of success, they are by no means a guarantee, and require extensive intervention with varied losses of mobility. Furthermore, continued progression of the deformity does occur and the associated deformities in the ribcage are far more difficult to correct. Future refinements are still likely possible, as the biology and mechanics of the spine continue to be studied by many researchers. However, to this day, the etiology or cause of the scoliotic deformity being treated remains unknown in the vast majority of cases (Willner, 1994). Before the physician can provide complete recovery, or ideally prevention, further research is required to provide the necessary understanding of the normal, and abnormal, functioning of the spine. Furthermore, prevention is only possible through knowledge of etiology. To investigate the underlying etiology of scoliosis, and in particular *why only some curves progress uncontrollably from small deformities to large incapacitating ones*, is the focus of this study.

## 1.2 Scoliosis

Scoliosis has classically been defined as an abnormal lateral deviation of the spine. However, the true three-dimensional nature of the deformity was recognized long ago (Adams, 1865) (Fig. 1.1A). Due to the use of anterior-posterior (A-P) radiographs in monitoring the condition, the three-dimensionality was ignored, and only the appearance in the coronal plane was examined using the classic Cobb angle (Cobb, 1948) (Fig. 1.1B). Today, scoliosis is again considered an abnormal three-dimensional (3-D) deformity of the spine, composed of a lateral deviation, an anterior-posterior deviation and an axial rotation (Dubousset, 1994). The vertebrae and ribcage are very distorted in large curves. Upon diagnosis, however, the vertebrae of a patient with a mild scoliosis usually appear normal and symmetric, as the curve at this stage is produced almost entirely by the deformations of the flexible discs.

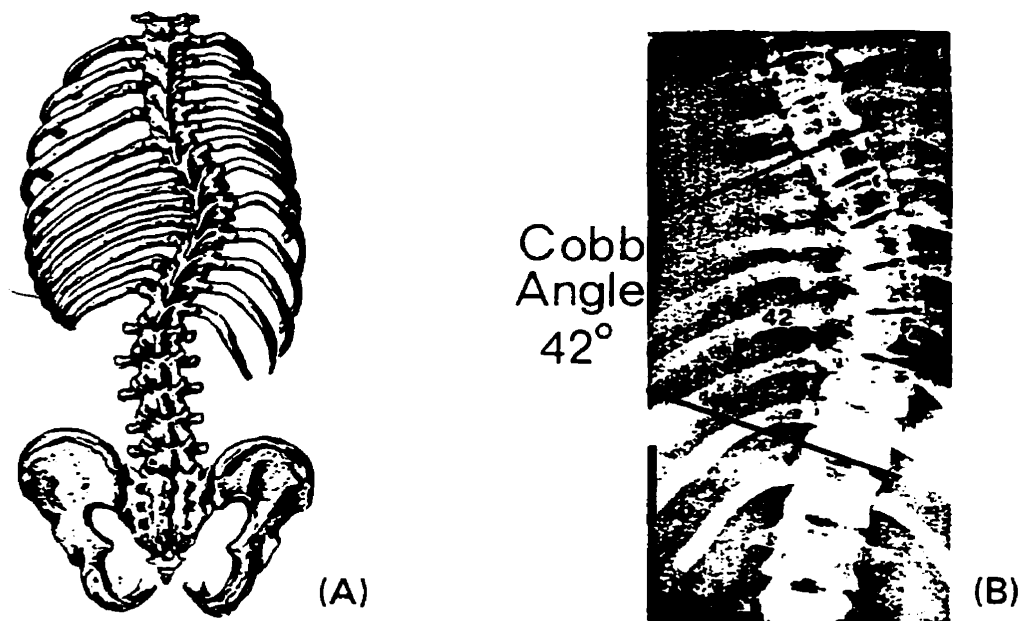


Figure 1.1: (A) Scoliosis is a three-dimensional deformity of the spinal column, with associated deformity to the ribcage (Keim and Hensinger, 1989). (B) A typical anterior-posterior (A-P) X-ray of a scoliotic patient, illustrating the classic two-dimensional measure of the deformity, the Cobb angle (Leatherman and Dickson, 1988).

### **1.2.1 Definition and Classification**

To distinguish between the many types of scoliosis, a classification system has been developed based on the underlying etiology. Accurate classification has greatly helped to understand the disease and enables the application of the most appropriate treatment. The Scoliosis Research Society developed a comprehensive classification system based on Cobb's (Cobb, 1948) initial suggestions (Goldstein and Waugh, 1973). Today, after a number of revisions, a comprehensive classification system encompassing all spinal deformities is available (see Table A.1, Appendix A).

The fact that about 90% of scoliosis patients are placed in the idiopathic category (unknown origin) is possibly the most prominent feature of the classification. Whether all these patients have indeed the same underlying cause for their deformity remains to be established. Nonetheless, upon presentation to a clinic or doctor, the vast majority of patients appear otherwise to be perfectly normal. The idiopathic category is further sub-divided by age of onset: infantile, juvenile and adolescent. The most common type is the adolescent.

### **1.2.2 Adolescent Idiopathic Scoliosis (AIS)**

Adolescent idiopathic scoliosis (AIS) is diagnosed when a curve of unknown origin is discovered between the age of 10 years and maturity. Although discovered in adolescence, the curve, quite likely, was present at an earlier age and only became prominent with the adolescent growth spurt. The distinction, thus, between juvenile and adolescent idiopathic scoliosis has become less clear in recent years. As a result, AIS is also referred to as "late onset" idiopathic scoliosis as opposed to "early onset" for the others. There are four distinct patterns: thoracic, thoracolumbar, lumbar and double (Fig. 1.2). The most common type is the right thoracic which generally extends from T4 to L1 (Robin, 1990). The spinous processes of the vertebrae are also always found to be characteristically rotated into the concavity of the curve, the maximum rotation coinciding with the curve apex (Fig. 1.3). At the time of diagnosis, the female/male ratio is close to 1:1, however, the ratio in

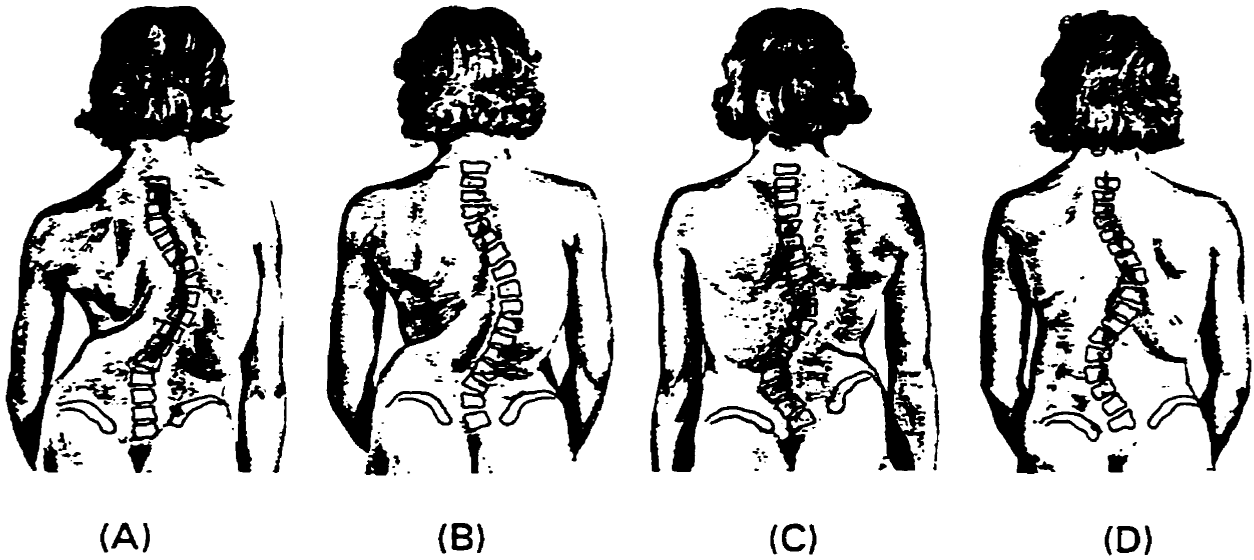


Figure 1.2: Illustration of the four common curve types found in AIS. A) Thoracic: B) Thoracolumbar; C) Lumbar: D) Double (Keim and Hensinger, 1989).

the most severe curves can reach 8:1 in favour of females (Robin, 1990; Weinstein, 1994; Stirling, 1996).

### 1.3 Motivation

The motivation for the present study originates in the natural history of AIS, which has been elucidated by the epidemiological and clinical studies on the general prevalence and progression tendencies of scoliotic deformities. The epidemiology of scoliosis is a rather controversial subject due to the large discrepancies that have been reported for the prevalence in the general population. From a review of these studies, several important points have emerged. If scoliosis is defined as any deviation from the mid-sagittal plane, then 10-15% in the adolescent age group suffer from the deformity (Brooks et al. 1975; Adair et al. 1977). Such a definition does not acknowledge that variations from “ideal” are very common in the normal population. If, on the other hand, scoliosis is defined more realistically as a deviation of  $10^\circ$  or more as measured by the Cobb angle, then only

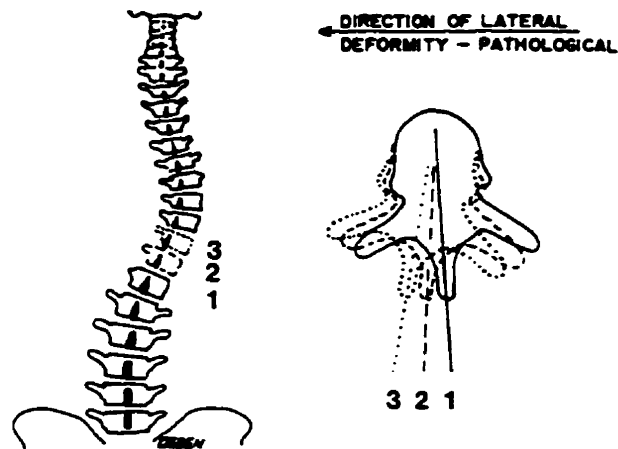


Figure 1.3: The vertebrae in AIS are always found to be rotated with the spinous processes oriented towards the concavity of the curve (White and Panjabi. 1990).

1-4% of adolescents are affected (e.g., Rogala et al, 1978; Asher et al, 1980; Lonstein et al, 1982; Dickson, 1983; Weinstein, 1994). Such relatively high rates of scoliosis were used to justify the establishment of large school screening programs. The objective was to diagnose scoliosis as early as possible so that brace treatment could be started and eventual surgery prevented. Careful analysis of the results of these programs has revealed that most small curves of  $10^\circ$  Cobb angle do not progress (e.g., Rogala et al, 1978; Dickson, 1983; Bailey et al, 1986). In fact, only about 10-20% of curves found in school screening programs can be classified as idiopathic scoliosis that is progressive (Dickson and Archer, 1984). The other curves are not true idiopathic scoliosis, or the curves remain small and stable or even recede. Further studies found that among patients originally prescribed brace treatment, but who did not actually receive a brace for a variety of reasons, only 25% were subsequently demonstrated to have had a progressive curve (Lonstein and Carlson, 1984; Miller et al, 1984). Recent studies suggest that controversy about the efficacy of bracing remains (Goldberg et al, 1993; Lonstein and Winter, 1994; Nachemson et al, 1995; Upadhyay et al, 1995). Clearly not all small curves found in school screening programs

or routine examinations are equal in terms of progression potential. Most, at least 80%, require no treatment at all. Of those that do progress, many will stabilize to about 30° Cobb angle. To predict which of the small curves will progress to a level requiring surgery remains a difficult task.

Many attempts have been made to develop indices and identify factors that predict progression. Some of the factors considered have been: type and degree of curvature, skeletal and physiological maturity, chronological age, family history, gender, stature, growth rate, among others. To date, no single factor has been found to accurately and consistently provide a positive prognosis of progression (Peterson et al, 1995). Nonetheless, some patterns have emerged. For example, a right thoracic curve of 30° in a young female is considered to be at high risk for progression (Robin, 1990; Lonstein and Winter, 1994), and must be monitored very closely. If there is a 5° increase in Cobb angle in the year following diagnosis, then the curve is usually deemed progressive, and bracing treatment or surgery is required (Lonstein and Carlson, 1984; Upadhyay et al, 1995). To further help the physician predict a progressive curve, attempts have been made, such as that by Harrington (1962), to develop an index or factor. He proposed that the geometry of the curve could be used to indicate the need for surgical intervention. Specifically, the Harrington factor is calculated by dividing the Cobb angle by the number of vertebrae in the curve. Lonstein and Carlson (1984) examined a number of single and combined factors to determine the prognosis of a curve. A progression factor was determined that included the Cobb angle, the Risser sign (a measure of skeletal age) and the chronological age. The progression factor predicted a much higher incidence of progression, the greater the Cobb angle and the lower the skeletal age at diagnosis. Most recently, Peterson et al (1995) found that a lower Risser sign (skeletal maturity), a more cephalad level of the apical vertebra, chronologic age and, surprisingly, an absence of imbalance were predictive of curve progression, yet still much uncertainty remained.

The natural history of scoliosis is gradually emerging. However, the physician is still not able to make a treatment decision with complete confidence. Though definite guidelines are available, the prognosis for a mild scoliotic curve cannot as yet be predicted. The

present study is motivated by the need *to identify the characteristics of a progressive curve and to develop predictive factors*. Furthermore, an increased understanding of a progressive curve would help to develop more effective treatment. Only when the potential for progression in a scoliotic patient can be accurately assessed, can a rational treatment regime be implemented by the physician.

## 1.4 Literature Review of the Etiology of Scoliosis

The literature related to scoliosis is truly extensive. A recent book by Robin (1990) has provided a thorough compilation of previous work on the etiology of AIS. Other reviews have been presented by Nachemson and Sahlstrand (1977), Bunnell (1988), Byrd (1988) and Willner (1994). This review attempts to summarize the current state of knowledge as it relates to the etiology of curve progression in AIS. As discussed in the section on motivation, it has only recently been illustrated that most scoliotic curves do not progress to large curves. Consequently, most studies regarding etiology do not distinguish between progressive and non-progressive scoliosis. Therefore, the most prominent etiological theories regarding both curve progression and AIS itself are covered. Though many of these theories are of a purely biological origin, the review emphasizes the mechanical consequences of the given biological deficit. The studies related to anthropometry and scoliosis are of direct importance to the present study. Consequently, a comprehensive review of these studies is presented in detail and summarized in Table 1.1. The other theories are reviewed in lesser detail and presented in Appendix B.

The association between growth, in particular, the adolescent growth spurt, and curve progression in scoliosis is well documented and has long been known (Bampfield, 1824; Calvo, 1957; Duthie, 1959; Burwell, 1971; Duval-Beaupere, 1971; James, 1967. Burwell et al, 1977; Willner, 1994). Furthermore, the belief that serious progression is no longer a concern following the cessation of rapid growth is strongly held, though there is clear evidence of progression in the adult years. Research into the exact association between growth and scoliosis is more recent. A large number of studies have been undertaken in

recent years to examine both the biological and hormonal basis of growth, as well as the gross anthropometric measures of growth rate and stature.

In a series of papers, Willner (1974a,b; 1975a,b) presented the first evidence that scoliotic boys and girls were taller than age matched controls. The differences were apparent before and during adolescence, but had largely disappeared once adulthood was reached. The results were found irrespective of whether corrections were made for the loss of height due to the deformity. Scoliotic girls were also found to be lighter and therefore, considering their increased height, were leaner than normal. Nordwall and Willner (1975) further demonstrated that scoliotic girls were taller, when the height was corrected for the deformity, than controls of either the same chronological or skeletal age. They further showed that in early adolescence, the skeletal development was more advanced in scoliotic girls, whereas in later adolescence, the reverse was true.

Burwell et al (1977) presented an extensive anthropometric study of infantile and adolescent idiopathic scoliosis and found no difference between the normals and scoliotics. However, they conceded that since no corrections were made for the deformity itself, then the scoliotics were likely taller than normal.

Clark (1977) studied growth velocity, standing and sitting height in scoliotic girls compared with normals. No difference in growth velocity was noted, however, it was concluded that the scoliotics would have been taller if corrections for the deformity had been made.

Schultz and Cisewski (1978) used a morphological factor that measured spine slenderness to predict progression in 20 of 26 patients. For non-progressive curves, the factor correctly predicted no progression in 13 of 22 patients. The spines of the non-progressive group were 34% less slender compared to the progressive group.

Drummond and Rogala (1980) found that the growth of adolescents with idiopathic scoliosis did not appear to differ from normal. However, when measurements were corrected for skeletal age, both boys and girls with scoliosis were found to be heavier and taller. They found a delay in the onset of puberty and skeletal immaturity in girls with AIS, particularly with larger curves ( $> 20^\circ$  Cobb angle).

Skogland and Miller (1981) used X-rays to measure the length and proportions of the

thoracolumbar spine in children with idiopathic scoliosis ( $< 40^\circ$  Cobb angle). The length of the thoracolumbar spine was measured both along the curve (termed corrected length) and as the shortest vertical distance top to bottom (termed uncorrected length). No significant difference in the length of the thoracolumbar spine was found between the controls and AIS patients for both measures of length. However, there was a tendency for longer spines in scoliotics (longer by 4 mm for girls and by 12 mm for boys), and the height of the T6 vertebra was significantly greater. Furthermore, the slenderness of the T6 and L4 vertebrae was found to be greater for scoliotics, particularly for girls less than 13 yrs and for all boys. It should also be noted, that had the method of Bjure et al (1968) been used to correct spine length (as used in previous studies) then a significantly greater length in scoliotics would have been found. The authors felt that this technique overestimated the length, particularly for curves under  $30^\circ$  of Cobb angle.

Low et al (1978) and Leong et al (1982) found scoliotics to be taller than normal when the height was corrected for the deformity. They also found the sitting-height/lower-limbs length ratio to be slightly greater in scoliotics. Furthermore, the pubertal growth duration was longer. This was argued to be the explanation for the greater height of scoliotics.

Buric and Momcilovic (1982) found the standing height of idiopathic scoliotics to be 5 cm greater than controls, while the sitting height was 2 cm greater. No significant difference was found in the weights of scoliotics and controls. The above comparisons were made at the same chronological age. When skeletal age was assessed, the scoliotics were found to be significantly more mature below the age of 12 yrs, and less mature thereafter.

Dickson and Sevitt (1982) reported that the children with progressive scoliosis were significantly taller than those with a non-progressive scoliosis. However, the children in both groups were growing at the same rates, and thus, they concluded that increased height was not likely to be an etiological factor for AIS, but rather an indicator of a bad prognosis.

In a review paper, Gross et al (1983a) argued that the literature consistently supported the view that scoliosis could be explained due to buckling in a purely mechanical manner. In an interesting analysis, they compared the partial weight (head, torso and arms) versus

the critical load (Euler) for normal boys and girls, and scoliotic girls for ages 11-13 yrs. The difference between the critical load and the partial weight was the smallest for the scoliotic girls. The difference for normal boys was also much greater than that for normal girls. The comparison, however, did not account for changes in spine stiffness with age, or for the scoliotic deformity, or for the distribution of body weight over the spine length. Nonetheless, the results illustrated a close relationship between body weight and critical load of the spine.

Schultz et al (1984) measured the spine morphology using X-rays of normal children, ages 10-16 yrs. The diameters in both the coronal and mid-sagittal planes were measured at T5, T10 and L3, as well as the length between T5-L3. The spines of girls were more slender than boys at all ages, with statistical significance at ages 12-16 yrs. In a review paper, Schultz (1984) summarized the data for similar measurements from scoliotics. The differences between scoliotic girls and the normals were inconsistent and only bordered on statistical significance.

Taylor and Twomey (1984) found the female thoracolumbar spine to grow more in length than the male from ages 9 to 13 yrs in normal children. From 8 yrs to maturity, the transverse diameters in the coronal plane of thoracic and lumbar vertebrae increased more in males than females. Therefore, these combined differences would result in a significantly more slender thoracolumbar spine in females compared to males from 8 yrs onwards.

Normelli et al (1985b) found no significant difference at the time of the menarche between scoliotic girls and the controls, using more contemporary anthropometric data. However, the authors noted that the difference was almost significant and concluded that the scoliotic girls would have been found taller if the heights had been corrected for the deformity. The scoliotic girls were found to be significantly lighter at the menarche compared to the normals.

Skogland et al (1985) reported a prospective study of 62 tall girls. A scoliosis curve measuring greater than  $10^\circ$  Cobb angle was found in 13 of the 62 girls. In addition, 14 girls had a curve of  $5-10^\circ$  and two of these had exceeded the threshold of  $10^\circ$  in an annual follow-up. This frequency for scoliosis was far higher than expected, and may indicate a

predisposition for scoliosis in girls with excessively tall stature.

Two studies by Nicolopoulos et al (1985a,b) examined the stature of healthy children and of those with AIS. As in the previous studies, the authors found the standing height of scoliotic girls to be greater than controls for ages 12 to 15 yrs. However, in contrast to previous reports, the authors found a significant change in cephalo-caudal proportions. They found no significant difference in the suprapelvic height between the scoliotic girls and the normals. Rather they found significant increases in the pelvic height and nearly significant increases in the subischial height. The authors concluded that girls with AIS have an ectomorphic growth pattern, where the trunk is shorter relative to leg length.

Archer and Dickson (1985) found the standing height of girls with AIS was significantly greater from 10 to 13 yrs in those with a curve greater than 15° compared to those with a curve less than 15°, or to those with a scoliosis due to pelvic tilt. On the other hand, they found no difference in the growth increments between the curves of different magnitude or the pelvic tilt scoliosis. Furthermore, they found no differences in standing height or increase in standing height between progressive, static or regressive curves. The authors noted that the increased standing height was found without the use of a correction factor such as that of Bjure et al (1968) used in previous studies. They were critical of its use, and argued that the increased height was due to an "uncoiling" of the normal sagittal kyphosis (which is central to the theory of Dickson et al (1984), outlined earlier). They also found no difference in skeletal development of the scoliotics and were critical of the use of inappropriate historical controls in previous works.

Veldhuizen et al (1986) used anterior-posterior X-rays of scoliotics and found no difference in the growth increments of the height or width of the vertebrae from those involved in the curve, and those outside the curve region. The slenderness index of height/width was increased in girls compared to boys, but was not different in the scoliotic region of the spine compared to the remaining vertebrae.

Shohat et al (1988) examined growth and ethnicity in scoliosis from a large population of military recruits at age 17. Scoliotics were significantly taller, lighter and thinner (weight/height) than the non-scoliotic controls, with no corrections made for height loss.

The more severe curves were found in taller, lighter and thinner individuals. Females were at increased risk of developing the more severe curves.

Carr et al (1989) developed an improved technique to correct for the height loss due to the scoliotic deformity. The technique used automated stereophotogrammetry (termed ISIS) to determine the true spinal length along the curves in both the sagittal and coronal planes. This technique, therefore, could determine the height loss, while recognizing the 3-D nature of a scoliotic curve. They found a mean height loss due to scoliosis of 2.2 cm using the ISIS technique, whereas the Bjure et al (1968) formula determined a mean height loss of 2.7 cm. This confirmed the suspicions of previous researchers that the formula of Bjure et al (1968) overcompensated for the deformity. On the other hand, they still found that even with changes in the sagittal plane (less kyphosis), a correction for height loss due to the deformity, ranging from 0 to 5.3 cm, had to be made to establish spine length.

Loncar-Dusek et al (1991) found that scoliotics grew faster or more intensely than their peers who did not have scoliosis. Scoliotic girls had a peak growth velocity of 8.1 cm/yr compared to the normals at 7.1 cm/yr. The authors noted, however, that the increased growth velocity in scoliotics need not imply an increased standing height at maturity.

Hagglund et al (1992) found that girls with AIS have an accelerated growth velocity in the prepubertal period. Two years before the peak growth velocity, scoliotic girls were significantly taller than controls. Furthermore, after adjustment for the fact that the menarche of scoliotic girls was earlier, they were still taller. At maturity, however, the scoliotic girls were only slightly taller than normal. Since the increased height was found in the prepubertal growth phase, the authors concluded that increased growth hormone (GH) activity was responsible.

Carr et al (1993) have recently examined the family stature of patients with idiopathic scoliosis. They found scoliotics to be 2.4 cm taller than normal. When the height was corrected for the deformity, using the ISIS technique developed by the authors, the scoliotics were 4.6 cm taller than normal. The authors found no difference in skeletal age from chronological age, nor did the pubertal ratings differ from normal. For scoliotics with a positive family history, their height was similar to normals, whereas those from unaffected

families were taller. Therefore, scoliotics with a positive family history appear not to need to grow as much to develop scoliosis. The scoliotics were also taller than their unaffected relatives, indicating that genetic factors alone have not caused the increased height.

Nissinen et al (1993) found in a longitudinal prospective study that both boys and girls who eventually had scoliosis displayed an increase of body height, sitting height and growth of sitting height. In pre-scoliotic girls, the sitting height was gained at an earlier age and the peak sitting height velocity was greater than normal. These factors were not, however, statistically significant in the logistic analyses.

Goldberg et al (1993) found that scoliotic girls had an earlier menarche and were taller than normal in early adolescence. At maturity, however, the height difference had disappeared. If the scoliotics were subdivided by curve severity or by progressive behaviour, there was no significant difference in the distribution of tall and short girls. The authors concluded that scoliotic girls had an earlier pubertal growth spurt, but that no abnormality in growth existed.

In a recent prospective study, Hazebroek-Kampschreur et al (1994) found that height was the strongest predictor for the development of scoliosis and kyphosis in both sexes. In particular, taller girls who had started their adolescent growth spurt at 11 years of age were at greatest risk to develop AIS and other trunk abnormalities at 13 years of age.

In spite of the extensive research in recent years into growth and stature, as outlined in the foregoing, a clear consensus is yet to emerge. Due to the large number of studies from different researchers, and from different countries, that have reported an increased standing height in scoliotics, this perhaps is the most confident finding. Whether or not the spine is longer, however, is another question. Only the study by Skogland and Miller (1981) measured directly the spine length in scoliotics using X-rays. They only found a significant increase if corrections were made using the technique by Bjure et al (1968), though there was a tendency for longer spines in scoliotics, which was not statistically significant. The recent ISIS technique possibly represents the best method today of assessing the true length of a spine. The study by Carr et al (1993) found increased standing height but did not examine directly spine length. Only when a technique such as ISIS, which can

measure the true length of the 3-D spine, is combined with accurate X-rays will the length of scoliotic spines be rigorously determined. The suggestion of increased spine slenderness in scoliotics needs also to be further substantiated. On the other hand, the difference in spine slenderness between boys and girls appears to be strongly supported. Though many of these studies have discussed the implications of an increased spine length in terms of a reduced Euler buckling load, the effect of the reported  $\approx 1-2$  cm increase in spine length has received little quantitative analysis. In particular, the increase has not been analyzed in terms of the weight carried by the spine and its slenderness through the years of growth.

Whether there is a growth anomaly is also not clear from these studies. Some have found altered skeletal development, whereas others have not, or have found differences which are not thought to be pathological. Several studies have searched for biochemical indications of growth abnormalities to explain the apparent increased stature of scoliotics (Misol et al, 1971; Willner et al, 1976; Skogland and Miller, 1980, 1981; Ahl et al, 1988). There appears to be evidence of increased growth hormone activity in scoliotics, particularly in early puberty, but the evidence for a primary abnormality is less clear.

Table 1.1: Summary of the studies related to anthropometry and scoliosis.

RESEARCHERS	COUNTRY	KEY FINDINGS AND COMMENTS	CORRECTIONS FOR DEFORMITY*
Willner, 1974a,b; 1975a,b	Sweden	Increased standing and sitting height in scoliotics Proportion between sitting and standing height undisturbed Decreased weight → leaner than normal Found in both cross-sectional and longitudinal studies	Irrespective  (Method of Bjure et al, 1968)
Nordwall and Willner, 1975	Sweden	Increased standing height in scoliotics Advanced skeletal age in early adolescence	Yes (Method of Bjure et al, 1968)
Burwell et al, 1977 (Symposium)	England	No anthropometric difference in scoliotics Argued that with corrections scoliotics are taller	No
Clark, 1977 (Symposium)	England	No difference in growth velocity Argued that with corrections scoliotics are taller	No
Schultz and Cisewski, 1978 (Abstract)	U.S.	Increased slenderness in progressive curves, in 20 out of 26 patients. Decreased slenderness in 13 of 22 non-progressive patients (X-rays)	
Drummond and Rogala, 1980	U.S. & Canada	Scoliotics are taller and heavier if corrected for skeletal age	No
Skogland and Miller, 1981	Norway	Only a tendency for longer spines in scoliotics Increased slenderness (particularly thoracic) in scoliotics (X-rays)	Yes (but not using method of Bjure et al, 1968) Length along curve in the coronal plane
Low et al, 1978 Leong et al, 1982	Hong Kong	Increased standing height in scoliotics	Yes (Method of Bjure et al, 1968)
Buric and Momcilovic, 1982	Yugoslavia	Increased standing and sitting height in scoliotics. No difference in weight	Yes (Method of Bjure et al, 1968) for curves > 30° Cobb angle
Taylor and Twomey, 1984	Australia	Increased spine slenderness in normal girls compared to boys	
Schultz et al, 1984	Sweden	Increased spine slenderness in normal girls compared to boys	

RESEARCHERS	COUNTRY	KEY FINDINGS AND COMMENTS	CORRECTIONS FOR DEFORMITY*
Normelli et al, 1985b	Sweden	Increased standing height if corrections had been made for the deformity. Decreased weight	No
Skogland et al, 1985	Norway	Increased incidence of scoliosis in tall girls	
Nicolopoulos et al, 1985a,b	England	Increased standing and sitting height in scoliotics due to taller pelvis	Yes (Method of Bjure et al, 1968)
Archer and Dickson, 1985	England	Increased standing height for > 15° Cobb No difference in growth velocity or development - Increase due to uncoiling (reduced kyphosis) of normal thoracic kyphosis. - Critical of Bjure et al (1968) correction method - Critical of improper historical controls	No
Veldhuizen et al, 1986	England	No difference in growth increments between regions of scoliotic spines (X-rays)	
Shohat et al, 1988	Israel	Scoliotics are taller and lighter, particularly in larger curves	No
Carr et al, 1989	England	Improved method to correct for height loss due to the deformity	Yes (Method of ISIS)
Loncar-Dusek et al, 1991	Yugoslavia	Increased peak growth velocity but no increased standing height at maturity	—
Hagglund et al, 1992	Sweden	Scoliotics are taller in pre-puberty	Yes (Method of Bjure et al, 1968)
Carr et al, 1993	England	Scoliotics are taller. No difference in skeletal age. Not taller if there is a positive family history. Taller than unaffected relatives	Yes (Method of ISIS, Carr et al, 1989)
Nissinen et al, 1993	Finland	Increased standing and sitting height, and growth velocity in scoliotics. Longitudinal study.	No
Goldberg et al, 1993	Ireland	Scoliotics are taller in early adolescence. No difference with curve severity or progression	Yes (Method of Bjure et al, 1968)

\* Due to the loss of height as a result of the deformity, it is necessary to "correct" the measured vertical height to determine the "actual" spine length.

## 1.5 Problem Identification and General Objective

The natural history of AIS reveals that to successfully establish the prognosis of a mild curve is as important and as difficult as determining the underlying etiology. Successful prediction of curve progression would reduce unnecessary bracing and radiology of essentially "stable" curves and lead to earlier diagnosis of progressive ones. Presently, there are a number of guidelines, such as age and curve magnitude, but establishing the prognosis remains a difficult task for the physician.

Since most mild curves do not progress, this is indicative that more than one factor must be present in a progressive scoliosis. One factor leads to the initial scoliosis, and a second factor leads to the progression. Both factors need not be pathological. In fact, the second factor need only be a catalyst that is harmlessly present in many people, but when combined with a small scoliosis can produce progression. Similarly, the initial scoliosis may simply represent the outer bounds of asymmetry naturally present in the population. The second factor that promotes the progression would then be the most important. This is but one of the problems in determining the etiology of a likely multifactorial disease.

Another difficulty is distinguishing between cause and effect. Many differences have been found in clinical studies between scoliotics and controls, yet the consequences of the deformity almost certainly causes many of the observed discrepancies. Only long term longitudinal clinical studies following a large population can conclusively prove that a given factor is associated with a progressive scoliosis. The difficulty, of course, is determining what to measure over the long term.

Experimental animal studies avoid the problem of cause and effect, but introduce other concerns. Though scoliosis has been produced in many animals, it is not clear that it represents a proper model for idiopathic scoliosis in humans. Firstly, the surgical alteration or removal of a part may produce scoliosis, but this level of deficit just simply has not been observed in scoliotics. Secondly, the morphology, stiffness, activating muscles and control systems are all quite different between humans and animals. In particular, the role of gravity is very different in quadrupeds. It is thus difficult to ascertain the validity and

implications of the results.

Even if the etiology of scoliosis and a progressive curve is purely biological, mechanics are still relevant to the understanding of the disease. Many, if not most, of the biological theories of scoliosis are manifested in a mechanical manner. Differences in morphology, hormone levels, and muscular-control systems, for instance, are all biological deficits which alter the mechanics of the spinal complex. An understanding of the relevant mechanics can only help to establish the prognosis and the potential for the final curve magnitude. In fact, progressive scoliosis could be described as a purely mechanical event, dictated by a change in the equilibrium states. A stable curve remains in equilibrium, whereas a progressive curve represents a search for a new and necessary equilibrium configuration.

The study of the mechanics of a scoliotic spine can also help to distinguish between cause and effect without the problems involved in clinical and experimental studies. By purely examining cause, a study of mechanics can determine if a given theory is plausible, and the level of alteration required for progression. The development of an analytical model provides the opportunity to examine a multitude of potentially causal factors.

Of the various etiological theories reviewed in the previous section and Appendix B, those related to growth and stature have only received limited consideration from a mechanical point of view. Yet clearly, changes in stature are inextricably associated with mechanics. This is particularly relevant for the following three reasons. Firstly, though the risk of progression in scoliosis is consistently shown to be associated with the adolescent growth spurt, the exact reasons for this correlation are not known. In particular, it is not known whether the correlation is due to the growth within the vertebrae, due to the changes to the gross anthropometric measures of the spine and trunk, or to some other purely biological relationship. After birth, the period of adolescence represents the most dramatic changes in the human form. Consequently, it is not unreasonable to assume that the association between growth and scoliosis is due to the changes in the gross morphology which occurs during the adolescent growth spurt. The mechanics of this event, and specifically for a scoliotic spine, have not been widely investigated despite the strong links with progression. Secondly, there continues to be reports, as highlighted in the foregoing

literature review, of altered growth and stature in scoliotics. These differences are not necessarily pathological, but could represent the upper limits or an identifiable subgroup with a given growth rate and stature. There have been concerns raised about the validity of these observations, and thus, there is a need to establish whether the observed changes could alter the mechanics sufficiently to cause progression. Thirdly, the differences in stature between males and females is often discussed in the scoliotic literature. However, the resultant mechanical differences has received far less attention. This is significant considering the dramatically different progression tendencies between males and females.

To further the understanding of the relationship between growth and progressive scoliosis, in particular a mechanical correlation, there are various possible approaches: clinical, experimental (in-vivo, in-vitro and animals) and models. The relationship between growth and progressive scoliosis originated in the clinical studies, however, they are restricted by the problem of cause and effect and the very large populations which must be studied due to the relatively small number of mild scoliotic curves that do progress. Experimental studies in animals are difficult to interpret in terms of mechanical concerns. Experimental in-vivo studies are intrinsically difficult and limited by the factors which can be studied. Experimental in-vitro studies could be very useful in order to examine stature, but the access to a sufficient adolescent specimen population is essentially impossible. On the other hand, a modelling approach appears very well suited at this point in time. The development of a model to analyze the mechanics of the adolescent growth spurt, and the relationship to idiopathic scoliosis, provides a means to assess the present clinical observations from a mechanical point-of-view. A model can then be used in concert with future clinical studies to establish if there is a mechanical basis to the link between scoliosis and growth. Therefore, the general objective of the present study can now be formulated as follows:

- i) Development of a model of a spine with a mild idiopathic scoliosis.
- ii) Investigation of the mechanics of curve progression during the critical growth spurt of adolescence.

This work is part of a longer term goal to contribute to the development of a rational methodology to establish the prognosis of a mild idiopathic scoliosis diagnosed in a young adolescent. The development of a model to study the changing mechanics of the growing spine in scoliosis represents a first step towards this goal.

## 1.6 Thesis Outline

Chapter 1 presented a general introduction to the subject of scoliosis and the motivation for studying this disorder. A literature review of the prominent theories for the etiology of scoliosis was presented, followed by the formulation of the general objective. Chapter 2 presents a review of spinal biomechanics as related to scoliosis and to previous models of the spine, followed by the formulation of the specific objectives. Chapter 3 presents the development of the governing equations of the spatial beam-column model of the spinal column. Chapter 4 presents the development of the ribcage FEM used to establish the elastic ribcage stiffness needed for the beam-column model. Chapter 5 presents the validation studies of the present spinal model in comparison with experiment and other spine models. Chapter 6 presents the analysis of the ribcage stiffness and the support provided to the spinal column. Chapter 7 presents the parametric analysis and the results of the effect of the adolescent growth spurt on curve progression due to simulated growth. Chapter 8 provides a discussion of the findings, the limitations of the present work, draws some conclusions and provides suggestions for future work. Appendix A presents a list of all known etiologies for scoliosis. Appendix B presents a review of various theories for the etiology of AIS. Appendix C presents a short review of relevant spinal anatomy to assist the reader. Appendix D presents a review of various approaches to modelling the spine not directly related to scoliosis. Appendix E presents an analysis of the potential errors of the present spine model and the limits on its applicability. Appendices F,G and H provide a listing of the various terms and coefficients in the governing equations.

## **Chapter 2**

# **REVIEW OF SPINAL BIOMECHANICS AND FORMULATION OF SPECIFIC OBJECTIVES**

### **2.1 Introduction**

Prior to the formulation of the specific objectives of this study, it is necessary to review the relevant spinal biomechanics needed to develop the present model of a scoliotic spine. A review of certain experimental studies is included as they are relevant to understanding the behaviour of the spinal column or are related to scoliosis. However, the review is concentrated on spinal modelling studies related to scoliosis, which is the area of the present study. An overview of spinal modelling is also presented in Appendix D to illustrate the various approaches and for completeness. The formulation of the specific objectives for this study concludes the chapter.

## **2.2 Review of Spinal Biomechanics**

Individual components of the spine such as the disc, vertebra, and ligaments have been extensively tested in experiments to determine their material properties. The joints of the spine and ribcage have been studied to determine stiffnesses or flexibilities through load-displacement tests. And to a limited degree, the spine as a whole has also been investigated to determine its kinematics, stiffness and stability characteristics. From this experimental data, models have been developed to represent the various tissues of the spine. There are excellent textbooks and papers which provide comprehensive discussions on the biomechanics of the spine and scoliosis (Schultz, 1976, 1984; Pope et al. 1984; Bunch and Patwardhan, 1989; White and Panjabi, 1990; Goel and Weinstein, 1990).

### **2.2.1 Experimental Studies**

Experimental studies into the mechanics of the whole spine with application to scoliosis are very rare. The study of Lovett (1905) was possibly the first to provide quantitative information on the mechanics of the normal spine using cadavers and live models, in order to gain insight into the pathological condition of scoliosis. The results illustrated the complex movements of the spine, in particular, the coupling behaviour between axial rotation and lateral bending, which varied along the spine length. It was concluded that the axial rotation component of scoliosis could not be explained by normal movements of the spine.

The next study to provide substantive quantitative information of spinal mechanics was by Lucas and Bresler (1961) and Lucas (1970). Whole adult ligamentous spines devoid of musculature and the ribcage were subjected to axial compression at T1 to investigate the stability of the column. For a spine fixed at the base and free at the top, a critical load of 19.1 N was found experimentally for buckling in the coronal plane. When the top was restrained laterally, but free to rotate (i.e., pinned), the critical load was 166.8 N. The spines were also subjected to a lateral load applied at the T1 vertebra. The lateral deflection of the spine was used to establish the lateral flexibilities at each motion segment, from which

an effective uniform stiffness for the whole spine was calculated. Using Euler's formula, a critical load of 20.4 N for the free top, and 167.2 N for the pinned top was calculated. The excellent agreement between the theoretical and experimental results illustrated that the adult ligamentous spine behaved as an elastic rod within the range of loads studied.

There are numerous studies in the literature which have reported 3-D flexibility data for the motion segments from adult spines (see White and Panjabi, 1990). Only the study of Miller and Skogland (1980a) determined the 3-D flexibility of an adolescent spine. Though only from a single specimen (an 11 year old boy), the results supported the impression that adolescents were more flexible than adults. The authors also attempted to correlate the flexibility data with morphological measurements and disc hydration at each spine level (Miller and Skogland, 1980b). No single geometric variable could explain all the changes in flexibility with spine level. Torsional and lateral bending flexibilities were most strongly correlated with variables at a given spine level.

Halsall (1980) and Halsall et al (1983) examined the lateral stiffness of intact cadaveric spines with the ribcage intact and severed. Lateral deflection of the spine was found to be linear up to a load of 250 N, which resulted in a flexibility of 0.1 mm/N at the T9 vertebra. When the results were compared with a beam model, excellent agreement for the lateral deflection along the spine was found between experiment and theory.

The studies reviewed above appear to be the only ones which provide quantitative data on the whole spine or the adolescent spine, with application to scoliosis.

### **2.2.2 Scoliosis Models**

The use of mechanical models to investigate the mechanics of scoliosis has a long history. More recently, analytical models have become sufficiently sophisticated to provide quantitative insights into the mechanics of scoliosis. They have been used to study the mechanics related to etiology, and to study the effects of various brace designs and internal fixation systems. For this review, the quantitative studies are grouped according to each particular model and research group, and summarized in Table 2.1. In the sections below, only those models which have been explicitly used to study etiology are discussed in detail.

## **Mechanical Models**

Early mechanical models by Feiss (1907) and Carey (1932), were constructed of metal, leather, wood, and springs, and were remarkably elaborate. These models provided a tool to examine the kinematics of the spine and to illustrate how a scoliotic deformity might arise. Other simpler models have been used by Rogers (1933), Arkin (1949), Somerville (1952), Roaf (1958, 1966), Lindahl and Raeder (1962), Olsen and Allen (1969), among others. Ultimately, these models could only provide qualitative information of spinal mechanics.

## **Euler Column Models**

The similarity of the spine to a structural column has been noted by all researchers to various degrees. Many have advocated that scoliosis is a stability failure, which can be described and predicted by Euler's formula. According to the well-known formula, the critical compressive load of a column is a function of the length, stiffness and end-conditions. Using this knowledge, the various structures of the spine have been discussed in terms of their ability to lower the critical load. In this context, the Euler model of a scoliotic spine has been employed for a long time. Only with the work of Lucas and Bresler (1961) did the Euler model provide the first quantitative information.

## **Quantitative Models**

In a long series of papers (1970-1993), Schultz and co-workers have developed a mathematical model to study the mechanics of scoliosis. The theory for the model was first outlined by Schultz and Galante (1970). In a subsequent paper, Schultz et al (1972), used the geometrical model to illustrate that scoliotic deformities could be reproduced within the normal range of motion of the spine with no vertebral asymmetries required. The next stage of development was to incorporate the quasi-static force-deformation properties of the spine (Belytschko et al (1973); Schultz et al (1973)). The spinal column was modelled as a collection of rigid bodies for the vertebrae, interconnected by several deformable elements.

Andriacchi et al (1974) incorporated the ribcage into the ligamentous spine model. The bony ribs and sternum were modelled as rigid bodies. The costovertebral, costotransverse,

costal cartilage and intercostal structures were modelled by deformable beams and springs. In comparison with the stability experiments on the spinal column by Lucas and Bresler (1961), the ribcage increased the buckling load by a factor of three to four, depending on the boundary conditions at the top of the spine. Takashima et al (1979) incorporated the active contractions of the trunk muscles into the spine and ribcage model. Distributed body weights were also included and applied at each vertebra, offset from the centre.

The model was then used by Haderspeck and Schultz (1981) to investigate what muscular loads could be involved in the progression of an idiopathic scoliosis. Based on the results, it was argued that progression was unlikely due to any malfunctions intrinsic to the trunk muscles. An increase in Cobb angle of  $6^\circ$ , which represented progression, was easily corrected by many muscle groups at low intensity. The findings were further explored in experimental studies by Portillo et al (1982), and Reuber et al (1983). Progression of scoliosis was proposed to result from an inability of the postural control system to adequately respond to the lateral bending moments imposed on a spine due to a small curve. If the muscular forces were too symmetric, all of the moments had to be resisted by the soft-tissues of the spine itself. Over time, these moments on the spine would lead to the permanent structural changes observed in large curves.

Further developments to the ribcage model of Andriacchi et al (1974) were reported by Closkey et al (1992). Five rigid cylinders, interconnected by deformable beam elements, were used to represent each rib. The response of the whole ribcage to frontal and lateral compressive loads was found to be in better agreement with experiments than the earlier rigid rib model by Andriacchi et al (1974). Recently, Closkey and Schultz (1993) used the deformable ribcage model to study the ribcage deformity in scoliosis.

Miller and Skogland (1980c) developed a model of the ligamentous spine modelled as a series of 17 flexible beam elements. Each beam was assigned a 3-D flexibility matrix determined from a single adolescent spine (Miller and Skogland, 1980a). A total of 146 paravertebral muscle slips were modelled, and symmetrical and asymmetrical configurations of the spine were analyzed in terms of the muscular response to maintain stability. The effects of an 8% increase in thoracic length and a 30% increase in lateral flexibility

were also studied to simulate growth. They concluded that the changes in displacements and loads on the spine indicated that curve progression via a growth mechanism cannot be excluded.

Lindbeck (1985) proposed a continuum model of the spine to analyze a functional scoliosis due to leg length inequality. The spine from L5 to T7 was idealized as a slender elastic beam. The spine and thorax above T7 were considered as a rigid body. The small displacement governing equations for the elastic axis were developed, and included an initial deformity. In a parametric analysis, it was found that to reproduce a functional scoliotic shape (measured on an X-ray), a uniform bending stiffness of around  $2 \text{ Nm}^2$  was required, which was in good agreement with experimental values reported in the literature.

Patwardhan and co-workers developed a biomechanical analog of curve progression based on the classical theory of beam-columns (Patwardhan et al, 1986). It was argued that progression can be likened to the plastic deformation of an initially curved beam-column, whereas a non-progressive curve remained in the elastic range. The transition was based on reaching a critical bending moment in the spine. The model was restricted to the coronal plane and therefore did not include the axial rotation component of a scoliotic deformity. An adjusted stiffness ( $EI$ ) was used to represent the overall behaviour of the spine. The model was used to parametrically investigate the progression characteristics of different types and magnitudes of curves, as well as the effectiveness of bracing different curves. A further investigation with the model was undertaken by Meade et al (1987) to analyze the progression characteristics of double curves.

Veldhuizen and Scholten (1987) used a discrete model of the spinal column to analyze the kinematics of a scoliotic spine compared to a normal spine. The model was essentially identical to the earlier model by Belytschko et al (1973), except for improved modelling of the facet joints. A scoliotic deformity would appear to have a different coupling pattern between lateral bending and axial rotation since the spinous processes are rotated into the concavity; a pattern which is opposite to the kinematics in the normal spine (Scholten and Veldhuizen, 1985). However, using X-rays and the model, the authors showed that with further lateral bending, a scoliotic deformity displayed a normal kinematic behaviour.

Scholten et al (1988) examined the stability of the spine with the discrete model and argued that the initiation of scoliosis could not be explained by buckling theory. Using a nonlinear analysis, the spine was found to be stable up to loads of two times body weight. The spine also remained stable even with a five-fold reduction of  $E$ . However, though the spine was found to be mathematically stable, the displacements predicted by these reductions were very large, and in a clinical setting would surely have been considered progression.

Stokes and Laible (1990) developed a FEM of the osseo-ligamentous thorax to investigate the initiation of scoliosis due to asymmetric rib growth. The nodal geometry was based on stereoradiographic reconstructions of an adolescent spine. The ribs, costal cartilages, and costotransverse joints were modelled by beam elements, and the intercostal tissue by spring elements. The motion segments were modelled by a two node element which incorporated experimentally measured stiffness matrices for the thoracic region.

Stokes and Gardner-Morse (1991) used a FEM of the ligamentous spine to analyze the interaction between lateral bending and axial rotation in scoliosis. The motion segments were represented by two methods. The first was similar to the method in the previous model, whereas in the second, an equivalent beam element was used which approximately matched the stiffness matrix of the other method. From the results, it was argued that the normal coupling of the motion segment could not explain the axial rotation in scoliosis and that the initial sagittal curvature was of greater importance in determining the coupling.

Noone et al (1991) developed a continuum model to investigate scoliosis due to bilateral muscular weakness with applications to paralytic scoliosis. A nonlinear continuum beam-column model of the spine in the coronal plane was developed. The moments due to two lateral muscles were also included as contraction forces producing a moment. The ability of the model to represent a scoliotic curve and the post-surgical shape of a corrected curve was demonstrated. The continuum model was also compared with a FEM model (Ghista et al, 1988) with good results.

Table 2.1: Summary of the models that have been developed to investigate the mechanics of scoliosis. The models are grouped according to the different primary researchers.

RESEARCHERS	MODEL TYPE*						COMMENTS & APPLICATION
	1	2	3	4	5	6	
Schultz and Galante, 1970	K	NL	---	3-D	---	MP	Geometric model of 3-D spine motion
Schultz et al., 1972	K	NL	---	3-D	---	MP	Geometric analysis of the 3-D scoliotic deformity
Belytschko et al., 1973	D	NL	NLE	3-D	SL	MP	Validation of whole isolated ligamentous spine model
Schultz et al., 1973	D	NL	LE	3-D	SL	MP	Properties and validation of model at motion segment level
Schultz and Hirsch, 1973	D	NL	LE	3-D	IL	MP	Analysis of Harrington rod correction
Andriacchi et al., 1974	D	L	LE	3-D	SL	MP	Incorporation of ribcage into the ligamentous spine model
Andriacchi et al., 1976	D	L	LE	3-D	BL	MP	Analysis of the Milwaukee brace to correct scoliosis
Takashima et al., 1979	D	L	LE	3-D	ML	MP	Incorporation of trunk muscles into the spine and ribcage model
Haderspeck and Schultz, 1981	D	L	LE	3-D	ML	MP	Analysis of muscular response to curve progression
Schultz et al., 1981	D	L	LE	3-D	ML	MP	Analysis of correction of scoliosis by muscle stimulation
Wynarsky and Schultz, 1991	O & D	L	LE	3-D	BL & ML	MP	Optimal correction possible by brace or muscle loads
Closkey et al., 1992	D	L	LE	3-D	SL	MP	Incorporation of a deformable ribcage into the model
Closkey and Schultz, 1993	D	L	LE	3-D	SL	MP	Analysis of the ribcage deformity in scoliosis
Miller and Skogland, 1980c	O & D	L	LE	3-D	ML	AP	Simulated growth of an adolescent spine
Yettram and Jackman, 1980	O	L	---	3-D	ML	---	Effectiveness of brace and correction devices in scoliosis

RESEARCHERS	MODEL TYPE*						COMMENTS & APPLICATION
	1	2	3	4	5	6	
Lindbeck, 1985	C	L	LE	2-D	SL	MP	Development of a beam-column model to represent a functional scoliosis
Patwardhan et al., 1986	C	L	LE	2-D	SL	MP	Development of a beam-column model to study curve progression
Meade et al., 1987	C	L	LE	2-D	SL	MP	Analysis of progression of double curves
Veldhuizen and Scholten, 1987	K	NL	-	3-D	---	MP	Analysis of the coupling behaviour of a scoliotic spine
Scholten et al., 1988	D	NL	LE	3-D	SL	MP	Analysis of the stability of the spine
Viviani et al., 1986	FEM	L	LE	2-D	IL	PP	Analysis of optimal correction of scoliosis using internal fixation
Ghista et al., 1988	FEM	L	LE	2-D	IL	PP	Analysis of optimal correction of scoliosis using internal fixation
Jayaraman et al., 1989	D	NL	LE	3-D	IL	MP	Analysis of different internal fixation systems
Stokes and Laible, 1990	FEM	NL	LE	3-D	GL	AP&MP	Thorax model to study asymmetric rib growth
Stokes and Gardner-Morse, 1991	FEM	L	LE	3-D	SL	MP	Analysis of axial rotation component in scoliosis
Stokes and Gardner-Morse, 1993	FEM	L	LE	3-D	IL	AP&MP	Analysis of Harrington distraction for correction of scoliosis
Noone et al., 1991	C	NL	LE	2-D	ML	MP	Development of a beam-column model for paralytic scoliosis

\* The type of model is described using 6 parameters. 1) K-kinematic, D-discrete (rigid bodies, springs, and deformable elements), FEM-finite element model, O-optimization, C-continuum beam-column; 2) L-geometric linear, NL-geometric nonlinear; 3) LE-linear elastic, NLE-nonlinear elastic; 4) 2-D-two dimensional; 3-D-three dimensional; 5) GL-induced growth loads, SL-general 3-D static loads, BL-static brace loads; ML-static muscle loads, IL-instrumentation loads; 6) PP-patient properties, MP-mature or adult properties; AP-adolescent properties.

## 2.3 Formulation of Specific Objectives

As discussed in Chapter 1, the general objective of the present study is to investigate the mechanics of curve progression during the adolescent growth spurt. Furthermore, it was proposed that the development of an appropriate model of a spine with a mild scoliosis provides a tool to efficiently and unambiguously investigate the many variables present during growth. It is clear from the foregoing review that the methods of approach, and choice of specific features incorporated in a model, are strongly guided by the desired application. Consequently, the present model is not intended as a general model of the spine, and cannot analyze many of the problems addressed by the other models. However, by focusing and optimizing the model to the present application, a relatively simple and efficient model is developed.

The choice of the specific features to incorporate in the present model is guided by a number of characteristics of both a progressive scoliosis and the spinal column itself. Firstly, curve progression in scoliosis is defined on a bi-annual or yearly basis. Consequently, the progression of scoliosis is essentially a quasi-static phenomenon. Though a spine is subjected to many dynamic loads during day-to-day activities, there is no evidence that curve progression occurs in this time frame. *Therefore, the development of a model solely for static analysis is appropriate (Item I).*

Secondly, though the trunk muscles can readily generate forces of sufficient magnitude to correct a scoliotic curve, they clearly do not respond adequately to a progressive scoliosis. The exact reason is not obvious. Though the muscles can generate high forces, these cannot be maintained for lengthy periods of time. Therefore, whether a sufficiently high magnitude of muscle force can be maintained over the time frame of curve progression is not clear. Alternatively, it is possible that the musculature is not always capable of responding to a progressive curve due to inappropriately oriented muscles or inadequate sensing by the postural system which must detect the curve. The trunk musculature and postural system have evolved to both maintain upright stability and to activate motion. Consequently, the muscles may simply not have a "built-in" ability to respond to a scoliotic

deformity. Therefore, irrespective of the exact reason, since both nonprogressive and progressive scoliotic curves are not corrected by the trunk muscles, it is difficult to assess their exact influence on scoliosis. Furthermore, though there are many suggestions of a deficit in the postural control system of scoliotics, which could lead to asymmetrical muscular actions, the exact mechanism is not clear at all. *Therefore, the development of a model incorporating only the passive response of the spine is appropriate (Item II).*

Thirdly, idiopathic scoliosis is a three-dimensional deformity of the spine, even in the earliest stages. Curve magnitude is routinely measured using the two-dimensional Cobb angle, which ignores the axial rotation and anterior-posterior deformities of scoliosis. However, the three-dimensional nature of scoliosis has also become clinically relevant in recent years. *Therefore, the model needs to be three-dimensional and capable of analyzing the lateral and anterior-posterior displacements, as well as the axial rotation of the spine (Item III).*

Fourthly, a scoliotic spine with a large deformity would require a geometrically nonlinear analysis due to the large displacements. The axial rotations and lateral displacements of the spine can become very large in the stages of a curve requiring bracing and surgery. However, the present study is interested in the earlier stages of a mild scoliosis, before the deflections become large. *Therefore, the development of a model for small to moderate displacements is appropriate (Item IV).* This issue is further discussed in the chapters on model development.

Fifthly, though the vertebrae of a spine with a large scoliosis are clearly deformed, those from a spine with only a mild scoliosis are only marginally deformed, if at all. Furthermore, these deformities are more likely a secondary effect, rather than a cause of the deformity. *Therefore, the model need not account for any changes to spinal mechanics that could result from deformed vertebrae (Item V).*

The five items outlined in the foregoing have focused the choices for the present model to a large extent on the basis of the characteristics of a *mild scoliosis*. However, there are still a number of aspects which must be considered with respect to the *spinal column* itself. The basic unit of the spinal column, the motion segment, is a complex structure with

varied tissues, properties and geometry. The modelling of the motion segment continues to be an area of active research with further refinements likely needed to accurately model the individual tissues. It is not necessary, however, to model the individual tissues directly, unless one is explicitly interested in their mechanics. The present model need only predict the displacements of the vertebrae to analyze progression. The stiffness characteristics of motion segments have been studied extensively and possibly are the best documented aspect of the spine. This data is ideal for the present model, since the characteristics of all the tissues of the motion segment are contained in the compact form of effective stiffnesses. *Therefore, it is adequate for the model to incorporate the stiffness characteristics of each motion segment at each level of the spine, as opposed to modelling directly the individual tissues (Item VI).*

From anatomical, experimental and modelling studies, it is clear that the ribcage plays an important role in supporting the spine. The spinal column is located between the right and left halves of the ribcage, and joins the two halves together to form the "barrel" structure of the ribcage and establish its strength. Since the spinal column is an integral part of this enclosed form, the relative displacements between the spine and ribcage are strongly restrained. *Therefore, the model needs to include the support of the ribcage (Item VII).* However, even though the ribcage is a complex spatial structure with varied material properties and geometry, its interaction with the spine is very specific. Each rib is joined to a vertebra of the spinal column at two joints. The present model takes advantage of this feature to provide a relatively simple representation of the passive ribcage support. It is understood that the active support of the ribcage through the trunk muscles could be more complex. However, as discussed above, the present model is only concerned directly with the passive response of the spine and ribcage.

The final point to consider for the development of the present model is the objective of analyzing the effect of the adolescent growth spurt on curve progression. The adolescent growth spurt has not been studied extensively in the previous models. A rigorous mechanical analysis of the various components such as spine length, vertebral dimensions, weight, ribcage support, among others, is required to fully discern their role during growth.

Recently, scoliosis models have attempted to "individualize" the models by incorporating either spinal stiffness or geometry directly from the adolescent patient. The drawback of this approach is the large populations required and the difficulty in establishing the variables or measures to compare the mechanics unambiguously between patients. Consequently, another approach is needed to establish which of the variables present during growth are most likely or most capable of affecting progression. The parametrization of the problem provides a means to efficiently analyze the variables present during growth, and to investigate the interdependent effects. *Therefore, the model must be amenable to a general parametric analysis* (Item VIII).

In addition, a model provides the means to simulate directly the effects of the adolescent growth spurt in a spine with a mild scoliosis. During growth, the stiffness properties, spine length and body weights are changing simultaneously. For a scoliotic curve of a given magnitude, at a certain age, a model can simulate the effects of different growth rates and patterns on curve progression tendencies in a simple and unambiguous manner. *Therefore, the model must be suitable for the simulation of different growth rates and patterns* (Item IX).

The two basic approaches to spine models have been the discrete and finite element representation versus the continuum. Both have been successful to varying degrees depending on the given application. The spine would appear to be a naturally discrete system due to the relatively rigid bodies, separated by a number of relatively flexible structures. On the other hand, a continuum model of the spinal column has been shown to provide an accurate analysis of its mechanics in a number of situations, including scoliosis, provided appropriate properties are adopted. Of course, the two models cannot provide entirely the same information. The discrete models, however, can quickly become expensive and data intensive, which can greatly restrict their ability to analyze the effects of a large number of parameters. Alternatively, the continuum models are excellent for a parametric analysis. However, previous models have suffered from the serious restriction of only two-dimensional representation in the coronal plane, with no axial rotation component. Furthermore, the ribcage has only been included in a lumped form or not at all.

For the present model, a hybrid approach is proposed. The scoliotic spinal column is to be modelled as an initially curved and twisted, spatial beam-column embedded in an elastic medium to represent the ribcage. The stiffness of the supporting ribcage is to be determined from numerical experiments using a finite element model. It is argued that once this representation of the ribcage is included into the governing equations of the beam-column, the model is sufficiently accurate and efficient to reach the general objective. Therefore, the present work is divided into four specific objectives:

- i) Development of the governing equations of an initially curved and twisted, spatial beam-column to represent a spinal column with a mild idiopathic scoliosis which incorporate the features outlined in Items I-VI.
- ii) Development of a finite element model of the ribcage and investigation of the stiffness it provides for the spinal column in view of the needs established in Items IV and VII.
- iii) Investigation of the mechanics of a scoliotic spine through a parametric analysis in order to address the needs expressed in Item VIII.
- iv) Investigation of the mechanical effect of growth on curve progression through simulation of the adolescent growth spurt in order to address the needs expressed in Item IX.

As outlined in the foregoing arguments, a number of assumptions have been made in order to develop a model to study curve progression during adolescent growth. Therefore, it must be reemphasized that this model cannot analyze many aspects of spinal biomechanics for which it was not intended. However, by focusing the development of the model to the present application, the goal was to create a model of relative simplicity and efficiency, but which incorporated sufficient features of spinal mechanics needed to investigate AIS.

# Chapter 3

## SPINAL COLUMN MODEL

### 3.1 Introduction

The governing equations of an initially curved and twisted, spatial beam-column, developed to represent a scoliotic spine, are presented in this chapter. An overview of beam-column theory is first presented to orient the reader with the general behaviour, terminology, assumptions and applications. This is followed by the development of the equations with the necessary modifications for application to the study of the mechanics of a scoliotic spine. In the final sections, the loads applied to the spine are described, followed by the geometry and properties of the spinal column. Several validation studies are outlined and the procedures for a parametric study and the simulation of the adolescent growth spurt are described.

### 3.2 Review of Beam-Column Theory and Behaviour

Beam-columns belong to a larger class of slender material bodies which are more generally referred to as rods. A rod is a one-dimensional material continuum in which one dimension is considerably greater than two other representative dimensions. The continuum, however, can undergo spatial displacement in three dimensions. There are many examples of rods, such as cables, wires, struts, bars, shafts, columns, beams, beam-columns.

fluid jets, strings of molecules, etc. A beam-column is in general a structural member that is subjected to axial compression, as well as bending due to lateral loads and moments. For a slender beam-column, the representative cross-sectional dimensions ( $b$  and  $d$ ) should be much less than the length dimension ( $L$ ). In engineering applications, the theory of beam-columns has provided excellent results if  $b/L$  and  $d/L < 0.1$ .

### In-Plane Beam-Column Behaviour

The most prevalent beam-column theory is that of Bernoulli-Euler, which is based on the assumption that cross-sections remain plane and normal to the deflection axis, and undergo no distortions (Fig. 3.1). These assumptions create inconsistencies in that shear forces are included for equilibrium with no resulting deformation. As a result, however, the governing equations can be readily developed by an equilibrium balance on an infinitesimal beam-column element. Consider a beam-column subjected to a distributed lateral load,  $q$ , and a compressive load,  $P$  (Fig. 3.2A). An infinitesimal or differential element for the beam-column is shown in Fig. 3.2B. Considering the lateral displacement,  $u$ , to be small, the forces on the element are summed in the horizontal direction to give

$$P \frac{d^2u}{dz^2} - \frac{dV}{dz} = q \quad (3.1)$$

Moments are then taken, and neglecting second order terms, to give

$$\frac{dM}{dz} = V \quad (3.2)$$

where  $M$  is the bending moment, and  $V$  is the shear force. For small displacements, the lateral displacement of the beam-column is related to the moment as follows:

$$EI \frac{d^2u}{dz^2} = -M \quad (3.3)$$

where  $EI$  is the bending stiffness of the beam-column in the plane of bending. This equation also inherently assumes that the cross-section is symmetric about the axes. Combining equations (3.1), (3.2) and (3.3), the governing differential equation is determined as

$$EI \frac{d^4u}{dz^4} + P \frac{d^2u}{dz^2} = q \quad (3.4)$$

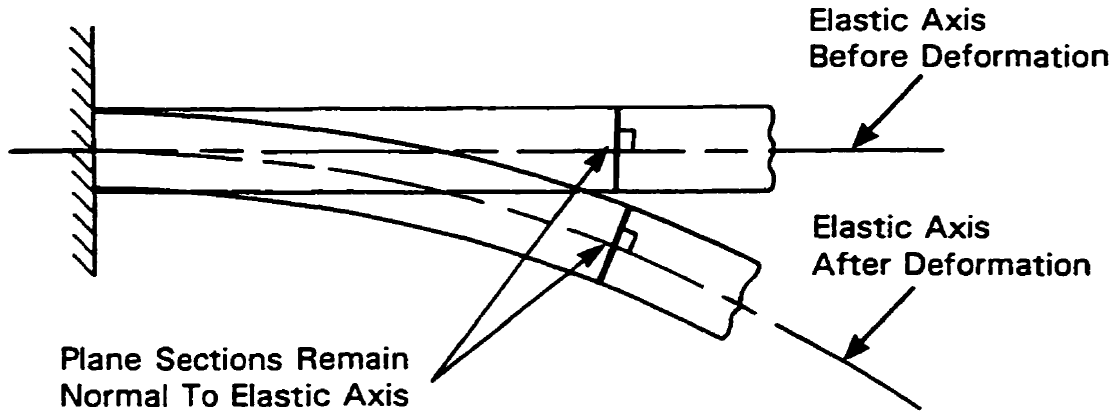


Figure 3.1: Illustration of the Bernoulli-Euler beam-column assumption that plane sections originally normal to the elastic axis remain normal after deformation.

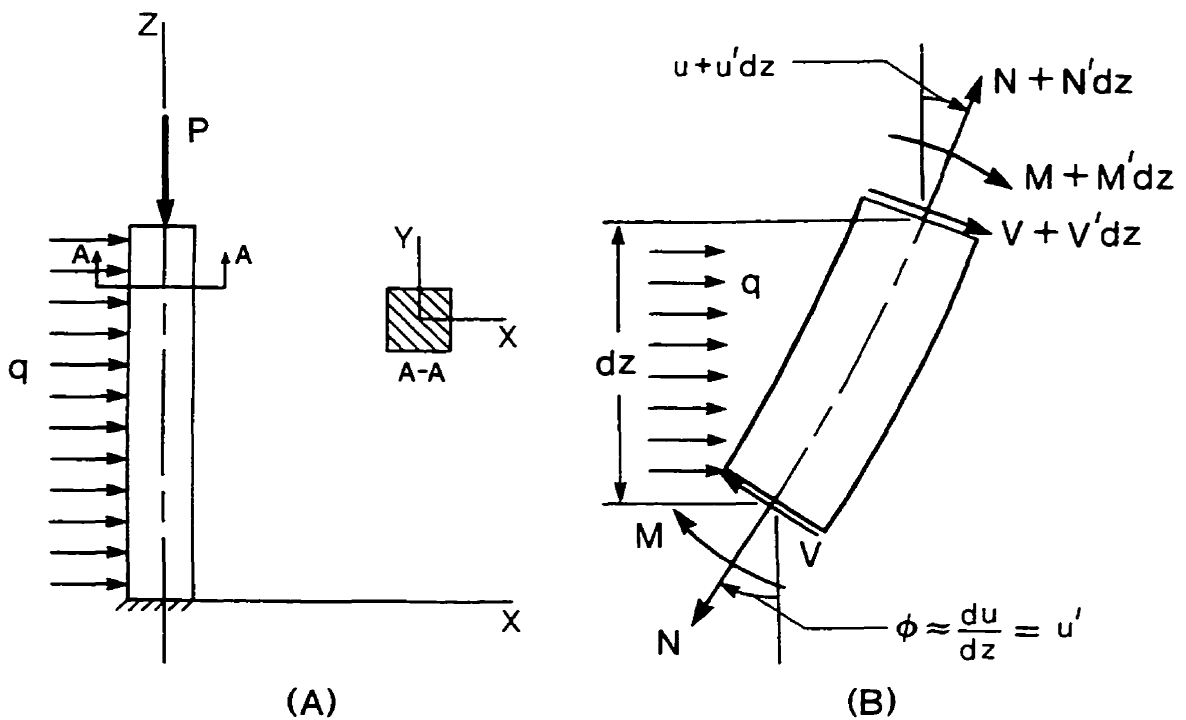


Figure 3.2: A) A beam-column subjected to an axial compression load,  $P$ , and a distributed lateral load,  $q$ . B) Differential element from the beam-column shown in a displaced position for small displacements.  $V$  is the shear force,  $N$  is the normal force, which is equal to  $P$  in the present example, and  $M$  is the bending moment acting on the cross-section.

for a constant  $EI$  along the length. This is the basic 4<sup>th</sup> order differential equation of a beam-column for bending in one plane. The solution of this equation determines the lateral displacement,  $u$ , of the elastic axis as a function of the length,  $z$ . With the associated boundary conditions, a large class of engineering structures are governed by this equation.

If there is no lateral load,  $q$ , then equation (3.4) is simplified to

$$\frac{d^4u}{dz^4} + \frac{P}{EI} \frac{d^2u}{dz^2} = 0 \quad (3.5)$$

This 4<sup>th</sup> order homogeneous equation governs the buckling of columns subjected to compressive end loads, and represents an eigenvalue problem. The solution for the lowest eigenvalue is the classical Euler critical load

$$P_{cr} = C \frac{EI}{L^2} \quad (3.6)$$

where  $C$  is a constant determined by the boundary conditions, and  $L$  is the column length.

The right hand side of equation (3.5) is zero, which established the eigenvalue problem. As a result, the deflections of the column are zero until the critical load,  $P_{cr}$ , is reached, at which point sudden failure occurs, and indeterminate displacements are predicted by this linear elastic theory. In reality, this mathematical situation is never reached due to small lateral loads, compression load eccentricity, or small initial displacements, collectively termed imperfections. The inclusion of these imperfections in equation (3.5) complicates the equation, and the problem is no longer an eigenvalue one. Instead a more general non-homogeneous equation is required to describe the problem. As a result, similar to the solution of the general beam-column equation, the deflection of the elastic axis is determined for all load magnitudes. The effect of imperfections is illustrated graphically in Fig. 3.3. The lateral load, load eccentricity, and the initial displacements can result in significantly large deflections, far below the critical load of the ideal column.

### Out-of-Plane Beam-Column Behaviour

The foregoing description of beam-column behaviour was confined to one plane and was thus termed in-plane behaviour. Out-of-plane behaviour or spatial behaviour can occur

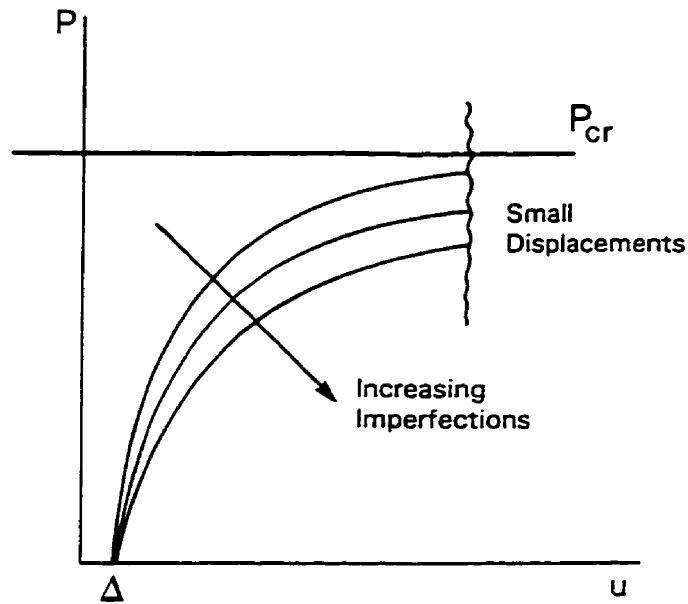


Figure 3.3: Effect of imperfections on the displacement behaviour of a column. An initial displacement,  $\Delta$ , causes immediate deflections, which can become large below the critical load. Other imperfections such as a small lateral load,  $Q$ , or a load eccentricity,  $e$ , causes a further increase in the displacements.

for a number of reasons. The most obvious is due to bending in either plane, or bi-axial bending. For a doubly symmetric beam-column subjected to an axial compression,  $P$ , with end eccentricities,  $e_x$  and  $e_y$ , in two orthogonal planes, then bending in either plane is produced (Fig. 3.4). Depending on the shape of the cross-section, significant twisting or axial rotation also occurs. Consider the situation where the bending stiffness in one plane,  $EI_x$ , is considerably greater than the stiffness in the other,  $EI_y$ . Even for a pure axial compression load, this structure can experience spatial buckling involving lateral displacements and axial rotations. For a lateral load applied in the stiffest plane, spatial buckling can also occur, generally referred to as lateral buckling. On the other hand, for a load applied in the weaker plane only bending would occur, the deflections governed by equation (3.4). To determine the buckling load or the deflection curve for lateral buckling, a new set of equations is needed.

Consider again the beam-column shown in Fig. 3.4. A balance of the forces and moments acting on a differential element is carried out, as before, except that the adjacent

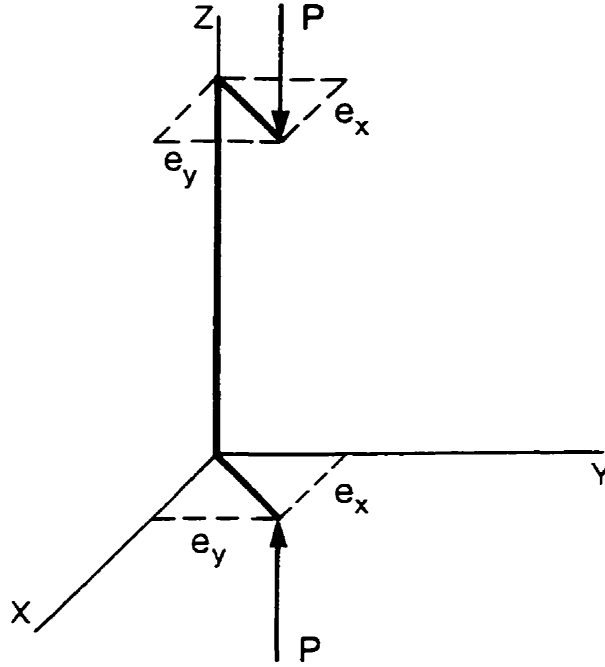


Figure 3.4: Illustration of a beam-column subjected to bi-axial bending due to an eccentric compression load  $P$ . Moments  $M_x$  and  $M_y$  are produced in each plane and the resulting deflection is spatial.

position is now displaced in space. The development is more extensive, but otherwise the method is the same. For small displacements, the following equations are obtained that describe the behaviour of this bi-axially loaded beam-column

$$\begin{aligned}
 EI_y \frac{d^4 u}{dz^4} + P \frac{d^2 u}{dz^2} - P e_y \frac{d^2 \theta}{dz^2} &= 0 \\
 EI_x \frac{d^4 v}{dz^4} + P \frac{d^2 v}{dz^2} + P e_x \frac{d^2 \theta}{dz^2} &= 0 \\
 GJ \frac{d^2 \theta}{dz^2} + P e_y \frac{d^2 u}{dz^2} - P e_x \frac{d^2 v}{dz^2} &= 0 .
 \end{aligned} \tag{3.7}$$

These are three linear homogeneous coupled differential equations. They determine the two lateral displacements,  $u$  and  $v$ , plus the axial rotation,  $\theta$ , of the beam-column, where  $EI_x$ ,  $EI_y$  are the bending stiffnesses in the two principal planes and  $GJ$  is the torsional rigidity, all of which are constant along the length.

If  $e_x$  and  $e_y$  are relatively small, the beam-column remains nearly straight up to the lowest critical load. There are three critical loads, one for each plane plus torsional buckling, the lowest of which governs the behaviour. The larger the values of  $e_x$  and  $e_y$ , the less

important are the critical loads because once again relatively large displacements can occur below the critical load. If either  $e_x$  or  $e_y$  is zero a different type of situation arises as all three equations are no longer coupled. Consider that  $e_x$  is zero and the compression load is only eccentric in the  $yz$  plane. The out-of-plane displacement,  $u$ , and axial rotation,  $\theta$ , are still determined by two coupled equations (1<sup>st</sup> and 3<sup>rd</sup> of 3.7). The in-plane displacement,  $v$ , is now independent and governed by the 2<sup>nd</sup> equation of (3.7). If again  $EI_x$  is greater than  $EI_y$ , then lateral-torsional buckling can occur governed by the two coupled equations.

So far, only symmetric cross-sections have been considered. For asymmetric sections, the equations are further complicated by what is termed the shear centre. At some point,  $S$ , of a cross-section, the resultant shear force,  $V$ , causes no axial rotation. For symmetric sections, the shear centre,  $S$ , is located at the geometric centre which locates the axes on the cross-section. For asymmetric sections, it is located at some other point, located at  $\langle \xi_0, \eta_0 \rangle$ , which can be determined. Therefore, for asymmetric sections, equations (3.7) are altered by incorporating the coordinates  $\xi_0$  and  $\eta_0$  with the load eccentricity terms  $e_x$  and  $e_y$ . The equations now describe the displacement of the shear centre instead of the geometric centre. The shear centre further couples the equations together. In general, thin-walled open cross-sections are most strongly affected by a shear centre, but any asymmetric solid section also contains a shear centre.

Imperfections of the spatial beam-column have the same effect as for the in-plane beam-column. Once again, the deflections can become substantial far below a critical load. As such, the general load-deflection behaviour of the beam-column can be of much greater importance than the critical load. To determine the spatial deflections of the beam-column, terms are added to equations (3.7) so that they are no longer homogeneous.

The behaviour of beam-columns has been studied in great depth by a number of researchers. In particular, the textbooks by Love (1920), Timoshenko and Gere (1961), Chen and Atsuta (1977) and Wempner (1981) all provide excellent analyses of the mechanics of beam-columns. Further complexities, not reviewed in the foregoing, such as more general loading, complex boundary conditions, distributed properties and nonlinearity, are discussed in these books.

## Directed Rods

As mentioned earlier, beam-columns belong to a larger class of bodies called rods, for which a much more general theory has been developed directly from a mathematical base in the field of continuum mechanics. By invoking the assumption that plane sections remain plane after displacement, the classical Bernoulli-Euler theory discussed in the foregoing has been developed to govern the behaviour of beam-columns. However, it is instructive to understand how this assumption relates to a more general theory.

A one-dimensional continuum can be described by a Cosserat or directed curve in space. A Cosserat curve is a material curve embedded in three-dimensional space, with two deformable vector fields (termed directors) attached to every point of the curve. A reference axis of the spatial rod is located in space, with respect to a Cartesian system, by a parametric representation  $\hat{r}(s)$ , where  $s$  is the curvilinear coordinate along the axis (Fig. 3.5). At each point on the axis defined by  $\hat{r}$ , there are a pair of directors  $\hat{d}_2$  and  $\hat{d}_3$ . Also shown in the figure is the Frenet triad formed by the unit tangent vector,  $\hat{t}$ , the unit principal normal,  $\hat{n}$ , and the unit binormal,  $\hat{b}$ , at each point on the axis. The plane defined by  $\hat{n}$  and  $\hat{b}$  represents the normal cross-section of the rod. In general, directors do not lie in the normal cross-section, and the projection of  $\hat{d}_2$  and  $\hat{d}_3$  on the cross-sectional plane can also be determined. The deformation of a rod, therefore, can be described by the tangent vector which models the axis, and the two directors which model the cross-section.

The modern foundations of directed curves was established by Ericksen and Truesdell (1958). This work served as a basis for the development of nonlinear theories of rods, as well as shells. Green and Laws (1966) developed a general theory of rods using two directors, whereas Cohen (1966) used three directors. The nonlinear theory of Cohen (1966) can account for axial extension of the rod axis, bending, transverse shear and deformation of the cross-section. These theories are developed with a broad generality and are applicable to all rods, as well as beam-columns. More recent papers have presented constrained theories of rods, where an internal constraint is imposed by a restriction of the possible class of motions. Naghdi and Rubin (1984) examined seven different constraints which can

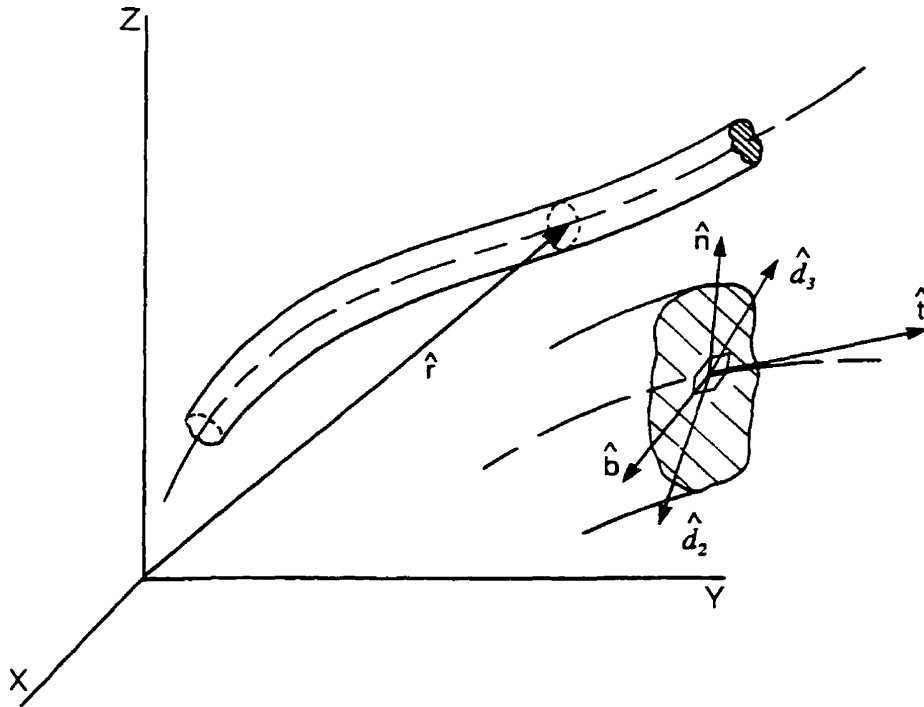


Figure 3.5: The axis of a spatial rod is specified by the position vector,  $\hat{r}$ , in a Cartesian system. At each point along a curve, a Frenet triad formed by the unit tangent vector,  $\hat{t}$ , the unit principal normal,  $\hat{n}$ , and the unit binormal,  $\hat{b}$ , can be defined. Two directors,  $d_2$  and  $d_3$ , are also shown, which need not lie in the plane defined by  $\hat{n}$  and  $\hat{b}$ .

be imposed on a nonlinear theory of rods, which was developed using a Cosserat curve and two directors. A nonlinear version of the Bernoulli-Euler beam theory was presented where the cross-sectional deformations and axial extension were excluded. This theory was very similar to an earlier work by Green and Laws (1973), which also developed a nonlinear Bernoulli-Euler beam using a different approach. Cohen and Sun (1992) considered six different constraints imposed on a general rod theory based on three directors. A nonlinear Bernoulli-Euler theory was developed by applying four of the constraints.

The strength of the director theories of rods lies in their generality and their development from basic principals, with no apriori assumptions. This generality also contributes to their weakness, with the associated complexity of the governing equations. The constrained theories of rods represent a compromise which simplifies the equations, thereby increasing the applicability of the theory.

### 3.3 Spatial Beam-Column Model of a Mild Scoliosis

Though many aspects of a scoliotic spine with regard to the kinematics, loads and boundary conditions have been included to various degrees in existing formulations of beam-column equations, the exact combination of features required to model a scoliotic spine has not been considered previously. Therefore, in this section, the assumptions and features of the scoliotic spine model are first detailed, followed by a derivation of the governing beam-column equations in a general form. Subsequently, they are applied specifically to the scoliotic spine.

To develop the equations, a variety of sources were consulted. In particular, the textbooks by Love (1920), Novozhilov (1953), Timoshenko and Gere (1961), Bolotin (1963), Washizu (1968), Chen and Atsuta (1977) and Wempner (1981) provided the overview of the general theory of spatial beam-columns. In general, however, the applications discussed in these books involved simplifications not appropriate to the modelling of the spine. A number of papers and reports provided more complex forms of the equations which were consulted in the development: Houbolt and Brooks (1958), Soltis and Christiano (1972), Hodges and Dowell (1975), Rosen and Friedmann (1978, 1979), Hodges and Ormiston (1980), Reissner (1983), Hodges (1985), Rosen and Rand (1986), Hodges (1987), Bauchau and Hong (1987, 1988), Tabarrok and Xiong (1989) and Koenig and Bolle (1993). Many of these studies were concerned with the spatial behaviour of initially curved and twisted beam-columns, with variable properties along the length, for the study of helicopter blades. This complexity of behaviour closely resembles the spinal column and served as a base to develop the equations. The properties, load conditions and initial shape are of course very different in the spine. The beam-columns considered in these studies were also either initially twisted or initially curved only in one plane, which remained constant along the length. The derivations began in a general form but were then restricted in the applications.

### 3.3.1 Assumptions and Features of the Present Model

As discussed in Chapter 1, beam-column theory can model a scoliotic spine provided that sufficient complexity is incorporated into the governing equations. The first consideration is whether a spine is slender enough to be considered as a beam-column. The cross-sectional dimensions of a vertebra generally decrease from the lumbar to the cervical region. The dimensions of a mid-thoracic vertebra are, therefore, representative of the column. The width,  $b$ , in the coronal plane of the vertebral body at  $T9$  is about 3.25 cm and the depth,  $d$ , in the mid-sagittal plane is about 2.74 cm (White and Panjabi, 1990). The length,  $L$ , of an adult spine might be anywhere from 43-55 cm on average. The slenderness ratios  $b/L$  and  $d/L$  are therefore less than the 0.1 value usually considered necessary for beam-column theory to apply (Chen and Atsuta, 1977). The theory approaches its limit in the coronal plane at the lumbar level, whereas in the upper thoracic region, the ratio is further reduced below the value at  $T9$ . The other concern is that in the mid-sagittal plane, the posterior elements increase the representative  $d$  value. However, the value of  $d$  for the vertebra can be nearly doubled to include the posterior elements (which is about their size) and still the theory would apply. Since most of the bending is resisted by the disc, the full dimensions of the posterior elements should not be required to establish a representative  $d$  value. For an adolescent spine, the ratios for  $b/L$  and  $d/L$  are also below 0.1 and beam-column theory should also be applicable.

The anterior portion of the spinal column comprised of the vertebral bodies, the disc and the anterior and posterior longitudinal ligaments is to be modelled as a spatial Bernoulli-Euler beam-column. Therefore, the spine is considered as a continuum where plane sections normal to the elastic axis before deformation remain plane and normal after deformation. The greatest concern with this assumption is that it implies that the deformation occurs at every point along the axis of the spine. In reality, the vertebrae are much more rigid compared to the disc and most deformation occurs in the disc. Therefore, a plane that is forced to be normal to the axis in the model is not likely to represent all planes along the actual spine (Fig. 3.6). Due to the alternating sequence of vertebra-disc-vertebra, it is reasonable to assume that plane sections would remain normal to the axis at one location,

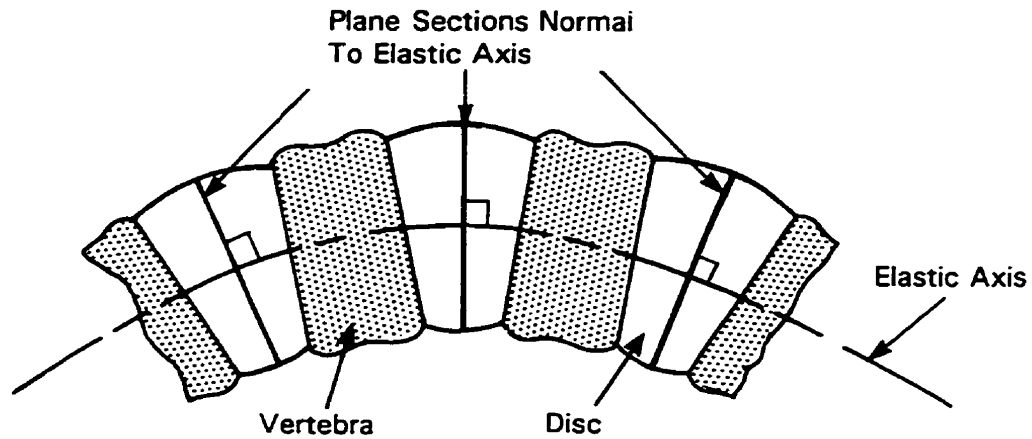


Figure 3.6: Illustration that the cross-sectional plane of the spine at all positions along the axis cannot remain normal to the elastic axis. Within each motion segment, however, at least one plane should remain normal after deformation.

at least, in each motion segment. Consequently, though there would be discrepancies between these locations, the errors should not accumulate along the spine length. The relative success of beam-column theory in describing the shape of a spine (as described in the literature review) indicates that this discrepancy cannot be overly significant in a global sense. The deflection of the elastic axis is still able to represent the motion of the vertebral centres.

The posterior elements, including the facet joints and the ligaments, are to be modelled partially by their effect on the shear centre of the beam-column. The cross-sectional shape of the vertebral bodies and discs are nearly elliptical, and as such, the shear centre should be located near the geometric centre. The centre of rotation (analogous to shear centre) of a motion segment is somewhat posterior to the disc centre, particularly in the lumbar spine (White and Panjabi, 1990). This is partly due to the facet joints which, in the lumbar region, resist axial rotation and force the centre of rotation posteriorly towards the locked facet joint (Shirazi-Adl et al, 1986a). The ligaments attached to the posterior elements also contribute to the position of the shear centre. Therefore, the definition of a shear centre that is not a function of motion is a limitation. On the other hand, it is argued that the shear centre can model first order effects of the posterior elements. i.e.,

the coupling between lateral bending and axial rotation, and a centre of rotation posterior to the disc centre. Furthermore, the overall effects of the posterior elements are also to be included by incorporating the bending stiffnesses and torsional rigidity for the motion segments at each spine level (White and Panjabi, 1990). Therefore, the different responses between flexion/extension could be included, as well as the stiffening behaviour provided by the facet joints through nonlinear or bilinear properties that vary over the spine length. However, though the properties vary over the length, the changes between adjacent motion segments are considered to be small and gradual enough that the rate of change of the stiffnesses is negligible.

The other assumptions implied by the Bernoulli-Euler theory are that the cross-section is not distorted and the axis is not extended. Again, it is argued that these are reasonable assumptions at present. The spine is most flexible in bending and axial rotation. The height of a person does change from going to a standing position from a supine one. However, the change is fairly small and divided by changes in the sagittal configuration, as well as the actual length of the spine as the discs are compressed. This present work is concerned with changes to the spine that occur over the period of a year, during which the small changes in length due to increased vertical loads are not likely to alter the mechanics.

A scoliotic spine with a large deformity would require a geometrically nonlinear analysis. The axial rotations and lateral displacements of the spine can become very large in the stages of a progressive curve requiring bracing and surgery. However, the present study is focused on the earliest stages of a mild scoliosis before the deflections become large. Furthermore, in a mild scoliosis there are minimal changes to the vertebrae, as the deformations are confined to the disc and remain small. Therefore, the present model is developed for small strains and moderate rotations.

The assumption of moderate rotations means that 2<sup>nd</sup> order terms are neglected compared to unity, but are retained compared to 1<sup>st</sup> order terms. Therefore, the most significant of the nonlinear terms are retained in the governing equations. In particular, the nonlinear terms that involve the interactions between the displacements in mutually orthogonal planes and the axial rotation of the beam-column are retained. These terms

could be of importance in modelling the three-dimensional deformity of a scoliotic spine, in which there is a correlation between the lateral displacements and the axial rotation. In a linear theory, these coupling terms do not emerge in the derivation. If an error of 10% in the predicted displacements is considered acceptable, then it can be shown that a change in Cobb angle up to  $18^\circ$  can be adequately predicted by moderate rotation theory. Furthermore, a change in axial rotation up to  $18^\circ$  can also be predicted. Beyond these values, errors greater than 10% can be expected in the predicted displacements. A mild scoliosis is usually considered to be in the range of  $10\text{-}30^\circ$  Cobb angle. Therefore, moderate rotation theory would appear to be ideal to model the spine with a mild scoliosis. Through the inclusion of the most significant nonlinear terms, the moderate theory extends substantially beyond a linear theory, yet remains significantly more efficient than a fully nonlinear theory. A fuller discussion of the potential errors is presented in Appendix E.

The natural curves of the spinal column, and the curves due to a mild scoliosis are to be included in the model as initial curvatures and twist. The sagittal profile of the spine is represented by an initial curvature in one plane, whereas a scoliotic spine involves initial curvatures in both planes, as well as an initial axial twist.

In a normal spine, the head and top of the spine are aligned centrally over the pelvis. In a scoliotic spine, the postural control system attempts to maintain this normal alignment in the presence of a lateral deviation of the spine. Consequently, the top of the spine usually remains close to its normal anatomic position, particularly for a mild scoliosis. There can be a lateral offset, however, on the order of a few centimeters. To simulate this overall balance, the displacements of the top of the spine are either specified or considered zero. Both pinned and fixed conditions can be considered for the rotations at the top. The bottom of the spine is considered to be fixed, as a cantilever, to the pelvis. These boundary conditions are not intended to represent the everyday activities of the spine, but rather the long term situation during the progression of the deformity. Over the long term, the top of the spine remains close to its anatomic position (Peterson et al, 1995).

To summarize, the anterior part of the spinal column is modelled as an initially curved and twisted, spatial Bernoulli-Euler beam-column undergoing moderate rotations and

small strains. The axial displacements, however, are considered negligible. The effect of the posterior elements on spinal kinematics is partially modelled by a shear centre. In addition, nonlinear and distributed properties along the spine are also included to further model the actions of the posterior elements.

### 3.3.2 Development of the Governing Differential Equations

The governing equations of the initially curved and twisted spatial beam-column model are presented in this section. The development proceeds from a general description of the geometry and kinematics before and after deformation, followed by the derivation of the generalized stress-strain relations, the equilibrium equations and finally, the boundary conditions. Since an existing formulation of the equations was not available in the literature, the present development proceeds from certain basic fundamentals which are presented for completeness.

#### Geometry Before Deformation

A fixed Cartesian coordinate system is defined by the triad of unit vectors  $\hat{i}_j$ .<sup>1</sup> Consider a spatial curve defined in parametric form by the position vector,  $\hat{r}_0(s)$ , as a function of arc length  $s$ . At each point along the curve, an orthogonal triad of unit vectors  $\hat{t}$ ,  $\hat{n}$  and  $\hat{b}$  is defined. The unit tangent vector to the curve is  $\hat{t}$ , while  $\hat{n}$  is termed the unit principal normal and  $\hat{b}$  the unit binormal. The unit tangent vector is given by

$$\hat{r}_{0,s} = \frac{d\hat{r}_0}{ds} = \hat{t} . \quad (3.8)$$

The unit normal and binormal are given by the Serret-Frenet equations (Struik, 1961; Thomas and Finney, 1980)

$$\begin{Bmatrix} \hat{t}_s \\ \hat{n}_s \\ \hat{b}_s \end{Bmatrix} = \begin{bmatrix} 0 & \mathcal{K} & 0 \\ -\mathcal{K} & 0 & \tau \\ 0 & -\tau & 0 \end{bmatrix} \begin{Bmatrix} \hat{t} \\ \hat{n} \\ \hat{b} \end{Bmatrix} \quad (3.9)$$

---

<sup>1</sup>Throughout, a subscript  $i$  or  $j$  is assigned values of 1,2 or 3.

where  $\mathcal{K}$  is the curvature and  $\tau$  is the geometric torsion. The triad  $\hat{t}$ ,  $\hat{n}$  and  $\hat{b}$  is generally referred to as the natural system of a space curve, which is fully described by the vector  $\hat{r}_0(s)$ , and equations (3.8) and (3.9).

Consider a second triad of orthogonal unit vectors,  $\hat{e}_i$ , defined at every point along the curve. The unit vector,  $\hat{e}_1$ , is also tangent to the curve and identical to  $\hat{t}$ , whereas  $\hat{e}_2$  and  $\hat{e}_3$  lie in the plane defined by  $\hat{n}$  and  $\hat{b}$ , but are rotated about  $\hat{e}_1$  or  $\hat{t}$  by an angle  $\alpha$ . The unit vectors,  $\hat{e}_i$ , are thus given by

$$\begin{Bmatrix} \hat{e}_1 \\ \hat{e}_2 \\ \hat{e}_3 \end{Bmatrix} = \begin{bmatrix} 1 & 0 & 0 \\ 0 & \cos \alpha & \sin \alpha \\ 0 & -\sin \alpha & \cos \alpha \end{bmatrix} \begin{Bmatrix} \hat{t} \\ \hat{n} \\ \hat{b} \end{Bmatrix}. \quad (3.10)$$

An alternate form of the Serret-Frenet equations is obtained (Love, 1920; Connor, 1976) by differentiating equation (3.10) and employing equation (3.9) to give

$$\begin{Bmatrix} \hat{e}_{1,1} \\ \hat{e}_{2,1} \\ \hat{e}_{3,1} \end{Bmatrix} = \begin{Bmatrix} \hat{e}_{1,s} \\ \hat{e}_{2,s} \\ \hat{e}_{3,s} \end{Bmatrix} = \begin{bmatrix} 0 & k_\eta & -k_\xi \\ -k_\eta & 0 & k_\zeta \\ k_\xi & -k_\zeta & 0 \end{bmatrix} \begin{Bmatrix} \hat{e}_1 \\ \hat{e}_2 \\ \hat{e}_3 \end{Bmatrix}. \quad (3.11)$$

The terms  $k_\xi$ ,  $k_\eta$  are curvatures, while  $k_\zeta$  is the twist of the curve, and are functions of  $\mathcal{K}$ ,  $\tau$  and  $\alpha$ . The terms  $k_\xi$ ,  $k_\eta$  and  $k_\zeta$  can be viewed as the projections of  $\mathcal{K}$  and  $\tau$ , defined in the  $\hat{t}$ ,  $\hat{n}$ ,  $\hat{b}$  system, onto the  $\hat{e}_i$  system. A general curvature vector can thus be defined as

$$\hat{k} = k_\zeta \hat{e}_1 + k_\xi \hat{e}_2 + k_\eta \hat{e}_3. \quad (3.12)$$

Since  $\hat{e}_i$  is an orthogonal system, then

$$(\hat{e}_i \cdot \hat{e}_j) = \delta_i^j \quad (3.13)$$

where  $\delta_i^j$  is the Kronecker delta symbol in three-dimensional space, and is defined by  $\delta_i^j = 1$  if  $i = j$  or 0 if  $i \neq j$ . Using equations (3.11) and (3.13), the curvatures and twist can also be expressed by

$$k_\xi = \hat{e}_1 \cdot \hat{e}_{3,1} = -\hat{e}_3 \cdot \hat{e}_{1,1}$$

$$k_\eta = \hat{e}_2 \cdot \hat{e}_{1,1} = -\hat{e}_1 \cdot \hat{e}_{2,1} \quad (3.14)$$

$$k_\zeta = \hat{e}_3 \cdot \hat{e}_{2,1} = -\hat{e}_2 \cdot \hat{e}_{3,1} .$$

Now consider that an axis of a beam-column is represented by the space curve  $\hat{r}_0(s)$ . The cross-section of the beam-column normal to the tangent,  $\hat{e}_1$ , is defined by the vectors  $\hat{e}_2$  and  $\hat{e}_3$  (Fig. 3.7). The position of any arbitrary point  $B$  on the cross-section is given by

$$\hat{r}(s, \xi, \eta) = \hat{r}_0(s) + \xi \hat{e}_2 + \eta \hat{e}_3 \quad (3.15)$$

where  $\xi, \eta$  are coordinates in the cross-section at position  $s$  along the axis. The curvature relations expressed in equations (3.11) or (3.14) describe the axis of the beam-column.

The basis vectors,  $\hat{g}_i$ , of this curvilinear coordinate system are given by

$$\hat{g}_i = \hat{r}_{,i} . \quad (3.16)$$

Inserting equation (3.15) into (3.16), and using (3.8) and (3.11) gives

$$\begin{Bmatrix} \hat{g}_1 \\ \hat{g}_2 \\ \hat{g}_3 \end{Bmatrix} = \begin{bmatrix} \sqrt{g} & -\eta k_\zeta & \xi k_\zeta \\ 0 & 1 & 0 \\ 0 & 0 & 1 \end{bmatrix} \begin{Bmatrix} \hat{e}_1 \\ \hat{e}_2 \\ \hat{e}_3 \end{Bmatrix} \quad (3.17)$$

where

$$g = (1 - \xi k_\eta + \eta k_\xi)^2 . \quad (3.18)$$

If  $\hat{k}$  was zero, then the undeformed configuration of the beam-column would be straight and untwisted. The basis vectors,  $\hat{g}_i$ , would then simply be identical to the  $\hat{e}_i$  system, which in turn would be aligned with the fixed  $\hat{i}_j$  system. However, because of the initial curvatures,  $\hat{k}$ , the  $\hat{e}_i$  and  $\hat{i}_j$  systems are not aligned. The axis of the undeformed beam-column is sufficiently described by equations (3.8) and (3.11), which are based on the parametric position vector,  $\hat{r}_0(s)$ , and the curvatures  $\hat{k}$ . The position of the undeformed beam-column in the fixed  $\hat{i}_j$  system can also be expressed in terms of an initial displacement vector,  $\hat{d}_0$ , and a rotation matrix,  $C_{ij}^0$ , as follows:

$$\hat{d}_0 = w_0 \hat{i}_1 + u_0 \hat{i}_2 + v_0 \hat{i}_3 \quad (3.19)$$

$$\hat{e}_i = C_{ij}^0 \hat{i}_j \quad (3.20)$$

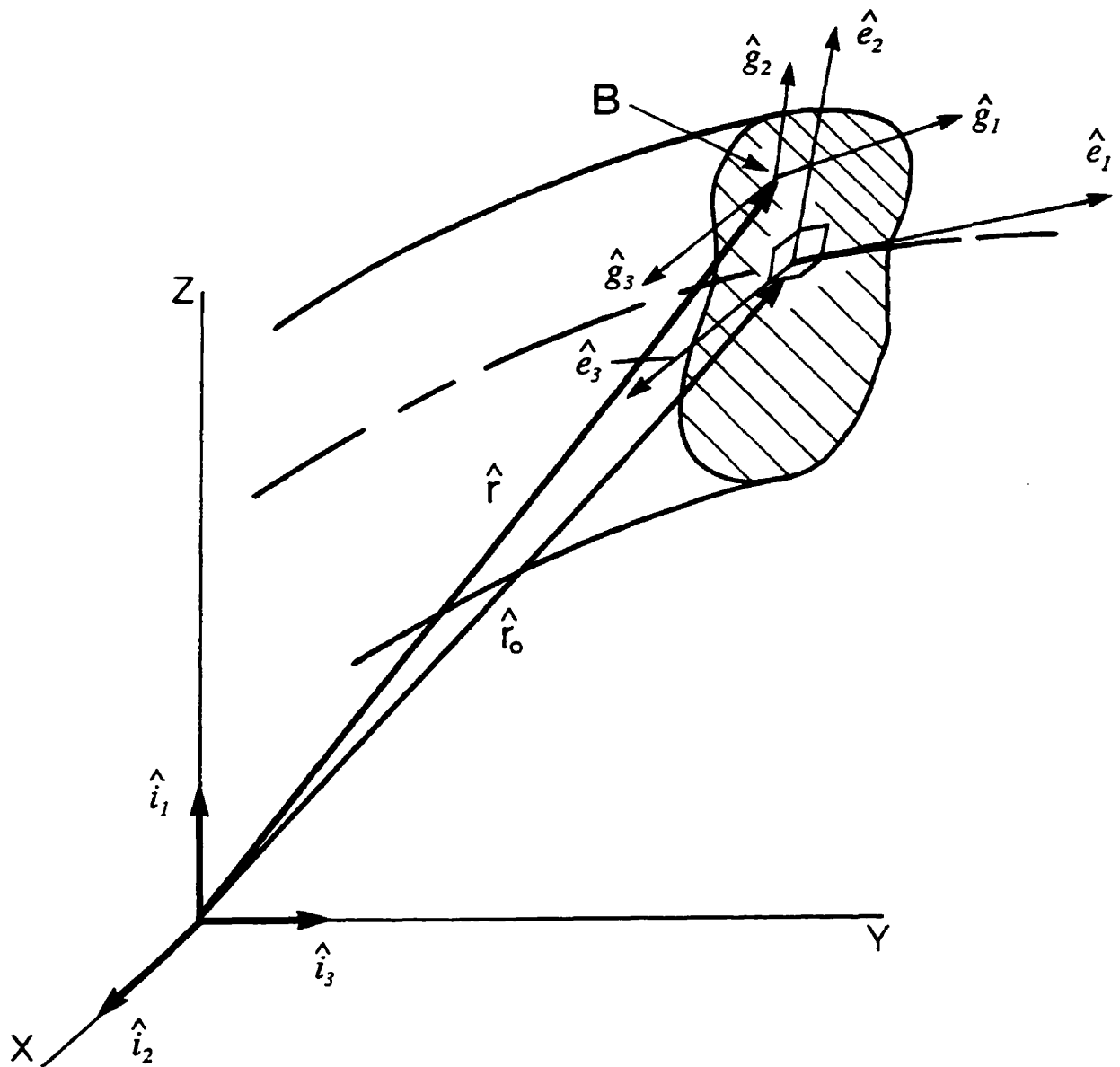


Figure 3.7: The axis of the initially curved and twisted beam-column is specified in the fixed system,  $\hat{i}_j$ , by the position vector  $\hat{r}_0$ . A point B in the plane of the cross-section is specified by the position vector  $\hat{r}$ . Also shown is the local system,  $\hat{e}_i$ , where  $\hat{e}_1$  is the unit tangent vector and  $\hat{e}_2, \hat{e}_3$  define the plane of the cross-section. At point B, the basis vectors,  $\hat{g}_i$ , are shown.

where  $w_0$ ,  $u_0$  and  $v_0$  are the displacements of every point along the beam-column axis in the directions  $\hat{i}_1$ ,  $\hat{i}_2$  and  $\hat{i}_3$  of the fixed system, respectively. The components of the rotation matrix  $C_{ij}^0$  are the direction cosines of the triad,  $\hat{e}_i$ , relative to the fixed  $\hat{i}_j$  system, and serve to describe the rotated position of the cross-section defined by  $\hat{e}_i$  in space.

### Geometry After Deformation

Under the action of loads, the beam-column is deformed from its initial position in space to a subsequent position described by the displacement of the axis. During the deformation, the cross-section is rotated to a new position in space. At every point along the deformed axis, an orthogonal triad of unit vectors,  $\hat{e}_i^*$ , is defined, where  $\hat{e}_1^*$  is the unit vector tangent to the deformed axis, and  $\hat{e}_2^*$ ,  $\hat{e}_3^*$  define the cross-section of the deformed beam-column. The triad,  $\hat{e}_i$ , of the undeformed beam-column is, therefore, displaced by a vector,  $\hat{D}_0$ , and rotated by  $C_{ij}^*$  to  $\hat{e}_i^*$ . The position vector of the deformed axis becomes

$$\hat{R}_0 = \hat{r}_0 + \hat{D}_0 \quad (3.21)$$

where

$$\hat{D}_0 = w\hat{e}_1 + u\hat{e}_2 + v\hat{e}_3 \quad (3.22)$$

and thus,

$$\hat{R}_0 = \hat{r}_0 + w\hat{e}_1 + u\hat{e}_2 + v\hat{e}_3 \quad (3.23)$$

The components  $w$ ,  $u$  and  $v$  of the displacement vector,  $\hat{D}_0$ , are in the directions  $\hat{e}_1$ ,  $\hat{e}_2$  and  $\hat{e}_3$ , respectively, of the undeformed configuration (Fig. 3.8). They could equally have been defined with respect to the triad  $\hat{e}_i^*$  of the deformed beam-column.

The rotation of the triad  $\hat{e}_i$  to  $\hat{e}_i^*$  is described by

$$\hat{e}_i^* = C_{ij}^* \hat{e}_j \quad (3.24)$$

If the rotation is large, it cannot be described by a vector and must be treated by other means such as Euler angles. Consider the following sequence of Euler type rotations,  $\theta_3$  about  $\hat{e}_3$ , followed by  $\theta_2$  about the rotated  $\hat{e}_2$ , and finally,  $\theta_1$  about the rotated  $\hat{e}_1$ . For

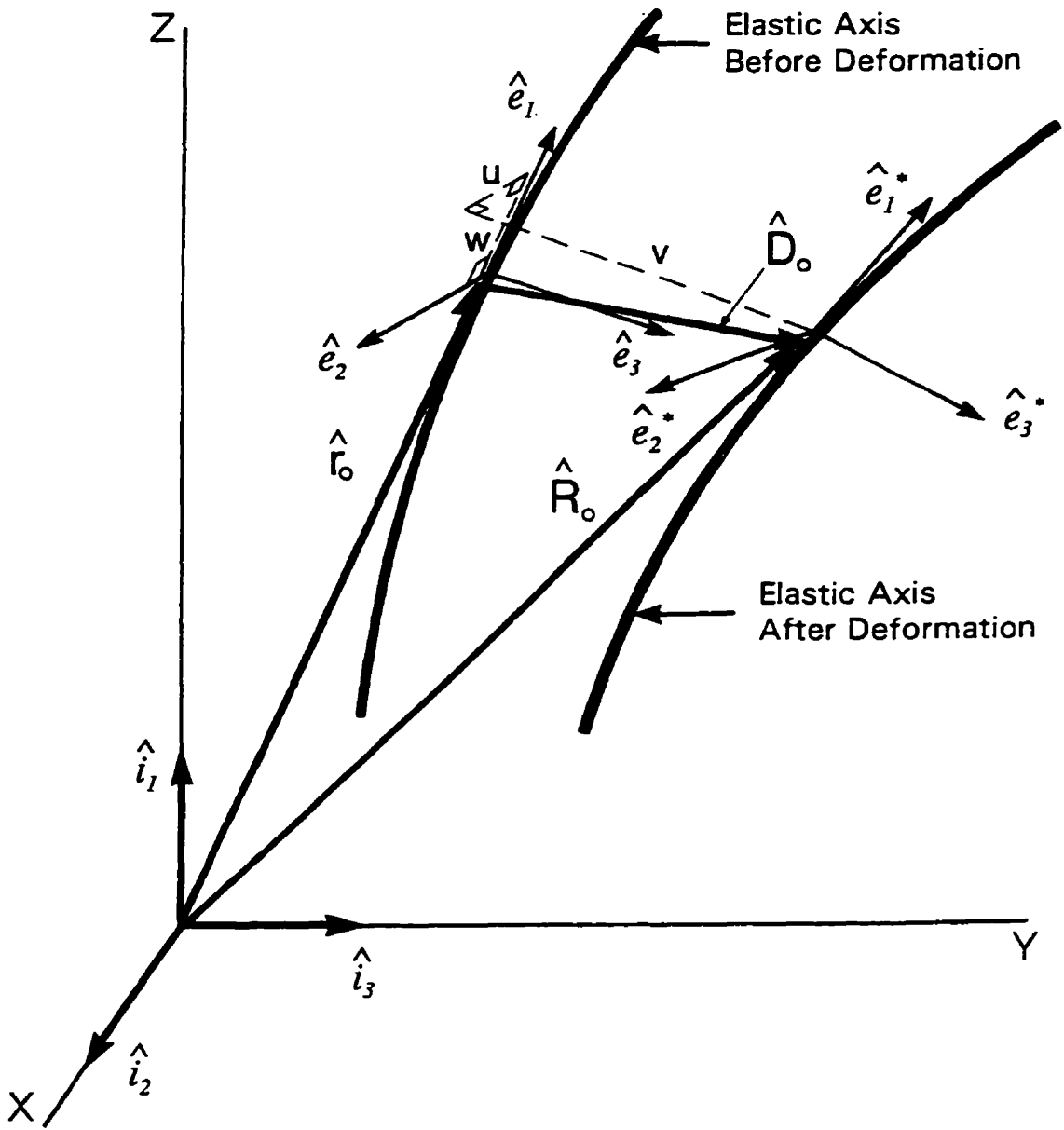


Figure 3.8: The elastic axis of the beam-column before and after deformation. The displacement,  $\hat{D}_0$ , of the beam-column is given by the components  $w$ ,  $u$  and  $v$ , expressed in the  $\hat{e}_i$  system, respectively. Also shown is the  $\hat{e}_i^*$  system of the deformed beam-column, where  $\hat{e}_1^*$  is the unit tangent vector of the deformed axis, and  $\hat{e}_2^*$  and  $\hat{e}_3^*$  define the plane of the cross-section of the deformed beam-column.

this sequence, the rotation matrix,  $C_{ij}^*$ , determined from the product of three matrices, becomes

$$C_{ij}^* = \begin{bmatrix} C_2 C_3 & C_2 S_3 & -S_2 \\ S_1 S_2 C_3 - C_1 S_3 & C_1 C_3 + S_1 S_2 S_3 & S_1 C_2 \\ C_1 S_2 C_3 + S_1 S_3 & -S_1 C_3 + C_1 S_2 S_3 & C_1 C_2 \end{bmatrix} \quad (3.25)$$

where  $C_i = \cos \theta_i$  and  $S_i = \sin \theta_i$ .

The rotations,  $\theta_i$ , are now related to the displacements,  $w$ ,  $u$  and  $v$ , by examining the deformation of a differential element,  $ds$ , of the beam-column (Peters and Ormiston, 1973; Hodges and Dowell, 1975; Chen and Atsuta, 1977; Rosen and Friedmann, 1979; Rosen and Rand, 1986). First, consider the unit tangent vector to the deformed axis given by

$$\hat{e}_1^* = \frac{\hat{R}_{0,1}}{D} = [(1 + d_1) \hat{e}_1 + d_2 \hat{e}_2 + d_3 \hat{e}_3] / D \quad (3.26)$$

where

$$\begin{aligned} d_1 &= w_{,1} - uk_\eta + vk_\xi \\ d_2 &= u_{,1} + wk_\eta - vk_\zeta \\ d_3 &= v_{,1} - wk_\xi + uk_\zeta \end{aligned} \quad (3.27)$$

and

$$D = |\hat{R}_{0,1}| = [(1 + d_1)^2 + d_2^2 + d_3^2]^{1/2} \quad (3.28)$$

The motion and deformation of the element can be described first as a rigid translation  $w$ ,  $u$  and  $v$ , plus a rigid rotation  $\theta_3$ ,  $\theta_2$  and  $\theta_1$ , of the  $\hat{e}_i$  to the  $\hat{e}_i^*$  system. Subsequently, the element is deformed by changing the dimensions and angles of the unit vectors,  $\hat{e}_i^*$ , to a system,  $\hat{G}_i$ , which are the basis vectors of the deformed beam-column. Consider the element  $ds$  on the axis of the beam-column shown in Fig. 3.9. The element is carried to point  $B_0$  by the displacements  $w$ ,  $u$ ,  $v$  not shown in the figure. The element is then stretched by  $d_1 ds$  in the  $\hat{e}_1$  direction and  $d_2 ds$  in the  $\hat{e}_2$  direction to deform from 1  $\rightarrow$  2, as indicated by the unit tangent vector of equation (3.26). In the process, the element is

defined to rotate through the angle  $\theta_3$  about  $\hat{e}_3$ . Subsequently, it is further stretched by  $d_3 ds$  in the  $\hat{e}_3$  direction and defined to rotate  $-\theta_2$  about  $\hat{e}_2$  to deform from 2  $\rightarrow$  3. Finally, the element is defined to rotate  $\theta_1$  about the  $B_0-3$  axis, which now represents the unit tangent vector,  $\hat{e}_1^*$ , of the deformed beam-column. This transformation from the undeformed to the deformed configuration is apparent from equation (3.26) which determines the direction of  $\hat{e}_1^*$ . Examining Fig. 3.9, the following relations can be determined

$$\sin \theta_3 = \frac{d_2}{D_1} \quad ; \quad \cos \theta_3 = \frac{(1+d_1)}{D_1} \quad (3.29)$$

$$\sin \theta_2 = -\frac{d_3}{D} \quad ; \quad \cos \theta_2 = \frac{D_1}{D} \quad (3.30)$$

where

$$D_1 = [D^2 - d_3^2]^{1/2} . \quad (3.31)$$

Also the angle  $\theta_1$  is replaced by  $\theta$ , which represents the axial rotation of the cross-section about the tangent to the axis.

At this point, there have been no assumptions beyond the Bernoulli-Euler model of a beam-column. The rotation matrix,  $C_{ij}^*$ , of equation (3.25), which is valid for large rotations, can be related to the displacements  $w$ ,  $u$ , and  $v$ , and the rotation  $\theta$ , of the axis through equations (3.27 - 3.31). As a result, the deformed axis is related to the undeformed by the four variables,  $w$ ,  $u$ ,  $v$  and  $\theta$ , which vary along the length. The substitution of equations (3.28 - 3.31) into (3.25) gives a rotation matrix of

$$C_{ij}^* = \begin{bmatrix} \frac{(1+d_1)}{D} & \frac{d_2}{D} & \frac{d_3}{D} \\ -\left(\frac{S_1 d_3 (1+d_1)}{DD_1} + \frac{C_1 d_2}{D_1}\right) & \left(\frac{C_1 (1+d_1)}{D_1} - \frac{S_1 d_2 d_3}{DD_1}\right) & \frac{S_1 D_1}{D} \\ \left(-\frac{C_1 d_3 (1+d_1)}{DD_1} + \frac{S_1 d_2}{D_1}\right) & -\left(\frac{S_1 (1+d_1)}{D_1} + \frac{C_1 d_2 d_3}{DD_1}\right) & \frac{C_1 D_1}{D} \end{bmatrix} . \quad (3.32)$$

For a large displacement analysis, equation (3.32) must be used to account for the geometric nonlinearities. The equation is now simplified to a situation referred to as moderate elastic rotations. The expressions for  $D$  and  $D_1$  given by equations (3.28) and

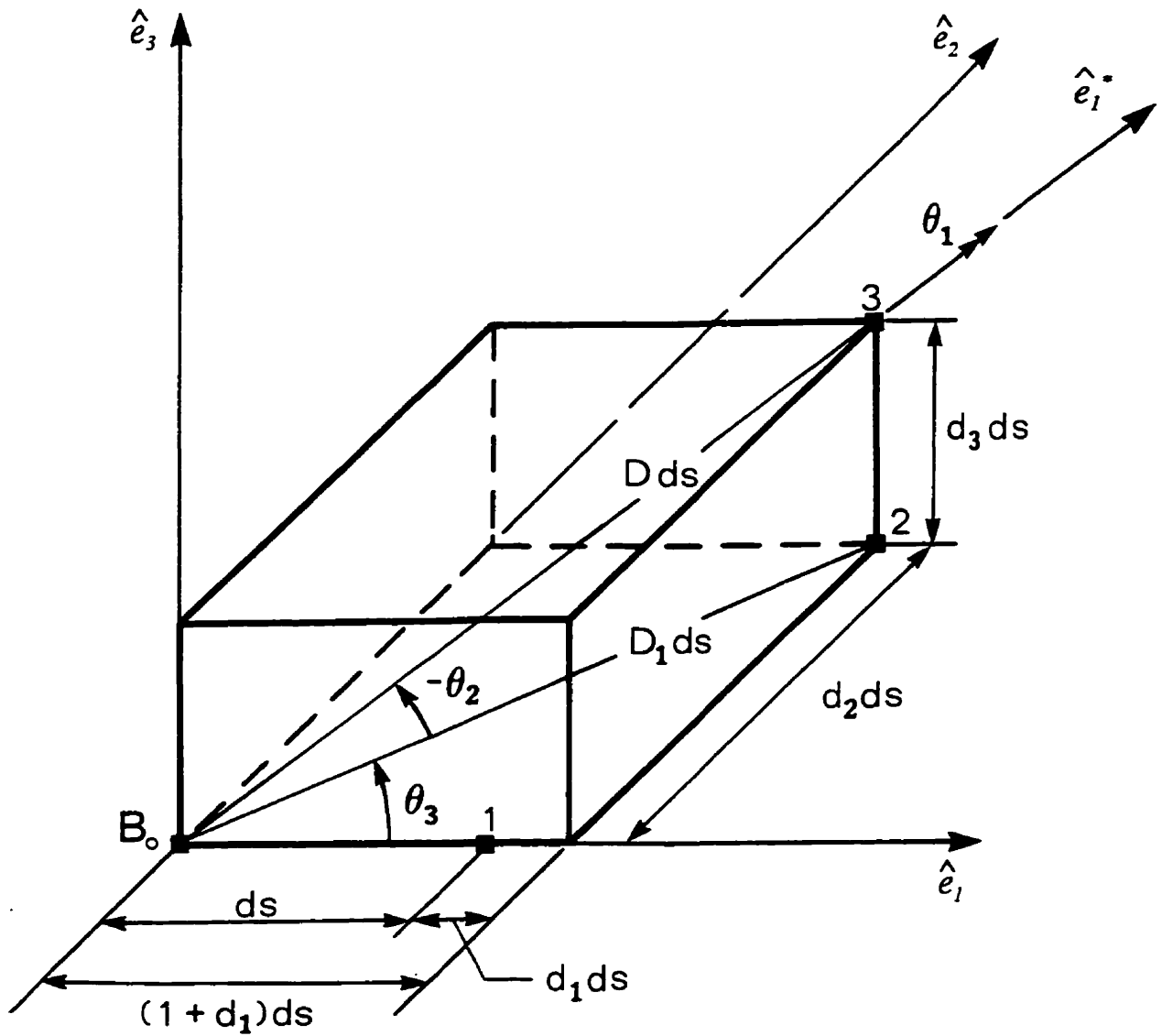


Figure 3.9: Illustration of the relationship between the displacement variables  $w$ ,  $u$  and  $v$ , where are a function  $d_1$ ,  $d_2$  and  $d_3$ , and the three Euler rotations of the cross-section of the beam-column. The cross-section of the undeformed beam-column, with unit tangent vector,  $\hat{e}_1$ , is carried through three Euler type rotations,  $\theta_3$ ,  $\theta_2$  and  $\theta_1$ , to the deformed position with unit tangent vector  $\hat{e}_1^*$ .

(3.31) are expanded in series form and substituted into equation (3.32). Similarly,  $\sin \theta$  and  $\cos \theta$  are also expanded in a series. If terms up to 2<sup>nd</sup> order are retained, then after some algebra, the rotation matrix becomes

$$C_{ij}^* = \begin{bmatrix} 1 - \frac{1}{2} (d_2^2 + d_3^2) & d_2 (1 - d_1) & d_3 (1 - d_1) \\ -d_2 (1 - d_1) - \theta d_3 & 1 - \frac{1}{2} d_2^2 - \frac{1}{2} \theta^2 & \theta \\ -d_3 (1 - d_1) + \theta d_2 & -(\theta + d_2 d_3) & 1 - \frac{1}{2} d_3^2 - \frac{1}{2} \theta^2 \end{bmatrix}. \quad (3.33)$$

Further reductions are made by assuming that  $d_1$ ,  $d_2^2$ ,  $d_3^2$  and  $\theta^2$  are small compared to unity. In the present model, the axial displacements along the beam-column are considered very small. Therefore,  $d_1$  is of  $\mathcal{O}(\epsilon^2)$ , similar to  $d_2^2$ ,  $d_3^2$  and  $\theta^2$  which are of  $\mathcal{O}(\epsilon^2)$ . However, terms of  $\mathcal{O}(\epsilon^2)$  are retained compared to terms of order  $\mathcal{O}(\epsilon)$ , but not compared to terms of  $\mathcal{O}(1)$ . For example, terms such as  $d_2 d_3$ ,  $\theta d_2$  and  $\theta d_3$  are retained compared to terms such as  $d_2$ ,  $d_3$  and  $\theta$ . This is referred to as moderate rotations, and the rotation matrix is simplified as follows:

$$C_{ij}^* = \begin{bmatrix} 1 & d_2 & d_3 \\ -(d_2 + \theta d_3) & 1 & \theta \\ -(d_3 - \theta d_2) & -(\theta + d_2 d_3) & 1 \end{bmatrix}. \quad (3.34)$$

If the rotations were small instead of moderate, the terms  $\theta d_3$ ,  $\theta d_2$  and  $d_2 d_3$  can also be dropped to give an anti-symmetric, linear rotation matrix.

As in the undeformed beam-column, a curvature vector,  $\hat{K}$ , can be defined as

$$\hat{K} = K_\zeta \hat{e}_1^* + K_\xi \hat{e}_2^* + K_\eta \hat{e}_3^* \quad (3.35)$$

where  $K_\zeta$  is twist, and  $K_\xi$ ,  $K_\eta$  are the curvatures of the deformed beam-column.<sup>2</sup> The curvatures and twist can, therefore, be defined by

<sup>2</sup>These terms are not exactly the curvatures and twist, but rather are  $(1 + \bar{\epsilon}_{11})$  times the exact values, where  $\bar{\epsilon}_{11}$  is the extensional strain of the axis. This has already been considered small earlier by assuming  $d_1 \ll 1$ , and this assumption is also considered later in the strain analysis (Wempner, 1981).

$$\begin{Bmatrix} \hat{e}_{1.1}^* \\ \hat{e}_{2.1}^* \\ \hat{e}_{3.1}^* \end{Bmatrix} = \begin{bmatrix} 0 & K_\eta & -K_\xi \\ -K_\eta & 0 & K_\zeta \\ K_\xi & -K_\zeta & 0 \end{bmatrix} \begin{Bmatrix} \hat{e}_1^* \\ \hat{e}_2^* \\ \hat{e}_3^* \end{Bmatrix}, \quad (3.36)$$

or alternatively,

$$\begin{aligned} K_\xi &= \hat{e}_1^* \cdot \hat{e}_{3.1}^* = -\hat{e}_3^* \cdot \hat{e}_{1.1}^* \\ K_\eta &= \hat{e}_2^* \cdot \hat{e}_{1.1}^* = -\hat{e}_1^* \cdot \hat{e}_{2.1}^* \\ K_\zeta &= \hat{e}_3^* \cdot \hat{e}_{2.1}^* = -\hat{e}_2^* \cdot \hat{e}_{3.1}^* \end{aligned} \quad (3.37)$$

To determine the curvatures and twist in terms of the rotation matrix, equation (3.24) and its derivatives with respect to  $s$  or  $l$  are substituted into equation (3.37), and employing equation (3.11), the following expressions are found

$$\begin{aligned} K_\xi &= (C_{11}^* C_{33}^* - C_{13}^* C_{31}^*) k_\xi + (C_{12}^* C_{31}^* - C_{11}^* C_{32}^*) k_\eta + (C_{13}^* C_{32}^* - C_{12}^* C_{33}^*) k_\zeta \\ &\quad + C_{11}^* C_{31.1}^* + C_{12}^* C_{32.1}^* + C_{13}^* C_{33.1}^* \\ K_\eta &= (C_{21}^* C_{13}^* - C_{23}^* C_{11}^*) k_\xi + (C_{22}^* C_{11}^* - C_{21}^* C_{12}^*) k_\eta + (C_{23}^* C_{12}^* - C_{22}^* C_{13}^*) k_\zeta \\ &\quad + C_{21}^* C_{11.1}^* + C_{22}^* C_{12.1}^* + C_{23}^* C_{13.1}^* \\ K_\zeta &= (C_{31}^* C_{23}^* - C_{33}^* C_{21}^*) k_\xi + (C_{32}^* C_{21}^* - C_{31}^* C_{22}^*) k_\eta + (C_{33}^* C_{22}^* - C_{32}^* C_{23}^*) k_\zeta \\ &\quad + C_{31}^* C_{21.1}^* + C_{32}^* C_{22.1}^* + C_{33}^* C_{23.1}^* \end{aligned} \quad (3.38)$$

The foregoing expressions for the deformed curvatures and twist could be determined in terms of any rotation matrix. If equation (3.34) for moderate rotations is used, the following expressions are found

$$K_\xi = k_\xi + \theta k_\eta - (d_2 + \theta d_3) k_\zeta - d_{3.1} + \theta d_{2.1}$$

$$\begin{aligned}
K_\eta &= -(\theta + d_2 d_3) k_\xi + k_\eta - (d_3 - \theta d_2) k_\zeta + d_{2,1} + \theta d_{3,1} \\
K_\zeta &= d_2 k_\xi + d_3 k_\eta + k_\zeta + \theta_{,1} + d_3 d_{2,1} .
\end{aligned} \tag{3.39}$$

This can further be reorganized into a combination of the initial curvatures and twist, plus linear terms and nonlinear terms as follows:

$$\begin{aligned}
K_\xi &= k_\xi + K_\xi^L + K_\xi^{NL} \\
K_\eta &= k_\eta + K_\eta^L + K_\eta^{NL} \\
K_\zeta &= k_\zeta + K_\zeta^L + K_\zeta^{NL}
\end{aligned} \tag{3.40}$$

where  $K_\xi^L$ ,  $K_\eta^L$  and  $K_\zeta^L$  are the linear terms

$$\begin{aligned}
K_\xi^L &= -d_{3,1} + \theta k_\eta - d_2 k_\zeta \\
K_\eta^L &= d_{2,1} - \theta k_\xi - d_3 k_\zeta \\
K_\zeta^L &= \theta_{,1} + d_2 k_\xi + d_3 k_\eta ,
\end{aligned} \tag{3.41}$$

and where  $K_\xi^{NL}$ ,  $K_\eta^{NL}$  and  $K_\zeta^{NL}$  are nonlinear contributions

$$\begin{aligned}
K_\xi^{NL} &= -\theta d_3 k_\zeta + \theta d_{2,1} \\
K_\eta^{NL} &= -d_2 d_3 k_\xi + \theta d_2 k_\zeta + \theta d_{3,1} \\
K_\zeta^{NL} &= d_3 d_{2,1} .
\end{aligned} \tag{3.42}$$

If the expressions for  $d_i$ , given in equation (3.27), are inserted into equations (3.41-3.42), then the deformed curvatures and twist are expressed in terms of four variables  $w$ ,  $u$ ,  $v$  and  $\theta$ , plus the initial curvatures  $k_\xi$ ,  $k_\eta$  and twist  $k_\zeta$ . The nonlinear terms of equation (3.42) result from retaining some higher order terms in the rotation matrix. For the linear case,  $K_\xi^{NL}$ ,  $K_\eta^{NL}$  and  $K_\zeta^{NL}$  are simply set equal to zero. For an initially straight beam-column,  $k_\xi$ ,  $k_\eta$  and  $k_\zeta$  are also set equal to zero. In this case, the curvatures and twist of the deformed beam-column are reduced to the well-known linear expressions

$$\begin{aligned}
K_\xi &= -v_{,11} \\
K_\eta &= u_{,11} \\
K_\zeta &= \theta_{,1} .
\end{aligned} \tag{3.43}$$

## Strain Analysis

The preceding sections have been primarily concerned with the geometry, kinematics and deformation of the axis of the beam-column. In order to establish the stress-strain relations, however, it is necessary to determine the deformation of all points of the beam-column, not just the elastic axis. As discussed earlier, the Bernoulli-Euler hypothesis is used to establish the deformation of the beam-column. As a result, the position of some point  $B$  on the cross-section of the beam-column can be described by

$$\hat{R}(s, \xi, \eta) = \hat{R}_0(s) + \xi \hat{e}_2^* + \eta \hat{e}_3^* \quad (3.44)$$

where  $\hat{R}$  is a position vector, and  $\xi, \eta$  are coordinates in the cross-section. Another term is often included in this expression to describe the warping of the cross-section in the tangential direction  $\hat{e}_1^*$ . This term is particularly important for thin walled open sections or composite beam-columns which can display significant warping of the cross-section. For slender solid sections, it is less of a factor and is not included in the present derivation.

The displacement of point  $B$  from the undeformed to the deformed configuration can be described by

$$\hat{U} = \hat{R} - \hat{r} \quad (3.45)$$

where  $\hat{r}$  is given by equation (3.15) and  $\hat{U}$  is the displacement vector of point  $B$  (Fig. 3.10). The basis vectors of the deformed beam-column are given by

$$\hat{G}_i = \hat{R}_{,i} \quad (3.46)$$

Equation (3.44) is differentiated, and using equations (3.26) and (3.36) the following expressions for the basis vectors are obtained

$$\begin{Bmatrix} \hat{G}_1 \\ \hat{G}_2 \\ \hat{G}_3 \end{Bmatrix} = \begin{bmatrix} \sqrt{G} & -\eta K_\zeta & \xi K_\zeta \\ 0 & 1 & 0 \\ 0 & 0 & 1 \end{bmatrix} \begin{Bmatrix} \hat{e}_1^* \\ \hat{e}_2^* \\ \hat{e}_3^* \end{Bmatrix} \quad (3.47)$$

where

$$G = (D - \xi K_\eta + \eta K_\xi)^2 \quad (3.48)$$

and  $D$  is given by equation (3.28). As before, for the rotation matrix,  $D$  is expanded as a series

$$D = (1 + 2\bar{e}_{11})^{\frac{1}{2}} = 1 + \bar{e}_{11} - \frac{1}{2} \bar{e}_{11}^2 + \dots \quad (3.49)$$

where

$$\bar{e}_{11} = d_1 + \frac{1}{2} d_1^2 + \frac{1}{2} d_2^2 + \frac{1}{2} d_3^2 \quad (3.50)$$

This expression in series form is valid for small  $\bar{e}_{11}$ , therefore,  $D$  is simplified such that

$$D = 1 + \bar{e}_{11} \quad (3.51)$$

It is now possible to determine the strains of the deformed beam-column using the basis vectors. The strains are determined by (Wempner, 1981)

$$\begin{aligned} e_{11} &= (\hat{G}_1 \cdot \hat{G}_1 - \hat{g}_1 \cdot \hat{g}_1) / 2(\hat{g}_1 \cdot \hat{g}_1) \\ e_{12} &= (\hat{G}_1 \cdot \hat{G}_2 - \hat{g}_1 \cdot \hat{g}_2) / 2 \sqrt{\hat{g}_1 \cdot \hat{g}_1} \\ e_{13} &= (\hat{G}_1 \cdot \hat{G}_3 - \hat{g}_1 \cdot \hat{g}_3) / 2 \sqrt{\hat{g}_1 \cdot \hat{g}_1} \end{aligned} \quad (3.52)$$

Due to the Bernoulli-Euler assumptions, the strains  $e_{22}$ ,  $e_{33}$  and  $e_{23}$  are easily found to be zero. This is in accordance with the assumption of no deformation of the cross-section of the beam-column. Using equations (3.17-3.18), (3.47-3.48) and (3.51), the strains become

$$\begin{aligned} e_{11} &= \frac{1}{2} \left[ (1 + \bar{e}_{11} - \xi K_\eta + \eta K_\xi)^2 - (1 - \xi k_\eta + \eta k_\xi)^2 \right. \\ &\quad \left. + (K_\zeta^2 - k_\zeta^2) (\xi^2 + \eta^2) \right] / g_{11} \\ e_{12} &= -\frac{1}{2} \eta (K_\zeta - k_\zeta) / \sqrt{g_{11}} \\ e_{13} &= \frac{1}{2} \xi (K_\zeta - k_\zeta) / \sqrt{g_{11}} \end{aligned} \quad (3.53)$$

where

$$g_{11} = \hat{g}_1 \cdot \hat{g}_1 = (1 - \xi k_\eta + \eta k_\xi)^2 + (\eta k_\zeta)^2 + (\xi k_\zeta)^2 \quad (3.54)$$

At this stage, the initial curvatures and twist are considered to be small such that, in combination with the assumption of a slender body,  $g_{11} \approx 1$ . Furthermore, the analysis is restricted to small strains, and the strain components are reduced to engineering strains.

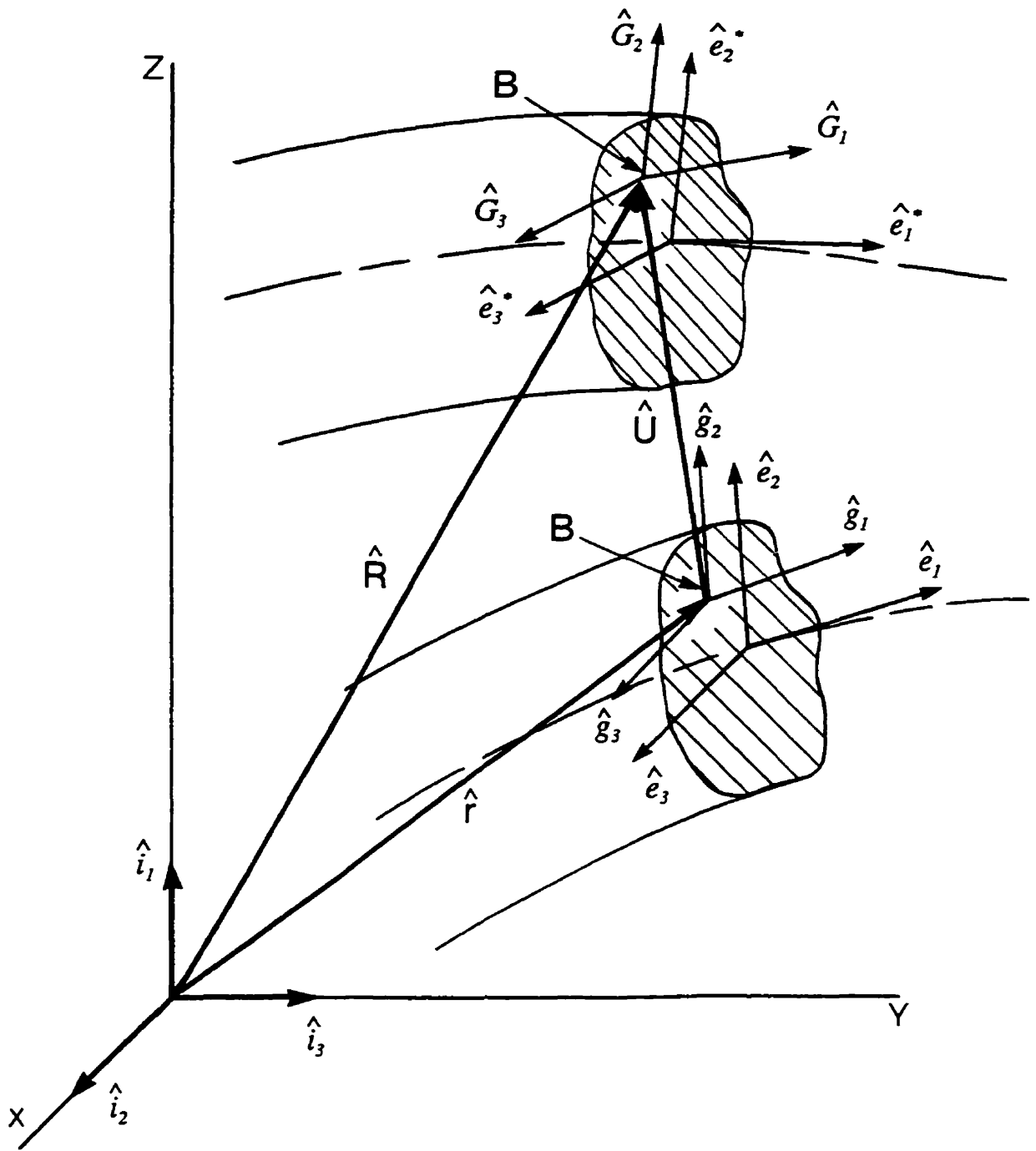


Figure 3.10: Illustration of the deformation of the beam-column from the initial to the deformed position. The displacement of a point B on the cross-section is given by  $\hat{U}$ . Also shown are the basis vectors,  $\hat{G}_i$ , of the deformed beam-column at point B.

Therefore, equation (3.53) becomes

$$\begin{aligned}
 \epsilon_{11} &= \bar{e}_{11} - \xi \bar{K}_\eta + \eta \bar{K}_\xi \\
 \gamma_{12} &= -\eta \bar{K}_\zeta \\
 \gamma_{13} &= \xi \bar{K}_\zeta
 \end{aligned} \tag{3.55}$$

where  $\epsilon_{11}$  is the axial strain,  $\gamma_{12}$ ,  $\gamma_{13}$  are the engineering shear strains, and  $\bar{K}_\xi = K_\xi - k_\xi$ ,  $\bar{K}_\eta = K_\eta - k_\eta$  and  $\bar{K}_\zeta = K_\zeta - k_\zeta$ . It is also apparent that the term,  $\bar{e}_{11}$ , introduced previously in equation (3.49), is the extensional strain of the elastic axis.

### Stress-Strain Relations

The material of the beam-column is assumed to be linear elastic, isotropic and homogeneous, and described by the Young's Modulus,  $E$ , and the Shear Modulus,  $G$ . The stresses acting on the cross-section can, therefore, be expressed as

$$\begin{aligned}
 \sigma_{11} &= E \epsilon_{11} = E (\bar{e}_{11} - \xi \bar{K}_\eta + \eta \bar{K}_\xi) \\
 \tau_{12} &= \bar{\tau}_{12} + G \gamma_{12} = \bar{\tau}_{12} - \eta G \bar{K}_\zeta \\
 \tau_{13} &= \bar{\tau}_{13} + G \gamma_{13} = \bar{\tau}_{13} + \xi G \bar{K}_\zeta
 \end{aligned} \tag{3.56}$$

where  $\bar{\tau}_{12}$  and  $\bar{\tau}_{13}$  are the components of the shear stresses which are due to the shear forces acting on the cross-section. These shear forces are required for equilibrium in the governing equations developed subsequently, but which do not deform the cross-section according to the Bernoulli-Euler assumptions, and therefore, do not emerge naturally from the strain analysis. Alternatively,  $\bar{e}_{12}$  and  $\bar{e}_{13}$  terms could have been introduced earlier in the strain analysis, in which case  $\bar{\tau}_{12} = 2G \bar{e}_{12}$  and  $\bar{\tau}_{13} = 2G \bar{e}_{13}$ . Either way, the addition is artificial for a Bernoulli-Euler beam-column. It is also possible to permit transverse shearing deformations, given by  $\bar{e}_{12}$  and  $\bar{e}_{13}$ , as a modification of the Bernoulli-Euler hypothesis, but this is not considered in the present derivation.

The stress vector which acts at some point  $B$  on the deformed cross-section can be

expressed as

$$\hat{S} = \sqrt{g_{11}} (\sigma_{11} \hat{G}_1 + \tau_{12} \hat{G}_2 + \tau_{13} \hat{G}_3) \quad (3.57)$$

where  $g_{11} \approx 1$ , due to relatively small initial curvatures, as previously mentioned in the strain analysis. Using equations (3.47-3.48) and (3.51), and applying the small strain assumptions made earlier, the stress vector becomes

$$\hat{S} = \sigma_{11} \hat{e}_1^* + \tau_{12} \hat{e}_2^* + \tau_{13} \hat{e}_3^* . \quad (3.58)$$

Also neglected in the equation are the effects of the axial stress in the shear terms. This nonlinear contribution can become important in beam-columns with an open section, when the axial stresses are high.

The stress vector is now integrated over the cross-section to determine the resultant force

$$\hat{F} = \int_A \hat{S} dA = N \hat{e}_1^* + V_\xi \hat{e}_2^* + V_\eta \hat{e}_3^* \quad (3.59)$$

where  $N$  is the axial load or normal force to the cross-section, and  $V_\xi$ ,  $V_\eta$  are the resultant shear forces. Therefore, using equation (3.56) and (3.58-3.59), the normal force is given by

$$N = \int_A \sigma_{11} dA = \int \int_A E (\bar{e}_{11} - \xi \bar{K}_\eta + \eta \bar{K}_\xi) d\xi d\eta \quad (3.60)$$

which can be simplified, for a homogeneous  $E$  over the cross-section, as follows:

$$N = (EA) (\bar{e}_{11} - \xi_0 \bar{K}_\eta + \eta_0 \bar{K}_\xi) \quad (3.61)$$

where

$$\begin{aligned} A &= \int \int_A d\xi d\eta \\ \xi_0 &= \frac{1}{A} \int \int_A \xi d\xi d\eta \\ \eta_0 &= \frac{1}{A} \int \int_A \eta d\xi d\eta . \end{aligned} \quad (3.62)$$

The term  $A$  is the cross-sectional area, and  $\xi_0$ ,  $\eta_0$  are the coordinates of the tension centre or neutral point of the cross-section. The shear forces are not integrated out specifically, as only the resultant is of necessity in the derivation.

The moment produced by the stress vector is determined by integrating the cross product of the stress vector and the moment arm at point  $B$ , measured from the origin of the cross-sectional coordinates. to give

$$\dot{M} = \int_A [(\xi \hat{e}_2^* + \eta \hat{e}_3^*) \times \hat{S}] dA = M_\zeta \hat{e}_1^* + M_\xi \hat{e}_2^* + M_\eta \hat{e}_3^* \quad (3.63)$$

where  $M_\zeta$  is the torsional moment, and  $M_\xi$ ,  $M_\eta$  are the bending moments. Substitution of equations (3.56) and (3.58) into equation (3.63) gives

$$\begin{aligned} M_\zeta &= \int_A (\xi \tau_{13} - \eta \tau_{12}) dA = \int \int_A (\xi \bar{\tau}_{13} - \eta \bar{\tau}_{12} + G \bar{K}_\zeta (\xi^2 + \eta^2)) d\xi d\eta \\ M_\xi &= \int_A \sigma_{11} \eta dA = \int \int_A E(\bar{e}_{11} - \xi \bar{K}_\eta + \eta \bar{K}_\xi) \eta d\xi d\eta \\ M_\eta &= - \int_A \sigma_{11} \xi dA = - \int \int_A E(\bar{e}_{11} - \xi \bar{K}_\eta + \eta \bar{K}_\xi) \xi d\xi d\eta . \end{aligned} \quad (3.64)$$

The two bending moments can be further expressed as

$$\begin{aligned} M_\xi &= (EA) \bar{e}_{11} \eta_0 + EI_{\xi\xi} \bar{K}_\xi - EI_{\xi\eta} \bar{K}_\eta \\ M_\eta &= -(EA) \bar{e}_{11} \xi_0 - EI_{\xi\eta} \bar{K}_\xi + EI_{\eta\eta} \bar{K}_\eta \end{aligned} \quad (3.65)$$

where

$$\begin{aligned} I_{\eta\eta} &= \int \int_A \xi^2 d\xi d\eta \\ I_{\xi\xi} &= \int \int_A \eta^2 d\xi d\eta \\ I_{\xi\eta} &= \int \int_A \xi \eta d\xi d\eta . \end{aligned} \quad (3.66)$$

If equation (3.61) is substituted into (3.65) for  $\bar{e}_{11}$ , then the bending moments become

$$\begin{aligned} M_\xi &= N \eta_0 + EI_{\xi\xi_0} \bar{K}_\xi - EI_{\xi\eta_0} \bar{K}_\eta \\ M_\eta &= -N \xi_0 - EI_{\xi\eta_0} \bar{K}_\xi + EI_{\eta\eta_0} \bar{K}_\eta \end{aligned} \quad (3.67)$$

where

$$\begin{aligned}
 I_{\xi\xi_0} &= I_{\xi\xi} - A\eta_0^2 = \int \int_A (\eta - \eta_0)^2 d\xi d\eta \\
 I_{\eta\eta_0} &= I_{\eta\eta} - A\xi_0^2 = \int \int_A (\xi - \xi_0)^2 d\xi d\eta \\
 I_{\xi\eta_0} &= I_{\xi\eta} - A\xi_0\eta_0 = \int \int_A (\xi - \xi_0)(\eta - \eta_0) d\xi d\eta .
 \end{aligned} \tag{3.68}$$

The terms  $I_{\xi\xi_0}$ ,  $I_{\eta\eta_0}$  and  $I_{\xi\eta_0}$  are determined with respect to the tension centre  $\langle \xi_0, \eta_0 \rangle$ . The bending moments about the origin of some axis of the beam-column have, therefore, been expressed in terms of properties determined about another point, the tension centre.

The torsional moment can also be reduced to the following

$$M_c = GJ \bar{K}_c + \int \int_A (\xi \bar{\tau}_{13} - \eta \bar{\tau}_{12}) d\xi d\eta \tag{3.69}$$

where

$$J = \int \int_A (\xi^2 + \eta^2) d\xi d\eta . \tag{3.70}$$

The second term in equation (3.69) is the torsional moment produced by the shear forces  $V_\xi$  and  $V_\eta$ , which act about the origin of the coordinate system on the cross-section. This term becomes zero by definition if the origin is termed the shear centre. The axis of the beam-column located at this point is then termed the elastic axis. This reflects the fact that some point on an elastic cross-section can always be found such that the resultant shear forces do not influence the torsional moment.

Therefore, combining equations (3.61), (3.65) and (3.69), where the origin about which the moments are determined is now the elastic axis, leads to the following equations

$$\begin{Bmatrix} N \\ M_\xi \\ M_\eta \\ M_c \end{Bmatrix} = E \begin{bmatrix} A & A\eta_0 & -A\xi_0 & 0 \\ A\eta_0 & I_{\xi\xi} & -I_{\xi\eta} & 0 \\ -A\xi_0 & -I_{\xi\eta} & I_{\eta\eta} & 0 \\ 0 & 0 & 0 & \frac{GJ}{E} \end{bmatrix} \begin{Bmatrix} \bar{e}_{11} \\ \bar{K}_\xi \\ \bar{K}_\eta \\ \bar{K}_c \end{Bmatrix} \tag{3.71}$$

which are referred to as the generalized stress-strain relations for a curved and twisted beam-column. The origin of the coordinates is located at the shear centre, and the equations include an offset  $\langle \xi_0, \eta_0 \rangle$  of the neutral point origin.

If the cross-section axes chosen are the principal axes, then by definition  $I_{\xi\eta} = 0$ . Further, if the neutral point or tension centre coincides with the origin ( $\xi_0 = \eta_0 = 0$ ), the equations become completely uncoupled and reduce to the familiar form

$$\begin{aligned} N &= EA \bar{e}_{11} \\ M_\xi &= EI_{\xi\xi} \bar{K}_\xi \\ M_\eta &= EI_{\eta\eta} \bar{K}_\eta \\ M_\zeta &= GJ \bar{K}_\zeta \end{aligned} \quad (3.72)$$

where  $EA$  is the extensional stiffness,  $EI_{\xi\xi}$ ,  $EI_{\eta\eta}$  are the bending stiffnesses, and  $GJ$  is the torsional rigidity.

### Equilibrium Equations

To derive the governing equations it is necessary to consider the equilibrium between the internal resultants due to deformation and the applied forces and moments. Consider a differential beam-column element,  $ds$ , shown in a deformed position in Fig. 3.11. A distributed force,  $\hat{f}$ , and a distributed moment,  $\hat{m}$ , per unit length<sup>3</sup> are assumed to act along the elastic axis. Summing the forces acting on the element to zero gives

$$\hat{F}_{,1} + \hat{f} = 0, \quad (3.73)$$

and similarly for the moments

$$\hat{M}_{,1} + \hat{e}_1^* \times \hat{F} + \hat{m} = 0 \quad (3.74)$$

where  $\hat{F}$  and  $\hat{M}$  are the internal forces and moments defined earlier.

To solve these vectorial equations, they must be expressed in component form to give six equations. The vectors can be resolved in either the deformed or the undeformed coordinate system. The internal resultants are most naturally expressed in the deformed or

---

<sup>3</sup>Due to the assumption of small extension of the elastic axis, the change in unit length is small.

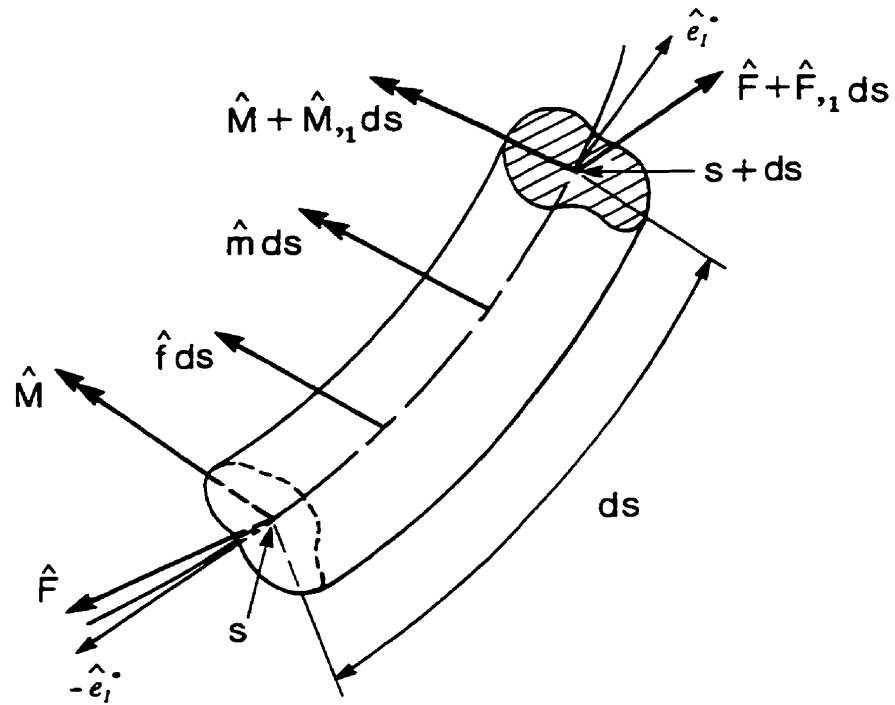


Figure 3.11: Differential element,  $ds$ , of the spatial beam-column subjected to an applied force,  $\hat{f}$ , and moment,  $\hat{m}$ , per unit length along the elastic axis.

local system, whereas the applied forces and moments depend on the given problem. If the applied loads are of a “follower” nature that depend on the deformation then they also are most naturally expressed in the deformed system. The other consideration is the magnitude of deformation. A small displacement analysis is better expressed in the undeformed system. Based on these considerations, the vectorial equations are now resolved into component form in the undeformed coordinate system,  $\hat{e}_i$ . Therefore, the applied forces and moments are expressed as

$$\begin{aligned}\hat{f} &= f_1 \hat{e}_1 + f_2 \hat{e}_2 + f_3 \hat{e}_3 \\ \hat{m} &= m_1 \hat{e}_1 + m_2 \hat{e}_2 + m_3 \hat{e}_3 \quad ,\end{aligned}\tag{3.75}$$

and the internal forces and moments as

$$\begin{aligned}\hat{F} &= F_1 \hat{e}_1 + F_2 \hat{e}_2 + F_3 \hat{e}_3 \\ \hat{M} &= M_1 \hat{e}_1 + M_2 \hat{e}_2 + M_3 \hat{e}_3 \quad .\end{aligned}\tag{3.76}$$

These components are related to those in the deformed system given by equations (3.59) and (3.63) by using equations (3.24) and (3.34) to give

$$F_1 = N + C_{21}^* V_\xi + C_{31}^* V_\eta \quad (3.77)$$

$$F_2 = C_{12}^* N + V_\xi + C_{32}^* V_\eta \quad (3.78)$$

$$F_3 = C_{13}^* N + C_{23}^* V_\xi + V_\eta \quad (3.79)$$

and

$$M_1 = M_\zeta + C_{21}^* M_\xi + C_{31}^* M_\eta \quad (3.80)$$

$$M_2 = C_{12}^* M_\zeta + M_\xi + C_{32}^* M_\eta \quad (3.81)$$

$$M_3 = C_{13}^* M_\zeta + C_{23}^* M_\xi + M_\eta \quad (3.82)$$

Equations (3.75) and (3.76) are now substituted into equations (3.73) and (3.74), and making use of equation (3.11), (3.24) and (3.34), the following six equations are obtained:

$$F_{1,1} + F_3 k_\xi - F_2 k_\eta + f_1 = 0 \quad (3.83)$$

$$F_{2,1} + F_1 k_\eta - F_3 k_\zeta + f_2 = 0 \quad (3.84)$$

$$F_{3,1} + F_2 k_\zeta - F_1 k_\xi + f_3 = 0 \quad (3.85)$$

$$M_{1,1} + M_3 k_\xi - M_2 k_\eta + C_{12}^* F_3 - C_{13}^* F_2 + m_1 = 0 \quad (3.86)$$

$$M_{2,1} + M_1 k_\eta - M_3 k_\zeta + C_{13}^* F_1 - F_3 + m_2 = 0 \quad (3.87)$$

$$M_{3,1} + M_2 k_\zeta - M_1 k_\xi - C_{12}^* F_1 + F_2 + m_3 = 0 \quad (3.88)$$

These are coupled nonlinear equations expressed in the undeformed system. Due to the Bernoulli-Euler assumptions, only 4 variables are needed to describe the motion of the beam-column. Therefore, only four equations are needed, as the shear resultants  $F_2$  and  $F_3$  can be eliminated. First, equations (3.87-3.88) are substituted into (3.83-3.86), then equations (3.87 and 3.88) are differentiated to give the following 4 equations

$$F_{1,1} + (k_\xi C_{13}^* - k_\eta C_{12}^*) F_1 + k_\xi M_{2,1} + k_\eta M_{3,1} + k_\eta k_\zeta M_2 - k_\xi k_\zeta M_3 + k_\xi m_2 + k_\eta m_3 + f_1 = 0 \quad (3.89)$$

$$[ M_{2,1} + M_1 k_\eta - M_3 k_\zeta ],_{,1} + (C_{13}^* F_1)_{,1} - F_{3,1} + m_{2,1} = 0 \quad (3.90)$$

$$[ M_{3,1} + M_2 k_\zeta - M_1 k_\xi ],_{,1} - (C_{12}^* F_1)_{,1} + F_{2,1} + m_{3,1} = 0 \quad (3.91)$$

$$M_{1,1} + (k_\xi - C_{12}^* k_\zeta) M_3 - (k_\eta - C_{13}^* k_\zeta) M_2 + (C_{12}^* k_\eta - C_{13}^* k_\xi) M_1 + C_{12}^* (M_{2,1} + m_2) + C_{13}^* (M_{3,1} + m_3) + m_1 = 0 \quad (3.92)$$

The shear forces  $F_2$  and  $F_3$  have not yet been fully eliminated as they remain present in the bending moment equations (3.90-3.91). Using equations (3.77-3.79), then  $F_1$  can be expressed in terms of  $F_2$  and  $F_3$  as follows

$$F_1 = N - C_{12}^* F_2 - C_{13}^* F_3 \quad (3.93)$$

This expression is valid only to the second order and was determined after dropping products of  $C_{ij}^*$  compared to unity, as was done previously. Similarly, using equations (3.87-3.88) for  $F_2$  and  $F_3$ , and using equation (3.93) for  $F_1$ , the following expressions are found

$$F_2 = -M_{3,1} - C_{12}^* C_{13}^* M_{2,1} + C_{12}^* N - k_\zeta (M_2 - C_{12}^* C_{13}^* M_3) + k_\xi M_1 - C_{12}^* C_{13}^* m_2 - m_3 \quad (3.94)$$

$$F_3 = M_{2,1} + C_{12}^* C_{13}^* M_{3,1} + C_{13}^* N + k_\zeta (C_{12}^* C_{13}^* M_2 - M_3) + k_\eta M_1 + C_{12}^* C_{13}^* m_3 + m_2 \quad (3.95)$$

which again are only valid for moderate rotations. It is now possible to express the four equations in terms of  $N$ ,  $M_1$ ,  $M_2$ , and  $M_3$ . Equations (3.93-3.95) are first substituted into equations (3.84-3.85) and then subsequently into (3.89-3.91) to eliminate the forces  $F_1$ ,  $F_2$  and  $F_3$ . Once again, products of  $C_{ij}^*$  are neglected compared to unity and following a lengthy algebraic reduction, the following equations are determined:

$$\begin{aligned}
& [N - C_{13}^* M_{2.1} + C_{12}^* M_{3.1}]_{,1} - [(k_\xi C_{12}^* + k_\eta C_{13}^*) M_1 - k_\zeta (C_{12}^* M_2 + C_{13}^* M_3)]_{,1} \\
& + (k_\xi C_{13}^* - k_\eta C_{12}^*) N + k_\xi M_{2.1} + k_\eta M_{3.1} + k_\zeta (k_\eta M_2 - k_\xi M_3) \\
& + k_\xi m_2 + k_\eta m_3 - (C_{13}^* m_2)_{,1} + (C_{12}^* m_3)_{,1} + f_1 = 0 \tag{3.96}
\end{aligned}$$

$$\begin{aligned}
& [M_{2.1} + C_{12}^* C_{13}^* M_{3.1}]_{,1} + (k_\eta M_1)_{,1} + [k_\zeta (C_{12}^* C_{13}^* M_2 - M_3)]_{,1} + (C_{13}^* N)_{,1} \\
& - (k_\xi - k_\zeta C_{12}^*) N + C_{13}^* (k_\xi - k_\zeta C_{12}^*) M_{2.1} - (k_\xi C_{12}^* + k_\zeta) M_{3.1} \\
& - k_\zeta (k_\xi C_{12}^* + k_\zeta) M_2 - C_{13}^* k_\zeta (k_\xi - k_\zeta C_{12}^*) M_3 + k_\xi (k_\xi C_{12}^* + k_\eta C_{13}^* + k_\zeta) M_1 \\
& + C_{13}^* (k_\xi - k_\zeta C_{12}^*) m_2 - (k_\xi C_{12}^* + k_\zeta) m_3 + (C_{12}^* C_{13}^* m_3)_{,1} + m_{2.1} + f_3 = 0 \tag{3.97}
\end{aligned}$$

$$\begin{aligned}
& [M_{3.1} + C_{12}^* C_{13}^* M_{2.1}]_{,1} - (k_\xi M_1)_{,1} + [k_\zeta (M_2 - C_{12}^* C_{13}^* M_3)]_{,1} - (C_{12}^* N)_{,1} \\
& - (k_\eta - k_\zeta C_{13}^*) N + (k_\eta C_{13}^* + k_\zeta) M_{2.1} - C_{12}^* (k_\eta - k_\zeta C_{13}^*) M_{3.1} \\
& - C_{12}^* k_\zeta (k_\eta - C_{13}^* k_\zeta) M_2 - k_\zeta (C_{13}^* k_\eta + k_\zeta) M_3 + k_\eta (k_\xi C_{12}^* + k_\eta C_{13}^* + k_\zeta) M_1 \\
& + (C_{13}^* k_\eta + k_\zeta) m_2 - C_{12}^* (k_\eta - C_{13}^* k_\zeta) m_3 + (C_{12}^* C_{13}^* m_2)_{,1} + m_{3.1} - f_2 = 0 \tag{3.98}
\end{aligned}$$

$$\begin{aligned}
& M_{1,1} + C_{12}^* M_{2.1} + C_{13}^* M_{3.1} - (k_\eta - k_\zeta C_{13}^*) M_2 + (k_\xi - k_\zeta C_{12}^*) M_3 \\
& - (k_\xi C_{13}^* - k_\eta C_{12}^*) M_1 + C_{12}^* m_2 + C_{13}^* m_3 + m_1 = 0 \tag{3.99}
\end{aligned}$$

These four equations govern the spatial behaviour of an initially curved and twisted beam-column undergoing moderate rotations expressed in the undeformed position. In the present form, they are generally referred to as *intrinsic* equations since they do not contain *explicit* displacement terms. If further substitutions are made, a set of *explicit* equations in terms of the four unknowns  $w$ ,  $u$ ,  $v$  and  $\theta$  can be determined.

## Boundary Conditions

All that remains to complete the derivation of the governing equations is to determine the boundary conditions. In complex structures, the exact boundary conditions are not always apparent. In these situations, the governing equations are often derived from a variational approach, as opposed to the Newtonian approach used in the foregoing. The boundary conditions emerge naturally from the variational approach and no further derivations are required. In the present application, the spatial beam-column is not subjected to any unusual or complex boundary conditions. Therefore, the well known standard boundary conditions of a beam-column are sufficient for the present model.

In general, the present beam-column can either be free, pinned or fixed at each end. These are the common boundary conditions of a beam-column, and are sufficient for the present model. These boundary conditions are enforced by specifying a set of either geometric or load constraints at the ends of the beam-column. For a free end, the internal forces and moments must satisfy the following

$$\begin{aligned} N = V_\xi = V_\eta &= 0 \\ M_\zeta = M_\xi = M_\eta &= 0 . \end{aligned} \quad (3.100)$$

The displacements at the free end are non zero, and can assume any value consistent with the given problem. For a pinned end, the internal moments and displacements must satisfy the following

$$\begin{aligned} M_\zeta = M_\xi = M_\eta &= 0 \\ u = v = \theta &= 0 . \end{aligned} \quad (3.101)$$

The internal shear forces,  $V_\xi$  and  $V_\eta$ , are non zero and represent the end reactions of the beam-column. The axial force,  $N$ , is also non zero if the beam-column is not free to slide in the axial direction. For a fixed end, the rotations and the displacements must satisfy the following

$$\begin{aligned}\theta = u_{,1} = v_{,1} &= 0 \\ w = u = v &= 0 .\end{aligned}\tag{3.102}$$

The internal forces and moments are non zero and represent the end reactions of the beam-column.

One set of the above boundary conditions must be satisfied at each end of the beam-column. Together with the governing equations, the displacements at all points along the beam-column can then be determined, and is generally referred to as a two-point boundary value problem.

### 3.3.3 Application to the Scoliotic Spine

In the preceding section, the governing equations of an initially curved and twisted, spatial beam-column were developed in a most general form. These equations are now adapted to specifically represent a spine with a mild scoliosis. To summarize, three basic sets of equations must be combined together to provide four *explicit* equations to solve for the four unknowns. From the preceding section, these are

1. Intrinsic equilibrium equations — (3.96-3.99)
2. Curvature-displacement equations — (3.27), (3.40-3.42)
3. Generalized stress-strain equations — (3.71).

Before combining these equations, consider first the cross-section of the spine (Fig. 3.12). The origin of the coordinate system is located somewhat posterior to the vertebral body centre, at the centre of rotation or shear centre of a motion segment. The tension centre is chosen to coincide with the vertebral body centre. As a result of the symmetry of the cross-section about the mid-sagittal plane, the tension centre is located at  $\langle 0, \eta_0 \rangle$  of the cross-section, i.e.,  $\xi_0 = 0$ . Furthermore, the local coordinate system is aligned with the principal axes. Therefore, equation (3.71) becomes

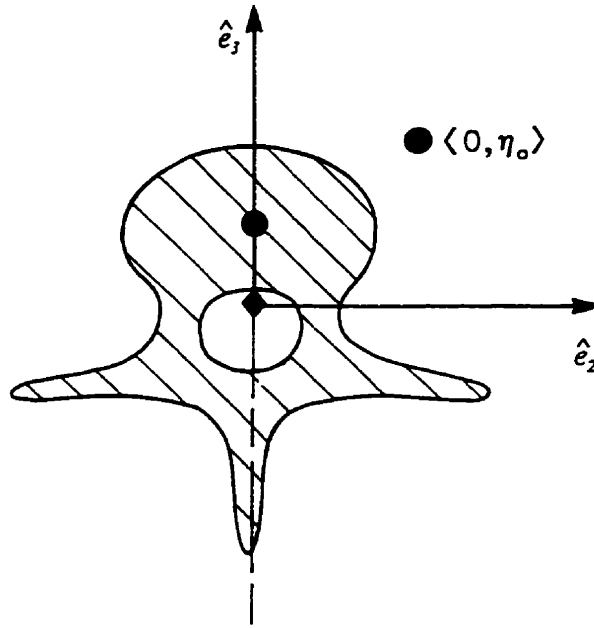


Figure 3.12: Location of the tension centre of the spine in relation to the shear centre. Due to symmetry, the tension centre is assumed to be offset only in the  $\hat{e}_3$  direction by  $\eta_0$ .

$$\begin{Bmatrix} N \\ M_\xi \\ M_\eta \\ M_\zeta \end{Bmatrix} = E \begin{bmatrix} A & A\eta_0 & 0 & 0 \\ A\eta_0 & I_{\xi\xi} & 0 & 0 \\ 0 & 0 & I_{\eta\eta} & 0 \\ 0 & 0 & 0 & \frac{GJ}{E} \end{bmatrix} \begin{Bmatrix} \bar{e}_{11} \\ \bar{K}_\xi \\ \bar{K}_\eta \\ \bar{K}_\zeta \end{Bmatrix}. \quad (3.103)$$

The longitudinal deformation,  $w$ , of the spine is assumed to be much less than the transverse components,  $u$  and  $v$ . Therefore, equation (3.27) is simplified to give

$$\begin{aligned} d_1 &= -uk_\eta + vk_\xi \\ d_2 &= u_{,1} - vk_\zeta \\ d_3 &= v_{,1} + uk_\zeta \end{aligned} \quad (3.104)$$

where the terms related to  $w$  have been dropped. In this case,  $N$  is considered the unknown as opposed to  $w$ , and  $M_\xi$ ,  $M_\eta$  are given by equation (3.67). Therefore, equation (3.103) is better expressed as<sup>4</sup>

<sup>4</sup>Note that since  $\xi_0 = 0$ , then  $EI_{\eta\eta} = EI_{\eta_0}$ .

$$\begin{Bmatrix} M_\xi \\ M_\eta \\ M_\zeta \end{Bmatrix} = \begin{bmatrix} \eta_0 & EI_{\xi\xi_0} & 0 & 0 \\ 0 & 0 & EI_{\eta\eta_0} & 0 \\ 0 & 0 & 0 & GJ \end{bmatrix} \begin{Bmatrix} N \\ \bar{K}_\xi \\ \bar{K}_\eta \\ \bar{K}_\zeta \end{Bmatrix}. \quad (3.105)$$

The curvatures and twist expressions were previously related to the variables  $d_1, d_2, d_3$ , as well as the initial curvatures  $k_\xi, k_\eta$  and twist  $k_\zeta$ . Direct substitution of equation (3.104) into equations (3.40-3.42) results in very lengthy expressions relating the curvatures and twist to the variables  $u, v$  and  $\theta$ . However, since the present study is only concerned with a mild scoliosis, then as discussed in Section 3.3.1, a moderate rotation theory was adequate to model the rotations. Consequently, the initial rotations  $u_{0,1}, v_{0,1}$  and  $\theta_0$  are also considered to be moderate and of the same order as  $u_{,1}, v_{,1}$  and  $\theta$ . The deformed curvature and twist expressions are, therefore, simplified by neglecting products of the initial and final rotations compared to one. Terms of  $\mathcal{O}(\epsilon^2)$  are neglected compared to terms of  $\mathcal{O}(1)$ , and terms of  $\mathcal{O}(\epsilon^4)$  are neglected compared to  $\mathcal{O}(\epsilon^2)$ , etc. The resulting curvature and twist expressions are thus valid for moderate rotations, and contain the influence of the initial curvatures and twist at the same order. Therefore, the curvatures and twist expressions become

$$\begin{aligned} \bar{K}_\xi &= K_\xi - k_\xi = -v_{,11} - 2u_{,1}k_\zeta - uk_{\zeta,1} + vk_\zeta^2 + \theta k_\eta + \theta u_{,11} \\ \bar{K}_\eta &= K_\eta - k_\eta = u_{,11} - 2v_{,1}k_\zeta - vk_{\zeta,1} - uk_\zeta^2 - \theta k_\xi + \theta v_{,11} \\ \bar{K}_\zeta &= K_\zeta - k_\zeta = \theta_{,1} + u_{,1}k_\xi + v_{,1}k_\eta + v_{,1}u_{,11} \end{aligned} \quad (3.106)$$

These expressions contain four distinct parts: initial curvatures and twist, pure linear terms, pure nonlinear terms, and combinations of linear terms with the initial curvatures and twist. Since the initial curvatures and twist are also considered moderate, the products of nonlinear terms with the initial curvatures and twist were dropped from these expressions due to the ordering scheme.

It is now possible to determine the *explicit* equations of the initially curved and twisted, spatial beam-column for moderate rotations and displacements. First, equations (3.80-

3.82) are substituted into equations (3.96-3.99), with the use of equation (3.34). Subsequently, equations (3.104-3.106) are also substituted to establish four equations in the four unknowns  $N$ ,  $u$ ,  $v$  and  $\theta$ . During this procedure, many more nonlinearities arise and are carefully excluded to maintain the ordering scheme used in the curvatures and twist equations. Furthermore, advantage is taken of certain features of the spinal column properties to simplify the equations. It is also assumed that  $EI_{\xi\xi_0}$ ,  $EI_{\eta\eta_0}$  and  $GJ$  are of the same order. The main effect of this assumption is that products of three terms or more of the rotations are neglected, since they can always be compared to unity. If, for instance, the spine was considerably stiffer in one direction compared to the others, then terms multiplying that stiffness would not be comparable to terms multiplying the other stiffnesses. Consequently, some higher order nonlinearities would have to be retained in the ordering scheme. However, the stiffness of the spine is of similar magnitude in both planes, and in torsion.

The stiffnesses  $EI_{\xi\xi_0}$ ,  $EI_{\eta\eta_0}$  and  $GJ$  are considered to vary over the spinal length. However, the spatial derivatives of the terms are considered negligible. Varied properties along the spine are to be included in a step-wise manner specified for each motion segment along the spine. The changes between successive motion segments are considered to be small and gradual, though the differences between the top of the thoracic and the bottom of the lumbar spine can be significant. It should be noted, however, that nonlinear terms involving the axial load are carefully retained since the axial load can be relatively large, and can be considered as the primary load on the spine.

There are many algebraic steps involved in this reduction that need not be detailed. During the algebraic reduction, the equations are reorganized in terms of the derivatives of the axial load,  $N$ , the displacements  $u$ ,  $v$ , and the axial rotation  $\theta$ . The final set of equations are best expressed in the following matrix form

$$\begin{aligned}
 & [M_4] \{t\}_{,1111} + [M_3] \{t\}_{,111} + [ [M_2] + [AM_2] ] \{t\}_{,11} \\
 & + [ [M_1] + [AM_1] ] \{t\}_{,1} + [ [M_0] + [AM_0] ] \{t\} = \{AM_c\} \quad (3.107)
 \end{aligned}$$

where  $[M_4]$ ,  $[M_3]$ ,  $[M_2]$ ,  $[M_1]$  and  $[M_0]$  are  $(4 \times 4)$  matrices that contain terms related to the internal reactions, and  $[AM_2]$ ,  $[AM_1]$ ,  $[AM_0]$  are  $(4 \times 4)$  matrices and  $\{AM_c\}$  is a vector related to the applied forces and moments. The four unknowns are expressed by the vector  $\{t\}$ , where

$$\{t\} = \begin{Bmatrix} N \\ u \\ v \\ \theta \end{Bmatrix} . \quad (3.108)$$

The components of the matrices are quite lengthy with both linear and nonlinear terms, and are given in Appendix F.

It is difficult to fully appreciate all the terms contained in the compact matrix form of equation (3.107). On the other hand, the fully expanded equations are very long with many terms. However, similar to the curvature and twist expressions, there are four types of terms that are contained in the components of the matrices. In order to illustrate the nature of the equations, consider the simplest form of the equations which can be fully expanded in a relatively compact form. If only the linear terms of the displacements  $u$ ,  $v$  and  $\theta$  are retained, and products of the initial curvatures and twist with the displacements are also dropped, the equations are considerably simplified. Then, the four governing equations become

$$\begin{aligned} N_{,1} - \eta_0 v_{,1} N_{,11} + \eta_0 (k_\xi - v_{,11}) N_{,1} + (k_\xi - v_{,11}) m_2 + (k_\eta + u_{,11}) m_3 \\ + m_{3,1} u_{,1} - m_{2,1} v_{,1} + f_1 = 0 \end{aligned} \quad (3.109)$$

$$-EI_{\xi\xi_0} v_{,1111} + \eta_0 N_{,11} + v_{,1} N_{,1} - (k_\xi - v_{,11}) N - k_\zeta m_3 + m_{2,1} + f_3 = 0 \quad (3.110)$$

$$\begin{aligned} EI_{\eta\eta_0} u_{,1111} + \eta_0 \theta N_{,11} - u_{,1} N_{,1} + 2\eta_0 (k_\zeta + \theta_{,1}) N_{,1} \\ - (k_\eta + u_{,11} - \eta_0 (k_{\zeta,1} + \theta_{,11})) N + k_\zeta m_2 + m_{3,1} - f_2 = 0 \end{aligned} \quad (3.111)$$

$$GJ\theta_{,11} - \eta_0 (k_\eta + u_{,11}) N + m_2 u_{,1} + m_3 v_{,1} + m_1 = 0 . \quad (3.112)$$

Note that products of  $N$  and the displacements  $u$ ,  $v$  and  $\theta$  are retained even though they represent a nonlinearity. Due to the relatively high axial stiffness of the spinal column, the axial load  $N$  can become large. Thus these terms are of fundamental importance in the equations as they are not a 2<sup>nd</sup> order effect. This nonlinearity is further discussed in the solution procedure detailed in the following section.

### 3.4 Solution

The governing equations (3.107) of the spinal column model are 4<sup>th</sup> order nonlinear, nonhomogeneous, coupled differential equations with variable coefficients. The nonlinearity is due to the inclusion of higher order terms in the displacements for moderate rotations, and for the combinations of the axial load with the displacements. The equations are nonhomogeneous due to the general loading, and the initial curvatures and twist. The coupling of the equations is due to the offset of the shear centre from the tension centre, the nonlinearity and the initial curvatures and twist once again. The coefficients are variable over the length due to distributed properties and loading, as well as, the initial curvatures and twist. In addition, boundary conditions are specified at either end of the beam-column, and therefore, the equations represent a two-point boundary value problem. The mechanics described by these equations were analyzed in this study using two separate approaches. First, a parametric analysis was performed using these equations to study the effect of a number of variables. Secondly, the equations were programmed into a loop to explicitly examine the changes during the adolescent growth spurt. In both cases, however, the equations had to be solved for a given set of boundary conditions, initial curvatures and twist, properties and loading conditions.

The equations (3.107) were reduced to a system of 1<sup>st</sup> order differential equations, and solved with a two-point boundary value problem solver available in the International Mathematical and Statistical Library (IMSL). In a preliminary analysis, both the multiple shooting technique (DB2PMS) and a finite difference technique (DB2PFD) were explored. The multiple shooting technique was found to be more efficient and stable and, therefore,

was used to solve the equations.

As mentioned earlier, two types of nonlinearities are involved in the equations, which are of a different nature. Since the axial displacements are assumed to be small, the axial load,  $N$ , becomes the unknown. As a result, products of  $N$  and its derivatives with the displacements are nonlinearities in the equations. The other nonlinearities are due to the products of the displacements and are considered 2<sup>nd</sup> order effects. The axial load nonlinearities are entirely different, since  $N$  can be relatively large and is not constrained in the ordering scheme. These terms, therefore, have a fundamental influence on the equations and behave very differently from the purely displacement nonlinearities. Consequently, the nonlinearities had to be treated separately, or convergence problems could have arisen due to differences in magnitude between the nonlinearities. Therefore, in the solution scheme, the axial load equation was solved separately from the three displacement equations.

The displacement equations of (3.107) (i.e., the 2<sup>nd</sup>, 3<sup>rd</sup> and 4<sup>th</sup>) contain 4<sup>th</sup> order derivatives for  $u$  and  $v$ , and 2<sup>nd</sup> order derivatives for  $\theta$ . They were reduced to a system of 10 1<sup>st</sup> order equations by the following substitution

$$\begin{aligned}
 u_1 &= u & v_1 &= v & \theta_1 &= \theta \\
 u_2 &= u_{,1} = u_{1,1} & v_2 &= v_{,1} = v_{1,1} & \theta_2 &= \theta_{,1} = \theta_{1,1} \\
 u_3 &= u_{,11} = u_{2,1} & v_3 &= v_{,11} = v_{2,1} \\
 u_4 &= u_{,111} = u_{3,1} & v_4 &= v_{,111} = v_{3,1}
 \end{aligned} \tag{3.113}$$

Since the two bending equations for  $u$  and  $v$  contained terms of the 2<sup>nd</sup> order derivative of  $\theta$ , then the torsion equation for  $\theta$  was substituted into the bending equations following the 1<sup>st</sup> order substitutions. Similarly, the bending equations for  $u$  and  $v$  were substituted into each other due to terms of the 4<sup>th</sup> order derivative of  $u$  and  $v$ . As a result, the displacement equations of (3.107) were expressed as a system of 1<sup>st</sup> order equations as follows:

$$\begin{Bmatrix} u_{1.1} \\ u_{2.1} \\ u_{3.1} \\ u_{4.1} \\ v_{1.1} \\ v_{2.1} \\ v_{3.1} \\ v_{4.1} \\ \theta_{1.1} \\ \theta_{2.1} \end{Bmatrix} = \begin{bmatrix} 0 & 1 & 0 & 0 & 0 & 0 & 0 & 0 & 0 & 0 \\ 0 & 0 & 1 & 0 & 0 & 0 & 0 & 0 & 0 & 0 \\ 0 & 0 & 0 & 1 & 0 & 0 & 0 & 0 & 0 & 0 \\ B_1 & B_2 & B_3 & B_4 & B_5 & B_6 & B_7 & B_8 & B_9 & B_{10} \\ 0 & 0 & 0 & 0 & 0 & 1 & 0 & 0 & 0 & 0 \\ 0 & 0 & 0 & 0 & 0 & 0 & 1 & 0 & 0 & 0 \\ 0 & 0 & 0 & 0 & 0 & 0 & 0 & 1 & 0 & 0 \\ C_1 & C_2 & C_3 & C_4 & C_5 & C_6 & C_7 & C_8 & C_9 & C_{10} \\ 0 & 0 & 0 & 0 & 0 & 0 & 0 & 0 & 0 & 1 \\ D_1 & D_2 & D_3 & 0 & D_4 & D_5 & D_6 & 0 & D_7 & D_8 \end{bmatrix} \begin{Bmatrix} u_1 \\ u_2 \\ u_3 \\ u_4 \\ v_1 \\ v_2 \\ v_3 \\ v_4 \\ \theta_1 \\ \theta_2 \end{Bmatrix} + \begin{Bmatrix} 0 \\ 0 \\ 0 \\ B_{11} \\ 0 \\ 0 \\ 0 \\ C_{11} \\ 0 \\ D_9 \end{Bmatrix} \quad (3.114)$$

Similarly, the axial load equation of (3.107) (i.e., the 1<sup>st</sup>) contains 2<sup>nd</sup> order derivatives of  $N$  and was, therefore, reduced to two 1<sup>st</sup> order equations by the following substitution

$$\begin{aligned} N_1 &= N \\ N_2 &= N_{,1} = N_{1.1} \end{aligned} \quad (3.115)$$

The second system of equations became

$$\begin{Bmatrix} N_{1.1} \\ N_{2.1} \end{Bmatrix} = \begin{bmatrix} 0 & 1 \\ A_1 & A_2 \end{bmatrix} \begin{Bmatrix} N_1 \\ N_2 \end{Bmatrix} + \begin{Bmatrix} 0 \\ A_3 \end{Bmatrix} \quad (3.116)$$

The coefficients  $B_1$ ,  $B_2$ , etc. for equations (3.114) and (3.116) are available in Appendix H.

For a solution, equation (3.114) required values for the axial load  $N$  and its derivatives, whereas equation (3.116) required values for the displacements  $u$ ,  $v$  and  $\theta$  plus the derivatives. Therefore, the solution scheme involved guessing values for the axial load, solving equation (3.114) for  $u$ ,  $v$  and  $\theta$  and then solving equation (3.116) for  $N$ . The output of one equation, therefore, served as the input to the other till convergence was achieved.

The other nonlinearity involving products of the displacements was solved by embedding the problem in a family of solutions which proceeded from the linear to the nonlinear case. The terms involving nonlinearities were multiplied by a factor  $C_{NL}$  and the solution proceeded from  $C_{NL} = 0.0$  to  $C_{NL} = 1.0$ , using the previous solution as guesses.

For the parametric analysis, the equations were solved using the scheme described above. For the explicit analysis of the adolescent growth spurt, a further loop was added in order to determine the model predictions during the years of growth. At each growth increment, the properties and loads were updated and the solution for  $N$ ,  $u$ ,  $v$  and  $\theta$  from the previous age was used as the initial configuration. A flow chart of the overall solution procedure is shown in Fig. 3.13.

### 3.5 Spinal Column Loads

In the present study, the spinal column was subjected to loads which originated from two separate sources: the applied body weight of the upper torso, and the passive reactions of the ribcage generated in response to the progression of a scoliotic spine. The ribcage loads are discussed separately in the final sections of Chapter 4, since they are determined from the FEM analysis of the ribcage. In this section, only the loads due to the applied body weight are considered.

The body weight was modelled as a distributed force,  $f_z^w$ , in the vertical direction,  $\hat{i}_1$ , of the fixed system. The body weight was assumed to act independent of the displacement of the spinal column. However, the body weight was considered to be offset from the vertical axis of the spine in the anterior direction. The potential of an offset in the lateral direction was also incorporated into the model. It is understood that possibly the body weight applied to a scoliotic spine might behave more like a follower force. In particular, as the vertebrae are rotated in a scoliotic spine during progression, the torso is also rotated to a certain degree. Therefore, the location of the centre of mass of the torso would change and the line of action of the body weight would be dependent on the spine motion. However, though the rotation of the ribcage and torso is moderately correlated to the axial rotation

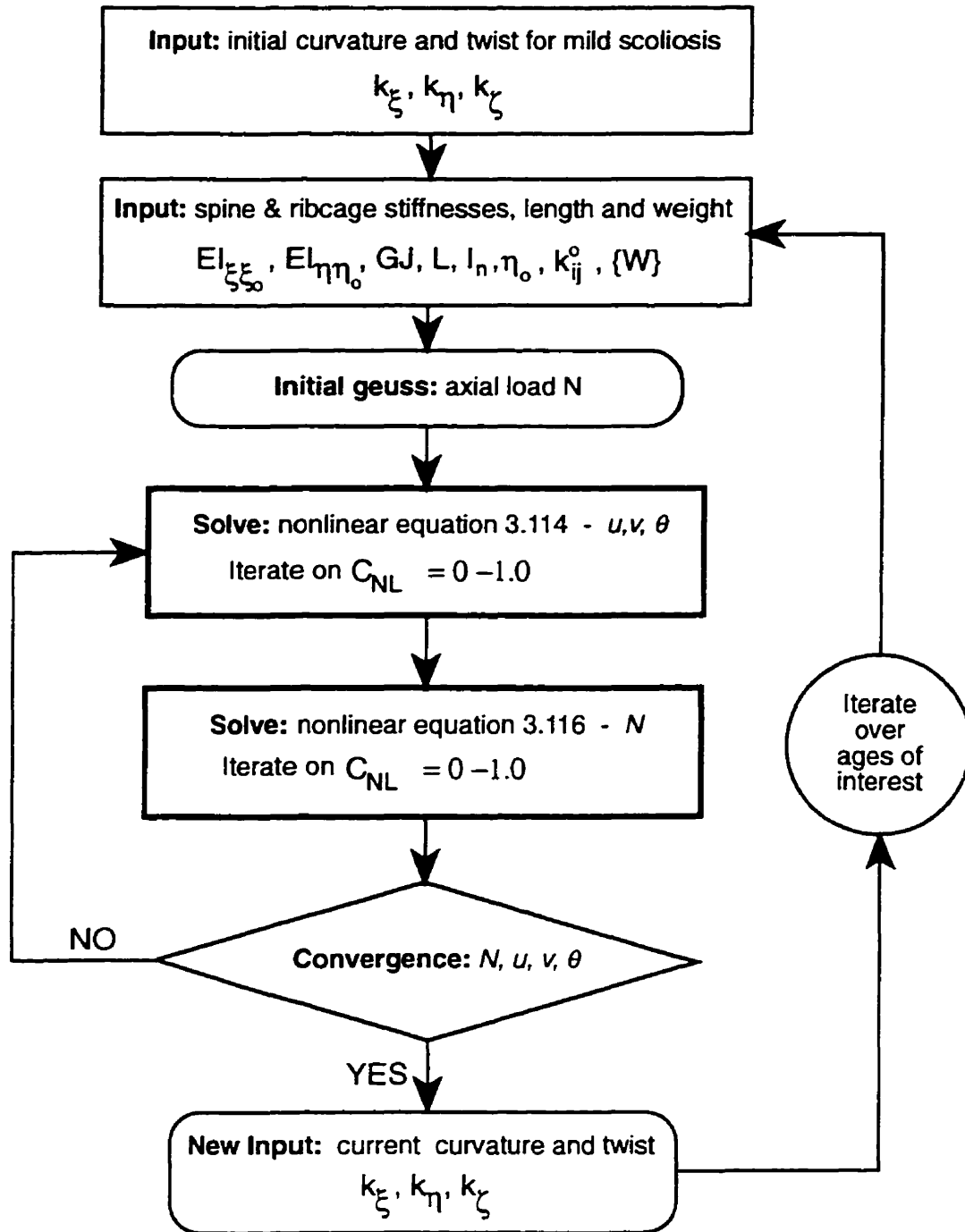


Figure 3.13: Flowchart of the overall solution procedure. Note that of the solution of each set of nonlinear 1<sup>st</sup> order equations involved a further loop which proceeded from a solution of the linear equations first, and then to the full nonlinearity using the previous step as a guess. Also, for the parametric analysis only the loop to solve both sets of nonlinear equations was performed.

of the spine in scoliosis, the exact relationship can be quite variable between patients (Aaro and Dahlborn, 1981; Closkey and Schultz, 1993). Furthermore, the top of the spine is usually only offset laterally a small amount relative to the bottom, and most of the torso is still predominantly centred over the pelvis, as in a normal spine. Also, the present model is only concerned with a mild scoliosis where the offsets of the torso are much less than in a large deformity. Therefore, it was felt reasonable to consider that the line of action of the body weight was independent of the spinal column displacements.

The distributed forces and moments of the applied body weight,  $\hat{f}^w$  and  $\hat{m}^w$ , which act at the point  $G_w < e_x, e_y >$  in the horizontal plane of the fixed system, can be expressed as follows:

$$\begin{aligned}\hat{f}^w &= -f_z^w \hat{i}_1 \\ \hat{m}^w &= -f_z^w e_y \hat{i}_2 + f_z^w e_x \hat{i}_3\end{aligned}\quad (3.117)$$

where  $f_z^w$  has been assumed to act in the negative  $\hat{i}_1$  direction.

In order to incorporate these forces and moments of the applied body weight into the governing equations, they must be related to the applied forces and moments in the undeformed coordinate system, in which the equations were originally resolved. This can easily be achieved through two steps. First, the moment equation of (3.117) must be modified to include the effect of the initial displacements, and secondly, the forces and moments must be rotated from the fixed to the undeformed system. The displacements of the spine in the initial configuration were originally defined in equation (3.19). In the horizontal plane of the fixed system, the elastic axis of the beam-column in the initial configuration is located at  $< u_0, v_0 >$  for a given point along the axis. Therefore, equation (3.117) is modified as follows:

$$\begin{aligned}\hat{f}^w &= -f_z^w \hat{i}_1 \\ \hat{m}^w &= -f_z^w (e_y - v_0) \hat{i}_2 + f_z^w (e_x - u_0) \hat{i}_3\end{aligned}\quad (3.118)$$

where  $\hat{m}^w$  is still resolved in the fixed system, but now acts about the origin of the initial configuration or undeformed system (Fig. 3.14), and  $\hat{f}^w$  remains the same.

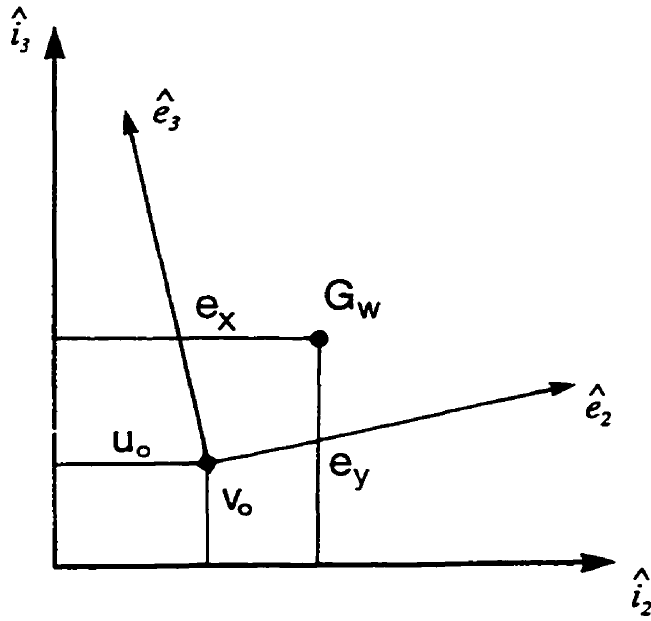


Figure 3.14: Location of the line of action of the body weight in the fixed system.

The force,  $\hat{f}^w$ , and the moment,  $\hat{m}^w$ , must now be resolved in the undeformed system through the rotation matrix  $C_{ij}^o$  (introduced in equation (3.20)), which relates the undeformed system,  $\hat{e}_i$ , to the fixed system  $\hat{i}_j$ . Therefore, the loading due to the applied body weight given in equation (3.118) can be expressed in the undeformed system using equation (3.20) as follows:

$$\begin{aligned}
 \hat{f}^w &= -f_z^w (C_{11}^o \hat{e}_1 + C_{21}^o \hat{e}_2 + C_{31}^o \hat{e}_3) \\
 \hat{m}^w &= -f_z^w [(C_{12}^o (e_y - v_0) - C_{13}^o (e_x - u_0)) \hat{e}_1 \\
 &\quad + (C_{22}^o (e_y - v_0) - C_{23}^o (e_x - u_0)) \hat{e}_2 \\
 &\quad + (C_{32}^o (e_y - v_0) - C_{33}^o (e_x - u_0)) \hat{e}_3] .
 \end{aligned} \tag{3.119}$$

The components of the rotation matrix,  $C_{ij}^o$ , have not been explicitly expressed up to this point. The initial curvatures and twist have, however, been restrained to moderate rotations similar to the deformed curvatures and twist. Therefore, the matrix,  $C_{ij}^o$ , can now be expressed in terms of moderate rotations similar to  $C_{ij}^*$ . Equation (3.34) for  $C_{ij}^*$  can easily be modified to determine an expression for  $C_{ij}^o$  by simply dropping the initial curvatures and twist from the  $d_i$  variables, and replacing  $u$ ,  $v$  and  $\theta$  by  $u_0$ ,  $v_0$  and  $\theta_0$ . The rotation matrix,  $C_{ij}^o$ , can be expressed in terms of the initial displacements for moderate

initial rotations as follows:

$$C_{ij}^o = \begin{bmatrix} 1 & u_{0.1} & v_{0.1} \\ -(u_{0.1} + \theta_0 v_{0.1}) & 1 & \theta_0 \\ -(v_{0.1} - \theta_0 u_{0.1}) & -(\theta_0 + u_{0.1} v_{0.1}) & 1 \end{bmatrix}. \quad (3.120)$$

Inserting equation (3.120) into (3.119), the components of the forces and moments of the applied body weight in the undeformed system are given by

$$\begin{aligned} f_1^w &= -f_z^w \\ f_2^w &= f_z^w (u_{0.1} + \theta_0 v_{0.1}) \\ f_3^w &= f_z^w (v_{0.1} - \theta_0 u_{0.1}) \end{aligned} \quad (3.121)$$

and

$$\begin{aligned} m_1^w &= f_z^w ( (e_x - u_0) v_{0.1} - (e_y - v_0) u_{0.1} ) \\ m_2^w &= f_z^w ( (e_x - u_0) \theta_0 - (e_y - v_0) ) \\ m_3^w &= f_z^w ( (e_x - u_0) + (e_y - v_0) \theta_0 + e_y u_{0.1} v_{0.1} ) \end{aligned} \quad (3.122)$$

or

$$\{\mathcal{W}\} = \begin{Bmatrix} f_1^w \\ f_2^w \\ f_3^w \\ m_1^w \\ m_2^w \\ m_3^w \end{Bmatrix} \quad (3.123)$$

which are valid for moderate initial rotations. The coordinates  $e_x$  and  $e_y$  can assume any value, provided the rotations do not become large.

Therefore, the applied body weight is now expressed in the undeformed system and can easily be incorporated into the governing equations through the components  $f_i$  and  $m_i$ . It should be noted that the components  $f_i^w$  and  $m_i^w$  are functions of the position along the

spine length. The applied body weight  $f_z^w$  can vary over the spine length, as can its point of application  $G_w < e_x, e_y >$  in the global system. Similarly, the initial displacements  $u_0$ ,  $v_0$  and  $\theta_0$  which represent the normal sagittal shape of the spine and the scoliotic deformity are not, in general, constant along the spine length.

The applied body weights of a young adult male and female (19-35 years old) were determined from extensive published data gathered between the 1930-1970's from the populations of Western societies (Western European, North American and Australian) (Tanner et al, 1965; McCammon, 1970; Eveleth and Tanner, 1976; Bayer and Bayley, 1976). The average weight of an adult was found to be 635 N (male - 690 N; female - 580 N). It is recognized that in any given population there are large variations in weight, and that variations in the means between Western countries also exist, nonetheless, the average weight between all of these studies was very consistent ( $\pm 1$  standard deviation  $< 1.5\%$ ). The total upper body weight of the trunk, arms and head was determined to be 64% of the total body weight (Ruff, 1950; Barter, 1957; Clauser et al, 1969), similar to that used by other authors (Takashima et al, 1979; Wong, 1979; Miller and Skogland, 1980c; Haderspeck and Schultz, 1981; Gross et al, 1983). This upper body weight was then distributed over the spine at each of the vertebral levels from T1 to L5, with the weight of the head and neck applied at T1, and the weight of the upper extremities distributed over T2 to T4, as in other models (Takashima et al, 1979; Haderspeck and Schultz, 1981; Scholten, 1986). The distributed weight at each spine level was converted to per unit length based on the intervertebral lengths (see Section 3.6). A different load distribution was used in the model of Miller and Skogland (1980c), where only the weight above T11 ( $\sim 40\%$  bodyweight) was applied to the spine distributed over the thoracic region. However, in preliminary investigations, the spinal displacements were found to be very similar for both of these load distributions for a spine with a fixed boundary condition at the bottom. The loads in the lumbar region remained nearly axial with very little bending moments, and therefore, the lateral displacements were minimally effected by the lumbar component of the body weight. The actual weight carried by the spine is probably somewhere between these two distributions.

The distributed upper body weights were applied at the centre of mass at each level of the spine as in previous models (Orne and Liu, 1971; Cramer et al, 1976; Takashima et al, 1979; Haderspeck and Schultz, 1981; Miller and Skogland, 1980c; Scholten, 1986; Kiefer et al, 1994). This position was located in the mid-sagittal plane, offset anterior to the vertebral centres by  $\Delta_g$ . Based on a recent study, the centre of mass in the male model was located 10 mm more anterior compared to the female (Pearsall and Reid, 1992). In Table 3.1, the distributed body weights and locations of the centres of mass used in the present model are presented for the seventeen levels of the spine.

## 3.6 Spinal Column Geometry

In this section, the variables and data used to describe the geometry of the spinal column are presented. First, the geometry of a normal spine for both an adult female and male is described, followed by the geometry of an initial mild scoliotic deformity. The variation of this geometry during the adolescent growth spurt is described in Section 3.10.

### 3.6.1 Normal Adult

To describe the geometry of the spinal column for the present beam-column model, a number of parameters were needed, which varied along the spine length. These were the location of the spinal axis in the sagittal plane ( $v_0$ ), the curvature in the sagittal plane ( $k_\xi$ ) and its derivatives, the position of the centres of the vertebral bodies relative to this axis ( $\eta_0$ ), the axial lengths between vertebral centres ( $l_n$ ), the representative cross-sectional dimensions for the width ( $b_n$ ) in the coronal plane and the depth in the sagittal plane ( $d_n$ ) of the vertebrae, and the vertical spine height ( $L$ ). The anthropometric data is described below and summarized in Table 3.2.

The “S” shape *curvature of the spine in the sagittal plane* has been quantified by the total included angle of the thoracic kyphosis, and the total included angle of the lumbar lordosis. These angles have been determined with noninvasive techniques which measured the back profile (Willner and Johnson, 1983; Carr et al, 1989a, 1991; Mellin and Poussa,

Table 3.1: The distributed body weights and locations of the centres of mass in an adult male and female as used in the present model.

Spine Level	Segmental Body Weight* (N)		Location of Centre of Mass ( $\Delta_g$ ) <sup>†</sup> (mm)	
	Male	Female	Male	Female
T1-T2	74	65	10.0	0
T2-T3	37	30.5	15.0	5.0
T3-T4	36	30	19.5	9.5
T4-T5	35	30	26.5	16.5
T5-T6	24	20	34.0	24.0
T6-T7	20	17	42.0	32.0
T7-T8	18	15	49.0	39.0
T8-T9	18	15	54.0	44.0
T9-T10	17	14	55.5	45.5
T10-T11	17	14	56.0	46.0
T11-T12	19	15.5	55.0	45.0
T12-L1	20	16.5	52.0	42.0
L1-L2	20	16.5	47.0	37.0
L2-L3	20	16.5	41.0	31.0
L3-L4	20	16.5	33.0	23.0
L4-L5	20	16.5	25.0	15.0
L5-S1	20	16.5	18.0	8.0

\* The body weight load per unit length ( $f_z^w$ ) was determined from these values based on the intervertebral lengths ( $l_n$ ) presented in Table 3.2.

† The anterior location of the centre of mass relative to the vertebral centre which was located at  $\langle 0, \eta_0 \rangle$ . Therefore, the location of the centre of mass in the fixed system was at  $\langle 0, \Delta_g + \eta_0 + v_0 \rangle$ , which meant that  $e_y - v_0 = \Delta_g + \eta_0$  in equation (3.122).

1992) and more directly from x-rays (Fons et al, 1980; Stagnara et al, 1982). Based on these results, the angle of thoracic kyphosis in the model was  $37^\circ$  and the angle of lumbar lordosis was  $50^\circ$  in both male and female adults. Some noninvasive type studies suggested a greater lordosis and lesser kyphosis in females (Willner and Johnson, 1983; Mellin and Poussa, 1992), which was not supported by an x-ray study (Stagnara et al, 1982). These discrepancies may have been due to the different techniques, since the noninvasive techniques tended to under predict the lordosis due to skin artifacts (Willner, 1981). Two other angles were also used to establish the shape. The tangent to the sagittal curve at the bottom was about  $32^\circ$  to the vertical, and at the top the tangent was about  $12^\circ$  to the vertical (Stagnara et al, 1982; Bernhardt and Bridwell, 1989). To represent this sagittal shape of the thoracolumbar spine, a 5<sup>th</sup> order polynomial was used similar to Cramer et al (1976) who used a 6<sup>th</sup> order polynomial to model the whole spine shape, including the cervical region. The top of the spine at the centre of vertebra T1 was assumed to be vertically aligned with the bottom at the L5-S1 motion segment, and a vertical line from L5-S1 to T1 was also assumed to pass through the T12-L1 level (this vertical position is described below). This sagittal alignment of T1 relative to L5-S1 has been used in most models (Schultz et al, 1972; Takahashi et al, 1979; Schultz et al, 1981; Scholten, 1986; Kiefer et al, 1995), though in others, T1 was slightly posterior (Orne and Liu, 1971; Cramer et al, 1976; Miller and Skogland, 1980c), and in others, the anterior-posterior position of T1 was studied as a variable (Schultz et al, 1981; Kiefer et al, 1994). In anatomy texts, T1 and L5-S1 were described to be in sagittal alignment (Grant, 1978; Gray, 1989), though a recent experimental study suggested that in adolescents there was an anterior offset of T1 relative to L5-S1 (Pearsall and Reid, 1992). Based on these constraints, it was then possible to determine the coefficients of the polynomial to represent the sagittal curve. The initial sagittal curvature and its derivative were then easily determined from the polynomial.

The 17 thoracolumbar vertebrae were characterized by *three dimensions of the vertebral bodies*; the width ( $b_n$ ), the depth ( $d_n$ ) and the height ( $h_n$ ). These dimensions were the average values obtained from a number of anthropometric studies, again based on populations from Western societies (Huber, 1930; Berry et al, 1987; Scoles et al, 1988; Panjabi

et al, 1991; Panjabi et al, 1992). Though techniques and definition of dimensions were somewhat varied, there was still remarkable consistency between the studies. For instance, the earlier data of Huber (1930) and the most recent data of Panjabi et al (1991, 1992) were very similar at all spine levels. Also, the average weight of 657 N and the average height of 167.8 cm in the subjects (average age: 46.3 years; range: 19-59 years) of the studies of Panjabi et al (1991, 1992) was very similar to the data used in the present model (weight - 635 N; height - 168.5 cm). The subjects of the study by Scoles et al (1988) were young males and females (20-40 years) from an extensive collection of skeletons collected between 1893 and 1938. The subjects for Berry et al (1985) were males and females taken from the same collection with an older age range of 50-70 years. Therefore, though the vertebral dimensions were determined from studies conducted over a longer time span than the studies used for other data, the consistency of the data provided confidence that these vertebral dimensions would correspond with the other anthropometric data. These data were all averaged to establish the dimensions of an "ideal" adult for model validation. However, other studies, which have not measured the dimensions of all vertebrae, have shown that in both the lumbar and thoracic regions the vertebrae in males and females were very different, both in total size and in the ratios of the dimensions (Brandner, 1970; Skogland and Miller, 1981; Schultz et al, 1984; Taylor and Twomey, 1984; Veldhuizen et al, 1986; Scoles et al, 1988; Gilsanz et al, 1994, 1994a). The results of these studies were used to scale the average data at all levels and establish the vertebral geometries of a male and female adult.

The *heights of the intervertebral discs* were specified as a fraction (0.3 - 0.45) of the adjacent vertebrae based on reported data (Todd and Pyle, 1928; Brandner, 1970; Taylor, 1975). The distances between vertebral centres ( $l_n$ ) were then calculated as the disc height plus half the vertebral height of each of the adjacent vertebrae. The summation of the 17 values for  $l_n$  gave the spine length along the sagittal curve, which was about 1.3% longer than the vertical height. The average spine length from the superior surface of T1 to the superior surface of S1 was 485 mm in the adult male and 448 mm in the adult female, with an average of 467 mm in the present model. The average vertical height was about 462

mm. Direct measurement of the vertical spine height from the middle of T1 to L5 in nine adults (male and female) was reported to be about 411 mm by Halsall (1980) and Halsall et al (1983), which was about 5% smaller than the present value of about 430 mm. Taylor and Twomey (1984) reported the vertical spine height from T1 to L4 to be 400 mm in females and 432 mm in males at adulthood. This corresponded very well with the current model values of 401 mm and 436 mm for females and males, respectively. The vertical height of the present adult model was about 7% smaller than that of Schultz et al (1973).

The *standing height* of a young adult male and female (19-35 years old) has been reported to be 175 cm and 162 cm, respectively (Tanner et al, 1965; McCammon, 1970; Eveleth and Tanner, 1976; Bayer and Bayley, 1976). Again, these data were representative of an average adult from Western society. The sitting height of adult males and females was reported to be 90.6 cm and 85.5 cm, respectively (Anderson et al, 1965; McCammon, 1970; Eveleth and Tanner, 1976). Therefore, the vertical height of the spine in the present model was 27.4% of the standing height and 52.8% of the sitting height in adult males, whereas in adult females, the spine height was 27.3% of the standing height and 51.7% of sitting height. Adult males have longer legs than females, but have a shorter pelvis, which explains why the spine length as a portion of standing height was similar in males and females, but differed slightly when expressed as a portion of the sitting height (Tanner, 1962; Anderson et al, 1965; McCammon, 1970; Karlberg and Taranger, 1976; Nicolopoulos et al, 1985). This reflects the data that the sitting height divided by the standing height is slightly greater in females. These values for the spine height as a percentage of the standing height were identical to that used by Gross et al (1983). Therefore, the present approach of determining the spine height as a summation of the heights of the vertebrae and discs resulted in excellent agreement with other independent measures, and determined the spine length as a fraction of the standing height.

As summarized by White and Panjabi (1990), the *centre of rotation* of the motion segment during axial rotation is posterior to the vertebral centres in the sagittal plane. This is largely due to the orientation of the facet joints. In the lumbar spine, the facet joints resist axial rotation very effectively, and consequently the centre of rotation is quite

posterior to the vertebral centres. In the thoracic spine, the facet joints are much less effective and the centre of rotation is closer to the vertebral centres. In a finite element analysis of the lumbar motion segment, Shirazi-Adl et al (1986a) showed that the centre of rotation was about 12 mm posterior to the vertebral centre, which agreed with earlier experimental work (Gregerson and Lucas, 1967; Cossette et al, 1971). In the thoracic spine, the centre of rotation was about 6 mm posterior (Gregerson and Lucas, 1967; White and Panjabi, 1990). These values were used for the parameter  $\eta_0$  in the thoracic and lumbar regions, with a transition zone from T10-L1. It is recognized that the centre of rotation of a motion segment is not constant during motion. However, this approach captured the primary effect that the centre of rotation was posterior to the vertebral centres.

### 3.6.2 Mild Scoliotic Deformity

Scoliosis is a three-dimensional deformity of the spine involving lateral and sagittal translations, as well as axial rotation of the vertebrae. In recent years, there have been increased attempts to develop a 3-D measure of the scoliotic curve to better represent the true geometry. However, there has yet to be the widespread acceptance of a single 3-D measure. The use of the Cobb angle in the coronal plane remains the most commonly used measure of a scoliotic curve, in conjunction with the lateral deviation and axial rotation at the apical vertebra. The strong correlation between the Cobb angle and the apical axial rotation, as well as the apical lateral translation has been reported by a number of authors (Aaro and Dahlborn, 1981; De Smet et al, 1984; Stokes et al, 1987; Drerup and Hierholzer, 1992; Kanayama et al, 1996). A scoliotic curve was also shown to be smooth, and could be represented by sinusoidal or polynomial curves (Stokes et al, 1987; Drerup and Hierholzer, 1992; Kanayama et al, 1996). Therefore, in the present study, similar to Kanayama et al (1996), 5<sup>th</sup> order polynomials were used to represent an initial mild scoliotic deformity. A thoracic scoliosis was initially created which spanned T5 to T12 with an apical vertebra at T9. Initial scoliotic curves with Cobb angles defined in the coronal plane of 10°, 20° and 30° were studied. The magnitude of axial rotation at the apical vertebra has been reported to be in the range of 0.31-0.39 times the Cobb angle (Aaro and Dahlborn, 1981; De Smet et al,

Table 3.2: Anthropometric data of an adult male and female for input to the spinal column model.

Spine			Male			Female		
Level	$n$	$\eta_0$	$b_n$	$d_n$	$l_n$	$b_n$	$d_n$	$l_n$
T2-T1	17	6.0	28.0	18.0	29.0 <sup>†</sup>	25.0	16.0	26.9 <sup>†</sup>
T3-T2	16	6.0	28.0	19.0	22.4	25.0	17.0	20.8
T4-T3	15	6.0	27.7	20.6	23.1	24.7	18.4	21.4
T5-T4	14	6.0	27.5	23.3	23.5	24.5	18.4	21.7
T6-T5	13	6.0	27.8	25.4	23.8	24.8	20.7	22.0
T7-T6	12	6.0	28.6	26.8	24.4	25.4	23.8	22.7
T8-T7	11	6.0	30.1	28.3	25.0	26.8	25.2	23.2
T9-T8	10	6.0	31.7	29.6	25.8	28.3	26.4	23.9
T10-T9	9	6.0	33.3	30.9	27.3	29.7	27.5	25.2
T11-T10	8	6.0	36.0	31.7	28.8	32.0	28.3	26.7
T12-T11	7	7.5	38.6	32.6	30.6	34.4	29.0	27.9
L1-T12	6	9.5	41.8	33.3	32.4	37.2	29.7	29.6
L2-L1	5	11.0	44.4	34.2	34.8	39.6	30.4	32.0
L3-L2	4	12.0	47.6	34.9	36.2	42.4	31.1	33.6
L4-L3	3	12.0	49.7	35.9	36.8	44.3	31.9	34.0
L5-L4	2	12.0	51.3	36.5	37.3	45.7	32.5	34.5
S1-L5	1	12.0	52.9	36.9	23.5 <sup>*</sup>	47.1	32.9	21.7 <sup>*</sup>

• All dimensions given in mm.  $\eta_0$  was assumed to be identical for male and female.

\* These dimensions were from the vertebral centre of L5 to the superior surface of S1.

† These dimensions were from the vertebral centre of T2 to the superior surface of T1.

1984; Stokes et al, 1987; Kanayama et al, 1996). Therefore, in the present model, for each of the initial Cobb angles investigated, the corresponding initial apical rotation was 0.35 times the Cobb angle, with the spinous processes rotated into the concavity. With these conditions, and the restraints of zero rotation and deviation at the top and bottom, the coefficients of the polynomials to represent the scoliotic curve were determined. The present study only considered a thoracic scoliosis and also did not consider initial abnormalities in the thoracic kyphosis of the spine as part of the scoliotic curve. Considerable controversy exists around whether the thoracic kyphosis is also disrupted in scoliosis (as outlined in Appendix B). Future studies can investigate other scoliotic curve patterns and the role of the thoracic kyphosis. At present, however, all model analyses were conducted on a thoracic scoliosis with an initial Cobb angle and apical axial rotation as described.

### 3.7 Spinal Column Material Properties

To specify the material properties of the spine, it was necessary to determine the following "effective" stiffnesses:  $EI_{\xi\xi_0}$ ,  $EI_{\eta\eta_0}$  and  $GJ$ . These stiffnesses were termed effective as they were intended to represent the whole motion segment stiffness due to the net contributions of the disc, ligaments and facet joints. The load-displacement response of the motion segments has been shown to vary over the spine length (White and Panjabi, 1990), and therefore these effective stiffnesses should also vary. A very extensive series of studies have been performed by many authors to establish the load-displacement response of the motion segment in the lumbar and thoracic spine. White and Panjabi (1990) have reviewed all these studies and summarized the results to establish average stiffness coefficients for the various regions of the spine. Based on these results, the effective stiffnesses of the thoracic and lumbar regions were calculated using the intervertebral lengths of the T6-T7 and L3-L4 motion segments (see Section 3.6) and are presented in Table 3.3.

The effective lateral bending stiffness ( $EI_{\eta\eta_0}$ ) determined by this procedure was in excellent agreement with the range of bending stiffness (1.5 - 7 Nm<sup>2</sup>) used by other continuum spine models (Lindbeck, 1985, 1987, 1988; Patwardhan et al. 1986; Hjalmar, 1988; Noone

Table 3.3: The average stiffness coefficients and calculated effective stiffnesses of the thoracic and lumbar regions of an adult.

		Thoracic Region*	Lumbar Region†
Axial	K (Nm/deg)**	2.53	5.00
Torque	GJ (Nm <sup>2</sup> )	3.3	10.0
Lateral	K (Nm/deg)	2.80	1.75
Bending	$EI_{\eta\eta_0}$ (Nm <sup>2</sup> )	3.7	3.5
Flexion/	K (Nm/deg)	2.51	1.72
Extension‡	$EI_{\xi\xi_0}$ (Nm <sup>2</sup> )	3.3	3.45

\*\* The K's were the stiffness coefficients reported by White and Panjabi (1990).

\* The calculation of the thoracic effective stiffnesses was based on the intervertebral length of T6-T7.

† The calculation of the lumbar effective stiffnesses was based on the intervertebral length of L3-L4.

‡ Note that the flexion and extension stiffnesses reported by White and Panjabi (1990) were combined.

et al. 1991). However, the stiffnesses used in these models were only determined in an adhoc procedure by adjusting the stiffnesses until the models agreed with *in vivo* descriptions of spine deformation. The present approach to determine the effective stiffnesses from independent studies of the motion segments provided a more rigorous basis for these values. The bending stiffness of the spine in the sagittal plane (flexion/extension) of the discrete model of Belytschko et al (1973) and Schultz et al (1973) was in the range 0.5 - 3.5 Nm<sup>2</sup> (as discussed by Scholten, 1986), which was also in excellent agreement with the present values.

The load-displacement response of the motion segment has also been shown to be nonlinear at higher loads and moments. However, examining the results of these studies (Panjabi et al, 1976; Schultz et al, 1979; Nachemson et al, 1979; Tencer and Ahmed, 1981), the stiffness was linear up to about 4-5° of rotation (bending or axial). This is within the range of applicability of the present model. For example, for a Cobb angle of 40° spanning eight vertebra, the intervertebral angles would only be 5° and a linear stiffness response

would still be expected. Therefore, only linear stiffnesses were included in the present model to investigate the mechanics of a mild scoliosis. These stiffnesses reported by White and Panjabi (1990) were generally intended to represent the elastic behaviour beyond the initial toe-in region of low stiffness common to biological materials, yet below the higher strain range where significant stiffening can occur. Therefore, the model may be slightly too stiff for very small deformations, but should have a reasonable stiffness in the range of interest. A nonlinear stiffness as a function of curvature could be implemented in the developed equations in future studies. Similarly, the present model could also be extended to include the differences in the flexion and extension stiffnesses. However, in the range of flexion and extension rotations of the present model, the stiffnesses in these opposite senses were assumed to be identical. In more extreme conditions of flexion and extension, this assumption would not be valid.

The motion segments have also been shown to display coupled motion. In particular, a lumbar motion segment subjected to a lateral bending moment was also found to rotate axially. These coupled stiffnesses are second order terms compared to the principal stiffnesses (White and Panjabi, 1990), but are significant during testing of motion segments. However, at the whole spine level they are less significant since the sagittal curvature of the spine also plays a dominant role in coupling behaviour (Scholten, 1986; Panjabi et al, 1989; Stokes et al, 1991). In the present model, the axial rotation and the lateral bending were coupled due to the anterior offset ( $\eta_0$ ) of the centre of rotation from the vertebral centres, as well as the initial twist and curvature, as seen in equations 3.111-3.112. This overall coupling was related to the axial load on the spine, and did not represent a direct coupling between lateral bending and axial rotation. However, it would be possible to include this coupled behaviour at the motion segment level through a term  $I_{\zeta\eta}$  in equation 3.103. Similarly, the flexion/extension behaviour could also be coupled to the lateral bending through a term  $I_{\xi\eta}$ . Therefore, at present, the axial rotation and lateral bending were coupled only due to the term  $\eta_0$ , and the sagittal curvature of the spine ( $\nu_0$ ), although further coupling could be implemented in the equations.

The effective stiffnesses presented in Table 3.3 were used as the base stiffnesses for the

lumbar and thoracic regions to estimate stiffnesses at other levels. The variation in the stiffness with vertebral level was assumed to be related to the changes in vertebral and disc geometry outlined in Section 3.6. Assuming an elliptical cross-section for the disc, the bending stiffnesses were proportional to  $\frac{b_n^3 d_n}{l_n}$  or  $\frac{b_n d_n^3}{l_n}$ , and the torsional stiffness was proportional to  $\frac{b_n^3 d_n^3}{l_n (b_n^2 + d_n^2)}$ . The bending and torsional stiffnesses as a function of spine level are presented in Fig. 3.15. This technique was previously used in the model developed by Schultz et al (1973). Miller and Skogland (1980c) found strong negative correlations between vertebral body size and axial torsion and lateral bending. Nachemson et al (1979) found that the load-displacement response of lumbar motion segments was very variable, but that specimens from the upper lumbar regions were 20% stiffer in lateral bending and torsion than those from the lower lumbar region, possibly associated with the decreased disc height in the upper lumbar region. They also found that motion segments from females were about 25% more flexible than male, and attributed this difference to the reduced vertebral and disc dimensions of the female specimens, rather than to a difference in material properties. Therefore, on the basis of the different geometry between a female and male spine reported in Section 3.6, the effective stiffnesses of an adult female and male over the spine length were estimated from the base values and presented in Table 3.4. The stiffnesses representative of a female were found to be about 70% of the male values.

### 3.8 Validation Studies of the Spinal Column

To validate the present spine model and approach, several comparisons with experiment were made for model predictions of the axial rotation and lateral bending response of the spine with ribcage supported included, and for the buckling load of the isolated spine. Additional validation studies were conducted for the isolated ribcage, and these are described in Chapter 4.

Lovett (1905) subjected a *whole spine with ribcage to axial torque* and determined the variation of axial rotation of the spine from a maximum of 54° at the top to zero at the bottom. The torque applied was unknown. In the present model, an axial torque was

Table 3.4: Effective stiffnesses of an adult at all spine levels of the present model.

Spine Level	Male			Female		
	$EI_{\eta\eta_0}$ (Nm <sup>2</sup> )	$EI_{\xi\xi_0}$ (Nm <sup>2</sup> )	$GJ$ (Nm <sup>2</sup> )	$EI_{\eta\eta_0}$ (Nm <sup>2</sup> )	$EI_{\xi\xi_0}$ (Nm <sup>2</sup> )	$GJ$ (Nm <sup>2</sup> )
T1-T2	2.73	2.26	2.90	1.90	1.57	2.01
T2-T3	3.21	2.61	3.06	2.23	1.82	2.13
T3-T4	3.60	2.98	3.23	2.50	2.07	2.25
T4-T5	3.95	3.32	3.42	2.75	2.31	2.38
T5-T6	4.23	3.65	3.70	2.94	2.54	2.57
T6-T7	4.37	3.89	3.89	3.03	2.71	2.71
T7-T8	4.55	3.92	4.15	3.16	2.73	2.88
T8-T9	4.74	3.97	4.42	3.29	2.76	3.07
T9-T10	4.87	4.04	4.87	3.38	2.81	3.38
T10-T11	4.81	4.11	5.61	3.34	2.86	3.90
T11-T12	4.60	4.10	6.49	3.19	2.85	4.51
T12-L1	4.48	4.08	7.86	3.11	2.83	5.46
L1-L2	4.32	4.05	9.47	3.00	2.82	6.58
L2-L3	4.15	4.04	10.77	2.88	2.81	7.48
L3-L4	4.13	4.07	11.80	2.87	2.83	8.20
L4-L5	4.63	3.89	12.83	3.22	2.70	8.92
L5-S1	5.39	3.63	13.53	3.74	2.53	9.40

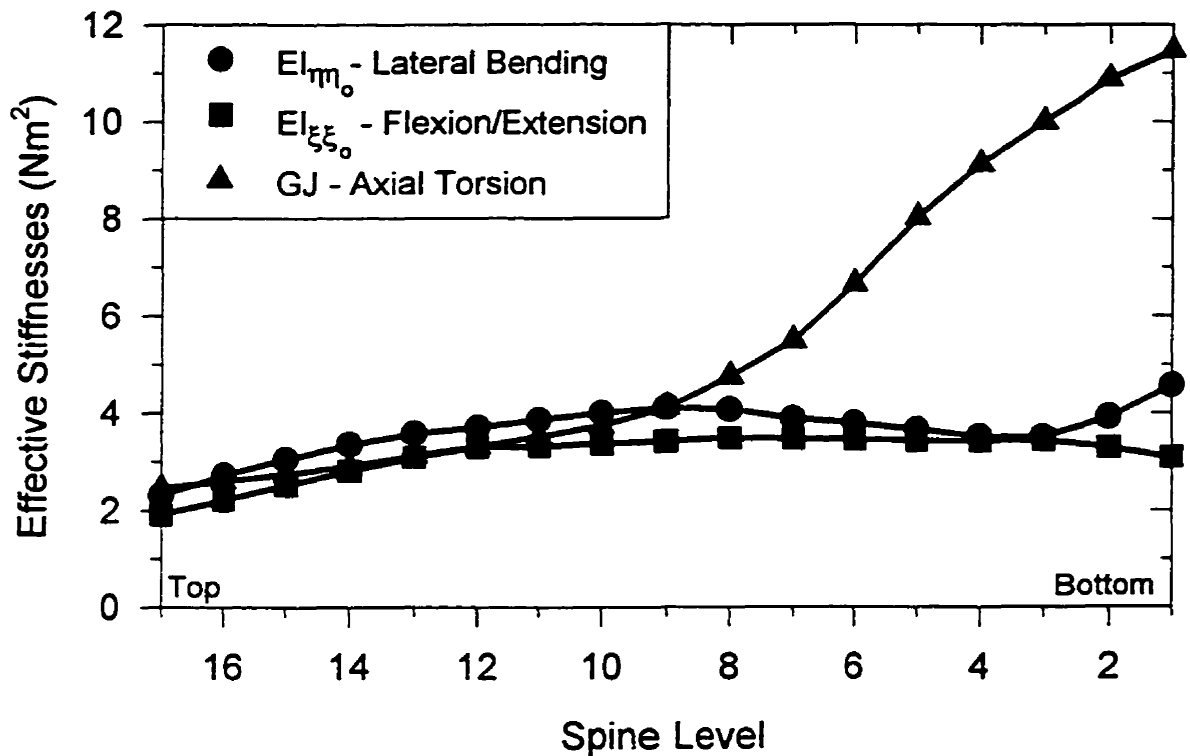


Figure 3.15: The average effective stiffnesses of an adult at each of the spine levels.

applied to the whole spine model at T1 until the maximum axial rotation matched that of the experiment. Comparisons were made with both the full 3-D ribcage stiffnesses included in the model and with all the stiffnesses except the lateral translational stiffness (see explanation and definition of these stiffnesses in Chapter 4).

Lucas and Bresler (1961) determined the *buckling load of an isolated spinal column* for a fixed bottom and free or pinned top. A buckling load of about 20 N was found for the free top, whereas a load of about 167 N was found for the pinned top. To simulate these experiments, a compressive axial load was applied at the top, with a very small lateral offset at T1. This imperfection was needed to provoke collapse of the model since a directly stability analysis was not done. The imperfection was only 0.1% of the spine height. This imperfection would also have been present in the experiment since the spinal column would not have been perfectly symmetric. The applied load at T1 was then increased in small increments until very large lateral displacements occurred.

The most important experiment for validation of the current model is that reported by Halsall (1980) and Halsall et al (1983). In this experiment, nine spines in whole fresh cadavers were subjected to a *lateral load applied at T9*. The top and bottom of the spine was clamped for a fixed-fixed beam bending experiment. The lateral load was applied slightly anterior to the spinal canal in one set of spines and slightly posterior in another set; which caused a coupled axial rotation in opposite senses in each set. The lateral flexibility at T9 was not significantly different between those two configurations with an average value of 0.1 mm/N for loads up to 250 N. This experiment was simulated by applying a 250 N load at T9 of the whole spine model with ribcage stiffnesses included (with/without the lateral translational stiffness). The load was applied at three different locations in the anterior-posterior direction: at the shear centre, 20 mm posterior and 6 mm anterior to the shear centre. The anterior and posterior positions were selected to represent the load application points in the experiment. This experiment provided ideal data to validate the combined lateral stiffness and rotational response of the whole spine model, in a configuration similar to scoliosis.

### **3.9 Procedure for Parametric Analysis of Whole Spine Model**

A set of seven parametric studies were conducted with the whole spine model to establish the relative effects of various parameters on the behaviour of the spinal column. Since progression of a scoliotic curve is defined as a 5 – 10° increase in Cobb angle (Lonstein and Carlson, 1984; Peterson et al, 1995; Upadhyay et al, 1995), the objective of this analysis was to establish the percentage change needed in the various parameters of the spine to produce a 5 – 10° change in Cobb angle. The base model was representative of a 9 year old female or 10-11 year old male. This age was chosen as the base since it represents the start of adolescence prior to the growth spurt. The effect of the growth spurt was analyzed through a separate and direct simulation (see Section 3.10). Since curves diagnosed at this age are most vulnerable to progression (Lonstein and Carlson, 1984), the goal was

to examine which anthropometric parameters were most critical to maintaining a stable non-progressive curve during the coming growth spurt. The body weight, spine length, and spine stiffnesses at this age are described in Section 3.10. The procedure to determine the ribcage stiffnesses at this age is described in Section 4.3.2.3. The mechanical properties and loads of this base model were then changed in small increments, while keeping all other parameters constant, until an increase in Cobb angle of greater than  $10^\circ$  was achieved. The seven parameters changed in the base model were: total upper body weight ( $W$ ), lateral bending stiffness ( $EI_{\eta\eta_0}$ ), torsional rigidity ( $GJ$ ), lateral translational stiffness of the ribcage ( $k_{11}^o$ ), lateral bending stiffness of the ribcage ( $k_{33}^o$ ), axial rotational stiffness of the ribcage ( $k_{66}^o$ ) and the spine length ( $L$ ). For each of these seven parametric studies, the analyses were repeated for an initial Cobb angle of  $10^\circ$ ,  $20^\circ$  and  $30^\circ$ , for a total of 21 separate studies. At each of these initial Cobb angles, there was an initial axial rotation of the apical vertebra, as described in Section 3.6.2. Though the effect of other parameters could also have been investigated, these were felt to be the most important, since they change with growth and are involved in the lateral and rotational response of the spine.

### 3.10 Simulation of Adolescent Growth Spurt

The spinal column and ribcage models were first developed to represent an “ideal” or “average” adult. These models were validated through comparison with experiments conducted on adults. To analyze the mechanics of an adolescent spine, these models were then systematically changed based on reported data in the literature. In this section, the changes to the body load, spine length and effective stiffnesses of the spinal column model required to simulate the adolescent growth spurt of a male and female are first described, followed by a description of changes made to simulate the accelerated growth patterns which have been reported in scoliotics, as outlined in Chapter 1. The changes required to model the adolescent ribcage are presented in Sections 4.4.2.1 and 4.4.2.3. A flowchart of this overall validation and analysis procedure is presented at the end of Chapter 4.

### 3.10.1 Normal Growth

The changes to the body weight and spine length during adolescence were taken from growth charts established in studies conducted between 1930 to 1970 on populations from Western societies (Tanner, 1962; Anderson et al, 1965; Tanner et al, 1966; McCammon, 1970; Bayer and Bayley, 1976; Eveleth and Tanner, 1976; Karlberg and Taranger, 1976; Tanner and Whitehouse, 1976; Lowrey, 1978). Though secular trends of an increased weight and height from the late 1850's to the 1950's are well documented (Tanner, 1962), the results of these studies from a more recent and shorter time range were found to be very consistent. The standard deviation of the average height and weight at a given age between these studies was always less than  $\pm 3\%$ . Tanner (1962) also reported that secular trends chiefly affected body size rather than the proportions, and that the increased weights and heights were present at all ages during adolescence. Secular trends in anthropometric data probably continue today as illustrated by Normelli et al (1985), who showed that the height and weight of Scandinavian children between 11 and 16 years of age was greater (2% for height at 16 years) compared to those found in earlier studies for a similar population (Willner, 1972; Karlberg and Taranger, 1976). Therefore, clearly care must be taken in using anthropometric data. For instance, the weight data from an earlier time range determined in the population of one country or ethnic group should not be combined with height data from more recent times of a different population. In the present study, by determining the average heights and weights from a broader spectrum of populations (though confined to Western societies to minimize variation) with overlapping time frames, these concerns were minimized. The drawback to this average cross-sectional approach was that care must be taken not to extrapolate these current results to a specific population with different anthropometric proportions. However, in the absence of longitudinal studies reporting all the anthropometric data needed, the use of a broad series of studies should limit any biasing of the model input data. These studies were also chosen because the time frame when they were conducted overlapped with the other studies used to establish vertebral dimensions and material properties (as described in other sections).

The *upper body weight* ( $W$ ) was determined to be 64% of the body weight and the *spine*

*height* ( $L$ ) was determined to be 27.5% of the standing height as discussed in Sections 3.5 and 3.6. These data are shown in Figs. 3.16 and 3.17, respectively, for a female and male from 9 to 18 years of age. These percentages were assumed to be constant at all ages. It is acknowledged that this may not be correct, but more detailed information to establish exact numbers as a function of age are not available. Since growth in standing height involves growth of the legs, pelvis, spine and head, it is difficult to more accurately establish the change in spine length as a percentage of the standing height. For instance, during adolescent growth, the legs grow slightly longer than the trunk, particularly in males (Tanner, 1962; McCammon, 1970; Karlberg and Taranger, 1976; Nicolopoulos et al. 1976). Therefore, if the spine length was assumed to be 27.5% of the standing height at adulthood, it may actually be closer to 28-29% at young adolescence. On the other hand, this change may be affected by the lack of growth in the head during adolescence, and the growth in height of the pelvis which may or may not differ between males and females (Anderson et al, 1965; Nicolopoulos et al, 1985). Therefore, because the spine length as a percentage of the standing height declines consistently from birth to maturity, the use of a constant number, which was established as a fraction of the adult height, should be conservative. Also, the peak increase of around 4% in height of the female spine compared to the male, between 12 and 13 years of age as used in the present model, was slightly less than the peak increase of around 6% reported in a separate study based on direct measurement of the spine height (Taylor and Twomey, 1984).

To determine the *effective stiffnesses* of an adolescent spine, both changes in the *material properties* and the *geometry* of an adolescent spine compared to those of an adult were included. The only reported data from young adolescent spines (11 year old boy and a 13 year old girl) is by Miller and Skogland (1980a), which suggests that the axial flexibility is twice as great as an adult and the bending flexibilities are 5 to 10 times greater. As argued by these authors (Miller and Skogland, 1980b), these differences were likely due to both geometry and material properties related to the increased hydration of the adolescent spine. The axial stiffness is proportional to the square of the cross-sectional dimension divided by the length ( $\sim E (b \times h)/L$ ) (Schultz et al, 1973). The reported vertebral dimensions

vertebral dimensions (Miller and Skogland, 1980b) of the 11 year old boy are only about 80% that of an adult (Berry et al, 1987; Scoles et al, 1988; Panjabi et al, 1991; Panjabi et al. 1992). Therefore, the axial stiffness should also be 80% of an adult or 25% more flexible ( $1/.8 \times 100$ ). The further increase in axial flexibility of the adolescent spine must be due to a decreased modulus around 60% of an adult spine to achieve the reported doubling of the axial flexibility ( $1/.6/.8 \times 100$ ). Similarly, the bending stiffnesses are proportional to the quadratic of the cross-sectional dimensions divided by the length ( $\sim E(b \times h^3)/L$ ), and therefore for adolescent dimensions only 80% of an adult, the bending flexibility should be increased by about 200% ( $1/.8^3 \times 100$ ). This again suggested that the modulus of an adolescent spine was around 20-40% of an adult spine to achieve the reported 5 to 10 fold increase in bending flexibility. Galante (1967) also reported a 50% reduction in stiffness of the annulus at childhood compared to adulthood. The decreased modulus of the adolescent spine was due possibly to increased hydration levels of the adolescent disc. The variation in disc hydration at different spine levels was also correlated to the variation in stiffness along the spine, indicating that disc hydration did affect the motion segment stiffness (Miller and Skogland, 1980b). This reduction of modulus is also consistent with reports of increased relaxation of the ligaments of young rabbits (Lam et al, 1993) which was related to an increased water content (Chimich et al, 1992). On the basis of these estimates, the "effective" modulus of the young adolescent motion segment was estimated to be only about 40% that of an adult. At other ages between young adolescence and adulthood, the reduction in modulus was determined from linear interpolation. Though the material properties could also be affected by the adolescent growth spurt, there was not enough data to establish this effect. On the basis of limited data, only a reasonable estimate for the maximum change in the material properties of the young adolescent compared to an adult was established. Further, since the adolescent growth spurt affects tissues differently throughout the body (Tanner, 1962), it was not possible to estimate how the growth spurt would affect the changes in material properties.

The *vertebral dimensions during adolescence* were determined from a number of studies which reported the growth of the vertebrae (Taylor and Twomey, 1984; Schultz et al, 1984;

Veldhuizen et al, 1986; Gilsanz et al, 1994). These studies do not provide comprehensive data of vertebral dimensions at all levels for all ages. However, they do provide data of the percentage increments in dimensions during adolescent growth of select thoracic and lumbar vertebrae for females and males. These data were then used to scale the vertebral dimensions of the present model which were determined from a more comprehensive data set. Then using the same technique used to scale the effective stiffness of an adult male and female, and the stiffnesses between levels (see Section 3.7), the effective stiffnesses were estimated for all ages during adolescence.

Combining these changes related to geometry and material properties, the net changes to the effective stiffnesses were determined for all ages during adolescence compared to adulthood. These effective stiffnesses as a function of age are shown in Fig. 3.18 for the T8-T9 spine level for both a male and female. At the other spine levels, the stiffnesses varied in a similar manner. At adulthood, the difference between males and females was greatest and agreed with the reported data of Nachemson et al (1979). Due to the earlier growth spurt of females, the stiffnesses were more similar in young adolescence. In later adolescence, the growth spurt of the males increased the stiffnesses. The vertebrae of a female spine are more slender compared to a male at all ages beyond 5 years, due to both greater heights and smaller widths (Taylor and Twomey, 1984). During adolescent growth, the width of female vertebrae do increase but never appear to exceed the widths of male vertebrae (Taylor and Twomey, 1984; Schultz et al, 1984; Veldhuizen et al, 1986; Gilsanz et al, 1994). Therefore, unless the material properties between males and females differed, it is very unlikely that the effective stiffnesses of a female spine could exceed those in a male. Overall, these data would suggest that a young adolescent spine would be about 6 times more flexible than an adult, which agreed with the experimental measurements of a 5-10 fold increase reported by Miller and Skogland (1980a).

### **3.10.2 Accelerated Growth in Scoliotics**

The adolescent growth of scoliotics has been reported to differ from normal controls as reviewed in Chapter 1. In general, scoliotics were found to be (2 - 4.5%) taller, particularly

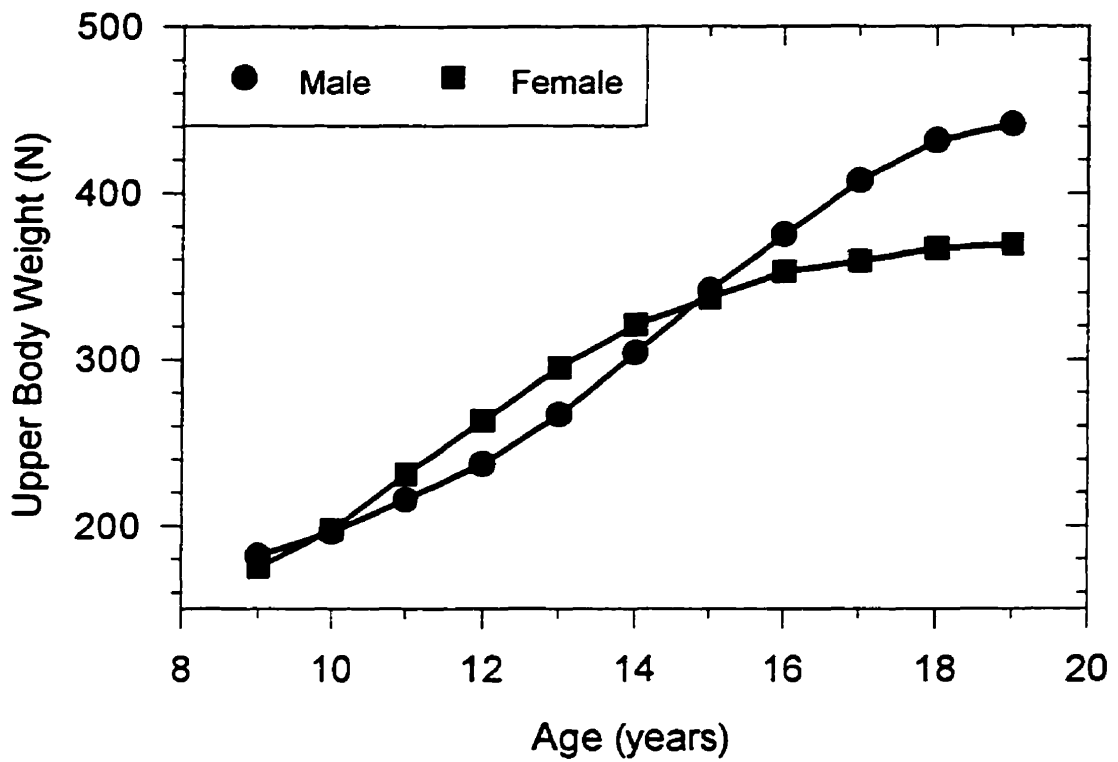


Figure 3.16: The upper body weight of a male and female from young adolescence to young adulthood.

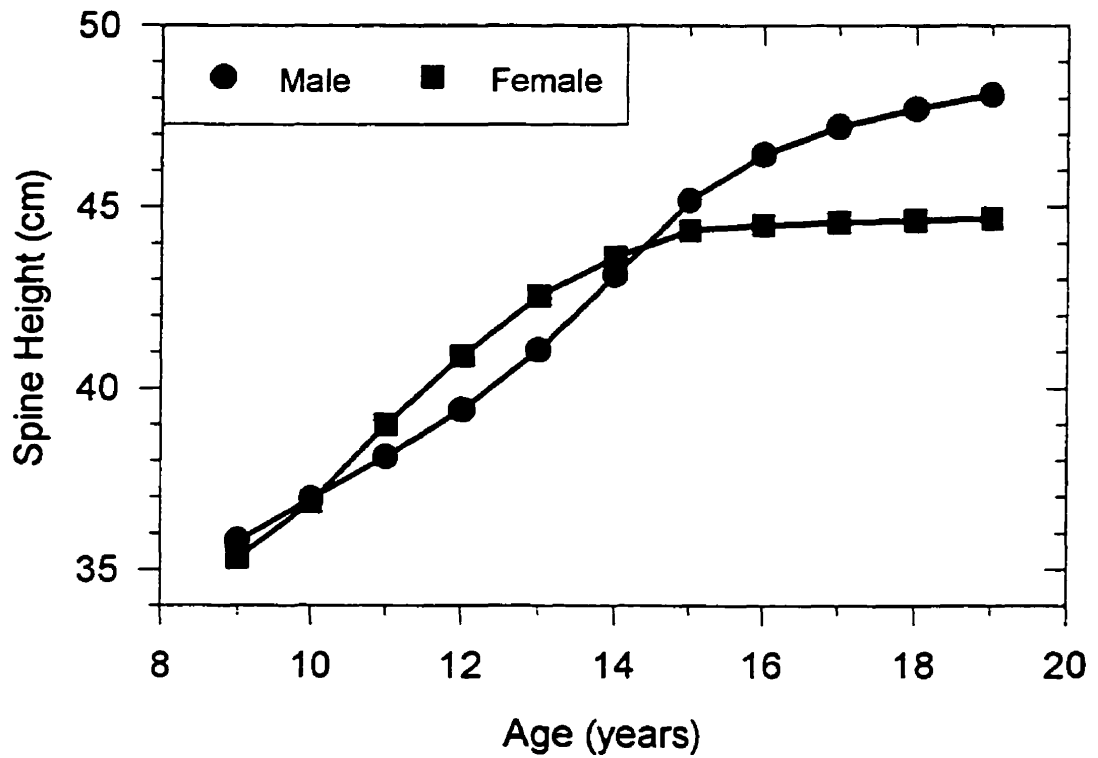


Figure 3.17: The vertical spine height of a male and female from young adolescence to young adulthood.

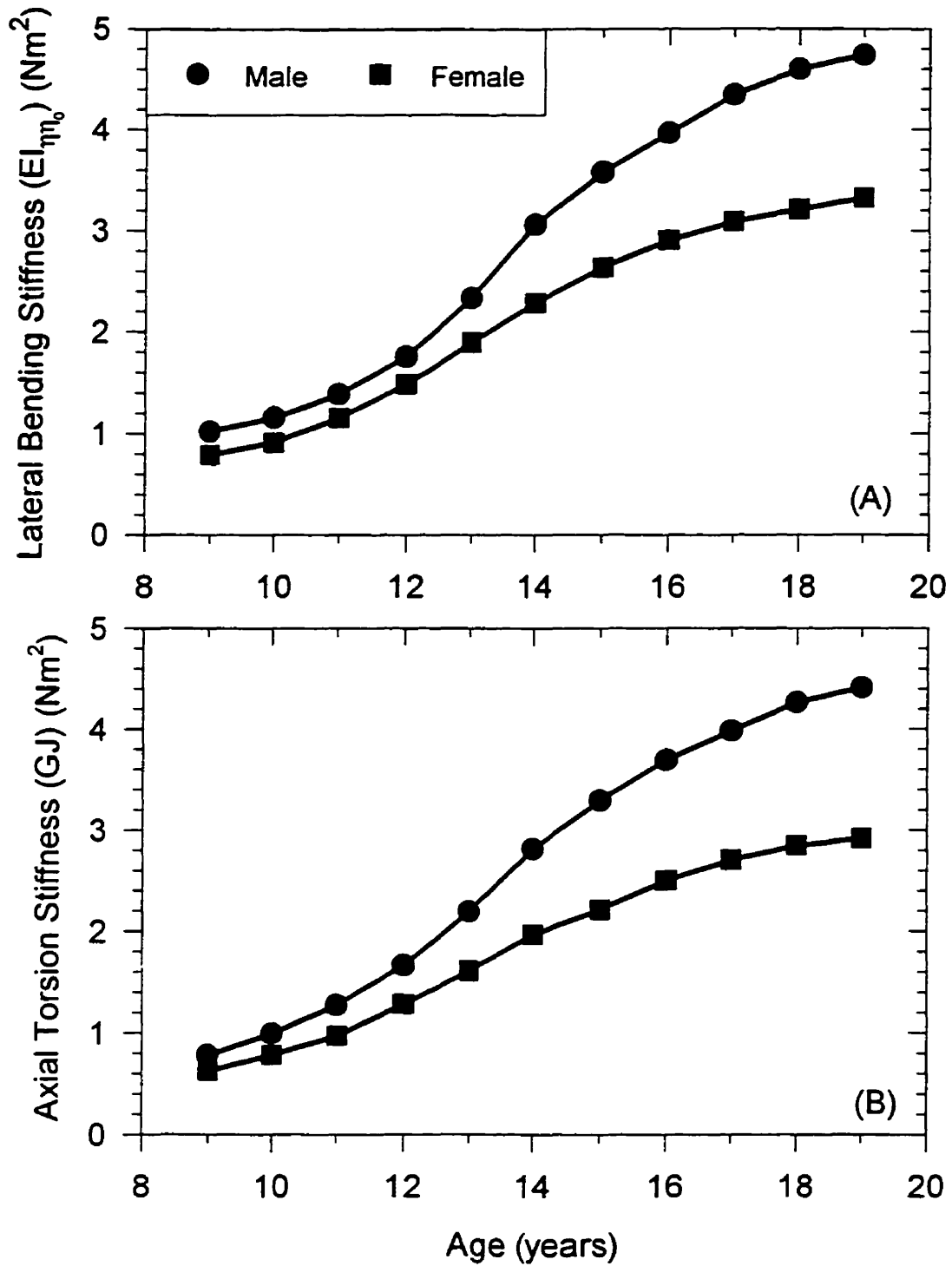


Figure 3.18: The effective stiffnesses at the T8-T9 spine level as a function of age for male and female. (A) Lateral bending stiffness -  $EI_{\eta\eta_0}$ ; (B) Axial torsion stiffness -  $GJ$ .

in early adolescence (Willner, 1974a,b, 1975a,b; Leong et al, 1982; Buric and Momcilovic, 1982; Normelli et al, 1985; Archer and Dickson, 1985; Hagglund et al, 1992; Carr et al, 1993; Goldberg et al, 1993). It was less clear if the growth was abnormal or aberrant, but rather just precocious. The sitting heights of scoliotics were also increased. However, whether the proportion of sitting height to standing height differed in scoliotics was less clear (Willner, 1975; Leong et al, 1982; Nicolopoulos et al, 1985; Upadhyay et al, 1991). On the other hand, though taller, the body weight of scoliotics was not found to be increased compared to normals. And at maturity, the body weight may have been even less. Therefore, scoliotics were in general taller and leaner, or more slender. This increased slenderness of body proportions may be reflected in the increased slenderness of the spines in scoliotics, as reported by Schultz and Cisewski (1978) and Skogland and Miller (1981).

The growth of vertebrae occurs through two mechanisms. Longitudinal or axial growth occurs at the superior and inferior growth plates, whereas increase in the transverse width and depth occurs through periosteal growth (Gooding and Neuhausser, 1965; Taylor, 1975; Skogland and Miller, 1981; Feik and Storey, 1983) . These two growth mechanisms are controlled by different factors. Longitudinal growth is governed by the hormonal system, whereas periosteal growth is influenced by mechanical factors. Therefore, a scoliotic with increased height, but normal weight, would also likely have a more slender spine.

On the basis of these reported alterations in the growth of scoliotics, the normal growth patterns reported in Section 3.10.1 were modified. In case I, the *spine length* was increased by 2% at all years during adolescence. In case II, the length was first increased by 2% at age 9 years. At other years, a linear reduction of this increase was implemented so that at maturity, there was no difference. Case III was similar to case II except an increase of 4.5% was implemented at 9 years of age. These changes were considered for both males and females. All other parameters of the model were not changed from the normal baseline values at each of the years during adolescence. These growth patterns were repeated for a mild scoliotic curve with an initial Cobb angle of 10, 20 and 30°. Therefore, a total of eighteen different simulations of adolescent growth patterns were performed.

## Chapter 4

# RIBCAGE MODEL

### 4.1 Introduction

The ribcage is a complex structure which provides support to the spinal column through a passive and an active mechanism. In both mechanisms, however, the support is predominantly achieved through the forces and moments generated between the individual ribs and the vertebrae at the costovertebral and costotransverse joints. As a passive structure, the ribcage provides elastic resistance to the deformation of the spine. As an active structure, the ribcage serves as a moment arm and a transmitter of forces generated by the trunk muscles. In the present chapter, a finite element model (FEM) of the ribcage is developed in order to conduct numerical experiments to determine the nature and magnitude of the passive support provided by the ribcage to the spine. A knowledge of these reactions is necessary to complete the beam-column model of the scoliotic spine presented in the preceding chapter.

A short description of the finite element method is first presented, followed by the development of the present model. In the final section of the chapter, a model for the ribcage stiffness is proposed and the procedure for the numerical experiments undertaken to establish the passive resistance of the ribcage is outlined.

## 4.2 Finite Element Model of the Ribcage

The finite element method is a means to discretize a continuous medium, in order to determine the behaviour of a given volume under a specific set of conditions. When applied to solid structures, the displacements, strains and stresses throughout the deformable material are determined for the applied loads and boundary conditions. The method is particularly useful for analyzing complex structures of varied geometry and material properties, and subject to general complex loading.

The basic approach is to subdivide the medium into a number of discrete elements, which are then systematically assembled to represent the whole structure. As the number of elements increases, the accuracy of the representation also increases. One of the most widely used finite element formulations is the displacement-based, which originated from the displacement method of structural analysis (Zienkiewicz, 1977; Cooke, 1981; Bathe, 1982). Today, there are many general displacement-based finite element programs available. All the common elements are included in these programs, and they are capable of solving problems with both material and geometric nonlinearities. These general displacement-based finite element programs are well suited to model the passive response of the ribcage in order to establish its stiffness characteristics.

The present finite element model is intended to be representative of an "ideal" ribcage. Unfortunately, however, the geometric and material property data of the individual components are primarily available only for the adult ribcage. As such, the ribcage model developed must be considered representative of an "ideal" adult. However, the gross dimensions of adolescent ribcages are available, and are considered as variables in the subsequent analysis, in order to fully investigate the passive resistance of the ribcage.

The first step in the development of a finite element model is to establish the appropriate structural model. The ribcage is composed of a number of different tissues which have specific geometries and properties. The ribs are the fundamental structures of the ribcage, that establish its shape and strength. They are long, slender curved bodies which are oriented in three-dimensions, and undergo general spatial motion. Consequently, in the

present model they were represented by spatial beam elements. A more detailed or finer model of the ribs was not required, since the present study was only interested in the gross rib motion, rather than a rigorous stress analysis of the cross-section. The costal cartilages were also modelled by beam elements, as they represent an extension of the ribs, albeit much more flexible. Only the first ten ribs were incorporated in the present model. Ribs 11 and 12 were not included since they do not form a closed loop. Consequently, these "floating" ribs are far less capable of bracing the spine.

The sternum is a thin rectangular structure that is comparatively much more rigid than any other component of the ribcage. In the present model, it was represented by a number of plate elements.

The costovertebral and costotransverse joints must be included in the ribcage model, since they are fundamental to the interaction between the spine and ribcage. Together, the costovertebral and costotransverse joints permit easy rotation about the rib neck axis. Other motions are relatively restrained. In the present model, the costovertebral joint was modelled as a pinned joint with some separation allowed between the rib and vertebra. The costotransverse joint was modelled by a beam element.

The passive responses of the intercostal muscles and tendonous tissues were modelled by a number of rod elements, arranged in a criss-cross pattern similar to the internal and external intercostal muscles. It was felt necessary to include the passive response of these muscles since they are an integral part of the ribcage which interconnect the ribs all along their length. The ribs are closely spaced, and any separation of the ribs would clearly be restrained passively by these muscles. Once the structural model of the ribcage was established, it was necessary to determine the geometry of the various components from which the nodal coordinates were calculated. The next step was to determine the number and choice of the specific elements, and their respective properties. This procedure is detailed in the following sections for each of the individual components of the ribcage.

## 4.2.1 Geometry and Nodal Coordinates

The geometry of the individual components of the ribcage are available in the literature. Furthermore, there are a number of guidelines available to direct the assembly of the individual components into a complete model of the ribcage. To supplement and confirm some of the geometric data in the literature, three skeletons, all in excellent condition, were selected from the collection in the Department of Anatomy, McGill University. Two males and one female were selected. Their age at death was unknown. Additionally, 10 ribs from various rib levels were selected to determine the wall thickness of the cortical shell. Geometric measurements were made using Vernier calipers ( $\pm 0.02$  mm) and a flexible tape measure ( $\pm 0.5$  mm). These geometric measurements were not intended as an exhaustive anthropometric study, but only intended to supplement the literature values. The overall accuracy of the model was validated in comparison with experiment and other models. The geometry of the individual components of the present model is described below, followed by the assembly procedure.

### 4.2.1.1 Ribs

The ribs are curved bones that change in geometry at each level of the spine. They are oriented in space, but do, however, lie nearly in a plane. Each rib was modelled by a number of spatial beam elements. As such, it was first necessary to establish the geometry of the elastic axis.

Roberts and Chen (1972) showed that the elastic axis of a rib was essentially coincident with the geometric centre. Furthermore, this axis could be described by arcs from two circles; one for the neck region, from the head to the angle, and another for the shaft region from the angle to the tip. Schultz et al (1974a) used part of a single circle to quantify the rib shaft geometry from the angle to a point near the tip. Other points were needed to specify the locations of the tip, the costotransverse joint and the rib head at the costovertebral joint. Wilson et al (1987) used a single circular arc to represent the rib from angle to tip. Other researchers described the entire rib shape from the head to the tip

using a parabolic arc (Dansereau and Stokes, 1988) or cubic Bezier polynomials (Kenyon et al, 1991).

In the present study, two circular arcs were used to model the rib geometry (Fig. 4.1). One circular arc was used for the neck region, based on the values of Roberts and Chen (1972). A second larger arc used to represent the shaft region was located relative to the rib head based on the values and method of Schultz et al (1974a). This method was chosen for its simplicity and ability to use the values of Schultz et al (1974a), which are from the largest database. The geometric data of Schultz et al (1974a) also contains a portion of costal cartilage at the tip. This length was estimated from comparison of measurements of the outer perimeter of their ribs with measurements of the present ribs, which did not include any costal cartilage.

The data used to construct the rib geometry in the present model is shown in Fig. 4.2. Also shown are the average values from Schultz et al (1974a), and those from the models of Andriacchi et al (1974), and Closkey et al (1992), which are based on the measured values. Where possible, comparison with the data from other researchers is also included. The geometric data used in the present model does not match exactly the experimental data, as the goal was to create an "ideal" ribcage. In the assembly procedure (detailed in a subsequent section), the use of the exact experimental data produced a somewhat irregular shaped ribcage. Consequently, adjustments were made to form a "smoother" shaped ribcage. However, the changes required were relatively small and the data compares well with the other models (Fig. 4.2).

A computer program was written to generate the nodal coordinates from the geometric data. The number of nodal points could be easily changed, and the final number was decided upon following a check for grid independence (detailed in the section on rib elements). The program also allowed for individual components to be adjusted, to create ribs of different size and shape, for assembly into different shaped ribcages.

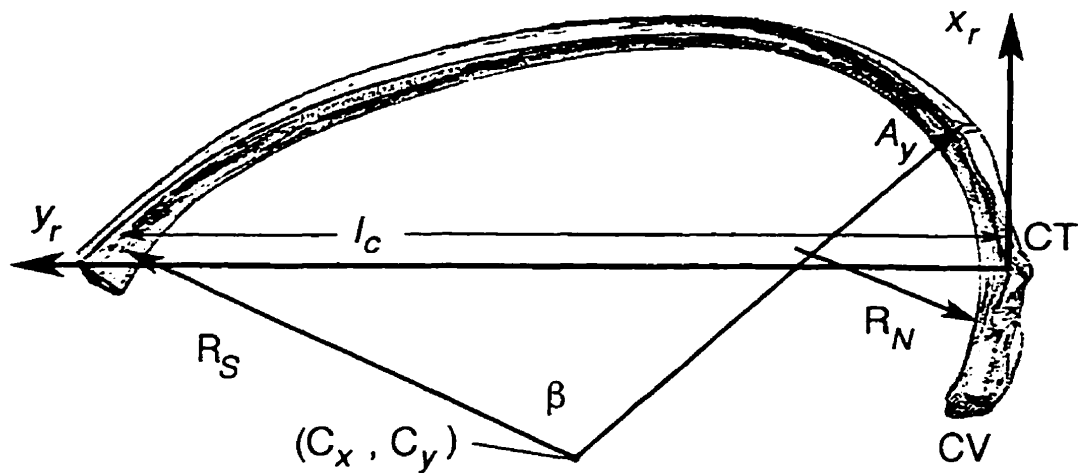


Figure 4.1: Geometric parameters used to quantify the rib geometry.  $R_N$  - radius of a rib in the neck region;  $R_S$  - radius of a rib in the shaft region;  $l_c$  - chord length of a rib;  $\beta$  - arc angle of a rib;  $C_x$  - lateral coordinate of the center of curvature of the shaft;  $C_y$  - anterior-posterior coordinate of the centre of curvature of the shaft;  $A_y$  - anterior-posterior coordinate of the rib angle;  $\beta$  - arc angle of the rib shaft. (Adapted from Gray, 1989).

#### 4.2.1.2 Costal Cartilages and Sternum

The dimensions of the sternum were established by the locations of the costosternal joints at seven points on either side (Fig. 4.3A). A local reference frame was defined, with the origin located at the xiphoid process. The values chosen for the present model are the averages from those in the literature (Schultz et al, 1974b), as well as from measurements made on the three skeletons.

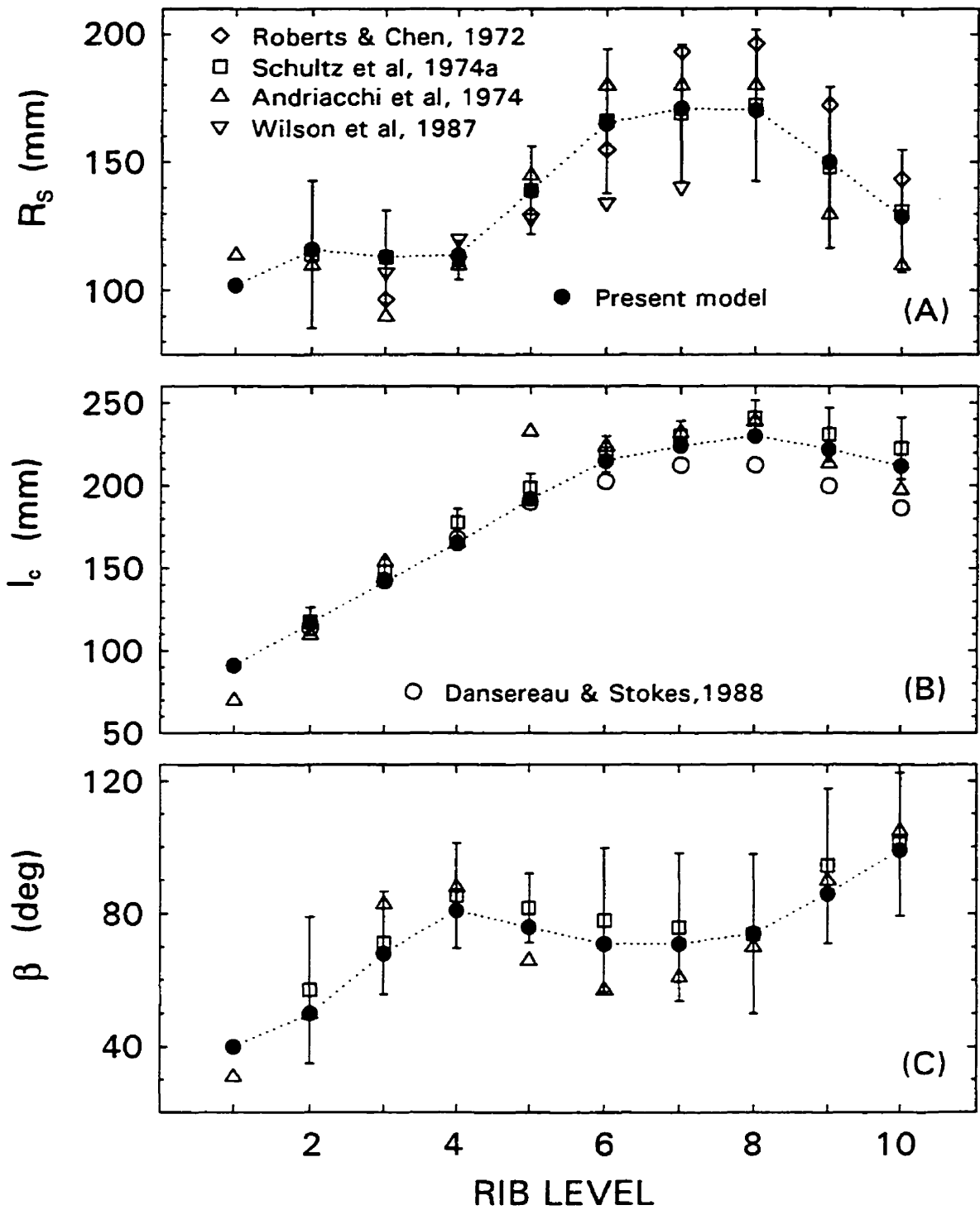


Figure 4.2: Geometry of the ribs at each level used in the present model and compared with experiments. A dotted line was added to interconnect the model data from the discrete levels to greater illustrate the changes as a function of rib level. (A)  $R_s$ ; (B)  $l_c$ ; (C)  $\beta$ ; (D)  $C_x$ ; (E)  $C_y$ ; (F)  $A_y$ .

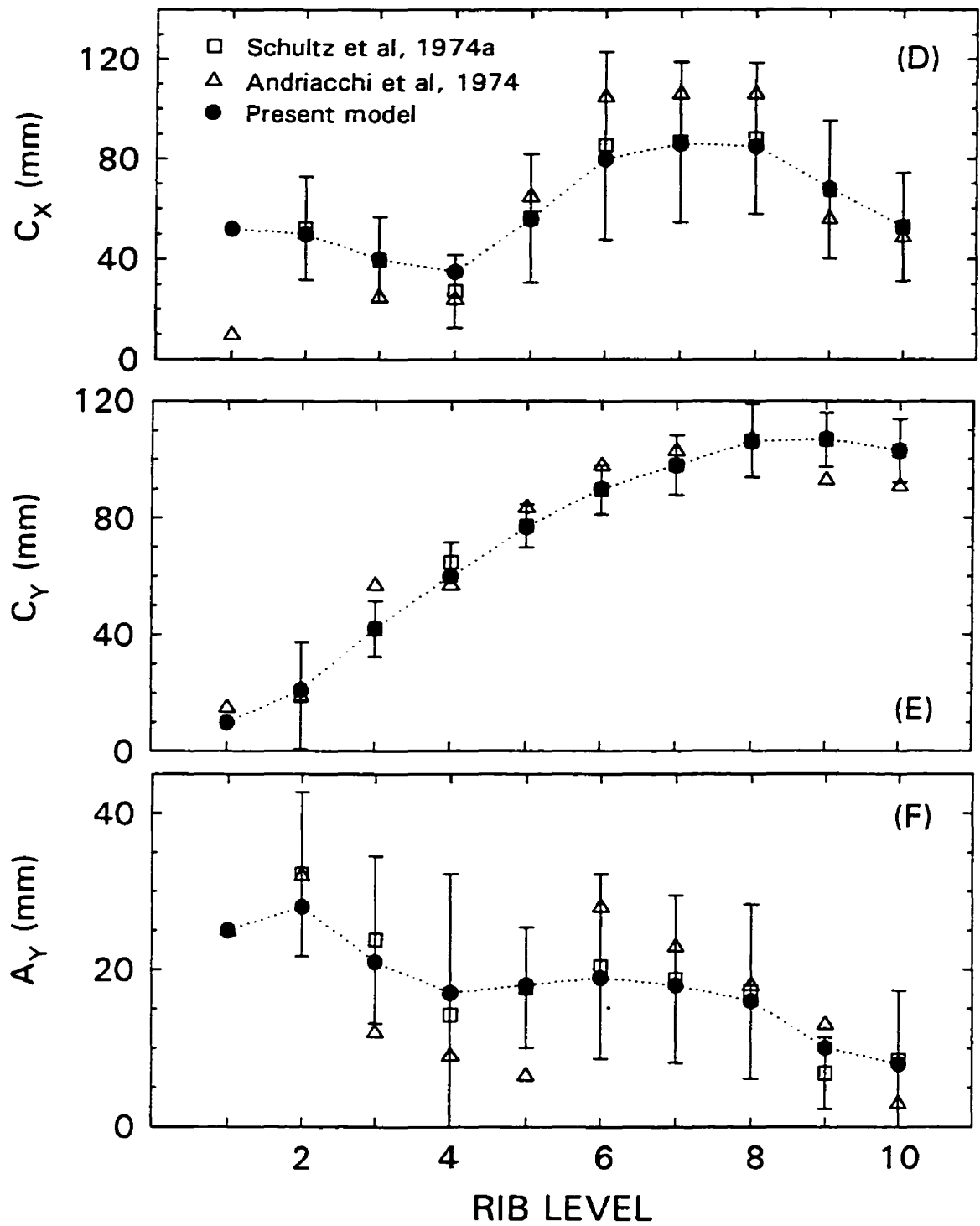


Figure 4.2. (Con'd) Geometry of the ribs at each level used in the present model and compared with experiments. A dotted line was added to interconnect the model data from the discrete levels to greater illustrate the changes as a function of rib level. (A)  $R_S$ ; (B)  $l_c$ ; (C)  $\beta$ ; (D)  $C_x$ ; (E)  $C_y$ ; (F)  $A_y$ .

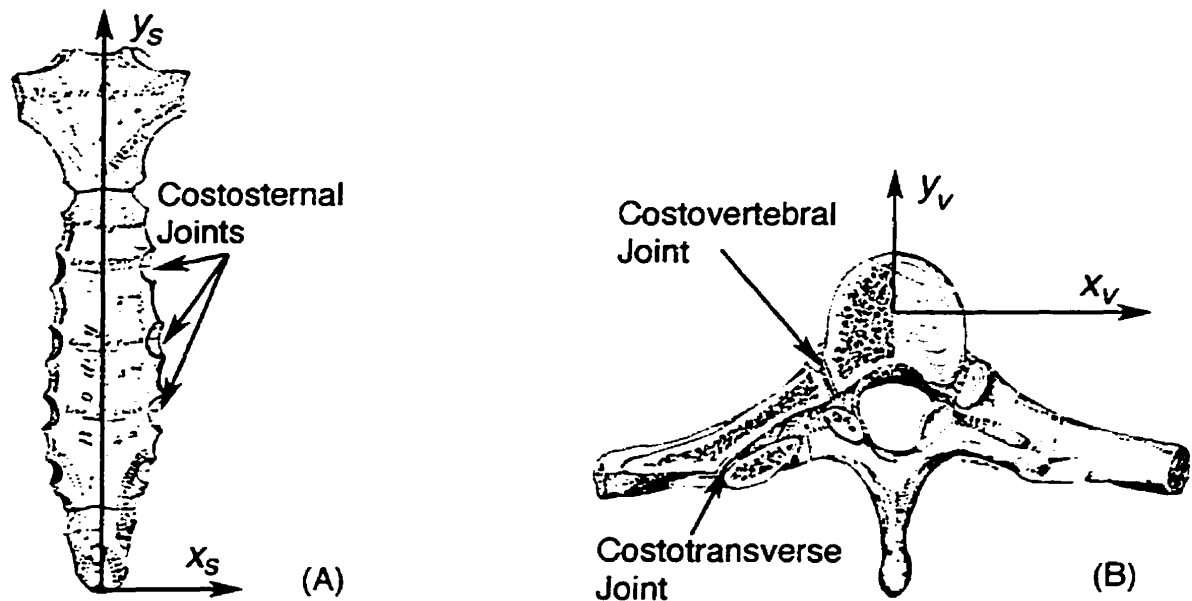


Figure 4.3: (A) Coordinate system  $x_s - y_s$  of the sternum to define the geometry of the costosternal joints; (B) Coordinate system  $x_v - y_v$  of a vertebra to define the geometry of the costovertebral and costotransverse joints. (Adapted from Gray, 1989).

The costal cartilages join the sternum to the anterior tips of the upper seven ribs. The geometry of the costal cartilages was thus established by the location of the sternum and the rib tips in space. As such, it was not necessary to specify their lengths directly. Rather, the costal cartilages were located automatically by the assembly procedure detailed in a subsequent section.

#### 4.2.1.3 Costovertebral and Costotransverse Joints

The ribs articulate with the vertebrae at the costovertebral and costotransverse joints on either side of each vertebra (Fig. 4.3B). These positions are easily distinguishable on a vertebra and have been reported by a number of researchers (Schultz et al, 1974b; Panjabi et al. 1991). Presently, measurements were also made from the three skeletons. The literature and present values were averaged for use in the present model.

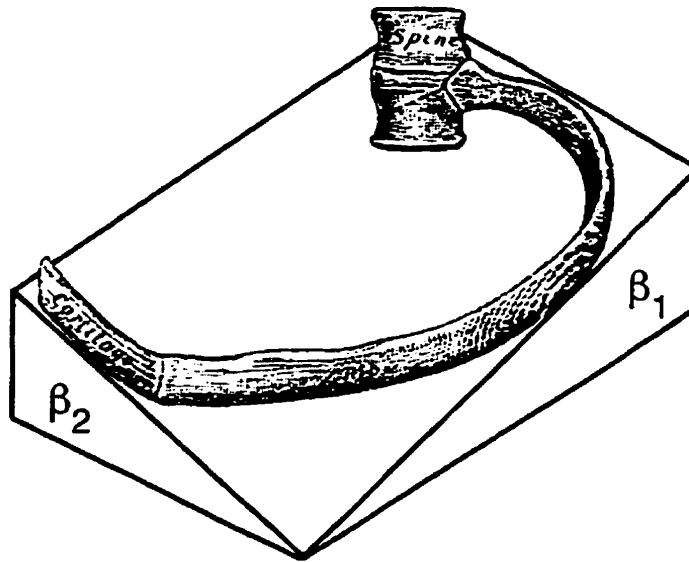


Figure 4.4: Orientation of a typical rib in space, as defined by the “pump handle” angle,  $\beta_1$ , and the “bucket handle” angle,  $\beta_2$ . (Adapted from Gray, 1989).

#### 4.2.1.4 Nodal Coordinates of the Assembled Ribcage

The nodal coordinates of the individual components of the ribcage were next assembled together to establish the full ribcage geometry. A number of values were needed for the assembly and were taken from the literature. First, the spatial position of the costovertebral and costotransverse joints had to be established. The geometry of these joints was previously specified relative to a local reference frame located at the vertebral centre. The coordinates of the vertebral centres were chosen to be identical to those in the beam-column model of a normal spine (see Section 3.6). The three-dimensional coordinates of the costovertebral and costotransverse joints were then determined by rotating the cross-sectional plane of each vertebra normal to the tangent of the thoracic kyphosis at the given rib level.

Next, the individual rib geometry, which has already been defined in a plane, was rotated through two rotations to locate the ribs in space (Fig. 4.4). These angles are similar to the “pump handle” angle and the “bucket handle” angle commonly used to refer to the spatial rib orientation and kinematics during respiration. The *thoracic index (TI)* is the ratio of the width to depth of the ribcage usually measured at mid-sternum, and the

*thoracic ratio (TR)* is the ratio of the width of the ribcage at each vertebral level to the length T1 - T12. Consequently, these measures of ribcage shape are largely determined by the bucket and pump handle angles. The values in the literature for the angles (Wilson et al, 1987; Dansereau and Stokes, 1988) were used as a guide, and subsequently adjusted till the ribcage shape ratios were in reasonable agreement with the values in the literature.

In the final step, the sternum was located in space in a plane 2-4 mm anterior to the rib tips. The exact anterior-posterior position was established by ensuring that the thoracic index corresponded to literature values. A computer program was written to assemble the individual rib geometry and determine the three-dimensional nodal coordinates of the ribcage. A flowchart of the procedure is shown in Fig. 4.5. This allowed for the easy assembly of any ribcage size or shape. A somewhat similar procedure was used by Kenyon et al (1991) to assemble the sixth rib and sternum from x-ray measurements.

#### **4.2.2 Elements and Material Properties**

As discussed in the foregoing, the spatial orientation of the ribs was established to ensure that the overall shape of the assembled ribcage agreed with literature values. In Fig. 4.6, the values for the *thoracic ratio* are compared to those in the literature. The overall shape of the ribcage in the coronal plane was found to be very similar to the measured values. The *TR* in the model was slightly larger (about 8-10%), in particular, in the lower ribs. This difference was due to the use of adult dimensions for the individual ribs, whereas the data available for the thoracic ratio was for an adolescent population. However, the difference was consistent with the general pattern of an increasing index with age (Openshaw et al, 1984; Grivas et al, 1991). In the present model, the *thoracic index* at the mid-sternum level was 1.4. This was found to be in excellent agreement with the values in the literature for *TI* of 1.33 - 1.44 (Davenport, 1934), 1.30 - 1.46 (Takahashi and Atsumi, 1955), 1.47 (Howatt and DeMuth, 1965), 1.26 - 1.33 (Davis and Troup, 1966), 1.54 (Openshaw et al, 1984) and 1.47 (Karlberg and Taranger, 1976). Therefore, the cross-sectional shape of the model was also reasonable in comparison with anthropometric measurements. Since the geometry of the individual components was combined from a variety of sources, it was

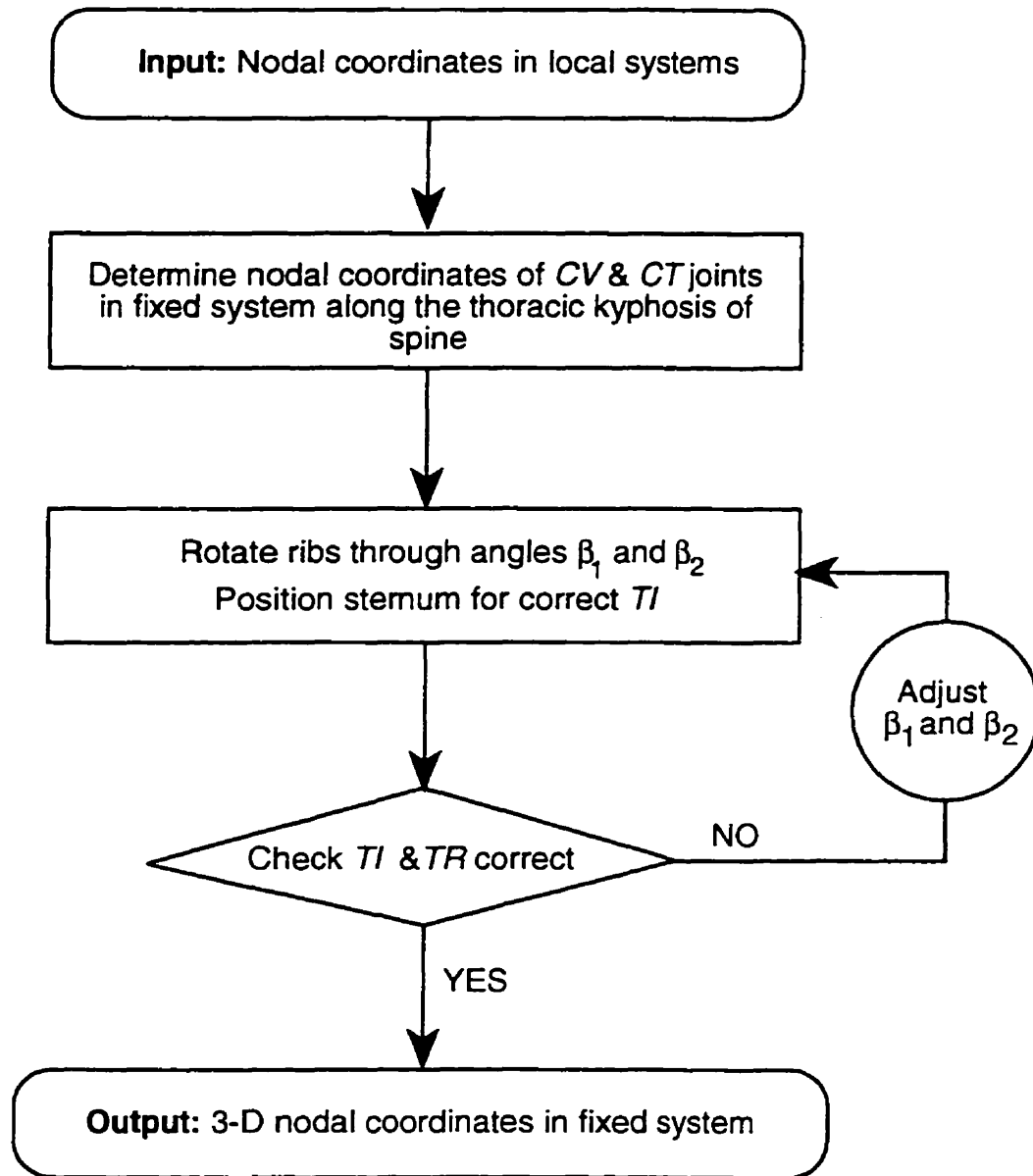


Figure 4.5: Flowchart of the assembly procedure to determine the 3-D nodal coordinates of the ribcage. The data was input in the local coordinate systems of the ribs, vertebrae and sternum, and output as three-dimensional data in the fixed global system.

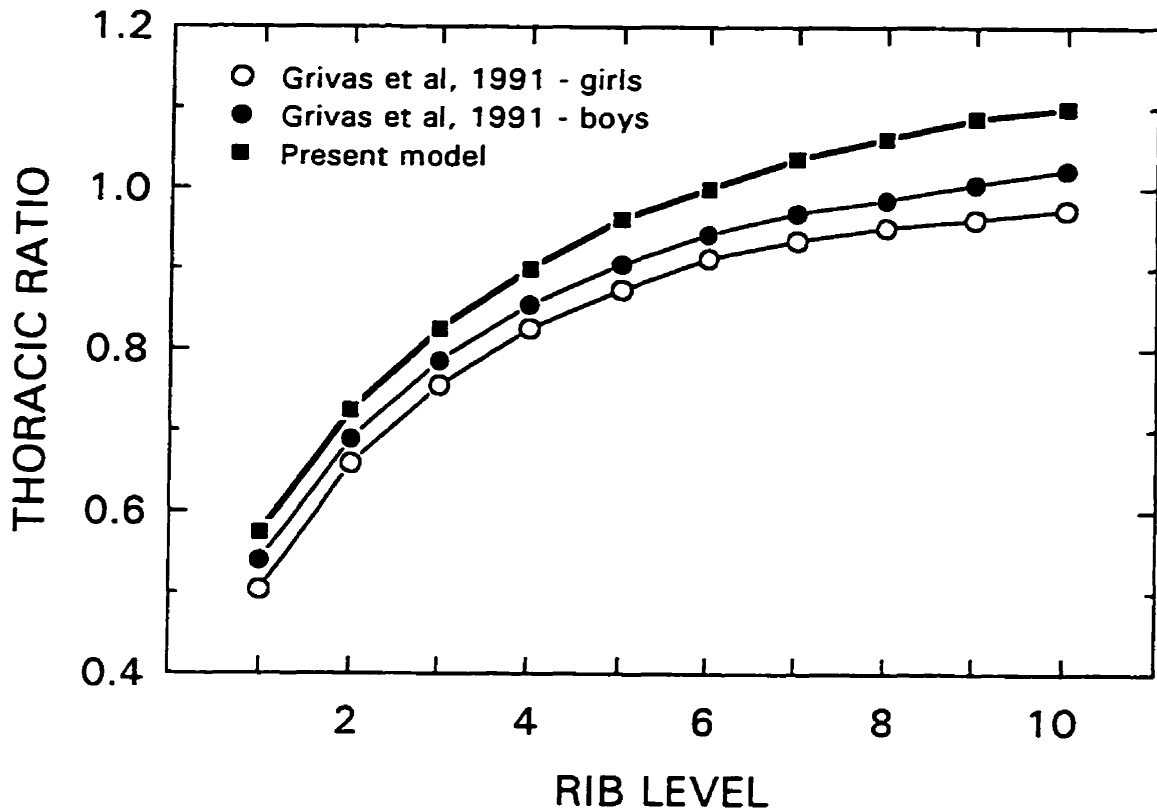


Figure 4.6: The thoracic ratio at each rib level in the present model and compared to clinical data in the literature.

important to ensure that the overall ribcage shape was reasonable.

The elements used to model the ribcage components are detailed in this section along with the respective material properties. Not all properties could be specified directly from the literature, but rather some had to be determined by numerical simulation of specific experimental tests. This procedure was used previously in other ribcage models (Andriacchi et al, 1974; Stokes and Laible, 1990; Closkey et al, 1992) and is outlined in the following sections. In these instances, the final property values are presented in Chapter 5. Additionally, measurements from the three skeletons were used to determine the rib cross-sectional properties.

#### 4.2.2.1 Ribs

Since the ribs are curved, it would be natural to model them with curved beam elements. However, the curved beam element formulations require that the principal axes

be aligned with the plane of the curved element defined by its radius of curvature. In the ribcage, the lower ribs could be adequately modelled by this curved beam element. In the upper ribs, however, the principal axes are not aligned with the plane of the rib in which it is curved. Consequently, it was not possible to use curved beam elements. Instead, straight beam elements were used, since the principal axes can be aligned with any direction. However, sufficient elements had to be used to ensure that the behaviour of the curved rib was adequately modelled. Therefore, two investigations were performed in order to check for grid independence, and for convergence of the straight beam model to a curved beam model. Ribs 2 and 8 were selected for the analysis, since rib 2 was highly curved and rib 8 was the longest.

The curved shapes of ribs 2 and 8 were modelled by both curved and straight beam elements, which were increased in number from 2 up to 18. The properties for ribs 2 and 8, which are described later, were used for the present analysis. The principal axes of the ribs were aligned with the plane of the curvature of the rib to allow comparison of the solutions of the curved and straight beam representations. The ribs were fixed in all directions at the rib head, and the tip was loaded simultaneously with three forces in mutually orthogonal directions (lateral, anterior and superior). The model predictions of the tip displacements were then checked for convergence since the load-displacement behaviour is of primary interest. To assess the predictions from the various grids, they were compared as a percentage difference from the predictions of the curved beam representation with 18 elements.

The convergence of the tip displacements as the number of elements was increased is shown in Fig. 4.7. For the curved beam representation, grid independence was achieved with as little as 5 or 6 elements for rib 8, and 3 elements for rib 2. The use of more curved elements produced changes in the predicted displacements of less than 0.5%. For the straight beam representation, grid independence was achieved with about 9 elements for both rib 2 and 8. Though the addition of straight elements after about 5 or 6 elements produced relatively small changes, nonetheless the predictions gradually approached the predictions of the representation with 18 curved beam elements. The addition of more

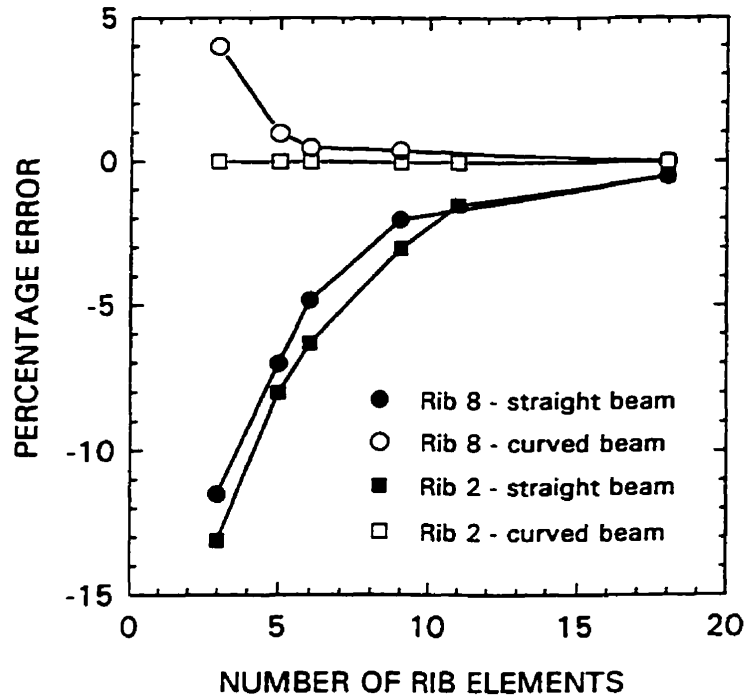


Figure 4.7: Grid independence check for the finite element representation of the ribs. Comparison between a curved and a straight beam representation are also shown.

than 9 elements produced changes of less than about 2%.

Therefore, on the basis of the foregoing, each bony rib was modelled by 9 elements for a total of 180 elements for the entire ribcage. Other investigations also showed that 3 of the 9 elements per rib should be used for the neck region of the rib, which has a higher curvature than the shaft region. Though possibly a slightly less number of elements could have been used, it was also desired to ensure that the curved rib shape was reasonably well represented with sufficient nodes for the attachment of the intercostal elements.

The cross-section of each rib was assumed to be elliptical in order to calculate the principal moments of inertia and cross-sectional area. Variations from a purely elliptical shape are due to grooves in the shaft region which contain nerves and veins (Fig. 4.8). These changes are unlikely to affect the overall behaviour of the rib, but rather only affect the local deformation. The cross-section of a rib also reveals a porous core of cancellous bone surrounded by a shell of cortical bone. The core was also assumed to be elliptical. The bending stiffness of a rib in one of the principal planes was, therefore, estimated as

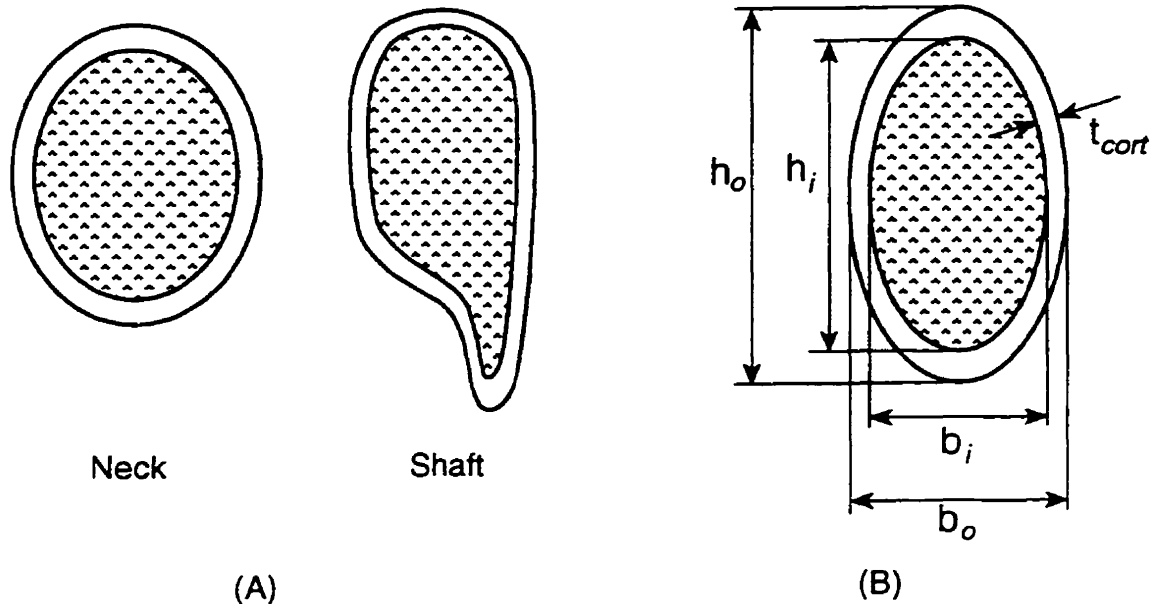


Figure 4.8: Cross-sectional geometric parameters of a rib. (A) Typical geometries in the shaft and neck regions; (B) Hollow elliptic model of the rib cross-section.  $h_o$  - major outer diameter;  $h_i$  - major inner diameter;  $b_o$  - minor outer diameter;  $b_i$  - minor inner diameter;  $t_{cort}$  - cortical wall thickness.

follows:

$$EI_1 = E_{cort}I_{cort} + E_{can}I_{can} \quad (4.1)$$

$$I_{cort} = \frac{\pi}{64} (h_o^3 b_o - h_i^3 b_i) \quad (4.2)$$

$$I_{can} = \frac{\pi}{64} h_i^3 b_i \quad (4.3)$$

where  $E_{cort}$ ,  $E_{can}$  were the Young's Moduli for cortical and cancellous bone, respectively. The dimensions of the rib cross-section given by  $h_o$ ,  $b_o$ ,  $h_i$  and  $b_i$  are shown in Fig. 4.8. The properties of cancellous bone can vary over quite a range, but in general are much less than cortical bone. Also, due to the cubic influence of the cross-sectional diameter on the moment of inertia, the contribution from the cancellous core to the bending stiffness was very small due to the smaller dimensions of the core. For the following properties (Granik and Stein, 1973; Keaveny and Hayes, 1993) and dimensions (Sedlin et al, 1963),

$$\begin{aligned}
h_0 &= 13 \text{ mm} & b_0 &= 6 \text{ mm} \\
h_i &= 11 \text{ mm} & b_i &= 4.5 \text{ mm} \\
E_{cort} &= 12000 \text{ MPa} & E_{can} &= 50 - 500 \text{ MPa}
\end{aligned}$$

the bending stiffness for the cortical shell was equal to  $4.2 \text{ Nm}^2$ , whereas the maximum possible (i.e., corresponding to  $E_{can} = 500 \text{ MPa}$ ) bending stiffness for the cancellous bone was  $0.15 \text{ Nm}^2$ . Therefore, the bending stiffness was clearly dominated by the cortical shell, and the contribution from the cancellous core was negligible (Granik and Stein, 1973). For an elliptical core inside an elliptical shell, the ratio of the diameters are proportional, and thus

$$t_c = \frac{h_i}{h_0} = \frac{b_i}{b_0} \quad (4.4)$$

where  $t_c$  is a measure of the wall thickness. Therefore, inserting equation (4.4) into (4.2), and dropping the cancellous bone contribution, the bending stiffness was given by

$$EI_1 = E_{cort} \frac{\pi}{64} h_0^3 b_0 (1 - t_c^4) \quad (4.5)$$

Similarly, the other properties were given by

$$EI_2 = E_{cort} \frac{\pi}{64} b_0^3 h_0 (1 - t_c^4) \quad (4.6)$$

$$GJ_R = G_{cort} \frac{\pi}{16} \frac{h_0^3 b_0^3}{(h_0^2 + b_0^2)} (1 - t_c^4) \quad (4.7)$$

$$A_R = \frac{\pi}{4} h_0 b_0 (1 - t_c^2) \quad (4.8)$$

where  $EI_1$ ,  $EI_2$  were the bending stiffnesses about the principal rib planes,  $GJ_R$  was the torsional rigidity, and  $A_R$  was the effective cross-sectional area. Therefore, using equations (4.5 - 4.8), the properties of the ribs were simply estimated by the specification of the major and minor diameters and the wall thickness.

The major and minor diameters were measured from the ribs of the three skeletons. Measurements were made at four locations on each rib from either side: one in the neck

region and three along the shaft. The measurements did not change greatly in the shaft region and were, therefore, averaged for each rib. On the other hand, the neck and shaft regions were clearly different for ribs 2-10 (Fig. 4.9). The major diameter was greater in the shaft region compared to the neck region, whereas the minor diameter was greater in the neck region. The major diameter of rib 1 was clearly different from the other ribs which reflected its unique shape. In Fig. 4.9C, the ratio of the major to minor diameters are compared for the neck and shaft regions. The neck region was found to be approaching a circular cross-section, whereas the shaft region was much more elliptic.

Sedlin et al (1963) reported values of  $12.9 \pm 1.97$  mm for the major diameter, and  $4.8 \pm 1.6$  mm for the minor diameter of the shaft region of an adult. Granik and Stein (1973) reported values of 16.5 mm for the major diameter and 7.4 mm for the minor diameter of the mid-shaft region of ribs 6 and 7. These values were in excellent agreement with the present values of about 14 mm for the major diameter and 7 mm for the minor diameter, for the shaft region of ribs 6 and 7.

The cross-sections of 10 ribs were examined and the cortical wall thickness was estimated to be 0.75 - 2.00 mm. This agreed with the values in the literature of 0.92 - 1.09 mm (Roberts and Chen, 1970) and 0.25 - 2.29 mm (Granik and Stein, 1973). Therefore, the value of  $t_c$  was estimated to be 0.8, which gave a wall thickness in the appropriate range.

Using equations (4.5 - 4.8), the cross-sectional properties for the ribs were determined for the neck and shaft regions at each rib level (Fig. 4.10). The major moment of inertia for rib 1 was clearly different from the other ribs in both the neck and shaft regions, which reflects its unique anatomy. The torsional constant and cross-sectional area were also quite different for rib 1 compared to the others. For the other ribs, the major moment of inertia was larger in the shaft region compared with the neck region, whereas the minor moment of inertia was larger in the neck region. These differences with rib level were, of course, directly related to the cross-sectional dimensions. A similar explanation can explain the variation in the torsional constant and effective cross-sectional area with rib level. Also shown in Fig. 4.10 are the values used in the present model. There were slight differences

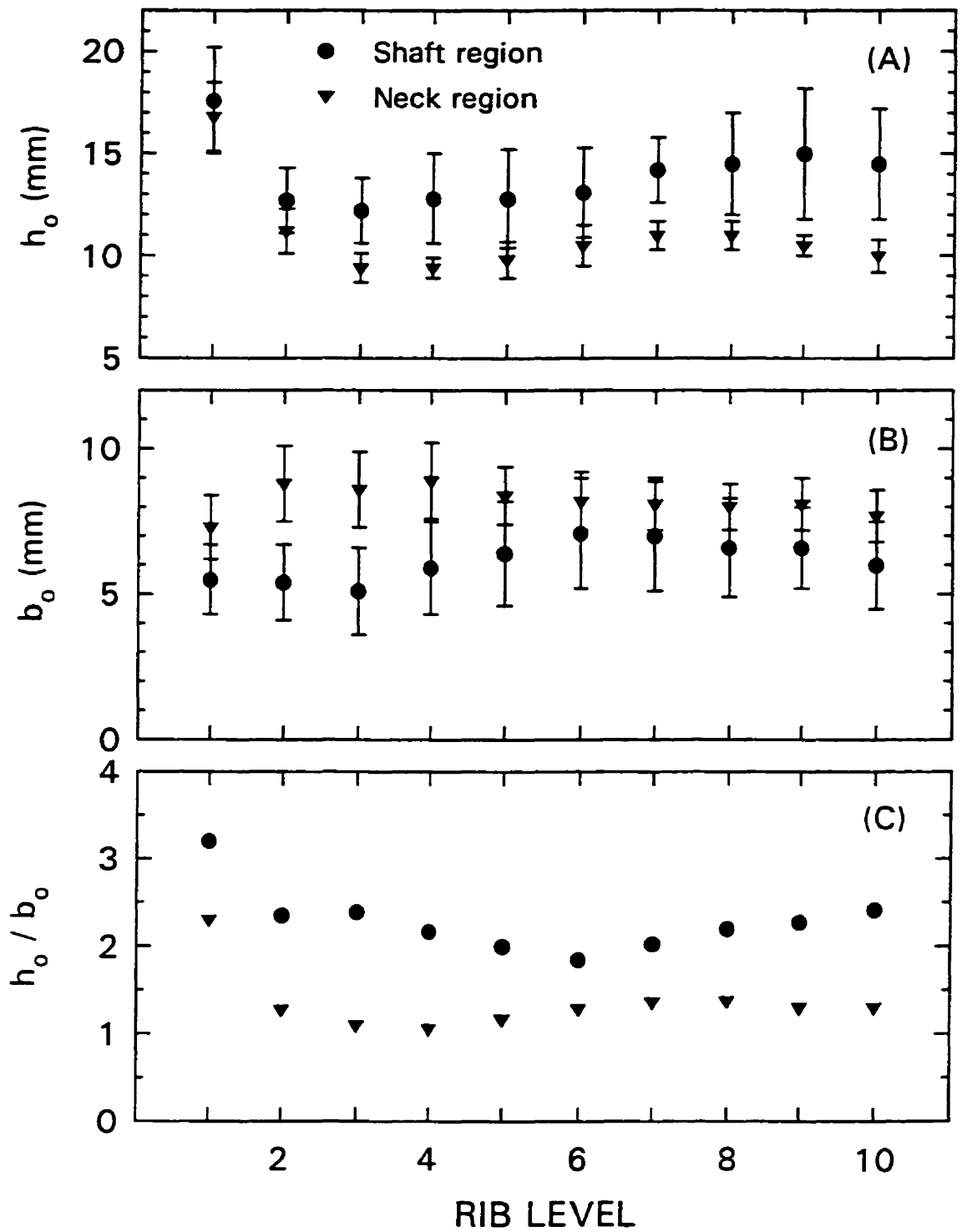


Figure 4.9: Cross-sectional geometry of the ribs at each level for the neck and shaft (average of 3 locations) regions, based on the measurements from three skeletons. (A) Major outer diameter,  $h_o$ ; (B) Minor outer diameter,  $b_o$ ; (C) Ratio of the major to minor outer diameters.

from the measurement values, due to the present concern of creating an "ideal" model.

The present cross-sectional properties were also in good agreement at all rib levels with those of Roberts and Chen (1970), which were based only on a single specimen. For example, at rib 7, they reported values of about  $700 \text{ mm}^4$  and  $200 \text{ mm}^4$  for the major and minor moments of inertia, respectively, a torsion constant of  $450 \text{ mm}^4$  and a cortical area of  $32 \text{ mm}^2$  in the shaft region. On the other hand, in the neck region, the major and minor moments were around  $300 \text{ mm}^4$ , the torsion constant around  $425 \text{ mm}^4$  and the area around  $33 \text{ mm}^2$ . They also reported the greatly increased values at the first and second ribs used in the present model. Saumarez (1986b) also commented on the significant differences between the neck and shaft regions. The minor moment of inertia for the mid-shaft region of ribs 6 and 7 was calculated explicitly by Stein and Granik (1976), based on the exact cross-sectional geometry, and reported to be in a range of about  $75\text{-}250 \text{ mm}^4$ , which agreed with the present value of about  $150 \text{ mm}^4$  (Fig. 4.10B). The cross-sectional area of cortical bone has also been reported to be in the range  $20\text{-}35 \text{ mm}^2$  (Stein and Granik, 1976),  $19\text{-}27 \text{ mm}^2$  (Takahashi and Frost, 1966),  $17\text{-}27 \text{ mm}^2$  (Sedlin et al, 1963; Sedlin, 1964) for the shaft region of the middle ribs in an adult. These values agreed well with the present area values of about  $27 \text{ mm}^2$  (Fig. 4.10D). The ratio of the cortical area to the total cross-sectional area has also been reported to be in the range  $0.29 - 0.56$  (Sedlin, 1964),  $0.28 - 0.58$  (Takahashi and Frost, 1966) and  $0.18 - 0.48$  (Santoro and Frost, 1968), again for the shaft region of the middle ribs from an adult. In the present study, the ratio was equal to  $(1 - t_c^2)$  or  $0.36$ , which agreed very well.

Since the rib cross-sections were elliptical, it was necessary to specify the orientation of the principal axes of the cross-sections. These orientations were specified for each rib using the immediately superior rib. The minor principal axis of a given beam element, at a given rib level, was oriented along the tangent to the outer surface of the ribcage. For rib 1, the minor principal axis of the given beam element was directed towards a central node located at the top of the ribcage. The orientation of the principal axes of the beam elements changed, therefore, between each rib level. A certain amount of "twist" along the rib length was also created by this procedure, as discussed by Roberts and Chen (1972).

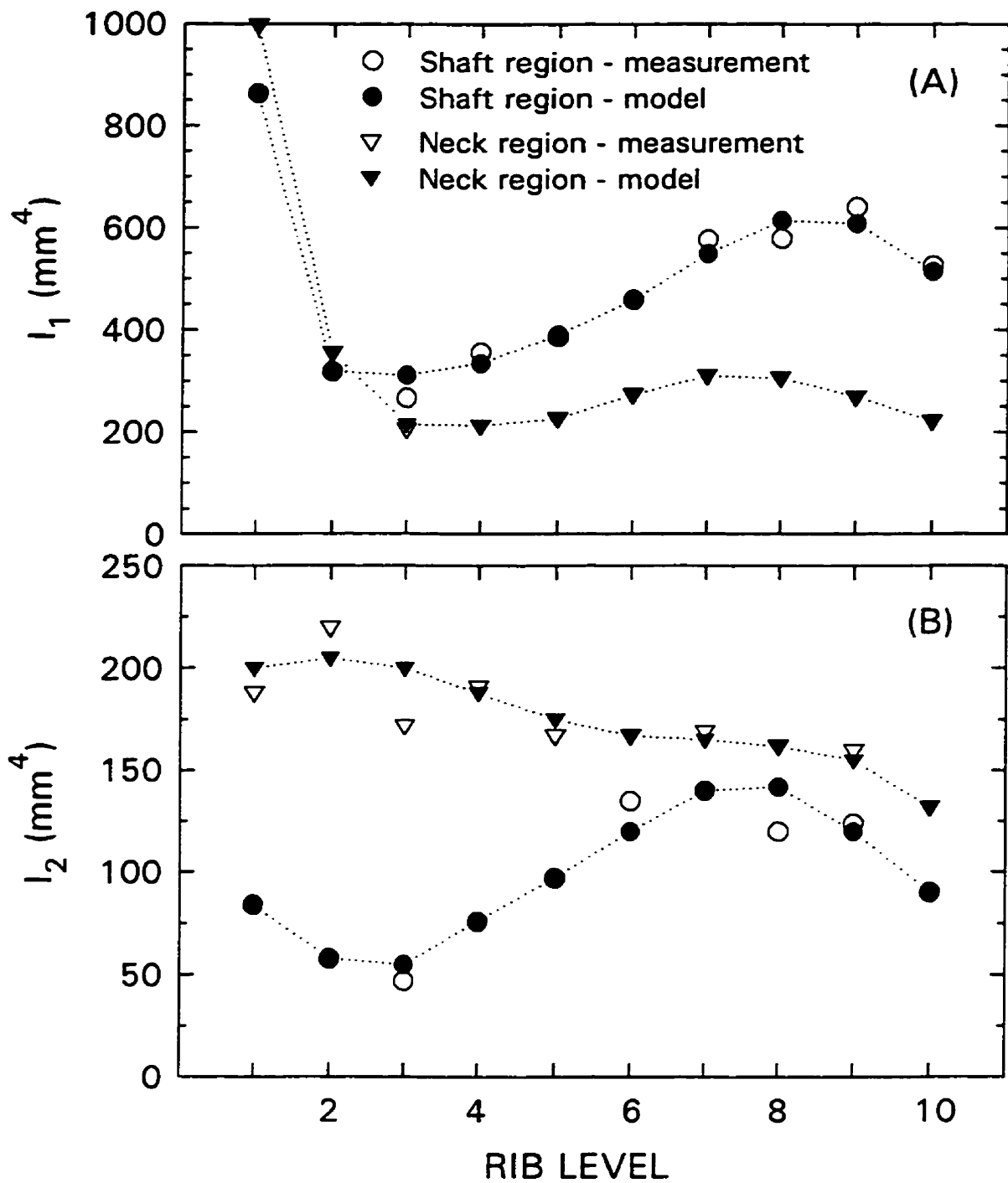


Figure 4.10: Cross-sectional properties of the ribs used in the beam elements and comparison with values in the literature [A dotted line was added to interconnect the data used in the model to greater illustrate the differences as a function of rib level.] (A) Major moment of inertia,  $I_1$ ; (B) Minor moment of inertia,  $I_2$ ; (C) Torsional constant,  $J_R$ ; (D) Cross-sectional area,  $A_R$ .

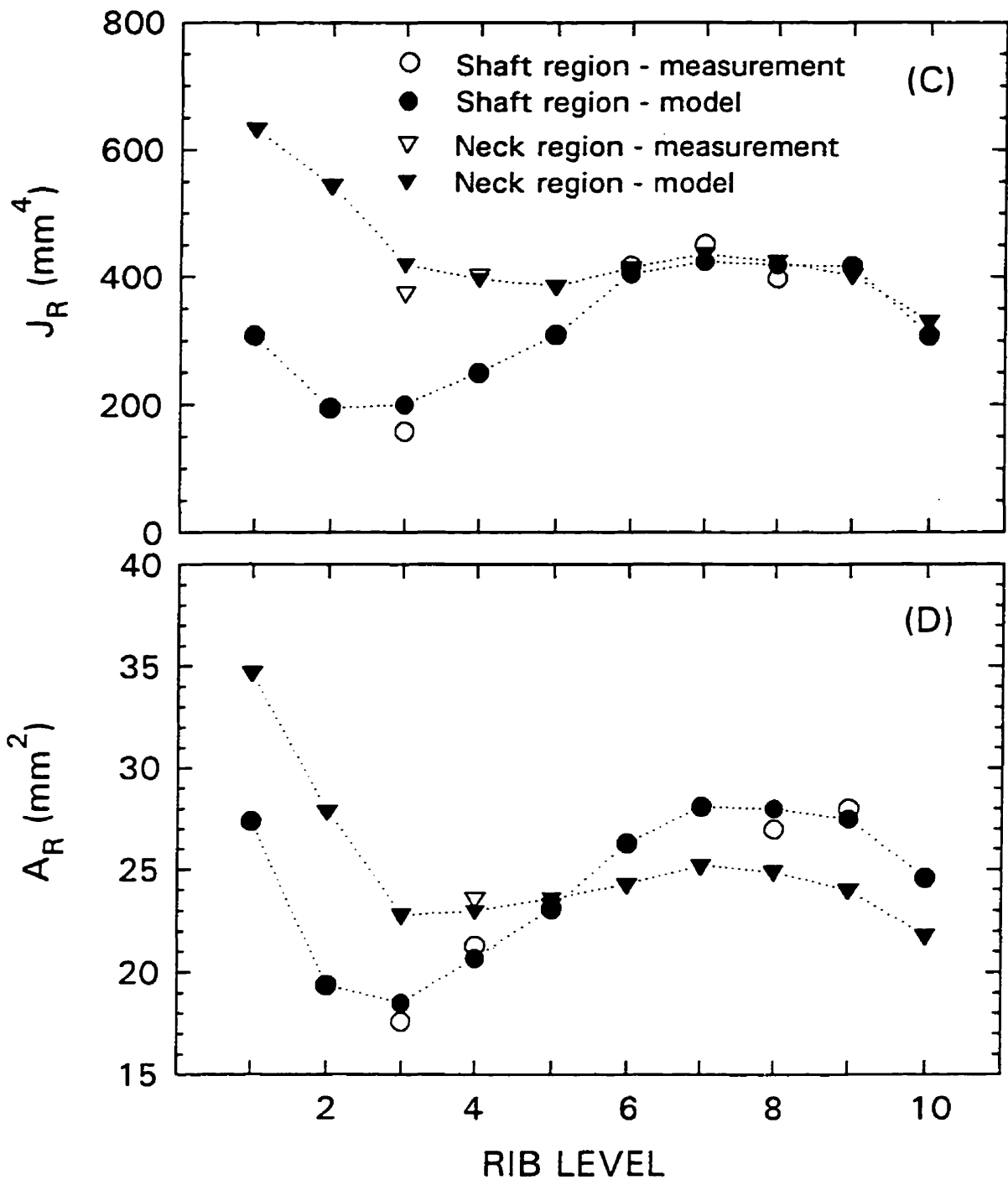


Figure 4.10 (Con'd) Cross-sectional properties of the ribs used in the beam elements and comparison with values in the literature [A dotted line was added to interconnect the data used in the model to greater illustrate the differences as a function of rib level.] (A) Major moment of inertia,  $I_1$ ; (B) Minor moment of inertia,  $I_2$ ; (C) Torsional constant,  $J_R$ ; (D) Cross-sectional area,  $A_R$ .

The present cross-sectional data was clearly from a limited specimen population and was only intended as an estimate of the properties which were not available with the other rib geometry. The overall validity of the rib behaviour, however, was checked by simulating the experiments on individual ribs by Schultz et al (1974a). A similar approach was used by Closkey et al (1992) to establish the stiffness values between the 5 rigid bodies of their rib model. In the experiments, individual ribs were loaded in three orthogonal directions at the tip, with respect to the local rib coordinate system: lateral/medial, anterior/posterior, and superior/inferior. The three-dimensional motion of the tip was recorded experimentally. However, only the principal translations in the direction of loading were reported for all ribs tested. The ribs tested also included part of the costal cartilages. Therefore, in the present simulation, one element from the costal cartilage (see Section 4.2.2.2) was added to the bony tips of ribs 1-6 and two elements for ribs 7-10.

Since the beam orientations were best specified in an assembled configuration of the ribcage, this numerical simulation was performed with the ribs in the assembled configuration. The loads at the rib tips, however, were oriented in the local coordinate system similar to the experiment, and the ribs were fixed in all directions at the costotransverse joint. The results of this validation check of the individual rib behaviour are presented in Chapter 5.

To examine the effect of the variation in cross-sectional property with rib level, three separate cases were also investigated, the results for which are presented in Chapter 5. In case A, the foregoing properties were used, which involved varied properties with rib level for both the neck and shaft region. In case B, one set of properties were used for the neck region and one set for the shaft region for rib levels 2-10, based on the following average values:

	Neck region	Shaft region
$I_1(\text{mm}^4)$	266	456
$I_2(\text{mm}^4)$	172	100
$J_R(\text{mm}^4)$	417	325
$A_R(\text{mm}^2)$	24.2	24.0

In case C, one set of properties were used for both the shaft and neck regions for rib levels 2-10, based on the following weighted average values (25% neck and 75% shaft):  $I_1 = 410 \text{ mm}^4$ ,  $I_2 = 118 \text{ mm}^4$ ,  $J_R = 348 \text{ mm}^4$  and  $A_R = 24 \text{ mm}^2$ . In all three cases, the properties for rib 1 remained the same due to its unique shape.

#### 4.2.2.2 Costal Cartilages and Sternum

The costal cartilages were modelled by beam elements joining the tips of the bony ribs to the sternum. Two elements were used for the costal cartilage at each rib level on either side, except for rib 7, where 3 elements were used due to the increased length of the cartilage. Based on the grid independence checks for the bony ribs, this seemed a reasonable number given the shorter length and lesser curvature of the costal cartilages. Additionally, one element per rib was used on either side to join ribs 8, 9 and 10 to the immediately superior rib (i.e., rib 8 to rib 7, etc.) at the tip. These lower ribs, termed "false" ribs, do not attach directly to the sternum, but rather act through an interchondral joint to the adjacent ribs. Ribs 6 and 7 were also interconnected at an interchondral joint, which was modelled by one beam element on either side. Therefore, the costal cartilages were modelled by 25 beam elements on either side for a total of 50 elements.

The sternum was modelled by six plane elements. Each element interconnected two adjacent rib levels of the seven "true" ribs attached directly to the sternum via the costal cartilages. The sternum was by far the stiffest structure of the ribcage and was found to displace essentially as a rigid body. The use of six elements was, therefore, more than adequate to model the displacement of the sternum. The costal cartilages and sternum are shown in Fig. 4.11 in an assembled configuration.

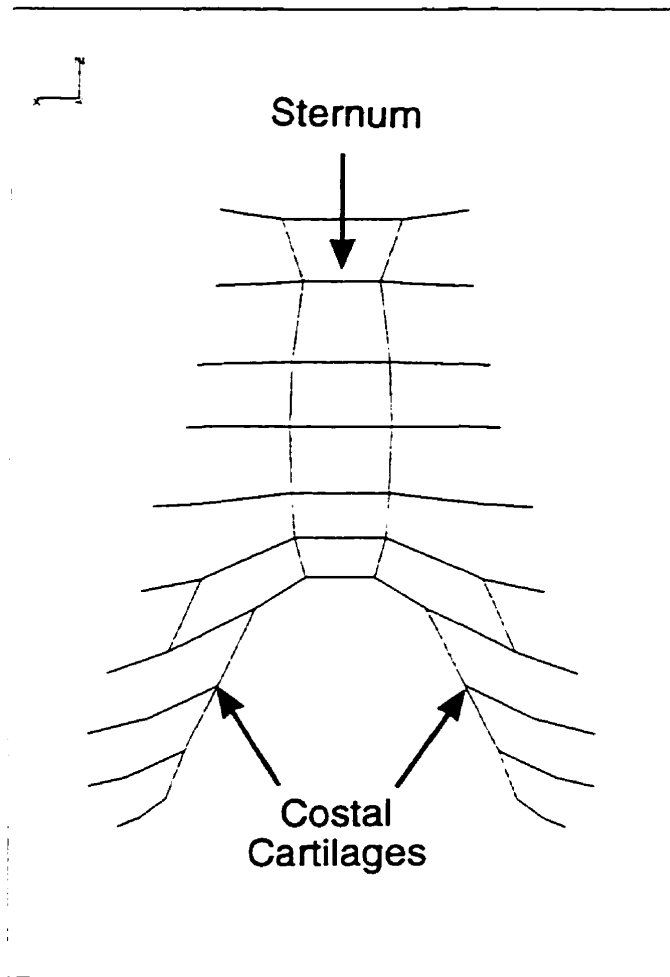


Figure 4.11: Costal cartilages and sternum of the finite element model shown in a frontal view. The beam elements of the costal cartilages are only illustrated by a line to represent the elastic axis.

The costal cartilages are attached to the sternum at the costosternal joints via a number of ligaments. It was not necessary, however, to model the ligaments and joints directly. Instead, in the present model, the costal cartilages were attached directly to the sternum. The properties of the costal cartilages were then chosen by simulating the experimental studies on the costal cartilage and sternum unit by Schultz et al (1974b). The combined effects of the ligaments and costosternal joint were, therefore, modelled collectively in the properties of the costal cartilages. Since the properties of the individual ligaments were not available, this represented the most viable approach and has been used in the other models (Andriacchi et al, 1974, Stokes and Laible, 1990, Closkey et al, 1992, Loring, 1992). However, it should be noted that the stress and strains within the costal cartilage elements were, consequently, not likely to be correct.

To simulate the experiments by Schultz et al (1974b), the costal cartilages and sternum were isolated from the ribcage model. Forces in the superior/inferior and anterior/posterior directions were applied to the costal cartilages at the average position of the 5 specimens tested. The cross-sectional properties of the costal cartilages were initially chosen to match the average rib shaft values with an  $E$  of 300 MPa. Through a trial and error approach, the properties were subsequently adjusted to match the experimental measurements. The final values chosen are presented in the validation results of Chapter 5.

#### 4.2.2.3 Costovertebral and Costotransverse Joints

The spatial orientation of the costovertebral and costotransverse joints leads to the unique kinematics between the ribs and the vertebrae. The dominant motion is a rotation about the rib neck axis that interconnects the two joints. This motion is central to respiration as the ribs rise up during inspiration by rotating about this axis. As a result, much of the changes in ribcage shape during respiration are due to the rigid body displacements of the ribs, as opposed to a deformation of the ribs.

To model this behaviour, the costovertebral joint was modelled as a pinned joint with no resistance to bending in any plane. The axial stiffness and torsional response of the joint was modelled by a rod element with bi-linear properties. A high compressive stiffness

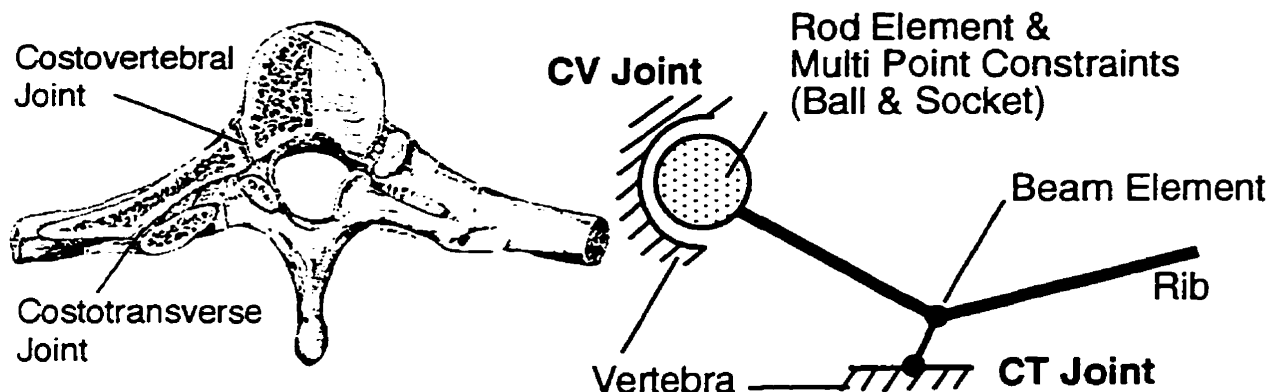


Figure 4.12: The structural model of the costovertebral and costotransverse joints.

was used to prevent penetration of the rib into the vertebra, a lower tensile stiffness was used to allow for some separation between rib and vertebra. Only one rod element was used at the costovertebral joints between the rib heads and the vertebrae. For most ribs, the rib head articulates with two adjacent vertebrae. However, the use of only one rod was found to be adequate to model the overall rib-vertebrae kinematics demonstrated in experimental studies.

The costotransverse joint was modelled by a beam element oriented normal to the rib neck axis. Once again, bi-linear properties were specified to prevent penetration and allow easier separation. A schematic illustration of the structural model of the costovertebral and costotransverse joints is shown in Fig. 4.12.

Similar to the costosternal joint, the ligaments of the costovertebral and costotransverse joints were not modelled explicitly, but rather were lumped into the overall behaviour of the joints. The choice of the appropriate material properties was determined, once again, through the numerical simulation of the experiments of Schultz et al (1974b). A small portion of each rib was loaded in three orthogonal directions at a point which was the average of the 5 specimens tested. The attachments of the costovertebral and costotransverse joints at the vertebrae were fixed in all directions. A trial set of material properties were

initially used and subsequently adjusted till agreement between experiment and model was established. The adjustment of the properties was quite straightforward, by keeping in mind that the predominant motion must be a rotation about the rib neck axis. The final set of properties for the beam and rod elements are presented in Chapter 5.

#### **4.2.2.4 Intercostal Structures**

To model the passive response of the intercostal muscles and tendonous attachments between each of the ribs, a number of rod elements were used. They were arranged in a criss-cross pattern between each rib similar to the external and internal intercostal muscles. Each node from one rib was attached to four other nodes; two on an adjacent superior and two on an adjacent inferior rib, except rib 1 and 10 which could only be attached inferiorly and superiorly, respectively. Therefore, 20 elements were used between each rib on either side, for a total of 360 elements. Since the muscular and tendonous tissues are incapable of resisting compressive forces, bi-linear properties were used for the intercostal elements. The compressive stiffness was assumed to be 10 times less than the tensile stiffness. This ensured that there was little compressive resistance between adjacent ribs, while preventing overlap and physical interaction. The tensile properties for these elements were determined by the numerical simulation of experiments on the lateral and anterior/posterior stiffness of the ribcage. This procedure is detailed in the following section.

#### **4.2.2.5 Assembled Ribcage**

The elements of the individual components of the ribcage were combined together into the assembled ribcage using the three-dimensional nodal coordinates. The assembled ribcage is shown in Fig. 4.13. In summary, the model was composed of 180 beam elements for the bony ribs, 50 beam elements for the costal cartilages, 6 plate elements for the sternum, 20 beam elements for the costotransverse joints, 20 rod elements for the costovertebral joints and 360 rod elements for the intercostal tissues, for a total of 636 elements. The nodal coordinates of the elements were defined by 283 grid points. Additionally, 20 other grid points were included in the model for the locations of the vertebral centres and

shear centres of the spinal column (see Section 3.6), for a total of 303 nodes.

The spinal column stiffnesses were not, of course, included in this model, but rather were part of the beam-column model. However, several constraints had to be included in the ribcage model to ensure compatibility with the spinal model. The spinal column model assumed that the spine was inextensible, due to high axial stiffness, and that no deformation of the cross-section occurred. Therefore, rigid body elements were included at each rib level to ensure that no cross-sectional deformation occurred between the costovertebral and costotransverse nodes on the vertebrae. The four nodes were thus rigidly linked at each rib level. Similarly, to prevent relative axial displacement between the rib levels, a rigid rod element was added between each node at the vertebral centres. These nodes were then pin-connected to the rigid body elements interconnecting the costovertebral and costotransverse joints. Therefore, 20 rigid body elements were also included in the ribcage model to represent the high axial and cross-sectional stiffness of the spinal column. Otherwise, no other constraints were imposed between the rib levels.

The overall deflection behaviour of the ribcage was validated by comparison with experimental results in the literature, as done for the previous models. Agostini et al (1966) subjected the muscle relaxed ribcage of three live males to a lateral squeezing force of up to 147 N. The subjects were in a sitting position during the experiment. The changes in the lateral diameter, as well as the anterior-posterior diameter (measured between the sternum and the vertebrae) were recorded at the level of the xiphoid process. The loads were applied to the ribcage through two plates (140 mm × 30 mm) positioned on either side, just ventral to the muscle latissimus dorsi and centred at the height of the xiphoid process. To simulate these experiments, lateral forces were applied to the two most lateral nodes on either side for ribs 5-8. Therefore, the lateral load was distributed over 8 nodes on either side. A net lateral force of 120 N was applied to either side. The vertebral centre node of the first vertebra was constrained against vertical displacement, since the high axial stiffness of the spinal column would prevent vertical motion. The vertebral centre node of the 10<sup>th</sup> vertebra was also constrained against displacement to simulate the vertical sitting position of the test subjects. To simulate the back support against which the volunteers

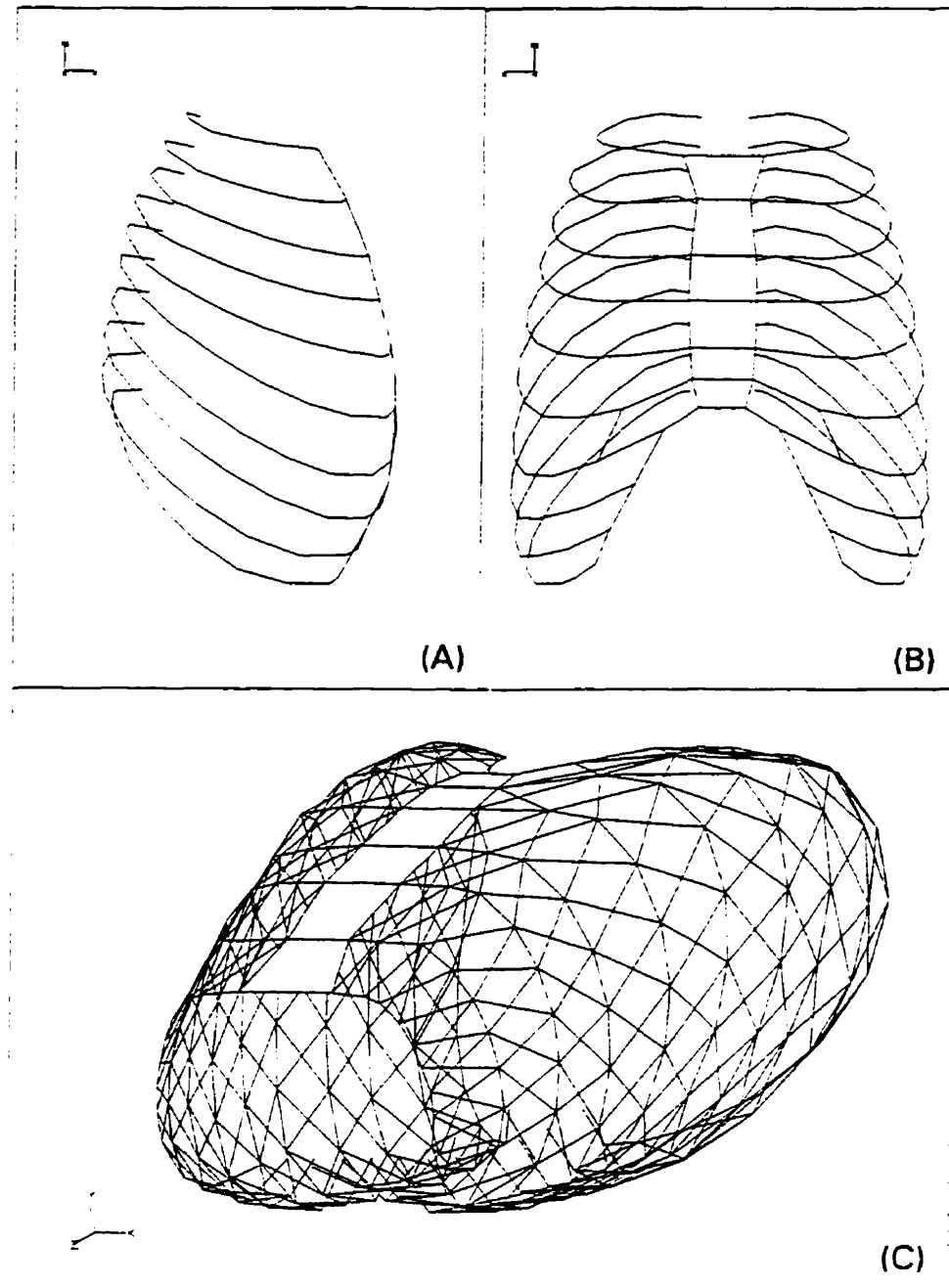


Figure 4.13: The finite element model of the assembled ribcage. (A) Lateral view; (B) Frontal view; (C) General view. Note that in (A) and (B) the intercostal elements were removed for clarity and only shown in (C). Also, beam and rod elements are only illustrated by a line to represent the elastic axis.

sat, the most posterior nodes on either side were constrained against anterior-posterior translation and completely unconstrained in other directions.

Nahum et al (1971) subjected both embalmed and fresh (unembalmed) cadavers to frontal compression loads on the sternum. A 152 mm diameter striker applied the compression load to the sternum, centred at the rib 4-5 level. The posterior of the ribcage was restrained by a rigid support. Loads of up to 616 N were applied. To simulate these experiments, a compression force of 500 N was applied to four nodes of the sternum, located at the junctions of ribs 4 and 5 with the sternum. The most posterior nodes on each rib of either side were constrained against anterior-posterior translation, to simulate the back support.

As discussed in the previous section, the tensile properties of the intercostal elements were chosen through trial and error to ensure a reasonable agreement between model predictions and the experiments just described. In preliminary investigations, it was found that the intercostals primarily affected the response of the ribcage to the lateral squeezing force, as opposed to the frontal compression force. Therefore, the intercostal values were chosen by first matching the model predictions to the experimental results for the lateral loads. The final property values are presented in Chapter 5, along with the validation of the overall ribcage response.

### 4.3 Solution

The analyses were performed using the general purpose finite element program MSC/Nastran (V65, MacNeal-Schwendler Corporation, Los Angeles, CA, USA). The program was implemented on a mainframe environment (IBM 3090-200E, with vector processing). The output was downloaded from the mainframe environment to a PC environment for analysis. The program FEMAP (V1.1, Enterprise Software Products, Harleysville, PA, USA) was used for post-processing of the nodal displacement data.

The solution sequences SOL24, SOL64 and SOL66 were used for linear, geometric nonlinearity, and geometric and material nonlinearity, respectively. Relatively small load

increments were usually required due to the high differences in stiffness properties between the bony and soft tissues structures, otherwise numerical divergence problems occurred. The bi-linear properties were handled through SOL66, however, usually only one load increment was required if geometric nonlinearity was not considered.

## 4.4 Equivalent Stiffness of the Ribcage

The finite element model of the ribcage, described in the previous sections, was developed in order to investigate the support provided for the spinal column through a passive mechanism. As a passive structure, the ribcage provides an elastic restraint against the deforming ribcage. The forces of the ribcage are transferred to the spine through the costovertebral and costotransverse joints. Therefore, the interaction between the spine and ribcage is very specific, occurring at four joints on each vertebra. In the present model, it is proposed to take advantage of this anatomical feature in order to provide a relatively simple means of incorporating the ribcage support into the spinal column model.

Previous models of the spine that have not directly modelled the ribcage, have either omitted its support entirely, or included it in a lumped form (see Chapter 2). The entire stiffness of the ribcage was modelled by increasing the thoracic bending stiffness, or considering the thoracic region of the spine as rigid. This was not felt to adequately model the three-dimensional ribcage support. In particular, the ribcage support is likely to vary with spine level due to the changing geometry of the ribcage. Furthermore, the ribcage support in a lateral-medial direction is likely to be different from that in an anterior-posterior direction. Therefore, in the following two sections, a model is first proposed for the representation of the three-dimensional stiffness of the ribcage, and secondly, a series of numerical experiments are outlined to establish the magnitude of the ribcage support.

### 4.4.1 Model of the Equivalent Stiffness of the Ribcage

Due to the specific nature of the spine and ribcage interaction, it is proposed that the passive response of the ribcage can be replaced by a 3-D elastic medium which surrounds

the spine. Furthermore, the properties of the elastic medium would vary with rib level. To illustrate the concept, consider only the lateral deformation of the spine. At each rib level, the relative displacement between the spine and ribcage is elastically restrained in the coronal plane (Fig. 4.14). The stiffness of the elastic restraint is a function of the collective actions of the various components of the ribcage, and their respective geometry and properties. Furthermore, there is both a "push" and a "pull" reaction from either side of the ribcage. Therefore, the total lateral stiffness of the ribcage can be replaced by a series of elastic springs for each rib level. The stiffnesses of the springs are clearly expected to be a function of rib level due to the changing geometry of the ribcage from top to bottom. The foregoing discussion was confined to only the lateral stiffness of the ribcage. An equivalent elastic stiffness for the ribcage could equally be specified for all other directions. Thus, the ribcage can be considered as a 3-D elastic medium which surrounds the spinal column and restrains its motion in all directions (Fig. 4.15). The 3-D elastic restraint, however, is transferred to the spine through four joints at each rib level. Therefore, the ribcage stiffness can and need only be specified at each rib level.

The experimental studies on the ribcage stiffness in the frontal and lateral directions, which were used to validate the present FEM model, showed that the passive response of the ribcage was linear in a large range. In a frontal direction, with loads up to 600 N, the displacements remained linear up to 60 mm (Nahum et al, 1971). In a lateral direction, changes to the ribcage diameter, with loads up to 120 N, remained very linear up to 24 mm (Agostini et al. 1966) and in an experiment on the lateral flexibility of both the spinal column and the ribcage, a linear response up to lateral loads of 250 N, with a lateral translation of 25 mm, was found (Halsall et al, 1983). The apex of a mild scoliotic curve might be displaced laterally 10 - 40 mm and even less in the sagittal plane. Consequently, if this full offset is transferred to the ribcage, a linear reaction can be expected all along the spine. Therefore, it was felt that the 3-D stiffness of the ribcage could be adequately specified with linear stiffnesses. A further discussion regarding this point is presented in Chapter 5 on the validation of the present FEM, where both linear and geometric nonlinear models are compared with experiment.

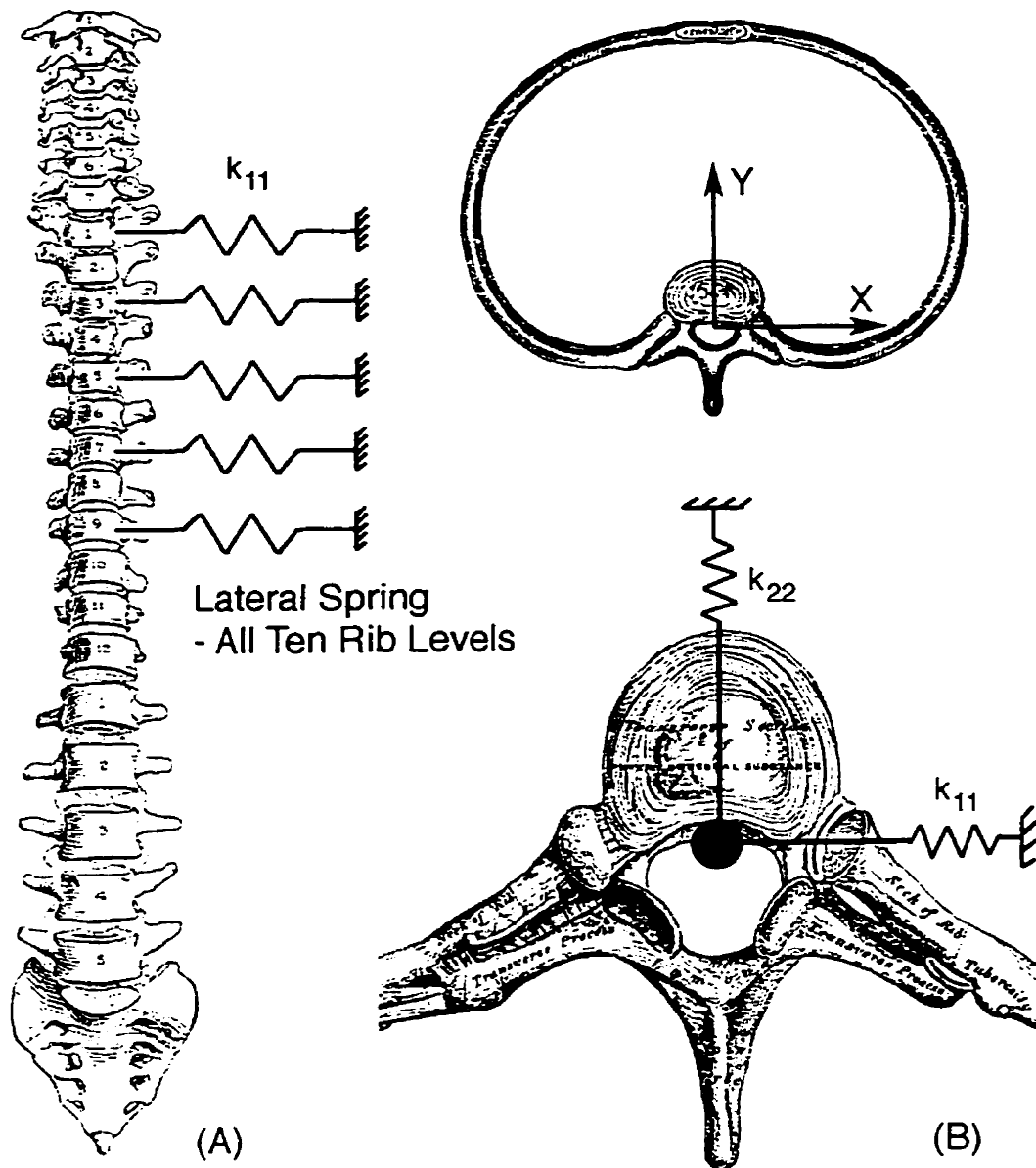


Figure 4.14: Model of the elastic restraint exerted by the ribcage against the spinal column in response to lateral bending in the coronal plane (Adapted from Gray, 1989). At each vertebral level, the collective actions of the ribcage are replaced by a spring acting in the coronal plane at a point  $S_R$  in the transverse plane. (A) Coronal plane view; (B) Transverse plane view at one vertebral level.

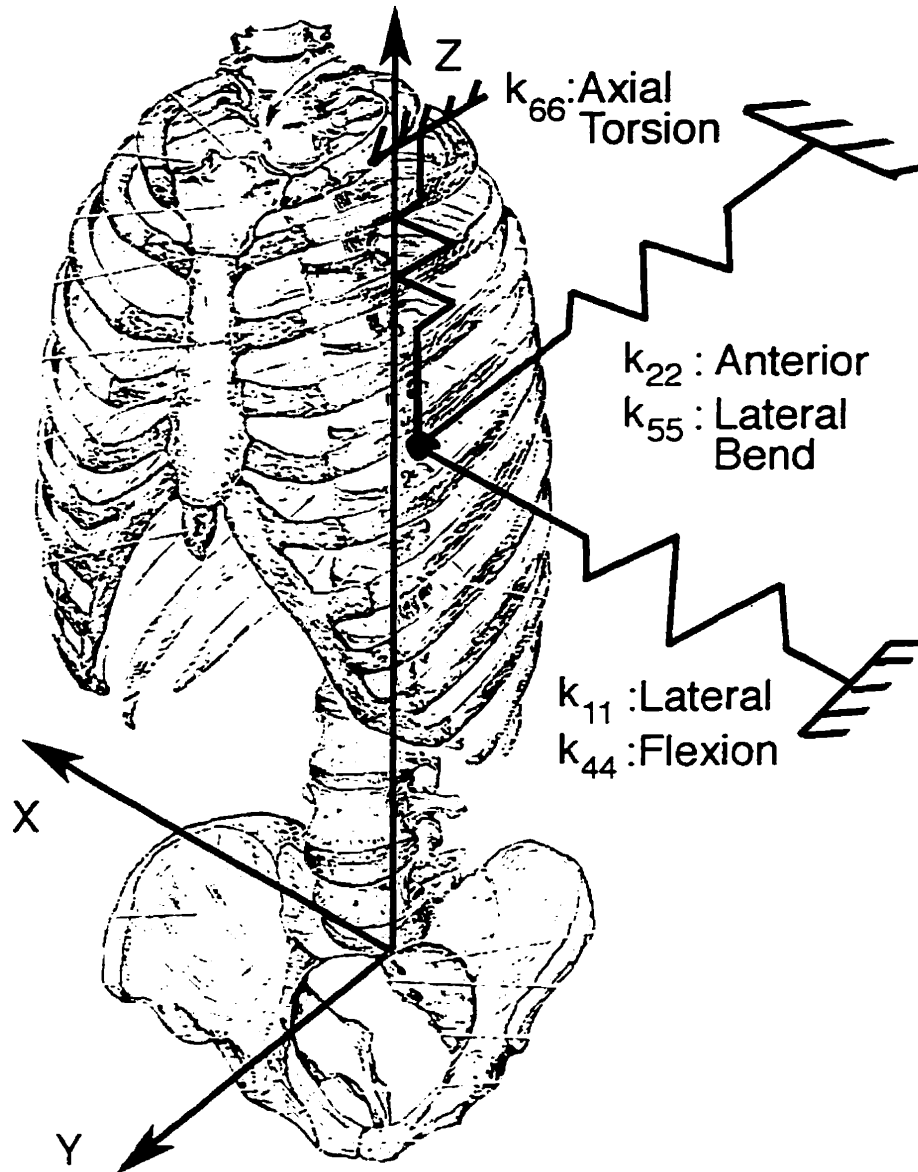


Figure 4.15: Three-dimensional model of the elastic restraint of the ribcage which surrounds the spinal column (Adapted from Gray, 1989). At each vertebral level, both translational and rotational springs are used to model the 3-D support of the ribcage.

In order to express the ribcage stiffness in a general form, consider a point  $S_R$  about which the stiffnesses are to be expressed. Three translations,  $T_x$ ,  $T_y$  and  $T_z$ , as well as three rotations,  $R_x$ ,  $R_y$  and  $R_z$ , expressed in the fixed system,  $i_j$ , are defined at point  $S_R$ . In general matrix form, the 3-D ribcage stiffness, at each rib level, can then be expressed as follows:

$$\begin{Bmatrix} \mathcal{F}_x \\ \mathcal{F}_y \\ \mathcal{F}_z \\ \mathcal{M}_x \\ \mathcal{M}_y \\ \mathcal{M}_z \end{Bmatrix} = \begin{bmatrix} k_{11} & k_{12} & k_{13} & k_{14} & k_{15} & k_{16} \\ & k_{22} & k_{23} & k_{24} & k_{25} & k_{26} \\ & & k_{33} & k_{34} & k_{35} & k_{36} \\ & & & k_{44} & k_{45} & k_{46} \\ & & & & k_{55} & k_{56} \\ & & & & & k_{66} \end{bmatrix} \begin{Bmatrix} T_x \\ T_y \\ T_z \\ R_x \\ R_y \\ R_z \end{Bmatrix} \quad (4.9)$$

where  $\mathcal{F}_x$ ,  $\mathcal{F}_y$  and  $\mathcal{F}_z$  are forces, and  $\mathcal{M}_x$ ,  $\mathcal{M}_y$  and  $\mathcal{M}_z$  are moments in the fixed system,  $i_j$ . The terms of the matrix,  $k_{11}$ ,  $k_{12}$ , ..., etc. are the stiffness values of the ribcage. The diagonal terms represent the principal stiffnesses, whereas the off-diagonal terms are coupled stiffnesses. For example,  $k_{11}$  is the lateral stiffness illustrated in Fig. 4.14 at a given rib level. The terms  $k_{12}$ ,  $k_{13}$ ,  $k_{14}$ ,  $k_{15}$  and  $k_{16}$  exist only if the force  $\mathcal{F}_x$  produces translations and rotations in the other directions, in addition to the principal translation  $T_x$ . At each rib level, a stiffness matrix can be defined, so that 10 matrices in total are required to describe the overall ribcage stiffness.

Due to the characteristics of the spine and symmetry, not all the terms of the stiffness matrix need be evaluated. First, due to the high axial stiffness of the spinal column, it was assumed to be inextensible. Even if axial deformation did occur, the ribcage is not well positioned to resist these motions. Consequently, the third row and third column can be dropped from equation (4.9). Second, due to symmetry about the mid-sagittal plane, some of the coupled stiffnesses must be zero. A force in the anterior-posterior direction ( $\mathcal{F}_y$ ) cannot produce a medial-lateral translation ( $T_x$ ), a lateral rotation ( $R_y$ ) or an axial rotation ( $R_z$ ). Therefore,  $k_{21}$ ,  $k_{25}$  and  $k_{26}$  must be zero, which in turn, implies that  $k_{12}$ ,  $k_{52}$  and  $k_{62}$  must also be zero. Similarly, a flexion-extension moment ( $\mathcal{M}_x$ ) cannot produce a

medial-lateral translation ( $T_x$ ), a lateral rotation ( $R_y$ ) or an axial rotation ( $R_z$ ). Therefore,  $k_{41}$ ,  $k_{45}$  and  $k_{46}$  must be zero, which again implies that  $k_{14}$ ,  $k_{54}$  and  $k_{64}$  must also be zero. Therefore, equation (4.9) can be simplified as follows:

$$\begin{Bmatrix} \mathcal{F}_x \\ \mathcal{F}_y \\ \mathcal{M}_x \\ \mathcal{M}_y \\ \mathcal{M}_z \end{Bmatrix} = \begin{bmatrix} k_{11} & 0 & 0 & k_{15} & k_{16} \\ & k_{22} & k_{24} & 0 & 0 \\ & & k_{44} & 0 & 0 \\ & & & k_{55} & k_{56} \\ & & & & k_{66} \end{bmatrix} \begin{Bmatrix} T_x \\ T_y \\ R_x \\ R_y \\ R_z \end{Bmatrix}. \quad (4.10)$$

The stiffness matrix is considerably simplified and only five principal stiffnesses remain, along with four coupled stiffnesses.

If point  $S_R$  is chosen as the shear centre of the motion segment, as described in Chapter 3, then the ribcage stiffness can be incorporated directly into the spatial beam-column equations. The governing equations of the beam-column determine the displacements of the elastic axis located at the shear centre, in response to forces and moments applied at the shear centre. In the beam-column equations, the forces and moments were specified per unit length. Therefore, equation (4.10) must be converted to a unit length basis. Since a stiffness matrix has been specified at each rib level, each matrix was divided by the distance between the vertebral centres at the given rib level (see Section 3.6). In this way, the applied forces and moments per unit length from the ribcage were specified in a step-wise manner along the spine. This is not an unreasonable approach since each rib articulates with a vertebra at two costovertebral joints which span the disc height. Furthermore, there are ligamentous attachments to the vertebrae both superior and inferior to the rib head. Therefore, the rib-vertebra interactions are spread over a distance nearly equal to the distance between the vertebral centres.

At a given rib level, the ribcage stiffnesses are expressed as follows:

$$\begin{Bmatrix} f_x^r \\ f_y^r \\ m_x^r \\ m_y^r \\ m_z^r \end{Bmatrix} = \begin{bmatrix} k_{11}^o & 0 & 0 & k_{15}^o & k_{16}^o \\ & k_{22}^o & k_{24}^o & 0 & 0 \\ & & k_{44}^o & 0 & 0 \\ & & & k_{55}^o & k_{56}^o \\ & & & & k_{66}^o \end{bmatrix} \begin{Bmatrix} T_x \\ T_y \\ R_x \\ R_y \\ R_z \end{Bmatrix} \quad (4.11)$$

where  $f_x^r$ ,  $f_y^r$ ,  $m_x^r$ ,  $m_y^r$  and  $m_z^r$  are the forces and moments per unit length, specified in the fixed system. The stiffness terms  $k_{11}^o$ ,  $k_{15}^o$ ,  $k_{16}^o$ , etc. are now specified per unit length. In order to incorporate these passive reactions of the ribcage into the beam-column equations, they must be transformed into the undeformed coordinate system, since the beam-column equations were resolved in that system. The applied ribcage forces and moments  $f_x^r$ ,  $f_y^r$ ,  $m_x^r$ ,  $m_y^r$  and  $m_z^r$ , in the fixed system, are related to the applied forces and moments,  $f_i^r$  and  $m_i^r$ , in the undeformed system, through the rotation matrix  $C_{ij}^o$ , originally defined in equation (3.20), which relates the undeformed system,  $\hat{e}_i$ , to the fixed system  $\hat{i}_j$ . Therefore, the following expressions are found for the applied forces

$$\begin{aligned} f_1^r &= f_x^r C_{12}^o + f_y^r C_{13}^o \\ f_2^r &= f_x^r C_{22}^o + f_y^r C_{23}^o \\ f_3^r &= f_x^r C_{32}^o + f_y^r C_{33}^o, \end{aligned} \quad (4.12)$$

and for the applied moments

$$\begin{aligned} m_1^r &= m_z^r C_{11}^o + m_x^r C_{12}^o + m_y^r C_{13}^o \\ m_2^r &= m_z^r C_{21}^o + m_x^r C_{22}^o + m_y^r C_{23}^o \\ m_3^r &= m_z^r C_{31}^o + m_x^r C_{32}^o + m_y^r C_{33}^o. \end{aligned} \quad (4.13)$$

The components of the matrix  $C_{ij}^o$  were specified in equation (3.121), and equations (4.12) and (4.13) can be rewritten as follows:

$$f_1^r = f_x^r u_{0,1} + f_y^r v_{0,1}$$

$$\begin{aligned}
f_2^r &= f_x^r + f_y^r \theta_0 \\
f_3^r &= -f_x^r (\theta_0 + u_{0,1} v_{0,1}) + f_y^r
\end{aligned} \tag{4.14}$$

and

$$\begin{aligned}
m_1^r &= m_z^r + m_x^r u_{0,1} + m_y^r v_{0,1} \\
m_2^r &= -m_z^r (u_{0,1} + \theta_0 v_{0,1}) + m_x^r + m_y^r \theta_0 \\
m_3^r &= -m_z^r (v_{0,1} - \theta_0 u_{0,1}) - m_x^r (\theta_0 + u_{0,1} v_{0,1}) + m_y^r .
\end{aligned} \tag{4.15}$$

Using equations (4.14) and (4.15), the ribcage reactions can be incorporated into the beam-column equations through the applied forces and moments,  $f_i$  and  $m_i$ , which are included in the formulation of the governing equations.

The ribcage forces and moments are best described as reactions, since they are zero unless the normal relative anatomic position between the spine and ribcage is changed. The greater the relative motion, the greater is the reaction. Consequently, they are functions of the displacement of the spine, and the sense of the force or moment is opposite to the direction of motion. It is, therefore, necessary to relate the deformation of the ribcage, given by  $T_x$ ,  $T_y$ ,  $R_x$ ,  $R_y$  and  $R_z$  in the fixed system, in a manner consistent with the displacement of the spinal column, which was expressed in the undeformed system.

First, consider the translations  $T_x$  and  $T_y$ , which can be related to the translations  $u$  and  $v$  of the elastic axis through the rotation matrix  $C_{ij}^o$ . The translations  $u$  and  $v$  are expressed in the undeformed system,  $\hat{e}_i$ , as follows (see equation 3.22)<sup>1</sup>:

$$\hat{D}_0 = u \hat{e}_2 + v \hat{e}_3 , \tag{4.16}$$

and in the fixed system,  $\hat{i}_j$ , as

$$\hat{D}_0 = (u C_{21}^o + v C_{31}^o) \hat{i}_1 + (u C_{22}^o + v C_{32}^o) \hat{i}_2 + (u C_{23}^o + v C_{33}^o) \hat{i}_3 . \tag{4.17}$$

The components in the  $\hat{i}_2$  and  $\hat{i}_3$  directions represent the translations  $T_x$  and  $T_y$ , respectively, of the elastic axis in the fixed system under the action of the applied loads. Additionally, there are the components  $u_0$  and  $v_0$  due to the initial displacements which are

---

<sup>1</sup>Note that the axial displacement  $w$  has been dropped in accordance with the assumptions of small axial displacements.

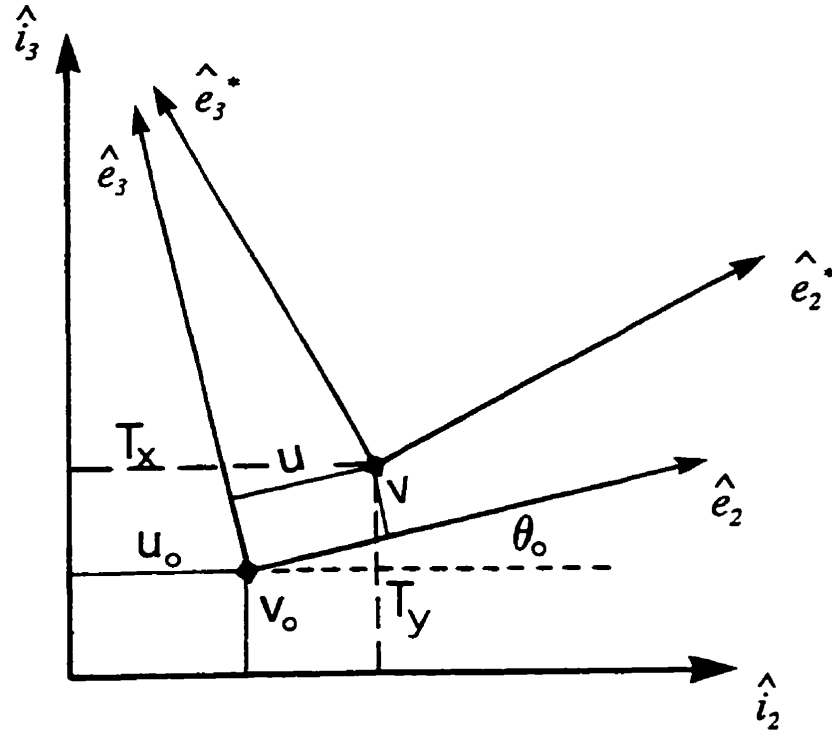


Figure 4.16: Translation of the shear centre as viewed in the transverse plane. Note that since the systems are not necessarily co-planar, then only the projections of the axes of the coordinate systems  $\hat{e}_i$  and  $\hat{e}_i^*$  onto the fixed system  $\hat{i}_j$  in the transverse plane are shown.

already defined in the fixed system. Using equation (4.17), and (3.121) for the components of  $C_{ij}^o$ , the translations  $T_x$  and  $T_y$  can then be expressed as follows (Fig. 4.16):

$$\begin{aligned} T_x &= u_0 + u - v\theta_0 \\ T_y &= v_0 + v + u\theta_0 \end{aligned} \quad (4.18)$$

These expressions represent the total translation of the elastic axis, expressed in the fixed system. They are a combination of both the initial configuration and the displaced configuration. However, the initial displacement,  $v_0$ , used to represent the initial sagittal profile of the spine should not result in a passive reaction from the ribcage. Since the ribcage is naturally curved to match the sagittal profile, it is expected that no passive reaction in the anterior-posterior direction would be present. Therefore, the translations  $T_x$  and  $T_y$

are better expressed as

$$\begin{aligned} T_x &= u_0 + u - v\theta_0 \\ T_y &= v + u\theta_0 \end{aligned} \quad (4.19)$$

where the initial anterior-posterior translation,  $v_0$ , has been dropped. The effects of the initial scoliotic shape given by  $u_0$  and  $\theta_0$ , however, are retained. If the scoliotic shape included an anterior-posterior component, then the effect of this on the ribcage reactions could be included through the  $v_0$  term of equation (4.18).

The rotations  $R_x$ ,  $R_y$  and  $R_z$  must also be related to the displacement variables of the beam-column. This was achieved by equating the terms of two separate rotation matrices, one involving expressions related to  $R_x$ ,  $R_y$  and  $R_z$  and the other involving the displacement variables of the beam column,  $u$ ,  $v$  and  $\theta$ . As discussed earlier, the passive response of the ribcage was considered to be linear in the range of motion of a mild scoliosis. Consequently, the ribcage response is independent of load history, and the rotations  $R_x$ ,  $R_y$  and  $R_z$  can be applied in any sequence. However, due to the nonlinearity of the beam-column model, it is necessary to express the rotations  $R_x$ ,  $R_y$  and  $R_z$  in a manner consistent with the beam-column equations. The deformed system,  $\hat{e}_i^*$ , can be related to the fixed system,  $\hat{i}_j$ , as follows:

$$\hat{e}_i^* = C_{ij} \hat{i}_j \quad (4.20)$$

where

$$C_{ij} = C_{ik}^* C_{kj}^o \quad (4.21)$$

The rotation matrix,  $C_{ij}$ , is the product of the two rotation matrices,  $C_{ik}^*$  and  $C_{kj}^o$ , which relate the intermediate undeformed system to the deformed and fixed systems, respectively.

Therefore, multiplying these matrices together, the following expression for  $C_{ij}$  is found:

$$C_{ij} = \begin{bmatrix} 1 & u_{0,1} + u_{,1} - \theta_0 v_{,1} - k_\zeta v & v_{0,1} + v_{,1} + \theta_0 u_{,1} + k_\zeta u \\ \left[ - (u_{0,1} + \theta_0 v_{0,1}) - (u_{,1} + \theta v_{,1}) \right. \\ \left. - \theta v_{0,1} + k_\zeta v \right] & 1 & \theta_0 + \theta - v_{0,1} u_{,1} \\ \left[ - (v_{0,1} - \theta_0 u_{0,1}) - (v_{,1} - \theta u_{,1}) \right. \\ \left. + \theta u_{0,1} - k_\zeta u \right] & \left[ - (\theta_0 + v_{0,1} u_{0,1}) \right. \\ & \left. - (\theta + v_{,1} u_{,1}) \right] & 1 \end{bmatrix} \quad (4.22)$$

where terms of  $\mathcal{O}(\epsilon^2)$  have again been neglected compared to unity. The rotation matrix,  $C_{ij}$ , represents the total rotation of the beam-column from a straight configuration, through an initial curvature and twist, to the spatially deformed configuration. The individual components of  $C_{ij}$  are, of course, the direction cosines of the deformed system,  $\hat{e}_i^*$ , relative to the fixed system  $\hat{i}_j$ . Due to the linearity of the ribcage stiffnesses, the rotations  $R_x$ ,  $R_y$  and  $R_z$  can be incorporated into the beam-column equations through any sequence of rotations. If a sequence of  $R_y$  about  $\hat{i}_3$ , followed by  $R_x$  about the rotated  $\hat{i}_2$ , followed by  $R_z$  about the rotated  $\hat{i}_1$  is used, then the rotation matrix is given by

$$C'_{ij} = \begin{bmatrix} C_x C_y & C_x S_y & -S_x \\ S_z S_x C_y - C_z S_y & C_z C_y + S_z S_x S_y & S_z C_x \\ C_z S_x C_y + S_z S_y & -S_z C_y + C_z S_x S_y & C_z C_x \end{bmatrix} \quad (4.23)$$

where  $C_x = \cos R_x$ ,  $C_y = \cos R_y$ ,  $S_x = \sin R_x$ , etc. The rotation matrix,  $C'_{ij}$ , of equation (4.23) relates the  $\hat{e}_i^*$  system to the  $\hat{i}_j$  system through three successive rotations  $R_y$ ,  $R_x$  and  $R_z$ . Therefore, the rotation matrix  $C'_{ij}$  must be identical to  $C_{ij}$  of equation (4.22) which also relates the  $\hat{e}_i^*$  system to the  $\hat{i}_j$  system. Using equation (4.23), the rotations  $R_x$ ,  $R_y$ , and  $R_z$  are given as follows:

$$\begin{aligned}
\sin R_x &= -C'_{13} \\
\tan R_y &= \frac{C'_{12}}{C'_{11}} \\
\tan R_z &= \frac{C'_{23}}{C'_{33}} .
\end{aligned} \tag{4.24}$$

If the rotation matrix for moderate rotations given in equation (4.22) is used for the components in equation (4.24), then the rotations are given by the following expressions.

$$\begin{aligned}
R_x &= -v_{0,1} - v_{,1} - \theta_0 u_{,1} - k_\zeta u \\
R_y &= u_{0,1} + u_{,1} - \theta_0 v_{,1} - k_\zeta v \\
R_z &= \theta_0 + \theta - v_{0,1} u_{,1} .
\end{aligned} \tag{4.25}$$

These expressions for  $R_x$ ,  $R_y$  and  $R_z$  are related to the rotations of the beam-column at the level of moderate rotations. It should be noted that if a different sequence of rotations is used, then slightly different expressions for  $R_x$ ,  $R_y$  and  $R_z$  are found. However, these differences are found to be 2nd order, which are considered negligible in the ordering scheme of moderate rotations.

Similar to the discussion for the translations, the initial sagittal profile should not cause a ribcage response. Therefore, if  $v_{0,1}$  only represents the normal sagittal profile of the spine, equation (4.25) should be simplified as follows:

$$\begin{aligned}
R_x &= -v_{,1} - \theta_0 u_{,1} - k_\zeta u \\
R_y &= u_{0,1} + u_{,1} - \theta_0 v_{,1} - k_\zeta v \\
R_z &= \theta_0 + \theta - v_{0,1} u_{,1}
\end{aligned} \tag{4.26}$$

where the  $v_{0,1}$  term has been dropped from the  $R_x$  expression. However, again, similar to the translations, the terms  $u_{0,1}$ ,  $\theta_0$  and  $k_\zeta$  are retained for the initial scoliotic shape.

It is now possible to express the ribcage reactions resolved in the undeformed system of the beam-column equations, as a function of the stiffnesses and of the displacement variables of the spine. Combining equations (4.11), (4.14), (4.15), (4.18) and (4.25), the following expressions for the ribcage reactions are found:

$$\begin{Bmatrix} f_1^r \\ f_2^r \\ f_3^r \\ m_1^r \\ m_2^r \\ m_3^r \end{Bmatrix} = [\mathcal{R}] \begin{Bmatrix} u_{.1} \\ v_{.1} \end{Bmatrix} + [\mathcal{D}] \begin{Bmatrix} u \\ v \\ \theta \end{Bmatrix} + \{ \mathcal{I} \} \quad (4.27)$$

where the components of  $[\mathcal{R}]$ ,  $[\mathcal{D}]$  and  $\{ \mathcal{I} \}$  are rather lengthy and are given in Appendix G. If only the principal stiffnesses are considered, then the expressions are somewhat simplified and given as follows:

$$\begin{aligned} f_1^r &= -[k_{11}^o u_{0.1} + k_{22}^o \theta_0 v_{0.1}] u - [k_{22}^o v_{0.1} - k_{11}^o \theta_0 u_{0.1}] v \\ &\quad - [k_{11}^o u_0 u_{0.1} + k_{22}^o v_0 v_{0.1}] \\ f_2^r &= -[k_{11}^o + k_{22}^o \theta_0^2] u - [(k_{22}^o - k_{11}^o) \theta_0] v - [k_{11}^o u_0 + k_{22}^o \theta_0 v_0] \\ f_3^r &= -[(k_{22}^o - k_{11}^o) \theta_0 - k_{11}^o u_{0.1} v_{0.1}] u - [k_{22}^o + k_{11}^o \theta_0^2 + k_{11}^o u_{0.1} v_{0.1}] v \\ &\quad - [k_{22}^o v_0 - k_{11}^o \theta_0 u_0 - k_{11}^o u_0 u_{0.1} v_{0.1}] \end{aligned} \quad (4.28)$$

and

$$\begin{aligned}
m_1^r &= -[ (k_{55}^o - k_{66}^o) v_{0,1} - k_{44}^o \theta_0 u_{0,1} ] u_{,1} + [ k_{44}^o u_{0,1} + k_{55}^o \theta_0 v_{0,1} ] v_{,1} \\
&\quad + [ k_{44}^o k_\zeta u_{0,1} ] u + [ k_{55}^o k_\zeta v_{0,1} ] v - k_{66}^o \theta \\
&\quad - [ k_{66}^o \theta_0 + (k_{55}^o - k_{44}^o) u_{0,1} v_{0,1} ] \\
m_2^r &= -[ (k_{55}^o - k_{44}^o) \theta_0 + k_{66}^o (u_{0,1} + \theta_0 v_{0,1}) v_{0,1} ] u_{,1} \\
&\quad + [ (k_{44}^o + k_{55}^o \theta_0^2) ] v_{,1} + [ k_{44}^o k_\zeta ] u + [ k_{55}^o k_\zeta \theta_0 ] v \\
&\quad + [ k_{66}^o (u_{0,1} + \theta_0 v_{0,1}) ] \theta - [ (k_{55}^o - k_{66}^o) \theta_0 u_{0,1} - (k_{44}^o + k_{66}^o \theta_0^2) v_{0,1} ] \\
m_3^r &= -[ k_{55}^o + k_{44}^o \theta_0^2 + k_{66}^o v_{0,1}^2 + (k_{44}^o - k_{66}^o) \theta_0 v_{0,1} u_{0,1} ] u_{,1} \\
&\quad - [ (k_{44}^o - k_{55}^o) \theta_0 + k_{44}^o u_{0,1} v_{0,1} ] v_{,1} - [ k_{44}^o k_\zeta (\theta_0 + u_{0,1} v_{0,1}) ] u \\
&\quad + [ k_{55}^o k_\zeta ] v + [ k_{66}^o (v_{0,1} - \theta_0 u_{0,1}) ] \theta \\
&\quad - [ (k_{55}^o + k_{44}^o v_{0,1}^2 + k_{66}^o \theta_0^2) u_{0,1} + (k_{44}^o - k_{66}^o) \theta_0 v_{0,1} ] . \tag{4.29}
\end{aligned}$$

It should be noted that in these expressions, the stiffnesses are not taken to be of the same order necessarily. Consequently, higher order terms related to the initial displacements are retained. For example, since  $k_{55}^o$  is not necessarily the same order as  $k_{44}^o$ , then terms such as  $k_{44}^o \theta_0^2$  cannot be dropped compared to  $k_{55}^o$ .

The total loads, from the ribcage and body weight, applied to the spinal beam-column model are as follows:

$$\begin{aligned}
\hat{f} &= \hat{f}^w + \hat{f}^r \\
\hat{m} &= \hat{m}^w + \hat{m}^r \tag{4.30}
\end{aligned}$$

or in component form expressed in the undeformed system,

$$f_1 = f_1^w + f_1^r$$

$$\begin{aligned}
f_2 &= f_2^w + f_2^r \\
f_3 &= f_3^w + f_3^r \\
m_1 &= m_1^w + m_1^r \\
m_2 &= m_2^w + m_2^r \\
m_3 &= m_3^w + m_3^r
\end{aligned}
\tag{4.31}$$

These components have been established (see equations 3.121, 3.122 and 4.27) and can easily be incorporated into the governing equations, given by equation 3.107, through the terms  $f_i$  and  $m_i$  included in the formulation. It should also be noted that there is a change of sign in the ribcage reactions given by equation 4.27 when they are substituted into equation 3.107. At this stage, the model is now complete with the passive reactions of the ribcage included in the beam-column model of the spine. The equations have been expressed in a compact matrix form with the components of the matrices available in the appendices.

It must also be noted that the general ribcage response given in equation (4.27) is composed of two basic parts: a response related to the initial configuration, and a response due to the deformation from the initial configuration to the final position. Therefore, prior to the deformation of the spine, a constant ribcage load related to the initial configuration, given by the array  $\{I\}$ , is applied to the spine. As discussed earlier, the component related to the normal sagittal profile is not included in these terms, which should only be related to a mild scoliosis, which is an "unnatural" configuration and could generate a response from the ribcage. This model also assumes that the ribcage response is purely elastic with no variation with time. However, in reality, most biological tissues are viscoelastic, and consequently, stress relaxation occurs. The time frame for stress relaxation of the ribcage response is likely much less than the yearly time frame of curve progression in scoliosis. Therefore, during progression the ribcage response could be less than that predicted by a purely elastic analysis. The exact viscoelastic characteristics of the whole spine are not available and it is not possible to simulate this effect directly. However, if at each increment of body load the array  $\{I\}$  is set equal to zero, the ribcage response would only be related to

the subsequent deformation. In other words, the ribcage reactions are completely relaxed after each load increment so that no constant ribcage load is included. This simulation of stress relaxation would represent the minimum ribcage response, whereas the inclusion of the constant load related to the initial configuration would represent the maximum ribcage response. In reality, the actual ribcage response would likely be somewhere between these extremes.

It is also apparent from equations (4.27-4.29) that the spine and ribcage interactions are functions of the initial scoliotic shape included in the terms of  $[\mathcal{R}]$  and  $[\mathcal{D}]$ . The components of these matrices are related to both the pure stiffness of the ribcage and to other terms involving the stiffnesses and the initial scoliotic shape. This, of course, reflects the changing geometric relationship between the initial configuration of a mildly scoliotic spine and the ribcage. The stiffnesses, however, remain constant, regardless of the changes, due to the assumed linearity of the ribcage response. In other words, the stiffness of a normal ribcage is assumed identical to that of a mild scoliosis.

The final point to consider with regard to the present model of the passive reactions of the ribcage are the boundary conditions used in the finite element model. The elastic stiffnesses used to surround the spine are intended to represent the relative stiffness between the spine and ribcage. Clearly, in day-to-day activities, the spine can undergo large motions which are nearly identical to the ribcage motions with little relative displacement. Consequently, only minimal passive bracing of the spine from the ribcage would occur in these situations. However, the present model is only concerned with the ribcage response to a mild scoliotic curve, and the relative displacement between the spine and ribcage during curve progression. Therefore, the boundary conditions of the ribcage should reflect its position during the progression of a mild scoliosis. In the stages of a mild scoliosis, the sternum remains close to its normal anatomic position (Closkey and Schultz, 1992). Thus, in the finite element model, the sternum is fixed in its anatomic position in order to establish the relative stiffnesses between the spine and ribcage. This is likely an oversimplification of the situation, and these stiffnesses can be considered as the upper bound.

#### 4.4.2 Procedure for the Numerical Experiments

As discussed in the foregoing section, the ribcage stiffness was incorporated into the beam-column equations through distributed forces and moments acting at the shear centre of the spine. The forces and moments were in turn expressed in terms of stiffness matrices specified at each rib level. To determine the nonzero terms of these matrices, a series of numerical experiments were performed with the developed FEM, and are described in this section. These experiments could have been performed in two separate ways. In the first technique, the shear centre is displaced in the principal directions one at a time. From the resultant reactions at the shear centre, it is possible to determine the stiffnesses. Alternately, pure forces and moments in each of the principal directions are applied one at a time. From the resultant displacements of the shear centre, it is possible to determine the flexibilities instead of the stiffnesses. These two techniques, generally referred to as the stiffness and the flexibility method, respectively, provide essentially the same information. However, in the flexibility method, it is necessary to invert the flexibility matrix to determine the stiffness matrix. Generally, in experimental situations, it is difficult to apply pure displacements, and the flexibility method is adopted (Panjabi et al, 1976). In the present model, if displacements had been applied to the rigid elements used to model the vertebrae, the reactions could not have been determined. Therefore, for the present analysis, it was necessary to adopt the flexibility approach. Equation (4.10) can be expressed in terms of flexibilities as follows:

$$\begin{Bmatrix} T_x \\ T_y \\ R_x \\ R_y \\ R_z \end{Bmatrix} = \begin{bmatrix} f_{11} & 0 & 0 & f_{15} & f_{16} \\ & f_{22} & f_{24} & 0 & 0 \\ & & f_{44} & 0 & 0 \\ & & & f_{55} & f_{56} \\ & & & & f_{66} \end{bmatrix} \begin{Bmatrix} \mathcal{F}_x \\ \mathcal{F}_y \\ \mathcal{M}_x \\ \mathcal{M}_y \\ \mathcal{M}_z \end{Bmatrix} \quad (4.32)$$

where  $f_{11}$ ,  $f_{22}$ ,  $f_{44}$  etc. are the principal flexibilities, and  $f_{15}$ ,  $f_{16}$ ,  $f_{24}$  and  $f_{56}$  are the coupled flexibilities.

Using equation (4.32), the flexibilities at each rib level were determined by applying,

one at a time, the forces and moments to the shear centre. The resultant principal and coupled displacements were determined, from which the flexibilities could be calculated. Consider, for example, the situation when a pure lateral force  $\mathcal{F}_x$  was applied. From the resultant displacements, the following flexibilities were then determined

$$\begin{aligned} f_{11} &= T_x/\mathcal{F}_x \\ f_{15} &= R_y/\mathcal{F}_x \\ f_{16} &= R_z/\mathcal{F}_x \end{aligned} \quad (4.33)$$

Similarly, the other flexibilities were determined from each of the loading conditions by the same procedure. Once the flexibility matrix at a given rib level was determined, it was inverted to determine the stiffness matrix. Note that for significant values of the coupled flexibilities the matrix must be inverted and not just the reciprocals of the flexibilities used for the stiffnesses. In this manner, the stiffnesses  $k_{11}$ ,  $k_{22}$  etc. were determined for each rib level and then the stiffnesses  $k_{11}^o$ ,  $k_{22}^o$  per unit length calculated. It should also be noted that through this procedure, both the “push” and “pull” reactions from either side of the ribcage were collectively contained in these stiffnesses.

#### 4.4.2.1 Sensitivity Analysis

In Chapter 5, the finite element model of the ribcage is first validated in a consistent manner by comparing the predictions of a model with *adult geometry* to experiments performed on *adults*. Cadaveric experimental data to validate an adolescent ribcage model is not available, and would be nearly impossible to obtain. Therefore, a series of *sensitivity analyses* were performed with the *adult ribcage model* in order to estimate the stiffnesses for a *young adolescent ribcage*. This sensitivity analysis was also used to estimate the differences in the ribcage stiffnesses between an *adult male* and *female* due to differences in geometry.

Changes in four separate parameters of the ribcage were considered: 1) gross ribcage geometry, 2) rib cross-sectional properties, 3) the lengths of the costal cartilages, and 4) material properties of the soft and bony tissues. These changes were considered separately

in order to understand how each change contributes to the overall difference when all the changes were combined. A summary of these changes in a total of ten models is presented in Table 4.1, and described in detail below. It should also be noted that the effect of changes in the ribcage stiffnesses was also investigated in the parametric analysis of the whole spine model presented in Chapter 7.

To investigate the effects of the *gross ribcage geometry* on the stiffnesses, three separate models were generated. In each of the models, the *width*, *depth* or *height* of the ribcage was reduced by 20%, respectively. These reduction values were based on anthropometric data of the thorax width, the biacromial distance, the thorax depth, the thorax circumference and the spine length of a nine year old girl and ten to eleven year old boy compared to their values in an adult (Tanner, 1962; Watson and Lowrey, 1962; Anderson et al. 1965; Howatt and DeMuth, 1965; Eveleth and Tanner et al, 1966; McCammon, 1970; Karlberg and Taranger, 1976; Tanner, 1976; Sinclair, 1978). These results were based on studies which were conducted on populations of Western societies which were similar to those used to establish the changes made to the spine model (see Chapter 3).

To investigate the effects of the *rib cross-sectional properties*, two separate changes were considered. The *major* and *minor diameters* of the outer cortical walls of the ribs were reduced by 20%, since the rib cross-sectional dimensions have reached about 80% of their adult value and the total rib areas about 60-65% ( $\sim .8^2 \times 100$ ) by the age of 9 and 10-11 years in girls and boys, respectively (Sedlin et al, 1963; Sedlin, 1964; Takahashi and Frost, 1966). However, though the gross dimensions are increasing, the *ratio of cortical to total area* decreases consistently from birth throughout life (Sedlin, 1964; Takahashi and Frost, 1966). This change was simulated by decreasing the ratio of the inner dimensions to the outer dimensions by 20% via the parameter  $t_c$  which gave a ratio of the cortical area to the total area of 0.6, which was reported for a 9 year old girl and 10-11 year old boy. Therefore, though the total rib cross-sections are smaller in adolescents compared to adults, they have thicker cortical walls, which should counteract the changes due to smaller ribs to a certain extent.

To investigate the effects of an increased *costal cartilage region*, the lengths of the costal

cartilages were increased by 30% to simulate an adolescent compared to an adult. In the growing adolescent, the rib tips become gradually ossified, such that the lengths of the costal cartilages are gradually decreased until adulthood. In the model of Stokes et al (1991), based on adolescent ribcage geometry, the properties of soft tissues were increased compared to the current model to achieve agreement with the lateral and anterior load experiments conducted on adults. These authors argued that this increase in modulus was needed to counteract the softening due to the increased region of costal cartilage in their model. They also noted that in comparison to the experiments on isolated ribs (Schultz et al, 1974a), their model predicted much larger displacements due to the increased lengths of the costal cartilages.

To investigate the effect of *material properties*, five other models were generated. In the first, the *cortical bone modulus* was reduced by 25% since the modulus has reached about 75% of a young adult value by about 10 years of age males and females (Currey and Butler, 1975; Carter and Spengler, 1978). This reduction of modulus is due to changes in bone mineral content and cortical bone density (Currey, 1988; Gilsanz et al. 1988; Geusens et al, 1991; Keaveny and Hayes, 1993; Gilsanz et al, 1994; Mora et al. 1994). In the other four models, the *moduli of the soft tissues* of the ribcage, i.e., the intercostals, the costal cartilages, the costovertebral and the costotransverse joints, were individually reduced by 60% compared to the adult values in each of the models, respectively. These changes to the soft tissue material properties were made based on the estimates of increased flexibility in a young adolescent spine (Miller and Skogland, 1980c), as outlined in Section 3.10.1. Since this increased flexibility was likely due to changes in the ligaments, as well as the discs, it was felt that this reported difference could be extended to the ligamentous soft tissue of the adolescent ribcage.

Table 4.1: Summary of the ten models developed to investigate the sensitivity of the ribcage stiffnesses to changes in geometry and material property parameters.

Model	Percentage Change of Ribcage Parameter Compared to Values in the Validated Model										
	Gross Ribcage Dimensions			Rib Cross-Sectional Dimensions		Material Properties					Costal Cartilage Lengths
	Width	Depth	Height	$h_o, b_o$	$t_c$	$E_{cort}$	$E_{IC}$	$E_{CC}$	$E_{CV}$	$E_{CT}$	
G-RW	-20										
G-RD		-20									
G-RH			-20								
G-RCS				-20	-20						
G-CC										+30	
MP-CRI						-25					
MP-IC							-60				
MP-CC								-60			
MP-CV									-60		
MP-CT										-60	

#### 4.4.2.2 Determination of Adult Ribcage Stiffnesses

The FEM of the ribcage was developed and validated from data of both male and female adults. Therefore, it was considered to be representative of an "average" adult with no distinction between male and female. This model was then used to determine equivalent ribcage stiffnesses using the procedure described at the start of Section 4.4.2. These stiffnesses were presented in Section 6.2 and have been used to validate the whole spine model.

To determine the *ribcage stiffnesses* of an *adult female and male*, linear interpolation and extrapolation were used based on the results of the foregoing sensitivity analysis. It is not clear if there are any differences in the material properties of the soft tissues between female and male adults (Nachemson et al, 1979). In the absence of reported differences, the material properties of the ribcage soft tissues were assumed to be identical in males and females. Similarly, differences in the bone mineral content of cortical bone between adult females and males have been reported (Geusens et al, 1991; Gilsanz et al, 1994), but, it was less clear if there were differences in bone mineral density, and therefore, bone modulus. Geusens et al (1991) have reported an increased bone mineral density in males, whereas others have argued that these differences were due to differences in bone size, which has not always been accounted for in the experimental methodology (Gilsanz et al, 1988; Katzman et al, 1991; Gilsanz et al, 1994). Therefore, in the absence of reported differences in the modulus of cortical bone between females and males, it was assumed to be identical.

The geometry of the ribcage in males and females has been reported to differ. Firstly, the outer dimensions of the individual *rib cross-sections* of an adult female were reported to be 77-86% of an adult male (Sedlin et al, 1963). This was consistent with the results that the total cross-sectional area of the adult female rib was only about 62% of the male (Sedlin, 1964; Takahashi and Frost, 1966; Santoro and Frost, 1968), since the total area would be proportional to the square of the dimensions ( $\sim .8^2 \times 100 = 64\%$ ). On the other hand, the area of cortical bone in the female was reported to be about 86% of the male value (Sedlin et al, 1963; Sedlin, 1964; Takahashi and Frost, 1966; Santoro and Frost,

1968). Therefore, the ratio of cortical area to total rib cross-sectional area was increased from  $\sim 0.31$  in a male to  $\sim 0.43$  in a female, which implied that the cortical wall thickness is greater in females. Since this ratio in the present model was given by  $(1 - t_c^2)$ , then  $t_c$  was about 0.76 in females and 0.83 in males. In the "average" FEM developed, a value for  $t_c$  of 0.8 was used and a ratio of cortical bone area to total cross-sectional area of 0.36. Therefore, these values were both midway between those of a male and female. On the basis of the foregoing, the outer dimensions of the female rib were assumed to be 80% of the male, and the parameter which established the cortical wall thickness,  $t_c$ , was assumed to be reduced by 10% in the female. Using the results of the sensitivity analysis for changes in these parameters, the effect of these differences between the male and female ribs on the ribcage stiffnesses was determined with linear interpolation and extrapolation.

The second difference in the geometry of the male and female ribcage included in the model was the gross dimension. The *gross depth*, *width* and *height* of the female ribcage have been reported to be about 92-94% of the corresponding dimensions in males (Watson and Lowrey, 1962; Tanner et al, 1966; Anderson et al, 1965; McCammon, 1970; Eveleth and Tanner, 1976; Karlberg and Taranger, 1976; Lowrey, 1978). These data were obtained again from a broad range of Western populations and were found to be very repeatable. Therefore, it was assumed for the present study that the gross depth, width and height of the adult female ribcage were only 93% of the corresponding male dimensions. The results of the sensitivity analysis of the "average" ribcage were then used to establish the differences in ribcage stiffness of a male and female due to changes in the gross ribcage dimensions.

Some studies have also suggested that the *thoracic ratio* and *thoracic index* of the ribcage also differ between males and females (Davenport, 1934; Takahashi and Atsumi, 1955; Howatt and DeMuth, 1965; Davis and Troup, 1966; Karlberg and Taranger, 1976; Grivas et al, 1991). However, these reported differences were not consistent and only around 2-3%. Therefore, the thoracic ratio and index were assumed to be the same in females and males.

The foregoing differences in the rib cross-section and the gross ribcage dimensions were

superpositioned to establish the final differences in the ribcage stiffnesses of an adult female and male. Further, the ribcage stiffnesses per unit length included the differences in spine length of the male and female which also contributed to differences in the final stiffness values. These final stiffnesses are presented in Section 6.4.

#### 4.4.2.3 Determination of Adolescent Ribcage Stiffnesses

The magnitude and sense of the changes used in the sensitivity analysis were based on the differences between a *9 year old girl* and an *adult female*, and a *10 to 11 year old boy* and an *adult male*. At these ages, boys and girls were reported to have about an equal percentage of their growth remaining to reach adulthood. For example, the ribcage width of a 9 year old girl was 80% of the value of that of an adult female, and similarly, the ribcage width of a 10 to 11 year old boy was also 80% of an adult male. However, in a female, growth is fully ended by 16 years whereas in a male, it is closer to 18 years. Therefore, the results from each of the sensitivity studies were superpositioned, and the total difference in the ribcage stiffnesses of a 9 year old girl or 10 to 11 year old boy compared to an adult was determined. These results are presented in Section 6.4.

To determine the *stiffnesses at other ages between the 9 or 10-11 year old and the adult*, interpolation could be readily employed due to the linearity of the model. The *increments of the gross ribcage dimensions* were determined from available growth charts (Tanner, 1962; Watson and Lowrey, 1962; Anderson et al, 1965; Howatt and DeMuth, 1965; Tanner et al, 1966; McCammon, 1970; Karlberg and Tanner, 1976; Eveleth and Taranger, 1976; Lowrey, 1978). These data were again from a broad population of Western societies, which demonstrated very close agreement in the yearly growth increments as a percent of the final dimension. Separate growth charts were used for females and males which included the differential adolescent growth spurts. The specific changes in the gross ribcage dimensions from young adolescence to adulthood are shown in Fig. 4.17.

The *increments in the individual rib cross-sectional properties* were based on the reported data for the changes with age in the rib dimensions (Sedlin et al, 1963), and total and cortical areas (Sedlin et al, 1963; Sedlin, 1964; Takahashi and Frost, 1966). Since the

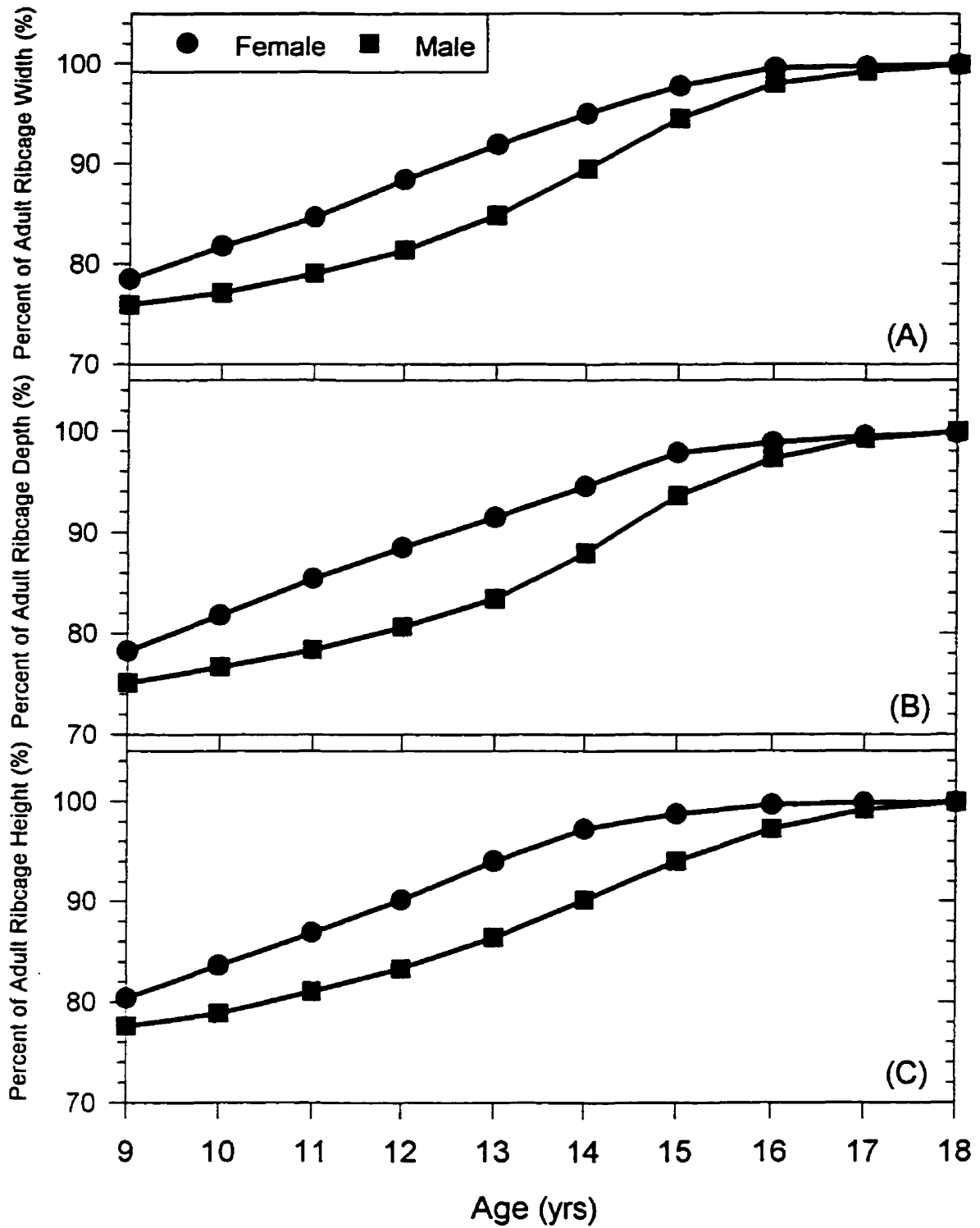


Figure 4.17: The ribcage dimensions as a percentage of the adult value for females and males from young adolescence to adulthood. (A) Gross ribcage width; (B) Gross ribcage depth; (C) Gross ribcage height. The earlier growth spurt of the females is evident.

data was not detailed enough, only uniform increments were used at all ages between the 9 or 10-11 year old and adult.

The increments for the material properties of the bone and soft tissues were also assumed to be uniform. As discussed in Section 3.10.2, there was not enough detailed information to implement variable increments due to the growth spurt.

These differences at each age were collectively superpositioned to establish the ribcage stiffnesses as a function of age. At each age, the *ribcage stiffnesses per unit length* were also determined using the changing spine length as detailed in Section 3.10. The final ribcage stiffnesses per unit length at all ages for male and female are presented in Section 6.4.

To summarize, the 3-D ribcage stiffnesses at all rib levels of an "average" adult were determined from a validated FEM of the ribcage. A sensitivity analysis was then conducted to establish the effect of changes in geometry and material properties of the ribcage on these stiffnesses. The results of this analysis were used to estimate the differences between an adult female and male ribcage, and the maximum changes in the stiffnesses of a young adolescent, both male and female, compared to an adult. Finally, using interpolation in conjunction with growth charts, the ribcage stiffnesses at all ages between young adolescence and adulthood were determined.

In Fig. 4.18, a flowchart is presented to illustrate the overall current approach of first developing both a spine and ribcage model based on data of an "average" adult, with no distinction between male and female. These models were then validated against experimental data collected from the mechanical testing of the adult spine and ribcage. Subsequently, the geometry of this validated "average" model and the applied body weight were changed to represent an adult male and female. Finally, the material properties and geometry of the male and female models, as well as the applied body weights, were further changed to represent the male and female adolescent. These models were then used to analyze the mechanics of curve progression during the adolescent growth spurt. This current approach differs significantly from previous studies, which have used models developed and validated solely for an "average" adult male (Schultz, 1984; Scholten, 1986), or developed with adolescent geometry yet validated against data determined from adults

(Stokes et Laible. 1991). In other models, it is even less clear if they are representative of an adult or an adolescent because they are not rigorously validated and the choice of properties are not clearly justified (Patwardhan et al, 1986; Lindbeck, 1988; Noone et al, 1991). It is argued that the current approach of first validating an adult model, and then systematically and consistently changing the mechanical parameters to develop an adolescent model should provide greater insight into the progression of scoliosis in adolescence.

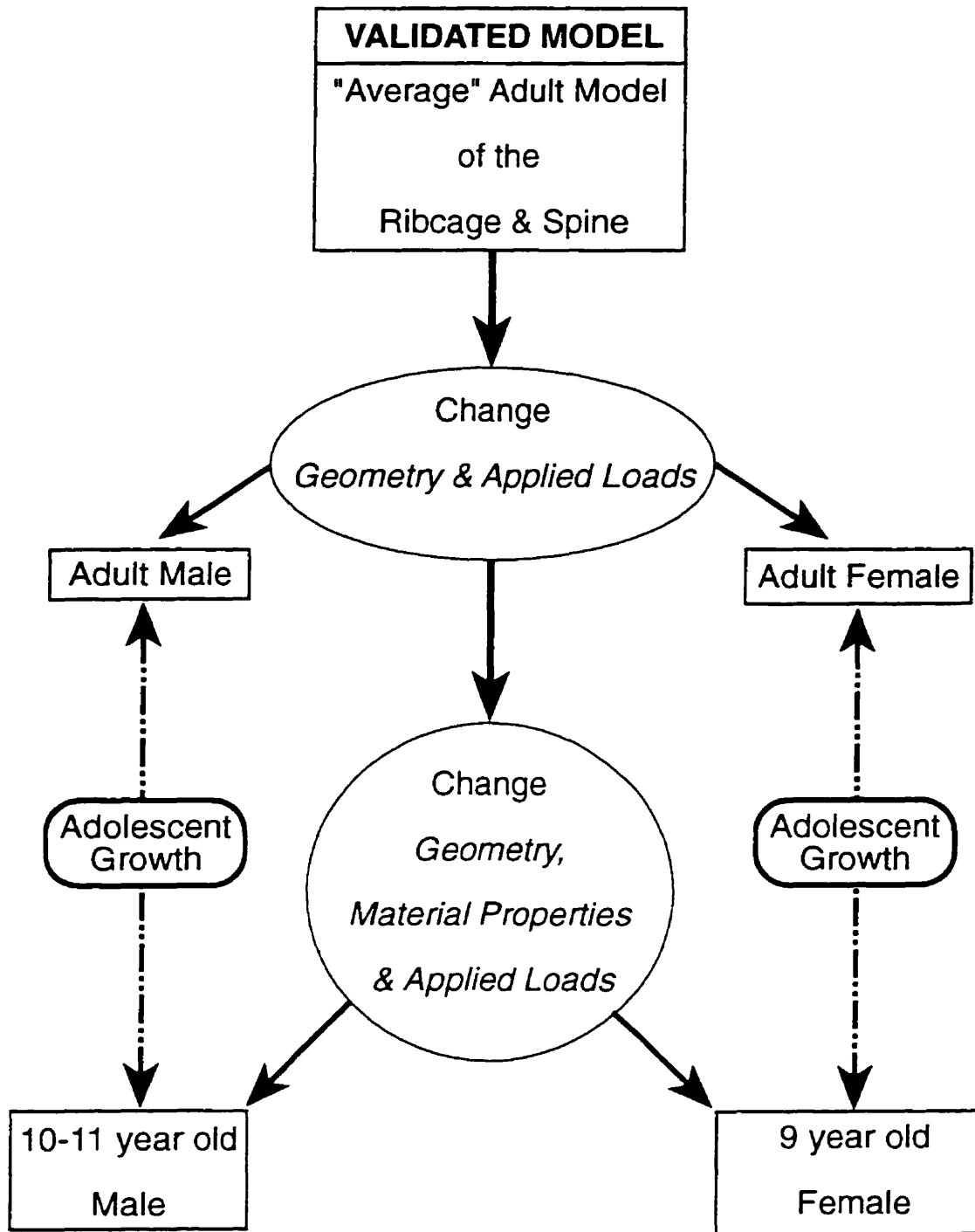


Figure 4.18: Flowchart of the current overall approach to model development, validation and analysis.

# Chapter 5

## VALIDATION OF THE PRESENT MODEL

### 5.1 Introduction

To validate the present analytic model, the predictions of the model were compared with the results of several experimental and model studies. Due to the nature of the present model, comparisons were first made for the predictions of the isolated ribcage followed by the spatial beam-column model with the incorporated equivalent ribcage stiffness. These validation studies were all conducted with “average” adult properties and loads for both the ribcage and spine models. It should be noted that the equivalent stiffness values of the ribcage are not presented until Chapter 6. However, the validation of the full spinal beam-column model with the ribcage stiffnesses is included in the present chapter in order to present the validation studies in a unified manner.

### 5.2 Finite Element Model of the Ribcage

First, the present finite element model predictions were compared with experimental results for the load-displacement behaviour of the individual components. As outlined in Chapter 4, this comparison was used to establish the final properties of some of the

elements. Next, the overall load-displacement behaviour of the assembled ribcage was compared with experiment, and one other set of properties determined. The present FEM of the ribcage was also compared with the other models in the literature.

### 5.2.1 Individual Ribcage Components

#### Ribs

As detailed in Chapter 4, the tips of the individual ribs were loaded with a 7.4 N force in medial/lateral, anterior/posterior and superior/inferior directions with respect to the rib coordinate system. The resulting deformations are reported in terms of the translations of the rib tips in the principal directions, respectively. Significant out-of-plane translations of the tips also occurred, which is in agreement with experimental observations. However, since only sample experimental results have been reported, these out-of-plane model predictions could not be validated. Similarly, the displacements along the rib length could not be compared with experimental results for a lack of data.

The present model predictions of the principal translations of the rib tips are shown in Fig. 5.1 for all ten ribs. The predictions were determined for three different sets (Cases A, B & C) of cross-sectional properties (see Chapter 4; Section 4.2.2.1.) in order to explore the effect of variation along a rib and between rib levels. Note that the comparisons were made for a geometrically linear analysis of the rib displacements, and therefore, no differences occurred for loads applied in opposite directions (i.e., medial/lateral, etc.). Regardless of the cross-sectional properties, the translations of the rib tips showed a clear variation with loading direction and rib level. The rib translations in the anterior/posterior directions were much less than in the other directions for ribs 2-10, whereas the medial/lateral and superior/inferior translations were of similar magnitude. The translations for rib 1 were similar in the medial/lateral and anterior/posterior directions, but were 3-4 mm larger in the superior/inferior direction. This behaviour was likely due to the orientation of the minor axis of rib 1 which was close to the transverse plane. The rib translations were in general maximum for ribs 7-8, for all loading conditions, which reflected the gross rib geometry. Ribs 7 and 8 were the longest ribs, and thus, the longer moment arm

for the superior/inferior and medial/lateral forces lead to increased translations. The anterior/posterior translations were also a reflection of the gross rib shape, but were also strongly influenced by the costal cartilage section at the tip. The anterior/posterior force was directed along an axis between the costotransverse joint and the tip. Therefore, the action of this force was affected by the medial/lateral offset of the curved rib from this axis. Though the radii were larger in lower ribs, the most lateral position of each rib changed little between ribs 4-8. The increase in the translations between ribs 1 and 4, therefore, was likely a result of the increased moment arm. The further increase in translations up to rib 8 was likely due to the increased length of the costal cartilage section on the rib. The subsequent decrease in the translations for ribs 9-10 was due to a combination of a decreased costal cartilage length and a decreased moment arm.

The foregoing description of the rib behaviour was found irrespective of the three sets of cross-sectional rib properties. There were, however, small differences and the use of Case A properties, which incorporated separate neck and shaft properties which varied with rib level, did provide a slightly better agreement with experiment. Therefore, the cross-sectional properties of Case A were used in all subsequent analyses.

In Fig. 5.2, the present model predictions of the rib tip translations are compared with the experimental measurements of Schultz et al (1974a) and the model predictions of Closkey et al (1992) for both a linear and a geometrically nonlinear analysis. Consequently, the results from forces applied in opposite directions are now presented separately due to differences in behaviour related to the updated geometry of a nonlinear analysis. Excellent agreement was found between the experimental results and the present model predictions for all loads and at most rib levels. The greatest differences occurred at rib 10 for all load directions except medial. There was no obvious reason for this discrepancy. However, it was possible that the costal cartilages were longer in the specimens compared with the present model, which could have contributed to the increased motion found experimentally. Alternatively, the cross-sectional properties in the present model could have differed from those in the experiment, which were not reported. The reductions in the model cross-sectional properties necessary to achieve agreement, however, appeared to be unreasonably

large. Examining the individual specimen data (Schultz et al, 1973a), it was noted that the displacements were double for one out of the five rib 10 specimens, in all directions, except medial. Consequently, the average experimental results from all five specimens were likely somewhat skewed at rib 10. If only the average of the four other specimens were used, then much closer agreement between the results of the experiment and the model predictions was found. The model predictions of Closkey et al (1992) also did not agree with the experimental results at rib 10, and were more similar to the present model.

The predictions of the present model were in close agreement with those from Closkey et al (1992). The largest differences occurred in ribs 2,4 and 6 for an anterior load. The present model translations were about 50% less, which resulted in better agreement with experiment. This better agreement was due possibly to the use of an elliptical cross-section in the present model, the orientation of which changed with rib level. Consequently, in the upper ribs, the major axis was better oriented to resist an anterior/posterior load, and contributed significantly to the anterior stiffness. In the model of Closkey et al (1992), beams at all rib levels were assigned the same stiffnesses.

The differences in the present model predictions from the linear and geometrically non-linear analyses were generally small at these load magnitudes. For a lateral force, the translations were predicted to be decreased for the nonlinear analysis, whereas they were increased for a medial load. Similarly, the nonlinear predictions were increased compared to the linear predictions for a posterior load, and decreased for an anterior load. These changes were at maximum only about 5 mm, and in general, much less than 10%. The differences between the linear and nonlinear predictions for superior/inferior loads were very small at less than 1%. More importantly, the agreement between the model predictions and experimental results was not significantly improved by the nonlinear analysis compared to the linear analysis. Therefore, at these load magnitudes, a linear analysis was clearly sufficient to predict the rib translations. This comparison, however, has only been performed at the given load magnitude. It is possible that for higher or lower loads, the model predictions would be less accurate. Furthermore, nonlinear material properties have not been considered either, since there are no values reported in the literature.

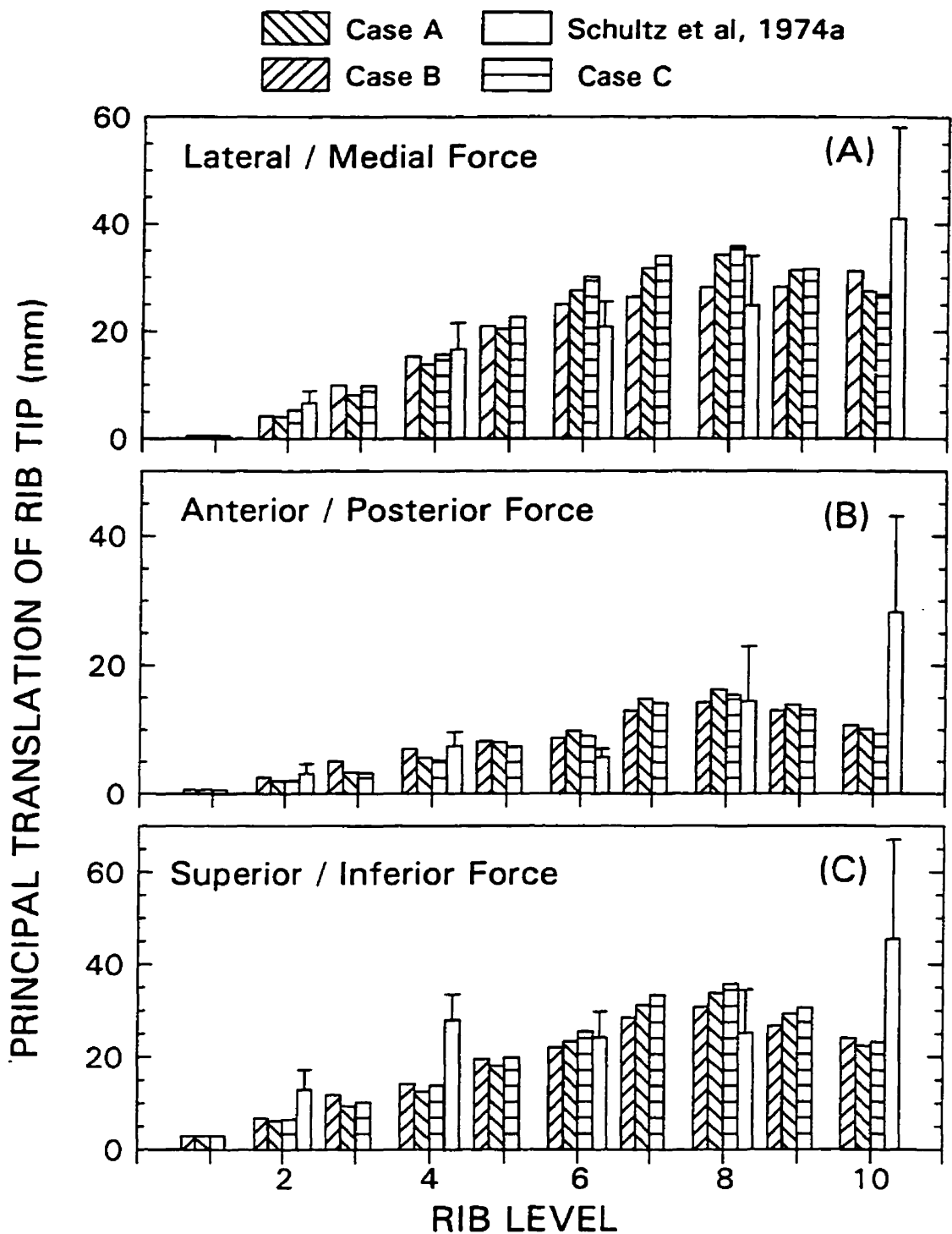


Figure 5.1: Predictions of the present model for the principal translations of the rib tips subjected to a force of 7.4 N for three different sets of rib cross-sectional properties. In comparison to the experimental results of Schultz et al (1974a) (averaged between opposite loading directions), the predictions using the cross-sectional properties of Case A were in closest agreement, although all cases were in good agreement. (A) Medial/Lateral Force; (B) Anterior/Posterior Force; (C) Superior/Inferior Force.

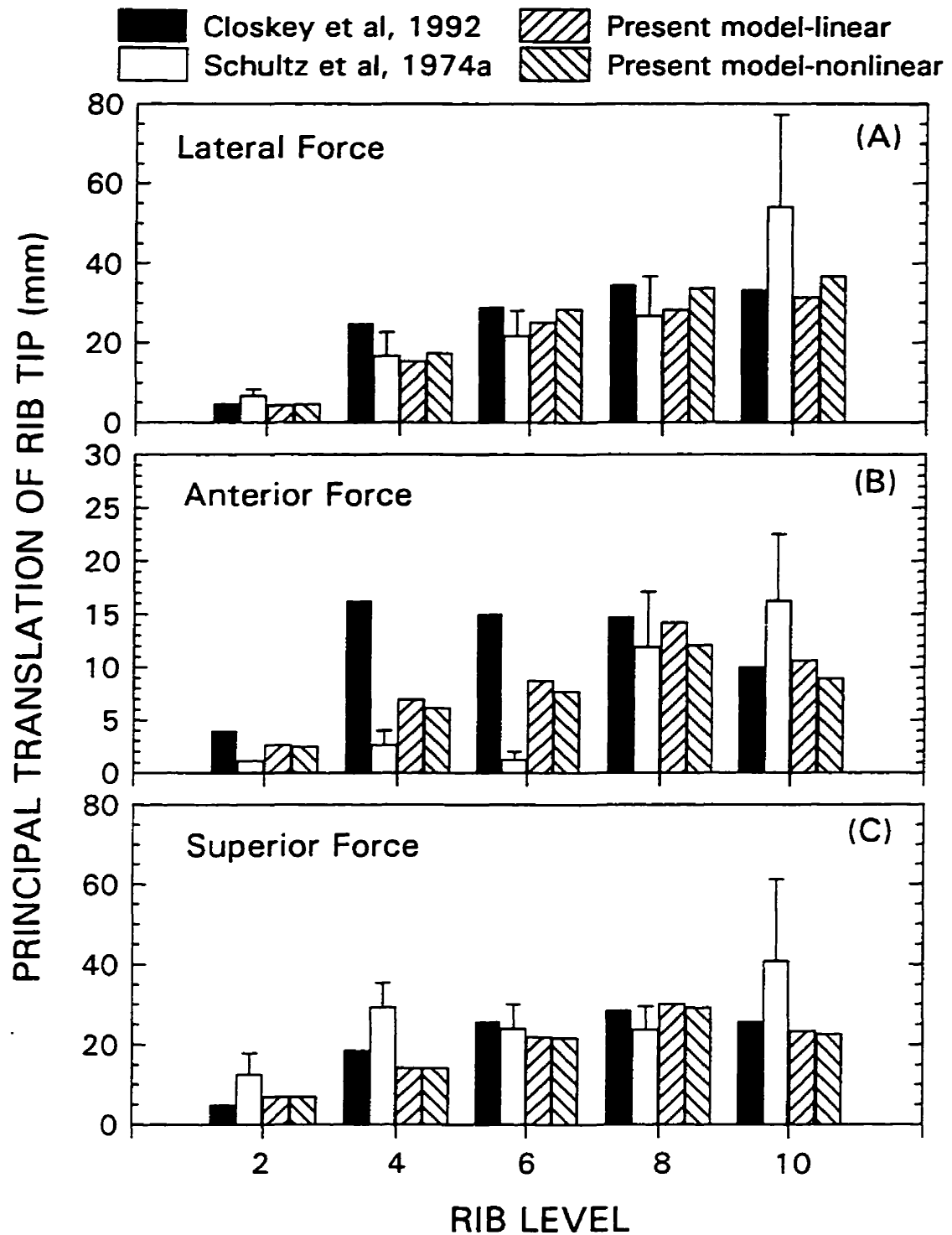


Figure 5.2: Predictions of the present model for the principal translations of the rib tips subjected to a force of 7.4 N for linear and geometrical nonlinear analyses. The predictions were generally in close agreement to other models (Closkey et al. 1992), and in better agreement with experiment (Schultz et al, 1974a) for rib levels 2, 4 and 6 for an anterior force. (A) Lateral Force; (B) Anterior Force; (C) Superior Force.

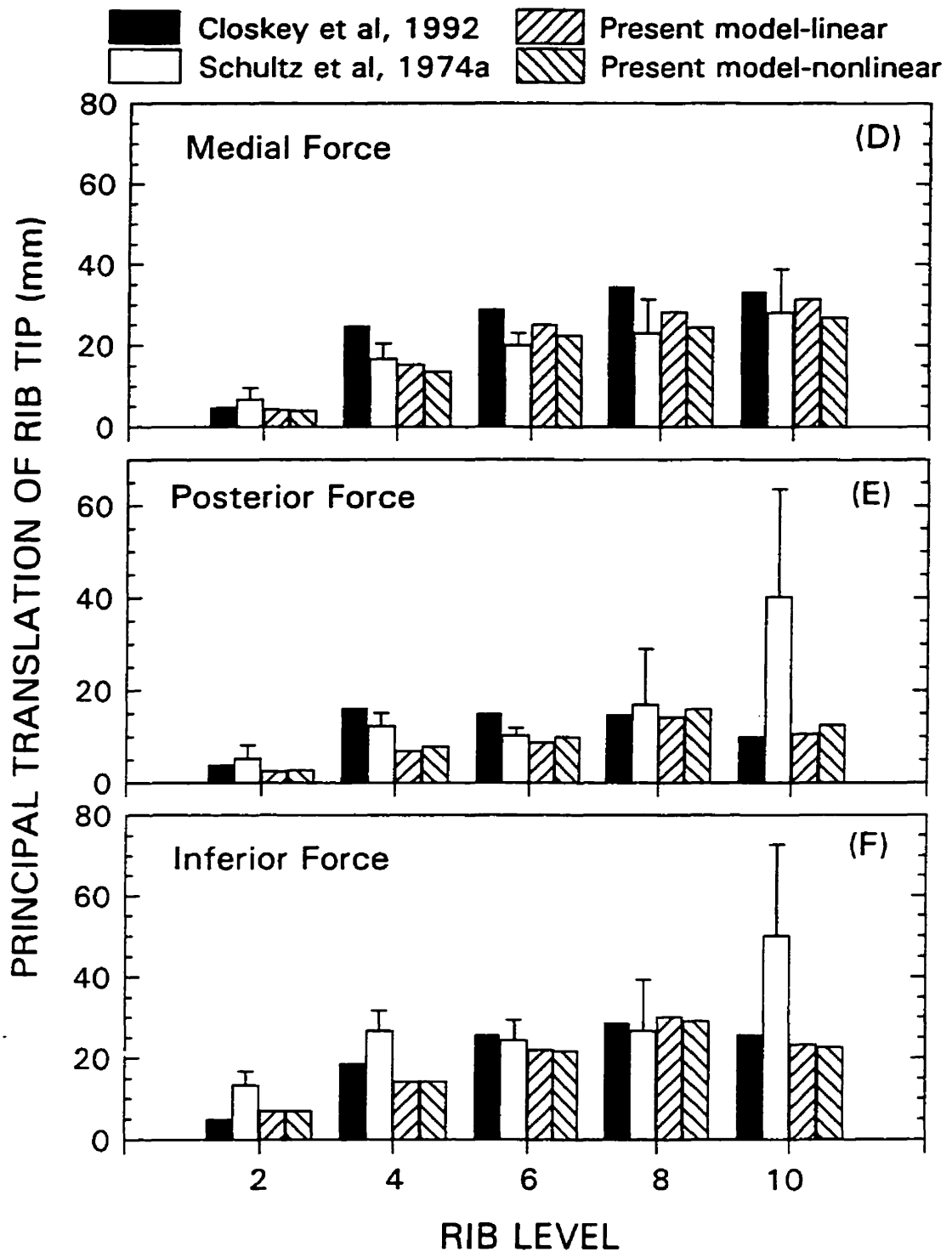


Figure. 5.2 (Con'd) Predictions for the present model of the principal translations of the rib tips subjected to a force of 7.4 N for linear and geometrical nonlinear analyses. The predictions were generally in close agreement to other models (Closkey et al. 1992), and in better agreement with experiment (Schultz et al. 1974a) for rib levels 2, 4 and 6 for an anterior force. (D) Medial Force; (E) Posterior Force; (F) Inferior Force.

It should also be noted that the nonlinear geometric analysis did predict a change in displacements from loads in opposite directions that was consistent with the experimental results. The posterior displacements were greater than the anterior displacements, and the lateral displacements were greater than the medial displacements, similar to the experimental results. The differences at these loads were not large, and the linear analysis predicted a value midway. At larger loads, however, the differences from opposite loads would only get larger, at which point the linear analysis would no longer predict displacements in either direction very well. These differences were easily explained due to the changing geometry with increasing load. As the anterior load was increased, the rib became straighter and the axial stiffness of the rib played a larger role. The predicted displacement from the nonlinear analysis was, therefore, reduced for the anterior load due to the high axial stiffness. On the other hand, as the posterior load was increased, the rib became more curved, and the lower bending stiffness played a larger role than the axial stiffness. The predicted nonlinear displacements were, therefore, increased for the posterior load. A similar analysis can also explain the difference between the nonlinear predictions for lateral and medial loads.

### **Costovertebral and Costotransverse Joints**

In order to establish the properties of the beam and rod elements used to simulate the costovertebral and costotransverse joints, a short segment of each rib was loaded with a 7.4 N force in three orthogonal directions, as described in Chapter 4. Excellent agreement was found between the predictions of the present model and those of the model of Andriacchi et al (1974), which was previously validated against the experimental results of Schultz et al (1974b) (Table 5.1). Since the load position was not exactly the same between the ribs from different cadavers and different rib levels in the experimental results, the reported results appeared rather variable. Therefore, presently, a more detailed comparison with the experimental results was not undertaken. There were, however, differences in the displacements between rib levels, which reflected the changing geometry of the costovertebral and costotransverse joints.

The property values of the costovertebral and costotransverse joints were thus assumed

Table 5.1: The present model predictions of the translations of a rib 6 segment loaded in three orthogonal directions about the costovertebral and costotransverse joints were found to be in excellent agreement compared to the model of Andriacchi et al (1974).

	Medial/Lateral (mm)	Anterior/Posterior (mm)	Superior/Inferior (mm)
Present Model	1.1	4.7	14.7
Andriacchi et al (1974)	1	5	11.5

Table 5.2: The present model predictions of the translations of a costal cartilage segment attached to rib 7 loaded in orthogonal directions about the costosternal joint were found to be in excellent agreement compared to the model of Andriacchi et al (1974).

	Anterior/Posterior (mm)	Superior/Inferior (mm)
Present Model	10.2	18.5
Andriacchi et al (1974)	10	14

to be the same for all rib levels in the present model: *costotransverse* -  $A = 10 \text{ mm}^2$ ,  $I_1 = 500 \text{ mm}^4$ ,  $I_2 = 500 \text{ mm}^4$ ,  $J = 500 \text{ mm}^4$ ,  $E_{\text{COMPRESSIVE}} = -1.5 \text{ MPa}$ ,  $E_{\text{TENSILE}} = 1.0 \text{ MPa}$ ; *costovertebral* -  $A = 10 \text{ mm}^2$ ,  $J = 500 \text{ mm}^4$ ,  $E_{\text{COMPRESSIVE}} = -0.3 \text{ MPa}$ ,  $E_{\text{TENSILE}} = 0.03 \text{ MPa}$ .

A nonlinear analysis was not performed since agreement between the model predictions and the experimental results was achieved with a linear analysis. Furthermore, nonlinear experimental load-displacement results or nonlinear properties have not been reported.

## Costal Cartilages

As described in Chapter 4, the costal cartilages were subjected to anterior/posterior and superior/inferior loads of 7.4 N with the sternum fixed, in order to establish appropriate properties of the costal cartilage elements. Excellent agreement was found between the present model predictions compared to the model predictions of Andriacchi et al (1974) which was previously validated against the experimental results of Schultz et al (1974b) (Table 5.2). The final properties of the beam elements used to model the costal cartilages at all levels were:  $A = 20 \text{ mm}^2$ ,  $I_1 = 150 \text{ mm}^4 = I_2$ ,  $J = 300 \text{ mm}^4$ ,  $E = 300 \text{ MPa}$ . Although difficult to compare directly due to differing dimensions, the Young's Modulus agrees with the value at 275 MPa used by Roberts and Chen (1970) and is smaller than the 480 MPa used by Stokes and Laible (1992). This difference is probably due to the larger region of costal cartilage in their model, which was reconstructed from an adolescent x-ray. Therefore, a stiffer costal cartilage was needed to achieve agreement with experiments conducted on adults. Again, a nonlinear analysis was not required since agreement was easily achieved with the linear analysis at the magnitude of loads considered.

### 5.2.2 Assembled Ribcage

The validation of the gross ribcage stiffness in both the lateral and anterior/posterior directions is presented in this section. As described in Chapter 4, the stiffness of the ribcage in response to a lateral squeezing force was first validated to establish the appropriate properties for the intercostal elements. In Fig. 5.3, the present model predictions for the change in ribcage diameter in both the lateral and anterior/posterior directions at the level of the xiphoid process due to a lateral squeezing force is presented. In comparison with the experimental measurements of Agostini et al (1966), on three live (muscle relaxed) males, excellent agreement was found. The present model prediction of the change in the lateral ribcage diameter was essentially identical compared to experiment, whereas the change in the anterior/posterior diameter was greater by less than 20%. A better comparison is the ratio of the percentage change of the anterior/posterior diameter to the percentage change of the lateral diameter, since this nondimensionalizes the ribcage dimensions which

may have differed between experiment and the model. Again, an excellent agreement was found with a ratio of -0.38 measured experimentally and a ratio of -0.41 predicted by the model. The properties of the intercostal elements needed to achieve this agreement were readily found through trial and error. The final values for the intercostal rod elements were  $A = 20 \text{ mm}^2$  and  $E = 2.5 \text{ MPa}$  in tension and  $0.25 \text{ MPa}$  in compression. The elements had negligible torsional stiffness.

This passive response of the intercostals had to be included in order to achieve agreement between experimental results and the model predictions. In simulations without intercostals, the ribs subjected to lateral loads displaced independent of the other ribs which is unrealistic. In particular, the change in the lateral ribcage diameter was much larger than observed experimentally. Without the intercostals, there was very small change in the anterior/posterior diameter which also did not agree with experiment. The inclusion of the intercostals stiffened the whole ribcage and ensured that the displacements from one rib were transferred to the adjacent ribs as seen in Fig. 5.4.

Most of the changes to the lateral diameter were due to rigid body rotations of the bony ribs about the rib-neck axis at the costovertebral and costotransverse joints. This was evident from examining the strains in the rib elements, which were found to be small. Nonetheless, the change in the ribcage diameter was partly due to deformation of the ribs. This rib motion is consistent with the actions of the ribs during respiration. On the other hand, the anterior/posterior changes were due mostly to the outward deformation of the flexible costal cartilage and to a lesser extent due to deformation of the bony ribs. This description of the change in ribcage diameters also explains why the intercostals predominantly affect changes to the lateral diameter. The intercostals are ideally oriented to resist the rigid body motion of the ribs relative to each other in directions normal to the plane in which they lie, but are poorly oriented to resist the outward expansion at the front of the ribcage.

In comparison with the results of the other models, the present model was more flexible than that of Andriacchi et al (1974), and therefore, was in much closer agreement with the experimental results. This result was not surprising due to the rigid ribs used in

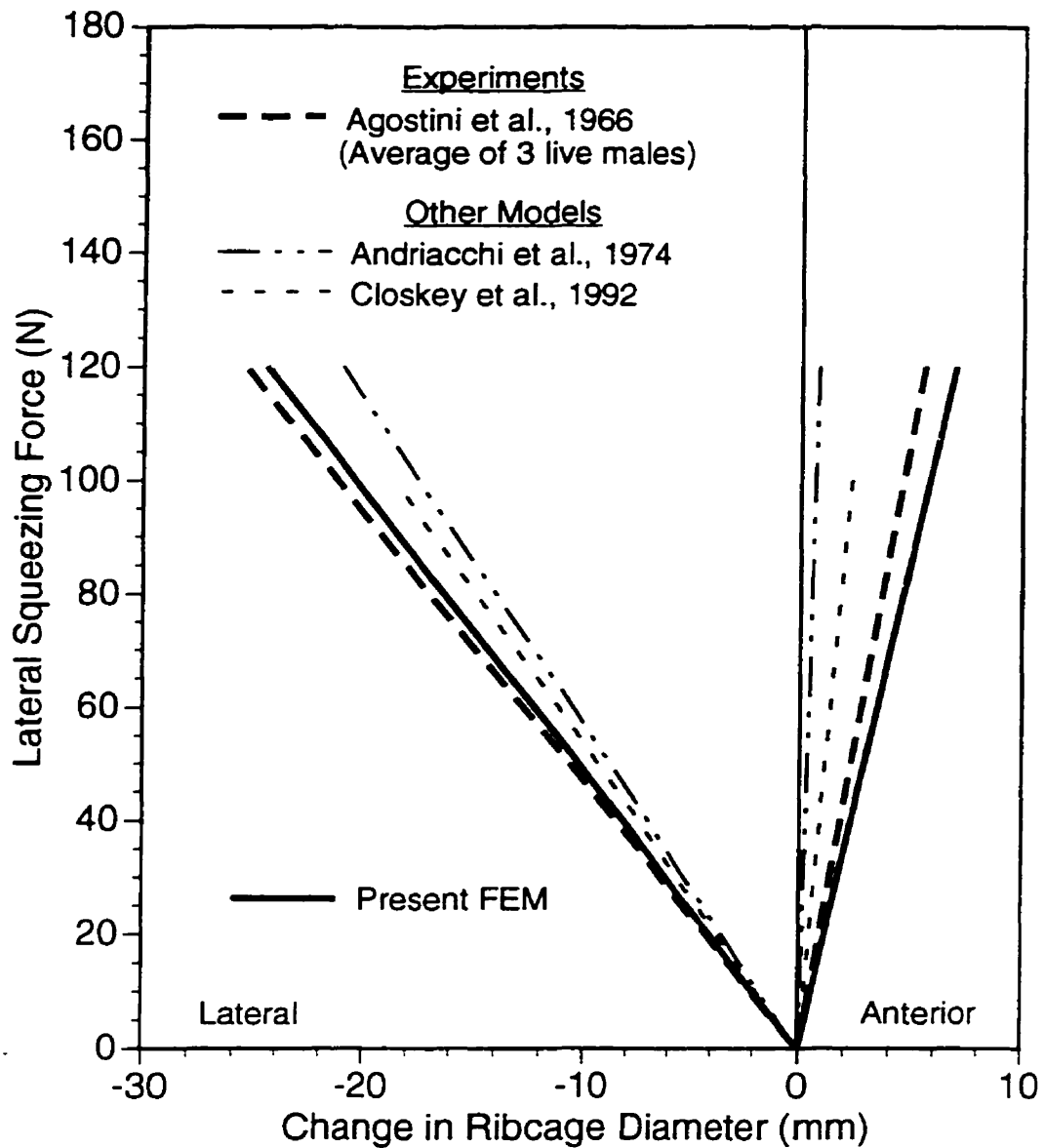


Figure 5.3: Comparison of the predictions of the present finite element model of the ribcage subjected to a lateral squeezing force compared with experiment and previous models. The predictions of the present model are only shown for a linear analysis to maintain clarity. Excellent agreement for the change in the lateral diameter was found in comparison to both experiment and previous models, whereas a better agreement with experiment was found for the change in anterior/posterior diameter.

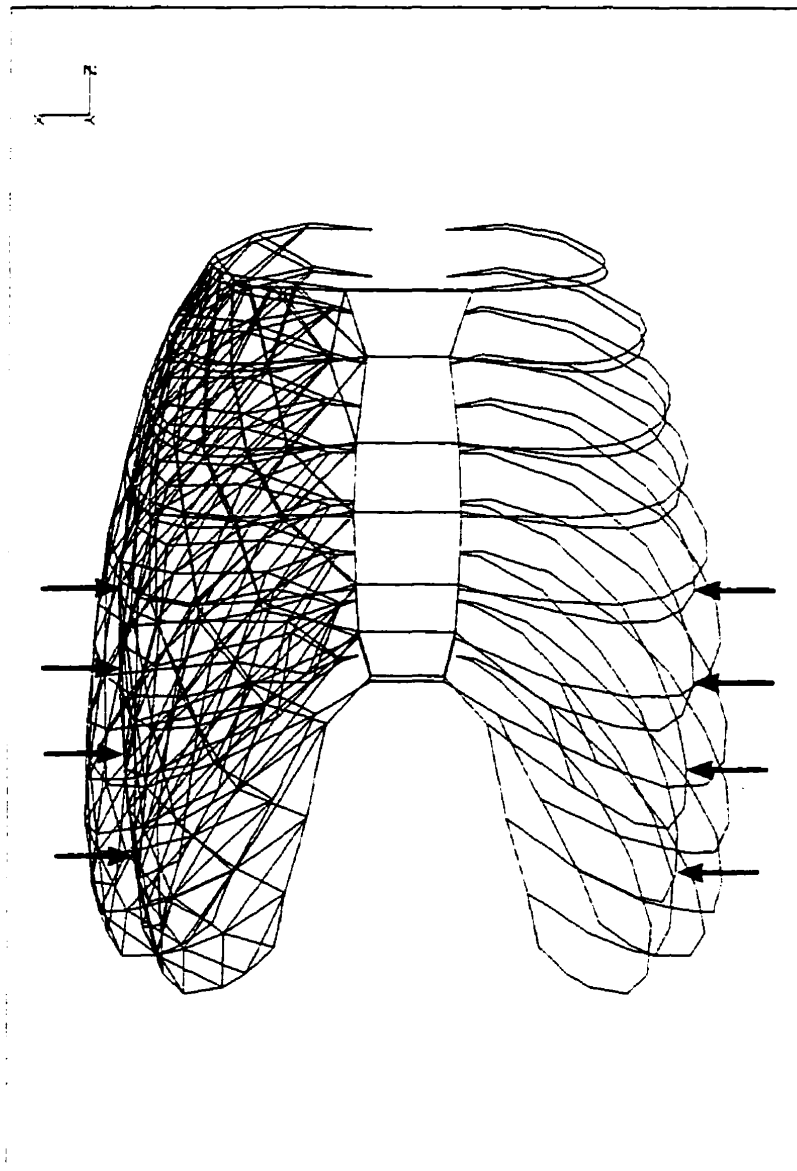


Figure 5.4: Deformed and undeformed configuration of the ribcage finite element model subjected to a lateral squeezing force centered at the level of the xiphoid process at the bottom of the sternum. The intercostal elements between the ribs ensured the coordinated action of all the ribs together.

the model of Andriacchi et al (1974). The change in the lateral ribcage diameter of the present model was very close to that of Closkey et al (1992). However, the change in the anterior/posterior diameter was about three times more in the present model, which resulted in better agreement with the experimental results. This difference was likely due to the pelvosternal springs included in the model of Closkey et al (1992) which restrained the anterior/posterior displacements of the sternum. This is further discussed below for the validation of the anterior/posterior displacements.

The property values of the intercostal elements used in the present model were in between that used in other models. Stokes and Laible (1990) used a similar criss-cross structure over 11 nodes per rib and a value of  $EA = 100 \text{ N}$  for the intercostals. In this model, with the intercostals also criss-crossed over 11 nodes per rib, a value of  $EA = 60 \text{ N}$  for the intercostals was chosen. Therefore, in the present model, the total intercostal stiffness was only about 60% that of the model by Stokes and Laible. Furthermore, they did not use bi-linear properties with negligible compressive stiffness as in the present model, and thus the difference in total stiffness is greater than 60%. This difference in stiffness is likely due to the larger region of costal cartilage in their model, which was re-constructed from adolescent x-rays, and validated against experimental data measured on adults. Consequently, to compensate for the larger costal region, the intercostals needed to be stiffer, as well as the costal cartilages as noted in the previous section. In the present validation, the properties of the intercostal elements were determined in a more consistent basis by comparing the response of a model with adult geometry to experiments conducted on adults. Though distributed differently along the ribs in the two models, the total stiffness of the intercostal elements between two ribs in the models of Andriacchi et al (1974) and Closkey et al (1992) was  $20 \text{ N/mm}$ . With an average normal distance of about  $30 \text{ mm}$  between ribs in the present model and 20 intercostal elements, this gives a total stiffness between two ribs of about  $40 \text{ N/mm}$ . This difference may partly explain the smaller changes in the anterior/posterior diameter due to a lateral squeezing force predicted by these models compared to the present model. In simulations with the present model, it was found that for small values of the intercostal stiffness, closer to the  $20 \text{ N/mm}$ , there was greater mo-

tion between the ribs and less anterior/posterior bulging. As the intercostal stiffness was increased to 40 N/mm, there was less inter-rib motion as the ribcage became stiffer, which in turn forced a greater anterior/posterior change of diameter, which agreed better with experiment.

In Fig. 5.5, the present model predictions in response to a frontal sternal load are compared with experimental results and the predictions of other models. The deformed ribcage is shown in Fig. 5.6. In comparison with experiment (Fig. 5.5A), the sternal displacement at the level of the xiphoid process was very similar to the unembalmed or fresh cadavers. The sternal displacement of the embalmed cadavers was at least 50% less, and was probably overly stiff to represent the passive stiffness of the ribcage in live subjects.

In comparison with the other models (Fig. 5.5B), the present model was found to be somewhat more flexible in the anterior/posterior direction. The models of Roberts and Chen (1972), which had rigid costovertebral and costotransverse joints, and of Andriacchi et al (1974), which had rigid ribs, predicted sternal displacements of only about 60% compared to the present model. The smaller displacements were consistent with the added rigidity in those models. The sternal displacement predicted by the model of Closkey et al (1992), with the pelvosternal springs, was only about 25% of the present model predictions and would appear to be much closer to the stiffness of an embalmed cadaver. However, without the pelvosternal displacements, the sternal displacement predicted by Closkey et al (1992) was much closer to the present model prediction. In the present model, there was a closer agreement in the anterior/posterior displacement with the fresh cadavers, which was felt to be a better representation of the passive stiffness in-vivo. The better agreement of the present model predictions with the anterior/posterior changes in ribcage diameter due to the lateral squeezing (Fig. 5.3) would also seem to justify the increased anterior/posterior flexibility of the present model.

The predictions of the present model for the geometric nonlinear analysis were about 30% larger at the highest loads compared to the linear analysis for the frontal sternal load (Fig. 5.5) and differed by less than 10% at the highest loads for the lateral squeezing loads (not shown in Fig. 5.3 for clarity). The experimental results, however, were very linear

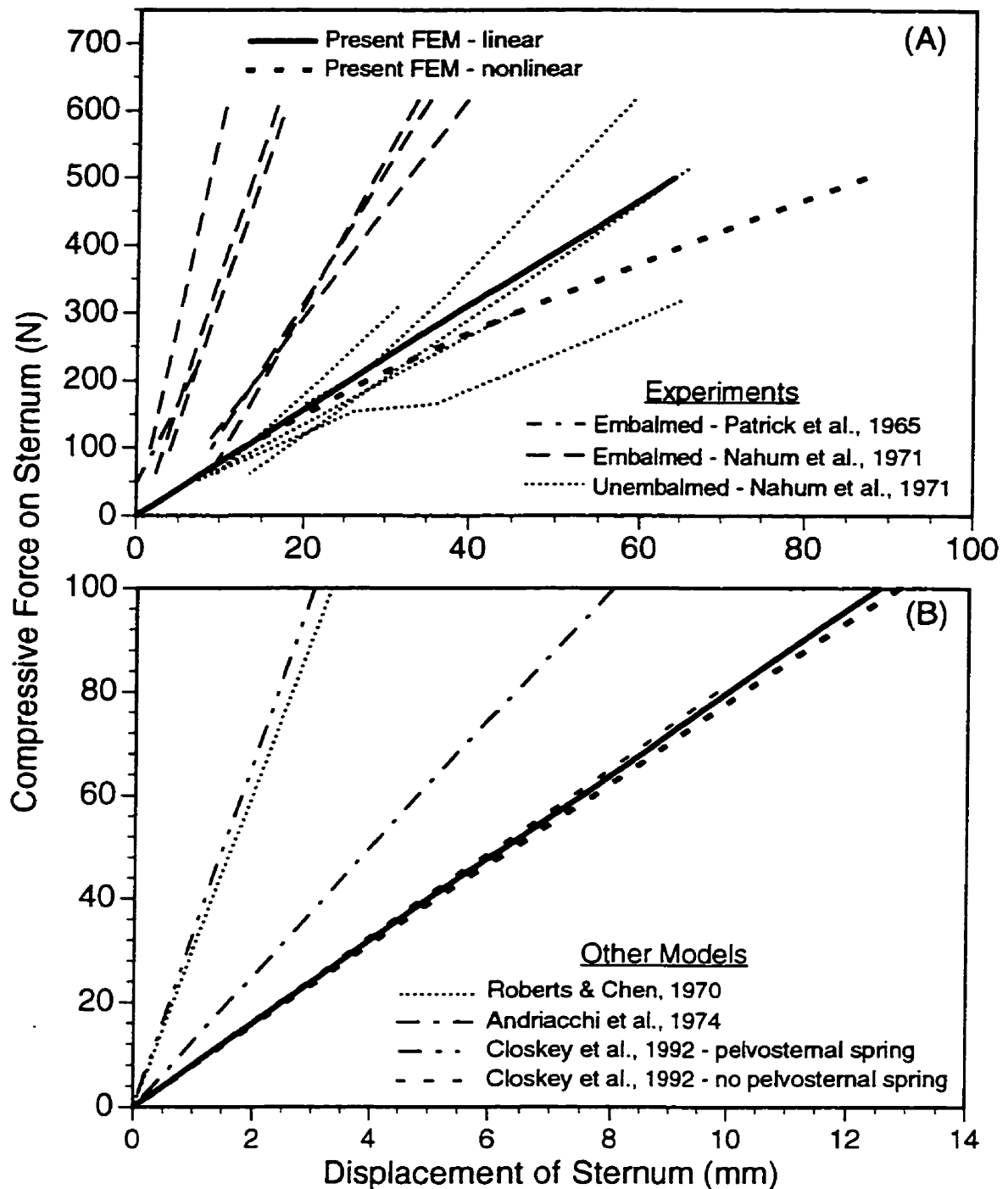


Figure 5.5: Comparison of the predictions of the present finite element model of the ribcage subjected to a sternal compressive load compared with experiment (A) and previous models (B). Excellent agreement with the experiments of unembalmed cadavers was found, and the present model was in general more flexible in the anterior/posterior direction compared with previous models.

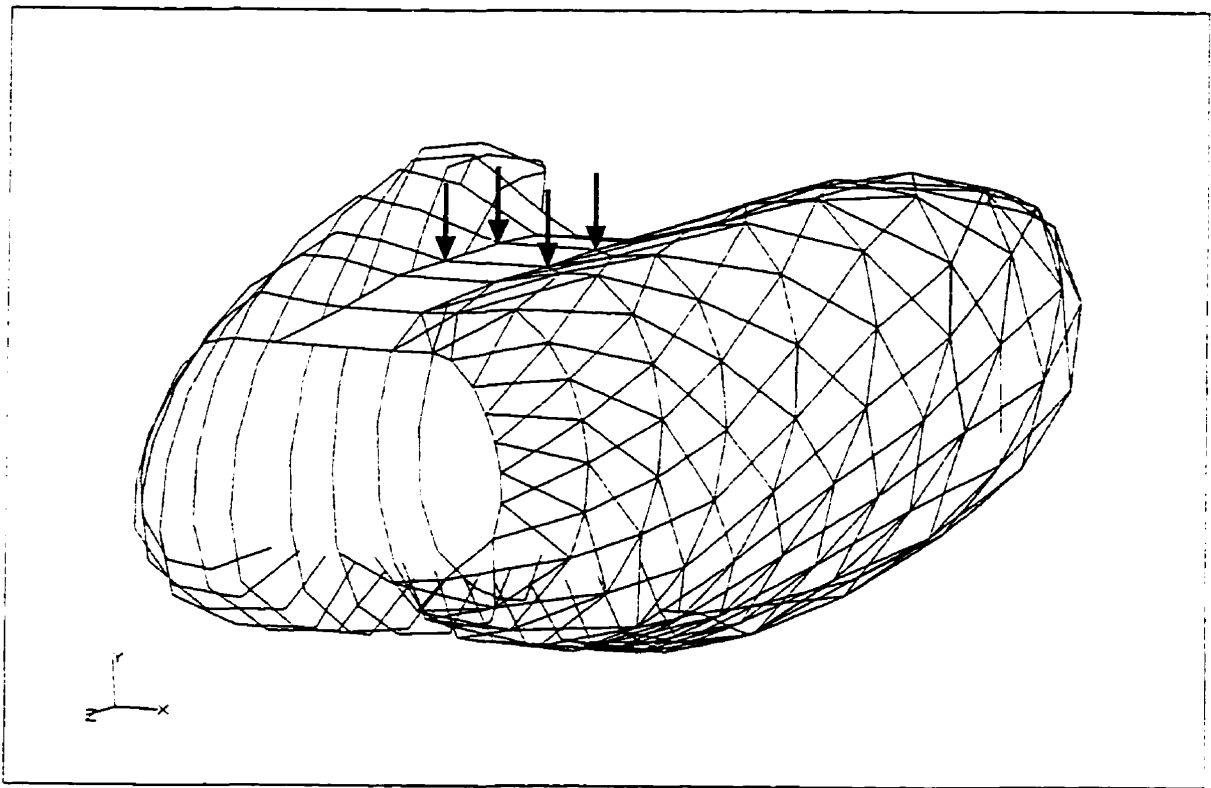


Figure 5.6: Deformed configuration of the finite element model of the ribcage subjected to a lower sternal load. The sternum undergoes a relatively large rotation due to the larger anterior displacements at the inferior portion.

for both loading directions. This illustrates that at these load magnitudes, there is likely a material nonlinearity which compensates for the geometric nonlinearity to produce a linear load-displacement response. Therefore, the sole use of a geometrically nonlinear analysis without material nonlinearity likely leads to incorrect displacement predictions. Without the knowledge of the nonlinear material properties, the load-displacement response of the ribcage is best predicted by a purely linear analysis. The stresses and strains within the various tissues of the ribcage, however, could be incorrect at the higher loads.

In summary, the present ribcage model was found to be in excellent agreement with the experimental load-displacement results for both the individual components and the overall ribcage. In comparison with the other models, the discrepancies were found to be reasonable, given the differences between the respective models. A better agreement with experiment was found in the anterior/posterior direction due to the increased flexibility of

the present model. Furthermore, a linear analysis was found to be sufficient to accurately predict the available experimental results.

### 5.3 Spatial Beam-Column Model of the Whole Spine

The present model prediction of the *axial rotation* at each spine level due to an applied axial rotation of  $54^\circ$  at T1 is compared with experiment and other models in Fig. 5.7. All models were in close agreement with experiment in the lumbar region of the spine, however, in the thoracic region all models underpredicted the experimental results. Excellent agreement was found between the present and previous models at all spine levels. The present model predictions were identical with or without the inclusion of the lateral translational stiffness. Since the application of the axial torque did not induce any lateral translation of the spine, the lateral stiffness did not play a role. Therefore, though the lateral translational stiffness of the ribcage was determined with the sternum fixed, which was not the case in this experiment, this discrepancy had no effect on this comparison.

The different results between the models and experiment could be due to three factors. First, the experimental results were only from one specimen, and due to the large variability in cadaveric testing routinely observed, this could easily explain the difference. Secondly, the present model was only considered accurate up to about  $18^\circ$  of axial rotation, and the other models were only linear. Clearly, the axial rotation of  $54^\circ$  applied to T1 meant that the accurate range of the models were exceeded. Therefore, the differences may be partly due to geometric nonlinearities not modelled. And thirdly, both the present and published models do not include material nonlinearity. Since most biological tissue demonstrates a material stiffening behaviour at large strains (White and Panjabi, 1990), the absence of this feature in these models could explain the lack of stiffening in the thoracic regions for higher axial rotations. However, the excellent agreement of the present continuum model with the published discrete models provided strong evidence of the ability of the present model to predict the axial rotation response of the spine.

The *buckling behaviour* of the model with a small imperfection is shown in Fig. 5.8 for

a model with properties based on the experiment of Lucas and Bresler (1961). For the free top, the lateral translation of T1 increased greatly as the critical load of 20.4 N was approached. Similarly, for the pinned top, the lateral translation at the middle of the spine was predicted to be very large as the applied load approached the critical buckling load of 167.2 N. These critical buckling loads were determined for a spine with a lateral bending stiffness of 1.90 N m<sup>2</sup> and a spine length of 479 cm. For the present model, the lateral bending stiffness was greater with an average value around 3.5 N m<sup>2</sup> and a spine length of 460 cm. Therefore, the buckling loads in the present model would be about 41 N for a free top and 334 N for a pinned top. The predictions of the lateral translations of the model with the current properties were also found to increase greatly as these critical loads were approached. These predictions were made for a straight spine subjected to an axial compressive load with only a very small lateral offset. In scoliosis, the "imperfection" is much larger due to the initial lateral curvature and axial rotation of the spine. Therefore, in a scoliotic spine much greater lateral translations coupled to the axial rotation occur at compressive loads below the buckling load of the straight spine.

For a *lateral load* of 250 N applied at the *shear centre* of T9 in the whole spine model with the full ribcage stiffness included, a maximum lateral translation of 18.8 mm was predicted, for a lateral flexibility of 0.075 mm/N (Table 5.3). If the lateral translational stiffness was not included in the model, then a lateral translation of 24.94 mm was predicted, for a lateral flexibility of 0.1 mm/N. These model predictions were in excellent agreement with the experimental results of Halsall (1980), Halsall et al (1983), who measured an average lateral flexibility of 0.1 mm/N at T9. For the lateral load applied at T9 *posterior* to the centre of rotation, the model predicted an axial rotation of about 5° with the spinous processes rotated into the convexity of the lateral curve. This model prediction was only slightly greater than the 4.5° of rotation measured in the experiment. For the lateral load applied at T9 *anterior* to the centre of rotation, the model predicted an axial rotation of 2° in the opposite sense (Fig. 5.9), which was also in agreement with experiment (Table 5.3). In this experiment, the cadavers were placed on a stainless steel table face down, and the spine at T1 and S5 was clamped in a fixed-fixed set-up. The anterior ribcage and

sternum were free to slide on the table which was kept well lubricated. However, due to the cadaveric weight and clamped spine condition at the top, the movement, and therefore, boundary conditions of the sternum were probably somewhere between fully fixed and completely free. The lateral translational stiffness of the present model was determined with the sternum fixed, and represented the stiffness due to relative lateral movement between the spine and ribcage. Therefore, with the lateral translational stiffness included, the model would be expected to predict a stiffer response compared with experiment, as was found. On the other hand, without the lateral stiffness included, the model would be expected to predict a softer stiffness which might better match experiment, which was also found. It was not possible to directly model the frictional interactions between table and cadaver, which must have occurred in the experiment. Therefore, the exact amount of relative lateral movement between the spine and ribcage in the experiment was unknown. Nonetheless, the predictions of the present model at the two extremes were in excellent agreement with this experiment, and provided validation of the combined lateral and axial rotation stiffness of the present model.

In summary, the spatial beam-column model was found to be in excellent agreement with experiment for axial rotation, lateral bending and axial buckling. In comparison with a discreet model, the axial rotations were also in excellent agreement. Further, the validation of the combined axial rotation and lateral bending response of the model provided confidence that the model can accurately investigate the mechanics of scoliosis.

Table 5.3: Comparison of the present model predictions with experiment for the combined lateral bending and axial rotation response due to a 250 N lateral load applied at vertebra T9.

Load Point*		Lateral Flexibility (mm/N)	Axial Rotation (deg)
Posterior -20 mm	Model - Full Ribcage	0.068	5.18
	Model - No Lateral	0.093	5.11
	Experiment <sup>†</sup>	0.10±0.03	4.5±1.8
Shear Centre	Model - Full Ribcage	0.075	-0.26
	Model - No Lateral	0.100	-0.37
Anterior +6 mm	Model - Full Ribcage	0.076	-1.77
	Model - No Lateral	0.100	-1.83
	Experiment <sup>†</sup>	0.09±0.04	-2.0±3.1

\* The anterior/posterior location of the lateral load applied to vertebra T9.

<sup>†</sup> Experimental measurements from nine specimens by Halsall (1980), Halsall et al (1993).

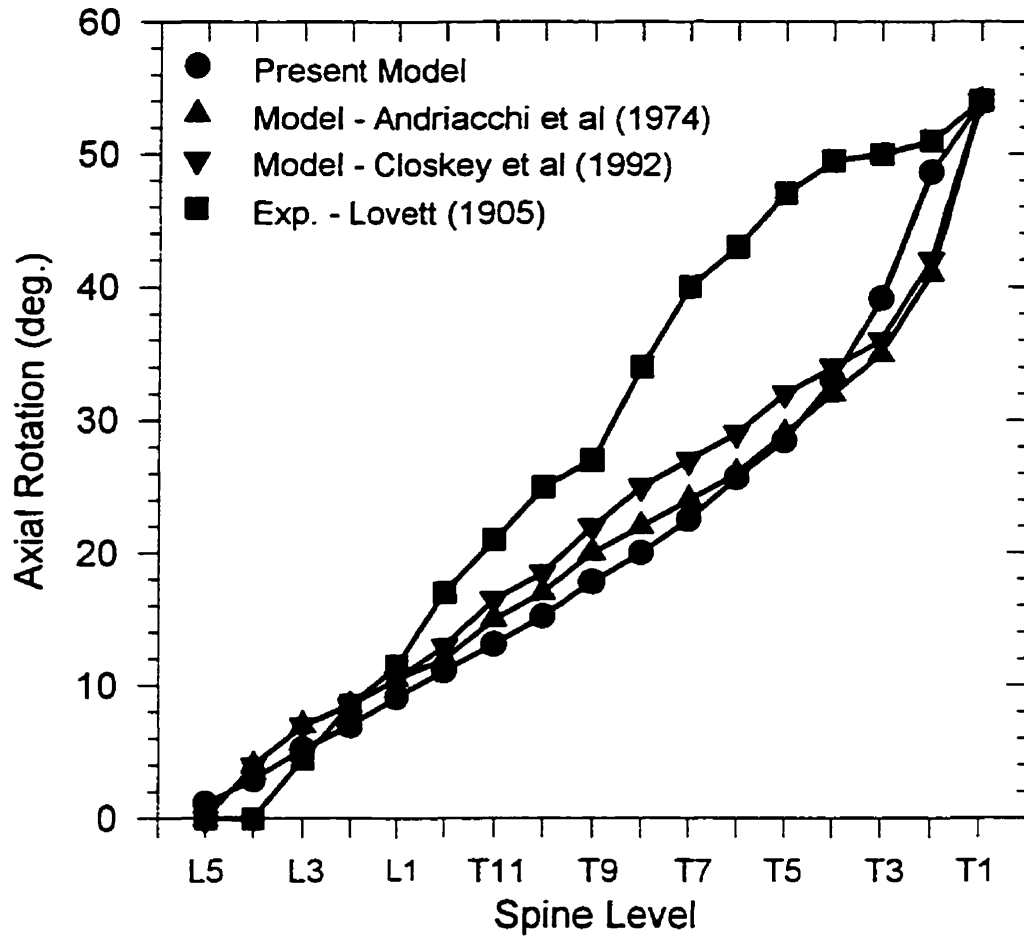


Figure 5.7: Comparison of the axial rotation at each spine level of the present model with experiment and other models for an axial rotation of  $54^\circ$  at T1.

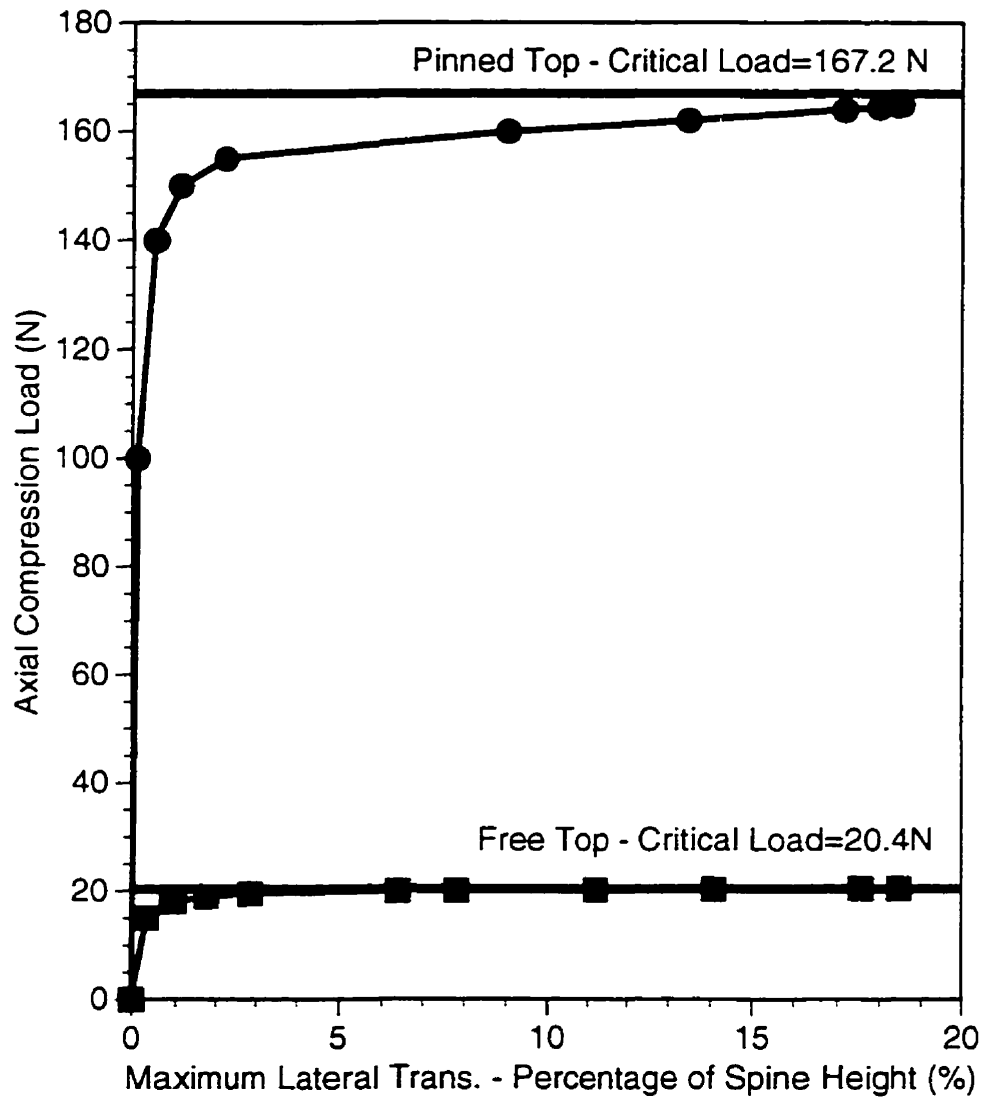


Figure 5.8: The lateral translations of the present model for an axial compressive load applied with a small imperfection for both a free and a pinned top. The properties used in the analysis matched those of the spines used in the experiment of Lucas and Bresler (1961).

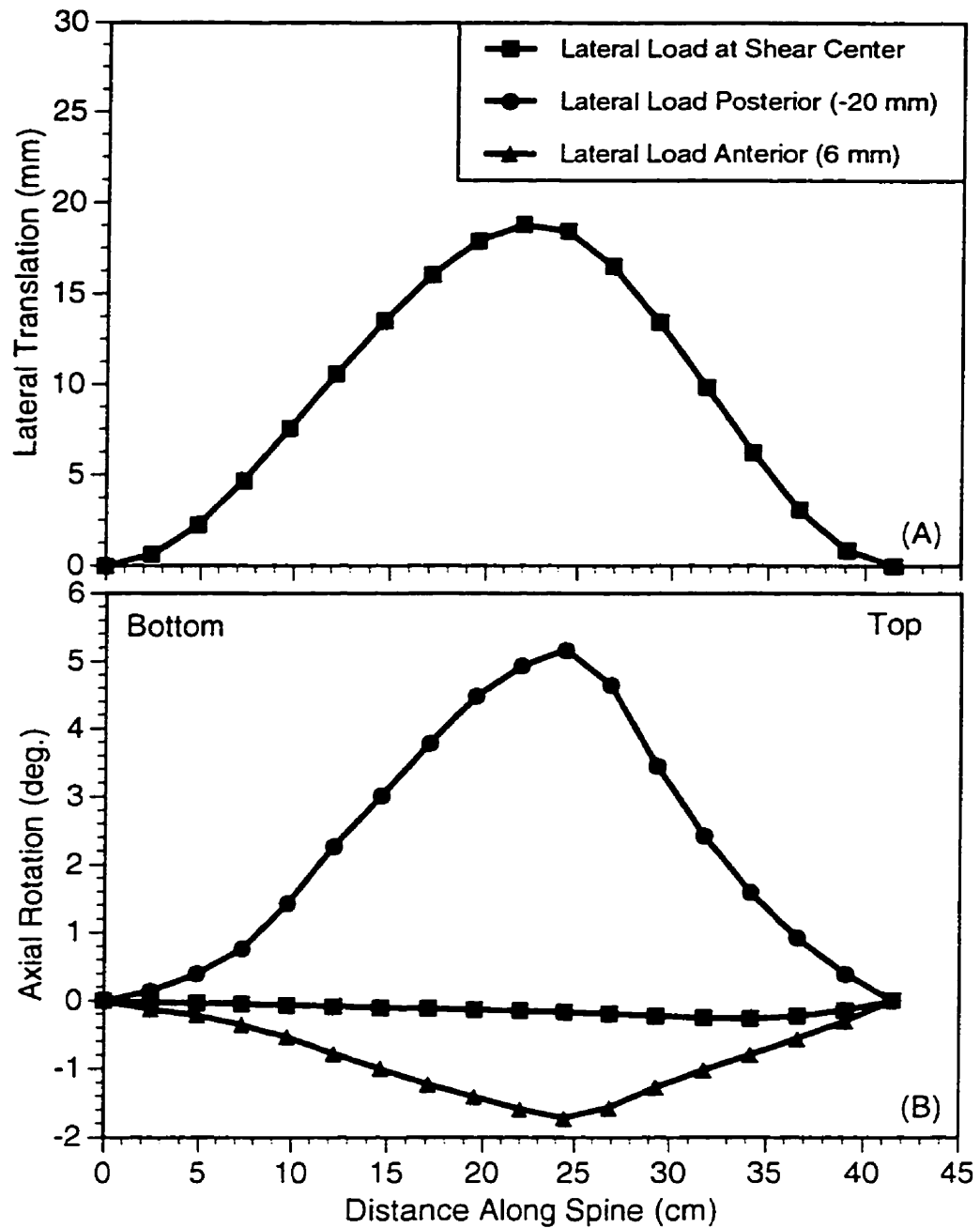


Figure 5.9: The model predictions for the lateral translation (A) and axial rotation (B) due to a lateral load applied at vertebra T9.

# Chapter 6

## RESULTS - RIBCAGE ANALYSIS

### 6.1 Introduction

In this chapter, the results of the numerical experiments to establish the equivalent ribcage stiffnesses of an adult ribcage are presented in the second section. The procedure for these experiments was outlined in Chapter 4. Subsequently, in the third section, several investigations are reported to assess the sensitivity of the ribcage stiffness to various factors. In the fourth section, the ribcage stiffnesses from adolescence to adulthood are presented based on estimates of changes in geometry and material properties. The stiffness properties presented in this chapter were incorporated into the spatial beam-column model of the spinal column, which was validated in Section 5.3 and subsequently analyzed in Chapter 7.

### 6.2 Equivalent Ribcage Stiffnesses of an Adult

In Table 6.1, the principal and coupled displacements due to loads applied independently in all directions at the shear centre are presented for rib 6. The coupled displacements were found to be less than the principal displacements by at least one, if not two orders of magnitude, in most loading directions. Very similar results were found for the coupled displacements at all of the rib levels. The possible exception was the coupled axial translation due to an anterior load which tended to be larger at all rib levels due to a

rotation downward of the whole ribcage. In the whole spine model, this motion would be easily resisted by the high axial stiffness of the spine. Consequently, the added axial load to the spine due to this coupled motion would only be a small component of the total axial load and should not significantly affect its behaviour. It would appear, therefore, that for loads applied to the ribcage at the location of the centre of rotation of the motion segments, the resultant displacements are primarily in the principal directions. It should also be noted that not all the coupled displacements were found to be symmetric as was assumed in Chapter 4. An anterior load should not produce a lateral translation due to the sagittal plane symmetry, and consequently in an elastic system neither should a lateral load produce an anterior translation. As seen in Table 6.1,  $f_{21}$  was indeed exactly zero as expected, however,  $f_{12}$  was only small. This was due to the use of bi-linear properties. For example, a lateral load caused the costotransverse joint on one side of the sagittal plane of symmetry to be in tension, whereas on the other it was in compression. In a truly elastic system, the tensile and compressive forces on either side of the symmetry plane would cancel, and there would be no net force available to cause an anterior translation. However, with bi-linear properties the magnitudes of the tensile and compressive forces differed and a net anterior force was produced causing the observed small coupled translation. The main point though was that all the coupled displacements were small. Similarly, there were small differences in the translations due to anterior versus posterior loading, but they were on the order of the coupled displacements. Therefore, it was felt necessary to consider only the principal stiffnesses of the ribcage for inclusion in the beam-column model, and only these are reported for all ribs.

In Fig. 6.1A, the load-displacement results are presented for lateral loads at all 10 rib levels. There was a clear increase in the lateral translation from rib 1 up to rib 10. At rib 10, the translations were about 5 times greater than at rib 1. As discussed for the individual rib behaviour, this was likely due to both the increased geometry of the lower ribs, and hence increased moment arm, as well as the increased lengths of the flexible costal cartilages. In the assembled ribcage, the orientations of the costovertebral and costotransverse joints also contribute to the differences in the lateral translations with rib

level. In the upper ribs, the rib neck axis is closer to the coronal plane, whereas in the lower ribs, it is closer to the sagittal plane. Consequently, for a lateral load, there was a greater rotation of the lower ribs about the rib neck axis. Due to this increased rotation, the more flexible soft tissues of the costovertebral and costotransverse joints must provide the resistance as opposed to the stiffer bony structure. Therefore, due to a number of factors, the lateral translations of the lower ribs were found to be much larger than that of the upper ribs.

In Fig. 6.1B, the load-displacement results are presented for anterior loads at all 10 rib levels. Similar to the results for the lateral loads, the anterior translations were found to increase from rib 1 up to rib 10. However, the anterior translations were less than the lateral translations at all rib levels except rib 10. In particular, for the upper ribs the translations were two to eight times less. In the lower ribs, the magnitude of the anterior translations was closer to the lateral translations. The differences in translations between the rib levels was likely due to the decreased lengths of the costal cartilages in the upper ribs. Similar to these load-displacement results, the moment-rotation results displayed a variation with rib level. The axial rotations were the smallest, and the flexion and lateral rotations were similar.

It is also worth noting that the load-displacement response, and therefore, stiffness at a given rib level is a function of that rib's interaction with all the other levels. Therefore, in this procedure to determine the ribcage stiffnesses, displacements were induced at all the rib levels in addition to the primary displacement at the given loaded rib level (Fig. 6.2). This level of interaction varied with rib level and further added to the variation of the rib stiffnesses. Consequently, the present procedure of sequentially loading each rib level of the intact ribcage captured the full and complex stiffness of the ribcage.

In Fig. 6.3, the principal ribcage stiffness values as determined from the load displacement results are presented. The anterior translational stiffness was greatest at the upper levels and decreased down to a similar value to the lateral translational stiffness at the lower levels (Fig. 6.3A). The axial rotational stiffness was greatest at the upper levels and decreased down to a similar magnitude to the lateral bending and flexion/extension

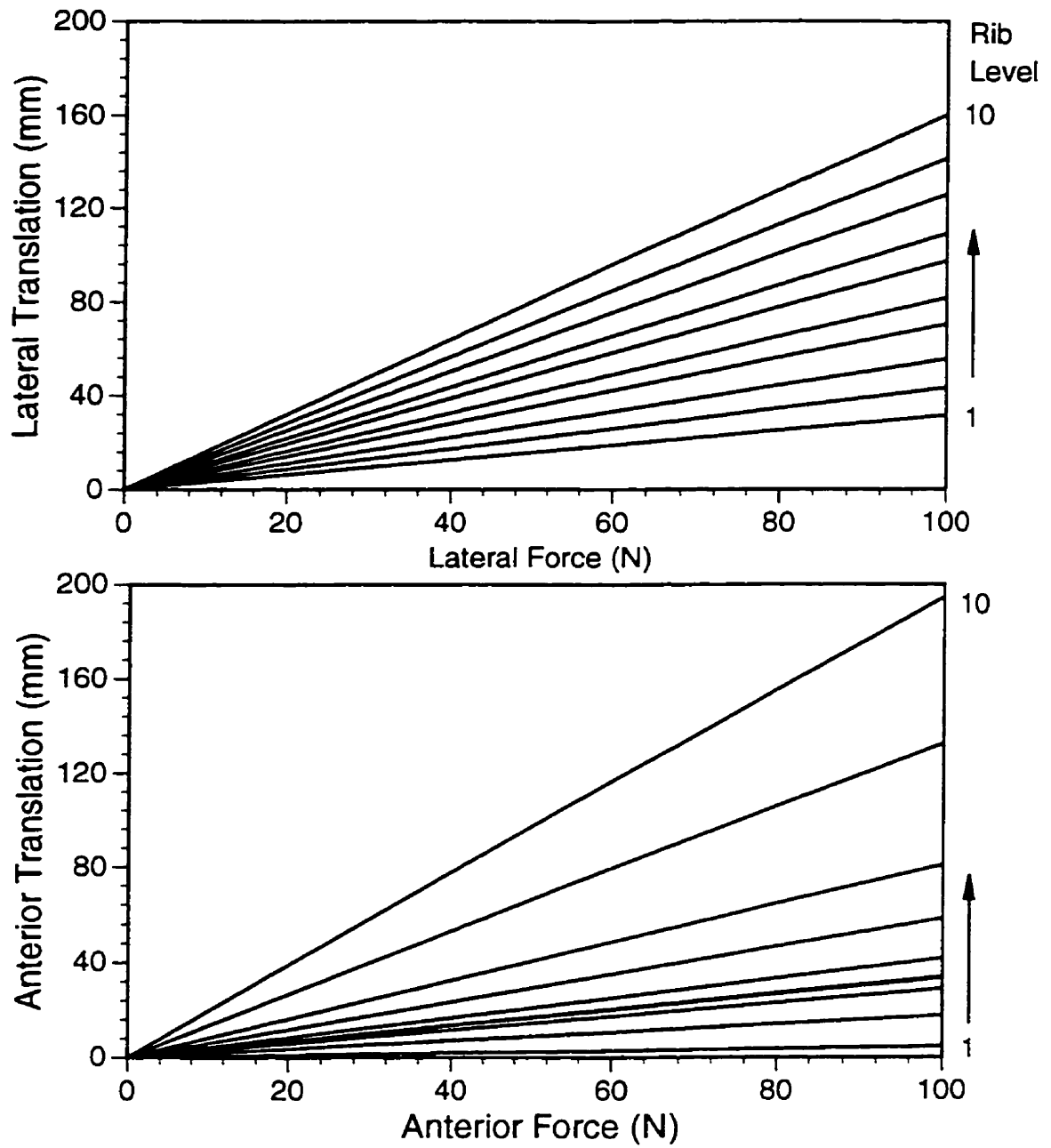


Figure 6.1: The load displacement results for a 100 N lateral load (A) and a 100 N anterior load (B) applied at the shear centres of the spine at all rib levels one at a time. There was a clear variation in the displacements with rib level for both anterior and lateral loads.

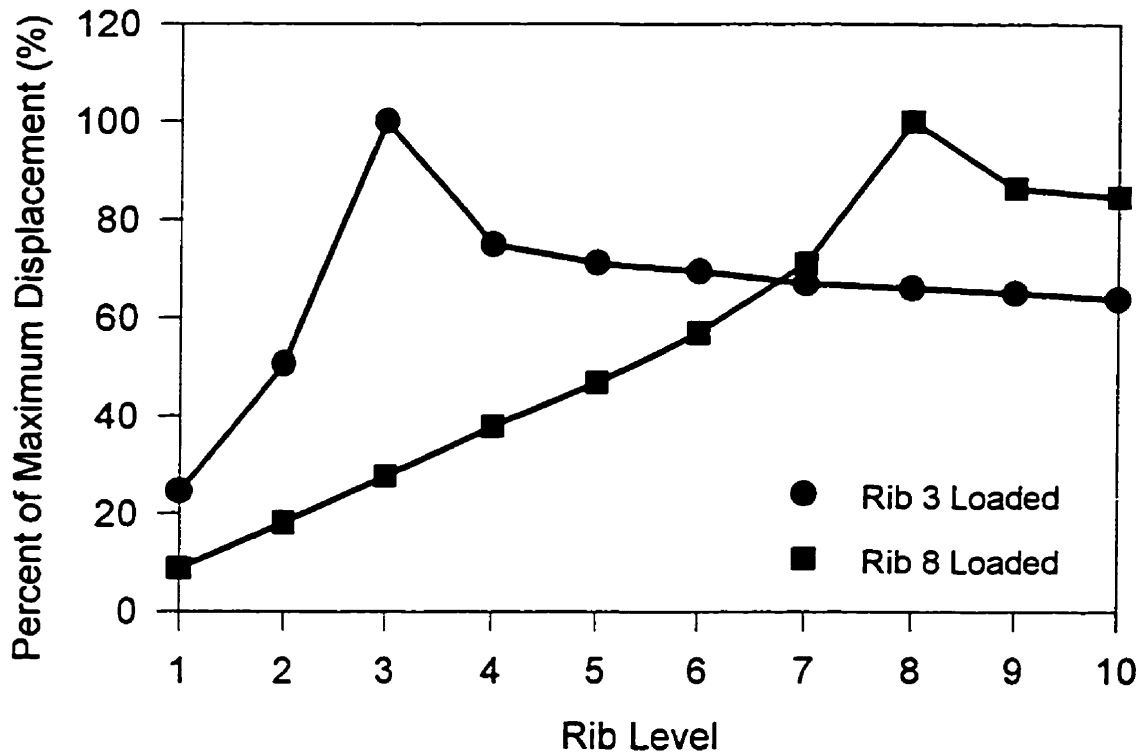


Figure 6.2: The lateral displacements of the shear centres at all the rib levels due to a lateral load (100 N) applied at the shear centre of rib level 3 and at rib level 8. The maximum displacements occurred at the primary loaded level and significant but lesser displacements were induced at the other rib levels. The principal stiffness determined from the load-displacement response at a given rib level was therefore affected by interaction of that given level with all the other rib levels, primarily through the intercostals due to relative movement between ribs.

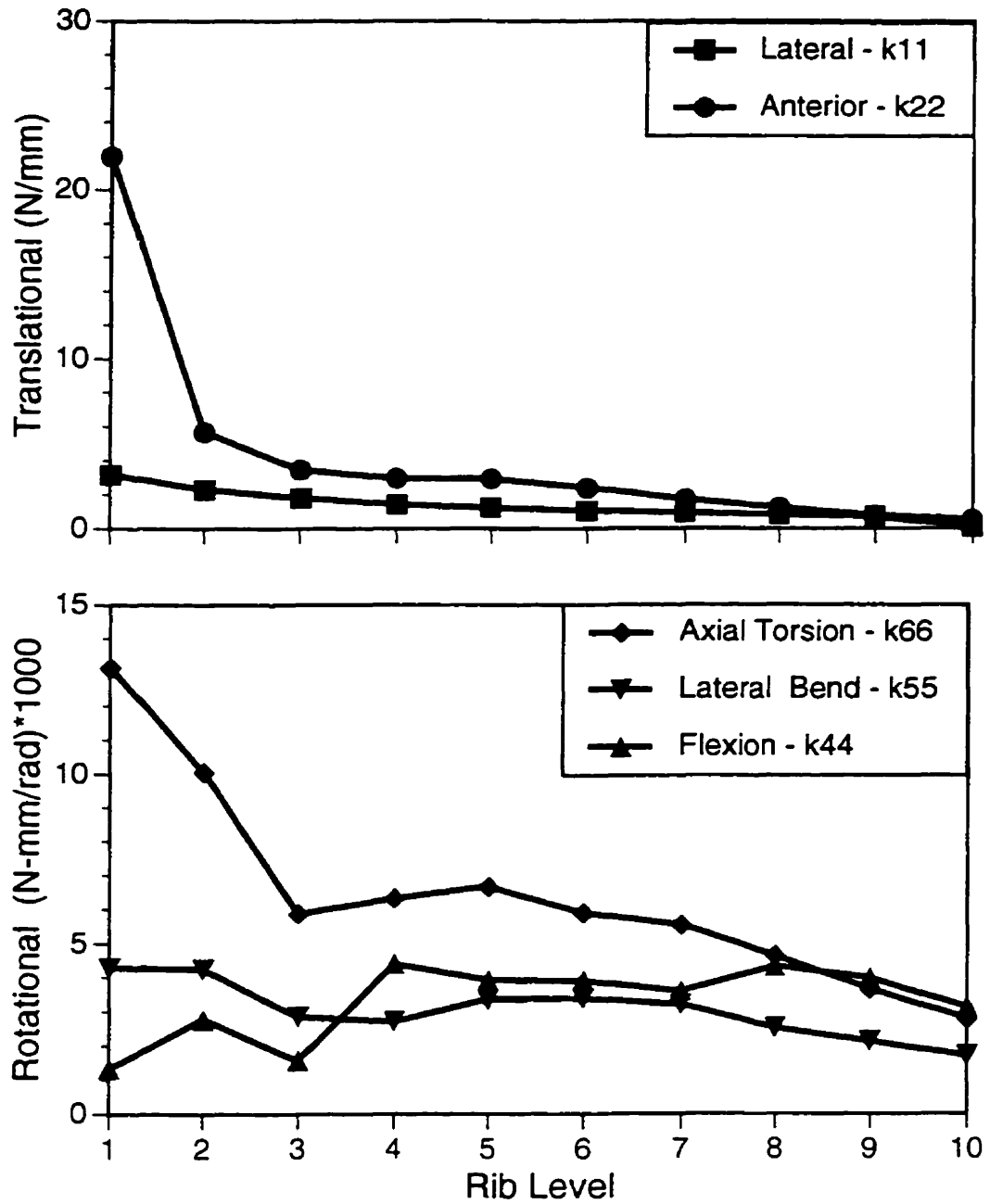


Figure 6.3: The translational (A) and rotational stiffnesses (B) as a function of rib level. The lateral and anterior translational stiffnesses were very similar at all rib levels except the first and second where the anterior stiffness increased greatly. The axial rotational stiffness was greater at most rib levels and the lateral bending and flexion/extension rotational stiffnesses were similar at all rib levels.

Table 6.1: The principal and coupled displacements of rib 6 subjected to 100 N loads and 1000 N-mm moments applied independently at the shear centre of the spine at this rib level. The coupled displacements are in general much less than the principal displacements.

	$T_x$ (mm)	$T_y$ (mm)	$T_z$ (mm)	$R_x$ (rad)	$R_y$ (rad)	$R_z$ (rad)
Lateral Load ( $\mathcal{F}_x$ )	<b>97.41</b>	1.40	1.75	-0.100	-0.119	-0.060
Anterior Load ( $\mathcal{F}_y$ )	$-4.3 \times 10^{-6}$	<b>41.63</b>	-6.04	-0.022	$1.1 \times 10^{-7}$	$5.2 \times 10^{-8}$
Flexion/Extension Moment ( $\mathcal{M}_z$ )	$-2.3 \times 10^{-4}$	-1.51	-1.74	<b>-0.257</b>	$-9.3 \times 10^{-6}$	$4.1 \times 10^{-6}$
Lateral Bending Moment ( $\mathcal{M}_y$ )	-1.23	0.20	0.12	$-8.6 \times 10^{-3}$	<b>0.295</b>	$-5.0 \times 10^{-2}$
Axial Moment ( $\mathcal{M}_x$ )	-0.53	0.53	0.05	$-7.6 \times 10^{-3}$	$-5.0 \times 10^{-2}$	<b>0.170</b>

rotational stiffnesses which did not vary greatly with rib level (Fig. 6.3B).

These results demonstrated that the passive ribcage provided primarily a resistance to axial rotation and anterior translation, particularly at the upper rib levels. At the lower rib levels, there was much less variation between the two translational stiffnesses or between the three rotational stiffnesses. Consequently, in the middle of the spine, there would not appear to be a preferential bracing of the spine in any given direction by the ribcage.

To incorporate these ribcage stiffnesses into the beam-column model, they were transformed to a per unit length value based on the intervertebral lengths presented in Section 3.6. This further increased the variation of the stiffnesses with rib level by a small amount due to the greater intervertebral distances in the lower thoracic spine. The final values of the principal ribcage stiffnesses per unit length for an adult ribcage are presented in Table 6.2.

Table 6.2: The principal ribcage stiffnesses per unit length at all the rib levels for an adult ribcage.

Rib Level	Translational		Rotational		
	Lateral- $k_{11}^o$ (kN/m <sup>2</sup> )	Anterior- $k_{22}^o$ (kN/m <sup>2</sup> )	Flexion/Extension- $k_{44}^o$ (N/rad)	Lateral Bend- $k_{55}^o$ (N/rad)	Axial- $k_{66}^o$ (N/rad)
1	158.0	1093.4	66.6	212.8	653.7
2	107.4	264.9	129.5	197.8	468.4
3	81.5	157.6	124.7	129.4	265.9
4	64.3	135.6	199.4	123.2	286.9
5	53.7	129.3	171.3	147.5	293.0
6	43.3	101.4	164.4	143.1	248.9
7	38.2	71.6	149.9	133.7	231.0
8	32.1	50.1	175.2	102.4	187.7
9	26.8	28.7	151.6	81.5	139.2
10	22.6	18.6	113.5	62.2	101.4

— Note these stiffnesses were representative of an “ideal” adult ribcage with no distinction between male and female.

### 6.3 Sensitivity Analysis of Ribcage Stiffnesses

The percentage changes in the ribcage stiffnesses due to variation of the geometry and material properties of the ribcage are presented in Figs. 6.4 - 6.8. The specific variations for this sensitivity analysis were outlined in Table 4.1 and the percentage changes were calculated as the difference between the stiffnesses of the altered ribcage minus those for the adult ribcage divided by the adult ribcage stiffness values (which were presented in Fig. 6.3). In each of the Figs. 6.4 to 6.8, the results due to changes in geometry are presented in (A), whereas in (B), the results due to changes in material properties are shown. Each figure presents the results for one of the five ribcage stiffnesses at all rib levels.

The lateral translational stiffness was most sensitive to changes in the gross depth of the ribcage where a decrease of 20% in depth resulted in a 30-35% increase in stiffness (Fig. 6.4A). This increase was likely due to the decreased moment arm for the lateral load which reduced the bending of the rib and thereby stiffened the ribcage. On the other hand, the lateral stiffness was least sensitive to changes in the gross width of the ribcage.

The lateral translational stiffness was most affected by the decreases in the material properties of the intercostal elements and the costal cartilages, where a 60% reduction of Young's modulus in each resulted in 25% reductions in lateral stiffness (Fig. 6.4B). A 60% reduction of the modulus of the costotransverse (CT) joints decreased the lateral stiffness by 30% and 20% at the first and second rib levels, respectively, but only by 10-15% at the other levels. This variation with rib level was likely due to the changing orientation of the CT joints which were least posterior to the shear centre of the vertebrae in the upper rib levels. Consequently, the CT joints of the upper ribs were exposed to greater shear forces due to a lateral load, as opposed to the lower ribs where the reaction forces in the CT joints were more normal to the joint line with less shear. Therefore, in the upper ribs, the soft tissue of the CT joints played a larger role in the lateral stiffness, which in turn was more sensitive to changes in the material properties of the CT joints.

The anterior translational stiffness was most sensitive to changes in the gross width of the ribcage, where a 20% reduction in width produced a 35-40% increase in the anterior

stiffness (Fig. 6.5A). This stiffening was again due to the reduction of the bending moment on the ribs, similar to the effect of the reduced depth on the lateral stiffness. On the other hand, the reduced depth had only a minimal effect on the anterior stiffness. Also the 30% increase in length of the costal cartilages produced a 20% decrease in anterior stiffness.

The anterior translational stiffness was most affected by decreases to the material properties of the costal cartilages, particularly in the lower ribs where the costal cartilages were more dominant due to their increased lengths (Fig. 6.5B). Changes to the material properties of the other tissues had a lesser effect on the anterior stiffness.

The flexion/extension rotational stiffness was increased the most by reduction of the gross ribcage width, which was counteracted by a nearly equal decrease in stiffness due to a reduction of the ribcage depth (Fig. 6.6A). The decrease in the flexion/extension stiffness due to reduction of the depth was consistent with the reduction of the moment arm or gross moment of inertia of the ribcage. The increase in the flexion/extension stiffness due a reduction of the width was related to the more complex transfer of load through the ribcage. In flexion/extension, the ribcage stiffness was related mostly to the deformation of the intercostals, the CT joints and the bending about the major axis of the ribs at their most lateral region. In reducing the width, there was a general reduction in the area over which the intercostals acted, yet the lateral region of the ribs was unaffected. There was a transfer of the load due to flexion/extension from the soft intercostals to the far stiffer ribs, and thus the increase in flexion/extension stiffness due to the reduction of the ribcage width.

The flexion/extension rotational stiffness was very sensitive to changes in the material properties of the CT joints, were a reduction of 60% in the modulus of the joints lead to a 50% reduction in flexion/extension stiffness (Fig. 6.6B). This was consistent with the location of the axis of rotation of the ribs through the CV and CT joints (see Fig. C.7B). This axis was aligned to permit easy raising and lowering of the ribs during respiration, which was partly a flexion and extension rotation of the ribs. Therefore, the CV joints had minimal rotational stiffness and the flexible CT joints carried most of the flexion moment. Thus, the flexion/extension stiffness was most sensitive to changes in the properties of the

CT joint. A 60% reduction in the modulus of the intercostals resulted in the next largest reduction of about 10% in the flexion/extension stiffness at the lower rib levels.

The lateral bending rotational stiffness was increased by changes to the gross ribcage depth and decreased by an equal amount by changes to the ribcage width (Fig. 6.7A). Similar to the explanation of the changes to the flexion/extension stiffness, these changes were consistent with reduction of the moment arms of the ribcage and a transfer of the moment to the stiffer axis of the ribs. The only difference was the opposite roles played by the ribcage depth and width, respectively, on these two rotational stiffnesses.

The lateral bending rotational stiffness was also very sensitive to a reduced modulus of the CT joints (Fig. 6.7B), where a 60% reduction in modulus of the CT joints resulted in a 45-50% reduction in the lateral bending stiffness. Lateral bending caused rigid body rotation of the ribs about the rib neck axis (see Fig. C7B), which was largely resisted by the relatively soft CT joints and therefore, the bending stiffnesses were sensitive to changes of the moduli of the CT joints. The intercostals resisted separation of the ribs and have a dominant role in the lateral bending stiffness, which explained the 20% reduction in lateral bending stiffness due to a 60% reduction in the modulus of the intercostals. Changes to the moduli of the costal cartilages only had a small effect since they were located close to the lateral bending axis of rotation and were not well suited to resist the lateral bending.

The axial rotational stiffness was increased about 5% by a 20% reduction of the gross ribcage height and reduced by 5-10% for a 20% reduction in ribcage width and depth (Fig. 6.8A). The increase in stiffness associated with the decrease of the ribcage height was likely due to increased contribution of the adjacent ribs to the stiffness at a given rib level as was illustrated previously (Fig. 6.2). The decrease of ribcage height meant that the ribs farthest from the given loaded level were closer, and thereby were subjected to greater axial rotation and added more rotational stiffness.

The axial rotational stiffness was most sensitive to changes in the material properties of the costotransverse joints (Fig. 6.8B), but to a slightly lesser extent than the other rotational stiffnesses. A reduction of 60% in the moduli of the CT joints resulted in a 40% reduction in the axial rotational stiffness at all rib levels. This again illustrated the

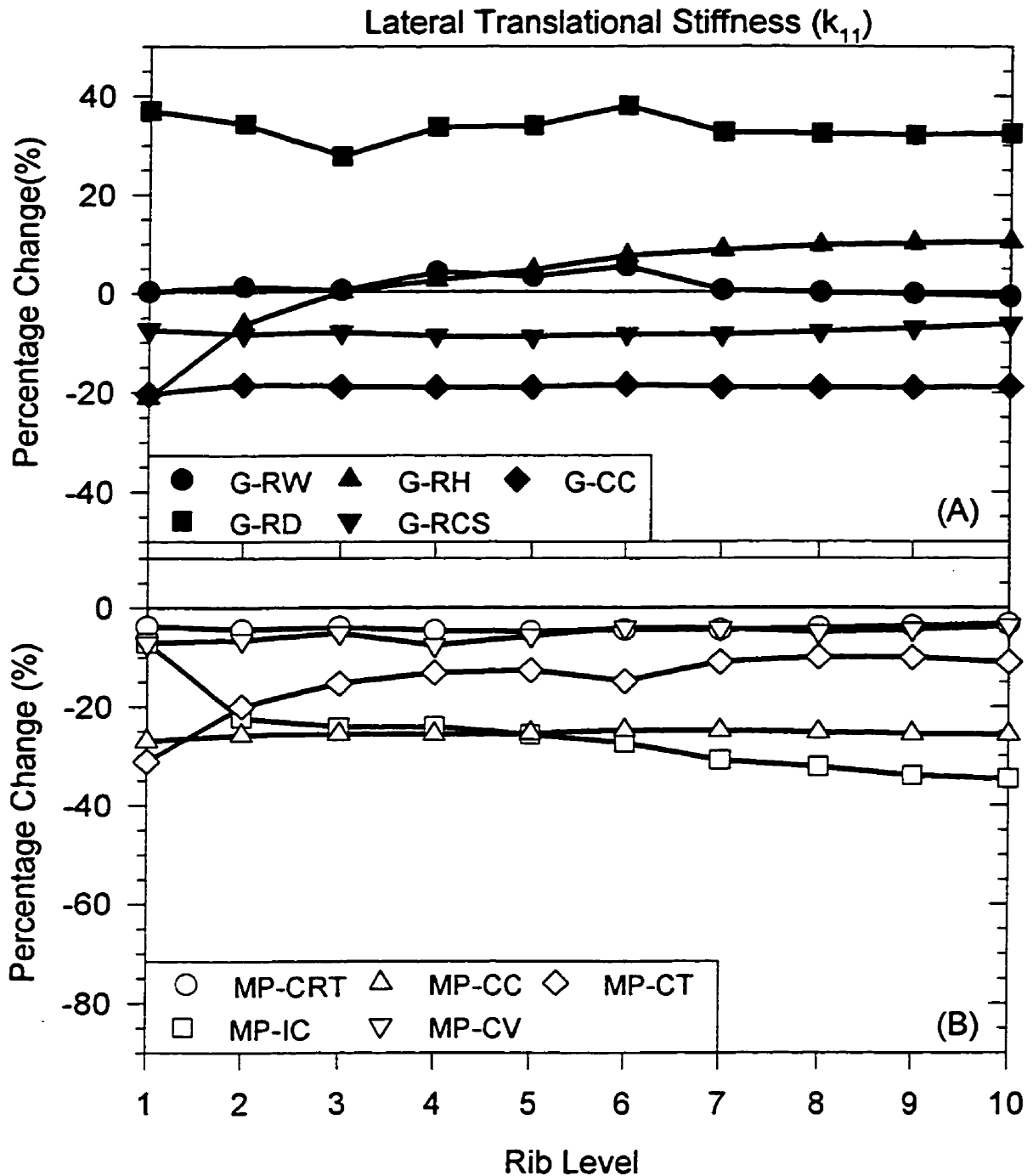


Figure 6.4: The percentage change in the lateral translational stiffness ( $k_{11}$ ) due to changes in the geometry (A) and the material properties (B) of the ribcage. The exact parametric changes to the geometry of the ribcage width (G-RW), ribcage depth (G-RD), ribcage height (G-RH), rib cross-section (G-RCS), costal cartilages (G-CC), and the material properties of the cortical rib bone (MP-CRT), the intercostals (MP-IC), the costal cartilages (MP-CC), the costovertebral joints (MP-CV) and the costotransverse joints (MP-CT) are detailed in Table 4.1.

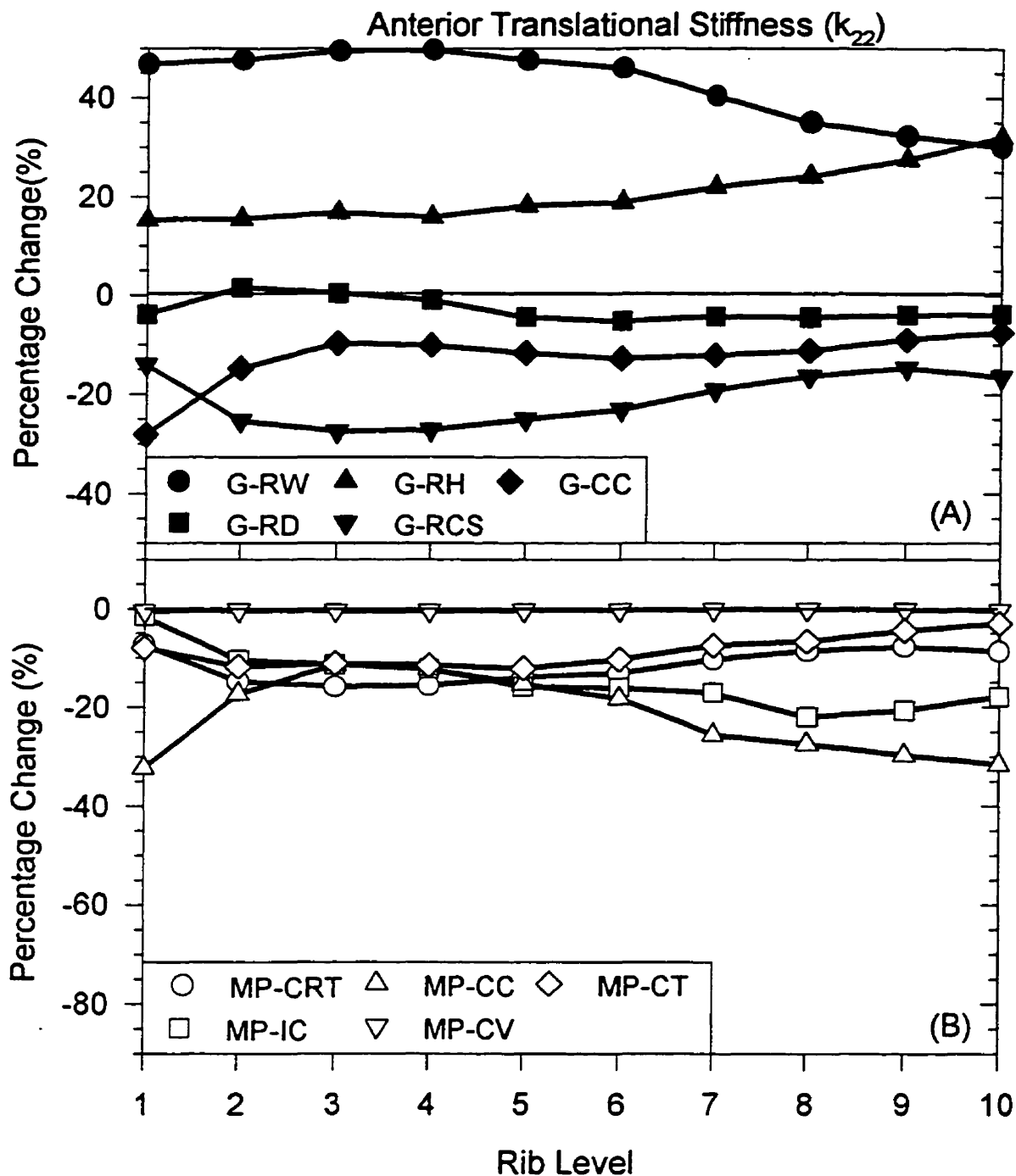


Figure 6.5: The percentage change in the anterior/translational stiffness ( $k_{22}$ ) due to changes in the geometry (A) and the material properties (B) of the ribcage. The exact parametric changes to the geometry of the ribcage width (G-RW), ribcage depth (G-RD), ribcage height (G-RH), rib cross-section (G-RCS), costal cartilages (G-CC), and the material properties of the cortical rib bone (MP-CRT), the intercostals (MP-IC), the costal cartilages (MP-CC), the costovertebral joints (MP-CV) and the costotransverse joints (MP-CT) are detailed in Table 4.1.

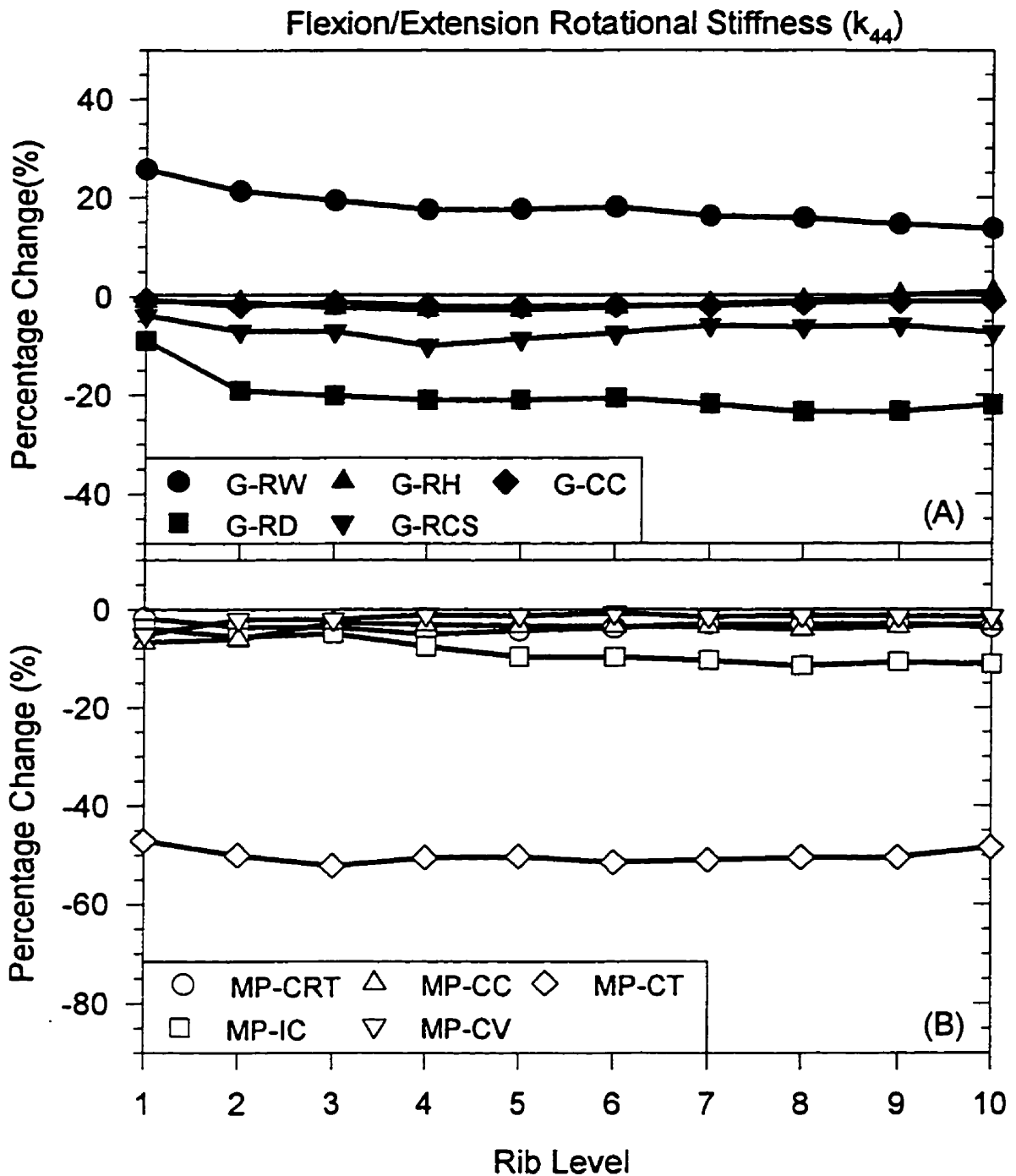


Figure 6.6: The percentage change in the flexion/extension rotational stiffness ( $k_{44}$ ) due to changes in the geometry (A) and the material properties (B) of the ribcage. The exact parametric changes to the geometry of the ribcage width (G-RW), ribcage depth (G-RD), ribcage height (G-RH), rib cross-section (G-RCS), costal cartilages (G-CC), and the material properties of the cortical rib bone (MP-CRT), the intercostals (MP-IC), the costal cartilages (MP-CC), the costovertebral joints (MP-CV) and the costotransverse joints (MP-CT) are detailed in Table 4.1.

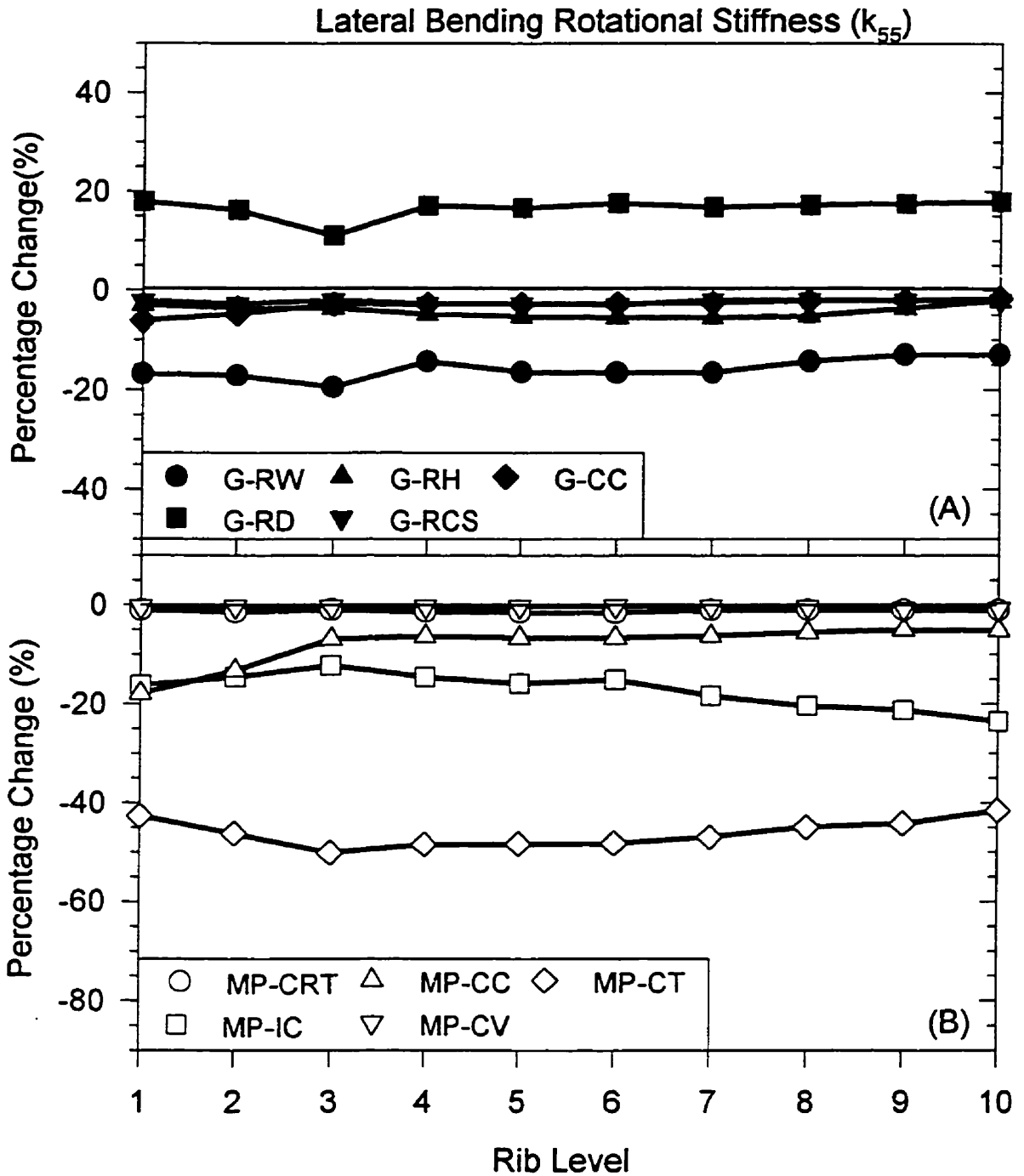


Figure 6.7: The percentage change in the lateral bending rotational stiffness ( $k_{55}$ ) due to changes in the geometry (A) and the material properties (B) of the ribcage. The exact parametric changes to the geometry of the ribcage width (G-RW), ribcage depth (G-RD), ribcage height (G-RH), rib cross-section (G-RCS), costal cartilages (G-CC), and the material properties of the cortical rib bone (MP-CRT), the intercostals (MP-IC), the costal cartilages (MP-CC), the costovertebral joints (MP-CV) and the costotransverse joints (MP-CT) are detailed in Table 4.1.

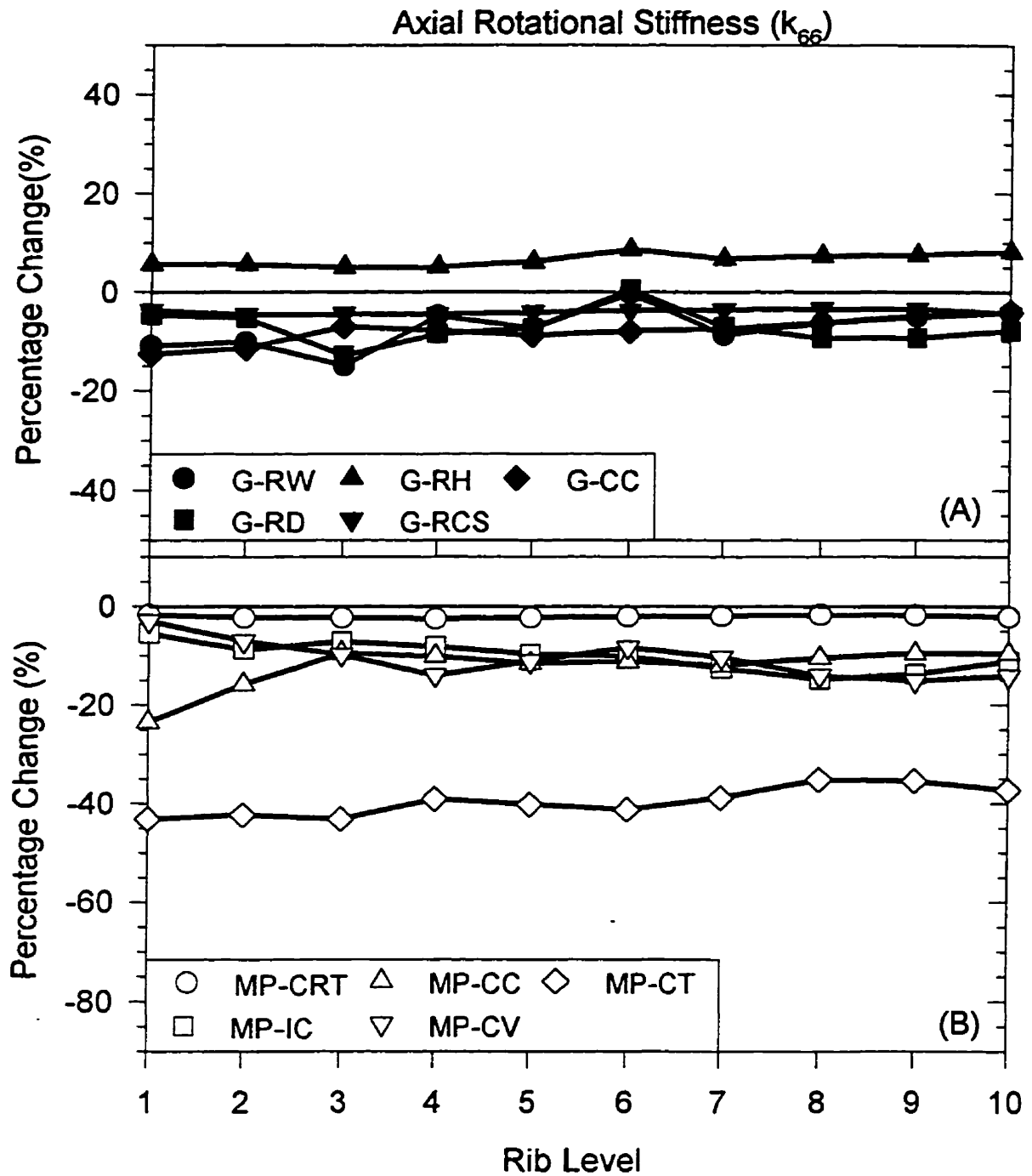


Figure 6.8: The percentage change in the axial rotational stiffness ( $k_{66}$ ) due to changes in the geometry (A) and the material properties (B) of the ribcage. The exact parametric changes to the geometry of the ribcage width (G-RW), ribcage depth (G-RD), ribcage height (G-RH), rib cross-section (G-RCS), costal cartilages (G-CC), and the material properties of the cortical rib bone (MP-CRT), the intercostals (MP-IC), the costal cartilages (MP-CC), the costovertebral joints (MP-CV) and the costotransverse joints (MP-CT) are detailed in Table 4.1.

dominant role of the CT joints in resisting any rigid body rotation of the ribs. Reduction by 60% in the moduli of the intercostals, the costal cartilages and the CV joints each resulted in about a 10% reduction in axial rotational stiffness.

## 6.4 Equivalent Ribcage Stiffnesses from Adolescence to Adulthood

The foregoing sensitivity analysis indicated that the ribcage stiffnesses were sensitive to changes in geometry and material properties. However, the changes in stiffness differed for the various directions of the ribcage. As discussed in Section 4.4.2.3., the collective summation of the results from the sensitivity analysis provided an estimate of the net difference in the ribcage stiffnesses of a young adolescent (9 year old female; 10-11 year old male) compared to an adult.

The net changes in geometry resulted in a 15-20% reduction in the ribcage rotational stiffnesses of a young adolescent compared to an adult (Fig. 6.9A). The translational stiffnesses were less affected by these net changes in geometry at all rib levels except at rib one. These relatively small differences, even after substantial changes in geometry, were due to the counteracting effects of the changes, where changes in geometry resulted in both increases and decreases in the ribcage stiffnesses as shown in previous section.

The net changes in material properties resulted in about a 55% reduction in all the ribcage stiffnesses, except the anterior translational which was only reduced 40-45% of a young adolescent compared to an adult (Fig. 6.9B). Since the ribcage was a structure composed of tissues of varied stiffnesses and orientations, the contributions of each to the overall ribcage stiffness was variable. Consequently, even substantial changes to the material properties of some tissues had only a minor effect, whereas changes to other tissues had a greater effect.

When combined, the changes in both the geometry and the material properties of a young adolescent ribcage (9 year old female; 10-11 year old male) compared to an adult lead to a net 40-65% reduction in the ribcage stiffnesses (Fig. 6.10). The differences in the

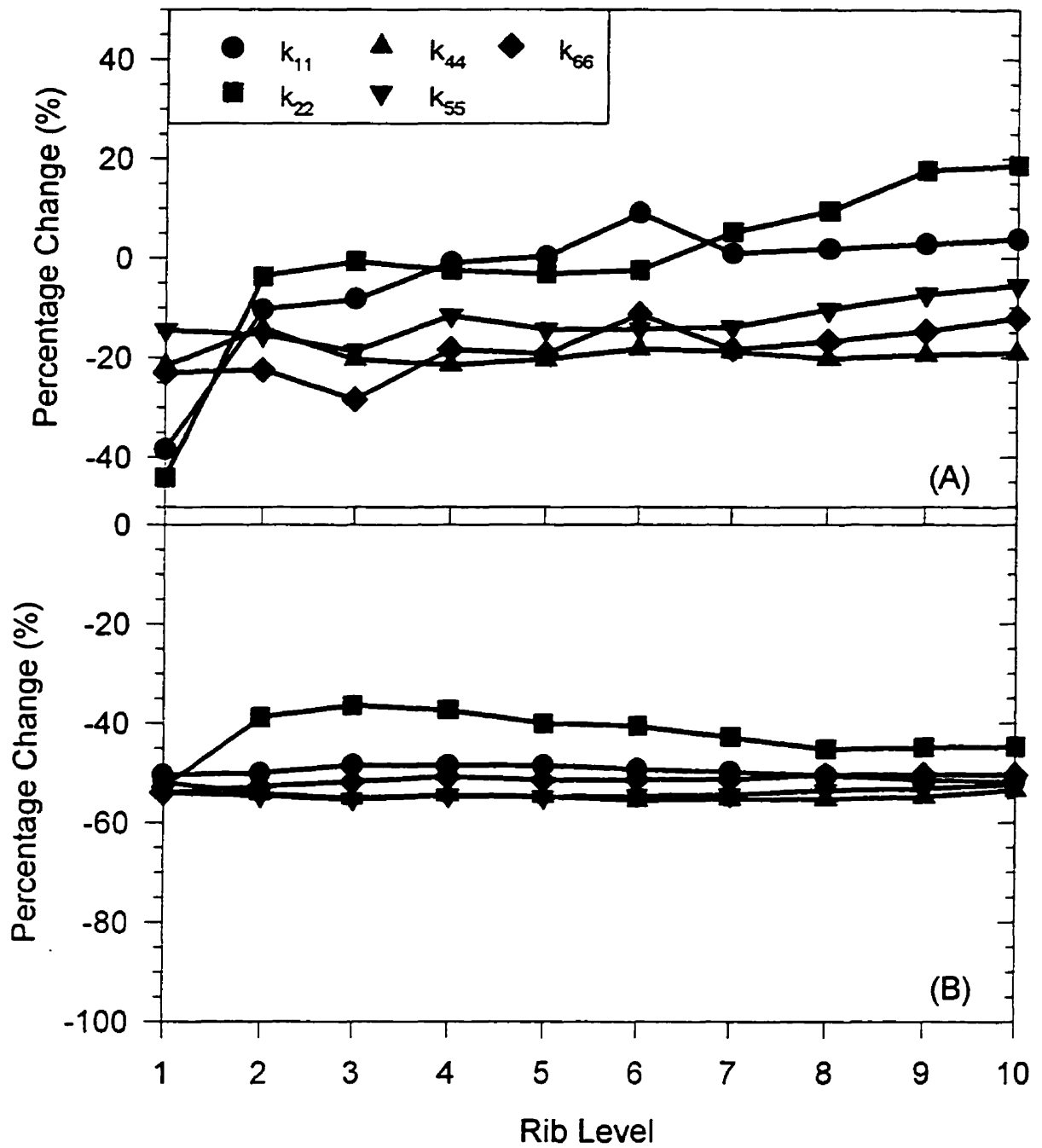


Figure 6.9: The net changes in the five ribcage stiffnesses at all rib levels due to differences in geometry (A) and material properties (B) of a young adolescent compared to an adult.  $k_{11}$ -lateral translational stiffness;  $k_{22}$ -anterior translational stiffness;  $k_{44}$ -flexion/extension rotational stiffness;  $k_{55}$ -lateral bending rotational stiffness;  $k_{66}$ -axial rotational stiffness.

three rotational stiffnesses between a young adolescent and an adult did not vary greatly with rib level, all being reduced 55-60%. The translational stiffnesses of a young adolescent were reduced about 65% at the first rib level, but at other rib levels, the anterior stiffness was only reduced about 50% and the lateral stiffness about 40%.

Based on *in vivo* measurements of trunk flexibility or mobility, Moll and Wright (1971) reported a 25% reduction in flexion, a 48% reduction in extension and a 31% reduction in lateral bending of an adult compared with an adolescent. Therefore, the current model predictions of a 40-60% reduction in ribcage stiffness was in excellent agreement with these *in vivo* results. Though clearly the ribcage is only a component of the trunk stiffness, it must be a dominant factor in the passive stiffness due to its size and structure. Therefore, this close agreement indicated that the net changes made to the ribcage model were very reasonable to establish the ribcage stiffnesses of a young adolescent.

The foregoing systematic changes established reasonable estimates for the net change in stiffness of a young adolescent ribcage compared to an adult at all rib levels. To incorporate these values into the spatial beam-column model, they were converted to per unit length similar to the adult stiffnesses presented in Table 6.2. Even though the effect of changes in the ribcage height have been included in the foregoing estimates, the reduced height of a young adolescent's ribcage and spine length has a further effect when determining the per unit length values. Since the intervertebral lengths of the adolescent's spine were less than an adult's (see Section 3.10), this led to a relative increase in the per unit length stiffnesses of the adolescent's ribcage, which counteracted to a certain extent the overall reduction in ribcage stiffness due to changes in the ribcage geometry and material properties. In Table 6.3, the ribcage stiffnesses per unit length of a 9 year old female or 10-11 year old male are presented. In comparison to the values of an adult presented in Table 6.2, there was a net reduction on the order of 35-50% of the ribcage stiffnesses per unit length.

The sensitivity analysis was also used to estimate the differences in ribcage stiffnesses between an adult male and female, based on differences in geometry (see Section 4.4.2.2). These values were then converted to per unit length based on the different intervertebral lengths (see Section 3.6), and represented the upper bounds of the final ribcage stiffnesses

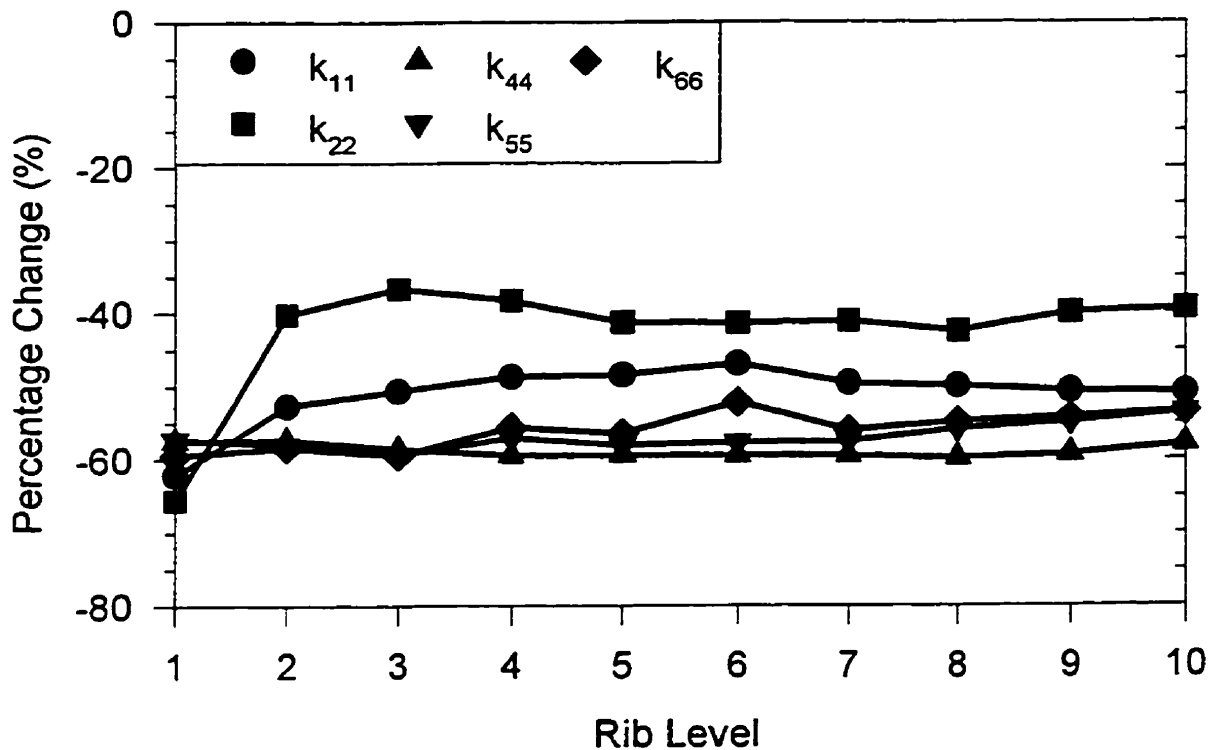


Figure 6.10: The net changes in the five ribcage stiffnesses at all rib levels due to the collective differences in geometry and material properties of a young adolescent compared to an adult.  $k_{11}$  – lateral translational stiffness;  $k_{22}$  – anterior translational stiffness;  $k_{44}$  – flexion/extension rotational stiffness;  $k_{55}$  – lateral bending rotational stiffness;  $k_{66}$  – axial rotational stiffness.

presented in Figs. 6.11-6.15.

To determine the ribcage stiffnesses per unit length at the intermediate ages during the adolescent growth spurt, interpolation was used as described in Section 4.4.2.3. These results are presented in Figs. 6.11 - 6.15 for each of the five ribcage stiffnesses for a female and male. Similar to other properties of the spine, the ribcage stiffnesses varied nonuniformly with age and the females reached their adult values earlier than males due to the different timing of the growth spurt. These final ribcage stiffnesses as a function of age were used in the analysis of the effect of the adolescent growth spurt on the progression potential of mild scoliotic curves presented in Section 7.3.

Table 6.3: The principal ribcage stiffnesses per unit length at all the rib levels of a young adolescent.

Rib Level	Translational		Rotational		
	Lateral- $k_{11}^o$ (kN/m <sup>2</sup> )	Anterior- $k_{22}^o$ (kN/m <sup>2</sup> )	Flexion/Extension- $k_{44}^o$ (N/rad)	Lateral Bend- $k_{55}^o$ (N/rad)	Axial- $k_{66}^o$ (N/rad)
1	74.9	471.1	35.4	113.8	331.3
2	63.5	198.0	69.1	103.8	243.8
3	50.3	124.8	76.5	65.7	134.8
4	41.2	104.6	101.2	66.2	159.3
5	34.7	95.0	87.1	77.5	164.8
6	28.7	74.3	83.4	75.7	148.9
7	24.1	52.7	76.1	71.1	127.1
8	20.1	36.0	88.2	56.6	106.0
9	16.6	21.5	77.3	46.1	79.7
10	13.9	14.1	59.7	36.2	59.0

— Note these stiffnesses were representative of a young adolescent, either a 9 year old female or 10-11 year old male.

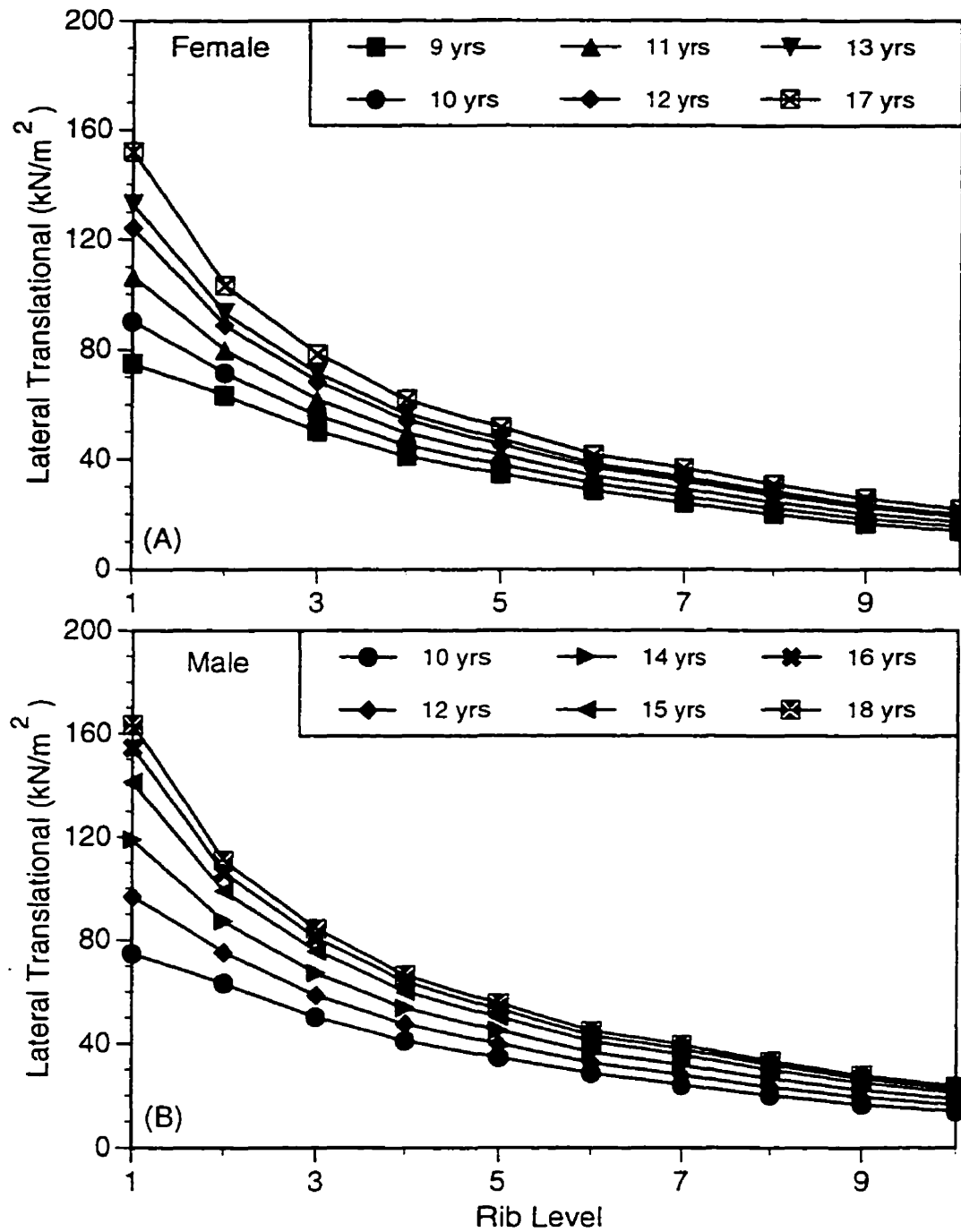


Figure 6.11: The lateral translational stiffness per unit length ( $k_{11}^0$ ) at each rib level as a function of age for a female (A) and male (B).

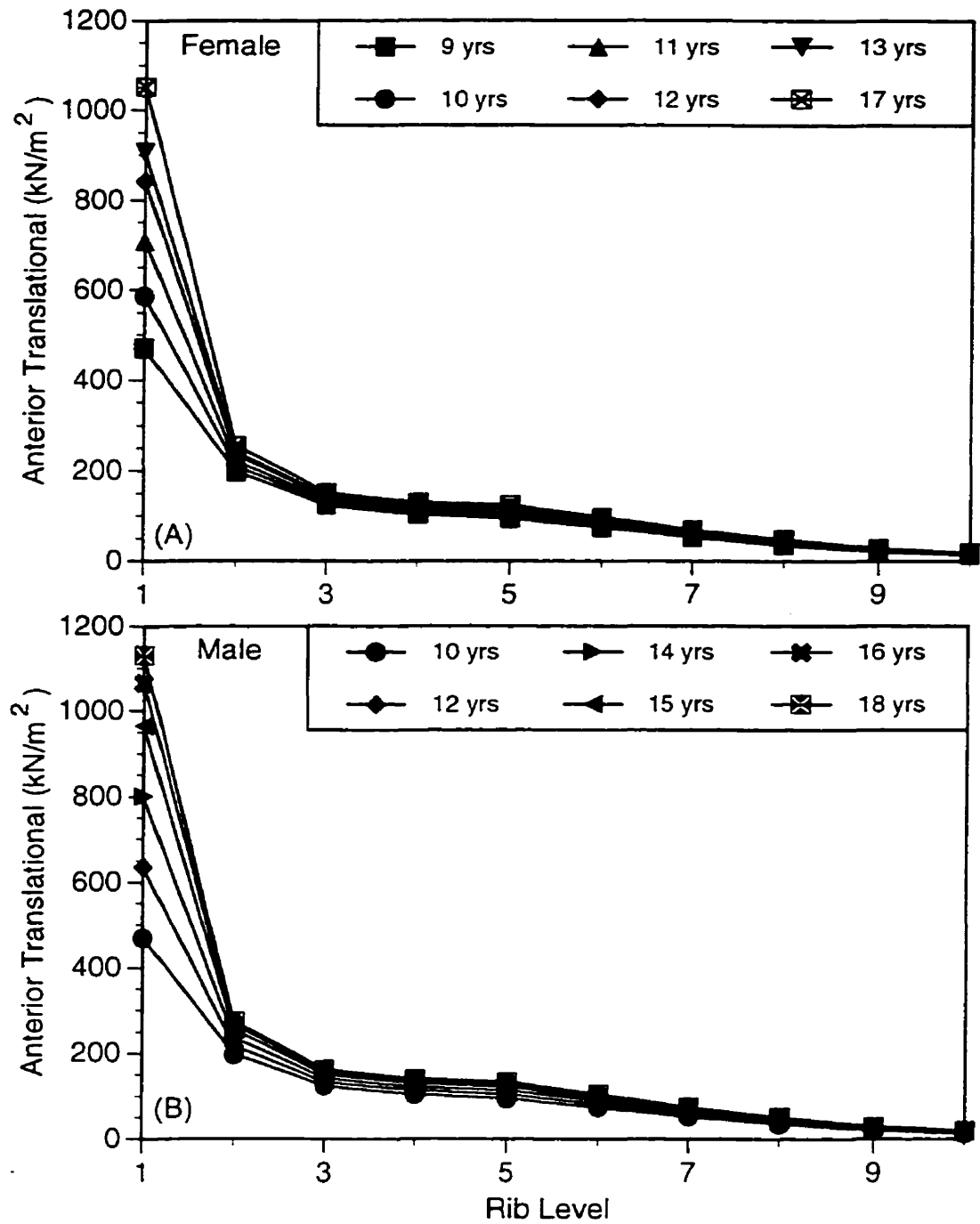


Figure 6.12: The anterior translational stiffness per unit length ( $k_{22}^o$ ) at each rib level as a function of age for a female (A) and male (B).

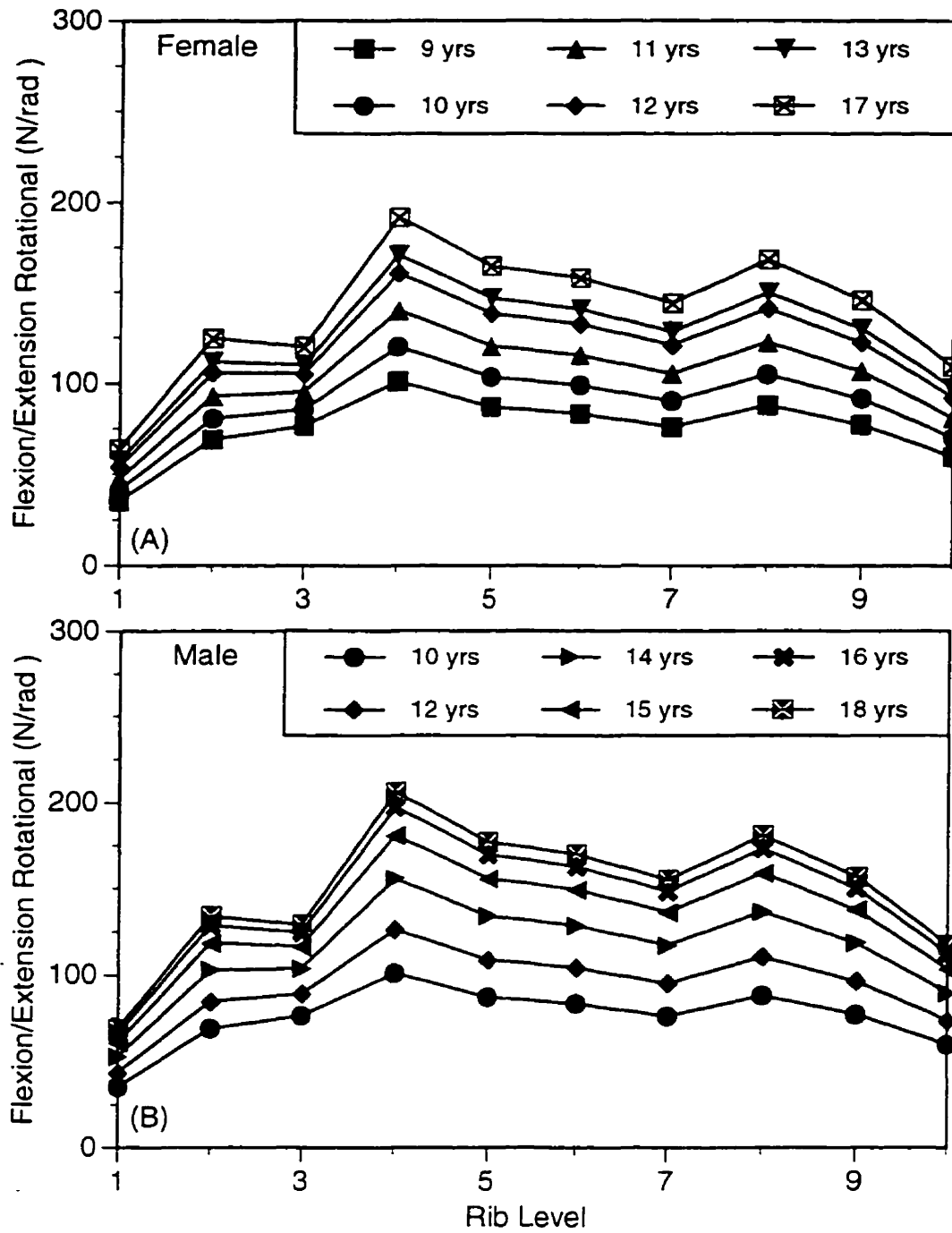


Figure 6.13: The flexion/extension rotational stiffness per unit length ( $k_{44}^o$ ) at each rib level as a function of age for a female (A) and male (B).

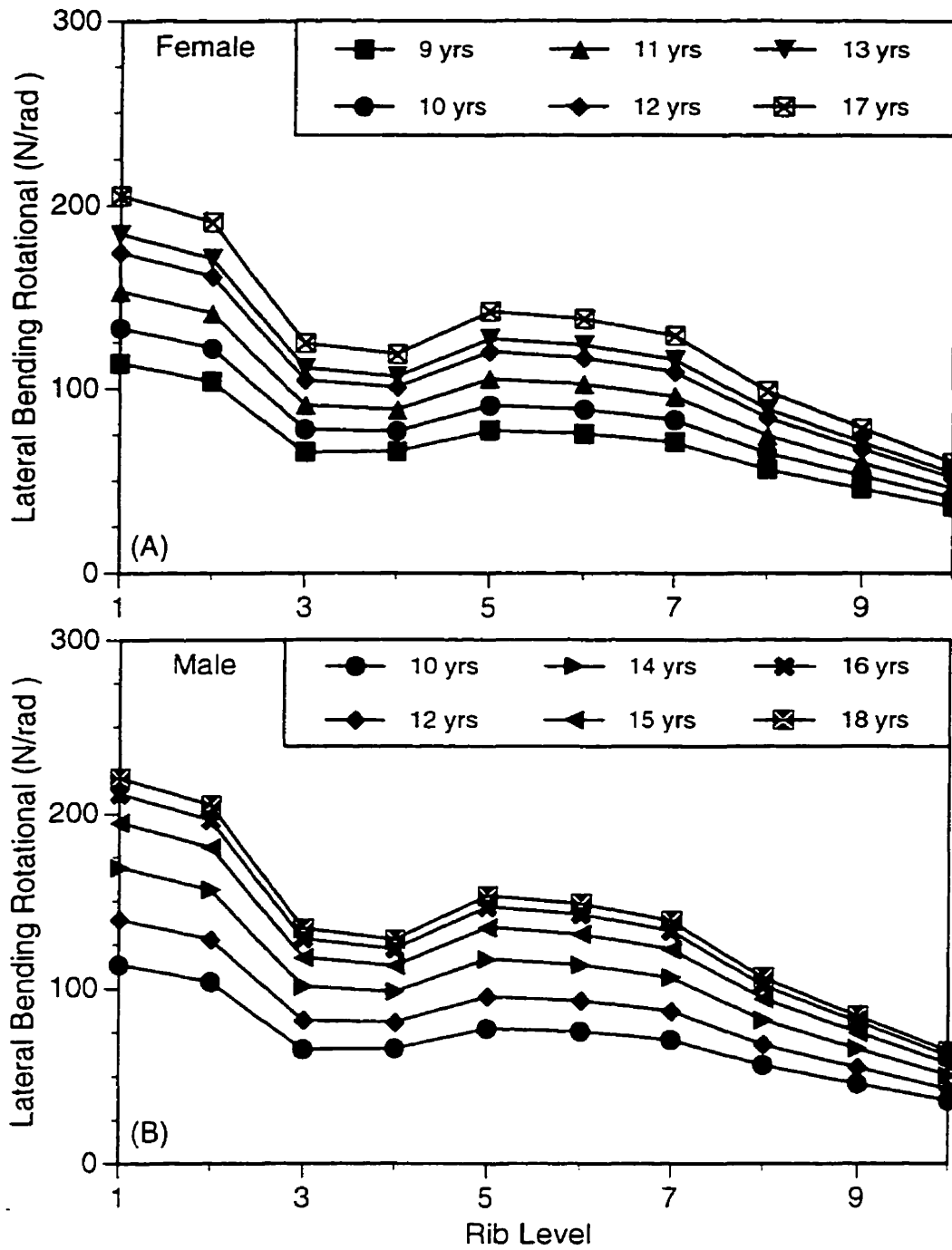


Figure 6.14: The lateral bending rotational stiffness per unit length ( $k_{55}^0$ ) at each rib level as a function of age for a female (A) and male (B).

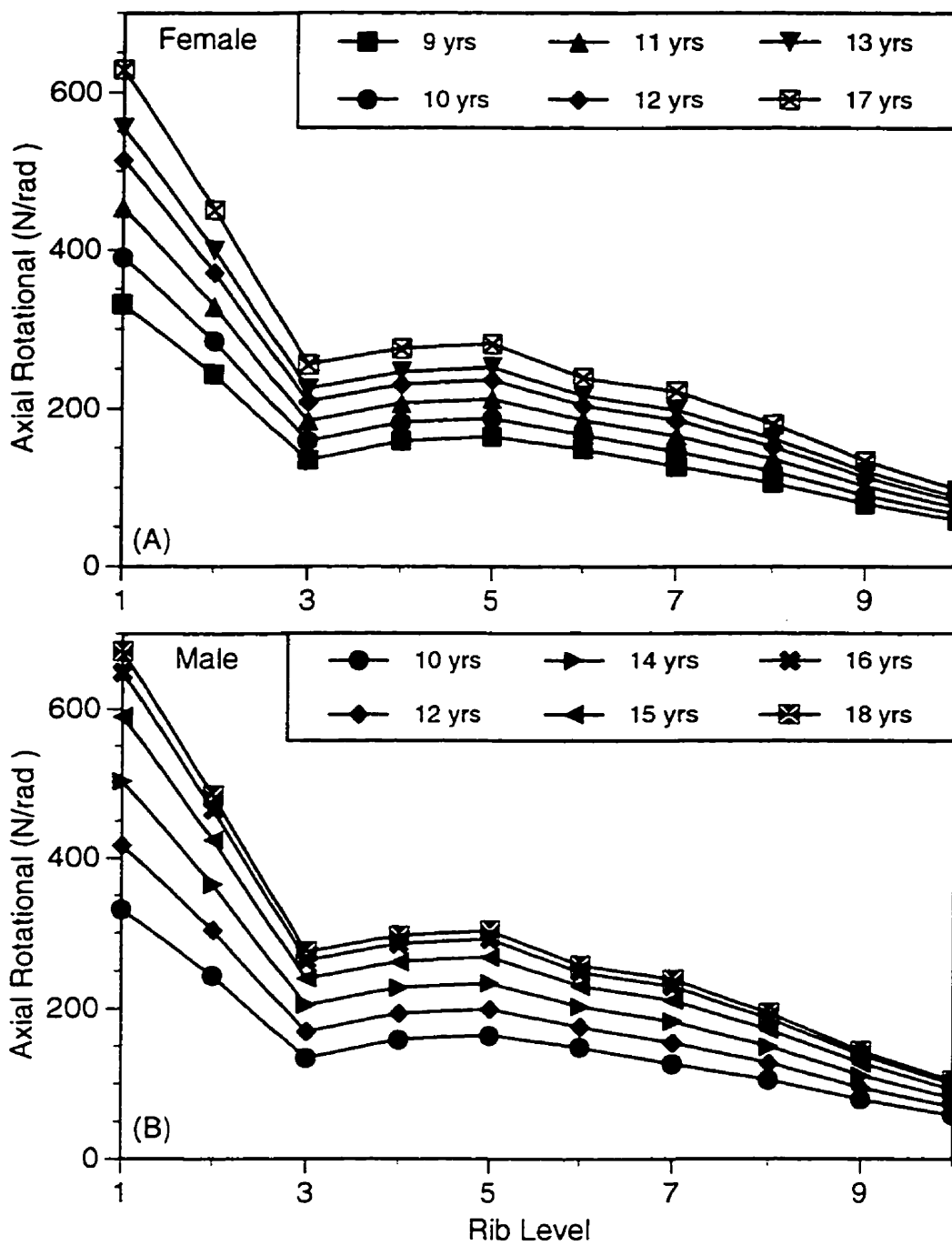


Figure 6.15: The axial rotational stiffness per unit length ( $k_{66}^o$ ) at each rib level as a function of age for a female (A) and male (B).

## Chapter 7

# RESULTS - SCOLIOTIC SPINE MODEL

### 7.1 Introduction

In this chapter, the results of the parametric analysis of the spatial beam-column model with incorporated ribcage stiffnesses are first presented. The procedure for this analysis was outlined in Section 3.9. Secondly, the results of the explicit analysis of the effect of the adolescent growth spurt on the progression of a mild scoliosis are presented for both normal and accelerated growth patterns in females and males, as outlined in Section 3.10.

### 7.2 Parametric Analysis of the Scoliotic Spine Model

The results of the parametric analysis of the spine model with a mild scoliosis are presented in Table 7.1. The model was clearly most sensitive to changes in spine height ( $L$ ). For the scoliotic spine with an initial Cobb angle of  $10^\circ$ , an increase of around 20% was needed to cause an increase of  $10^\circ$  in Cobb angle. However, for an initial Cobb angle of  $30^\circ$ , an increase in spine length of only around 5% was required. The scoliotic spine was also quite sensitive to changes in the applied upper body weight ( $W$ ), particularly for an

initial Cobb angle of  $30^\circ$ , where only a 10% increase in weight was needed to increase the Cobb angle by  $10^\circ$ .

The scoliotic spine was not overly sensitive to changes in the effective lateral bending stiffness ( $EI_{\eta\eta_0}$ ) and axial torsion stiffness ( $GJ$ ) of the spine. For an initial Cobb angle of  $10^\circ$ , the stiffnesses needed to be reduced by more than 40% to produce an increase of  $10^\circ$  in Cobb angle. The model sensitivities were very similar for the changes to each of these stiffnesses; likely related to the fairly close correlation between the lateral translation and axial rotation at the curve apex with the Cobb angle.

Changes to the lateral translational stiffness of the ribcage had the most effect on the scoliotic spine compared to the other ribcage stiffnesses. For an initial Cobb angle of  $30^\circ$ , a reduction of around 14% in the lateral ribcage stiffness was needed for an increase of  $10^\circ$  in Cobb angle. Reduction of the axial torsional stiffness of the ribcage had the next largest effect on the increase in Cobb angle. Overall, the initial Cobb angle did not affect the sensitivities of the ribcage stiffness parameters as greatly as the spinal column parameters.

These results indicated that a substantial change to the individual parameters was required to increase the Cobb angle  $10^\circ$  for an initial Cobb angle of  $10^\circ$ . Therefore, it is very unlikely that progression of a very mild scoliosis could occur solely due to growth, since it is unreasonable to expect a change in these parameters in one year by these percentages. On the other hand, for an initial Cobb angle of  $30^\circ$ , the percentage changes of the applied weight and spine length needed to increase the Cobb angle  $10^\circ$  could conceivably occur in the period of a year. Furthermore, for a Cobb angle of  $30^\circ$ , a change of  $10^\circ$  is a conservative definition of progression, since a change of only  $5^\circ$  is usually used at this curve magnitude to define progression (Lonstein and Carlson, 1984).

In this analysis, the changes to the parameters were considered separately. The vulnerability to progression would be greatly increased if, for example, both the weight and length increased simultaneously as in growth. Clearly, a significant increase in stiffness of the spine and ribcage would be needed to counteract this potential progression. In the next section, the results of the explicit simulation of adolescent growth is presented, which considered the simultaneous changes to these parameters during growth.

Table 7.1: The sensitivity of the scoliotic spine model to changes in various mechanical parameters.

Parameter	Initial Cobb Angle		
	10°	20°	30°
$W$	+ 35.7	+16.3	+10.3
$L$	+19.7	+8.3	+5.1
$EI_{\eta\eta_0}$	-44.9	-28.5	-16.5
$GJ$	-52.0	-32.6	-18.9
$k_{11}^o$	-32.1	-21.0	-14.2
$k_{55}^o$	-91.3	-70.5	-60.3
$k_{66}^o$	-51.0	-40.2	-32.4

— The sensitivity is expressed as the percentage difference in the parameter relative to the baseline value for a 9 year old female or 10-11 year old male required to cause an increase in Cobb angle of 10°. The parameters analyzed were upper body weight ( $W$ ), spine height ( $L$ ), lateral bending stiffness ( $EI_{\eta\eta_0}$ ), axial torsion stiffness ( $GJ$ ), lateral translational stiffness of the ribcage ( $k_{11}^o$ ), lateral bending stiffness of the ribcage ( $k_{55}^o$ ) and axial rotational stiffness of the ribcage ( $k_{66}^o$ ).

## 7.3 Effect of the Adolescent Growth Spurt on Curve Progression

### 7.3.1 Normal Growth Pattern

For a female spine with an *initial Cobb angle of 10°*, the model predicted only a very small increase of less than 2° in the Cobb angle, which peaked at 11 years of age and subsequently declined (Fig. 7.1A). In a male spine, the Cobb angle first declined slightly between the ages of 10 and 13 years, and then increased very slightly during the male growth spurt. For both males and females, the lateral translation and axial rotation of the apical vertebra were also minimally affected by normal growth of a spine with an initial Cobb angle of 10° (Fig. 7.1B-C).

For a spine with an *initial Cobb angle of 20°*, the Cobb angle increased about 5° during normal growth of a female, peaked at 11 years and then declined to the initial Cobb angle (Fig. 7.2A). In a male, the Cobb angle increased only about 1-2° during the later adolescent years.

For a spine with an *initial Cobb angle of 30°*, the Cobb angle increased quite substantially by about 9° during normal growth of a female (Fig. 7.3A). The lateral translation at the curve apex was about 36 mm with an axial rotation of 12° (Fig. 7.3B-C). The change in Cobb angle of a male during growth still only reached a peak of about 3.5° at 18 years of age.

These results showed that the mechanical changes associated with normal growth in a female could result in a sufficient increase in Cobb angle to be classified as clinically progressive for an initial Cobb angle of 20-30°. In a male, the predictions of the increase in Cobb angle would all be considered non-progressive. These results also showed that the progression of the curve stabilized and even declined in later years of adolescence for both females and males. The peak increases in Cobb angle were predicted to occur at the peak of the adolescent growth spurt (11-12 years in females; 14-15 years in males).

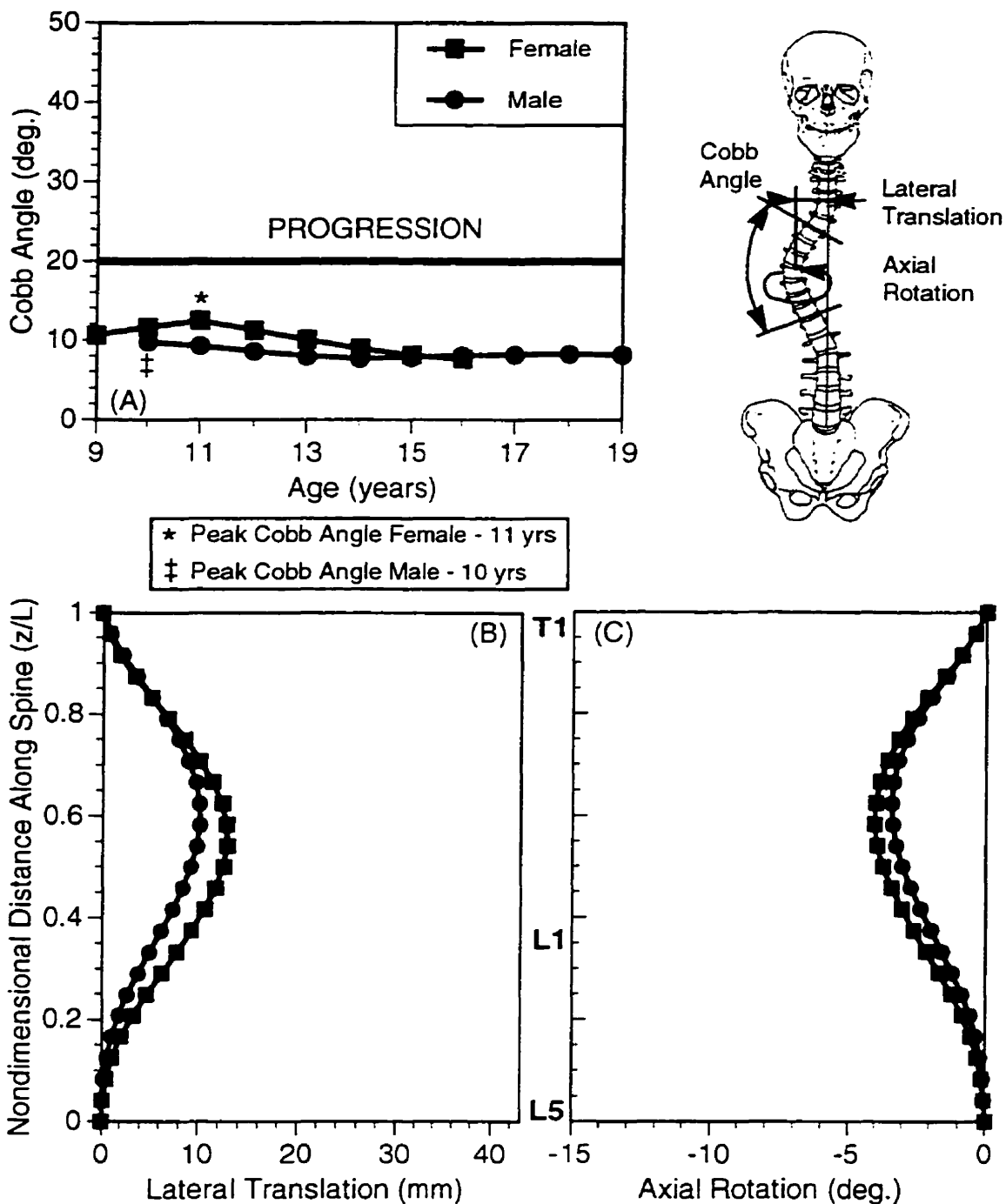


Figure 7.1: The model predictions of the effect of normal growth in males and females on curve progression of a mild scoliosis in a spine with an initial Cobb angle of 10°. (A) The Cobb angle of the scoliotic curve at each age of adolescence. (B) The lateral translation of the vertebral centres along the spine at the age of peak increase in Cobb angle. (C) The axial rotation of the vertebrae along the spine at the age of peak increase in Cobb angle.

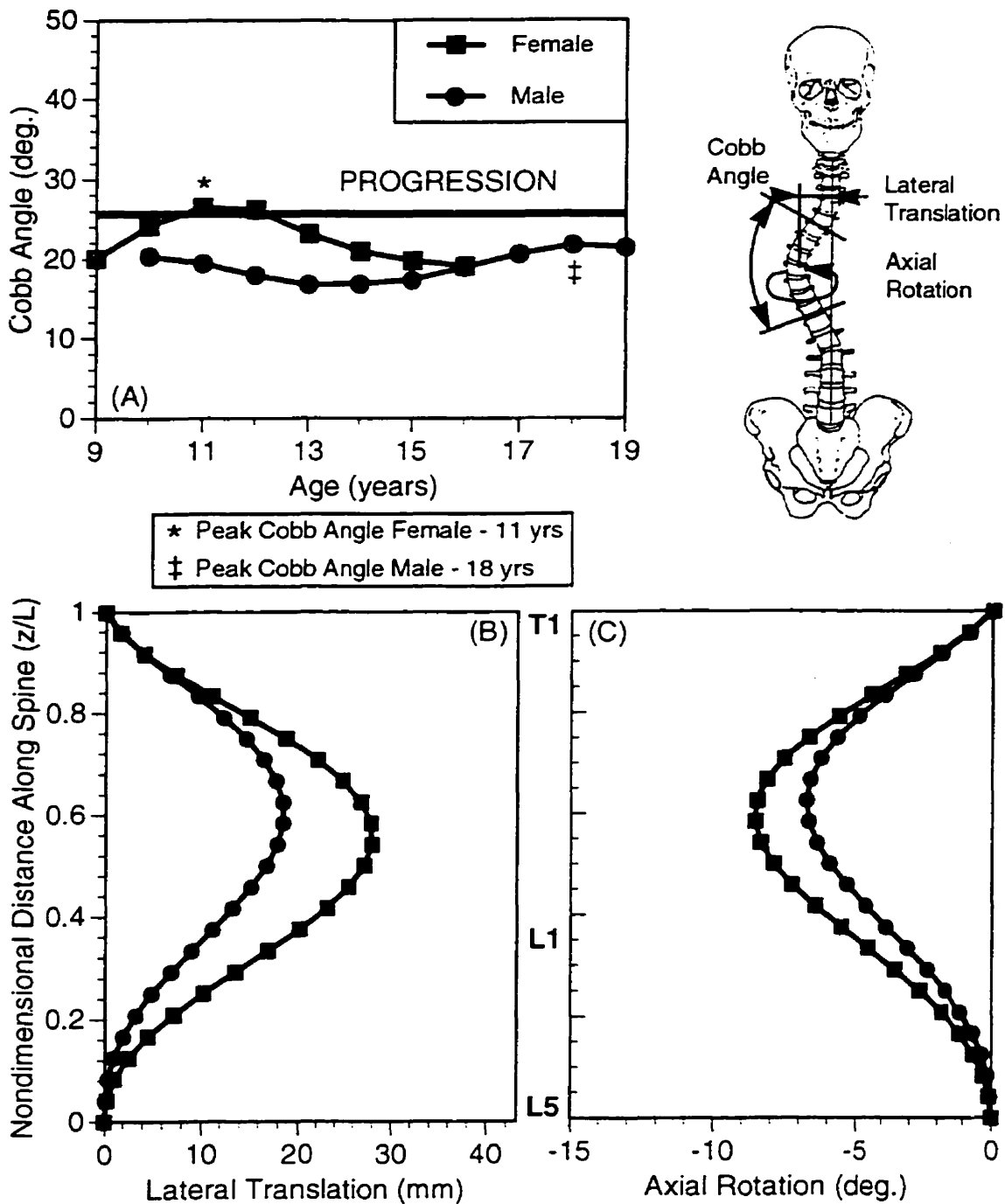


Figure 7.2: The model predictions of the effect of normal growth in males and females on curve progression of a mild scoliosis in a spine with an initial Cobb angle of 20°. (A) The Cobb angle of the scoliotic curve at each age of adolescence. (B) The lateral translation of the vertebral centres along the spine at the age of peak increase in Cobb angle. (C) The axial rotation of the vertebrae along the spine at the age of peak increase in Cobb angle.

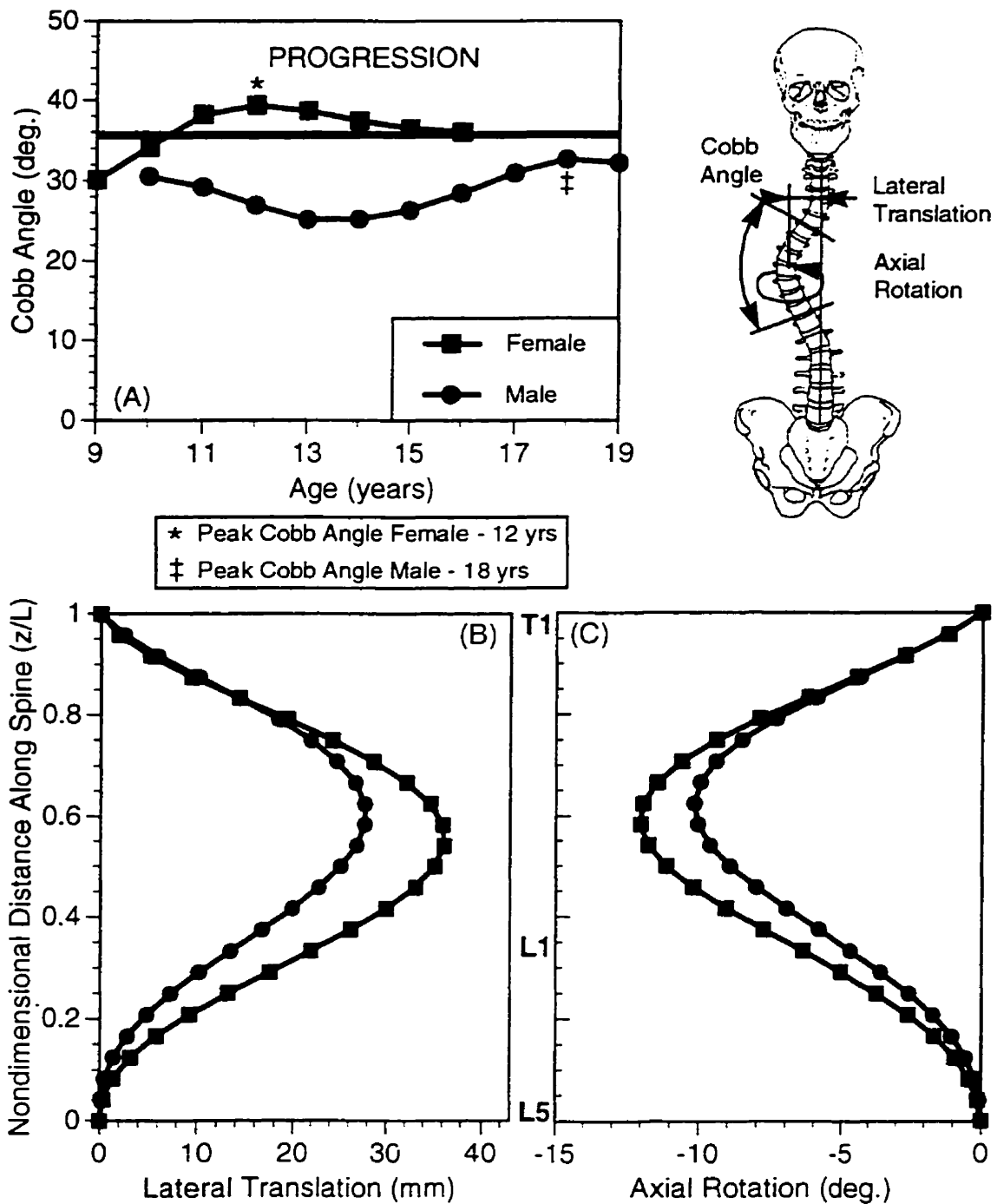


Figure 7.3: The model predictions of the effect of normal growth in males and females on curve progression of a mild scoliosis in a spine with an initial Cobb angle of  $30^\circ$ . (A) The Cobb angle of the scoliotic curve at each age of adolescence. (B) The lateral translation of the vertebral centres along the spine at the age of peak increase in Cobb angle. (C) The axial rotation of the vertebrae along the spine at the age of peak increase in Cobb angle.

### 7.3.2 Accelerated Growth Pattern

An accelerated growth pattern was predicted by the model to have a significant effect on the progression of a scoliotic curve. For a female spine with an initial Cobb angle of  $10^\circ$ , the Cobb angle was increased about  $2.5^\circ$  for the *growth pattern of Case I*, where the spine length was increased 2% at each age of adolescence (Fig. 7.4A). In a male on the other hand, the Cobb angle increased less than  $1^\circ$  for the Case I growth pattern (Fig. 7.4B). Therefore, compared with the results for the normal growth pattern, the Cobb angle was found to be only slightly increased in a female and male due to the 2% increase in spine length. This effect was increased by a greater initial Cobb angle. For a female spine with an initial Cobb angle of  $30^\circ$ , the Cobb angle was increased about  $13^\circ$  at the peak of the growth spurt at 12 years of age (Fig. 7.4A).

In the *growth pattern of Case II*, the spine length was first increased by 2% at 9 years of age in a female and at 10-11 years of age in a male. Subsequently, this length increase was linearly reduced until there was no difference in spine length from normal at maturity. The model predictions of curve progression during this growth pattern were very similar to the results of Case I. The peak increase in Cobb angle was slightly less, but still for a female spine with an initial Cobb angle of  $30^\circ$ , the Cobb angle was increased about  $11.5^\circ$  at 12 years of age (Fig. 7.5A).

The *growth pattern of Case III* was similar to Case II, except the initial increase in spine length was 4.5%. This growth pattern had a more dramatic effect. For a female spine with an initial Cobb angle of  $10^\circ$ , the Cobb angle was increased about  $6^\circ$  for the growth pattern of Case III between the ages of 10-12 years, before declining at later years (Fig. 7.6A). For an initial Cobb angle of  $30^\circ$ , the Cobb angle was increased nearly  $18^\circ$  in a female spine between 11 and 13 years of age. The effect of this growth pattern on males was also more significant. For a male spine with an initial Cobb angle of  $30^\circ$ , the Cobb angle was increased about  $4^\circ$  (Fig. 7.6B).

The effect of the Case III growth pattern was also to increase the span of years (centered around the peak of the growth spurt) when the Cobb angles were predicted to be larger. This was due to the fact that in a larger number of the early years of adolescence, the spine

length was significantly increased. Further, due to the more sustained period of larger Cobb angles, this likely contributed to the progression in a degenerative loop. These increased Cobb angles in earlier years made the spine more sensitive to increases in length and weight. Consequently, even though the yearly increments of these parameters were decreasing, they still had a significant effect on curve progression after the peak of the growth spurt.

These results show that the mechanical changes associated with an accelerated growth pattern could lead to increased Cobb angles compared to those associated with a normal growth pattern. However, for a curve with an initial Cobb angle of  $10^{\circ}$ , the increase in Cobb angle was still not enough to be classified as progressive. Similarly, in males, the changes in Cobb angle associated with the accelerated growth rates would also not be classified as progressive clinically.

In Figure 7.7, the correlation of the axial rotation of the spine at the curve apex with the Cobb angle is shown for the curve progression predicted in a female for the accelerated growth rate of Case III. As observed clinically, there was a close correlation between increases in Cobb angle and axial rotation of the spine. The spine continued to rotate axially during progression with the spinous processes rotated into the concavity of curve.

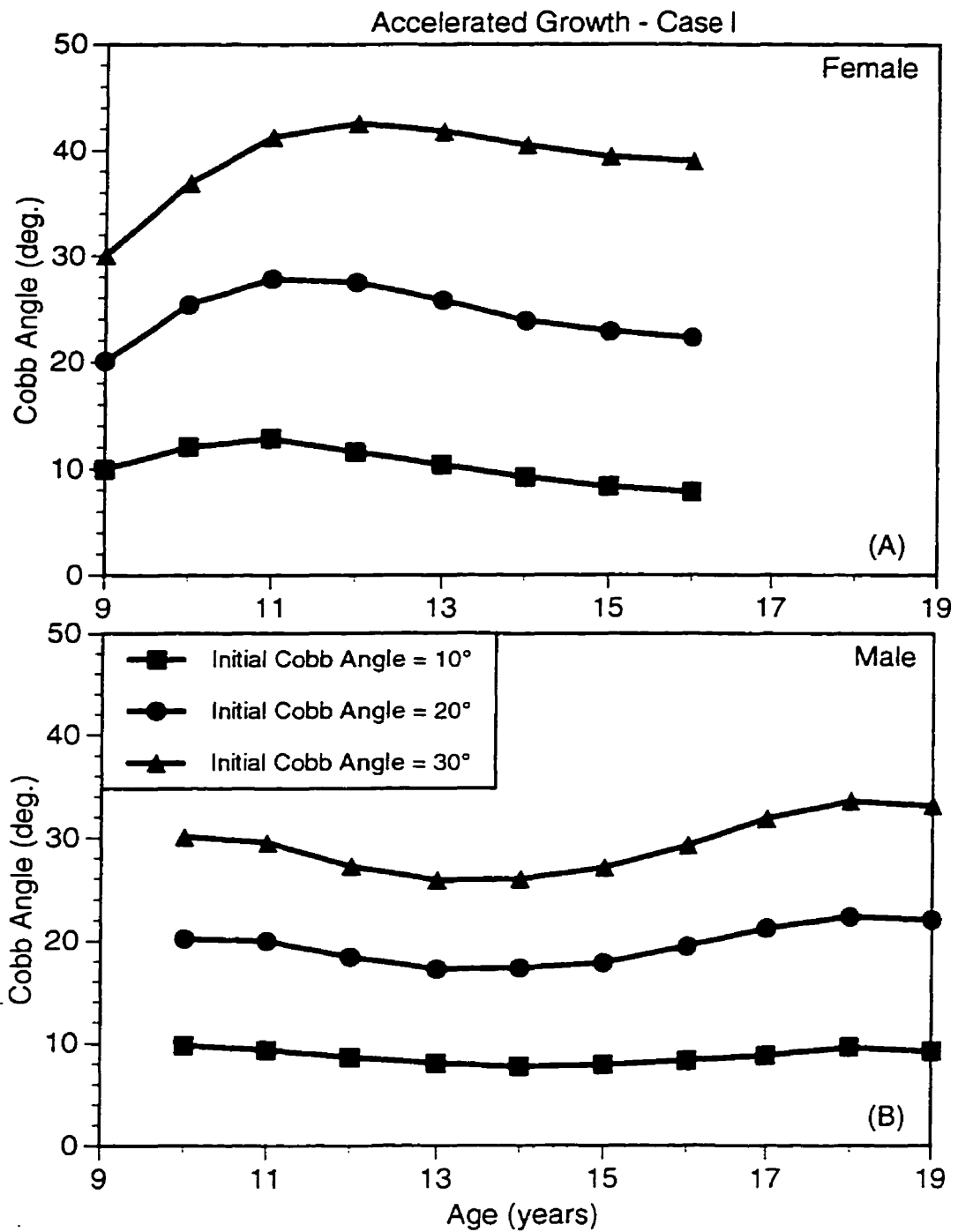


Figure 7.4: The model predictions of the effect of the accelerated growth pattern of Case I on the Cobb angle of a mild scoliotic curve with an initial Cobb angle of 10, 20 and 30°. (A) Female; (B) Male.

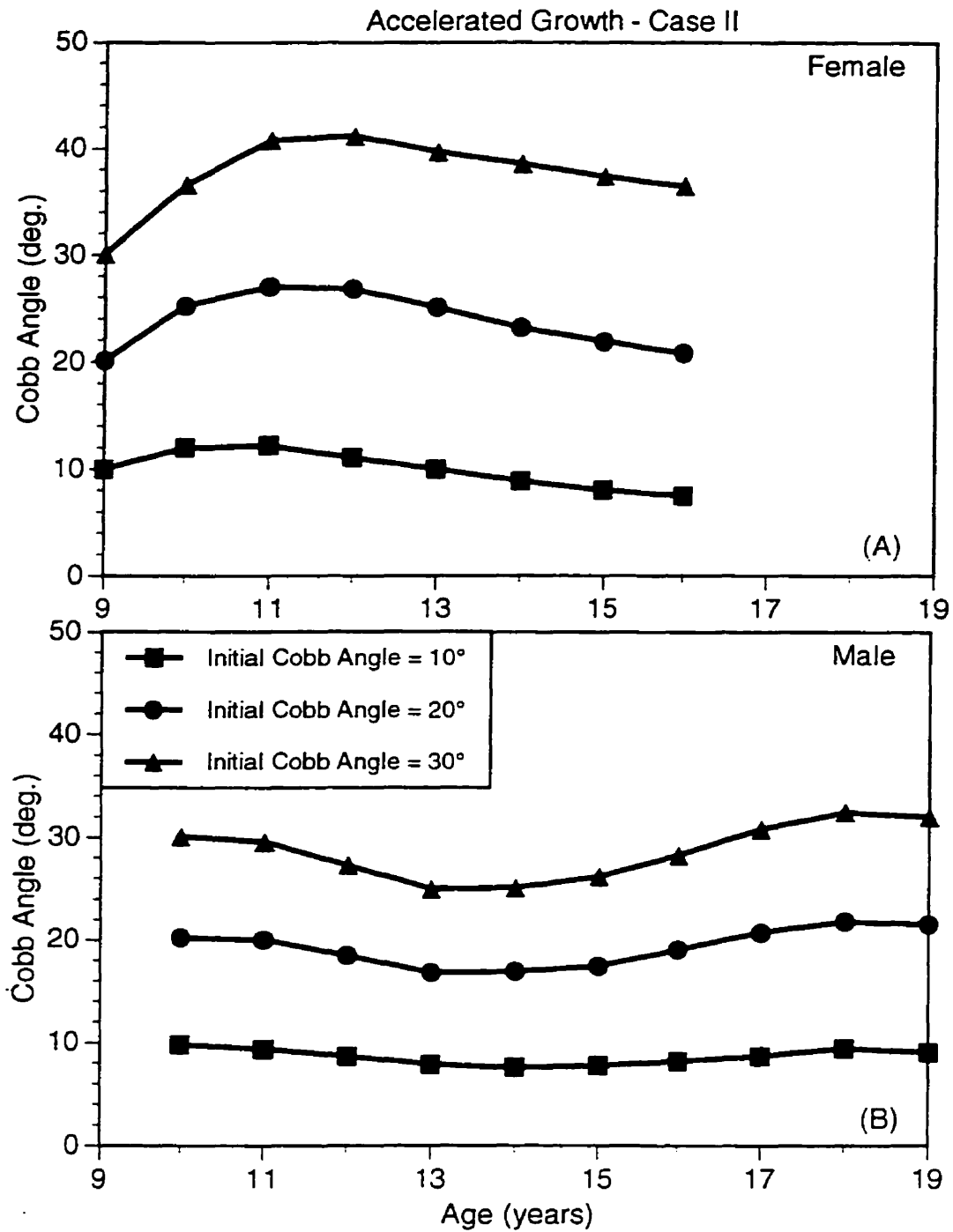


Figure 7.5: The model predictions of the effect of the accelerated growth pattern of Case II on the Cobb angle of a mild scoliotic curve with an initial Cobb angle of 10, 20 and 30°. (A) Female; (B) Male.

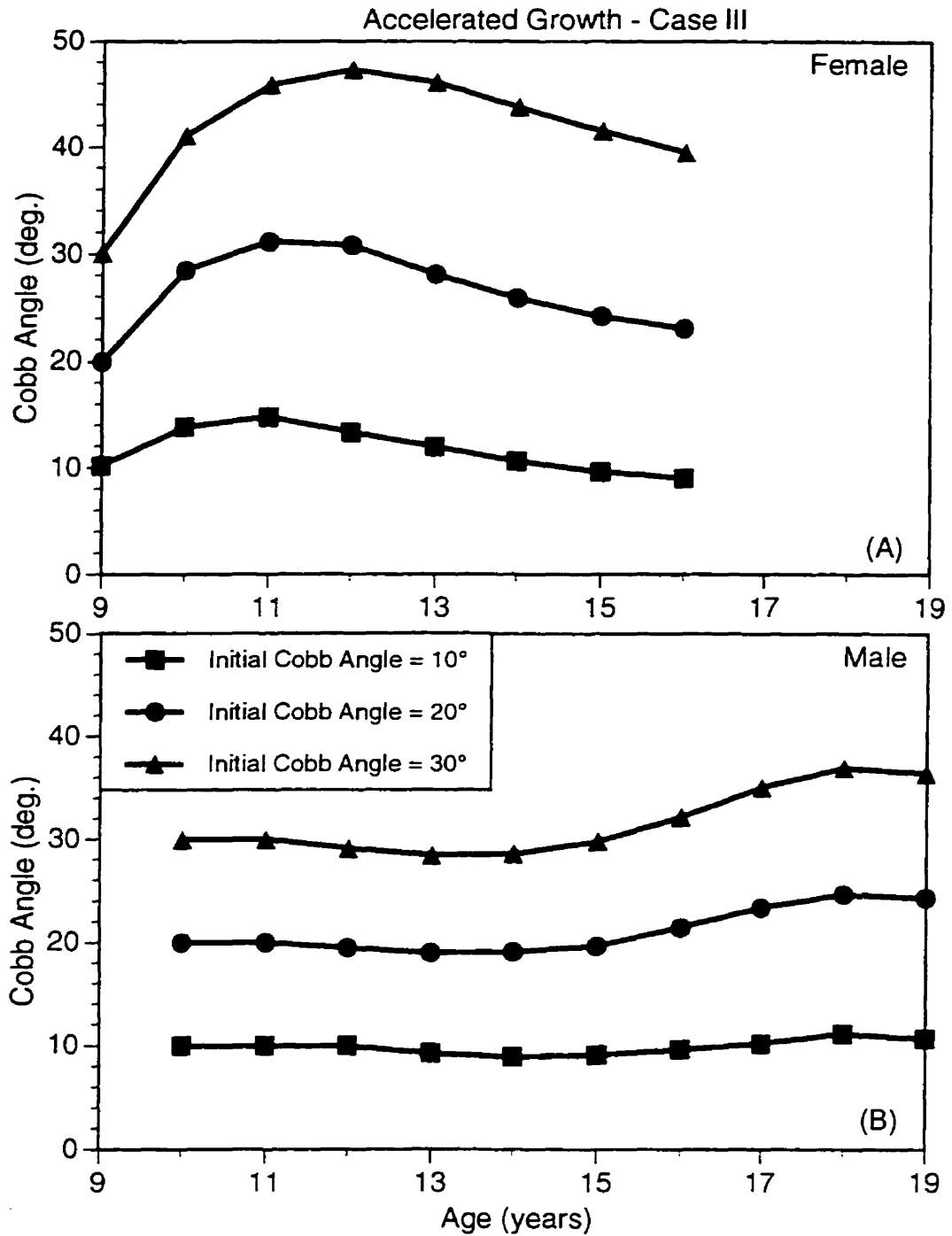


Figure 7.6: The model predictions of the effect of the accelerated growth pattern of Case III on the Cobb angle of a mild scoliotic curve with an initial Cobb angle of 10, 20 and 30°. (A) Female; (B) Male.

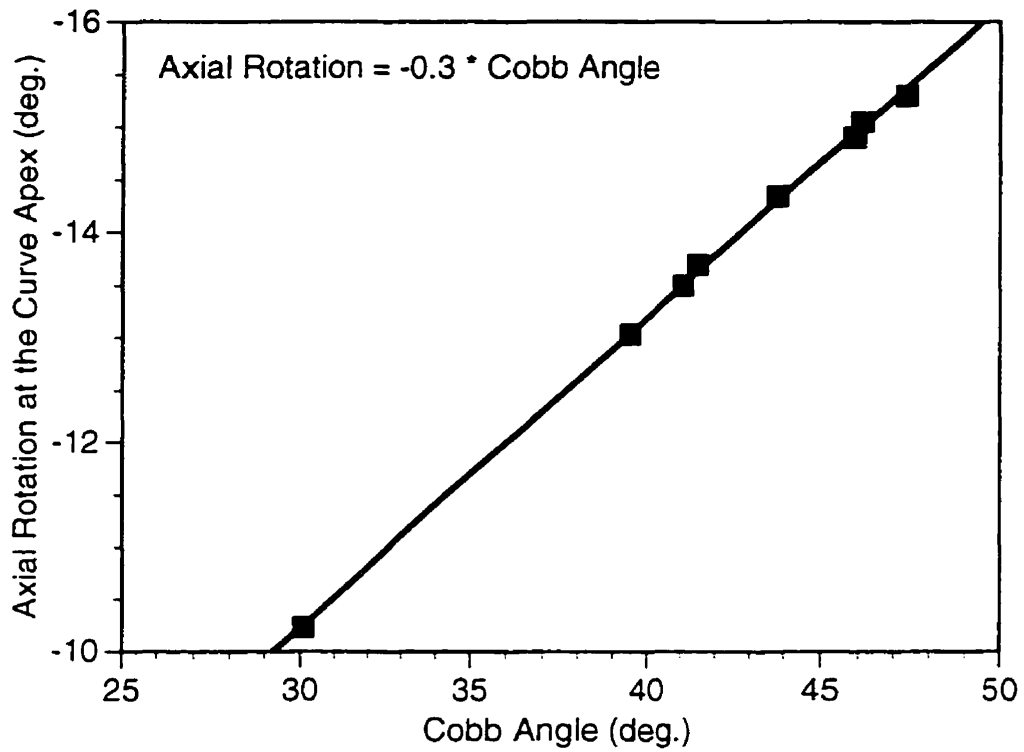


Figure 7.7: The correlation of the axial rotation of the spine at the curve apex with the Cobb angle during curve progression for the accelerated growth of Case III in a female.

# Chapter 8

## DISCUSSION AND CONCLUSIONS

### 8.1 Introduction

This study was motivated by the need to better predict the progression of spinal deformity in adolescent idiopathic scoliosis. The current objective was to develop a model of a spine with a mild scoliosis, and to identify mechanical factors associated with the critical growth spurt of adolescence which might explain why only some curves progress uncontrollably from small to large incapacitating deformities. In this chapter, the possible mechanical factors that affect curve progression are first discussed based on the results of the parametric analyses of the ribcage and spine. Secondly, the mechanical effect of growth on curve progression is discussed based on the results of the simulation of the adolescent growth spurt. The present results are then compared with previous work, followed by a discussion of the limitations of the present study. Next, the clinical significance of the current findings are presented, and following a summary, a set of conclusions are stated. The chapter concludes with some suggestions for future studies.

## 8.2 Mechanical Factors Affecting Curve Progression in Scoliosis

The particular mechanics of curve progression in scoliosis is best understood by first noting that the mechanics of a curved rod are very different from a straight one. For instance, a straight rod subjected to axial compression remains perfectly straight until the critical buckling load is reached. A curved rod, on the other hand, deflects laterally for even the smallest axial load due to the induced bending moment. Consequently, the magnitude of the initial curvature can be as important to consider as the loading in order to predict the deflection of a curved rod.

The human spinal column is a long, slender structure curved in one plane, but straight in the other, and is surrounded by the ribcage, which provides lateral support similar to a beam on an elastic foundation. Scoliosis is a deformity of the spinal column which leads to three-dimensional curvature, as well as axial rotation. This work attempted to better understand the *progression behaviour* of the scoliotic spine by developing and analyzing a model of an *initially curved and twisted, spatial beam-column embedded in an elastic medium* (Chapters 3 and 7). Due to the complexity of this system, a hybrid approach was developed whereby the *stiffness of the ribcage* was first analyzed with a *finite element model* (Chapters 4 and 6). This stiffness data was then incorporated directly into the continuum beam-column model of the scoliotic spine.

One of the significant findings of this study was the specific variation of the ribcage stiffness with orientation and rib level (Section 6.2). It was found to be stiffest at the upper ribs for anterior-posterior translation and axial rotation. In the lower ribs, the translational stiffnesses and the rotational stiffnesses were very similar. Consequently, the ribcage provides essentially uniform or isotropic support to the middle of the spinal column. In a thoracic or thoracolumbar scoliosis, which is the type of scoliosis of interest in this study, the apical vertebra is in the middle region of the spine, and there should be no preferential forces or moments exerted on the spine by the ribcage. In other words, though the ribcage provides essential support to the spine, other factors are likely to determine

the relative magnitudes of the anterior-posterior and lateral translations, and the relative degree of lateral tilt and axial rotation in a spine with a thoracic or thoracolumbar scoliosis.

The prediction of a high axial rotational stiffness of the ribcage in the upper ribs is of interest because of the potential effect on the axial rotation of the spine. The combination of the ribcage axial stiffness with the high torsional rigidity of the lumbar vertebrae would provide two strong rotational restraints at the top and bottom of the thoracic region of the spine. A rod curved like the spine in the sagittal plane is forced to rotate axially when subjected to lateral bending like in a scoliotic curve (Scholten, 1986). Therefore, in a thoracic or thoracolumbar scoliosis, the ends of the curve would be restrained against axial rotation as the lateral bending progresses. These boundary conditions of restrained axial rotation should reduce the magnitude of axial rotation along the spine caused by lateral bending of a curved rod.

The sensitivity analysis of the ribcage indicated that it is truly a complex composite structure (Section 6.3). It is composed of tissues of varied properties and orientations, and the bony and soft tissues each play a specific role under different loading conditions. Therefore, changes to the geometry of the ribcage were found to both increase and decrease the stiffness of the ribcage depending on the direction. When these changes to geometry were combined, the translational stiffnesses were found to be minimally affected by geometry compared with the rotational stiffnesses. Similarly, changes to the material properties of the cortical bone had little effect on the ribcage stiffness, whereas changes to the properties of the intercostals and costotransverse joints were far more dominant. Overall, the sensitivity analysis indicated that the ribcage stiffnesses were most affected by the gross ribcage size and the material properties of the costotransverse joints. Interestingly, changes to the geometry and properties of the costal cartilages did not have the largest effect, even though they are of relatively low modulus and occupy a large region of the ribcage. They had a dominant effect on the anterior/posterior translational stiffness as would be expected, since they are loaded about their weakest bending axis during anterior/posterior loads. However, for the other loading directions, they had less of a role. In particular, for all rotational stiffnesses, the costotransverse joints and intercostals were

found to provide the primary restraint to the nearly rigid body rotations of the ribs.

An important prediction of this study was that the stiffness of an adolescent ribcage would be reduced the most compared to an adult for axial rotation and lateral or flexion/extension bending, and least for anterior loads (Section 6.4). Again, this may be somewhat unexpected due to the larger region of costal cartilage in an adolescent. As previously stated, the costal cartilages did dominate the anterior/posterior stiffness, however, this stiffness was affected the least by the changes to the costotransverse joints which affected all the other stiffnesses to a greater extent. The costotransverse joints are best oriented to resist compressive loads between the spine and ribcage in the anterior/posterior direction. Therefore, even with a reduction of properties they were still very effective at resisting anterior/posterior loading. Consequently, the anterior/posterior stiffness of an adolescent was not reduced as greatly as the other ribcage stiffnesses compared to an adult.

The predictions of the ribcage model also suggested that the female ribcage stiffness would be reduced compared to a male (Section 6.4). This difference was primarily due to the differences in gross ribcage dimensions in a female. The smaller cross-section of the female rib also contributed to this difference, but this was somewhat mitigated by the thicker cortical walls.

The significance of these parametric analyses of the ribcage is that the support of the spine by the ribcage is complex and substantially different in an adolescent compared to an adult. Therefore, to understand the mechanics of curve progression in an adolescent, this difference in the ribcage stiffness must be recognized.

The parametric analysis of the spatial beam-column model with the incorporated ribcage stiffnesses, demonstrated the very significant effects of the initial scoliotic curve on the mechanics of progression (Section 7.2). In particular, as the initial Cobb angle was increased, the deformation of the scoliotic spine became very sensitive to changes in length and weight. For an initial Cobb angle of  $30^\circ$ , an increase in length of only 5% resulted in an increase of  $10^\circ$  in the Cobb angle. This, of course, is related to the fact that the critical load of a straight spine is related to the inverse square of the length. This

is significant because a 5% increase in spine length is not unusual during the adolescent growth spurt (Tanner, 1962; McCammon, 1970; Karlberg and Tanner, 1976). However, for a smaller initial Cobb angle of  $10^\circ$ , an increase of nearly 20% in length was needed to increase the Cobb angle by  $10^\circ$ . This indicates that the smaller initial curve is not overly vulnerable to progression due solely to rapid growth. The progression of a scoliotic curve was also most sensitive to the lateral translational stiffness of the ribcage, compared with the other directional stiffnesses. This is due to the fact that at the apex of the curve, the lateral stiffness is essentially normal to the curved spine and therefore, most effective at restraining the scoliosis.

The significance of these parametric analyses of the scoliotic spine is that for a mild scoliotic curve in a young adolescent, the changes required in the individual parameters to cause curve progression are too large to occur in a year due to growth, except possibly for an initial Cobb angle of  $30^\circ$ . Nonetheless, these results do demonstrate the different mechanics of the curved scoliotic spine compared to the straight normal spine. In a scoliotic spine, a change in any mechanical parameter due to growth must cause a change in Cobb angle. Therefore, whether these changes are sufficient to cause progression depends on the stiffness of the spine and ribcage and the sensitivity of the system at a particular stage of growth. A normal spine, on the other hand, is much more tolerant of changes due to growth since increases in weight and length do not automatically cause bending of the straight spine. Therefore, to fully understand the effect of the adolescent growth spurt on curve progression, the simultaneous changes to all the mechanical parameters of the spine must be considered.

### **8.3 Effect of Adolescent Growth on Curve Progression**

During adolescent growth, the spine length and applied body weight, as well as spinal and ribcage stiffnesses are all changing. Clearly, in the normal spine, synchronicity of these factors is maintained as the increased length and weight during growth are counteracted

by an increased spinal and ribcage stiffness. For a scoliotic spine with additional curvature and twist, there is a greater burden on the supporting stiffness to maintain stability and prevent curve progression.

A significant finding from the simulation of the adolescent growth spurt was that for a minimal scoliotic curve with an initial Cobb angle of  $10^\circ$ , then only a very small progression of the curve was predicted for both males and females with normal growth (Section 7.3.1). On the other hand, for a larger Cobb angle of  $30^\circ$ , normal growth in a female was found to lead to substantially greater progression of the curve compared to a male during their respective growth spurts. This was due to the earlier growth spurt of female adolescents combined with a more slender spine compared to males. Consequently, in females there was a greater initial increase in Cobb angle as the growth spurt began and the weight and length increased. However, even as the female growth spurt slowed down, the curve still progressed somewhat due to the now larger Cobb angle of the scoliotic curve, which was more sensitive to even relatively small increases in weight and length. In a male, on the other hand, there was an initial decrease in the Cobb angle and consequently, when the male growth spurt occurred, the spine and ribcage stiffnesses were sufficient to resist the tendency for curve progression.

Matched by chronological age during adolescence, the female spine is both longer (Taylor and Twomey, 1984) and subjected to greater body weight (Tanner, 1962; McCammon, 1970; Karlberg and Taranger, 1976) from about 11 to 13 years of age compared to a male. However, at no age during adolescence are the dimensions or cross-sectional area of the spine greater in females (Brandner, 1970; Taylor and Twomey, 1984; Schultz et al, 1984; Gilsanz et al, 1994). Therefore, even during this adolescent period of increased weight in females the vertebral bodies do not seem to get broader. As demonstrated by both Taylor and Twomey (1984) and Veldhuizen et al (1986), there is minimal horizontal growth of the female vertebrae compared to the surge in vertical height during the growth spurt. Whereas in males, during their later growth spurt, the horizontal growth of the vertebrae is greater and seems to better match the increase in height. In fact, starting as early as 5 years of age, the vertebrae of females are more slender than males (Taylor and Twomey,

1984). Though clearly the bending and torsional stiffnesses of the spine are related to many factors, the cross-sectional dimensions must have a substantial role. If the cross-sectional dimensions of the female vertebrae are consistently less than in a male, it is very unlikely that the bending stiffness of a female spine could be greater than a male. Therefore, in the female growth spurt, the increase in length of the spine and applied weight do not seem to be matched by a sufficient increase in the vertebral cross-section and therefore, bending and torsional stiffness.

The most significant finding from the simulation of the increased stature or accelerated growth observed in scoliotics was that the magnitude of the increase was sufficient to significantly alter the mechanics of the scoliotic spine (Section 7.3.2). For a young female adolescent, an increase of 4.5% in spine length lead to substantial increases in Cobb angle during the growth spurt. Again, however, in a male the same percentage increase in length lead to a much smaller increase in Cobb angle.

There appears to be interacting factors which explain these results. First, the female spine is more slender as discussed, and is already more vulnerable to progression. An initial increase of 4.5% in length further increases the slenderness of the female spine destabilizing an already sensitivity system. In a male, the increase had much less effect due to greater initial stability. The other factor is that once an increase in Cobb angle has occurred, the system becomes much more sensitive to changes in the applied weight and slenderness. And in a destabilizing loop, even though the increased stature in early adolescence is disappearing, it is still sufficient to affect the progression at later years.

These simulations of the adolescent growth spurt suggest that the changing mechanics of the spinal complex during growth could be associated with curve progression in a female. If the female is also of increased stature in early adolescence, this system is much less stable, and mechanical factors could indeed play a role in the progression observed in these individuals.

The current model predictions of the progression of a scoliotic curve would undoubtedly be reduced to a certain degree by asymmetrical muscular contractions. Therefore, the very small increase predicted during a normal adolescent growth spurt for a spine with an initial

Cobb angle of  $10^\circ$  may not occur *in vivo* and be observed clinically. The curve increases for a larger initial Cobb angle would also likely be less *in vivo*. However, these results do show that the female spine is much more vulnerable to progression during the adolescent growth spurt relative to the male. This increased potential for progression would then place a far greater burden on the supporting postural system to provide support to the spine.

Finally, this simulation of curve progression also showed the close correlation of the increase in Cobb angle with the axial rotation and lateral deflection which has been reported in the literature (Aaro and Dahlborn, 1981; De Smet et al, 1984; Stokes et al, 1987; Stokes, 1989; Drerup and Hierholzer, 1992; Kanayama et al, 1996). In particular, as the Cobb angle increased, the spinous processes of the vertebrae continued to be rotated into the concavity of the curve as observed clinically (Section 7.3.2). The mild scoliosis in the present model was implemented with an initial axial rotation of the spinous processes into the concavity of the curve. The present model cannot explain why this characteristic configuration occurs originally, however, interestingly the model predicts that the vertebrae continue to rotate in the same sense as the deformity progresses. Numerous researchers have commented on the need for a posterior tether and/or an uncoiling of the natural sagittal curvature to cause this characteristic rotation (Somerville, 1952; Deane and Duthie, 1973; Dickson et al, 1984; Jarvis et al, 1988). These features may be needed to cause the original rotation, but appear unnecessary to cause the continued rotation during progression. In the present model, posterior tether was not simulated and the sagittal curvature remained a kyphosis in the thoracic region. Therefore, it would seem that the continued rotation of the vertebrae during progression must be related to a different cause. As discussed in Sections 3.3 and 3.8, the lateral bending and axial rotation of the spine were inherently coupled due to the anterior location of the line of action of the applied body weight relative to the centre of rotation of the vertebrae. The rotation and bending were further coupled due to the initial scoliotic deformity (see equations 3.109-112). Therefore, the continued rotation of the vertebrae into the concavity of the scoliotic curve could be related to the natural coupling which occurs in a curved rod subjected to off-axis loads.

## 8.4 Comparison with Previous Work

As presented in Chapter 2, Schultz and co-authors (1971-1993) have developed a discrete model of the whole spine and ribcage to investigate the mechanics of scoliosis. The geometry, material properties and applied loads in the model were intended to be representative of an average American male (Schultz et al, 1973; Andriacchi et al. 1974; Takashima et al, 1979). The current study differs in that the spinal column and ribcage models were first developed to represent an average adult with no distinction between male and female. This validated model (Chapter 5) was then systematically changed to represent an adult male and female, and subsequently, further changed to represent an adolescent between the age of 9 years and adulthood (Sections 3.8-10 and 4.4.2). The significance of this different approach is that the current model includes the relative changes in the geometry and properties during the adolescent spurt. To extrapolate the findings of an adult model to the adolescent spine may not be correct, even in a linear model, unless care is taken. Because the weight and length, for example, do not change by the same percentages from young adolescence to adulthood, this difference must be accounted for to correctly model the adolescent spine. Therefore, the current approach of first validating an adult model, and then systematically changing this model based on published anthropometric data, should contribute to a further understanding of curve progression.

The most similar study to the present one is that of Miller and Skogland (1980c). They developed a discrete model of the isolated spinal column based on adolescent geometry. In their model, they also included the material properties determined from their experiments on an adolescent spine (Miller and Skogland, 1980a). The effect of growth was simulated by increasing the spine length 8% and the flexibility 30% in separate analyses. They concluded that both linear growth and alterations in material properties may affect the loading of the adolescent spine and should not be ruled out as being responsible for the progression of a minimal curve. The present results of the parametric analyses are in agreement with this study. In particular, in both studies, a more significant effect was found for changes in spine length compared to changes in spine stiffness. However, these authors did

not consider the effect of increased weight during growth and more importantly, did not systematically consider the effects of these simultaneous changes. Therefore, it is difficult to fully interpret their findings since to properly investigate the effects of growth, the changes to all parameters must be considered. The present study attempted to more rigorously investigate the effects of the changing mechanical factors during growth, by first validating the present model against available adult data, and then systematically investigating the adolescent growth spurt. Therefore, the present study extends the findings of these authors, and bridges the gap in the literature between this adolescent based model and the adult based model of Schultz and co-authors, in order to fully investigate the mechanics of curve progression during growth in adolescent idiopathic scoliosis.

Patwardhan et al (1986) investigated the mechanics of a progressive scoliosis with a two dimensional continuum beam-column model. They demonstrated the critical importance of the initial Cobb angle on the mechanics of progression. However, this model did not include the ribcage and could not analyze the axial rotation or the effect of sagittal curvature of the spine. This model was not rigorously validated and it was not clear if the loads and properties were representative of an adult or an adolescent. It is difficult, therefore, to compare directly their predictions for Cobb angle increase since they were dependent on the properties used in their model, which differed from the current model. The present model maintains the simplicity of this model for parametric analyses, but incorporates significant new features to better model the spine. The same conclusions regarding the effect of the initial Cobb angle were demonstrated, however, due to validation and better representation of the spine, the present results are likely to be more reliable.

## 8.5 Limitations

There are five general limitations of the present study which must be reviewed in order to reasonably assess the quality of the results. Firstly, the progression of a scoliotic curve has only been investigated from a *theoretical or modelling point-of-view*. Clearly, any findings from a model based study must ultimately be substantiated by the results of a

clinical study. Due to the natural history of AIS, very large populations must be followed, ideally in a longitudinal study, in order to provide an adequate number of progressive cases for analysis, which is a very expensive and difficult study. Equally, to explore the mechanics of curve progression with an experimental study would be extremely difficult due to the large number of adolescent specimens needed. Therefore, as outlined in Chapter 1, it was felt that the best approach was to develop a model of the spine and to rigorously validate it first against experimental data determined from adults. Subsequently, this validated model was systematically changed to represent an adolescent with a mild scoliosis based on extensive published differences of the geometry, and to a lesser extent, the differences in material properties between adolescents and adults. Most previous models used to study scoliosis have either used adult geometry and properties, or a mixture of adolescent geometry and adult properties which was still validated against adult experiments (see Section 2.2). The present modelling approach is argued to be a more systematic, and therefore, better validated approach to investigate the mechanics of the adolescent scoliotic spine (see Fig. 4.18). An analytical study also has clear advantages over a purely clinical or experimental study to test and explore the mechanics of etiologic theories. In particular, parametric analyses can establish the key or dominant factors in a complex mechanical system, which otherwise would not be evident. And the ability to simulate a process such as the adolescent growth spurt is ideally suited to models. Therefore, the development of the present model provides an efficient means to assess the present clinical observations regarding growth and curve progression in scoliosis (see Section 1.4). In the longer term, the concomitant use of the model with clinical studies should help to further understand the mechanics of a progressive curve.

Secondly, there are a number of assumptions which have been made in the development of the present model. These have been highlighted in the formulation of the specific objectives and in the chapters on model development (Chapters 3 and 4). The most significant assumption is the use of a *beam-column model to represent the spinal column*. It must be conceded that there are limitations to such a continuum model, which is used to represent a structure arguably closer to a discrete system. However, a number of features have been

included in the present model in order to improve on previous continuum models. In particular, the three-dimensionality and the inclusion of the ribcage support is felt to have greatly improved the applicability of the continuum model to the spinal column. Furthermore, in comparison with the available experimental results, the present model predictions were found to be in good agreement (Chapter 5). The present approach of including the ribcage support directly into the beam-column equations, and then reducing these higher order governing equations to a 1<sup>st</sup> order system of differential equations resulted in a very efficient model of the whole spinal structure. This was ideal for the present objectives of conducting a parametric analysis and simulating a process with many variables. In future studies, the model can be used to efficiently explore the mechanics of this spatial system and better understand the three-dimensionality of the scoliotic curve. Therefore, it is argued that the present beam-column model can adequately predict the behaviour of the mildly scoliotic spine, provided the limits of the theory are respected. The development of the equations for moderate rotations provides a range of applicability which is particularly suited to the study of a mild scoliosis. The use of the present model, however, to study the large deflections of the spine involved in a large structural scoliosis would clearly be inappropriate. Furthermore, the model is only capable of predicting the displacements of the spine and cannot predict the behaviour of the individual tissues of the spine. It is worth noting that recent measures of the three-dimensional curvature of scoliosis are based on continuous functions describing the location of the vertebrae as a spatial arc (Stokes et al, 1987; Drerup and Hierholzer, 1992; Kanayama, 1996). These curvature measures could be merged very efficiently with the present model to analyze the mechanics of more complex scoliotic deformities.

The third limitation of the present study is the *exclusion of a direct representation of the muscles and the postural control system* needed to maintain the vertical position of the spine in the model. In the formulation of the specific objectives (Section 2.3), it was argued that the development of a model, which only included the passive behaviour of the spine was not unreasonable. The actions of the muscles have only been included in the present model in terms of their gross effects on the boundary conditions. By considering the top of

the spine and the sternum of the ribcage to be fixed, this was felt to model the long term conditions present during a progressive scoliosis. The greatest concern is the exclusion of the potential muscular response to the asymmetrical conditions of a progressive scoliosis. However, in a mild scoliosis, these effects are reduced. The convex side activity of the muscles is most prominent in curves beyond 25-30° of Cobb angle (Reuber et al. 1983). The restriction of the present study to only mildly scoliotic curves is argued to minimize the potential muscular effects. However, it must be conceded that the increases in Cobb angle which have been suggested to be progressive in the present study could be mitigated *in vivo* to a certain extent. On the other hand, it is not clear exactly how significant this factor is in the long term clinical setting, since the activity of the muscles on the convex side is present in both progressive and non-progressive curves (Reuber et al. 1983). Therefore, though the magnitudes of the present predictions could be influenced by the muscular response, it is still felt that the direct comparison of the progressive tendencies due to different growth patterns and the systematic variation of parameters is not invalidated by the exclusion of muscles in the present study.

The fourth limitation of the present study is the unavailability of a *comprehensive source of data* for both the *material properties* and the *anthropometry of the adolescent spine and ribcage*. In the present study, these data have been gathered from a number of different studies (Sections 3.7-.8 and 4.4). Ideally, this anthropometric data would have been determined on a longitudinal basis following a group of adolescents over a number of years. However, to determine the internal spine dimensions, the routine x-raying of normal or scoliotic children over a number of years at sufficiently frequent intervals is not an ethically plausible solution. Possibly, the use of a non ionizing technique for imaging such as magnetic resonance may offer a solution, but still at great expense. It would also be impossible to obtain the material properties of the spine and ribcage tissues of these same individuals. And as discussed previously, it is also essentially impossible to attain a sufficiently large number of adolescent cadaveric spines for determination of material properties. Given these restraints, the present use of data from separate sources was felt to be appropriate. However, a number of precautions were taken to best ensure the

validity of the present model predictions. First, both the ribcage model and the spatial beam-column were developed with adult properties and geometry, and validated against experimental data determined from adults. This ensured that the overall spine model and the specific approach employed was valid. Second, to investigate the effect of the adolescent growth spurt on the mechanics of a scoliotic spine, the changing geometry was taken from the large number of studies which have published growth charts for various anthropometric measures of the spine and ribcage. These data were from a broad series of studies restricted to populations of Western Society. The weakest estimates were for the material properties of the adolescents. However, the overall reduction in stiffness of the ribcage and whole spine model of a young adolescent compared to an adult was in good agreement with reported increases in flexibility of the trunk (Moll and Wright, 1971), the lumbar spine (Hilton et al, 1979) and joints in general (Fairbank et al, 1984; Silman et al, 1987) for an adolescent. Therefore, it is argued that first validating the model with adult features in a consistent manner against experimental data from adults, and then systematically changing this model to represent a growing adolescent is the best approach to overcome the limitations of using data from varied sources. However, due to this average nature of the present model, care must be taken in extrapolating the results to specific populations where all the data for each of the model parameters would not be available.

The final limitation of the present study is the use of *time-independent properties*, even though most biological tissues demonstrate time-dependent behaviour of stress relaxation and creep. This time-dependent response can be represented constitutively as an inherent viscoelasticity, or as a poroelasticity with movement of a fluid relative to a solid phase of the tissue, or even by a combined approach. In the present study, only elastic properties were used because the progression of scoliosis occurs, and is even defined to have occurred, on a yearly basis. This time frame is far greater than any time constant which has been measured for biological tissue, and therefore, progression of scoliosis is a slow quasi-static phenomenon. Nonetheless, there may still be some concerns with the present model since it contains material properties which were taken from studies which were not all performed necessarily at a quasi-static rate. These studies were conducted in general over a time

frame of several minutes, however, significant stress relaxation of biological tissue can occur over the period of hours (White and Panjabi, 1990). Also, the model was validated against experimental studies which again were not performed at very slow rates. Therefore, these validated "elastic" stiffnesses may include a time-dependent stiffening, as observed in biological tissue, and be overly large. This could have two effects on the present model predictions. First, the long term ribcage resistance and bracing of a scoliotic spine may actually be less *in vivo* than in the present model. Second, if the spine stiffness was also less in the long term, then there would be a greater tendency for the scoliotic curve to progress. Further, since the present model cannot analyze or represent creep of the spine, it is possible that curve magnitudes predicted by this elastic model could become larger with creep. Therefore, the overall predictions of the present model for curve progression are likely to be conservative.

## 8.6 Clinical Significance

As discussed in Section 1.3, adolescent idiopathic scoliosis with an initial Cobb angle greater than  $10^\circ$  has a prevalence of 1-4% in an adolescent population. More importantly, however, only an unpredictable 15-25% of these mild scoliotic curves will progress to larger deformities during adolescence. Furthermore, the ratio of females to males for progressive curves can reach 10:1 for larger curves (Weinstein, 1994). A recent study suggested that if males are screened in later adolescence then the prevalence of scoliosis in boys is found to be increased (Karol et al, 1993). However, the overwhelming evidence is that severe progression occurs predominantly in females. A large number of studies (Section 1.4), have reported that scoliotics are taller than normal, particularly in early adolescence. However, it was less clear if the growth rate was abnormal, or rather just accelerated, such that at the start of adolescence, prior to the growth spurt, they were of increased stature.

The association between the adolescent growth spurt and curve progression has long been known (Willner, 1994). As stated by Lonstein (1996), "One of the most important aspects of spinal problems is growth, because it is growth that produces the progression of

spinal deformities". What remains unknown, however, is which aspect of growth is correlated with curve progression. Clearly growth is a complex process that involves multiple changes to the body. However, the adolescent growth spurt is the most dramatic change in body size after birth (Tanner, 1962). The present study therefore, attempted to determine the effect of these gross mechanical changes on the progression of a scoliotic curve.

The adolescent growth spurt is dramatically illustrated by the variable growth velocity of the standing height from birth to maturity (Fig. 8.1). The distinctly earlier spurt in females is readily evident. However, the change in height and spine length is only one component of growth. To fully understand the effect of adolescent growth on the mechanics of curve progression, it must be recognized that the spine length, body weight, spinal and ribcage stiffnesses are all changing simultaneously during growth. Furthermore, for the system to remain stable, all these parameters must remain synchronous. In Fig. 8.2, the ratio of the upper body weight to the critical buckling load (determined as a straight fixed-fixed beam-column) during the years of adolescent growth is shown for a male and female based on the data used in the current study. If this ratio exceeds one, then the column becomes unstable, whereas for values of the ratio below one, the system is theoretically stable. The ratio for the female spine is found to be significantly greater than that for a male. This indicates that the female spine has a much smaller margin of safety before the spine becomes unstable. Furthermore, this ratio changes dramatically throughout adolescence in both males and females, and is seen to peak during the years of the growth spurt (10-13 years in a female and 14-17 years in a male). Overall, a female spine appears to be about 35-50% less stable compared to a male. As discussed previously, this is partly due to the increased slenderness of the female spine. However, when considered in conjunction with the increased weight the female spine is subjected to in early adolescence during the growth spurt, the difference is even more pronounced. This simple comparison is only a component of curve progression, however, it clearly illustrates the different mechanics of the male and female spine. As argued earlier, the mechanics of a curved spine are much more complex, and to adequately predict progression, the spinal curvature as well as the ribcage stiffness must also be assessed. Nonetheless, the closer the applied weight is to the

critical load of a straight spine, the more vulnerable to progression it will be with even relatively small amounts of curvature.

Clinical studies have established a set of guidelines to evaluate the potential for progression in a scoliotic patient (Lonstein and Carlson, 1984; Weinstein, 1994; Peterson et al., 1995). The worst prognosis for serious curve progression is for a young female (9-10 years), who is skeletally immature, with a Cobb angle of at least  $20^\circ$  at diagnosis. The results of the present analysis clearly indicate that the changing mechanics of the adolescent spine during the growth spurt are likely to have a role in this prognosis. In particular, the much smaller region of safety of the female spine in early adolescence could readily explain the increased prevalence of progression in young females. Also, the significant difference in progression which was predicted by the model for an initial curve in the  $20\text{-}30^\circ$  range of Cobb angle compared with a smaller curve agrees with these clinical predictions. Therefore, the clinical guidelines for progression, where an increase of  $10^\circ$  is defined as progression for curves under  $20^\circ$ , but only an increase of  $5\text{-}6^\circ$  degrees for curves greater than  $20^\circ$ , is consistent with the mechanics of curve progression demonstrated here. Further, the current model predicts that once a patient has passed the peak of the growth spurt, there is unlikely to be a continued progression of the curve and it may even recede (Section 7.3). This suggests that mechanical factors associated with growth could explain why young and skeletally immature patients are most vulnerable to progression. As illustrated in Fig. 8.2, the spine appears to be least stable at the peak of the growth spurt, particularly in females, but also in males. Therefore, until the patient has passed the peak of their growth spurt, there appears to be an increased risk for progression due to mechanical factors. It must be noted that in the current study, all analyses have been referenced to a person's chronological age in years. However, it is recognized that the skeletal age and maturity is a much more accurate assessment of the remaining potential growth. The peak growth spurt in females was around 11-12 years of age in the present model, and would need to be shifted to understand the progression potential of a specific individual who was of greater or lesser skeletal maturity at this chronological age.

Overall, the current model predictions are found to be in excellent agreement with the

clinical findings of increased risk for curve progression in young females of slightly increased stature with an initial Cobb angle greater than  $20^{\circ}$ . This suggests that the inclusion of mechanical factors related to weight, stature and stiffness properties could improve the prediction of curve progression. Though some studies have considered mechanical factors such as spine slenderness (Schultz and Cisewski, 1979; Skogland and Miller, 1981; Lonstein and Carlson, 1984) to predict curve progression, no study appears to have considered all the combined factors of weight, stiffness and slenderness together, as well as initial Cobb angle, which more accurately characterizes the mechanical state of the spine. The development of the present model enables the analysis of the mechanics of the scoliotic spine during adolescent growth, and should contribute to the development of predictive factors which integrate mechanics with the current clinical guidelines.

Although either normal or accelerated growth is unlikely to fully explain curve progression, the mechanical effects of growth may have a role in progression if scoliosis is thought of as a two factor problem. Lonstein (1996) states, "There may actually be two mechanisms: one for the development of idiopathic scoliosis and another related to curve progression". The present study was only concerned with the progression characteristics of a curve due to mechanical changes associated with growth. The cause of the initial mild scoliosis was not considered. However, recent studies suggest subtle abnormalities in the postural control system of scoliotics could be the underlying cause of scoliosis (Willner, 1994). If this abnormality was also present in a young female adolescent of increased stature growing rapidly, it could be very vulnerable to progression. The decreased mechanical stability would place a much greater burden on the weakened postural system to maintain stability. In this way, the two factors would combine to cause curve progression during growth. On the other hand, for a person of smaller stature or later in adolescence with an increased mechanical stability, the mild scoliosis might occur due to the defect but no progression would occur as the postural system would not be unduly taxed. A person with a straight spine, though growing rapidly and of tall stature should have no difficulty maintaining stability, since the straight spine can carry a much greater load compared to a curved one with a mild scoliosis. In this two-factor progression scenario, the mechanical

effects of growth need not be abnormal, just accelerated. Therefore, the current model predictions strongly suggest that mechanical factors can explain the progression of larger scoliotic curves during adolescent growth. However, to best explain why only some scoliotic curves progress, the mechanics of growth may need to be considered as only a component of a multi-factorial disorder that causes adolescent idiopathic scoliosis.

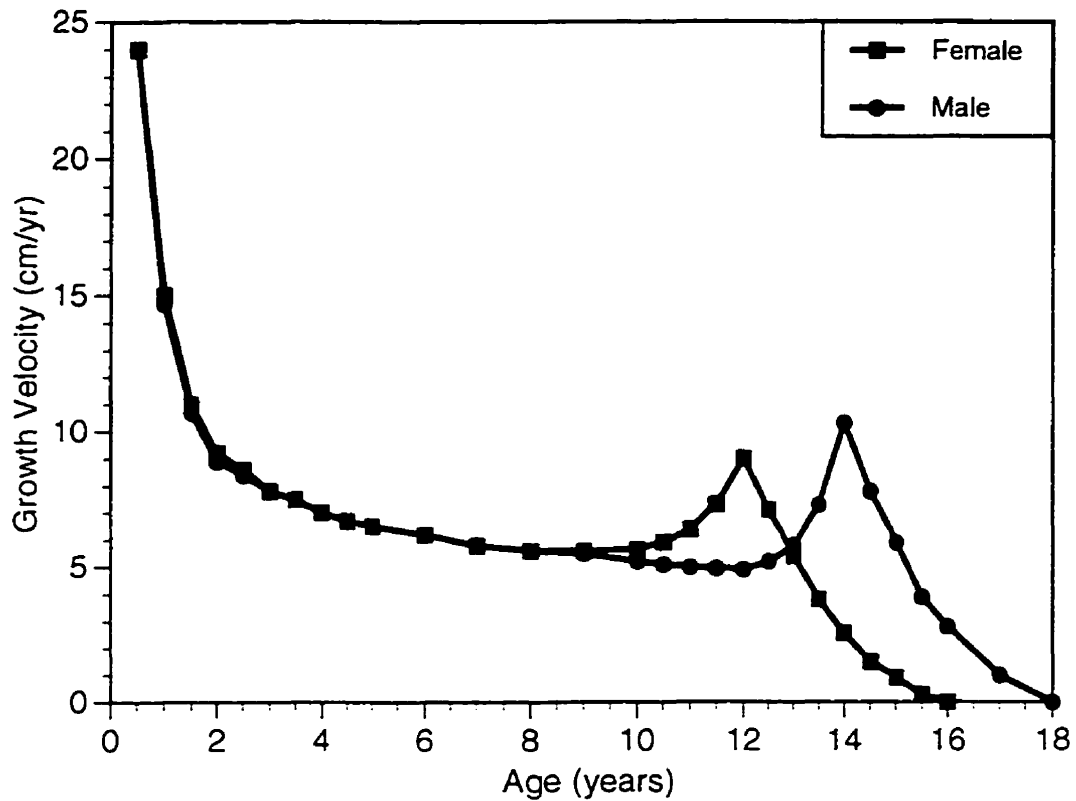


Figure 8.1: The growth velocity of standing height from birth to maturity for a female and male (Tanner et al, 1966).

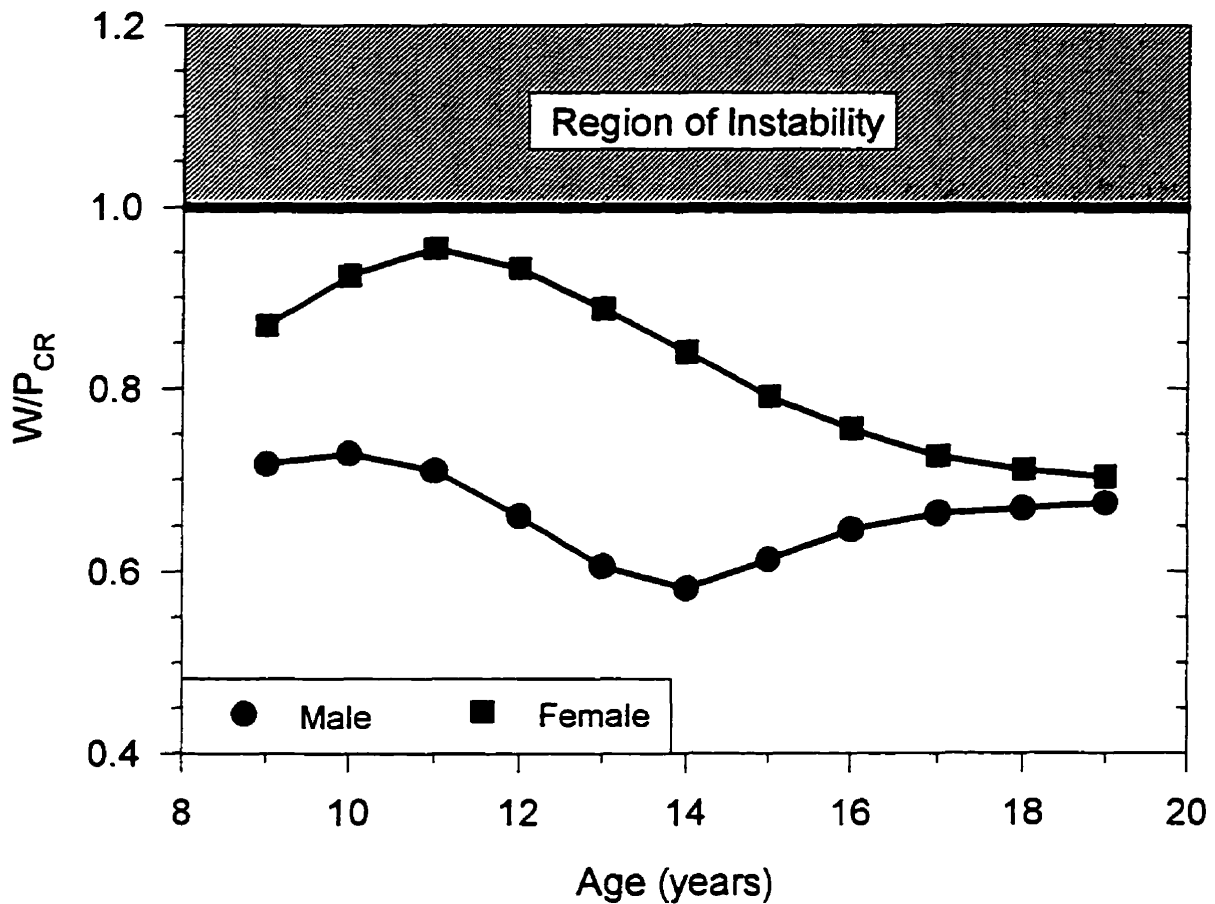


Figure 8.2: The ratio of the upper body weight to the critical load of a fixed-fixed beam-column for a male and female during adolescence. A margin of safety exists between the value of this ratio and when it equals one, which indicates an unstable system.

## 8.7 Summary and Conclusions

An initially curved and twisted, spatial beam-column model was developed as an analog for an adolescent spine with a mild scoliosis to investigate the mechanics of curve progression. The governing equations were developed for small strains and moderate rotations. The spine was embedded in a three-dimensional elastic medium to represent the ribcage. A finite element model of the ribcage was developed, and a series of numerical experiments were conducted with the model to establish the stiffness of the ribcage for incorporation into the beam-column model. Both the ribcage and spine models were validated in a consistent and systematic approach of comparing models with adult geometry

and properties, to experiments conducted on adults. A series of parametric studies were then conducted with these models to better understand the mechanics of this system. The geometry, material properties and applied loads of the spine were then changed in a systematic manner to simulate both normal and accelerated growth patterns during adolescence. These analyses were used to establish the role of mechanical factors associated with the adolescent growth spurt in the progression of a mild scoliotic curve.

On the basis of this study, the following set of conclusions was determined:

1. The three-dimensional stiffness of the ribcage varied with rib level and orientation, however, in the middle to lower ribcage the variation was least. The ribcage stiffness was greatest for anterior/posterior translation and axial rotation in the upper ribs.
2. The ribcage stiffness was most sensitive to changes in the gross ribcage geometry and the material properties of the costotransverse joints, and least sensitive to changes in the properties of the ribs. Further, the anterior stiffness was least affected, whereas the rotational stiffnesses were most affected by these changes.
3. An adolescent ribcage was considerably less stiff compared to an adult, and a male ribcage was slightly stiffer than that of a female.
4. The progression of a mild scoliosis was most sensitive to the initial Cobb angle, the spine length, the applied weight and the lateral translational stiffness of the ribcage.
5. A normal adolescent growth pattern in both females and males should not cause progression of scoliotic curves with a Cobb angle less than  $20^{\circ}$ .
6. Normal growth could lead to progression of a scoliotic curve in a female with an initial Cobb angle greater than  $20^{\circ}$  prior to the adolescent growth spurt.
7. The adolescent spine of a female compared to a male has an increased vulnerability to progression, due to its slenderness in relation to the weight carried during the adolescent years of growth, which may explain the clinical data of increased prevalence of progression in young females.

8. The mechanical changes associated with the reported increased stature in early adolescence of scoliotics could also be factors in the progression of a mild scoliosis in females, but not males.

## 8.8 Future Studies

On the basis of the current results, and the limitations surrounding them, a number of future studies are suggested:

1. To better validate models of an adolescent spine, experimental studies are needed. Even though adolescent cadaveric studies are likely never to be possible, more *in vivo* studies of the overall trunk flexibility and ribcage stiffness could reasonably be performed. The use of magnetic resonance imaging to view both the unloaded and control loaded spines of scoliotics and normals would provide tremendous data for model validation. Further, cadaveric studies of whole spines are needed. If whole spines from adults of different stature were acquired and tested, these data would help better validate both the overall model, and the predicted effect of anthropometric stature on the whole spine behaviour.
2. To extend the present model, the inclusion of muscles and in particular, a simulation of the postural control loop would be the best improvement. Deficiency of the postural control system has been suggested to be an etiologic factor in the development of a mild scoliosis. The effect of this deficiency on the mechanics of the growing spine is unknown. Possibly, the results of the present study, which suggest that clinically reported accelerated growth patterns essentially reduced the stability of the spine, would be amplified if the postural system was deficient. In this way, a progressive loop could be created, whereby a decreased spine stability due to accelerated growth placed a greater burden on the deficient postural control system, which was then unable to provide sufficient support.

3. Patwardhan et al (1986) suggested that reaching a critical bending moment in the spine was necessary for curve progression. A recent experimental study by Stokes et al (1996) provided a means to determine a value for such a moment by establishing the effect of abnormal loads on the growth of the vertebrae. If the value of a moment which disrupted vertebral growth could be established, it would be very instructive to incorporate this into the analysis of the present results. In this way, it would be possible to better assess the progression potential of scoliotic curves during growth.
4. Many other features of a scoliotic curve can be investigated efficiently with this model. A reduced sagittal curvature has been suggested as factor in the etiology of scoliosis. This could be easily analyzed with the present model to understand the interaction between the sagittal curvature, the lateral curvature and the axial rotation. The centre of gravity, and lateral offset are also likely to affect the mechanics of this system. In particular, the coupling between axial rotation and lateral curvature. In the present analysis, the top of the spine was considered fixed, but the effect of a pinned top should also be investigated. Also, the full three-dimensionality of the scoliotic curve could be analyzed using more recent measures of the 3-D curvature to better understand the mechanics of different curve patterns. The benefit of the current model is that these varied features can be analyzed very efficiently.
5. The results of this study also suggest that the changing geometry of the growing spine in scoliotics and normals would be worth measuring more accurately. An imaging technique such as magnetic resonance offers the best opportunity for such measurements. The present model approach could then be used to develop individualized models of both scoliotics and normals, which could be followed in a longitudinal clinical study. Combining models with longitudinal clinical studies offers the best chance to fully establish the role of mechanics in the progression of a curve during the adolescent growth spurt.

## STATEMENT OF ORIGINALITY

In the present work, an explicit analysis of the *mechanical influence of the adolescent growth spurt on curve progression* in idiopathic scoliosis was conducted through a *systematic* examination of a *number* of anthropometric variables related to growth. To the author's knowledge, this represents an original contribution to the study of curve progression in adolescent idiopathic scoliosis. In addition, the following points are also considered as an original contribution to knowledge:

### Spine Model Development

The present model is considered unique in these two aspects:

- The governing equations of an *initially curved* and *twisted*, spatial beam-column were developed for small strains and *moderate rotations*, to represent a spine with a mild scoliosis.
- The passive behaviour of the ribcage was modelled as a *three-dimensional elastic medium*, represented by *unique stiffness matrices* at each rib level, which were *incorporated directly* into the spatial beam-column equations governing the spine. The stiffnesses were determined through a series of *numerical experiments* conducted on a finite element model of the ribcage.

### Analysis

The following items are considered to elucidate a new understanding of curve progression:

- The adolescent spine of a female compared to a male has an increased vulnerability to curve progression, due to its *slenderness* in relation to the *weight carried* during the adolescent years of growth.
- The changes in stature which have been clinically observed in patients with AIS are of a *magnitude* to significantly alter the *mechanics* of the adolescent spine, making it more vulnerable to curve progression.

## REFERENCES

- Aaro S. and Dahlborn M. (1981) The longitudinal axis rotation of the apical vertebra, the vertebral, spinal and ribcage deformity in idiopathic scoliosis studied by computed tomography. *Spine*, 6:567-572.
- Adair I.V., van Wijk M.C. and Armstrong G.W.D. (1977) Moire topography in scoliosis screening. *Clin. Orth.*, 129:165-171.
- Adams W. (1865) *Lectures on the Pathology and Treatment of Lateral and other Forms of Curvatures of the Spine*. Churchill & Sons, London.
- Adler N., Bleck E.E., Rinsky L.A. and Young W. (1986) Balance reaction and eye-hand co-ordination in idiopathic scoliosis. *J. Orth. Res.*, 4:102-107.
- Agadir M., Sevastik B., Sevastik J., Persson A. and Isberg B. (1988) Induction of scoliosis in the growing rabbit by unilateral rib-growth stimulation. *Spine*, 9:1065-1069.
- Agostini E., Mognoni P., Torri G. and Miserocchi G. (1966) Forces deforming the ribcage. *Resp. Phys.*, 2:105-117.
- Ahl T., Albertsson-Wikland K. and Kalen R. (1988) Twenty-four hour growth hormone profiles in pubertal girls with idiopathic scoliosis. *Spine*, 13:139-142.
- Andersson M., Hwang S.C. and Green W.T. (1965) Growth of the normal trunk in boys and girls during the second decade of life. *J. Bone Jt. Surg.*, 47A:1554-1564.
- Andriacchi T.P., Schultz A.B., Belytschko T.B. and Dewald R.L. (1976) Milwaukee brace correction of idiopathic scoliosis. A biomechanical analysis and a retrospective study. *J. Bone Jt. Surg.*, 58:806-815.
- Andriacchi T., Schultz A., Belytschko T. and Galante J. (1974) A model for studies of mechanical interactions between the human spine and rib cage. *J. Biomech.*, 7:497-507.
- Archer I.A. and Dickson R.A. (1985) Stature and idiopathic scoliosis. A prospective study. *J. Bone Jt. Surg.*, 67B:185-188.
- Arkin A.M. (1950) The mechanism of rotation in combination with lateral deviation in the normal spine. *J. Bone Jt. Surg.*, 32A:180-188.
- Asher M.A., Green P. and Orvid J. (1980) A six year report on spine deformity screening in Kansas school children. *J. Kans. Med. Soc.*, 81:568-571.
- Avicenna (1595) (cited in Robin, 1990)

- Bagnall K.M., Raso V.J., Hill D.L., Moreau M., Mahmood J.K., Jiang H., Russell G., Bering M. and Buzzell G.R. (1996) Melatonin levels in idiopathic scoliosis: Diurnal and nocturnal serum melatonin levels in girls with adolescent idiopathic scoliosis. *Spine*, 21:1974-1978.
- Bailey S.J., Buckingham A. and Janzen T. (1986) Evaluation of school screening for scoliosis. *J. Bone Jt. Surg.*, 68B:855.
- Bampfield R.W. (1824) *An Essay on Curvatures and Diseases of the Spine - Including all Forms of Spinal Distortion*. Longman, Hurst, Rees, Orme, Brown and Green, London.
- Barrack R.L., Whitecloud T.S., Burrk S.W., Cook S.D. and Harding A.F. (1984) Proprioception in idiopathic scoliosis. *Spine*, 9:681-685.
- Barter J.T. (1957) Estimation of the mass of body segments. *WADC Technical Report* 57-260. Wright Patterson Air Force Base, Ohio.
- Bathe K. (1982) *Finite Element Procedures in Engineering Analysis*. Prentice-Hall, Englewood Cliffs.
- Bauchau O.A. and Hong C.H. (1987) Large displacement analysis of naturally curved and twisted composite beams. *J. AIAA*, 25:1469-1475.
- Bauchau O.A. and Hong C.H. (1988) Nonlinear composite beam theory. *J. Appl. Mech.*, 55:156-163.
- Bayer L.M. and Bayley N. (1976) *Growth Diagnosis*. 2nd Edition, University of Chicago Press, Chicago.
- Bean J.C., Chaffin D.B. and Schultz A.B. (1988) Biomechanical model calculation of muscle contraction forces: A double linear programming method. *J. Biomech.*, 21:59-66.
- Belytschko T.B., Andriacchi T.P., Schultz A.B. and Galante J.O. (1973) Analog studies of forces in the human spine: Computational techniques. *J. Biomech.*, 6:361-371.
- Belytschko T.B., Kulak R., Schultz A.B. and Galante J.O. (1974) Finite element stress analysis of an intervertebral disc. *J. Biomech.*, 7:277-285.
- Belytschko T.B., Schwer L. and Schultz A.B. (1976) A model for analytic investigation of three-dimensional head spine dynamics. AMRL-TR-76-10 Aerospace Medical Division, Wright-Patterson Air Force Base.
- Bergmark A. (1989) Stability of the lumbar spine: A study in mechanical engineering. *Acta Orth. Scand.*, 60, Suppl. 230:1-54.

- Bernhardt M. and Bridwell K.H. (1989) Segmental analysis of the sagittal plane alignment of the normal thoracic and lumbar spines and thoracolumbar junction. *Spine*, 14:717-721.
- Berry J.L., Moran J.M., Berg W.S. and Steffee A.D. (1987) A morphometric study of human lumbar and selected thoracic vertebrae. *Spine*, 12:362-367.
- Bisgard J.D. (1934) Thoracogenic scoliosis. Influence of thoracic disease and thoracic surgery on the spine. *Arch. Surg.*, 29:417-455.
- Bisgard J. and Musselman H. (1940) Scoliosis: Its experimental production and growth correction: growth and fusion of vertebral bodies. *Surg. Gynecol. Obstet.*, 70:1029-1036.
- Bjure T., Grimby G. and Nachemson S. (1968) Correction of body height in predicting spirometric values in scoliotic patients. *Scand. J. Clin. Lab. Invest.*, 21:190-192.
- Blount W.P., Schmidt A.C., Keever E.D. and Leonard E.T. (1958) The Milwaukee brace in the operative treatment of scoliosis. *J. Bone Jt. Surg.*, 40A:511-525.
- Bogduk N. and Twomey L.T. (1987) *Clinical Anatomy of the Lumbar Spine*. Churchill Livingstone, London.
- Bolotin V.V. (1963) *Nonconservative Problems of the Theory of Elastic Stability*. Pergamon Press, Oxford.
- Bradford D.S., Oegema T.R. and Brown D.M. (1977) Studies in skin fibroblasts of patients with idiopathic scoliosis. *Clin. Orth.*, 126:111-118.
- Brandner M.E. (1970) Normal values of the vertebral body and intervertebral disk index during growth. *Am. J. Roent.*, 110:618-627.
- Brooks H.L., Azen S.P., Gerberg E., Brooks R. and Chan L. (1975) Scoliosis: A prospective epidemiological study. *J. Bone Jt. Surg.*, 57A:968-972.
- Bunch W.H. and Patwardhan A.G. (1989) *Scoliosis: Making Clinical Decisions*. C.V Mosby Co., St. Louis.
- Bunnell W.P. (1988) The natural history of idiopathic scoliosis. *Clin. Orth. Rel. Res.*, 229:20-25.
- Buric M. and Momcilovic B. (1982) Growth pattern and skeletal age in school girls with idiopathic scoliosis. *Clin. Orth. Rel. Res.*, 170:238-242.
- Burwell R.G. (1971) The relationship between scoliosis and growth. "Scoliosis and Growth", ed. PA Zorab, Churchill Livingstone, Edinburgh, pp. 131-150.

- Burwell R.G., Cole A.A., Cook T.A., Grivas T.B., Kiel A.W., Moulten A., Thirwall A.S., Upadhyay S.S., Webb J.K. and Wernys- Holden S.S. (1992) Pathogenesis of idiopathic scoliosis: The Nottingham Concept. *Acta Orth. Bel.*, 58, Suppl. 1:33-58.
- Burwell R.G. and Dangerfield P.H. (1992) Pathogenesis and assessment of scoliosis. In: *Surgery of the Spine: A Combined Orthopaedic and Neurosurgical Approach*. Eds. Findlay G. and Owen R. Blackwell Scientific Publications, London, pp. 365-408.
- Burwell R.G., Dangerfield P.H. and Vernon C.C. (1977) Anthropometry and scoliosis. "Scoliosis", ed. PA Zorab, Academic Press, London, pp. 123-162.
- Butterworth T.R. Jr and James C. (1969) EMG studies in idiopathic scoliosis. *South. Med. J.*, 52:1008-1010.
- Bylund P., Jansson E., Dahlberg E. and Eriksson E. (1987) Muscle fiber types in thoracic erector spinae muscles. Fiber types in idiopathic and other forms of scoliosis. *Clin. Orth.*, 214:222-228.
- Byrd J.A. (1988) Current theories on the etiology of idiopathic scoliosis. *Clin. Orth. Rel. Res.*, 229:114-119.
- Calvo I.J. (1957) Observations on the growth of the female adolescent spine and its relation to scoliosis. *Clin. Orth.*, 10:40-46.
- Cameron N. (1993) Assessment of growth and maturation during adolescence. *Horm. Res.*, 39 (Suppl 3):9-17.
- Carey E.J. (1932) Scoliosis: etiology, pathogenesis and prevention of experimental rotatory lateral curvature of the spine. *J. Amer. Med. Ass.*, 98:104-110.
- Carr A.J., Jefferson R.J., Weisz I. and Turner-Smith A.R. (1989) Correction of body height in scoliotic patients using ISIS scanning. *Spine*, 14:220-222.
- Carr A.J., Jefferson R.J., Turner Smith A.R., Weisz I., Thomas D.G., Stavarakis T. and Houghton G.R. (1989a) Surface stereophotogrammetry of thoracic kyphosis. *Acta Orth. Scand.*, 60:177-180.
- Carr A.J., Jefferson R.J. and Turner-Smith A.R. (1991) Familial back shape in adolescent scoliosis. A photogrammetric population study. *Acta Orthop. Scand.*, 62:131-135.
- Carr A.J., Jefferson R.J. and Turner-Smith A.R. (1993) Family stature in idiopathic scoliosis. *Spine*, 18:20-23.
- Carter D.R. and Spengler D.M. (1978) Mechanical properties and composition of cortical bone. *Clin. Orth. & Rel. Res.*, 135:192-217.
- Chen W. and Atsuta T. (1977) *Theory of Beam-Columns. Vol. 2: Space Behaviour and Design*, McGraw-Hill, New York.

- Chimich D., Shrive N., Frank C., Marchuk L. and Bray B. (1992) Water content alters viscoelastic behaviour of the normal adolescent rabbit medial collateral ligament. *J. Biomech.*, 25:831-837.
- Clark S. (1977) Longitudinal growth studies in normal and scoliotic children. "Scoliosis". ed. PA Zorab. Academic Press, London. pp. 165-180.
- Clauser C.E., McConville J.T. and Young J.W. (1969) Weight, volume and center of mass of segments of the human body. *AMRL Technical Report 69-70*. Wright Patterson Air Force Base, Ohio.
- Closkey R.F. and Schultz A.B. (1993) Ribcage deformities in scoliosis: Spine morphology, ribcage stiffness and tomographic imaging. *J. Orthop. Res.*, 11:730-737.
- Closkey R.F., Schultz A.B. and Luchies C.W. (1992) A model for studies of the deformable rib cage. *J. Biomech.*, 25:529-539.
- Cobb J.R. (1948) Outline for the study of scoliosis. *AAOS Instr. Course Lect.*, 5:261.
- Cohen H. (1966) A nonlinear theory of elastic directed curves. *Int. J. Eng. Sci.*, 4:511-524.
- Cohen H. and Sun Q.X. (1992) A further work on directed rods. *J. Elasticity*, 28:123-142.
- Connor J.J. (1976) *Analysis of Structural Member Systems*. Ronald Press Co., New York.
- Cook R.D. (1981) *Concepts and Applications of Finite Element Analysis*. 2nd Ed. John Wiley & Sons, New York.
- Cossette J.W., Farfan H.F., Robertson G.H. and Wells R.V. (1971) The instantaneous center of rotation of the third lumbar intervertebral joint. *J. Biomech.*, 4:149-156.
- Cotrel Y. (1970) Le corset de plâtre EDF dans la traitement de la scoliose idiopathique. *Med. Hyg.*, 28:1032-1040.
- Cotrel Y. and Dubousset J. (1984) Nouvelle technique d'osteosynthese rachidienne segmentaire par voie posterieure. *Rev. Chir. Orth.*, 70:489-495.
- Cotterhill P.C., Kostuik J.P., D'Angelo G., Ferrie G.R. and Maki B.E. (1986) An anatomical comparison of the human and bovine thoracolumbar spine. *J. Orthop. Res.*, 4:298-303.
- Cramer H.J., Liu K.Y. and von Rosenberg D.U. (1976) A distributed parameter model of the inertially loaded human spine. *J. Biomech.*, 9:115-130.
- Crisco J.J. and Panjabi M.M. (1992) Euler stability of the human ligamentous lumbar spine. Part I: Theory. *Clin. Biomech.*, 7:19-26.

- Crisco J.J., Panjabi M.M., Yamamoto I. and Oxland T.R. (1992) Euler stability of the human ligamentous lumbar spine. Part II: Experiment. *Clin. Biomech.*, 7:27-32.
- Currey J.D. and Butler G. (1975) The mechanical properties of bone tissue in children. *J. Bone Jt. Surg.*, 57A:810-814.
- Currey J.D. (1988) The effect of porosity and mineral content on the Young's modulus of elasticity of compact bone. *J. Biomech.*, 12:131-139.
- Dai Q.G. and Liu K.Y. (1992) Failure analysis of a beam-column under oblique-eccentric loading: Potential failure surfaces for cervical spine trauma. *J. Biomech. Eng.*, 114:119-128.
- Dansereau J. and Stokes I.A.F. (1988) Measurements of the three dimensional shape of the ribcage. *J. Biomech.*, 21:893-901.
- Davenport C.B. (1934) The thoracic index. *Human Biology*, 6:1-23.
- Davis P.R. and Troup J.D.G. (1966) Human thoracic diameters at rest and during activity. *J. Anat.*, 100:397-410.
- De Smet A.A., Asher M.A., Cook L.T., Goin J.E., Sheuch H.G. and Orrick J.M. (1984) Three-dimensional analysis of right thoracic idiopathic scoliosis. *Spine*, 9:377-381.
- Deane G. and Duthie R.B. (1973) A new projectional look at articulated scoliotic spines. *Acta Orth. Scand.*, 44:351-365.
- Deng Y.C. and Goldsmith W. (1987) Response of a human head/neck/upper-torso replica to dynamic loading. II. Analytical/numerical model. *J. Biomech.*, 20:487-497.
- Dickson R.A. (1983) Scoliosis in the community. *Brit. Med. J.*, 286:615-618.
- Dickson R.A. and Archer I.A. (1984) Scoliosis in the community. "Management of Spinal Deformities", eds. Dickson RA & Bradford DS. Butterworth, London: pp. 77-100.
- Dickson R.A., Lawton J.O., Archer I.A. and Butt W.P. (1984) The pathogenesis of idiopathic scoliosis. Biplanar spinal asymmetry. *J. Bone Jt. Surg.*, 66B:8-15.
- Dickson R.A. and Sevitt E.A. (1982) Growth and idiopathic scoliosis: A longitudinal cohort study. *J. Bone Jt. Surg.*, 64B:385.
- Dietrich M., Kedzior K. and Zagrajek T. (1991) A biomechanical model of the human spinal system. *J. Eng. Med.*, 205-H1:19-26.
- Drerup B. and Hierholzer E. (1992) Evaluation of frontal radiographs of scoliotic spines - Part II. Relations between lateral deviation, lateral tilt and axial rotation of vertebrae. *J. Biomech.*, 25:1443-1450.

- Drummond D.S. and Rogala E.J. (1980) Growth and maturation of adolescents with idiopathic scoliosis. *Spine*, 5:507-511.
- Dubousset J. (1994) Three dimensional analysis of the scoliotic deformity. Chapter 22. In: *The Pediatric Spine: Principles and Practice*, Ed. Weinstein S.L., Raven Press, New York.
- Durning R.P., Scoles P.V. and Fox O.D. (1980) Scoliosis after thoracotomy in tracheo-oesophageal fistula patients. *J. Bone Jt. Surg.* 62A:1156-1169.
- Duthie R.B. (1959) The significance of growth in orthopaedic surgery. *Clin. Orth.* 14:7-19.
- Duval-Beaupere G. (1971) Pathogenic relationship between scoliosis and growth. In: Zorab P.A. (ed): *Scoliosis and Growth*. Proceedings of a Third Symposium held at the Institute of Diseases of the Chest. Churchill Livingstone, Edinburgh, London, p. 58.
- Enneking W.G. and Harrington P. (1969) Pathological changes in scoliosis. *J. Bone Jt. Surg.*, 51A:165-184.
- Ericksen J.L. and Truesdell C. (1958) Exact theory of stress and strain in rods and shells. *Arch. Rat. Mech. Anal.*, 1:295-323.
- Eveleth P.B. and Tanner J.M. (1976) *Worldwide Variation in Human Growth*. Cambridge University Press, Cambridge.
- Fairbank J.C.T., Pynsent P.B. and Phillips H. (1984) Quantitative measurements of joint mobility in adolescents. *Ann. Rheum. Dis.*, 43:288-294.
- Feik S.A. and Storey E. (1983) Remodeling of bone and bones: growth of normal and abnormal transplanted caudal vertebrae. *J. Anat.*, 136:1-14.
- Feiss H.O. (1907) Mechanics of lateral curvature. Part II: Demonstration of models to illustrate the mechanical tendencies of posture in the normal. *Am. J. Orth. Surg.*, 4:323-339.
- Fisher R.L. and DeGeorge F.V. (1967) A twin study of idiopathic scoliosis. *Clin. Orth.*, 55:117-126.
- Fon G.T., Pitt M.J. and Thies A.C. (1980) Thoracic kyphosis: range in normal subjects. *Am. J. Radiol.* 134:979-983.
- Ford D.M., Bagnall K.M., McFadden K.D., Greenhill B.J. and Raso V.J. (1984) Paraspinal muscle imbalance in adolescent idiopathic scoliosis. *Spine*, 9:373-376.
- Galante (1967) Tensile properties of the human annulus fibrosus. *Acta. Orth. Scand.*, Suppl. 100.

- Garland H.G. (1934) Hereditary scoliosis. *Brit. Med. J.*, i:328.
- Geusens P., Cantatore F., Nijs J., Proesmans W., Emma F. and Dequeker J. (1991) Heterogeneity of growth of bone in children at the spine, radius and total skeleton. *Growth, Develop. and Aging*, 55:249-256.
- Ghista D.N., Viviani G.R., Subbaraj K., Lozada P.F., Srinivasan and Barnes G. (1988) Biomechanical basis of optimal scoliosis surgical correction. *J. Biomech.*, 21:77-88.
- Gilad I. and Nissan M. (1985) Sagittal evaluation of elemental geometrical dimensions of human vertebrae. *J. Anat.*, 143:115-120.
- Gilsanz V., Boechat M.I., Gilsanz R., Loro M.L., Roet F. and Goodman W.G. (1994a) Gender differences in vertebral sizes in adults: Biomechanical implications. *Radiology*, 190:678-682.
- Gilsanz V., Boechat M.I., Roe T.F., Loro M.L., Sayre J.W. and Goodman W.G. (1994) Gender differences in vertebral body sizes in children and adolescents. *Radiology*, 190:673-677.
- Gilsanz V., Gibbens D.T., Roe T.F., Carlson M., Senac M.O., Boechat M.I., Huang H.K., Schultz E.E., Libanati C.R., and Cann C.C. (1988) Vertebral bone density in children: Effect of puberty. *Radiology*, 166:847-850.
- Glisson F. (1672) *De Rachidite sine Morbo Puerilli*. London. (Cited in Robin, 1990).
- Goel V.K., Kim Y.E., Lim T.H. and Weinstein J.N. (1988) An analytical investigation of the mechanics of spinal instrumentation. *Spine*, 13:1003-1011.
- Goel V.K. and Weinstein J.N. (1990) *Biomechanics of the Spine: Clinical and Surgical Perspective*. CRC Press, Boca Raton.
- Goldberg C.J., Dowling F.E. and Fogarty E.E. (1993) Adolescent idiopathic scoliosis - early menarche, normal growth. *Spine*, 18:529-535.
- Goldstein L.A. and Waugh T.R. (1973) Classification and terminology of scoliosis. *Clin. Orth. Rel. Res.*, 93:10-22.
- Gooding C.A. and Neuhauser E.B.D. (1965) Growth and development of the vertebral body in the presence and absence of normal stress. *Am. J. Roentgenol.*, 93:338-394.
- Granik G. and Stein I. (1973) Human ribs: Static testing as a promising medical application. *J. Biomech.*, 6:237-240.
- Grant J.C.B. (1978) *Grant's Atlas of Anatomy*. Ed.: Anderson J.E. 7<sup>th</sup> edition. Williams and Wilkins Co., Baltimore.
- Gray H. (1989) *Gray's Anatomy*. Ed.: Williams P.L., Warwick R., Dyson M., Bannister L. 37<sup>th</sup> edition. Churchill Livingstone, London.

- Green A.E. and Laws N. (1966) A general theory of rods. *Proceed. Royal Soc., A*-293:145-155.
- Green A.E. and Laws N. (1973) Remarks on the theory of rods. *J. Elasticity*, 3:179-184.
- Gregerson G.G. and Lucas D.B. (1967) An in vivo study of the axial rotation of the human thoracolumbar spine. *J. Bone Jt. Surg.*, 49:247-263.
- Gregoric M., Pecak F., Trontelj L.J. and Dimitrijevic M.R. (1981) Posture control in scoliosis. A statokinesimetric study in patients with scoliosis due to neuromuscular disorders and in patients with idiopathic scoliosis. *Acta Orth. Scand.*, 52:59-63.
- Grivas T.B., Burwell R.G., Purdue M., Webb J.K. and Moulten A. (1991) A segmental analysis of thoracic shape in chest radiographs of children. Changes related to spinal level, age, sex, side and significance for lung growth and scoliosis. *J. Anat.*, 178, 21-38.
- Gross C., Graham J., Neuwirth M. and Pugh J. (1983a) Scoliosis and growth: an analysis of the literature. *Clin. Orth.*, 175: 243-250.
- Gross C., Gross M. and Alexander D. (1983b) Scoliotic spinal anthropometry. *Bull. Hosp. Jt. Dis.*, 43, 84-91.
- Haas S.L. (1939) Experimental production of scoliosis. *J. Bone Jt. Surg.*, 21: 963-968.
- Haderspeck K and Schultz A. (1981) Progression of idiopathic scoliosis: analysis of muscle actions and body weight influences. *Spine*, 6: 447-455.
- Hadley N.A., Ponsetti I.V., Solursh M. (1991) Ligamentous elastic fiber pathology in adolescent idiopathic scoliosis. *Transactions of the 37th ORS*, p. 616.
- Hagglund G., Karlberg J. and Willner S. (1992) Growth in girls with adolescent idiopathic scoliosis. *Spine*, 17: 108-111.
- Halsall A.P. (1980) A study of human spine flexibility with respect to scoliosis surgery. *Masters Thesis*, University of Toronto.
- Halsall A.P., James D.F., Kostuik J.P. and Fernie G.R. (1983) An experimental evaluation of spinal flexibility with respect to scoliosis surgery. *Spine*, 8:482-488.
- Harrington P.R. (1962) Treatment of scoliosis: correction and internal fixation of spine instrumentation. *J. Bone Jt. Surg.*, 44A:591-610.
- Hazebroek-Kampschreur A.A.J.M., Hofman A., van Dijk A.P. and van Linge B. (1994) Determinants of trunk abnormalities in adolescence. *Int. J. Epidemiol.*, 23:1242-1247.
- Hess J.L. and Lombard C.F. (1958) Theoretical investigations of dynamic response of man to high vertical acceleration. *J. Aviat. Med.*, 29, 66-74.

- Herman R., Mixon J., Fisher A., Maulucci R. and Stuyck J. (1985) Idiopathic scoliosis and the central nervous system: A motor control problem. The Harrington Lecture, 1983 Scoliosis Research Society. *Spine*, 10:1-14.
- Hibbs R.H. (1917) The treatment of deformities of the spine caused by poliomyelitis. A report of 8 cases in which operation was performed. *J. Am. Med. Ass.*, 69:787-791.
- Hilton R.C., Ball J. and Benn J.T. (1979) In-vitro mobility of the lumbar spine. *Ann. Rheum. Dis.*, 38:378-383.
- Hjalmars S. (1981) A continuum model of the human spine as an anisotropic beam. *Proceed. of the 4th Conference on Continuum Models of Discrete Systems*, North-Holland Pub. Co., Stockholm.
- Hjalmars S. (1988) A beam model of the human spine under muscular action. *J. Tech. Phys.*, 29:43-49.
- Hodges D.H. (1985) Nonlinear equations for dynamics of pretwisted beams undergoing small strains and large rotations. *NASA TP-2470*.
- Hodges D.H. (1987) Nonlinear beam kinematics for small strains and finite rotations. *Vertica*, 11:573-589.
- Hodges D.H. and Dowell E.H. (1975) Nonlinear equations of motion for the elastic bending and torsion of twisted nonuniform rotor blades. *NASA TN D-7818*.
- Hodges D.H. and Ormiston R.A. (1980) On the nonlinear deformation geometry of Euler-Bernoulli beams. *NASA TP-1566*.
- Houbolt J.C. and Brooks G.W. (1958) Differential equations of motion for combined flapwise bending, chordwise bending and torsion of twisted nonuniform rotor blades. *NACA Report 1346*.
- Howatt W.F. and DeMuth G.R. (1965) Configuration of the chest. *Pediatrics*, 35:177-184.
- Huber G.C. (1930) *Piersol's Human Anatomy: Including Structure and Development and Practical Considerations*. 9<sup>th</sup> edition, J.B. Lippincott Co., Philadelphia.
- James J.I.P. (1967) *Scoliosis*. Livingstone, Edinburgh.
- Jarvis J.G., Ashman R.B., Johnston C.E. and Herring J.A. (1988) The posterior tether in scoliosis. *Clin. Orth. Rel. Res.*, 227:126-134.
- Jayaraman G., Zbib H.M. and Jacobs R.R. (1989) Biomechanical analyses of surgical correction techniques in idiopathic scoliosis: Significance of bi-planar characteristics of scoliotic spines. *J. Biomech.*, 22:427-437.

- Jordanoglou J. (1970) Vector analysis of rib movement. *Resp. Physio.*, 10:109-120.
- Kanayama M., Tadano S., Kaneda K., Ukai T. and Abumi K. (1996) A mathematical expression of three dimensional configuration of the scoliotic spine. *J. Biomech. Eng.*, 118:247-252.
- Kaneko T. (1968) Histopathologic-histochemical studies on back muscles in scoliosis. *J. Jap. Orth. Ass.*, 42:13-28.
- Karaharju E.O. (1967) Deformation of vertebra in experimental scoliosis. *Acta Orth. Scand. (Supp.)*, 105.
- Karlberg P. and Taranger J. (1976) The somatic development of children in a Swedish urban community. *Acta Ped. Scand.*, Suppl. 258.
- Karol L.A., Johnston C.E., Browne R.H. and Madison M. (1993) Progression of the curve in boys who have idiopathic scoliosis. *J. Bone Jt. Surg.*, 75A:1804-1810.
- Katzman D.K., Bachrach L.K., Carter D.R. and Marcus R. (1991) Clinical and anthropometric correlates of bone mineral acquisition in healthy adolescent girls. *J. Clin. Endocrinol. Metab.*, 73:1332-1339.
- Kawata S. (1976) Experimental scoliosis produced by stereotoxic destruction of posterior part of the hypothalamus in bipedal rats. *Shikoku Acta Med.*, 32:125.
- Keaveny T.M. and Hayes W.C. (1993) Mechanical properties of cortical and trabecular bone. Chapter 10, In: *Bone*, Ed. Hall B.K., CRC Press, Boca Raton.
- Keifer A., Shirazi-Adl A. and Parianpour M. (1994) On the equilibrium positions of the human spine in neutral posture. *ASME BED*, 28:87-88.
- Keifer A., Shirazi-Adl A. and Parianpour M. (1995) Stabilizing mechanisms of human spine in neutral postures. *ASME BED*, 31:85-86.
- Keim H.A. and Hensinger R.N. (1989) Spinal deformities: scoliosis and kyphosis. *Clinical Symposia*, 41:1-32.
- Keeson W., Crowe A. and Hearn M. (1992) Proprioceptive accuracy in idiopathic scoliosis. *Spine*, 17:149-155.
- Kenyon C.M., Pedley T.J. and Higenbottam T.W. (1991) Adaptive modelling of the human ribcage in median sternotomy. *J. Appl. Physiol.*, 70:2287-2302.
- Koenig H.A. and Bolle N.A. (1993) Non-linear formulation for elastic rods in three-space. *Int. J. Non-Linear Mech.*, 28:329-335.
- Kojima T. and Kurokawa T. (1992) Quantitation of three-dimensional deformity of idiopathic scoliosis. *Spine*, 17:S22-S29.

- Kulak R.F., Belytschko T.B. and Schultz A.B. (1976) Nonlinear behaviour of the human intervertebral disc under axial load. *J. Biomech.*, 9:301-317.
- Laible J.P., Pflaster D.S., Krag M.H., Simon B.R. and Haugh L.D. (1993) A poroelastic - swelling finite element model with application to the intervertebral disc. *Spine*, 18:659-669.
- Laible J.P., Pflaster D.S., Simon B.R., Krag M.H., Pope M. and Haugh L.D. (1994) A dynamic material parameter estimation procedure for soft tissue using a poroelastic finite element model. *J. Biomech. Eng.*, 116:19-29.
- Lam T.C., Frank C.B. and Shrive N.G. (1993) Changes in the cyclic and static relaxations of the rabbit medial collateral ligament complex during maturation. *J. Biomech.*, 26:9-17.
- Langenskiold A. and Michelsson J.E. (1961) Experimental progressive scoliosis in the rabbit. *J. Bone Jt. Surg.*, 43B:116-120.
- Langenskiold A. and Michelsson J. (1962) The pathogenesis of experimental progressive scoliosis. *Acta Orthop. Scand. (Suppl)*, 59:1-26.
- Latham F. (1957) A study in body ballistics: Seat ejection. *Proceed. Royal Soc.*, B-147:121.
- Lavaste F., Skalli W., Robin S., Roy-Camille R. and Mazel C. (1992) Three-dimensional geometrical and mechanical modelling of the lumbar spine. *J. Biomech.*, 26:1153-1164.
- Leatherman K.D. and Dickson R.A. (1988) *The Management of Spinal Deformities*. Wright, London.
- LeFebvre J., Triboulet-Chessenant A. and Missirlui M.F. (1961) Electromyographic data in idiopathic scoliosis. *Arch. Phys. Med.*, 42:710-711.
- Lemmers L.G., Sanders M.M., Cool J.C. and Grootenboer H.J. (1991) The cause of axial rotation of the scoliotic spine. *Clin. Biomech.*, 6:179-184.
- Leong J.C.Y., Low W.D., Mok C.K., Kung L.S. and Yau A.C.M.C. (1982) Linear growth in Southern Chinese female patients with adolescent idiopathic scoliosis. *Spine*, 7:471-475.
- Lin H.S., Liu Y.K., Ray G. and Nikravesh P. (1978) Systems identification for material properties of the intervertebral joint. *J. Biomech.*, 11:1-14.
- Lindahl O. and Raeder E. (1962) Mechanical analysis of forces involved in idiopathic scoliosis. *Acta Orth. Scand.*, 32:27-38.

- Lindbeck L. (1985) Analysis of functional scoliosis by means of an anisotropic beam model of the human spine. *J. Biomech.*, 107:281-285.
- Lindbeck L. (1987) Analysis of the asymmetrically loaded spine by means of a continuum beam model. *J. Biomech.*, 20:753-765.
- Lindbeck L. (1988) Anthropometric and biomechanical characteristics of the spine. *J. of Tech. Phys.*, 29:1.
- Liu K.Y. and Dai G. (1989) The second stiffest axis of a beam-column: Implications for cervical spine trauma. *J. Biomech. Eng.*, 111:122-127.
- Loncar-Dusek M., Pencina M. and Prebeg Z. (1991) A longitudinal study of growth velocity and development of secondary gender characteristics versus onset of idiopathic scoliosis. *Clin. Orth. Rel. Res.*, 270:278-282.
- Lonstein J.E. (1996) *Lovell and Winter's Pediatric Orthopaedics*, Chapter 17. Eds. Morrissy R.T. and Weinstein S.L.. Lippincott-Raven, Philadelphia.
- Lonstein J., Bjorklund S., Wanninger M. and Nelson R. (1982) Voluntary school screening for scoliosis in Minnesota. *J. Bone Jt. Surg.*, 64A:481-487.
- Lonstein J.E. and Carlson J.M. (1984) The prediction of curve progression in untreated idiopathic scoliosis during growth. *J. Bone Jt. Surg.*, 66A:1067-1071.
- Lonstein J.E. and Winter R.B. (1994) The Milwaukee brace for the treatment of adolescent idiopathic scoliosis. *J. Bone Jt. Surg.*, 76A:1207-1221.
- Loring S.H. (1992) Action of human respiratory muscles inferred from finite element analysis of ribcage. *J. Appl. Physiol.*, 72:1461-1465.
- Lowrey G.H. (1978) *Growth and Development of Children*. Year Book Medical Publishers, Chicago.
- Love A.E.H. (1926) *A Treatise on the Mathematical Theory of Elasticity*. University Press, Cambridge.
- Lovett R.W. (1905) The mechanism of the normal spine and its relation to scoliosis. *Bost. Med. Surg. J.*, 153:349-358.
- Lovett R.W. (1916) *Lateral Curvature of the Spine and Round Shoulders*. 3rd edit. Blakiston, Philadelphia.
- Low W.D., Mok C.K., Leong J.C.Y., Yau A.C.M.C and Lisowski F.P. (1978) The development of Southern Chinese girls with adolescent idiopathic scoliosis. *Spine*, 3:152-156.
- Loynes R.D. (1972) Scoliosis after thoracoplasty. *J. Bone Jt. Surg.*, 54B:484-498.
- Lucas D.B. (1970) Mechanics of the spine. *Bull. Hosp. J. Diseases*, 31:115-131.

- Lucas D.B. and Bresler B. (1961) Stability of the ligamentous spine. *Tech. Report 40*, Biomech. Lab., UCSF.
- Luo Z. and Goldsmith W. (1991) Reaction of a human head/neck/torso system to shock. *J. Biomech.*, 24:499-510.
- Luque E.R. (1982) Segmental spine instrumentation for correction of scoliosis. *Clin. Orth.*, 163:192-198.
- Machida M., Dubousset J., Imanura Y., Iwaya T., Yamada T. and Kimura J. (1993) An experimental study in chickens for the pathogenesis of idiopathic scoliosis. *Spine*, 18:1609-1615.
- MacLaughlin S.M. and Oldale K.N.M. (1992) Vertebral body diameters and sex prediction. *Annals of Hum. Biol.*, 19:285-292.
- Malina R.M. (1975) *Growth and Development - The First Twenty Years in Man*. Burgess Publishing Co., Minneapolis.
- Mattson G.K., Haderspeck-Grib K., Schultz A. and Nachemson A. (1983) Joint flexibilities in structurally normal girls and girls with idiopathic scoliosis. *J. Orth.*, 1:57-62.
- McCummon R.W. (1970) *Human Growth and Development*. Charles C. Thomas Publisher. Springfield.
- McGill S.M. (1992) A myoelectrically based dynamic three-dimensional model to predict loads on lumbar spine tissues during lateral bending. *J. Biomech.*, 25:395-414.
- McGill S.M. and Norman R.W. (1986) Partitioning of the L4-L5 dynamic moment into disc, ligamentous, and muscular components during lifting. *Spine*, 11:666-678.
- McKenzie J.A. and Williams J.F. (1971) The dynamic behaviour of the head and cervical spine during whiplash. *J. Biomech.*, 4:477-490.
- Meade K.P., Bunch W.H., Vanderby R., Patwardhan A.G. and Knight G.W. (1987) Progression of unsupported curves in adolescent idiopathic scoliosis. *Spine*, 12:520-526.
- Mehta M. (1972) The rib-vertebra angle in the early diagnosis between resolving and progressive infantile scoliosis. *J. Bone Jt. Surg.*, 54B:230-243.
- Mellin G., Harkonen H. and Poussa M. (1988) Spinal mobility and posture and their correlations with growth velocity in structurally normal boys and girls aged 13 to 14. *Spine*, 13:152-154.
- Mellin G. and Poussa M. (1992) Spinal mobility and posture in 8 to 16 year old children. *J. Orth. Res.*, 10:211-216.

- Michelsson J. (1965) The development of spinal deformity in experimental scoliosis. *Acta Orthop. Scand. (Suppl)*, 81:1-91.
- Miller J.A.A., Nachemson A.L. and Schultz A.B. (1984) Effectiveness of braces in mild idiopathic scoliosis. *Spine*, 9:632-635.
- Miller J.A.A. and Skogland L.B. (1980a) On the load-displacement behaviour of adolescent spinal motion segments. An experimental study using autopsy specimens. Chapter IV. In: On the importance of growth in idiopathic scoliosis: A biochemical, radiological and biomechanical study. *Ph.D. Thesis*, University of Oslo.
- Miller J.A.A. and Skogland L.B. (1980b) The relation of specimen geometry, disc hydration and annulus collagen fibre orientation to motion segment flexibility in the adolescent spine. Chapter V. In: On the importance of growth in idiopathic scoliosis: A biochemical, radiological and biomechanical study. *Ph.D. Thesis*, University of Oslo.
- Miller J.A.A. and Skogland L.B. (1980c) Musculoskeletal interactions in the adolescent spine. A study of the effect of some geometric and material property changes in a three-dimensional mathematical model. Chapter VI. In: On the importance of growth in idiopathic scoliosis: A biochemical, radiological and biomechanical study. *Ph.D. Thesis*, University of Oslo.
- Misol S., Ponseti I.V., Samaan N. and Bradbury J.T. (1971) Growth hormone blood levels in patients with idiopathic scoliosis. *Clin. Orth.*, 81:122-125.
- Moll J.M.H. and Wright V. (1971) Normal range of spine mobility: An objective clinical study. *Ann. Rheum. Dis.*, 30:381-386.
- Mora S., Goodman W.G., Loro M.L., Roe T.F., Sayre J. and Gilsanz V. (1994) Age related changes in cortical and cancellous vertebral bone density in girls. *Am. J. Roent.*, 162:405-409.
- Nachemson A.L. and Sahlstrand T. (1977) Etiologic factors in adolescent idiopathic scoliosis. *Spine*, 2:176-184.
- Nachemson A.L., Schultz A.B. and Berkson M.H. (1979) Mechanical properties of human lumbar spine motion segments - influences of age, sex, disc level and degeneration. *Spine*, 4:1-8.
- Naghdi P.M. and Rubin M.B. (1984) Constrained theories of rods. *J. Elasticity*, 14:343-361.
- Nahum A.M., Gadd C.W., Schneider D.C. and Kroell C.K. (1971) The biomechanical basis for chest impact protection: Force-deflection characteristics of the thorax. *J. Trauma*, 11:874-882.

- Nicolopoulos K.S., Burwell R.G. and Webb J.K. (1985a) Stature and its components in adolescent idiopathic scoliosis. Cephalo-caudal disproportion in the trunk of girls. *J. Bone Jt. Surg.*, 67B:594-601.
- Nicolopoulos K.S., Burwell R.G. and Webb J.K. (1985b) Stature and its components in healthy children, sexual dimorphism and age related changes. *J. Anat.*, 141:105-114.
- Nissinen M., Heliovaara M., Seitsamo J. and Poussa M. (1993) Trunk asymmetry, posture, growth and risk of scoliosis. A three-year follow-up of Finnish prepubertal school children. *Spine*, 18:8-13.
- Noone G., Mazumdar J. and Ghista D. (1991) Continuous model of the human scoliotic spine. *J. Biomed. Eng.*, 13:473-80.
- Nordwall A. (1973) Studies in idiopathic scoliosis. *Acta Orth. Scand.* (Suppl.), 150.
- Nordwall A. and Willner S. (1975) A study of skeletal age and height in girls with idiopathic scoliosis. *Clin. Orth. Rel. Res.*, 110:6-10.
- Normelli H., Sevastik J. and Akrivos J. (1985a) The length and ash weight of the ribs of normal and scoliotic persons. *Spine*, 10:590-592.
- Normelli H., Sevastik J., Ljung G., Aaro S. and Jonsson-Soderstrom A.M. (1985b) Anthropometric data relating to normal and scoliotic Scandinavian girls. *Spine*, 10:123-126.
- Novozhilov V.V. (1953) *Foundations of the Nonlinear Theory of Elasticity*. Graylock Press. Rochester.
- Oegema T.R., Bradford D.S., Cooper K.M. and Hunter R.E. (1983) Comparison of biochemistry of proteoglycans isolated from normal, idiopathic scoliosis and cerebral palsy spines. *Spine*, 8:378-387.
- Ohlen G., Aaro S. and Bylund P. (1988) The sagittal configuration and mobility of the spine in idiopathic scoliosis. *Spine*, 13:413-416.
- Olsen G.A. and Allen J.H. (1969) The lateral stability of the spine. *Clin. Orth.*, 65:143-156.
- Openshaw P., Edwards S. and Helms P. (1984) Changes in ribcage geometry during childhood. *Thorax*, 39:624-627.
- Orne D. and Liu K.Y. (1971) A mathematical model of spinal response to impact. *J. Biomech.*, 4:49-71.
- Pal G.P. (1991) Mechanism of production of scoliosis: A hypothesis. *Spine*, 16:288-292.
- Panjabi M.M. (1973) Three-dimensional mathematical model of the human spine structure. *J. Biomech.*, 6:671-680.

- Panjabi M.M., Brand R.A. and White A.A. (1976) Three-dimensional flexibility and stiffness properties of the human thoracic spine. *J. Biomech.*, 9:185-192.
- Panjabi M.M., Yamamoto I., Oxland T. and Crisco J. (1989) How does posture affect coupling in the lumbar spine? *Spine*, 14:1002-1011.
- Panjabi M.M., Takata K., Goel V., Federico D., Oxland T., Duranceau J. and Krag M. (1991) Thoracic human vertebrae. Quantitative three-dimensional anatomy. *Spine*, 16:888-901.
- Panjabi M.M., Goel V., Oxland T., Takata K., Duranceau J., Krag M. and Price M. (1992) Human lumbar vertebrae: Quantitative three-dimensional anatomy. *Spine*, 17:299-306.
- Pare A. (1634) *Collected Works*. (Translation J. Johnson), London. (Cited in Robin, 1990).
- Patwardhan A.G., Bunch W.H., Meade K.P., Vanderby Jr. R. and Knight G. (1986) A biomechanical analog of curve progression and orthotic stabilization in idiopathic scoliosis. *J. Biomech.*, 19:103-117.
- Pedrini V.A., Ponseti I.V., Pyevich M. and Pedrini M. (1990) Function-related differences in elastin and collagen content of animal ligamenta flava. *Transactions of the 36th ORS*, p. 527.
- Pearsall D.J. and Reid J.G. (1992) Line of gravity relative to upright vertebral posture. *Clin. Biomech.*, 7:80-86.
- Pedriolle R. and Vidal S. (1985) The idiopathic scoliosis curve: evolution and prognosis. *Spine*, 10:785-791.
- Peters D.A. and Ormiston R.A. (1973) The effects of second order blade bending on the angle of attack of hingeless rotor blades. *J. Am. Helicopter Soc.*, 18:45-49.
- Peterson L., Nachemson A.L. et al. (1995) Prediction of progression of the curve in girls who have adolescent idiopathic scoliosis of moderate severity. *J. Bone Jt. Surg.*, 77A:823-827.
- Piggott H. (1971) Posterior rib resection in scoliosis. *J. Bone Jt. Surg.*, 53B:663-671.
- Ponseti I.V., Pedrini V. and Dohrman S. (1972) Biochemical analysis of intervertebral discs in idiopathic scoliosis. *J. Bone Jt. Surg.*, 54A:1793.
- Pope M.H., Stokes I.A.F. and Moreland M. (1984) The biomechanics of scoliosis. *CRC Crit. Rev. Biomed. Eng.*, 11:157-188.
- Portillo D., Sinkora G., McNeill T., Spencer D. and Schultz A. (1982) Trunk strengths in structurally normal girls and in girls with idiopathic scoliosis. *Spine*, 7:551-554.

- Poussa M., Harkonen H. and Mellin G. (1989) Spinal mobility in adolescent girls with idiopathic scoliosis and its structurally normal controls. *Spine*, 14:217-219.
- Poussa M. and Mellin G. (1992) Spinal mobility and posture in adolescent idiopathic scoliosis at three stages of curve magnitude. *Spine*, 17:757-760.
- Prasad P. and King A.I. (1974) An experimentally validated dynamic model of the spine. *J. Appl. Mech.*, 41:546-550.
- Raso V.J., Russell G.G., Hill D.L., Moreau M. and McIvor J. (1991) Thoracic lordosis in idiopathic scoliosis. *J. Pediat Orth.*, 11:599-602.
- Reber J.G. and Goldsmith W. (1979) Analysis of large head-neck motions. *J. Biomech.*, 12:211-222.
- Reissner E. (1983) Further considerations on the problem of torsion and flexure of prismatic beams. *Int. J. Solids Struct.*, 19:385-392.
- Reuber M., Schultz A., McNeill T. and Spencer D. (1983) Trunk muscle myoelectric activities in idiopathic scoliosis. *Spine*, 8:447-456.
- Riddle H.V.F. and Roaf R. (1955) Muscle imbalance in the causation of scoliosis. *Lancet* i, 1245-1247.
- Risser J.C. and Fergusson A.B. (1936) Scoliosis: its prognosis. *J. Bone Jt. Surg.*, 18:667-670.
- Risser J.C., Lauder C.H., Norquist D.M. and Craig W.O. (1953) Three types of body casts. *AAOS Instr. Course Lect.*, 10:131-142.
- Roaf R. (1958) Rotation movements of the spine with special reference to scoliosis. *J. Bone Jt. Surg.*, 40B:312-332.
- Roaf R. (1966) The basic anatomy of scoliosis. *J. Bone Jt. Surg.*, 48B:786-792.
- Roaf R. (1980) *Spinal Deformities*. Pitman Medical, London.
- Roberts S.B. and Chen P.H. (1970) Elastostatic analysis of the human thoracic skeleton. *J. Biomech.*, 3:527-545.
- Roberts S.A. and Chen P.H. (1972) Global geometric characteristics of typical human ribs. *J. Biomech.*, 5:191-201.
- Robin G.C. (1990) *The Aetiology of Idiopathic Scoliosis: A Review of a Century of Research*. CRC Press, Freund Publishing, Boca Raton.
- Rogala E.J., Drummond D.S. and Gurr J. (1978) Scoliosis: incidence and natural history. A prospective epidemiological study. *J. Bone Jt. Surg.*, 60A:173-176.

- Rogers S.P. (1933) Mechanics of scoliosis. *Arch. Surg.*, 26:962-969.
- Rosen A. and Friedmann P. (1978) Nonlinear equations of equilibrium for elastic helicopter or wind turbine blades undergoing moderate deformation. *NASA CR-159478*.
- Rosen A. and Friedmann P. (1979) The nonlinear behaviour of elastic slender straight beams undergoing small strains and moderate rotations. *J. Appl. Mech.*, 46:161-168.
- Rosen A. and Rand O. (1986) Numerical model of the nonlinear behaviour of curved rods. *Comp. Struct.*, 22:785-799.
- Roth P.B. (1911) Report on a thousand cases of scoliosis. *Brit. Med. J.*, ii:493-497.
- Ruff S. (1950) Brief acceleration - less than one second. *German Aviation Medicine*. 1:584.
- Sahgal V., Shah A., Flanagan N., Schjaffer M., Kane W., Subrami V. and Singh H. (1983) Morphological and morphometric studies in muscle in idiopathic scoliosis. *Acta Orth. Scand.*, 54:242-251.
- Sahlstrand T., Ortengren R. and Nachemson A. (1978) Postural equilibrium in idiopathic scoliosis. *Acta Orth. Scand.*, 49:354-365.
- Santoro F. and Frost H.M. (1968) Correlation of the transverse sizes of 6th and 11th ribs in normal and osteoporotic individuals. *Henry Ford Hosp. Med. J.*, 16:87-96.
- Saumarez R.C. (1986a) An analysis of possible movements of human upper rib cage. *J. Appl. Physio.*, 60:678-689.
- Saumarez R.C. (1986b) An analysis of action of intercostal muscles in human upper rib cage. *J. Appl. Physio.*, 60:690-701.
- Sayre L.A. (1877) *Spinal Disease and Spinal Curvature. Their Treatment by Suspension and the Use of Plaster of Paris Bandage*. Smith & Elder, London.
- Scholten P.J.M. and Veldhuizen A.G. (1985) The influence of spine geometry on the coupling between lateral bending and axial rotation. *Eng. in Med.*, 14:167-171.
- Scholten P.J.M. (1986a) Idiopathic scoliosis - some fundamental aspects of the mechanical behaviour of the human spine. *Ph.D. Thesis*, Free University, Amsterdam.
- Scholten P.J.M. and Veldhuizen A.G. (1986) The bending stiffness of the trunk. *Spine*, 11:463-467.
- Scholten P.J.M., Veldhuizen A.G. and Grootenboer H.J. (1988) Stability of the human spine: A biomechanical study. *Clin. Biomech.*, 3:27-33.
- Schultz A.B. (1976) A biomechanical view of scoliosis. *Spine*, 1:162-171.

- Schultz A.B. (1984) Biomechanical factors in the progression of idiopathic scoliosis. *Ann. Biomed. Eng.*, 12:621-630.
- Schultz A.B., Belytschko T.B., Andriacchi T.B. and Galante J.O. (1973) Analog studies of forces in the human spine: mechanical properties and motion segment behaviour. *J. Biomech.*, 6:373-383.
- Schultz A.B., Benson D.R. and Hirsch C. (1974a) Force-deformation properties of human ribs. *J. Biomech.*, 7:303-309.
- Schultz A.B., Benson D.R. and Hirsch C. (1974b) Force-deformation properties of human costo-sternal and costo-vertebral articulations. *J. Biomech.*, 7:311-318.
- Schultz A.B. and Cisewski D.J. (1978) Morphological factors in progression of adolescent idiopathic scoliosis. *Transactions of the 24th ORS*, p. 251.
- Schultz A.B. and Galante J.O. (1970) A mathematical model for the study of the mechanics of the human vertebral column. *J. Biomech.*, 3:405-416.
- Schultz A.B., Haderspeck K. and Takashima S. (1981) Correction of scoliosis by muscle stimulation: biomechanical analysis. *Spine*, 6:468-476.
- Schultz A.B., Haderspeck K., Warwick D. and Portillo D. (1983) Use of the lumbar trunk muscles in isometric performance of mechanically complex standing task. *J. Orth. Res.*, 1:77-91.
- Schultz A.B. and Hirsch C. (1973) Mechanical analysis of Harrington rod correction of scoliosis. *J. Bone Jt. Surg.*, 55A:983-992.
- Schultz A.B., Larocca H., Andriacchi T. and Galante J.O. (1972) A study of geometrical relationships in scoliotic spines. *J. Biomech.*, 5:409-420.
- Schultz A.B., Sorensen S.E. and Andersson G.B.J. (1984) Measurements of spine morphology in children, ages 10-16. *Spine*, 9:70-73.
- Schultz A.B., Warwick D.N., Berkson M.H. and Nachemson A.L. (1979) Mechanical properties of human lumbar spine motion segments - Part I: Responses in flexion, extension, lateral bending, and torsion. *J. Biomech. Eng.*, 101:46-57.
- Schwartzmann J.R. and Miles M. (1945) Experimental production of scoliosis in rats and mice. *J. Bone Jt. Surg.*, 27:59-69.
- Scoles P.V., Linton A.E., Latimer B., Levy M.E. and DiGiovanni B.F. (1988) Vertebral body and posterior element morphology: The normal spine in middle life. *Spine*, 13:1082-1086.
- Sedlin E.D. (1964) The ratio of cortical area to total cross-section area in rib diaphysis: A quantitative index of osteoporoses. *Clin. Orth.*, 36:161-168.

- Sedlin E.D., Frost H.M. and Villaneuva A.R. (1963) Variations in cross-section area of rib cortex with age. *J. Geront.*, 18:9-13.
- Sevastik J., Aaro S., Lindholm T.S. and Dahlborn M. (1978) Experimental scoliosis in growing rabbits by operations on the ribcage. *Clin. Orth.*, 136:282-286.
- Sevastikoglou J.A., Aaro S., Elmstedt E., Dahlborn M. and Levander R. (1980) Bone scanning of the spine and thorax in idiopathic thoracic scoliosis. *Clin. Orth. & Rel. Res.*, 149:172-176.
- Shirazi-Adl S.A., Shrivastava S.C. and Ahmed A.M. (1984) Stress analysis of the lumbar disc-body unit in compression. A three-dimensional nonlinear finite element study. *Spine*, 9:120-134.
- Shirazi-Adl A., Ahmed A.M. and Shrivastava S.C. (1986a) Mechanical response of a lumbar motion segment in axial torque alone and combined with compression. *Spine*. 11:914-927.
- Shirazi-Adl A., Ahmed A.M. and Shrivastava S.C. (1986b) A finite element study of a lumbar motion segment to pure sagittal plane moments. *J. Biomech.*, 19:331-350.
- Shirazi-Adl A. and Parnianpour M. (1993a) On the global spinal postural stability: Role of flexion moment as a stabilizing mechanism. *1993 Advances in Bioengineering*, BED-Vol. 26:369-372.
- Shirazi-Adl A. and Parnianpour M. (1993b) Nonlinear response analysis of the human ligamentous lumbar spine in compression. On mechanisms affecting the postural stability. *Spine*, 18:147-158.
- Silman A.J., Day S.J. and Haskard D.O. (1987) Factors associated with joint mobility in an adolescent population. *Ann. Rheum. Dis.*, 46:209-212.
- Shohat M., Shohat T., Nitzan M., Mimouni M., Kedem R. and Danon Y.L. (1988) Growth and ethnicity in scoliosis. *Acta Orth. Scand*, 59:310-313.
- Simon B.R., Wu J.S.S., Carlton M.W., Evans J.H. and Kazarian L.E. (1985) Structural models for human spinal motion segments based on a poroelastic view of the intervertebral disc. *J. Biomech. Eng.*, 107:327-335.
- Sinclair D. (1978) *Human Growth after Birth*. 3<sup>rd</sup> edition. Oxford University Press. London.
- Skogland L.B. and Miller J.A.A. (1980) Growth related hormone in idiopathic scoliosis - an endocrine basis for accelerated growth. *Acta Orth. Scand.*, 51:779-789.
- Skogland L.B. and Miller J.A.A. (1981) The length and proportions of the thoracolumbar spine in children with idiopathic scoliosis. *Acta Orth. Scand*, 52:177-185.

- Skogland L.B., Miller J.A.A., Skottner A. and Fryklund L. (1981) Serum somatomedins and non-dialysable urinary hydroxyproline in girls with idiopathic scoliosis. *Acta Orth. Scand.*, 52:307-313.
- Skogland L.B., Steen H. and Trygstad O. (1985) Spinal deformities in tall girls. *Acta Orth. Scand.*, 56:155-157.
- Snellman O. (1973) Growth and remodelling of the ribs in normal and scoliotic pigs. *Acta Orth. Scand.*, 149:28-41.
- Soechting J.F. and Paslay P.R. (1973) A model for the human spine during impact including musculature influence. *J. Biomech.*, 6:195-203.
- Soltis L.A. and Christiano P. (1972) Finite deformation of biaxially loaded columns. *J. Struct. Div. Proceed. ASCE*, ST-12, 2647-2662.
- Somerville E. (1952) Rotational lordosis in the development of the single curve. *J. Bone Jt. Surg.*, 34B:412-427.
- Spencer G.S.G. and Eccles M.J. (1976) Spinal muscle in scoliosis. Part 2. The proportion and size of type I and type II skeletal muscle fibres measured using a computer controlled microscope. *J. Neurol. Sci.*, 30:143-154.
- Spencer G.S.G. and Zorab P.A. (1976) Spinal muscle in scoliosis. Part 1. History and histochemistry. *J. Neurol. Sci.*, 30:137-142.
- Spilker R.L. (1980) Mechanical behaviour of a simple model of an intervertebral disk under compressive loading. *J. Biomech.*, 13:895-901.
- Spilker R.L., Daugirda D.M. and Schultz A.B. (1984) Mechanical response of a simple finite element model of the intervertebral disc under complex loading. *J. Biomech.*, 17:103-112.
- Stagnara P., de Mauroy J.C., Dran G., Gonon G.P., Costanzo G., Dimnet J. and Pasquet A. (1982) Reciprocal angulation of vertebral bodies in a sagittal plane: Approach to references for the evaluation of kyphosis and lordosis. *Spine*, 7:335-342.
- Stein I.D. and Granik G. (1976) Rib structure and bending strength: An autopsy study. *Calif. Tiss. Res.*, 20:61-73.
- Stokes I.A.F. (1989) Axial rotation component of thoracic scoliosis. *J. Orth. Res.*, 7:702-708
- Stirling A.J., Howel D., Millner P.A., Sadiq S., Sharples D. and Dickson R.A. (1996) Late-onset idiopathic scoliosis in children six to fourteen years old. *J. Bone Jt. Surg.*, 78A:1330-1336.

- Stokes I.A.F., Bigalow L.C. and Moreland M.S. (1987) Three-dimensional spinal curvature in idiopathic scoliosis. *J. Orth. Res.*, 5:102-113.
- Stokes I.A.F. (1989) Axial rotation component of thoracic scoliosis. *J. Orthop. Res.*, 7:702-708.
- Stokes I.A.F., Dansereau J. and Moreland M.S. (1989) Ribcage asymmetry in idiopathic scoliosis. *J. Orth. Res.* 7:599-606.
- Stokes I.A.F. and Gardner-Morse M. (1991) Analysis of the interaction between vertebral lateral deviation and axial rotation in scoliosis. *J. Biomech.*, 24:753-759.
- Stokes I.A.F. and Garder-Morse M. (1993) Three-dimensional simulation of Harrington distraction instrumentation for surgical correction of scoliosis. *Spine*, 18:2457-2464.
- Stokes I.A.F. and Laible J.P. (1990) Three-dimensional osseo-ligamentous model of the thorax representing initiation of scoliosis by asymmetric growth. *J. Biomech.*, 23:589-595.
- Stokes, I.A.F., Spence H., Aronsson D.D. and Kilmer N. (1996) Mechanical modulation of vertebral body growth. *Spine*, 21:1162-1167.
- Struik D.J. (1961) *Lectures on Classical Differential Geometry*. Addison-Wesley Publishing Co., Reading.
- Sundaram S.H. and Feng C.C. (1977) Finite element analysis of the human thorax. *J. Biomech.*, 10:505-516.
- Tabarrok B. and Xiong Y. (1989) On the buckling equations for spatial rods. *Int. J. Mech. Sci.*, 31:179-192.
- Takahashi E. and Atsumi H. (1955) Age differences in thoracic form as indicated by thoracic index. *Human Biology*, 27:65-71.
- Takahashi H. and Frost H.M. (1966) Age and sex related changes in the amount of cortex of normal human ribs. *Acta Orth. Scand.*, 37:122-130.
- Takashima S.T., Singh S.P., Haderspeck K.A. and Schultz A.B. (1979) A model for semi-quantitative studies of muscle actions. *J. Biomech.*, 12:929-939.
- Tanner J.M. (1962) *Growth at Adolescence*. 2<sup>nd</sup> edition. Blackwell Scientific Publications, Oxford.
- Tanner J.M., Whitehouse, R.H. and Takaishi M. (1966) Standards from birth to maturity for height, weight, height velocity and weight velocity: British children, 1965. Part I. *Arch. Dis. Child L.*, 41:454-635.
- Taylor J.R. (1975) Growth of human intervertebral discs and vertebral bodies. *J. Anat.*, 120:49-68.

- Taylor J.R. and Twomey L.T. (1984) Sexual dimorphism in human vertebral body shape. *J. Anat.*, 138:281-286.
- Taylor T.K.F., Ghosh P. and Bushell G.R. (1981) The contribution of the intervertebral disc to the scoliotic deformity. *Clin. Orth.*, 156:79-90.
- Tencer A.F. and Ahmed A.M. (1981) The role of secondary variables in the measurement of the mechanical properties of the lumbar intervertebral joint. *J. Biomech. Eng.*, 103:129-137.
- Thomas G.B. and Finney R.L. (1980) *Calculus and Analytic Geometry. Part II: Vectors, Functions of Several Variables, Infinite Series and Differential Equations*, Addison-Wesley Publishing Company, Reading, Massachusetts.
- Todd T. and Pyle S. (1928) A quantitative study on the vertebral column by direct and roentgenoscopic methods. *Am. J. Phys. Anthrop.*, 12:321-338.
- Toth R. (1967) Multiply degree-of-freedom nonlinear spine model. *19th Ann. Conf. on Engng. in Med. and Biol.*
- Timoshenko S.P. and Gere J.M. (1961) *Theory of Elastic Stability*. McGraw-Hill. New York.
- Ueno K. and Liu Y.K. (1987) A three-dimensional finite element model of a lumbar intervertebral joint in torsion. *J. Biomech. Eng.*, 109:200-209.
- Upadhyay S.S., Nelson I.W., Ho E.K.W., Hsu L.C.S. and Leong J.C.Y. (1995) New prognostic factors to predict the final outcome of brace treatment in adolescent idiopathic scoliosis. *Spine*, 20:537-545.
- Veldhuizen A.G., Baas P. and Webb P.J. (1986) Observations on the growth of the adolescent spine. *J. Bone Jt. Surg.*, 68B:724-728.
- Veldhuizen A.G. and Scholten P.J.M. (1987) Kinematics of the scoliotic spine as related to the normal spine. *Spine*, 12:852-858.
- Veldhuizen A.G. and Scholten P.J.M. (1990) Flexibility in structurally normal young females and in young females with idiopathic scoliosis. *Clin. Biomech.* 5:117-126.
- Veliskakis K.P. (1973) Increased generalized ligamentous laxity in idiopathic scoliosis. *J. Bone Jt. Surg.*, 55A, 435.
- Venn G., Mehta M.H. and Mason R.M. (1983) Solubility of spinal ligament collagen in idiopathic and secondary scoliosis. *Clin. Orth.*, 177:294-301.
- Viviāni G.R., Ghista D.N., Lozada P.J., Subbaraj K. and Barnes G. (1986) Biomechanical analysis and simulation of scoliosis surgical correction. *Clin. Orth. Rel. Res.*, 208:40-47.

- Washizu K. (1968) *Variational Methods in Elasticity and Plasticity*. Pergamon Press, Oxford.
- Waters R.L. and Morris J.M. (1973) An in vivo study of normal and scoliotic interspinous ligaments. *J. Biomech.*, 6:343-348.
- Watson E.H. and Lowrey G.H. (1962) *Growth and Development of Children*. 4<sup>rmth</sup> edition, Year Book Medical Publishers, Chicago.
- Weinstein S.L. (1994) Adolescent idiopathic scoliosis: prevalence and natural history. Chapter 21. In: *The Pediatric Spine: Principles and Practice*. Ed. Weinstein S.L., Raven Press, New York.
- Wempner G.A. (1981) *Mechanics of Solids with Applications to Thin Bodies*. Sijthoff and Noordhoff, Rockville.
- White A.A. and Panjabi M.M. (1990) *Clinical Biomechanics of the Spine*. 2nd Edit. J.B. Lippincott Co., Philadelphia.
- Williams J.L. and Belytschko T.B. (1983) A three-dimensional model of the human cervical spine for impact simulation. *J. Biomech. Eng.*, 105:321-331.
- Willner S. (1974a) Growth in height of children with scoliosis. *Acta Orth. Scand.*, 45:854-866.
- Willner S. (1974b) Study of growth in girls with adolescent idiopathic structural scoliosis. *Clin. Orth.*, 101:129-135.
- Willner S. (1975a) A study of height, weight and menarche in girls with idiopathic structural scoliosis. *Acta Orth. Scand.*, 46:71-83.
- Willner S. (1975b) The proportion of legs to trunk in girls with idiopathic structural scoliosis. *Acta Orth. Scand.*, 46:84-89.
- Willner S. (1981) Spinal pantograph – a non-invasive technique for describing kyphosis and lordosis in the thoraco-lumbar spine. *Acta Orth. Scand.*, 52:525-529.
- Willner S. (1994) Adolescent idiopathic scoliosis: etiology. Chapter 20. In: *The Pediatric Spine: Principles and Practice*. Ed. Weinstein S.L., Raven Press, New York.
- Willner S. and Johnson B. (1983) Thoracic kyphosis and lumbar lordosis during the growth period in children. *Acta Paed. Scand.*, 72:873-878.
- Willner S., Nillsson K.O., Kastrup K. and Bergstrand C.G. (1976) Growth hormone and somatomedin-A in girls with adolescent idiopathic scoliosis. *Acta Paed. Scand.*, 65:547-552.

- Wilson T.A., Rehder K., Krayner S., Hoffman E.A., Whitney C.G. and Rodarte J.B. (1987) Geometry and respiratory displacement of human ribs. *J. Appl. Physiol.*, 62:1872-1877.
- Wong T. (1979) Idiopathic scoliosis and the stability of the human spine. *M.Sc. Thesis.* University of Waterloo.
- Woodburne R.T. (1983) *Essentials of Human Anatomy.* 7<sup>th</sup> edition. Oxford University Press, Oxford.
- Wynarsky G.J. and Schultz A.B. (1991) Optimization of skeletal configuration: Studies of scoliosis correction biomechanics. *J. Biomech.*, 24:721-732.
- Wynne-Davies R. (1968) Familial (idiopathic) scoliosis: a family study. *J. Bone Jt. Surg.*, 50B:24-30.
- Xiong B., Sevastik J., Hedlund R. and Sevastik b. (1994) Sagittal configuration of the spine and growth of the posterior elements in early scoliosis. *J. Orth. Res.*, 12:113-118.
- Yahia L., Rivard C.H., Newman N. and Rhalmi S. (1992) Spinal ligaments and idiopathic scoliosis. In: *International Symposium on 3-D Scoliotic Deformities*, Ed. J. Dansereau, Gustav Fischer Verlag, Stuttgart, pp. 434-443.
- Yamada K., Ikata T., Yamamoto H., Nakagaway Y., Tanaka H. and Tezuka A. (1969) Equilibrium function in scoliosis and active corrective plaster jacket for the treatment. *Tokushima J. Ex. Med.*, 16:1-7.
- Yarom R. and Robin G.C. (1979) Muscle pathology in idiopathic scoliosis. *Isr. J. Med. Sci.*, 15:917-924.
- Yettram A.L. and Jackman M.J. (1980) Equilibrium analysis for the forces in the human spinal column and its musculature. *Spine*, 5:402-411.
- Zaleske D.J., Ehrlich M.G. and Hall J.E. (1980) Association of glycosaminoglycan depletion and degradative enzyme activity in scoliosis. *Clin. Orth.*, 148:177-181.
- Zetterberg C., Aniansson A. and Grimby G. (1983) Morphology of the paravertebral muscles in adolescent idiopathic scoliosis. *Spine*, 8:457-462.
- Zetterberg C., Bjork R., Ortengren R. and Andersson G.B.J. (1984) Electromyography of the paravertebral muscles in idiopathic scoliosis. *Acta Orth. Scand.*, 55:304-309.
- Zienkiewicz O. (1977) *The Finite Element Method*, 3rd Edit. McGraw-Hill. New York and London.
- Zuk T. (1962) The role of spinal and abdominal muscles in the pathogenesis of scoliosis. *J. Bone Jt. Surg.*, 44B:102-105.

# **Appendix A**

## **Classification System for Spinal Deformities**

Table A.1: Etiological classification system for spinal deformities developed in accordance with the Scoliosis Research Society (Leatherman and Dickson, 1988).

<b>PRIMARY, PROGRESSIVE OR STRUCTURAL DEFORMITIES</b>
<p><i>Idiopathic deformities</i></p> <ol style="list-style-type: none"> <li>1. Idiopathic scoliosis               <ol style="list-style-type: none"> <li>a. Early-onset (before 5 years of age)</li> <li>b. Late-onset (after 5 years of age)*</li> </ol> </li> <li>2. Idiopathic kyphosis               <ol style="list-style-type: none"> <li>a. Type I – classical Scheuermann’s disease</li> <li>b. Type II – “apprentice’s spine”</li> </ol> </li> </ol>
<p><i>Congenital deformities</i></p> <ol style="list-style-type: none"> <li>1. Bone deformities</li> <li>2. Cord deformities</li> <li>3. Bone and cord deformities</li> <li>4. Syndromes in which congenital spine deformities are prevalent</li> </ol>
<p><i>Neuromuscular deformities</i></p> <ol style="list-style-type: none"> <li>1. Cerebral palsy</li> <li>2. Poliomyelitis</li> <li>3. True “neuromuscular disorders”</li> <li>4. Familial dysautoromia</li> <li>5. Malignant hyperpyrexia</li> </ol>
<p><i>Deformities in association with neurofibromatosis</i></p> <ol style="list-style-type: none"> <li>1. Dystrophic deformities</li> <li>2. Idiopathic-type deformities</li> </ol>

\* Late-onset scoliosis also includes adolescent idiopathic scoliosis (AIS).

Table A.1 (Continued)

<i>Mesenchymal deformities</i>
1. Heritable disorders of connective tissue
2. Mucopoly saccharidoses
3. Bone dysplasias
4. Metabolic bone disorders
5. Endocrine disorders
<i>Traumatic disorders</i>
1. Vertebral
2. Extravertebral
<i>Deformity due to infection</i>
1. Pyogenic infection
2. Tuberculosis
<i>Deformity due to tumours</i>
1. Intradural tumours
2. Syringomyelia
3. Paravertebral childhood tumours
4. Primary extradural tumours
5. Metastatic spinal disease
<i>Miscellaneous conditions</i>
<i>Spinal deformity in adults</i>
1. True adult deformities
2. Adult-presenting deformities
<i>Spondylolisthesis</i>
1. Dysplastic
2. Isthmic
3. Degenerative
4. Traumatic
5. Pathological
<b>SECONDARY, NON-PROGRESSIVE OR NON-STRUCTURAL DEFORMITIES</b>
<i>Pelvic tilt scoliosis</i>
<i>Irritative lesions</i>
<i>Hysterical scoliosis</i>

## Appendix B

# Etiological Theories for Idiopathic Scoliosis

In this appendix, various theories for the cause of idiopathic scoliosis are reviewed and summarized in Table B.1. The theories are grouped according to the tissue, structure or system that they primarily affect. This review is intended to provide the reader with an overview of the varied approaches which have been considered in the etiology of scoliosis. In each area, the review attempts to summarize the current state of the literature and to show that there is no clear definitive cause for adolescent scoliosis and thus the term idiopathic.

### Genetic

Early researchers, such as Roth (1911), Lovett (1916) and Garland (1934), commented on the number of families associated with scoliosis. There are other reports on the tendency for twins to be affected (Fisher and DeGeorge, 1967). One of the more authoritative works was by Wynne-Davies (1968) which suggested a dominant or multiple gene inheritance pattern. Attempts, however, to identify genes have not been successful, and only the increased incidence in certain families can be accepted. Furthermore, a multiple gene inheritance pattern can also indicate a combination of genetic and environmental factors.

## Intervertebral Disc

A number of studies have examined the collagen and proteoglycan content of the disc in scoliotics (Ponseti et al, 1972; Zaleske et al, 1980; Taylor et al, 1981; Oegema et al, 1983). Definite changes at the cellular level have been found in the nucleus and the annulus, which were postulated to alter the structural integrity of the disc. Furthermore, differences in the disc between the convex and concave side of the curve have been observed, as well as differences due to the location of the disc in the curve, i.e., closer or farther from the apex. However, these latter findings are difficult to interpret unambiguously, because the changes in the disc could be due to the deformity itself, rather than being causative.

## Vertebra

Experimental studies in animals (Haas, 1939; Bisgard and Musselman, 1940; Langenskiold and Michelsson, 1962; Michelsson, 1965; Karaharju, 1967) have produced scoliosis by destroying the vertebral growth centre on one side. However, the deformities in the vertebrae are more likely secondary (Enneking and Harrington, 1969; Sevastikoglou et al, 1980) to the scoliotic curve due to the Heuter-Volkman principle, which governs the response of the epiphyseal growth plates at the superior and inferior surfaces of the vertebrae. Similarly, the changes in the laminae and pedicles are likely due to Wolff's law which governs the remodelling of bone due to mechanical loads.

Recently, the Heuter-Volkman principle has been proven directly in a rat tail model, where increased compression during growth retarded the development of the vertebrae, whereas tension had the opposite affect leading to longer vertebrae (Stokes et al, 1996). These authors hypothesized that this mechanism could be critical in the progression of a scoliotic curve where the increased bending moment on the spine due to the scoliotic curve would lead to wedging of the vertebra via the Heuter-Volkman principle. This in turn would lead to more progression and a larger moment which would only lead to further wedging in a progressive circle. This mechanism is very attractive to explain the progression of a curve, but does not indicate why some curves progress and others do not, since this mechanism would be present in all curves. If it could be shown that a certain load is

required before the growth is affected, the magnitude of which might vary between individuals, then this might explain different progression tendencies. However, there is no data to support this idea at present. Therefore, it has been shown that the Heuter-Volkman principle likely explains the gradual wedging of the vertebrae in a scoliotic curve, but its role in directly causing progression remains unclear.

### **Ligaments and Tendons**

Both the collagen and the elastin content of the ligaments and tendons have been investigated in patients with AIS. No biomechanical (Nordwall, 1973; Waters and Morris, 1973) or biochemical (Bradford et al, 1977; Venn et al, 1983) abnormalities have been found in the collagen from scoliotics. The findings for the elastin content are less clear. Veliskakis (1973) found an increased number of elastin fibres, whereas Nordwall (1973) found no difference. There have also been several recent studies reporting differences in the elastin content for scoliotics (Pedrini et al, 1990; Hadley et al, 1991; Yahia et al, 1992).

The overall laxity of the ligamentous system has also been studied by determining the trunk bending and joint stiffnesses of scoliotics. Mattson et al (1983) found that normals had increased lateral bending flexibility (as measured by range of motion) compared to scoliotic girls. Also, the flexibility of other joints was not increased for the scoliotics. A recent study of Veldhuizen and Scholten (1990) reported similar flexibility results. Though these studies have not determined directly the spinal flexibility, they do show that scoliotics do not suffer from a systemic increased flexibility.

### **Muscles**

Successful attempts have been made to produce scoliosis in animal models through resection or damage to various muscles (Schwartzmann and Miles, 1945; Langeskiold and Michelsson, 1961). However, the curves did not always include the characteristic axial rotation component of AIS and did not have the same progression tendencies. Furthermore, in AIS there is no obvious gross damage to the muscular tissue. This is further supported by the study of Portillo et al (1982), which found no trunk muscular strength difference between mild scoliotics and normals.

Many studies have reported findings of asymmetrical muscular activity, as measured by EMG (electromyograph), between the convex and concave side (e.g., Riddle and Roaf, 1955; LeFebvre et al, 1961; Zuk, 1962). It would appear, however, that the asymmetrical muscular activity is a secondary response to the curve. The asymmetry disappears following fusion (Butterworth and James, 1969) and is more pronounced in larger curves (Reuber et al, 1983; Zetterberg et al, 1984).

The pathophysiology of the muscles of AIS patients has been examined from many different angles (Kaneko, 1968; Spencer and Eccles, 1976; Spencer and Zorab, 1976; Yarom and Robin, 1979; Sahgal et al, 1983; Zetterberg et al, 1983; Ford et al, 1984; Bylund et al, 1987). As yet, however, there is no clear evidence that the observed differences in muscular tissue are not once again secondary adaptations.

### **Ribcage**

Removal of ribs due to fracture or tumor, for example, can result in scoliosis in humans (Bisgard, 1934; Piggot, 1971; Loynes, 1972; Durning et al, 1980). Scoliosis has also been produced in experimental studies in animals by resection of ribs (Langenskiold and Michelsson, 1961; Michelsson, 1965; Snellman, 1973; Sevastik et al, 1978). However, the implications of these studies for AIS are less clear, since the ribcage in AIS is fully intact.

Other researchers have studied the ribcage for more subtle defects which could be implicated in etiology. Mehta (1972) investigated the prognostic value of the rib-vertebra-angle-difference or RVAD in the progression of a curve for infantile idiopathic scoliosis. Further investigations of the ribcage have focused on rib lengths and asymmetrical growth of the ribs (Normelli et al, 1985a; Agadir et al, 1988; Stokes et al, 1989), and on the importance of symmetrical support from the ribcage (Pal, 1991).

A recent theory proposed by Burwell and co-workers (Burwell and Dangerfield, 1992; Burwell et al, 1992), attempts to unify the many and varied observations from scoliotics into a general, multi-factorial view of etiology. Their observations (Grivas et al 1991) of altered morphology in the ribcages of scoliotics are the basis for this unified theory. However, it is not known whether the observed changes in scoliotics in the morphology of the

ribcage can significantly alter its mechanical support.

### **Sagittal Plane Curves**

Adams (1865) showed that idiopathic scoliosis in the thoracic region was in reality a lordosis plus axial rotation. The normal thoracic kyphosis had become a lordosis about the apex of the curve. Somerville (1952) again reaffirmed the 3-D nature of idiopathic scoliosis. However, the origin of the lordosis at the curve apex was not clear, as there was no evidence of a primary growth disturbance in the posterior elements. Roaf (1966), and Deane and Duthie (1973) also implicated a thoracic lordosis in the etiology of idiopathic scoliosis. More recently, Dickson et al (1984) argued that scoliosis is the result of a combination of a thoracic lordosis (a reduced kyphosis is sufficient) plus a small lateral deviation in the coronal curve. When these conditions arise, then with repeated flexion, the vertebrae are forced to rotate axially, producing the idiopathic scoliotic deformity. The distinguishing feature of this theory from previous ones is that no pathological condition is required. The small lateral deviation is common in many people and during the adolescent growth spurt the thoracic kyphosis is reduced.

Several recent papers have all shown a decrease in the thoracic kyphosis in scoliotics (Ohlen et al, 1988; Poussa et al, 1989; Carr et al, 1991; Raso et al, 1991; Kojima and Kurokawa, 1992; Poussa and Mellin, 1992). Not all researchers, however, agree that all scoliotic curves are lordotic (De Smet et al, 1984; Stokes et al, 1987). Furthermore, Xiong et al (1994) have recently shown that changes to the vertebrae occur in all planes simultaneously in the early stages.

A decrease in mobility with forward flexion was also noted in scoliotics (Poussa et al, 1989; Poussa and Mellin, 1992). However, the authors acknowledge that their gross measurements of trunk mobility do not necessarily imply a more rigid thoracic curve (Mellin and Poussa, 1992). Without a decreased flexibility of the spine in the sagittal plane that rendered the lordosis comparatively rigid, it is difficult to accept the mechanics of this theory. The lateral and torsional buckling of the spine to one side with flexion can only occur if the lordosis is relatively rigid. Otherwise, the spine would simply be flexed into

the original kyphosis with applied flexion and remain in the sagittal plane.

### **Postural Equilibrium**

The idea that idiopathic scoliosis is the result of a deficit in the postural control system is one of the most prominent theories today. The search for the actual deficit, however, has been less successful, as all aspects of the system from the sensory nerves, to the muscles, to the brain, to the vestibular system have been studied. The research in this area began with Yamada et al (1969) who found equilibrium dysfunction in 81% of patients. However, there were similar problems with other types of scoliosis and the amount of dysfunction also correlated positively with the curve magnitude, which again raised the question of cause and effect.

Sahlstrand et al (1978) found that scoliotics demonstrated increased sway compared with normals, particularly when blindfolded. They concluded that in scoliotics there existed disturbed proprioception, related to the optic and possibly the vestibular systems. Herman et al (1985) argued that in scoliotics there was visuo-spatial perceptual impairment. As a result, scoliotics recalibrate their equilibrium system and develop asymmetrical muscular action. Contradictory findings have, however, been presented by Gregoric et al (1981) which could not find any significant change in postural sway and by Adler et al (1986) which found decreased sway in scoliotics. Proprioception has also been investigated by Barrack et al (1984) and Keeson et al (1992), for example, and found to be dysfunctional or asymmetrical in scoliotics.

Based on the observations of the foregoing authors and others, attempts have been made to develop experimental animal models of the proposed etiologies. Alterations to the brain stem have been successful in producing scoliosis in rats (Kawata, 1976), for example. A recent study produced scoliosis in chickens through removal of the pineal gland (Machida et al, 1993). However, in humans no differences in the quantity of melatonin, which is controlled by the pineal gland, was found in scoliotics compared to normals (Bagnall et al, 1996). More studies are needed to measure the melatonin levels more closely during the early stages of scoliosis and during progression.

Table B.1: Summary of the various etiological theories for AIS, subdivided according to the primary tissue, structure or system involved.

ETIOLOGICAL THEORY	RESEARCHERS	KEY FINDINGS
Genetic	Roth, 1911 Lovett, 1916 Garland, 1934 Fisher and DeGeorge, 1967 Wynne-Davies, 1968	History of scoliosis in the family History of scoliosis in the family History of scoliosis in the family Occurrence of scoliosis in twins Dominant or multiple gene inheritance pattern
Intervertebral Disc	Ponseti et al, 1972 Zaleske et al, 1980 Taylor et al, 1981 Oegema et al, 1983	Biochemical changes in the nucleus observed in scoliotics Biochemical changes are secondary Biochemical changes are secondary Biochemical changes are secondary, as they occur in different types of scoliosis
Vertebra	Haas, 1939 Bisgard and Musselman, 1940 Langenskiold and Michelsson, 1962 Michelsson, 1965 Karaharju, 1967 Enneking and Harrington, 1969 Sevastikoglou et al, 1980  Stokes et al, 1996	Experimental scoliosis in growing dogs Experimental scoliosis in goats Experimental scoliosis in rabbits Experimental scoliosis in pigs Experimental scoliosis Vertebral asymmetries are secondary effects No asymmetrical growth activity in vertebrae of progressive curves Experimental validation of the Heuter-Volkman principle
Ligaments and Tendons Collagen	Nordwall, 1973 Waters and Morris, 1973 Bradford et al, 1977 Venn et al, 1983	No mechanical difference between scoliotics and normals No mechanical difference between scoliotics and normals No biochemical difference between scoliotics and normals No biochemical difference between scoliotics and normals

ETIOLOGICAL THEORY	RESEARCHERS	KEY FINDINGS
<p>--- Elastin</p> <p>- Joint stiffness</p>	<p>Veliskakis, 1973                      Nordwall, 1973                      Pedrini et al, 1990                      Hadley et al, 1991                      Yahia et al, 1992</p> <p>Mattson et al, 1983                      Veldhuizen and Scholten, 1990</p>	<p>Increased number of elastin fibres in ligaments from scoliotics                      No difference between scoliotics and normals                      Importance of elastin for stability                      Differences found at the molecular level                      Decreased amount of elastin fibres in ligaments from scoliotics</p> <p>Scoliotics are not more flexible than normals                      Scoliotics are not more flexible than normals</p>
<p>Muscles</p> <p>— Gross musculature</p> <p>-- EMG</p> <p>--- Pathophysiology</p>	<p>Schwartzmann and Miles, 1945                      Langeskiold and Michelsson, 1961                      Portillo et al, 1982</p> <p>Riddle and Roaf, 1955                      LeFebvre et al, 1961                      Zuk, 1962</p> <p>Butterworth and James, 1969                      Reuber et al, 1983                      Zetterberg et al, 1984</p> <p>Kaneko, 1968                      Spencer and Zorab, 1976                      Spencer and Eccles, 1976                      Yarom and Robin, 1979</p>	<p>Experimental scoliosis by muscle excision in rats and mice                      Experimental scoliosis by muscle excision in rabbits                      No difference in muscular strength between scoliotics and normals</p> <p>Increased muscular activity on convex side                      Increased muscular activity on convex side                      Increased muscular activity on convex side                      Increased muscular activity on convex side; decreases after fusion                      Increased muscular activity on convex side; only in larger curves                      Increased muscular activity on convex side; proportional to curve magnitude</p> <p>Neurogenic atrophy in paraspinal muscles in scoliotics                      Histochemical differences of muscle fibre types in scoliotics                      Histomorphometric differences of muscle fibre types in scoliotics                      Histochemical and electron microscope differences in paraspinal and gluteus maximus muscles of scoliotics</p>

ETIOLOGICAL THEORY	RESEARCHERS	KEY FINDINGS
	Sahgal et al, 1983 Zetterberg et al, 1983  Ford et al, 1984  Bylund et al, 1987	Decrease in type II (fast twitch) fibres on concave side Increase in type I (slow twitch) fibres on convex side; argued to be secondary Increase in type I (slow twitch) fibres at curve apex in the multifidus Altered proportions of type I/type II fibres in scoliotics
Ribcage --- Rib resection (humans)  Rib resection (animal model)  Rib asymmetries & morphology	Bisgard, 1934 Piggot, 1971 Loynes, 1972 Durning et al, 1980  Langenskiold and Michelsson, 1961  Michelsson, 1965  Snellman, 1973 Sevastik et al, 1978  Mehta, 1972 Sevastik et al, 1978 Sevastikoglou et al, 1980 Normelli et al, 1985a Agadir et al, 1988 Stokes et al, 1989 Pal, 1991 Grivas et al, 1991	Scoliosis following thoracic disease and surgery Posterior rib resection to correct scoliosis Scoliosis following thoracoplasty Scoliosis following thoracoplasty  Experimental scoliosis in the rabbit following rib resection Experimental scoliosis in the rabbit following rib resection Experimental scoliosis in pigs Experimental scoliosis in growing rabbits following ribcage operations  Prognostic value of the RVAD in curve progression Asymmetric rib growth can initiate scoliosis Some asymmetry in rib growth in progressive scoliosis Asymmetric rib lengths in scoliotics Asymmetric rib growth can initiate scoliosis Asymmetric rib lengths in scoliotics Asymmetric rib forces causes scoliosis Narrowing of lower chest with increasing age is a factor in scoliosis

ETIOLOGICAL THEORY	RESEARCHERS	KEY FINDINGS
Sagittal Plane Curves	Adams, 1865 Somerville, 1952 Roaf, 1966 Deane and Duthie, 1973  Dickson et al, 1984 Jarvis et al, 1988 Ohlen et al, 1988 Poussa et al, 1989 Raso et al, 1991  Carr et al, 1991 Poussa and Mellin, 1992 Kojima and Kurokawa, 1992	Importance of lordosis in scoliosis Thoracic lordosis due to failure of growth in the posterior elements Thoracic lordosis due to lengthening of the vertebral bodies Thoracic lordosis due to inhibition of growth in the posterior elements Thoracic lordosis is a limit of the normal lateral curves Thoracic lordosis is due to an unknown posterior tether Reduced thoracic kyphosis in the lateral profile Reduced thoracic kyphosis in the lateral profile Reduced thoracic kyphosis or lordosis in the sagittal plane of the apical vertebra Reduced thoracic kyphosis in the lateral profile Reduced thoracic kyphosis in the lateral profile Thoracic lordosis in a vertebral reference frame
Postural Equilibrium	Yamada et al, 1969 Kawata, 1976 Sahlstrand et al, 1978 Gregoric et al, 1981 Barrack et al, 1984 Herman et al, 1985 Adler et al, 1986 Keeson et al, 1992 Machida et al, 1993	Equilibrium dysfunction observed in scoliotics Experimental scoliosis in rats related to brain stem Increased postural sway in scoliotics No evidence of postural problems in scoliotics Asymmetry in positioning of lower limbs in scoliotics Visuo-spatial disorder in scoliotics Scoliotics have less sway than normal Asymmetrical spatial orientation in scoliotics Experimental scoliosis in chickens related to brain stem
Growth Biochemical	Misol et al, 1971 Willner et al, 1976 Skogland and Miller, 1980  Skogland and Miller, 1981 Ahl et al, 1988	Serum growth hormone levels are normal in scoliotics Increased secretion of growth hormone in scoliotics Increased response to growth hormone stimulation in early puberty in scoliotics Could not confirm an increased growth rate in scoliotics Increased secretion of growth hormone in early puberty of scoliotics

# Appendix C

## Anatomy of the Spine

### C.1 Introduction

This appendix presents a description of the relevant anatomy of the spine, including the structures that comprise the spinal column, as well as those which provide external support. The description begins with the intervertebral joint which is the basic “building block” of the spine, followed by a description of the spinal column itself, to illustrate the variations in form along its length. The subsequent sections describe the external support provided by the ribcage and the trunk musculature. Throughout this description, emphasis is placed on the functional anatomy of the various structures of the spinal complex, with particular reference to those most implicated in the etiology of scoliosis. This anatomical review is a compilation from many sources (e.g., Grant, 1978; Gray, 1989), and is only intended as an overall description to assist the reader.

### C.2 Intervertebral Joint

An *intervertebral joint*, also termed a *motion segment*, is defined to comprise two adjacent vertebrae plus the interconnecting ligaments and disc (Fig. C.1A). Although there are significant differences in the morphology of the intervertebral joint at different levels of the spine, nonetheless, the basic features remain the same.

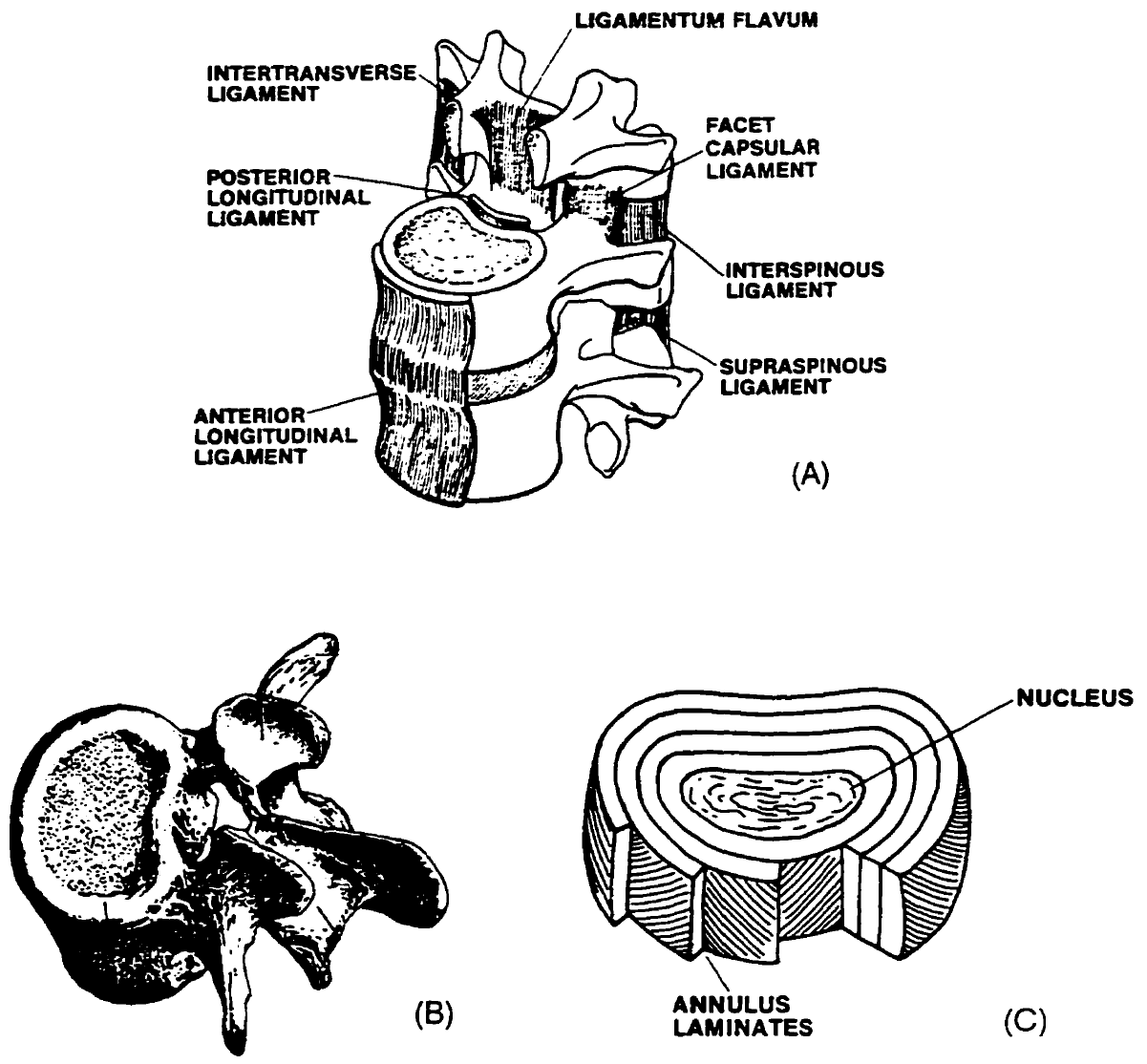


Figure C.1: A) An intervertebral joint or motion segment comprised of two vertebrae, plus the interconnecting disc, ligaments and facet joints (Grant, 1978). B) A typical vertebra from the lumbar region of the spine (Gray, 1989). C) An intervertebral disc is composed of a nucleus, surrounded by a series of fibrous bands.

## Vertebra

Each vertebra consists of an *anterior* or *vertebral body*, which is roughly an elliptical cylinder, and a posterior ring, termed the *neural arch* (Fig. C.1B). The neural arch is composed of two *pedicles* and two *laminae* which are united to enclose a space termed the *spinal foramen* which serves to protect the spinal cord. At the junction of the laminae, the *spinous process* arises and extends posteriorly, while at the junction of the laminae and the pedicles, two *transverse processes* arise and extend laterally to each side. There are a total of four *articular processes* (two superior and two inferior) which also arise at the junction of the laminae and the pedicles on either side. These structures, extraneous to the anterior body, are also collectively termed the *posterior elements*. As a general description, the vertebral bodies serve to carry the body weight and distribute this load to the flexible intervertebral disc, whereas the posterior elements serve as levers for the attachment of ligaments and muscles to provide stiffness and motion, respectively.

## Intervertebral Disc

The intervertebral disc is located between two adjacent vertebral bodies. It is comprised of three distinct structures: the *nucleus pulposus*, the *annulus fibrosus* and the *cartilaginous endplates*. The nucleus pulposus is a gel-like substance with a high water content making it nearly incompressible, and it occupies 30-50% of the cross-sectional disc area. The annulus fibrosus is composed of a series of bands containing collagenous fibres embedded in a ground substance, similar to a composite material. The fibres are inclined at an angle of about 30° with respect to the horizontal plane of the disc; the angle of inclination changing alternately from one band to another (Fig. C.1C). The ordered pattern of the annulus fibrosus arises gradually from the periphery of the nucleus, and the annulus completely surrounds the nucleus. The cartilaginous endplates are composed of hyaline cartilage and represent a transition zone between the disc and the vertebrae. The endplates gradually become ossified with increasing age.

The intervertebral disc provides the three-dimensional flexibility between the adjacent vertebrae. The disc is subjected to an axial compression load which in the lower spine can

often exceed body weight during heavy lifting. As an incompressible fluid, the nucleus exerts pressure on the inner wall of the annulus in response to the compressive load. In turn, the fibres of the annulus are tensed to contain this pressure. Concurrent to resisting the axial compression, the disc permits extensive bending in the sagittal and coronal planes, as well as axial rotation.

## Ligaments

There are seven *ligaments* that interconnect two adjacent vertebrae (Fig. C.1A). The ligaments are mainly composed of collagen and function as uniaxial structures that only resist tension. Their function, therefore, is primarily determined by their location and orientation.

The *anterior longitudinal ligament* extends over the anterior surfaces of all vertebrae and discs, whereas the *posterior longitudinal ligament* extends over the posterior surfaces. Due to their locations, the anterior and posterior longitudinal ligaments primarily resist extension and flexion, respectively. However, they also significantly resist disc bulging, anterior/posterior shear and axial rotation. The *ligamenta flava* interconnect the laminae of adjacent vertebrae on either side. They are the most elastic ligaments in the body and are pre-tensioned in the neutral position. Their location is best suited to resist flexion and axial rotation. Between the adjacent spinous processes is the *interspinous ligament*, while the *supraspinous ligament* extends over the posterior tips of the spinous processes. Both these ligaments primarily resist flexion, although they can also provide resistance to axial rotation. The *intertransverse ligament* joins the transverse processes of adjacent vertebrae and is most effective at resisting lateral bending and axial rotation. The *capsular ligament* is a sac-like structure which encloses the facet joint (described below) formed by the superior and inferior articular processes on either side. It is most effective at resisting the relative motion between the superior and inferior processes.

The seven ligaments function together to provide stiffness and stability to the intervertebral joint while allowing sufficient physiological motion, with minimal expenditure of muscle energy. They best achieve this function through their non-linear stiffness prop-

erties. Near the neutral position, the ligaments are less stiff compared with a deformed position, where the stiffness can be considerably greater. In this manner, the ligaments are best able to permit motion at lower loads while providing protection and stability to the intervertebral joint at higher traumatic loads.

### Facet Joints

The *facet* or *apophyseal joints* are formed between two adjacent vertebrae from the articular processes, which contain the articular facets, along with the cartilaginous articular surfaces and capsular ligaments. The facet joints are formed between the superior articular facets of the inferior vertebra, and the inferior articular facets of the adjacent superior vertebra (Fig. C.1A). The articulating surfaces of the facets are composed of cartilage which allows free relative movements. Concurrently, the superior and inferior processes are bound by the capsular ligament.

The general function of the facet joints is to permit relative motion between the vertebrae in one sense, while constraining the motion in another. The configuration of the joint, and therefore its function, varies greatly between different spine levels, and is further explained in the following section.

## C.3 Spinal Column

The *spinal* or *vertebral column* consists of a total of 33 vertebrae, plus the interconnecting discs and ligaments. The spinal column is divided into four major regions from bottom to top: sacral, lumbar, thoracic and cervical (Fig. C.2). The main functions of the spinal column are to transfer load between the pelvis and the upper body, to provide sufficient flexibility during physiological motions and to protect the delicate spinal cord. These functions are achieved through a complex balance between the characteristics of the basic element of the spinal column, the intervertebral joint, and the gross form of the column with its four distinct regions. In a lateral view, the cervical region is curved convex anteriorly (lordosis), the thoracic region is concave anteriorly (kyphosis), the lumbar

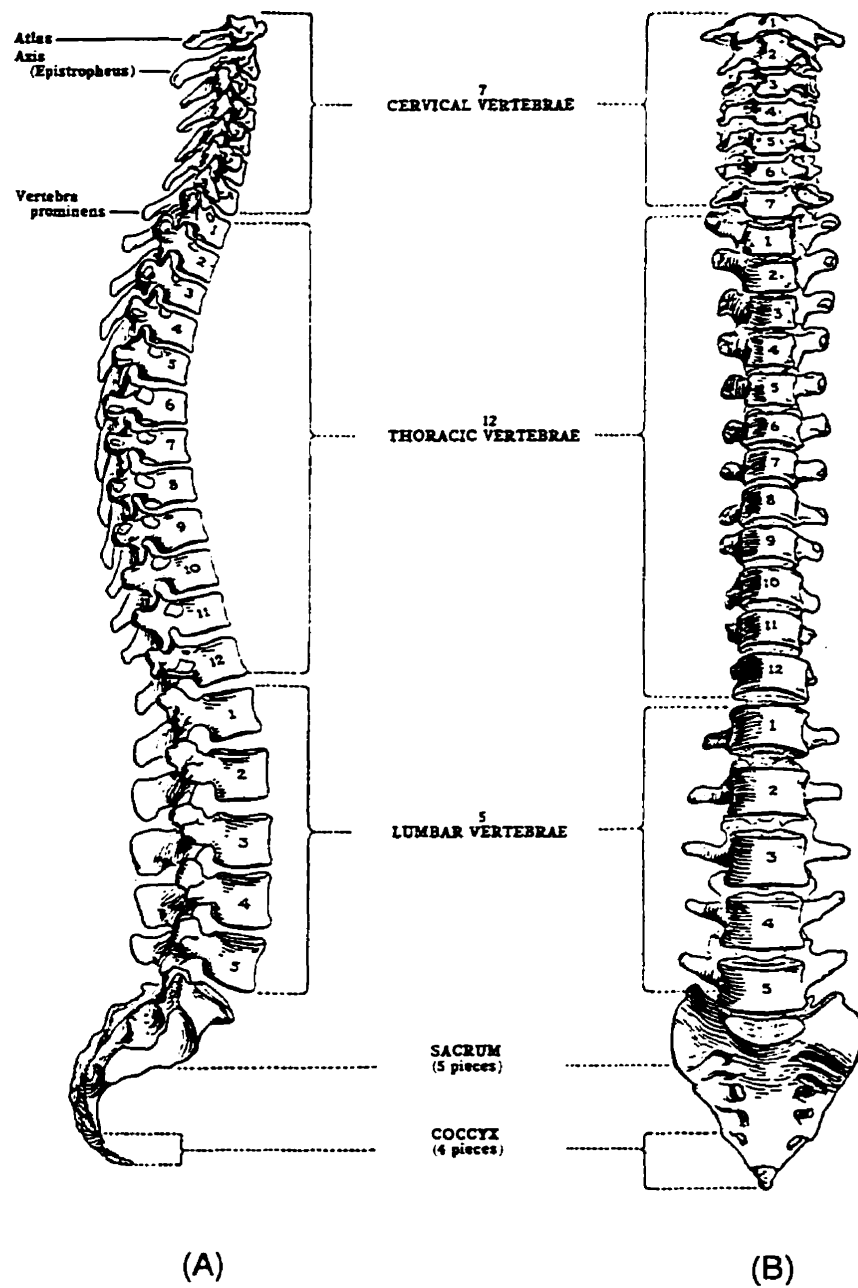


Figure C.2: The spinal or vertebral column is composed of 33 vertebrae and divided into four regions: sacral, lumbar, thoracic and cervical (Grant, 1978). A) Lateral view; B) Anterior view.

region is convex anteriorly (lordosis) and the sacral region is concave anteriorly (kyphosis). These four major curves in the lateral view allow for the internal organs to be carried more efficiently over the pelvis, provide increased flexibility and provide a shock absorbing capacity. In a frontal view, the spine is normally straight except for a slight right curvature found in many individuals. This curve is likely due to the location of the heart and aorta, and to the preponderance of right-handed individuals. In addition to the lateral curves, there are other significant differences between the spinal regions, as described below.

### **Sacral Region**

The *sacral region* consists of five fused sacral vertebrae and three or four fused coccygeal segments. This fused mass is firmly attached with the pelvis. Although there are many disorders of this region, it is not involved greatly with scoliosis.

### **Lumbar Region**

The *lumbar region* consists of five vertebrae (L1-L5), which are the largest and strongest in the spine. The lumbar lordosis is largely the result of wedge shaped discs. The facet joints are primarily oriented perpendicular to the transverse plane, at an angle to the mid-sagittal plane increasing caudally from a value of about  $25^{\circ}$  at L1 to  $55^{\circ}$  at L5 (Fig. C.3A). This orientation enables the lumbar facets to provide effective resistance to axial rotation. The lumbar facets are also significantly curved, which restricts slipping between the inferior and superior processes, and provides further resistance to axial rotation. The lower lumbar facets are also tilted such that the superior facets face cephaladly to a certain degree. This enables them to carry some of the vertical load, which is greatest at the lower levels, and thereby reduce the stress in the disc.

### **Thoracic Region**

The *thoracic region* consists of 12 vertebrae (T1-T12), which gradually change in shape to match the adjoining regions, caudally and cephaladly. The T12 vertebra is very similar to the L1 vertebra, whereas the T1 vertebra is more similar to the cervical vertebrae

than to the other thoracic vertebrae. The size of the vertebrae increases from T1-T12 to accommodate the increasing vertical load, similar to the lumbar vertebrae. The thoracic kyphosis is more the result of wedge shaped vertebrae, as opposed to wedge shaped discs, as in the lumbar region. The facet joints of the thoracic region are significantly different compared with the lumbar region. The superior facets are directed posteriorly, while the inferior facets are directed anteriorly (Fig. C.3B). The left and right facets can thus be considered as small arcs of a circle. As a result, the facet joints in the thoracic region are unable to provide a geometric restraint to axial rotation. They are also angled at about  $60^\circ$  to the transverse plane, which helps to resist extension.

The transverse and spinous processes of the thoracic region also differ from the lumbar region. The spinous processes become longer and more caudally directed. The transverse processes also become longer with an articular process near the tip which articulates with the ribcage. The vertebral bodies of the thoracic region also contain additional articular processes which articulate with the head of the rib. These articular processes, unique to the thoracic vertebrae, are described in further detail in the next section on the ribcage.

### **Cervical Region**

The *cervical region* consists of seven vertebrae (C1-C7), which are the smallest in the spine. The vertebral bodies are significantly broader in the coronal plane. The facet joints are oriented towards the transverse plane to permit easy axial rotation and bending in either plane. The first and second cervical vertebra differ markedly from the others and are also termed the atlas and the axis, respectively. These names reflect their function in providing a junction to the head with maximum mobility.

## **C.4 Ribcage**

The *ribcage* has several important functions. Firstly, it provides a protective barrier for the vital internal organs against traumatic impact. Secondly, it provides attachment points for the trunk musculature, with large moment arms, which allow the muscles to

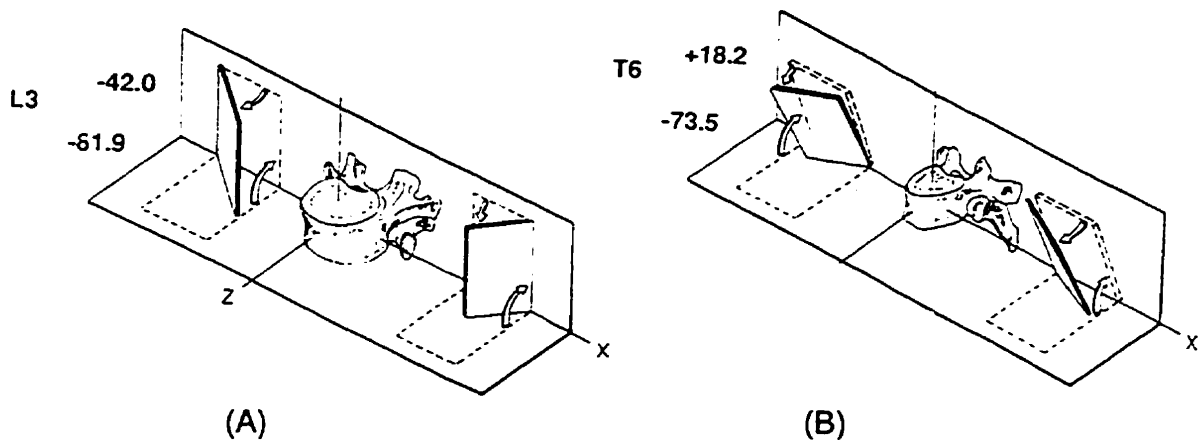


Figure C.3: Typical orientations of the facet joints from two regions of the spine (White and Panjabi, 1990). A) Lumbar facets; B) Thoracic facets.

efficiently move the spine. Thirdly, the ribcage plays an important role in respiration. The ribcage diameter changes substantially with inspiration and expiration helping the lungs to function. Fourthly, the ribcage provides much needed stiffness to the spine during both passive and active situations.

The ribcage is composed of a number of components which together give it its conical shape and establish its function (Fig. C.4). The *ribs* are the main components, with 12 on either side. They are attached to the central *sternum* via the *costal cartilages* which provide a direct attachment for the first seven ribs, termed true ribs. The other five ribs are called false ribs as their tips are not attached directly to the sternum. The ribs are attached to the spinal column via the *costovertebral* and *costotransverse joints*. Spatially, the ribs are inclined to the transverse plane, with the anterior tips being lower. The space between the ribs is termed the *intercostal space*. A more detailed description of these components is presented below.

## Ribs

The *ribs* are long curved arcs of bone which prescribe the basic shape of the ribcage. The *head* of a rib is the swollen proximal end which is formed by two articular facets. The facets, in contact with two successive thoracic vertebrae, form the costovertebral joints.

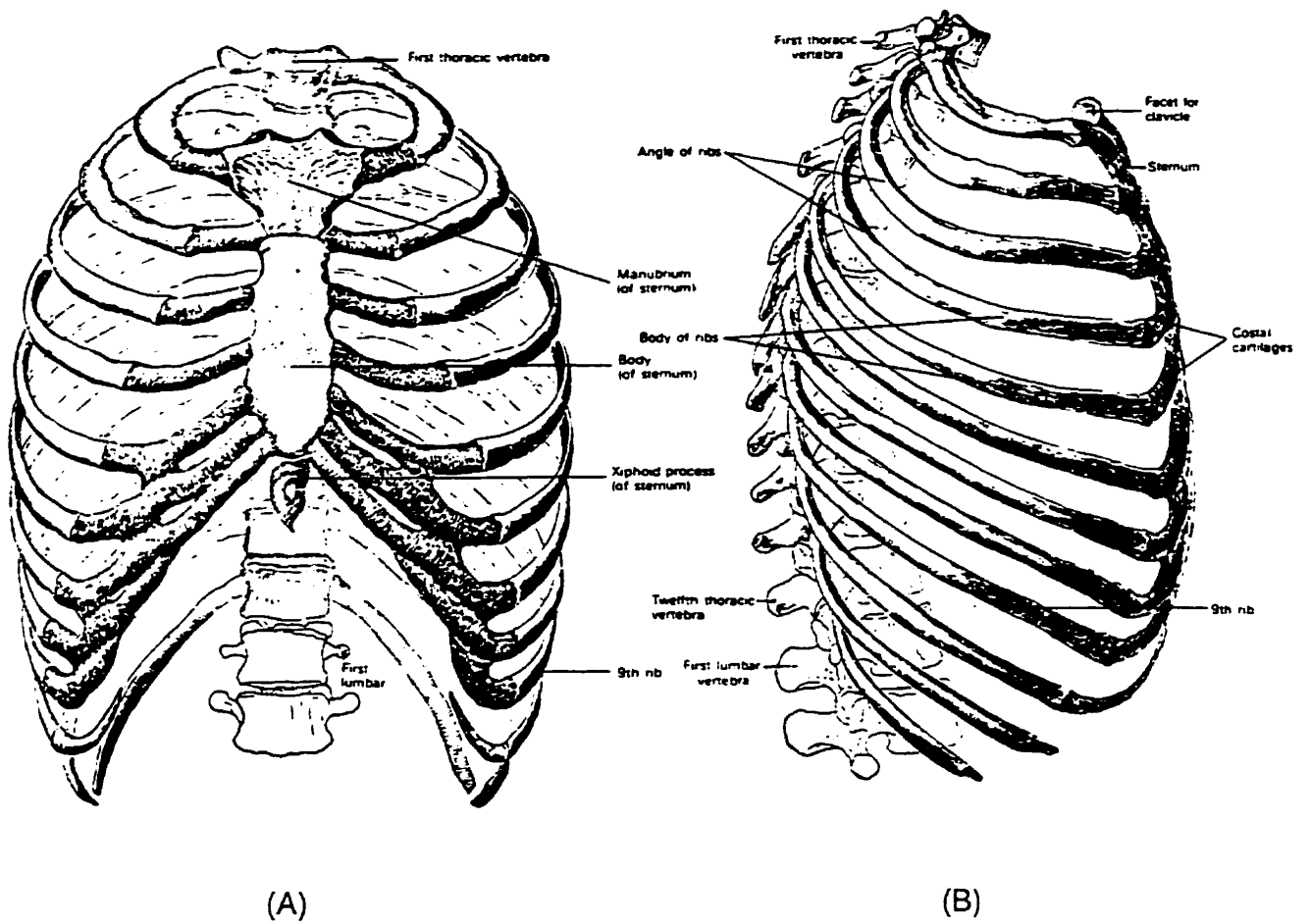


Figure C.4: Typical views of the ribcage devoid of musculature (Grant, 1978). A) Anterior; B) Lateral.

The *neck* is a short segment which extends from the head of the rib to the articulation of the rib with the transverse process at the costotransverse joint. The *tubercle* is located at the postero-inferior point of each rib and articulates with the transverse process of the lower of the two adjacent vertebrae at the given rib level. The *angle* is a sharp curve in the rib found lateral to the tubercle, and marks a change in the rib as it turns anteriorly and the curvature decreases. The *shaft* forms the main body of the rib and extends from the angle to the anterior tip in a smooth arc. The *sternal end* or *anterior tip* of the rib is an oval depression into which the costal cartilage is attached. The cross-section of a rib is more or less elliptical, particularly in the shaft region. The discrepancies from a pure oval form are due to the grooves to which the muscles and ligaments are attached. The rib is composed of a cortical shell which surrounds porous cancellous bone.

The foregoing general description of a rib applies best to ribs 3-9. These ribs are very similar with only changes in their gross dimensions. Rib 7 or 8 is generally the longest. The first rib is unique in that it is much smaller with broad, flat surfaces facing upwards. The second rib is twice the size of the first, and represents a compromise between the first and the other more standard ribs. Rib 10 is unifacetal but otherwise is similar to ribs 3-9. Ribs 11-12 are also unifacetal and are also called "floating ribs", since they do not join with the other ribs and the sternum through the costal cartilages.

## Sternum

The *sternum* or *breastbone* is a broad, flat bone situated in the middle of the anterior wall of the ribcage (Fig. C.4). In the adult, it is composed of three separate portions. The first portion is the *manubrium*, the middle and largest is the *corpus sterni* and the inferior portion is the *xiphoid process*.

## Costal Cartilages

The *costal cartilages* are solid elliptic bars of white hyaline cartilage which join the ribs with the sternum (Fig. C.4). The cartilage can be regarded as an extension of the rib itself. The first seven ribs are directly attached to the sternum via the costal cartilages.

Ribs 8-10 are connected to the lower edge of the cartilage of the cephalad rib. The costal cartilages provide for much of the expansion in ribcage dimensions, as they are much more flexible than the ribs themselves.

The costal cartilages are fitted into the depression in the anterior tips of the ribs. The two are held together by the periosteum, which is the outer layer of dense fibrous tissue which surrounds bone. The junction between the costal cartilage and the rib is termed the *costochondral joint*. This type of joint is termed a *synarthrosis* with no appreciable motion between the rib and cartilage. At the other end of the cartilage, it is joined to the sternum for the first seven ribs at the *costosternal joint*. This joint is an *arthrodial* articulation which permits some gliding between a concave and a convex surface. There are also a number of ligaments which connect the costal cartilage to the sternum.

### **Costovertebral Joint**

The *costovertebral* or *CV joint* is formed by the heads of the ribs and the thoracic vertebrae (Fig. C.5). As mentioned earlier, for ribs 2-9, there are two articulations with each rib head and the upper and lower successive thoracic vertebrae. The other ribs have only a single articulation at the rib head. The costovertebral joints are *arthrodial*, with only a small amount of sliding between the rib and vertebra. The joint is connected by a capsular ligament, an anterior costovertebral ligament which attaches the rib to the vertebra at three parts, and an interarticular ligament which attaches to the intervertebral disc for ribs 2-9.

### **Costotransverse Joint**

The tubercle of a rib is joined to an adjacent transverse process by an *arthrodial* joint termed the *costotransverse* or *CT joint* (Fig. C.5). The joint is connected by the anterior, middle, and posterior portions of the costotransverse ligament and a capsular ligament.

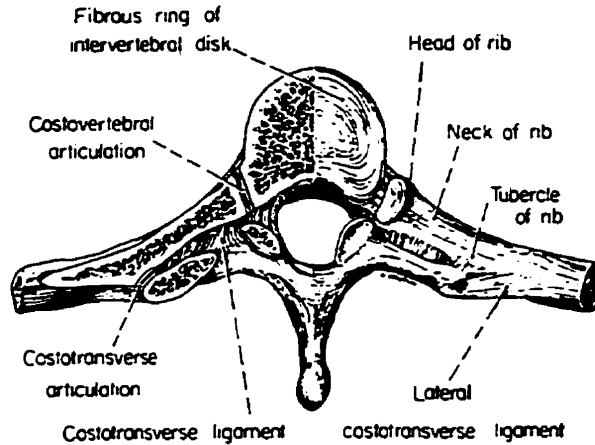


Figure C.5: Transverse view of the costovertebral joint and costotransverse joint (Gray, 1989).

## C.5 Trunk Musculature

The musculature of the trunk is a truly complex system with a very high degree of redundancy. Though there are many muscles of various forms, they can be broadly divided into three groups: *intrinsic*, *extrinsic* and *respiratory*. This division is based on their primary functions, though they are not explicitly confined to these roles.

### Intrinsic

The *intrinsic* category refers to those muscles which are closest to the spinal column (Fig. C.6A). These muscles provide stability to the spinal column and control the local relative movements between the vertebrae. They can be further divided into deep, intermediate and superficial categories depending on their relative location to the spinal column.

### Extrinsic

The *extrinsic* category refers to those muscles which interconnect the spine and ribcage to other parts (Fig. C.6B). In particular, the lumbar spine and ribcage are connected to

the pelvis through a number of muscles. These muscles are again needed for stability, but also are used to activate the large trunk motions of day-to-day activities.

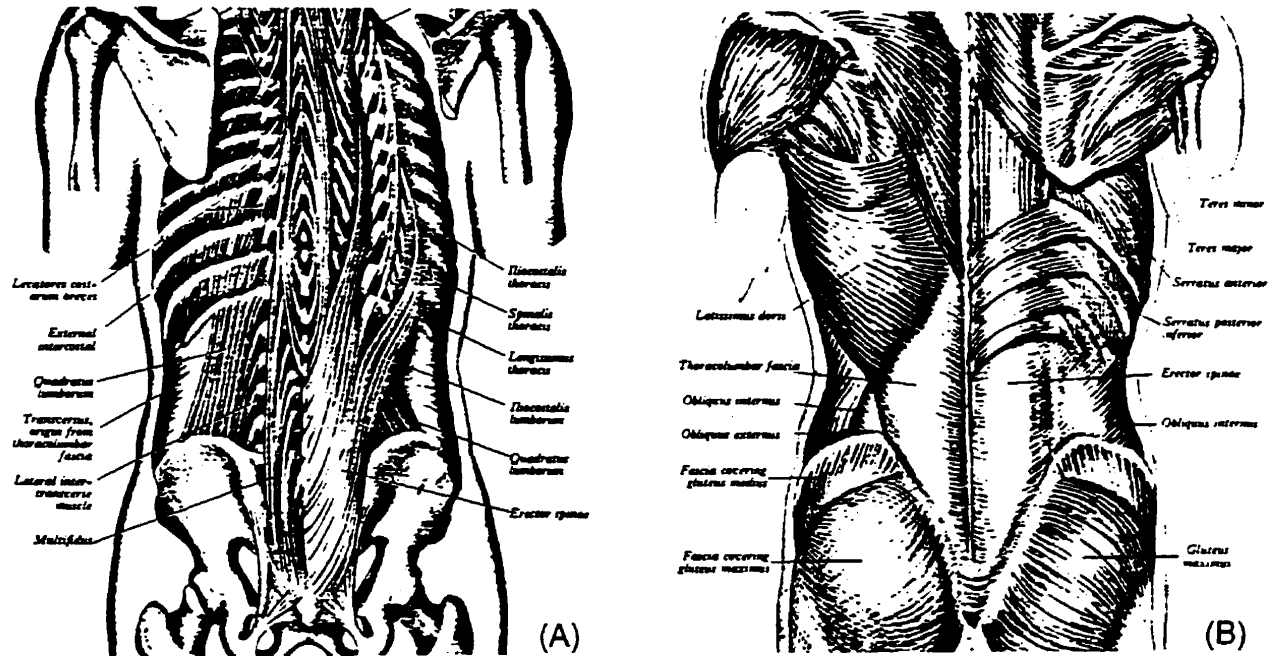


Figure C.6: An illustration of some of the trunk muscles (Gray, 1989). A) Intrinsic; B) Extrinsic.

### Respiratory

The *respiratory* category refers to those muscles which are an integral part of respiration (Fig. C.7A). These muscles are active during both inspiration and expiration and enable the lungs to breath through changes to the volume of the thoracic cavity. During respiration, the ribs undergo a rotation about an axis aligned with the neck of the rib, referred to as the rib neck axis (Fig. C.7B).

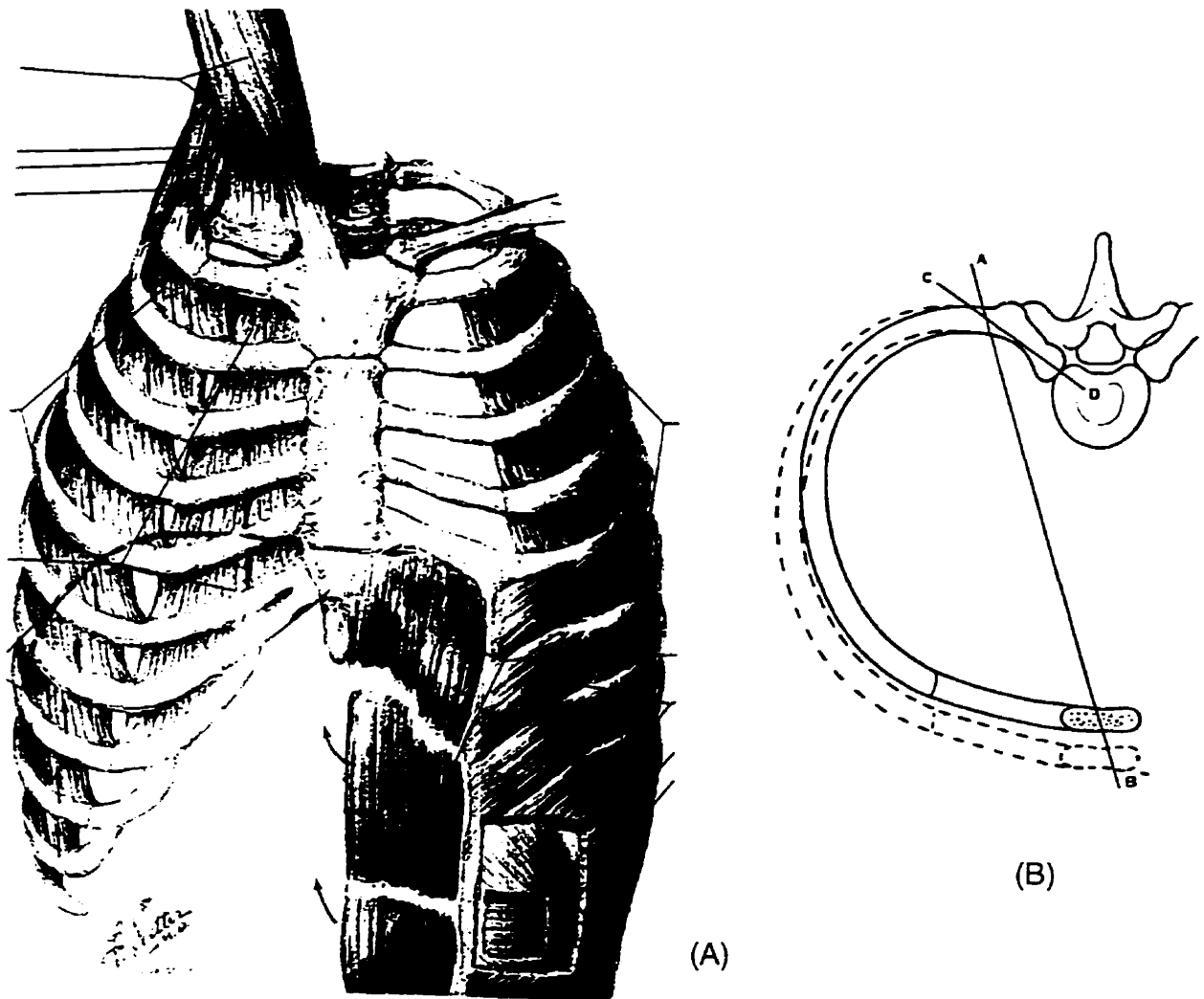


Figure C.7: A) An illustration of some of the respiratory muscles which serve to raise and lower the ribcage structure during respiration (Gray, 1989); B) The rib-neck axis (line C-D), about which the rib rotates during respiration (Woodburne, 1983).

# Appendix D

## Spine Models

In this appendix, various models of the spine, developed for applications other than scoliosis, are reviewed to illustrate the varied engineering techniques which have been employed. To compare the various approaches to the quantitative analysis of the spine, the models are divided into the following groups: Whole Spine, Cervical Spine, Intervertebral Joint and Disc, Multisegmental, Trunk Muscles and Ribcage. A summary of these models is presented in Table D.1. In the sections below, only those models which could potentially be extended to an explicit scoliosis model are discussed in some detail.

### Whole Spine Models

The first models developed to provide substantive quantitative information of spinal mechanics were dynamic models for studying airplane pilot ejections. These were primarily interested in the axial response of the spine. Both discrete and continuum models were used, and damping and viscoelastic effects were also included (Latham, 1957; Hess and Lombard, 1958; Toth, 1967). The next phase of models investigated the spinal response in the sagittal plane, for the study of whiplash and automobile crashes (Orne and Liu, 1971; Soechting and Paslay, 1973; Prasad and King, 1974). Another development in the dynamic analysis of the spine was by Cramer et al (1976). A continuum model of the spine, represented as a curved homogeneous beam-column subject to eccentric inertial loading, was developed. Other detailed models of the whole body dynamics have been recently

developed by Deng and Goldsmith (1987) and by Luo and Goldsmith (1991).

The static behaviour of the whole spine has not been as extensively studied as the dynamic. Lindbeck (1987, 1988) developed a continuum model of the spine, based on an earlier proposal by Hjalmar (1981). The muscle-relaxed spine, from L5 to T8, was modelled as a slender elastic beam. The ribcage was considered as a rigid body. The ability of the model to determine the lateral deflections and curvatures of an asymmetrically loaded spine in the coronal plane was demonstrated. The inclusion of muscular forces in the model was proposed by Hjalmar (1988). A very extensive FEM model of the whole trunk has been proposed by Dietrich et al (1991), but only limited applications were presented.

A recent study by Shirazi-Adl and Parnianpour (1993a) examined the stability of the thoracolumbar spine. The model was similar to the simplified nonlinear FEM of the lumbar spine (Shirazi-Adl and Parnianpour, 1993b), but extended to the whole spine. The ribcage was modelled by increasing the beam element stiffnesses five-fold in the thoracic region. The study was primarily interested in the stability in the sagittal plane with application to the lumbar spine.

### **Cervical Spine Models**

There are also numerous models in the literature which have been used to investigate the cervical spine (McKenzie and Williams, 1971; Belytschko et al. 1976; Reber and Goldsmith, 1979). One of the most comprehensive models was by Williams and Belytschko (1983). A three-dimensional finite element model was developed for transient analysis and validated for both lateral and frontal impacts. More recently, a continuum beam-column has been used to investigate the failure of the cervical spine (Liu and Dai, 1989; Dai and Liu, 1992). The equations of a beam-column subjected to eccentric end loads were developed for small strains and small displacements.

### **Multisegmental Models**

Crisco and Panjabi (1992) modelled the lumbar spine as a collection of five rigid bodies interconnected by angular springs. The buckling load predicted by the model agreed with

experimental results (Crisco et al, 1992) when linear properties were assigned to the springs. Exponentially nonlinear properties were needed to accurately predict the postbuckling behaviour measured experimentally (Crisco et al, 1992). The model was also extended to the thoracolumbar spine to simulate the experiment of Lucas and Bresler (1961). The buckling load predicted by the model was slightly higher than the experimental value and the Euler critical load.

A more extensive FEM model of the lumbar spine was proposed by Shirazi-Adl and Parnianpour (1993b) to study stability. Two types of models were developed. In the first, the discs and ligaments were modelled in fine detail (7155 elements), the facets by contact gap elements, and each vertebra by two beam elements and two rigid bodies to represent the anterior body and the posterior structures. The second model considered each vertebra as a rigid body and each disc as a spatial beam element with appropriately adjusted stiffnesses. The simplified model was developed to investigate a large number of cases to determine values for an appropriate horizontal support and flexion moment to maintain stability. The authors noted that such a parametric analysis was essentially impossible in the detailed model due to the computational costs.

### **Ribcage Models**

Roberts and Chen (1970) developed a three-dimensional finite element model of the thorax to investigate its response to a frontal load. Each rib was modelled by five beam elements with varied properties along the length and between ribs. The costovertebral and costosternal joints were assumed rigid. The displacement of the sternum was found to be reasonable when compared with experimental values.

Another FEM of the thorax was developed by Sundaram and Feng (1977) to study the response when subjected to frontal compressive forces. Two separate models were created. The first was very similar to that of Roberts and Chen (1970), whereas the second incorporated a representation of the internal organs and the passive resistance of certain trunk muscles. The results were discussed in terms of potential injuries due to chest impact.

There are several models developed specifically to study the ribcage during respiration (Jordanoglou, 1970; Saumarez, 1986a,b; Wilson et al, 1987; Kenyon et al, 1991; Loring, 1992). These models were primarily concerned with the kinematics of the ribs and the changes in ribcage volume during respiration.

Table D.1: Summary of spine models to illustrate the various techniques employed. This is only intended as a representative list, and also does not include scoliosis models (See Table 2.1).

STRUCTURE	RESEARCHERS	MODEL TYPE*					APPLICATION
		1	2	3	4	5	
Whole Spine	Latham, 1957	D	L	LE	1-D	DL	Axial impact
	Hess and Lombard, 1958	C	L	LE	1-D	DL	Axial impact
	Toth, 1967	D	L	VE	1-D	DL	Axial impact
	Orne and Liu, 1971	D	NL	VE	2-D	DL	Axial, sagittal impact
	Soechting and Paslay, 1973	C	L	LE	2-D	DL	Sagittal impact
	Panjabi, 1973	D	L	LE	3-D	SL & DL	Proposed model
	Prasad and King, 1974	D	NL	VE	2-D	DL	Sagittal impact
	Cramer et al, 1976	C	NL	LE	2-D	DL	Sagittal impact
	Deng and Goldsmith, 1987	D	NL	VE	3-D	DL	Sagittal impact
	Lindbeck, 1987, 1988	C	L	LE	2-D	SL	Asymmetrical loading in coronal plane
	Hjalmar, 1988	C	L	LE	2-D	ML	Asymmetrical loading in coronal plane
	Dietrich, 1991	FEM	NL	NLE	3-D	ML	Model of muscle stablized trunk
	Luo and Goldsmith, 1991	D	NL	VE	3-D	DL	Sagittal impact
	Shirazi-Adl and Parnianpour, 1993a	FEM	NL	NLEC	3-D	SL	Spine stability
Cervical Spine	McKenzie and Williams, 1971	D	NL	VE	2-D	DL	Whiplash
	Belytschko et al, 1976	FEM	NL	LE	3-D	DL	Whiplash
	Reber and Goldsmith, 1979	D	NL	VE	2-D	DL	Whiplash
	Williams and Belytschko, 1983	FEM	NL	NLE	3-D	DL	Frontal and lateral whiplash
	Liu and Dai, 1989	C	L	LE	2-D	SL	Stability, failure analysis
	Dai and Liu, 1992	C	L	LE	2-D	SL	Stability, failure analysis
Intervertebral Joint	Belytschko et al, 1974	FEM	L	LEO	AX	SL	Disc pathomechanics
	Kulak et al, 1976	FEM	L	NLEO	AX	SL	Disc pathomechanics
	Lin et al, 1978	FEM	L	LEO	3-D	SL	Disc pathomechanics
	Spilker, 1980	FEM	L	LEI	AX	SL	Disc pathomechanics
	Shirazi-Adl et al, 1984, 1986a, 1986b	FEM	NL	NLEC	3-D	SL	Disc pathomechanics
	Spilker et al, 1984	FEM	L	LEI	AX	SL	Disc pathomechanics
	Simon et al, 1985	FEM	NL	PE	AX	CL	Disc pathomechanics
	Ueno and Liu, 1987	FEM	NL	NLEC	3-D	SL	Disc pathomechanics
	Laible et al, 1993,1994	FEM	NL	PE	3-D	CL	Disc pathomechanics

STRUCTURE	RESEARCHERS	MODEL TYPE*					APPLICATION
		1	2	3	4	5	
Multisegmental	Goel et al, 1988	FEM	NL	NLEC	3-D	SL	Spinal instrumentation
	Lavaste et al, 1992	FEM	NL	NLEC	3-D	SL	Spinal instrumentation
	Crisco and Panjabi, 1992	D	NL	NLE	2-D	SL	Euler lumbar stability
	Shirazi-Adl and Parnianpour, 1993b	FEM	NL	NLEC	3-D	SL	Lumbar stability
Trunk musculature	Schultz et al, 1983	O	L	---	3-D	ML	Lumbar loads
	McGill and Norman, 1986	O	L	---	2-D	ML	Lumbar loads
	Bean et al, 1988	O	L	---	3-D	ML	Lumbar loads
	Bergmark, 1989	D	L	L	3-D	ML	Lumbar loads and stability
	McGill, 1992	O	L	---	3-D	ML	Lumbar loads
Ribcage	Jordanoglou, 1970	K	NL	---	3-D	---	Respiration kinematics
	Roberts and Chen, 1970	FEM	L	LE	3-D	SL	Frontal loads
	Sundaram and Feng, 1977	FEM	L	LE	3-D	SL	Frontal loads
	Saumarez, 1986a,b	K&D	NL	---	3-D	SL	Respiration mechanics
	Wilson et al, 1987	K	NL	---	3-D	---	Respiration kinematics
	Kenyon et al, 1991	K	NL	---	3-D	---	Respiration kinematics
	Loring, 1992	FEM	L	LE	3-D	SL	Respiration mechanics

\* The type of model is described by 5 parameters: 1st) D-discrete (springs, dampers and rigid bodies), O-optimization, C-continuum, K-kinematic, FEM-finite element model; 2nd) L-geometric linear, NL-geometric nonlinear; 3rd) LE-elastic, VE-viscoelastic, LEO-linear elastic orthotropic, LEI-linear elastic isotropic, NLEC-nonlinear elastic composite, PE-poroelastic; 4th) 1-D-one dimensional, 2-D-two dimensional, 3-D-three dimensional, AX-axisymmetric; 5th) DL-dynamic loads, MI-muscle loads; SL-static loads, CL-creep loads; ---: Not applicable.

# Appendix E

## Error Analysis of the Beam-Column Model

During the derivation of the governing equations of the spatial beam-column model (Chapter 3), several assumptions were made regarding the magnitude of certain terms in order to simplify the equations. In the present appendix, these assumptions are assessed in terms of the magnitude of errors that could be expected.

The present spatial beam-column was developed for the situation referred to as small strains and moderate rotations. This assumption was first implemented in the rotation matrix,  $C_{ij}^*$ , given in equation (3.35), which related the undeformed system,  $\hat{e}_i$ , to the deformed system,  $\hat{e}_i^*$ . In this matrix terms of  $\mathcal{O}(\epsilon^2)$  were neglected compared to terms of  $\mathcal{O}(1)$ , however, terms of  $\mathcal{O}(\epsilon^2)$  were retained compared to terms of  $\mathcal{O}(\epsilon)$ . In other words, terms of  $\mathcal{O}(\epsilon)$  were not neglected compared to the terms of  $\mathcal{O}(1)$ . Therefore, the ordering scheme was as follows:

$$\begin{aligned}d_1 & \text{ --- } \mathcal{O}(\epsilon^2) \\d_2 & \text{ --- } \mathcal{O}(\epsilon) \\d_3 & \text{ --- } \mathcal{O}(\epsilon) \\ \theta & \text{ --- } \mathcal{O}(\epsilon)\end{aligned}\tag{E.1}$$

and consequently,  $d_1$ ,  $d_2^2$ ,  $d_3^2$  and  $\theta^2$  were neglected compared to unity. This situation was referred to as moderate rotations, since nonlinear terms involving products of the rotations were retained in the rotation matrix. In neglecting  $d_1$ ,  $d_2^2$ ,  $d_3^2$  and  $\theta^2$  compared to unity, this also implied small strains, which was implemented in equation (3.55).

To assess the potential error of neglecting second order terms, and to illustrate the difference between linear and moderate rotations, consider an error of 10% as acceptable. In a linear theory, the axial rotation,  $\theta$ , and the bending rotations,  $d_2$  and  $d_3$ , would be neglected compared to unity. Consequently,  $\theta$ ,  $d_2$  and  $d_3$  must be less than 0.1 so that they can be dropped from the equations with an error of less than 10%. On the other hand, for moderate rotations, it was the products of rotations or second order terms that were neglected compared to unity. Therefore,  $\theta^2$ ,  $d_2^2$  and  $d_3^2$  must be less than 0.1 for moderate rotation theory to be valid at an error of less than 10%. In other words,  $\theta$ ,  $d_2$  and  $d_3$  must be less than  $\sqrt{0.1}$ .

The implications of this difference are very pertinent for a mild scoliosis. For the linear theory the maximum change in axial rotation must be less than 0.1 rad or about  $6^\circ$ , whereas for the moderate rotation theory, the change in axial rotation need only be less  $\sqrt{0.1}$  rad or about  $18^\circ$ , for a 10% error. Alternatively, with moderate rotation theory, a change in axial rotation of  $6^\circ$  can be predicted with an error of less than 1%, whereas the linear theory would have an error of 10%. The Cobb angle is essentially the inclusive angle between the normals to the tangents at the inflection points of the scoliotic curve, viewed in the coronal plane. Therefore, the Cobb angle is proportional to  $d_2$  and a change about  $6^\circ$  can be adequately predicted by a linear model theory. For moderate rotations, however, a change in Cobb angle of  $\sqrt{0.1}$  or about  $18^\circ$  can be predicted with an error of less than 10%.

## Appendix F

# Components of the Main Governing Equations in Matrix Form

The four governing equations are best expressed in a compact matrix form (see equation 3.108). In the present appendix, the components of these matrices are presented. The governing equations in matrix form are as follows:

$$\begin{aligned} & [M_4] \{t\}_{.1111} + [M_3] \{t\}_{.111} + [ [M_2] + [AM_2] ] \{t\}_{.11} \\ & + [ [M_1] + [AM_1] ] \{t\}_{.1} + [ [M_0] + [AM_0] ] \{t\} = \{AM_c\} \end{aligned} \quad (\text{F.1})$$

The nonzero components of these matrices are listed in the following pages.

### Matrix $M_4$

$$\begin{aligned}
 m_{22}^4 &= \mathcal{U}_1 \\
 m_{23}^4 &= \mathcal{U}_2^{N\mathcal{L}} \theta \\
 m_{32}^4 &= \mathcal{V}_1 \\
 m_{33}^4 &= \mathcal{V}_2^{N\mathcal{L}} \theta
 \end{aligned} \tag{F.2}$$

### Matrix $M_3$

$$\begin{aligned}
 m_{22}^2 &= \mathcal{U}\mathcal{N}_4^{N\mathcal{L}} N v_{.1} \\
 m_{23}^3 &= \mathcal{U}_3 + \mathcal{U}_3^{N\mathcal{L}} \theta_{.1} \\
 m_{32}^3 &= \mathcal{V}_3 + \mathcal{V}\mathcal{N}_3^{N\mathcal{L}} N u_{.1} + \mathcal{V}_3^{N\mathcal{L}} \theta_{.1}
 \end{aligned} \tag{F.3}$$

### Matrix $M_2$

$$\begin{aligned}
 m_{22}^2 &= \mathcal{U}\mathcal{N}_5 N \\
 m_{23}^2 &= \mathcal{U}_6 \\
 m_{24}^2 &= \mathcal{U}_7 + \mathcal{U}\mathcal{N}_7 N + \mathcal{U}_7^{N\mathcal{L}} v_{.11} \\
 m_{31}^2 &= \mathcal{V}\mathcal{N}_{12}^{PP} \\
 m_{32}^2 &= \mathcal{V}_4 + \mathcal{V}\mathcal{N}_4 N + \mathcal{V}\mathcal{N}_4^{P,N\mathcal{L}} N_{.1} u_{.1} \\
 m_{33}^2 &= \mathcal{V}\mathcal{N}_5 N \\
 m_{34}^2 &= \mathcal{V}_6 + \mathcal{V}_6^{N\mathcal{L}} u_{.11} \\
 m_{42}^2 &= \mathcal{T}_2 + \mathcal{T}\mathcal{N}_2 N + \mathcal{T}_2^{N\mathcal{L}} v_{.11} \\
 m_{43}^2 &= \mathcal{T}_3 + \mathcal{T}\mathcal{N}_3^{N\mathcal{L}} N \theta \\
 m_{44}^2 &= \mathcal{T}_1
 \end{aligned} \tag{F.4}$$

**Matrix  $M_1$**

$$\begin{aligned}
 m_{21}^1 &= \mathcal{U}\mathcal{N}_{13}^{\mathcal{P}} \\
 m_{22}^1 &= \mathcal{U}\mathcal{N}_8 N + \mathcal{U}\mathcal{N}_8^{\mathcal{P}} N_{,1} \\
 m_{23}^1 &= \mathcal{U}_9 + \mathcal{U}\mathcal{N}_9 N + \mathcal{U}\mathcal{N}_9^{\mathcal{P}} N_{,1} + \mathcal{U}\mathcal{N}_9^{\mathcal{PPNL}} N_{,11} u_{,1} + \mathcal{U}\mathcal{N}_9^{\mathcal{PNL}} N_{,1} u_{,11} \\
 m_{24}^1 &= \mathcal{U}_{10} + \mathcal{U}\mathcal{N}_{10}^{\mathcal{P}} N_{,1} \\
 m_{32}^1 &= \mathcal{V}_7 + \mathcal{V}\mathcal{N}_7 N \\
 m_{33}^1 &= \mathcal{V}\mathcal{N}_8^{\mathcal{P}} N_{,1} \\
 m_{34}^1 &= \mathcal{V}_9 + \mathcal{V}\mathcal{N}_9 N \\
 m_{42}^1 &= \mathcal{T}_4 \\
 m_{43}^1 &= \mathcal{T}_5 + \mathcal{T}\mathcal{N}_5 N + \mathcal{T}_5^{\mathcal{NL}} u_{,111}
 \end{aligned} \tag{F.5}$$

**Matrix  $M_0$**

$$\begin{aligned}
 m_{21}^0 &= \mathcal{U}\mathcal{N}_{13} \\
 m_{23}^0 &= \mathcal{U}_{11} + \mathcal{U}\mathcal{N}_{11}^{\mathcal{P}} N_{,1} + \mathcal{U}\mathcal{N}_{11} N \\
 m_{24}^0 &= \mathcal{U}_{12} + \mathcal{U}\mathcal{N}_{12}^{\mathcal{PP}} N_{,11} \\
 m_{31}^0 &= \mathcal{V}\mathcal{N}_{12} \\
 m_{32}^0 &= \mathcal{V}_{10} + \mathcal{V}\mathcal{N}_{10} N + \mathcal{V}\mathcal{N}_{10}^{\mathcal{P}} N_{,1} \\
 m_{34}^0 &= \mathcal{V}_{11} + \mathcal{V}\mathcal{N}_{11} N + \mathcal{V}\mathcal{N}_{11}^{\mathcal{P}} N_{,1} \\
 m_{41}^0 &= \mathcal{T}\mathcal{N}_9 \\
 m_{42}^0 &= \mathcal{T}\mathcal{N}_6 N \\
 m_{43}^0 &= \mathcal{T}\mathcal{N}_7 N \\
 m_{44}^0 &= \mathcal{T}\mathcal{N}_8 N
 \end{aligned} \tag{F.6}$$

Matrix  $AM_2$

$$am_{22}^2 = ACU_1$$

$$am_{23}^2 = ACU_2$$

$$am_{32}^2 = ALCV_1$$

$$am_{33}^2 = ALCV_2$$

Matrix  $AM_1$

$$am_{22}^1 = ACU_3$$

$$am_{23}^1 = ACU_4$$

$$am_{24}^1 = ACU_5$$

$$am_{32}^1 = ALCV_3$$

$$am_{33}^1 = ALCV_4$$

$$am_{34}^1 = ALCV_5$$

$$am_{42}^1 = ACT_1$$

$$am_{43}^1 = ACT_2$$

Matrix  $AM_0$

$$am_{22}^0 = ACU_6$$

$$am_{23}^0 = ACU_7$$

$$am_{24}^0 = ACU_8$$

$$am_{32}^0 = ALCV_6$$

$$am_{33}^0 = ALCV_7$$

$$am_{34}^0 = ALCV_8$$

$$am_{42}^0 = ACT_3$$

$$am_{43}^0 = ACT_4$$

$$am_{44}^0 = ACT_5$$

Array  $AM_c$

$$am_2^c = -ACU_9$$

$$am_3^c = -ALCV_9$$

$$am_4^c = -ACT_6$$

(F.7)

Components of the "U equation".

$$U_1 = EI_{\eta\eta_0}$$

$$UN_2^{NL} = EI_{\eta\eta_0} - EI_{\xi\xi_0}$$

$$U_3 = -2(EI_{\xi\xi_0} + EI_{\eta\eta_0})k_\zeta \quad UN_3^{NL} = 2EI_{\eta\eta_0} - 2EI_{\xi\xi_0} - GJ$$

$$UN_4^{NL} = \eta_0$$

$$UN_5 = k_\xi \eta_0 - 1$$

$$U_6 = -(5EI_{\eta\eta_0} + EI_{\xi\xi_0})k_{\zeta,1}$$

$$U_7 = -(EI_{\eta\eta_0} + GJ)k_\xi \quad UN_7^{NL} = EI_{\eta\eta_0} - EI_{\xi\xi_0} - 2GJ \quad UN_7 = \eta_0$$

$$UN_8 = \eta_0 k_{\xi,1}$$

$$UN_8^P = k_\xi \eta_0 - 1$$

$$U_9 = -4EI_{\eta\eta_0}k_{\zeta,11}$$

$$UN_9 = \eta_0 k_{\eta,1} + 2k_\zeta$$

$$UN_9^P = 2k_\eta \eta_0$$

$$UN_9^{P,NL} = \eta_0$$

$$UN_9^{PP,NL} = \eta_0$$

$$U_{10} = -(2EI_{\eta\eta_0} + GJ)k_{\xi,1}$$

$$UN_{10}^P = 2\eta_0$$

$$U_{11} = -EI_{\eta\eta_0}k_{\zeta,111}$$

$$UN_{11} = k_{\zeta,1}$$

$$U_{12} = -EI_{\eta\eta_0}k_{\xi,11}$$

$$UN_{12}^{PP} = \eta_0$$

$$UN_{13} = \eta_0 k_{\zeta,1} - k_\eta$$

$$UN_{13}^P = 2k_\zeta \eta_0$$

Components of the "V equation".

$$\mathcal{V}_1 = -EI_{\xi\xi_0}$$

$$\mathcal{V}_2^{NL} = EI_{\xi\xi_0} - EI_{\eta\eta_0}$$

$$\mathcal{V}_3 = -2(EI_{\xi\xi_0} + EI_{\eta\eta_0})k_\zeta$$

$$\mathcal{V}_3^{NL} = 2EI_{\xi\xi_0} - 2EI_{\eta\eta_0} + GJ$$

$$\mathcal{VN}_3^{NL} = \eta_0$$

$$\mathcal{V}_4 = -(5EI_{\xi\xi_0} + EI_{\eta\eta_0})k_{\zeta,1}$$

$$\mathcal{VN}_4 = -\eta_0 k_\eta$$

$$\mathcal{VN}_4^{PNL} = -\eta_0$$

$$\mathcal{VN}_5 = 1$$

$$\mathcal{V}_6 = (EI_{\xi\xi_0} + GJ)k_\eta$$

$$\mathcal{V}_6^{NL} = EI_{\xi\xi_0} - EI_{\eta\eta_0} + 2GJ$$

$$\mathcal{V}_7 = -4EI_{\xi\xi_0}k_{\zeta,11}$$

$$\mathcal{VN}_7 = 2k_\zeta$$

$$\mathcal{V}_9 = (2EI_{\xi\xi_0} + GJ)k_{\eta,1}$$

$$\mathcal{VN}_8^P = 1 + \eta_0 k_\xi$$

$$\mathcal{V}_{10} = -EI_{\xi\xi_0}k_{\zeta,111}$$

$$\mathcal{VN}_9 = -2\eta_0 k_\zeta$$

$$\mathcal{VN}_{10} = k_{\zeta,1}$$

$$\mathcal{V}_{11} = EI_{\xi\xi_0}k_{\eta,11}$$

$$\mathcal{VN}_{10}^P = k_\zeta$$

$$\mathcal{VN}_{11} = -\eta_0 k_{\zeta,1}$$

$$\mathcal{VN}_{11}^P = -2k_\zeta \eta_0$$

$$\mathcal{VN}_{12}^{PP} = \eta_0$$

$$\mathcal{VN}_{12} = -(k_\xi + \eta_0 k_\zeta^2)$$

(F.9)

Components of the “ $\theta$  equation”.

$$T_1 = GJ$$

$$T_2 = (GJ + EI_{\eta\eta_0}) k_\xi$$

$$T_3 = (GJ + EI_{\xi\xi_0}) k_\eta$$

$$T_4 = GJ k_{\xi,1}$$

$$T_5 = GJ k_{\eta,1}$$

$$T_2^{N^L} = GJ + EI_{\xi\xi_0} - EI_{\eta\eta_0}$$

$$T_5^{N^L} = GJ$$

$$TN_2 = -\eta_0$$

$$TN_3^{N^L} = -\eta_0$$

$$TN_5 = 2k_\zeta \eta_0 \quad (F.10)$$

$$TN_6 = k_\zeta^2 \eta_0$$

$$TN_7 = k_{\zeta,1} \eta_0$$

$$TN_8 = k_\xi \eta_0$$

$$TN_9 = -k_\eta \eta_0$$

Components of the “ $U$  load equation”.

$$\begin{aligned}
 ACU_1 &= R_{61} \\
 ACU_2 &= R_{62} \\
 ACU_3 &= D_{61} + R_{61.1} + R_{51}k_\zeta - R_{61}k_\eta u_{,1} - R_{41.1}v_{,1} - I_6k_\eta \\
 ACU_4 &= D_{62} + R_{62.1} + R_{52}k_\zeta + (R_{52}k_\eta - R_{42.1}) v_{,1} + I_5k_\eta - I_{4.1} \\
 ACU_5 &= D_{63} - D_{43}v_{,1} - D_{43}k_\zeta u \\
 ACU_6 &= D_{61.1} - D_{21} + D_{51}k_\zeta + D_{51}k_\eta v_{,1} - I_{4.1}k_\zeta \\
 ACU_7 &= D_{62.1} - D_{22} + D_{52}k_\zeta - D_{62}k_\eta u_{,1} \\
 ACU_8 &= D_{63.1} + D_{53}k_\zeta - D_{63}k_\eta u_{,1} + (D_{53}k_\eta - D_{43.1}) v_{,1} - D_{43.1}k_\zeta u \\
 ACU_9 &= -I_2 + I_{6.1} + I_5k_\zeta
 \end{aligned} \tag{F.11}$$

Components of the “ $V$  load equation”.

$$\begin{aligned}
 ACV_1 &= R_{51} \\
 ACV_2 &= R_{52} \\
 ACV_3 &= D_{51} + R_{51.1} - R_{61}k_\zeta - (R_{61}k_\xi + R_{41.1}) u_{,1} - I_6k_\xi + I_{4.1} \\
 ACV_4 &= D_{52} + R_{52.1} - R_{62}k_\zeta + R_{52}k_\xi v_{,1} - R_{42.1}u_{,1} + I_5k_\xi \\
 ACV_5 &= D_{53} - D_{43}u_{,1} + D_{43}k_\zeta v \\
 ACV_6 &= D_{31} + D_{51.1} - D_{61}k_\zeta + D_{51}k_\xi v_{,1} \\
 ACV_7 &= D_{32} + D_{52.1} - D_{62}k_\zeta + D_{62}k_\xi u_{,1} + I_{4.1}k_\zeta \\
 ACV_8 &= D_{53.1} - D_{63}k_\zeta + (D_{53}k_\xi - D_{43.1}) u_{,1} + D_{53}k_\xi v_{,1} + D_{43.1}k_\zeta v \\
 ACV_9 &= I_3 + I_{5.1} - I_6k_\zeta
 \end{aligned} \tag{F.12}$$

Components of the “ $\theta$  load equation”.

$$ACT_1 = R_{51}u_{.1} + R_{61}v_{.1} + R_{61}k_{\zeta}u - R_{51}k_{\zeta}v + R_{41} + I_5 + W_5$$

$$ACT_2 = R_{52}u_{.1} + R_{62}v_{.1} + R_{62}k_{\zeta}u - R_{52}k_{\zeta}v + R_{42} + I_6 + W_6$$

$$ACT_3 = D_{51}u_{.1} + D_{61}v_{.1} + D_{61}k_{\zeta}u - D_{51}k_{\zeta}v + D_{41} + (I_6 + W_6)k_{\zeta}$$

$$ACT_4 = D_{52}u_{.1} + D_{62}v_{.1} + D_{62}k_{\zeta}u - D_{52}k_{\zeta}v + D_{42} - (I_5 + W_5)k_{\zeta}$$

$$ACT_5 = D_{53}u_{.1} + D_{63}v_{.1} + D_{63}k_{\zeta}u - D_{53}k_{\zeta}v + D_{43}$$

$$ACT_6 = I_4 + W_4$$

(F.13)

## Appendix G

# Matrix Components for the Ribcage Loads

In the present appendix, the components of the matrices for the ribcage loads are presented (see equation 4.27).

$$\begin{Bmatrix} f_1 \\ f_2 \\ f_3 \\ m_1 \\ m_2 \\ m_3 \end{Bmatrix} = [\mathcal{R}] \begin{Bmatrix} u_{,1} \\ u_{,1} \end{Bmatrix} + [\mathcal{D}] \begin{Bmatrix} u \\ v \\ \theta \end{Bmatrix} + \{ \mathcal{I} \} \quad (\text{G.1})$$

$$\begin{aligned}
\mathcal{R}_{11} &= -k_{15}^o u_{0,1} + k_{16}^o v_{0,1} u_{0,1} \\
\mathcal{R}_{12} &= +k_{15}^o \theta_0 u_{0,1} + k_{24}^o v_{0,1} \\
\mathcal{R}_{21} &= -k_{15}^o + k_{16}^o v_{0,1} + k_{24}^o \theta_0^2 \\
\mathcal{R}_{22} &= +k_{15}^o \theta_0 + k_{24}^o \theta_0 \\
\mathcal{R}_{31} &= +k_{15}^o (\theta_0 + u_{0,1} v_{0,1}) - k_{16}^o v_{0,1} (\theta_0 + u_{0,1} v_{0,1}) \\
\mathcal{R}_{32} &= -k_{15}^o \theta_0 (\theta_0 + u_{0,1} v_{0,1}) + k_{24}^o \\
\mathcal{R}_{41} &= -k_{65}^o + k_{66}^o v_{0,1} + k_{44}^o \theta_0 u_{0,1} + k_{55}^o v_{0,1} + k_{56}^o v_{0,1}^2 \\
\mathcal{R}_{42} &= +k_{65}^o \theta_0 + k_{44}^o u_{0,1} - k_{55}^o \theta_0 v_{0,1} \\
\mathcal{R}_{51} &= +k_{65}^o (u_{0,1} + \theta_0 v_{0,1}) - k_{66}^o v_{0,1} (u_{0,1} + \theta_0 v_{0,1}) + k_{44}^o \theta_0 - k_{55}^o \theta_0 + k_{56}^o v_{0,1} \theta_0 \\
\mathcal{R}_{52} &= -k_{65}^o \theta_0 (u_{0,1} + \theta_0 v_{0,1}) - k_{44}^o - k_{55}^o \theta_0^2 \\
\mathcal{R}_{61} &= +k_{65}^o (v_{0,1} - \theta_0 u_{0,1}) - k_{66}^o v_{0,1} (v_{0,1} - \theta_0 u_{0,1}) - k_{44}^o \theta_0 (\theta_0 + u_{0,1} v_{0,1}) - k_{55}^o + k_{56}^o v_{0,1} \\
\mathcal{R}_{62} &= -k_{65}^o \theta_0 (v_{0,1} - \theta_0 u_{0,1}) - k_{44}^o (\theta_0 + u_{0,1} v_{0,1}) + k_{55}^o \theta_0
\end{aligned} \tag{G.2}$$

$$\begin{aligned}
D_{11} &= -k_{11}^o u_{0,1} - k_{22}^o \theta_0 v_{0,1} + k_{24}^o k_\zeta v_{0,1} \\
D_{12} &= +k_{11}^o \theta_0 u_{0,1} + k_{15}^o k_\zeta u_{0,1} - k_{22}^o v_{0,1} \\
D_{13} &= -k_{16}^o u_{0,1} \\
D_{21} &= -k_{11}^o - k_{22}^o \theta_0^2 + k_{24}^o k_\zeta \theta_0 \\
D_{22} &= +k_{11}^o \theta_0 + k_{15}^o k_\zeta - k_{22}^o \theta_0 \\
D_{23} &= -k_{16}^o \\
D_{31} &= +k_{11}^o (\theta_0 + u_{0,1} v_{0,1}) - k_{22}^o \theta_0 + k_{24}^o k_\zeta \\
D_{32} &= -k_{11}^o \theta_0 (\theta_0 + u_{0,1} v_{0,1}) - k_{15}^o k_\zeta (\theta_0 + u_{0,1} v_{0,1}) - k_{22}^o \\
D_{33} &= +k_{16}^o (\theta_0 + u_{0,1} v_{0,1}) \\
D_{41} &= -k_{61}^o - k_{42}^o \theta_0 u_{0,1} + k_{44}^o k_\zeta u_{0,1} - k_{51}^o v_{0,1} \\
D_{42} &= +k_{61}^o \theta_0 + k_{65}^o k_\zeta - k_{42}^o u_{0,1} + k_{51}^o \theta_0 v_{0,1} + k_{55}^o k_\zeta v_{0,1} \\
D_{43} &= -k_{66}^o - k_{56}^o v_{0,1} \\
D_{51} &= +k_{61}^o (u_{0,1} + \theta_0 v_{0,1}) - k_{42}^o \theta_0 + k_{44}^o k_\zeta - k_{51}^o \theta_0 \\
D_{52} &= -k_{61}^o \theta_0 (u_{0,1} + \theta_0 v_{0,1}) - k_{65}^o k_\zeta (u_{0,1} + \theta_0 v_{0,1}) + k_{42}^o - k_{51}^o \theta_0^2 - k_{55}^o k_\zeta \theta_0 \\
D_{53} &= +k_{66}^o (u_{0,1} + \theta_0 v_{0,1}) - k_{56}^o \theta_0 \\
D_{61} &= +k_{61}^o (v_{0,1} - \theta_0 u_{0,1}) + k_{42}^o \theta_0 (\theta_0 + u_{0,1} v_{0,1}) - k_{44}^o k_\zeta (\theta_0 + u_{0,1} v_{0,1}) - k_{51}^o \\
D_{62} &= -k_{61}^o \theta_0 (v_{0,1} - \theta_0 u_{0,1}) - k_{65}^o k_\zeta (v_{0,1} - \theta_0 u_{0,1}) + k_{42}^o (\theta_0 + u_{0,1} v_{0,1}) + k_{51}^o \theta_0 + k_{55}^o k_\zeta \\
D_{63} &= +k_{66}^o (v_{0,1} - \theta_0 u_{0,1}) - k_{56}^o
\end{aligned} \tag{G.3}$$

$$\begin{aligned}
\mathcal{I}_1 &= -k_{11}^o u_0 u_{0,1} - k_{15}^o u_{0,1} u_{0,1} - k_{16}^o \theta_0 u_{0,1} - k_{22}^o v_0 v_{0,1} + k_{24}^o v_{0,1} v_{0,1} \\
\mathcal{I}_2 &= -k_{11}^o u_0 - k_{15}^o u_{0,1} - k_{16}^o \theta_0 - k_{22}^o v_0 \theta_0 + k_{24}^o v_{0,1} \theta_0 \\
\mathcal{I}_3 &= +k_{11}^o u_0 (\theta_0 + u_{0,1} v_{0,1}) + k_{15}^o u_{0,1} (\theta_0 + u_{0,1} v_{0,1}) \\
&\quad + k_{16}^o \theta_0 (\theta_0 + u_{0,1} v_{0,1}) \\
\mathcal{I}_4 &= -k_{61}^o u_0 - k_{65}^o u_{0,1} - k_{66}^o \theta_0 - k_{42}^o v_0 u_{0,1} + k_{44}^o v_{0,1} u_{0,1} \\
&\quad - k_{51}^o u_0 v_{0,1} - k_{55}^o u_{0,1} v_{0,1} - k_{56}^o \theta_0 v_{0,1} \\
\mathcal{I}_5 &= +k_{61}^o u_0 (u_{0,1} + \theta_0 v_{0,1}) + k_{65}^o u_{0,1} (u_{0,1} + \theta_0 v_{0,1}) + k_{66}^o \theta_0 (u_{0,1} + \theta_0 v_{0,1}) \\
&\quad - k_{42}^o v_0 + k_{44}^o v_{0,1} - k_{51}^o u_0 \theta_0 - k_{55}^o u_{0,1} \theta_0 - k_{56}^o \theta_0^2 \\
\mathcal{I}_6 &= +k_{61}^o u_0 (v_{0,1} - \theta_0 u_{0,1}) + k_{65}^o u_{0,1} (v_{0,1} - \theta_0 u_{0,1}) + k_{66}^o \theta_0 (v_{0,1} - \theta_0 u_{0,1}) \\
&\quad + k_{42}^o v_0 (\theta_0 + u_{0,1} v_{0,1}) - k_{44}^o v_{0,1} (\theta_0 + u_{0,1} v_{0,1}) - k_{51}^o u_0 - k_{55}^o u_{0,1} - k_{56}^o \theta_0
\end{aligned} \tag{G.4}$$

# Appendix H

## Components of the Solution Matrix

In the present appendix, the components of the matrices for the solution of the two systems of 1<sup>st</sup> order equations (see equations (3.114) and (3.116)) are presented. The main equations from these matrices are here repeated, where the variables  $N_1$ ,  $N_2$ ,  $u_1$ ,  $u_2$ ,  $u_3$ ,  $u_4$ ,  $v_1$ ,  $v_2$ ,  $v_3$ ,  $v_4$ ,  $\theta_1$ ,  $\theta_2$  are defined in equations (3.113) and (3.115)

$$\begin{aligned}N_{2,1} &= A_1 N_1 + A_2 N_2 + A_3 \\u_{4,1} &= B_1 u_1 + B_2 u_2 + B_3 u_3 + B_4 u_4 + B_5 v_1 + B_6 v_2 + B_7 v_3 \\&\quad + B_8 v_4 + B_9 \theta_1 + B_{10} \theta_2 + B_{11} \\v_{4,1} &= C_1 u_1 + C_2 u_2 + C_3 u_3 + C_4 u_4 + C_5 v_1 + C_6 v_2 + C_7 v_3 \\&\quad + C_8 v_4 + C_9 \theta_1 + C_{10} \theta_2 + C_{11} \\\theta_{2,1} &= D_1 u_1 + D_2 u_2 + D_3 u_3 + D_4 v_1 + D_5 v_2 + D_6 v_3 \\&\quad + D_7 \theta_1 + D_8 \theta_2 + D_9\end{aligned}\tag{H.1}$$

The coefficients of these equations are now listed. It should be noted that these coefficients are a function of terms presented in Appendices F and G.

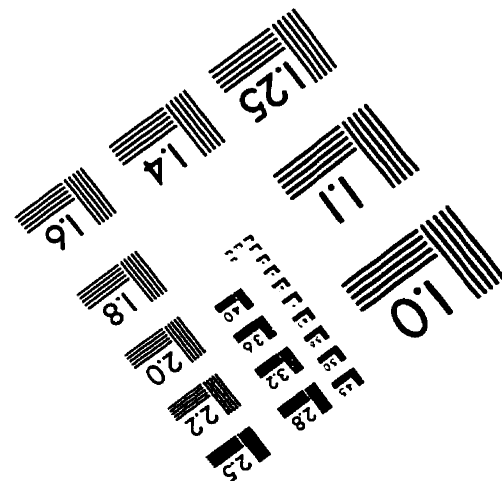
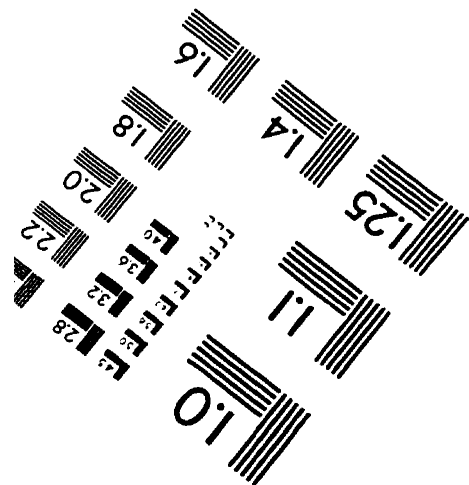
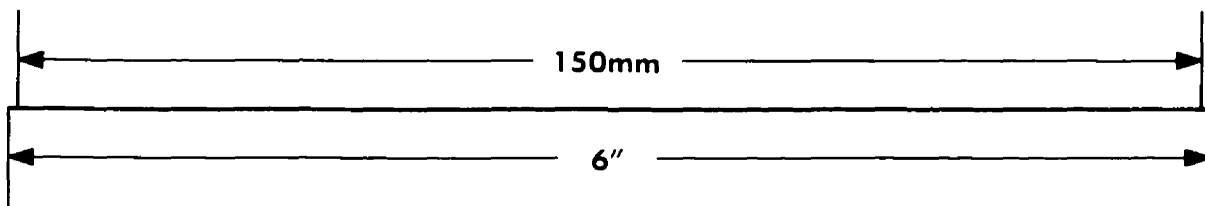
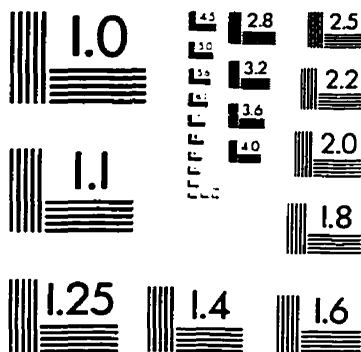
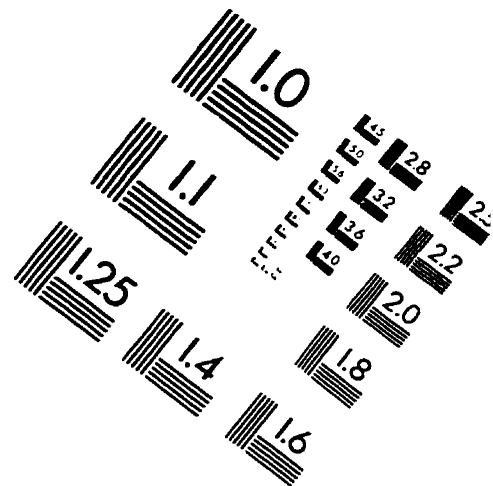
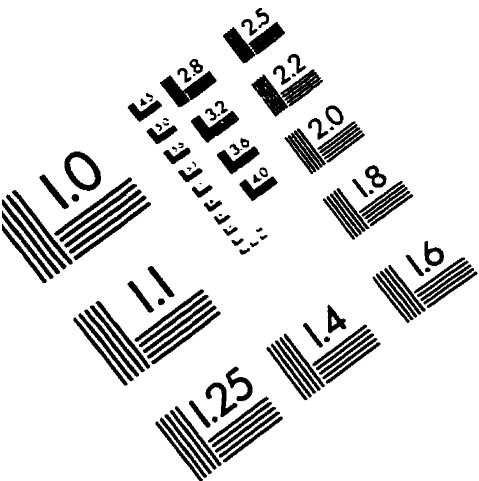
$$\begin{aligned}
B'_1 &= -am_{22}^0/m_{22}^4 & C'_1 &= -[m_{32}^0 + am_{32}^0]/m_{32}^4 \\
B'_2 &= -[m_{22}^1 + am_{22}^1]/m_{22}^4 & C'_2 &= -[m_{32}^1 + am_{32}^1]/m_{32}^4 \\
B'_3 &= -[m_{22}^2 + am_{22}^2]/m_{22}^4 & C'_3 &= -[m_{32}^2 + am_{32}^2]/m_{32}^4 \\
B'_4 &= -m_{22}^3/m_{22}^4 & C'_4 &= -m_{32}^3/m_{32}^4 \\
B'_5 &= -[m_{23}^0 + am_{23}^0]/m_{22}^4 & C'_5 &= -am_{33}^0/m_{32}^4 \\
B'_6 &= -[m_{23}^1 + am_{23}^1]/m_{22}^4 & C'_6 &= -[m_{33}^1 + am_{33}^1]/m_{32}^4 \\
B'_7 &= -[m_{23}^2 + am_{23}^2]/m_{22}^4 & C'_7 &= -[m_{33}^2 + am_{33}^2]/m_{32}^4 \\
B'_8 &= -m_{23}^3/m_{22}^4 & C'_8 &= 0 \\
B'_9 &= -[m_{24}^0 + am_{24}^0]/m_{22}^4 & C'_9 &= -[m_{34}^0 + am_{34}^0]/m_{32}^4 \\
B'_{10} &= -[m_{24}^1 + am_{24}^1]/m_{22}^4 & C'_{10} &= -[m_{34}^1 + am_{34}^1]/m_{32}^4 \\
B'_{11} &= -[m_{21}^1 + m_{21}^0 - am_2^c]/m_{22}^4 & C'_{11} &= -[m_{31}^2 + m_{31}^0 - am_3^c]/m_{32}^4 \\
B'_{12} &= -m_{24}^2/m_{22}^4 & C'_{12} &= -m_{34}^2/m_{32}^4
\end{aligned} \tag{H.2}$$

$$\begin{aligned}
B_1 &= B'_1 + D_1 B'_{12} - \mathcal{U}_2^{N\mathcal{L}} (C'_1 + D_1 C'_{12}) \theta_1 \\
B_2 &= B'_2 + D_2 B'_{12} - \mathcal{U}_2^{N\mathcal{L}} (C'_2 + D_2 C'_{12}) \theta_1 \\
B_3 &= B'_3 + D_3 B'_{12} - \mathcal{U}_2^{N\mathcal{L}} (C'_3 + D_3 C'_{12}) \theta_1 \\
B_4 &= B'_4 - \mathcal{U}_2^{N\mathcal{L}} C'_4 \theta_1 \\
B_5 &= B'_5 + D_4 B'_{12} - \mathcal{U}_2^{N\mathcal{L}} (C'_5 + D_4 C'_{12}) \theta_1 \\
B_6 &= B'_6 + D_5 B'_{12} - \mathcal{U}_2^{N\mathcal{L}} (C'_6 + D_5 C'_{12}) \theta_1 \\
B_7 &= B'_7 + D_6 B'_{12} - \mathcal{U}_2^{N\mathcal{L}} (C'_7 + D_6 C'_{12}) \theta_1 \\
B_8 &= B'_8 - \mathcal{U}_2^{N\mathcal{L}} C'_8 \theta_1 \\
B_9 &= B'_9 + D_7 B'_{12} - \mathcal{U}_2^{N\mathcal{L}} [(C'_9 + D_7 C'_{12}) \theta_1 + (C'_{11} + D_9 C'_{12})] \\
B_{10} &= B'_{10} + D_8 B'_{12} - \mathcal{U}_2^{N\mathcal{L}} (C'_{10} + D_8 C'_{12}) \theta_1 \\
B_{11} &= B'_{11} + D_9 B'_{12}
\end{aligned} \tag{H.3}$$

$$\begin{aligned}
C_1 &= C'_1 + D_1 C'_{12} - \mathcal{V}_2^{N\mathcal{L}} (B'_1 + D_1 B'_{12}) \theta_1 \\
C_2 &= C'_2 + D_2 C'_{12} - \mathcal{V}_2^{N\mathcal{L}} (B'_2 + D_2 B'_{12}) \theta_1 \\
C_3 &= C'_3 + D_3 C'_{12} - \mathcal{V}_2^{N\mathcal{L}} (B'_3 + D_3 B'_{12}) \theta_1 \\
C_4 &= C'_4 - \mathcal{V}_2^{N\mathcal{L}} B'_4 \theta_1 \\
C_5 &= C'_5 + D_4 C'_{12} - \mathcal{V}_2^{N\mathcal{L}} (B'_5 + D_4 B'_{12}) \theta_1 \\
C_6 &= C'_6 + D_5 C'_{12} - \mathcal{V}_2^{N\mathcal{L}} (B'_6 + D_5 B'_{12}) \theta_1 \\
C_7 &= C'_7 + D_6 C'_{12} - \mathcal{V}_2^{N\mathcal{L}} (B'_7 + D_6 B'_{12}) \theta_1 \\
C_8 &= C'_8 - \mathcal{V}_2^{N\mathcal{L}} B'_8 \theta_1 \\
C_9 &= C'_9 + D_7 C'_{12} - \mathcal{V}_2^{N\mathcal{L}} [(B'_9 + D_7 B'_{12}) \theta_1 + (B'_{11} + D_9 B'_{12})] \\
C_{10} &= C'_{10} + D_8 C'_{12} - \mathcal{V}_2^{N\mathcal{L}} (B'_{10} + D_8 B'_{12}) \theta_1 \\
C_{11} &= C'_{11} + D_9 C'_{12}
\end{aligned} \tag{H.4}$$

$$\begin{aligned}
D_1 &= -[m_{42}^0 + am_{42}^0]/m_{44}^2 \\
D_2 &= -[m_{42}^1 + am_{42}^1]/m_{44}^2 \\
D_3 &= -m_{42}^2/m_{44}^2 \\
D_4 &= -[m_{43}^0 + am_{43}^0]/m_{44}^2 \\
D_5 &= -[m_{43}^1 + am_{43}^1]/m_{44}^2 \\
D_6 &= -m_{43}^2/m_{44}^2 \\
D_7 &= -[m_{44}^0 + am_{44}^0]/m_{44}^2 \\
D_8 &= 0 \\
D_9 &= -[m_{41}^0 - am_{41}^c]/m_{44}^2
\end{aligned}
\tag{H.5}$$

# IMAGE EVALUATION TEST TARGET (QA-3)



**APPLIED IMAGE . Inc**  
 1653 East Main Street  
 Rochester, NY 14609 USA  
 Phone: 716/482-0300  
 Fax: 716/288-5989

© 1993, Applied Image, Inc., All Rights Reserved